THE EFFECT OF NON-ENZYMATIC GLYCATION OF KERATINS ON THE PHYSICAL PROPERTIES OF PLANTAR EPIDERMIS IN TYPE II DIABETIC AND NON-DIABETIC INDIVIDUALS

A thesis

presented to University College London

in fulfilment of the regulations

for the degree of

Doctor of Philosophy

by

Farina Hashmi

Department of Medicine

University College London

ProQuest LLC
789 East Eisenhower Parkway
P.O. Box 1346
Ann Arbor, MI 48106-1346

Abstract

As keratin is the principle structure of the plantar stratum corneum, it has been postulated that changes in this protein, associated with non-enzymatic glycation, may contribute to abnormalities in the development of plantar callus in diabetes consequently leading to ulceration of plantar skin. The clinical appearance of the skin in the diabetic state has been described as being thicker and less flexible than non-diabetic skin, particularly in the hands.

A group of six Type II diabetic patients and six age and sex matched controls were initially selected for the verification of the methods of analysis to be used on a larger sample group.

Epidermal keratin extraction protocols were tested and their validity confirmed using immunoblot analyses.

The early glycation product, furosine and the advanced glycation end-products pentosidine and carboxymethyllysine were the glycation products chosen for quantification in plantar callus tissue. The quantification of furosine and pentosidine were successfully achieved using high performance liquid chromatography assays. The qualitative detection of CML was achieved using gas chromatography/ mass spectrometry (GC/MS).

In response to the lack of sensitivity of the GC/MS detection method for CML, polyclonal and monoclonal antibodies were developed. Screening of these antibodies identified a lack of specificity for CML detection and quantification.

In addition to the quantification of the glycation compounds in plantar epidermal tissues; the flexibility and thickness of the skin on three different sites on the feet were measured. The epidermal thickness was measured using high frequency ultrasound imaging and the mechanical properties of the epidermis were tested using vertical negative pressure methods.

The selected group of Type II diabetic subjects (n=103), in the final clinical study, showed a statistically significant increase in levels of pentosidine in plantar callus specimens compared with the control group (n=87). The quantity of furosine and pentosidine measured in the callus samples did not correlate with those measured in blood serum. The HbA1c levels showed no association between glycation of plantar epidermal proteins and glycaemic control.

The echogeneic images captured by ultrasonography were thickest on the plantar metatarsal sites, followed by the medial longitudinal arch and finally the dorsal skin sites. The epidermal thickness in the PMA region was greater in diabetics in comparison to controls and an association with neuropathy was suggested.

Pedal skin exhibited viscoelastic properties. The magnitude of the elastic component, measured immediately after the negative displacing pressure was removed, was significantly greater in diabetic skin than controls on all three sites on the foot. Plantar diabetic skin was significantly less plastic than non-diabetic plantar skin.

Acknowledgement

I would like to express my sincere thanks to my friends and colleagues at the Department of Medicine, University College London, Archway Campus. I feel privileged to have worked with such a professional and compassionate team of people.

In particular I would like to thank the following people:

Professor James Malone-Lee, my supervisor, for his support, guidance and enthusiasm throughout the process of this PhD. I am indebted to him for his constant encouragement leading to the completion of this thesis.

Professor Elizabeth Hounsell (School of Biological and Chemical Sciences, Birkbeck College, UK), my biochemistry supervisor, for her encouragement and support.

Professor Chris Fry for his help, patience and admirable teaching skills.

Dr Steven Goodrick for sharing his expert and invaluable scientific knowledge and for his friendship.

Dr Vidya Mohamed-Ali for her technical expertise and support with the work carried out in Chapter 6.

Shirley Burnett, Maria Christofi and Gurmesh Lohia for their help with the recruitment of patients for this thesis.

Jean Jones and Marcia Nickle for their help with patient recruitment and for their friendship.

Professor Paul Thornalley and his group (Department of Biochemistry, University of Essex, UK), for welcoming me to their laboratories and for their contributions to Chapter 3.

Dr Nikolay Paramonov (School of Biological and Chemical Sciences, Birkbeck College, UK) for teaching me many analytical chemistry techniques and Osnat Hakimi for her contributions to Chapter 5 as part of her final year BSc project.

Finally, I would like to thank the Dr William M. Scholl Podiatric Research and Development Fund for the financial support that allowed this work to proceed.

Foreword

This thesis incorporates the scientific disciplines of biochemistry, physics and clinical sciences, therefore the chapters have been organised according to their disciplines rather than the standard PhD format. The arrangement of each experimental chapter includes a literature review of methods, followed by the experimental methods and results, finishing with a discussion of the findings. At the end of Chapters 4, 7 and 8, the data collected from the non-diabetic subjects were statistically analysed and discussed. The data from diabetic subjects was compared to the control data in Chapter 9. This chapter includes the volunteer recruitment process in detail. The final chapter discusses all the results.

CONTENTS

List of Figures

List of Plates

List of Tables

List of Abbreviations

AGE	advanced glycation end-product
AG	aminoguanadine
A-V	arterio-venous
BMI	body mass index
BSA	bovine serum albumin
CE	cell envelope
C	carboxy group
CM	cell medium
CML	carboxymethyllysine
Da	daltons
dH_2O	deionised water
DNA	deoxyribonucleic acid
DVT	deep vein thrombosis
E	Young's modulus
EBM	epidermal basement membrane
EDTA	ethylene diamine tetra-acetic acid
EGTA	ethylene glycol-bis-(β-aminoethyl ether) N,N,N',-tetra acetic acid
ELISA	enzyme-linked immunosorbent assay
GC/MS	gas chromatography mass spectrometry
3 – DG	3 – deoxyglucasone
GO	glyoxal
HAT	hypoxantahine aminpterin thymidine
HAV	hallux abducto valgus
HbA1c	haemoglobin A1c
HBFA	heptafluorobutyric acid
HGPRT	hypoxanthine-guanine phosphoribosyltransferase
HMF	hydroxymethylfuraldehyde
HPLC	high performance liquid chromatography
IDDM	insulin dependent diabetes mellitus
Ile	isoleucine
IF	intermediate filament
IGF – 1	insulin-like growth factor
IgG	immunoglobulin G
IgM	immunoglobulin M

IL-6	interleukin – 6
K	keratin
KLH	keyhole limpet haemocyanin
l	litre
LDL	low density lipoprotein
LEA	lower extremity amputation
L/F	left foot
Leu	leucine
Met	methionine
MF	microfilament
MGO	methylglyoxal
M	molar
mbar	millibar
mg	milligram
μg	microgram
min	minutes
ml	millilitre
μl	microlitre
MLA	medial longitudinal arch
mm	millimetre
mM	millimolar
μm	micrometre
MS	mass spectrscopy
MT	microtubules
MTJ	midtarsal joint
MTPJ	metatarsophalangeal joint
m/z	mass charge ratio
η	viscosity
N	amino group
NEG	non-enzymatic glycation
ng	nanogram
NIDDM	non-insulin dependent diabetes mellitus
O/C	onychocryptosis
O/M	onychomycosis
OPA	*o*-phthaldialdehyde
O/X	onychauxis

PBS	phosphate buffer saline
PBST	phosphate buffer saline tween
PEG	polyethylene glycol
PM	pyridoxamine
PMA	plantar metatarsal area
PUVA	psoralens ultraviolet A
PVD	peripheral vascular disease
r	correlation coefficient
RAGE	receptor for advanced glycation end products
R/F	right foot
RIA	radioimmunoassay
RIS	reactive intermediate species
RNA	ribonucleic acid
ROM	range of motion
ROS	reactive oxygen species
RT	room temperature
s	seconds
SC	stratum corneum
SD	standard deviation
SDS	sodium dodecyl sulphate
SDS-PAGE	sodium dodecyl sulphate – polyacrylamide gel electrophresis
SIM GC-MS	ion selective monitoring gas chromatography mass spectroscopy
ROS	reactive oxygen species
STJ	sub-talar joint
τ	time constant
TBA	thiobarbituric acid
TFA	trifluoracetic acid
TFAA	trifluoracetic acid anhydride
Tg	thyroglobulin
Val	valine
WHO	World Health Organisation

Chapter 1 Review of Literature

1.1 Introduction to Callus, Ulceration and the Diabetic Foot

Corn and callus formation is a common occurrence affecting all age groups, particularly the elderly [1-7] and people with diabetes [8;9]. In the case of diabetes, the development of callus is one of the most common problems associated with the feet [10], and in such a high-risk group, is a warning sign for ulceration [11;12]. Neuropathy, vascular insufficiency and trophic changes add to the risk [13]. The neuropathic ulcer is invariably associated with the presence of callus [13]. Infection often complicates ulceration, which can cause overwhelming tissue destruction and subsequent lower extremity amputation (LEA).

Clinical observational data suggest that there is variation in callus texture in the diabetic foot from dry to macerated, but invariably it is thick and bulky. Only one paper has described the plantar callus of diabetic individuals as being "unusually hard" [14]. Since high vertical pressures and shear stresses imposed on the skin, encourage the development of callus it could be possible that formation of plantar diabetic callus is either a reaction to abnormal pressures or an abnormality of the specific area compromising the response to normal pressures. This poses the question - is there a connection between diabetes and the quality of the skin, in particular at the extremities?

Despite the increased awareness of the long-term diabetic complications, statistics for diabetic foot pathologies are still distressing. The prevalence of active foot ulceration varies around the world (Table 1.1), and is the most common cause of hospitalisation for diabetic patients in Western countries [15]. It is estimated that approximately 15% of people with diabetes, world–wide, will at some stage develop diabetic foot ulceration [12;16;17]. In studies of causal pathways leading to LEA, foot ulcers precede approximately 84% of amputations [12]. Lower extremity amputation in patients with diabetes is associated with high postoperative mortality and a high rate of secondary amputation, accumulating considerable health care costs [18].

Published data on the distribution of the risk factors of ulceration and amputation, in the British population of people with diabetes alone, is lacking. The length of stay in hospital for patients with diabetes is almost twice that of the non-diabetic population and the risk of hospital mortality in diabetics is almost three times that of non-diabetics [19]. The costs for treating these complications account for 25% of the hospital costs of diabetes care, but the indirect costs can be much more [17], for example the fitting of artificial limbs costs approximately £8500 per patient.

Table 1.1. The prevalence and cost of diabetic foot ulceration worldwide.

	UK	USA	Europe	Africa
Prevalence of Active Foot Ulceration	4 – 10%	1%	1%	11%
Annual Hospital Amputations per Year	£13.4 million	£350 million	Unknown	Unknown

A health problem of this scale merits attention. Plantar callus in the diabetic population is of major importance. There is not a great volume of research devoted to the etiology of callus. As the development of the callus is a key component of the pathophysiology of ulceration in diabetic patients it is a good target for initiating an exploration for preventative measures. The purpose of this thesis is to understand better the mechanisms of the development of callus and to contribute to the growing body of knowledge on preventable complications in the diabetic foot. The public health benefits of this research may be realised in the accurate and early detection of people with diabetes at greatest risk of developing foot ulceration, so that resources may be appropriately directed to preventative health programs.

1.2 Diabetic Foot Pathologies

Of the many diabetic complications, some of the most unpleasant affect the lower extremities. The remarkable factors associated with the diabetic foot are neuropathy, macrovascular and microvascular disease [20]. These processes may occur exclusively or together in varying degrees, placing the patient at risk of ulceration, infection, gangrene and ultimately amputation (Fig. 1.1–1.4). With regards to foot ulceration, there is a complex interaction between these

pathologies and other contributory factors, such as altered foot pressures; secondary to structural foot deformities and limited joint mobility [21].

1.2.1 Peripheral Neuropathy

Diabetic peripheral neuropathy is described as the presence of signs and symptoms of peripheral nerve dysfunction excluding other causes [22] and encompasses distal sensory motor polyneuropathy, autonomic neuropathy and mononeuropathy. Nerve damage of this kind occurs in up to 25% of people with diabetes mellitus 10 years post diagnosis and increases to 50% after 20 years duration of the disease [22;23]. Sensory polyneuropathy is the most common of the diabetic peripheral neuropathies, affecting 30% of diagnosed diabetic patients [22]. The clinical features of diabetic neuropathy are outlined in Table 1.2.

1.2.1.1 Peripheral Motor Neuropathy

The classic signs of peripheral motor neuropathy in the foot are a high medial longitudinal arch (*pes cavus*), and clawed or retracted lesser toes, with prominent metatarsal heads (Fig. 1.5 & 1.6). The clawing of the lesser toes is due to intrinsic muscle atrophy, as a result of the denervation of the muscles, leading to the excessive influence of the extensors. The foot becomes rigid and the shock absorption abilities diminish. This characteristic posture exposes the skin to high pressure points, particularly over the metatarsal heads, dorsal interphalangeal joints and the apices of the toes [16] and increases the susceptibility of these areas to ulceration [12]. The vulnerability of the plantar metatarsal area is further compounded by the atrophy of the plantar metatarsal fat pad as well as its anterior displacement as a result of retraction of the lesser toes [23]. The combination of insensitivity to pain, lack of proprioception and high pressures under the relatively exposed metatarsal heads, leads to callus and ulcer formation [24] (Fig. 1.7&1.8).

Figure 1.1. Dry digital gangrene in a neuroischaemic foot.

Figure 1.2. Necrosis secondary to popliteal artery thrombosis.

Figure 1.3. Necrosis indicated by blue – black discolouration surrounded by cellulitis and haemorrhage in a neuropathic foot.

Figure 1.4. Ulceration, discharge and necrosis in a neuroischaemic foot.

Pictures taken - Managing the Diabetic Foot [25]

Table 1.2. Features of neuropathy

	Motor Neuropathy	Autonomic Neuropathy	Sensory Neuropathy
Symptoms		• May be asymptomatic or severe • May accompany sensory polyneuropathy, or manifest as a pure autonomic affect	1) Non-painful and asymptomatic, or 2) Paraesthesia of feet and occasionally hands, or 3) Shooting pains and burning sensation, pins and needles sensation, in the legs and feet, especially at night.
Signs	***Cranial nerve lesions*** • Double vision due to damage to nerves that supply the eye • facial nerve palsy ***Isolated peripheral lesions*** • lateral cutaneous nerve of the thigh • femoral, sciatic and peroneal nerves affected ***Diabetic amyotrophy*** • proximal, painful, weakness and wasting of the leg and digital muscles • anterior compartment syndrome • loss of reflexes, but not loss of sensation • extensor plantar responses • decreased nerve conduction times	***Cardiovascular*** • postural hypotension • vagal denervation of the heart, with high resting heart rates • greater blood flow through superficial tissues, presenting in the foot as a warm and red ***Gastrointestinal tract*** • diarrhoea • delayed gastric emptying ***Sudomotor*** • facial and upper body sweating at meal times • loss of sweating in the feet ***Endocrine effect*** • Impaired or upset renin, glucagon or catecholamine release • Failure of metabolic response to hypoglycaemia ***Impotence*** • May present as the earliest feature of autonomic neuropathy	• Loss of vibration sense in feet • Loss of pain sensation in feet • Loss of thermal sensitivity in feet • Reduced or absent limb tendon reflexes
Outcomes			• Mild to moderate reduction on pain sensation • Muscle weakness and denervation of intrinsic foot muscles, leading to pes cavus
Outcomes of chronic neuropathy (after 20 year +)			• Glove and stocking anaesthesia • Impaired joint position sense, contributing to Charcot joint formation • Sensory ataxia, impaired gait and positive Romberg's sign • Deep trophic ulceration • Bladder atony and impotence

(Adapted from Assessment of the Lower Limb [26].

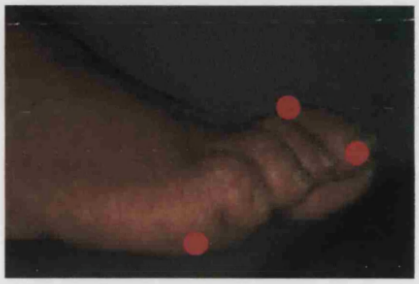

Figure 1.5. Clawed Toes (Secondary to *pes cavus*)
A fixed flexion deformity at the interphalangel joints.

Figure 1.6. *Pes Cavus*
The dorsum of the foot is domed due to a high medial longitudinal arch.

● **Points commonly associated with callus formation and ulceration.**

Figure 1.7. Ulceration over the dorsal aspect of the proximal interphalangeal joint of the third toe which is clawed

Figure 1.8. Ulceration of the apex of the fourth toe with overlying callus.

Pictures taken from - Managing the Diabetic Foot [25]

1.2.1.2 Peripheral Sensory Neuropathy

Neuropathic anaesthesia tends to follow a "glove and stocking" pattern affecting all modalities of sensation, although not necessarily to the same extent. Early signs of impending loss of sensation are feelings of vague numbness, paraesthesia, shooting pains, hyperaesthesia and atypical sensations such as burning pains. Acute neuropathy presenting early may improve with tight glycaemic control, but chronic longstanding changes are irreversible (Table 1.2).

1.2.1.3 Peripheral Autonomic Neuropathy

Autonomic dysfunction frequently coexists with sensory neuropathy and is characterised by reduced or absent perspiration along with increased blood flow. The resulting denervation of the sweat glands causes the skin to become dry and predisposes it to fissuring and callus formation [27]. The increase in blood flow occurs as a result of autonomic neuropathy of the vasomotor nerves to the foot causing the skin temperature to increase and the dorsal veins in the foot to become more prominent when the individual is supine. These changes are a result of arterio-venous (A-V) shunting that diverts blood away from the bones and the capillaries of the skin, causing Charcot foot collapse and skin atrophy respectively (Fig.1.9–1.12).

1.2.2 Peripheral Ischaemia

In long–term diabetes mellitus, both micro- and macrovascular disease is evident, particularly in the periphery. These pathologies manifest as arteriosclerosis, atheroma and median calcification and involve arteries below the knee. There is little evidence to support the thinking that microcirculatory disease is the sole cause of diabetic foot ulceration [12]. For instance, a thickening of the basement membrane surrounding muscle capillaries is a well established lesion in diabetes, but a similar lesion is not found in the capillaries of the skin [23]. The clinical signs of ischaemia are summarised in Table 1.3.

Figure 1.9. The Charcot Foot
Bone and joint damage in the metatarsal-tarsal region leads to the rocker-bottom deformity in which there is displacement and subluxation of the tarsus downwards, and the medial convexity, which results from displacement of the talonavicular joint or from tarsometatarsal dislocation. Both are often associated with a bony prominence.

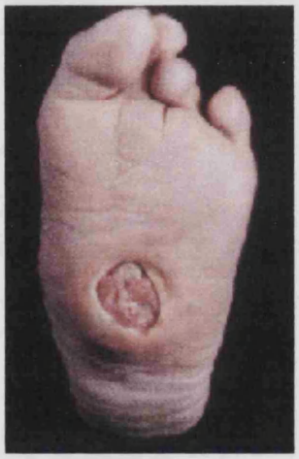

Figure 1.10. Ulceration over the bony prominence on the plantar surface of a rocker bottom deformity

Figure 1.11. Charcot foot showing a rocker bottom deformity.

Points commonly associated callus formation and ulceration.

Figure 1.12. Distended veins over the dorsum of the foot and ankle in the neuropathic foot.

Pictures taken from - Managing the Diabetic Foot [25]

1.2.3 Peripheral Neuro– ischasemia

Many patients with diabetes develop signs and symptoms of neuropathy and ischaemia. The coincidence of neuropathy places the foot at a greater risk of ulceration, as the normal warning symptoms of a compromised circulation, pain, is absent.

1.3 Hyperkeratosis and the Diabetic Foot

Hyperkeratosis is a thickening of the keratinised layers of the skin, in particular the stratum corneum (SC). In the foot it presents in the form of callus (a discreet area of thickened SC) or Heloma (a small area of callus containing a deep centre or nucleus of parakeratotic cells), which presses into the underlying skin. Callus presents in different ways in each different foot type in diabetes (Table 1.3 and Fig. 1.13 & 1,14).

It is known that the majority of people who suffer from corns and callus have increased forefoot loading [28;29]. The formation of callus is thought to be a normal protective response to trauma, partly due to abnormal anatomy and foot mechanics. If the mechanical trauma is removed, the skin will revert back to its normal structure. However, whilst this seems plausible, it has yet to be tested since the investigative methods for properly exploring this proposition have not yet been available.

An understanding of foot biomechanics will not answer all the questions, since lifestyle must also come into play through factors such as mobility, cadence, daily activities and footwear. The biochemical and clinical nature of callus tissue is discussed later.

Tables 1.3. The four types of diabetic foot and the presentations of callus.

	Clinical Signs and Symptoms	Callus Presentation
Normal	• No noticeable changes but at risk of developing fungal, bacterial and viral infections.	• Dry fissures around the heels occur in conjunction with dermatophyte infection.
Neuropathic	• Warm, with bounding pulses. • Characterised by Charcot joints and deep trophic ulcers, with associated infection. • Cavoid type foot shape with clawing of the lesser toes and trigger first toes. • Prominent joints. • Prone to ulceration.	• Skin is dry and prone to fissures. • Callus forms readily at areas of high pressures, particularly in cavoid and Charcot type foot.
Ischaemic	• Cold with thin, dry and atrophic skin. • Nail and hair growth is compromised. • Pulses are reduced or absent • Loss of muscle bulk in the lower limb. • Intermittent claudication and/or rest pain • Patchy dry gangrene and ulceration	• Plantar callus is thin, glass – like and difficult to debride. • Painful Heloma Mille form within the dry and inelastic skin. • Hyperkeratotic skin lesions and thickened nails may be underlain by tissue breakdown.
Neuro-ischaemia	• Similar to the ischaemic foot and limb i.e. temperature, paucity of blood supply and ulceration. • Foot will be relatively pain free	• Callus formation is similar to the neuropathic foot type.

(Note that the extrinsic factors such as poor footwear and activity levels also contribute to the build-up of callus.)

Figure 1.13. Plantar callus with extravasation

Figure 1.14. Dry skin with fissures on the periphery of the calcaneum

Taken from – Managing the Diabetic Foot [25]

1.4 Diabetic Foot Ulceration

Diabetic ulcers result in the loss of full skin thickness with exposure of dermal and, potentially, subdermal tissues. There are both physiological and mechanical events leading to foot ulceration (Fig. 1.15).

The neuropathic ulcer is associated with an excessive build-up of hyperkeratotic tissue, around its periphery. In contrast, an ischaemic ulcer has minimal callus on and around it (Table 1.4 & Figs. 1.16 -1.19).

Table 1.4. Comparison of neuropathic and ischaemic ulcers

Neuropathic	Ischaemic
Pain free	Excessively painful
Hyperkeratotic edges	Slight Hyperkeratosis
May be macerated	Usually dry unless infected
Occur on areas of pressure and shear	Occur at extremities
Medium to large	Initially small
Undermined walls	Vertical walls
Yellow purulent slough	Thick adherent slough
Copious discharge	Seropurulent discharge
General/ local neuropathy	Associated signs of ischaemia

Investigations into the aetiologies of plantar diabetic ulcers have, for many years, concentrated on pressure studies and limited interest has been directed to the formation of callus.

Non–enzymatic glycation (NEG) of the connective tissue collagen, abundant in dermal tissues and joint tendons, may influence the formation of diabetic ulcers. The process of glycation of collagen has an effect on the biomechanics of the tissue, mainly cross–linking of the collagen fibres, causing the reduction in the mobility of the tendons and skin of the foot. This leads to a lack of shock absorption during gait, both locally at high pressure points and generally throughout the foot. This is discussed in more detail in sections 1.24 onwards.

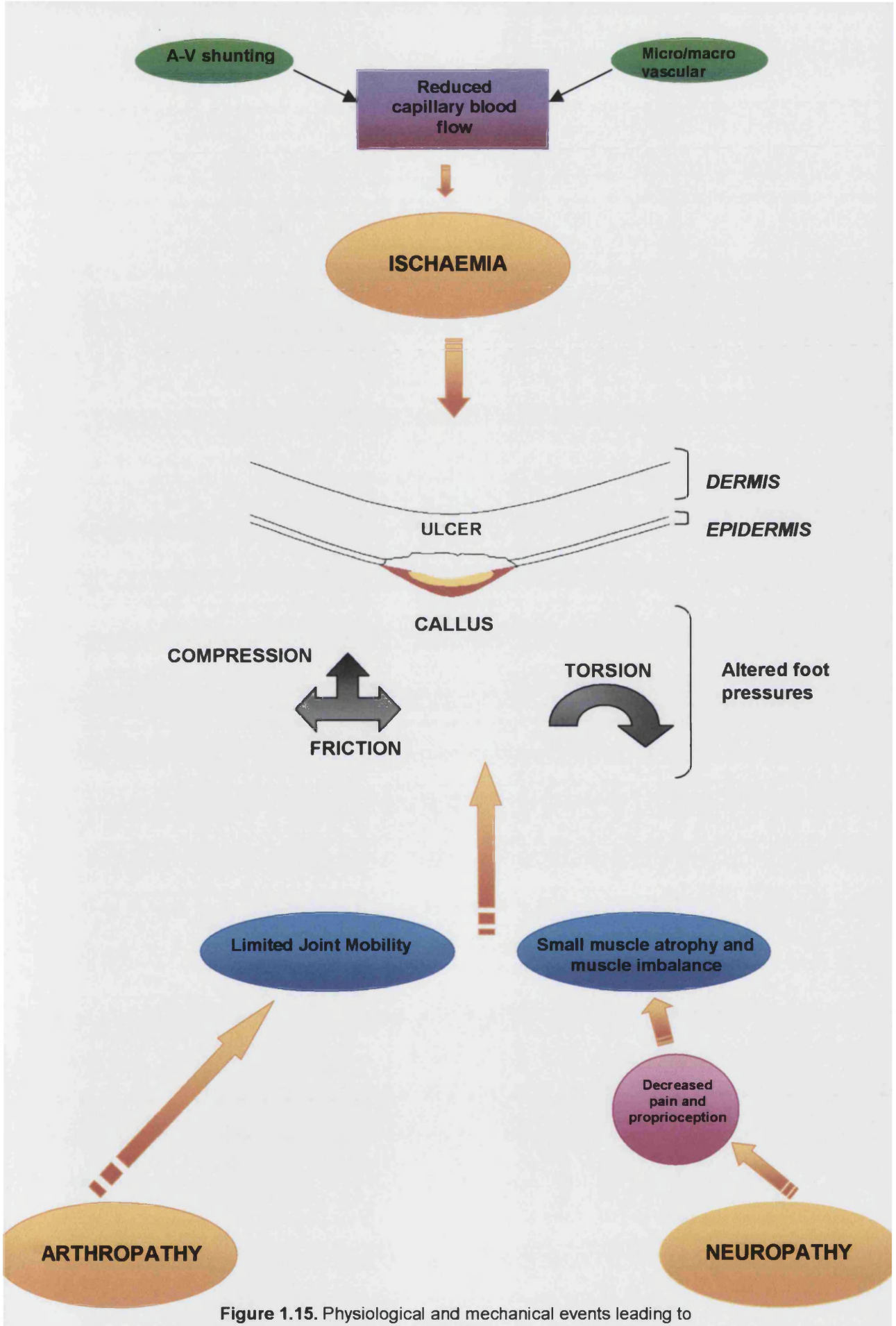

Figure 1.15. Physiological and mechanical events leading to ulceration

Figure 1.16. Callus over a neuropathic ulcer.

Figure 1.17. Neuropathic foot with plantar ulcer surrounded by callus.

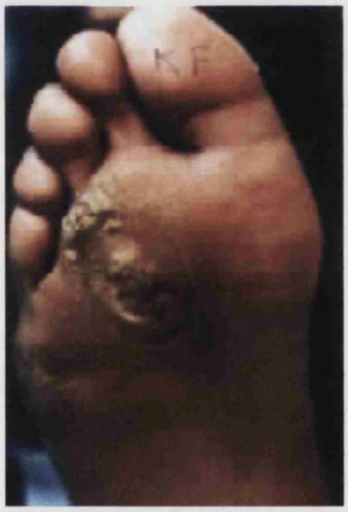

Figure 1.18. Callus over and surrounding a plantar ulcer.

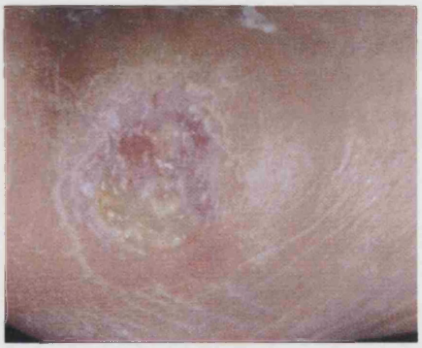

Figure 1.19. Neuro-ischaemic ulcer over the medial aspect of the 1st metatarsal-phalangeal joint.

Taken from – Managing the Diabetic Foot [25]

1.5 Causes of Plantar Ulceration

The two prerequisites for the formation of diabetic plantar ulcers are neuropathy[12;15] and elevated plantar pressures [30]. This is supported by the observation that neuropathic ulcers commonly form on the plantar aspect of the forefoot [23], the most common sites being the hallux and the 1st and 5th metatarsal heads. Limited mobility of the sub–talar joint (STJ) and 1st metatarsalphalangeal joint (MTPJ), is most prevalent in Type II diabetes [21;31] and may influence plantar foot pressures. This might explain why Type II diabetics present with more plantar callus in these areas than Type I diabetics [32].

Callus acts as a foreign body elevating plantar pressures further [11;33]. These data showed that callus was a better predictor of ulceration than foot pressure measurements. This is explained by two main schools of thought: firstly, callus may be a manifestation of long–term exposure to high pressure (from footwear) whereas foot pressure in many studies has been measured without shoes on; and secondly, the pressure required to produce callus may vary between individuals, but once it has formed it is at this point that the abnormal response to local pressures leads to ulceration. Finally, foot pressure systems measure only vertical pressure, but callus and ulceration develop in response to vertical and horizontal forces, and callus may represent a better measure of "total pressure".

Although the argument that high pressure causes damage to tissues is logical, the evidence is conflicting. It has been shown that diabetic patients with neuropathy tend to have high plantar pressures compared to non–diabetic controls and diabetic patients without neuropathy [23] and the vertical dynamic plantar pressures are especially high in those patients with a history of plantar neuropathic ulcers [27]. However, there is also contradictory data that show plantar pressures not to be elevated in insensate feet [16].

There is argument about the threshold pressure above which it is likely that injury to the tissue will occur. Boulton *et al* (1983) [27] have suggested a value of 1 MPa (measured between the foot and the floor), but ulcers have been observed in patients with considerably lower plantar pressures [34]. An example of a plantar

pressure distribution in a patient who has experienced a plantar ulcer is shown in Figure 1.20a. A comparison of the location of the ulcer with the peak pressure plot provides convincing evidence of the association between ulceration and high pressure. In contrast, the pressure distribution in Fig. 1.20b is from a patient with higher pressures and similar loss of sensation, but this individual has not experienced a plantar ulcer. These examples emphasise not only the importance of a multifactorial approach to the evaluation of risk in the diabetic foot, but it also renders uncertain the use of direct pressure measurement as predictive tool for plantar ulceration.

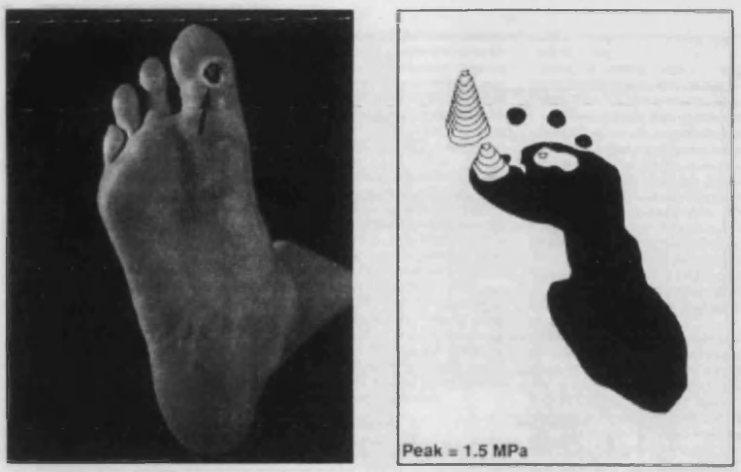

Figure 1.20a. (Left) Foot photograph from a patient with loss of protective sensation, hallux rigidus, and an ulcer (indicated by arrow) under the great toe.
(Right) Diagram depicting peak plantar pressure during late support phase of gait for the same patient. Contour intervals are 125kPa (taken from Sims DS *et al* 1988)[23].

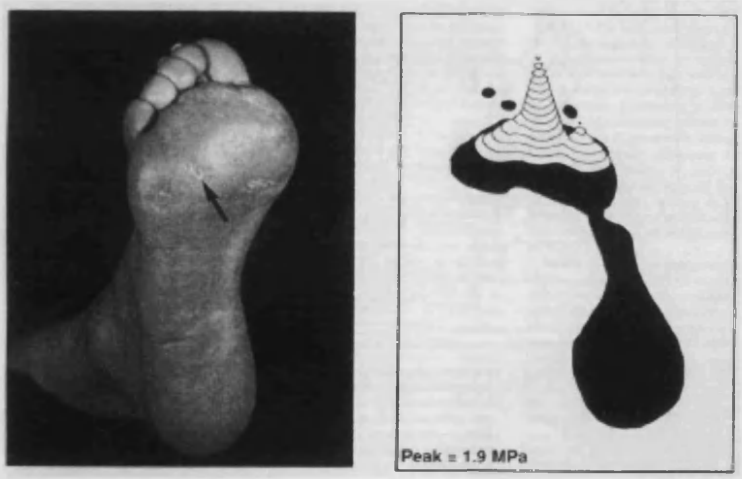

Figure 1.20b. (Left) Foot photograph from a patient with loss of protective sensation, marked equinus deformity, heavy callus formation (indicated by arrow), and absent history of ulceration.
(Right) Diagram depicting peak plantar pressures during late support phase of gait for the same patient (taken from Sims DS *et al* 1988)[23].

1.6 Dermal Manifestations of Diabetes Mellitus

Diabetes is accompanied by widespread biochemical, morphological and functional abnormalities of connective tissues such collagen and elastin, reflected as reduced elastic recoil of lung tissue [35]; elastic fibre fraying in Type I and II diabetic skin and resistance to digestion of collagen in diaphragmatic tendons [36].

Virtually all people who suffer with diabetes develop skin manifestations at some stage of the disease progression. Some of the manifestations might be explained on the basis of the attachment of glucose to dermal collagen proteins, and the metabolism of this combination, collectively termed non–enzymatic glycation (NEG). The NEG of skin changes its structure, function and colour. The biochemistry of NEG, and its relation to skin proteins, will be discussed in more detail later.

1.6.1 Diabetic Hand Syndrome

Limited joint mobility affecting the small joints of the hands (cheiroarthropathy) of diabetic patients has been recognised for some time and presents in conjunction with thick, tight, waxy skin on the dorsum of the hands [37-41]. This collection of pathologies have been attributed to neuropathy [42], duration of diabetes [37;43;44], retinal microvascular disease [43] and NEG of tendon and skin collagen [36;45].

The earliest description of this phenomenon was the observation that insulin dependent diabetes mellitus (IDDM) was often complicated with painful stiff hands. Subsequently, Rosenbloom and Frias (1974) [46] described three adolescent patients with long-standing IDDM, restricted joint mobility, thick tight waxy skin, growth impairment and maturational delay. This was substantiated further by similar observations in a larger cohort (n=309) of IDDM [47] and NIDDM patients [48]. Others claimed that although there was a weak correlation between skin thickening and duration of diabetes, skin thickness did not correlate with cheiroarthropathy [39].

1.6.2 Diabetic Thick Skin

Diabetic thick skin shows characteristic features different from those seen in scleroderma [38;40]. It presents as thickened and indurated skin at the extremities. The observation may range from clinically inapparent, but a measurable, increase in skin thickness unassociated with symptoms, to clinically apparent thickening of skin involving the fingers, hands and upper back region [49].

Pulsed ultrasound techniques have demonstrated forearm skin to be thicker in diabetics in comparison to non-diabetics [50]. Contrary to the pattern seen in non–diabetics, skin thickness in diabetics may increase with age. This may be associated with longer duration of diabetes. It is supported by evidence of the reduction in skin thickness following pump administration of insulin and tight control of blood sugar levels [51].

As most studies have concentrated on upper extremity skin, it is not valid to conclude that diabetic skin is thickened at other sites. In the case of the lower extremities, the pathogenesis of this condition has been attributed to factors such as neuropathy [41;42]; duration of diabetes [37;43;44]; and microvascular disease [47] and there are conflicting views about the effects of diabetes on skin thickness. Malik *et al* (1992) [52], found no significant difference in skin thickness on the extremities (dorsum of the foot) between diabetics and their non-diabetic counterparts. The inconsistency between studies is partly explained by the methods used for determining skin thickness, such as pinching the skin, giving a purely qualitative estimation [37]. Studies that have used ultrasound equipment, where an accurate measurement of thickness is achieved, have reported thicker skin in diabetics compared to non–diabetics [40]. Using ultrasonography techniques, Huntley and Walter (1990) [40] were unable to confirm a correlation between skin thickness, glycaemic control or duration of the disease, on the thigh, forearm and dorsum of the foot. The greatest differences were found at the thigh and the least at the foot, suggesting that the increased skin thickness is not necessarily uniform in diabetics nor a universal occurrence in diabetes. No studies of this kind have been carried out on the plantar aspect of the foot of diabetics where the majority of neuropathic ulcers form. Only one published study

has investigated plantar skin, in a small number of non-diabetic volunteers (n=9), using ultrasound imaging [53]. It has only been assumed, therefore, that the skin of the lower extremities of diabetics is thicker.

Whether the change in capillary blood flow, increased NEG, polyol accumulation[54;55] or other metabolic disorders are responsible for these findings has yet to be ascertained. All these observations establish joint contracture and waxy skin as complications of diabetes. Although they are multifactorial in origin, it is believed that the NEG of collagen plays an important role in the stiffening of connective tissues around the joints and the thickening of the skin [56]. A direct role of hyperglycaemia that relates to the increase in the NEG of proteins is implied [45;51].

1.6.3 Yellow Skin and Nails

Diabetic skin and nails often have a yellow hue [57] as a result of the accumulation of advanced glycation end–products (AGEs). The colour is best appreciated on the palmar and plantar sites because of the sparse competition with melanocytes in these areas (Fig. 1.21). All the nails are affected by the yellow colouration but it is most commonly seen on the distal edge of the nail of the hallux, as the protein turnover in this nail is very slow (more than one year). The level of AGEs in the nail plate have not been measured to date, but one study of the fingernails has demonstrated that diabetics have high levels of fructose–lysine (furosine), a marker of early glycation [58]. The yellow colouration of the skin and nails is seen in elderly non-diabetic people, NEG is part of the normal aging process. It is also noted in lymphatic odema from neoplasia of hypoplasia [59]. The significance of this observation in skin and nail tissue of diabetics is undetermined. One of the obvious questions is whether or not the yellow nails and skin can be used as a quantifiable indicator of the degree of NEG for other tissues of the body.

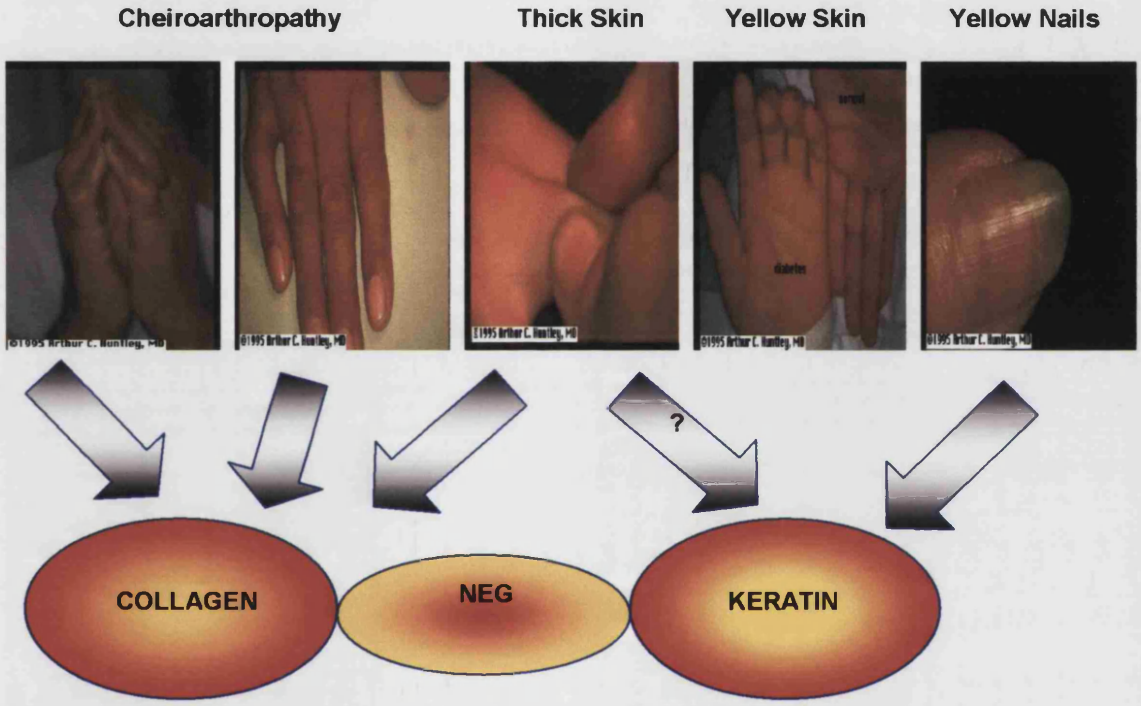

Figure 1.21. Illustration of cheiroarthropathy and its relationship with keratin and collagen. All photograph taken from reference [60]

1.7 Skin

The skin is comprised of two layers, the dermis and the epidermis. The principle fibrous proteins of the dermis are elastin and collagen and those of the epidermis are collectively termed keratins (~65% of epidermal proteins) [61]. There are many keratins and they vary in structure and function [62].

In the dermis the collagen and elastic fibres are laid down extracellularly but remain under the influence of fibroblasts. In contrast, keratin is laid down intracellularly and the keratinocytes (responsible for keratin synthesis) die in the terminal stages of the synthesis of keratin when the intermolecular cross-linkages are formed.

1.7.1 The Epidermis

The epidermis is made up of a keratinizing, multilayered (stratified), squamous epithelium. It is constantly being renewed, a protective adaptation, which compensates for wear and damage at the skin surface. This is most noticeable following injury and in some pathological states.

Although the basic organisation of the skin is the same throughout the body, the epidermis on the plantar aspect of the foot has several unique features [53], one being that it is considerably thicker than that on other parts of the body (1.4 and 0.1mm, respectively), particularly the SC layer. This correlates with the larger size and number of stratum corneum cells in palmar and plantar skin in comparison to other sites of the body [63].

1.7.2 The Structure and Function of the Epidermis

The epidermis is sub–divided into several distinct strata, each layer differing in the extent of cell differentiation (Fig. 1.22). It has five main functions: (1) protection against desiccation and external injury, such as chemical, thermal, microbial and photic stresses; (2) touch, pressure, pain and temperature sensation; (3) thermoregulation via insulation and via vasculature and evaporation of sweat. Hands, feet and ears act as heat exchangers; (4) metabolic functions including Vitamin D synthesis in the epidermis, storage of energy in the form of triglycerides in the dermis, and the skin as a whole has an immunological role particularly through the production of cytokines; and (5) it has a high coefficient of friction, which aids stability during locomotion.

Stratum Corneum

This is the outer most layer of the skin, and is made up of flattened squames, where the cellular structures have been lost and the cell contents and membrane converted to keratin and phospholipids. Desmosomic connections are still visible, but the most superficial layers lose their adherence to one another and desquamate. The adherence cells are enmeshed within a complex of lipid waxes, sterols and other products of keratinocyte lysis.

Stratum Lucidum

This lies superficial to the stratum granulosum, and is only seen as a clear homogenous line in glaborous skin. The cells are very flat, arranged in lamellae.

Stratum Granulosum

The cells of this layer lie superficial to the stratum spinosum, and they no longer mitose. It is two to four cells thick, and acts as the junction between the clearly living deeper cells and clearly dead cells of the outer epidermis. The cytoplasm contains a population of basophilic granules of keratohyalin made from transformed cell organelles and lysosomes containing hydrolytic enzymes. True keratin does not develop in this layer, but the disulphide bone characteristic of keratin is seen in this layer.

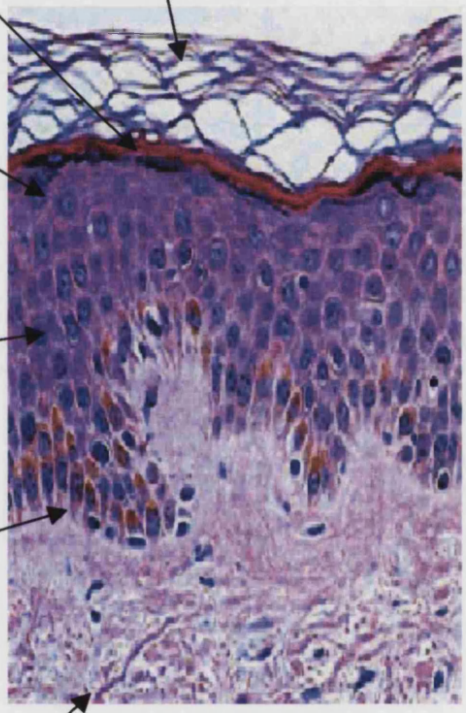

Stratum Spinosum

This lies just superficial to the stratum basale. The cells at this point can still undergo maturation and produce highly specialised structures involved in the process of keratinisation. It is comprised if several layers of polyhedral cells

Stratum Basale

This is the deepest layer of the epidermis and lies at the dermoepidermal junction. It is made up of one layer of living columnar cells (except in pathological states when more layers are found). The cells undergo frequent mitosis and the daughter cells formed are called keratinocytes, the principal cell type of the epidermis. These proliferating cells maintain the cell population of the epidermis.

Epidermal Basement Membrane

The epidermal basement membrane (EBM) is a dynamic structure, undergoing constant remodelling, that forms a continuous interface between the epidermis and the dermis (the dermo– pidermal – junction) and, as such it is thought to have a number of essential functions, including the support and attachment of epidermal cells, the regulation and nutritional transport between the dermis and the epidermis, and the control of epidermal development and organisation. The EBM appears to play an integral part in such physiological and pathological processes as wound healing, and blistering.

Figure 1.22. Schematic diagram illustrating the layers of the epidermis. Taken from reference [64].

1.7.3 Keratinisation

As the basal keratinocytes migrate upwards through the layers of the epidermis, they undergo remarkable morphological, biochemical and functional changes during the process of terminal differentiation (Fig. 1.23). The keratinocyte cells become polyhedral in shape, and flatten as they enter the SC layer. Originally about 6 micrometres in width, the cell in the horny layer flattens to 30 micrometres. The terminally differentiating cells lack a nucleus and are filled with keratin fibres. This process is called keratinisation [65]. This culminates in the formation of the SC layer, which provides a durable, pliable and effective barrier of tightly packed dead cells (modified keratinocytes called corneocytes).

When the cells reach the surface of the SC they are lost, a process called desquamation. The adhesion between the cells of the SC is influenced by intercellular lipid content [66], intercellular desquamin content [67] and the intercellular proteolytic degradation of cohesive structure [68]. An alteration in the distribution of these substances has an effect on the desquamation process. The time it takes for a single basal cell to migrate through the epidermis and desquamate (the epidermal turnover time) is between 40 and 56 days [69;70]. The time required for an individual cell to reach the surface, is greater for a thick SC. Epidermal turnover time of the SC on the forearm, back and thigh appears to decrease with age [71].

1.7.4 Hyperkeratosis

Hyperkeratosis is an excessive increase in the thickness of the SC (callus). It is a common feature of many chronic diseases such as lichen planus, psoriasis and chronic discoid lupus. In the case of hyperkeratosis on the foot, it is more of a response to mechanical trauma, resulting in the formation of callosities. Little is known about the persistence of callosities when the source of the mechanical trauma has been removed.

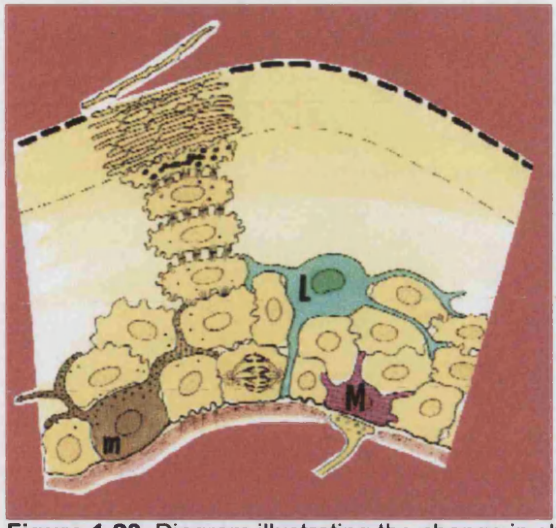

Figure 1.23. Diagram illustrating the change in shape of keratinocytes during keratinisation. Picture taken from reference [72].
m-melanocyte, **L**-Langerhans cell, **M**-Merkel cell

1.7.4.1 Hyperkeratosis and Mechanical Trauma

The SC shows locational variations both in structure and thickness, depending on the degree of mechanical trauma that the site is subjected to, for example the skin of the forearm is thinner than that on the sole of the foot. The skin, therefore, has an adaptive response to physical trauma. When callus plaques begin to form there is an alteration in the homeostatic mechanisms, which maintain normal epidermal thickness. Depending on the type and frequency of application, the epidermis responds to friction by either blistering (an acute response to friction) or by thickening (a chronic response). MacKenzie (1974) [73] attributed the chronic response to a decrease in the rate of desquamation as opposed to an increase in cell proliferation [66]. He suggested that friction induces an alteration in cell differentiation in the epidermis, leading to the formation of 'hard' keratins like that of hair and nails, that do not desquamate as readily as 'soft' keratins.

Springetts' model of callus formation (Fig. 1.24) suggests that tissues subjected to stress are stimulated to produce growth factors and inflammatory mediators [74]. These chemicals increase the transit time of epidermal cells resulting in the accumulation of immature cells, appearing in the form of callus at the surface of the skin.

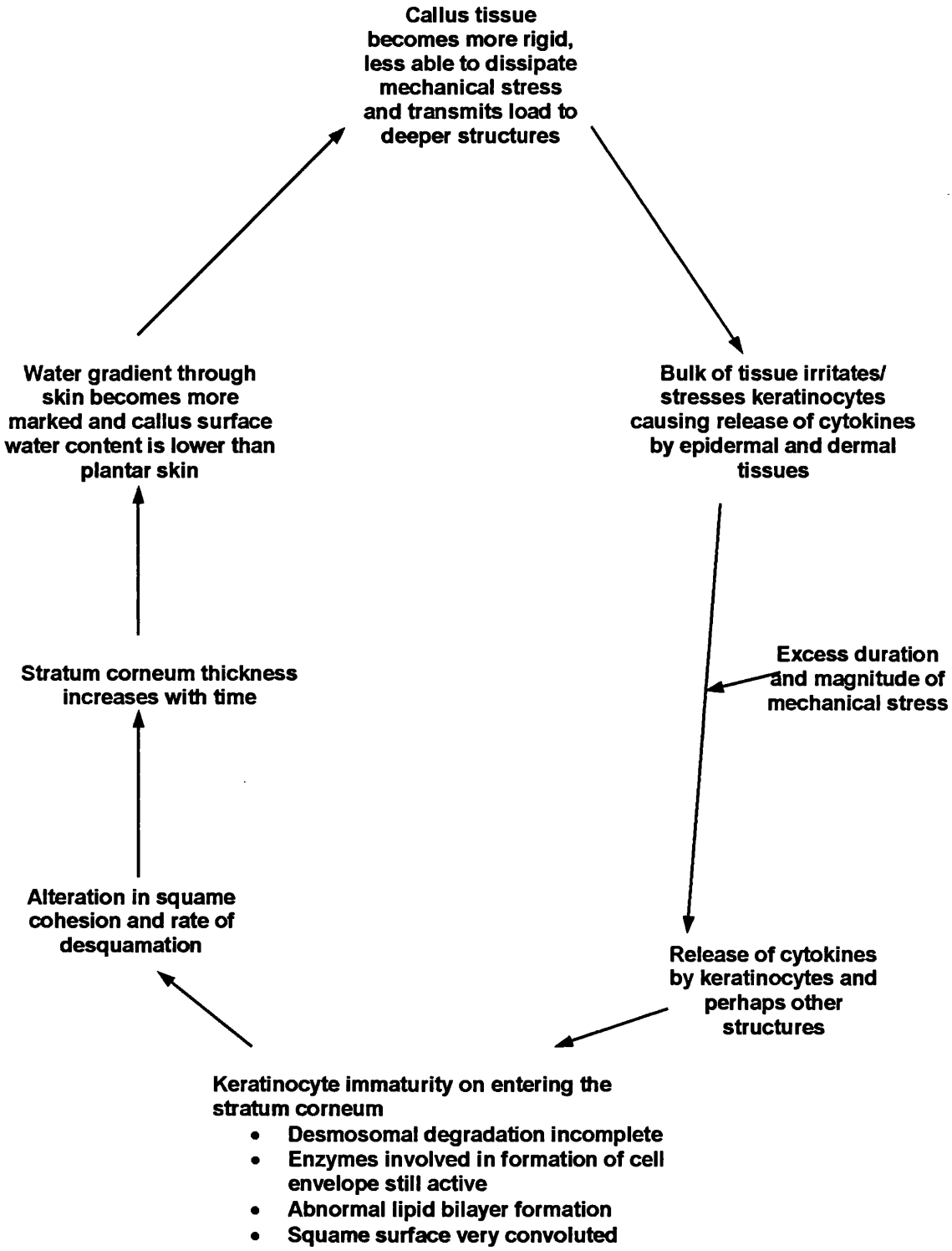

Figure 1.24. A proposed model for callus formation [74]

1.7.4.2 Stratum Corneum Cells and Mechanical Trauma

The cellular architecture of the SC is responsible for the major role it plays in the protective function of the epidermis. The SC cell surface is comprised of a series of projections and depressions, which complement those of adjacent cells [75], resulting in the strong cohesion between the cells of the SC which are arranged in tightly packed columns. The maintenance of this ordered stacking depends on the relatively slow rate of cell turnover. In the palmar and plantar regions this system is disrupted due to the high rate of cell proliferation [75]. The epidermis copes with this random stacking system by allowing faster surface clearance of cells and more massive SC [75].

A higher rate of cell proliferation results in cells moving much faster through the viable epidermis, and does not allow sufficient time for complete differentiation producing less dense corneocytes with a less ordered structure [63] When subjected to physical trauma corneocytes become thicker than those of normal skin and a large numbers of cells are formed (Tables 1.5 & 1.6) [63].

Proliferation is controlled by negative feedback mediated by endogenous hormone-like mitotic inhibitors. When injury occurs, these substances are lost and proliferation takes place. These inhibitors are glycoproteins called chalones. The epidermal glycoproteins, termed chalones, control cell division and desquamation. This is an important safety mechanism. It does not, however, explain why epidermis varies in thickness from one body site to another.

Table 1.5. Thickness of corneocytes at different sites on the human body [76]

Site	Mean Thickness (μm±SD)
Forehead	0.28±0.10
Axilla	0.22±0.05
Upper arm, lateral	0.28±0.03
Lower arm, ventral	0.23±0.05
Lower arm, dorsal	0.27±0.06
Paraumbilical region	0.29±0.05
Shoulder blade	0.23±0.07
Upper thigh	0.34±0.09
Lower leg	0.34±0.03
Palm	0.31±0.13
Sole	0.42±0.13

Table 1.6. The number of corneocytes counted at different sites on the human body [77]

Body area	Mean	Average % nucleated
Forehead	61,800	9.9
Axilla	104,000	2.3
Arm	152,500	0.7
Palm	96,400	2.6
Abdomen	134,000	0.4
Thigh	124,000	2.0
Heel	228,000	0.2

1.8 Keratins

Proteins are macromolecules that execute, regulate and mediate most biological functions in the cell as well as in the intercellular matrix. Each different protein in the organism performs a different task. To ensure that these reactions are beneficial to the organism, the proteins need to be efficient and specific in their function. Structural changes within proteins cause incorrect folding, leading to a loss or a modification of their biological activities. A number of processes can lead to this type of behaviour, including the introduction of covalent modifications such as oxidation and glycation.

Keratins, are the main fibrous proteins of the epidermis and are one of the most abundant proteins in the human body. Their molecular weights range from 40–70 kDa, implying approximately 350–550 amino acids per molecule [78]. They occur primarily as extracellular, insoluble fibres, which account for the major part of the organic mass of the epidermis, hair and nails. They possess unique structural and functional properties depending on the inter- and intra–molecular cross–linking of the keratin fibrils.

1.8.1 The Structure of Keratins

Keratin proteins adopt two types of structural conformations: α–helical (in the skin of mammals) and β–pleated (in the feathers of birds and the scales of reptiles).

1.8.1.1 Keratin Intermediate Filament Proteins

The intermediate filament proteins (IFs) are major components of the cytoskeleton (10–15nm in diameter) of most eukaryotic cells including keratinocytes, and they display considerable structural and functional heterogeneity. The other two major filament systems are actin microfilaments (MFs) (7–10nm in diameter), and microtubules (MTs) (25nm in diameter) [79]. The IFs are the most dynamic of the three filament types. In particular, reversible dissociation–association of IF dimers can occur along the entire filament length and not just at the two ends as is with the other two filament types. The

integrated network formed by the three filament systems is responsible for the mechanical integrity of the cell and is critically involved is such processes as cell division, motility and plasticity.

Epidermal keratinocytes contain an abundance of IF proteins, the correct formation of which is essential for normal differentiation. The filaments are synthesized in and retained by the inner living cell layers and eventually constitute the major component (up to 2/3 of the total mass) of the terminally differentiated SC. Keratins are the most diverse proteins and, unlike other IF proteins, are heteropolymers comprising of at least one Type I (acidic, pH range 4.5–6) keratin and one Type II (neutral–basic, pH 6.5–8.5) keratin. To date, 16 human Type I keratin IF proteins have been described, ranging in size from 40 to 65 kDa and 13 larger Type II keratins (50–70 kDa).

1.8.1.1.1 The Primary Sequence of Keratin Intermediate Filaments

All IF proteins exhibit a characteristic 'tripartite' structure, which includes the α–helical central domain, the 'rod' (highly conserved in size 310–315 amino acid residues), and the non–helical 'head' (amino terminal) and 'tail' (carboxyl terminal) domains located at either end of the rod domain [79]. The characteristic features of the central rod domain reveals a pronounced heptad repeat $(a\text{-}b\text{-}c\text{-}d\text{-}e\text{-}f\text{-}g)_n$, where portions *a* and *d* are occupied by apolar amino acid residues (e.g. Leu, Ile, Met or Val) and the other positions are occupied by polar or charged residues. This gives rise to an alpha–helical twist in the polypeptide chain favouring the formation of a coiled–coil structure, and producing a characteristic pattern of charged and hydrophobic residue (Fig. 1.25 & 1.26). The coiled–coil structure defines the overall elongated shape of an IF dimer. The IF proteins have 4 coiled–coil domains (1A, 1B, 2A and 2B) which are separated by short linear regions or linker segments (L1, L12 and L2) (Fig. 1.27). The elementary unit of an IF is long (~47 nm) and thin (~2–3 nm) central rod-like dimer domain, which accounts for roughly 38 kDa in molecular weight terms. Thus, the smallest keratin (K19), which is only 40 kDa, possesses a rod domain with only a minimal amount of amino (N) and carboxy (C) terminal sequences.

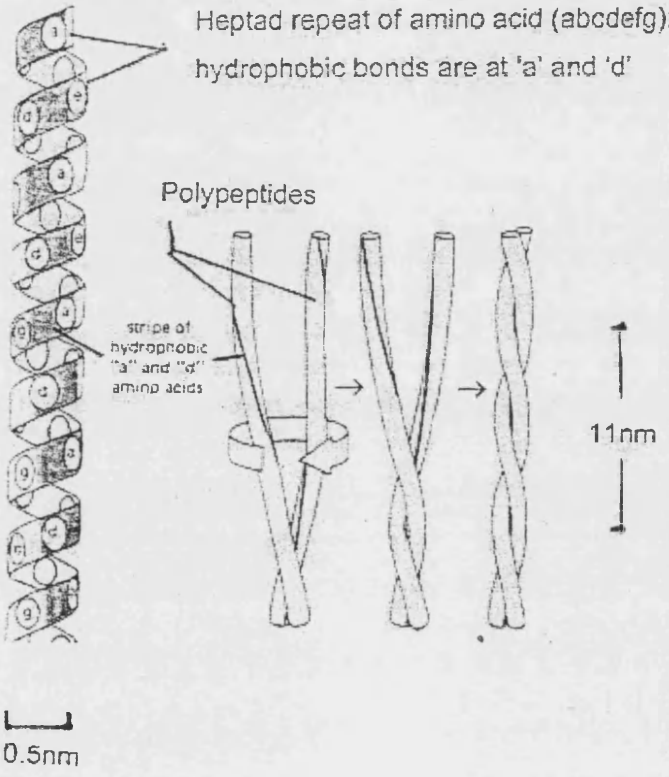

Figure 1.25. Coiled–coil parallel heterodimer formation.

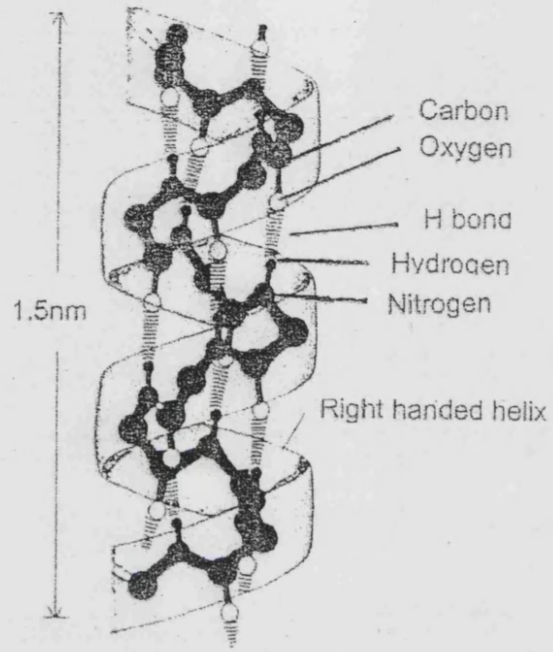

Figure 1.26. The alpha helix secondary structure. Alpha helix with the hydrogen bonds holding the chain in a coil. There are 18 amino acids per five turns of the coil and there are always two amino acid groups distance between the hydrogen bonds.

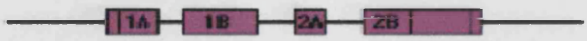

Figure 1.27. Homologous regions of keratin intermediate filaments

It is these N- and C- terminal sequences that are responsible for the heterogeneity of the IF proteins in terms of size (2–32 kDa) and composition. Although the rod domain structure is highly conserved in Type I and II keratins, the terminal sequences (especially the C–termini) are often unique and have specialised primary and secondary structures which differ not only between types of IF proteins but between different keratins too.

1.8.1.1.2 Structure of the Elementary Intermediate Filament Dimer

Two dimers condense to form an anti–parallel staggered tetramer which in the case of keratins has two Type I and two Type II subunits [80]. These aggregate with other tetramic units to form and 8–chain unit and eventually a filament of 10–15nm diameter [81] (Fig. 1.28). An additional non-random periodic distribution of acidic and basic residues in the rod has been suggested to play a role in intermolecular ionic associations (Table 1.7). A series of zones alternating acidic and basic residues seem to repeat at ~9.5 residue intervals along the molecule, or 3 times every 28 residues [62]. This charge periodicity may reflect the importance of electrostatic interactions in stabilising associations between coiled–coil dimers or higher ordered structures. The filaments form a lattice structure that has approximately 32 polypeptide chains in cross–section, which often aggregate together to form tonofilament bundles and run through the cellular cytoplasm terminating at the desmosomal complexes that rivet the adjacent keratinocytes together.

Scanning transmission electron microscopy shows the filaments to appear 'fuzzy' at the surface and the density falls off at the periphery. This indicates that the N–and C–terminal sequences, which are extensive for the larger keratins, lie on the surface of the filament and protrude into the cytoplasm. Studies of epidermal keratins suggest that the termini are on the surface, as proteolytic modification and phosphorylation of intact filaments produces molecular alterations to the terminal sequences. As the IF proteins all differ in the nature of their terminal sequences, and these are accessible to the surrounding cellular environment, it appears that the function of individual IF proteins is dictated by the nature of these heterogenous terminal ('surface') structures.

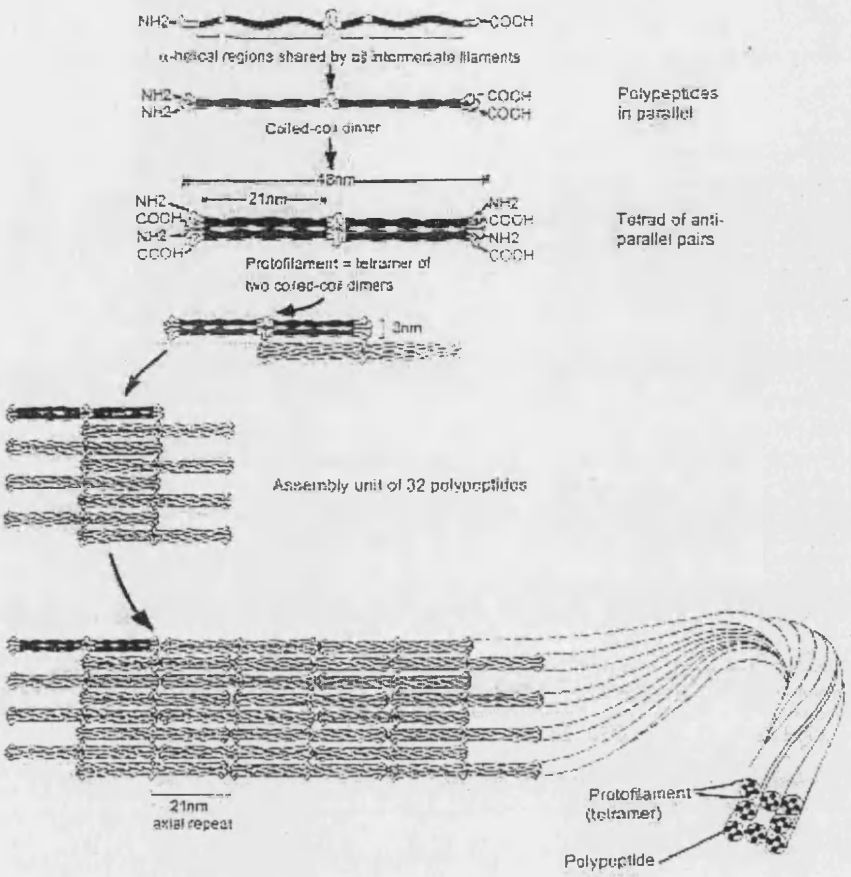

Figure 1.28. Model of intermediate filament construction. The monomer shown in **a** pairs with another monomer to form coiled – coil dimer **b**. The dimers then line up to form an anti – parallel tetramer **c**. The final 10nm rope like intermediate filaments are packed together in a helical array.

1.8.2 Mechanical Properties of Keratins

The mechanical properties of keratins are a function of the geometrical form and the intrinsic properties of the filament matrix. The combination of the linearly elastic, high modulus fibres, embedded in a viscoelastic low modulus matrix has a biological value in being able to distribute any applied stress evenly over the filaments, thus preventing the propagation of cracks or points of rupture. The α–helical structure in conjunction with the long length of the keratin filaments allows for bending and stretching. The keratin filament matrix is an aqueous environment with cysteinyl residues in a reduced form. In the final stages of synthesis the cysteinyl residues are oxidized in pairs to yield disulphide cross–linkages which stabilize the matrix (Table 1.7). When the keratin is eventually exposed to the environment, there is a reduction in water content, accompanied by shrinkage, and a profound change in the mechanical properties of the matrix causing it to become stiffer and brittle. Little is known about the proportion of matrix proteins in 'soft' keratins, therefore, it is difficult to determine their contribution to the mechanical properties of the epidermis.

Keratinocytes specialise in making keratins, but other proteins include involucrin, fillagrin and loricrin to mention but a few. These are matrix and cross–linking proteins which, like keratin IF proteins are expressed to a high level to provide structural integrity to tissues.

Table 1.7. The three main chemical bonds involved with the structure of keratins.

	Disulphide Bonds	**Hydrogen Bonds**	**Salt Bonds**
Atoms involved	-S – S – (cysteine residues)	- NH & - C=O	- C=O negatively charged - - N – H positively charged
Bond interaction energies	30 – 100 cals/molecule	2 - 10 cals/molecule	10 – 20 cals/molecule
Chemical characteristics	- Resistance to digestion. - Resistance to hydrolysis.	Can be ruptured by 6M urea	- Bonds cross – link polypeptide chains. - Difficult to rupture. - Ruptured by alkalies – but also rupture disulphide bonds.

1.8.3 Keratin Expression in the Epidermis

It seems very likely that different keratins provide cells with subtly different properties of resistance and plasticity to equip them with the ability to resist the physical stresses of each particular body site. During normal keratinisation the expression of epidermal keratins alters during terminal differentiation. The basal cells of the epidermal proliferative compartment are composed largely of K5 and K14, providing crucial mechanical support within the basal region [82]. As cells become committed to terminal differentiation, they switch on two other keratin genes: K1 and K10 [62]. Biochemical, immunological and *in situ* hybridisation data show that K5 and K14 are progressively down–regulated and that the filament system in the upper suprabasal cells not only increases in density but also changes in composition, as more K1–K10 appears. When the cells reach the upper granular layer, the filament system is composed almost entirely of K1 and K10. These filaments are then proteolytically modified, becoming smaller and more acidic as the organelles are removed and the dead corneocytes are formed. When the skin is damaged there is an over production of K6 and K16 at the expense of K1 and K10.

1.8.4 Keratin Expression in Plantar Epidermis

Although, K2 and K9 are generally minor components in the epidermis, they are abundant in palmar and plantar epidermis [83]. The raised papillary ridges overlying the primary epidermal ridge take most of the compression stress on this skin. This is also the region where the palmo–plantar specific keratin K9 is most highly expressed [84], strongly suggesting that the function of K9 is to provide additional reinforcement in this stress–bearing epidermis [84]. Keratins K6 and K16 are also constitutively expressed in palmar and plantar epidermis and are expressed in response to any wounding or perturbation of the epidermis such as hyperproliferation [85;86]. The expression of K16 in the intervening secondary ridge zones may provide areas of plasticity and elasticity in between stiffer K9–expressing patches, as well as strengthening the epidermis [87] to prevent it from being torn apart [84].

1.9 Advanced Glycation End Products and Diabetes

Glycation* is a complex, series of parallel and sequential non-enzymatic reactions of glucose, α-oxaldehydes and other saccharide derivatives with proteins, nucleotides and lipids, resulting in structural modifications of the proteins involved[87]. Also known as the 'Maillard reaction', the process was first discovered in 1912 by the French food chemist L.C. Maillard who noted the browning of amino acids when heated with sugar [88]. Food chemists continued to work on the chemistry of the Maillard reaction, leading to the hypothesis that a similar reaction could also occur between other amino substances other than in foods [89] .It is the AGEs that form cross–links between proteins, having effects on their chemical and physical behaviour. AGEs have been proposed in hypotheses to explain a number of diabetic and age–related complications [90]. Although the basic chemistry of the process was described more than ninety years ago, it is only in the last twenty years that extensive, clinical research in this area has taken place[91].

Alterations in the structural and functional properties of proteins as a result of AGE formation are implicated in key diabetic pathologies, in particular diabetic microvascular disease [92;93], neuropathy [94] and nephropathy [95], as well as being implicated in a wide range of other pathologies such as cartilage pathology, in rheumatoid arthritis [96]; amyloid plaques in Alzheimer's disease [97]; and nephron structural change in end stage renal disease [98] .

The pathophysiological changes that result from AGE accumulation, follow 3 general mechanisms:

- ***Extracellular AGEs and matrix dysfunction*** – The functional properties of several important matrix components are altered by AGE formation. The first matrix protein to be seen to undergo intermolecular covalent, bonds

* Protein glycosylation is the chemical addition of carbohydrate or glycosyl groups to peptides or proteins, to produce glycopeptides or glycoproteins. Glycosyl transferases are used in this biochemical reaction. Glycation is a less controlled reaction by which a sugar ketone or aldehyde group becomes attached to the free amino groups of proteins or amino acids without the assistance of an enzyme. This attachment occurs at the free amine group of lysine or arginine, which is not involved in the peptide bond.

via AGEs, was collagen [99]. AGE formation on collagen also covalently cross–links soluble plasma proteins such as low-density lipoproteins [100] and immunoglobulins. These trapped plasma proteins contribute to the characteristic nature of the narrowing of the vascular lumen in diabetes. The structure and function of intact vessels appear to be altered by these AGE–induced abnormalities in the extracellular matrix [101].

- ***Cellular receptors for AGEs*** – Monocytes and macrophages were the first cells on which the high affinity receptor for AGE was identified [101]. As a response to receptor binding by AGE–proteins, the macrophages produce cytokines (IL–6, IGF–1 and TNF-alpha). These cytokines are produced at levels that have been shown to increase glomerular synthesis of Type IV collagen and to stimulate proliferation of arterial smooth muscle cells and macrophages [101;102]

- ***Intracellular glycation*** - Haemoglobin was the first protein for which intracellular NEG was demonstrated to reflect time–integrated glucose concentration. These modifications involved the Amadori product, not AGEs and alter the protein function in the target tissues. Intracellular AGE formation may also affect DNA function causing mutations and potential deleterious effects on gene expression.

Current understanding of how chronic hyperglycaemia leads to the pathophysiological features of diabetic complications is due, in part, to the better understanding of the role of AGEs. The chemical processes and pathways that ultimately lead to AGE formation have yet to be fully clarified. Not all AGEs have been isolated; those that have been characterised are heterogeneous in nature and have a tendency to be unstable during isolation. There is currently no universally accepted method of detecting AGEs, no internal standards or any internationally recognised standard unit of measurement. These inconstancies make the comparisons of results between different research groups difficult. Although the actions of AGEs are complex and not fully understood, the currently known AGEs produce the same chemical outcome.

1.9.1 The Chemistry of Glycation – The Formation and Structure of AGEs

1.9.1.1 The Hodge Pathway

The Hodge pathway represents the classic two–stage glycation reaction.

1.9.1.1.1 Stage 1 – Formation of Amadori Products

Most studies of glycation reactions have investigated the modification of N–terminal amino groups in circulating and tissue proteins by the carbonyl groups of the free glucose [103]. The range of extent of glycation is typically 0.1-1% of lysine and arginine residues in proteins [104]. The first step is a concentration dependent process [105] involving the binding of glucose to a protein and the formation of early glycation products (Schiff's base). A Schiff's base is an unstable and reversible product that exists mainly in the form of cyclic glycosylamine, for example fructoseamine. With time it either dissociates or undergoes a further reversible rearrangement, to form a Amadori or Heyns product, depending on whether the implicated sugar is an aldose or a ketose, respectively [104]. An example of an Amadori product is fructose–lysine or furosine (Fig. 1.29).

1.9.1.1.2 Stage 2 – Formation of AGEs

The early glycation products follow complex degradation reactions such as dehydration, condensation and oxidation, to become AGEs [106]. Examples of known AGEs are pentosidine and N^{ε}- (carboxymethyl)lysine (CML) [107] (Fig. 1.30 & 1.31). Pentosidine and CML are termed glycoxidation products [108-111] as both glycation and free radical oxidation reactions are required for their formation from reducing sugars. Oxidation of polyunsaturated fatty acids may also lead to the formation of CML, suggesting the role of lipid oxidation AGE formation [112;113].

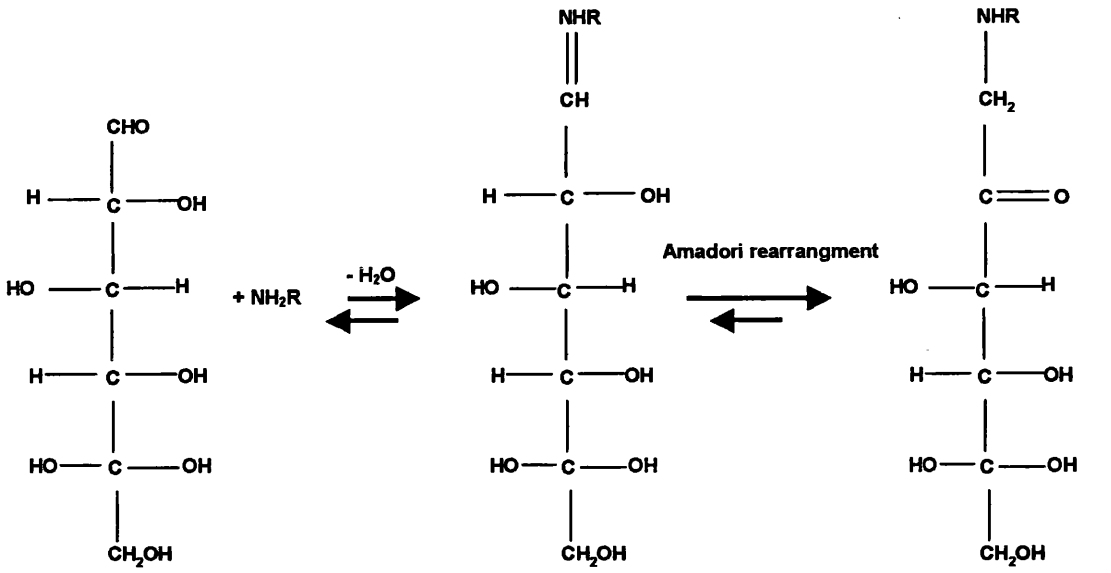

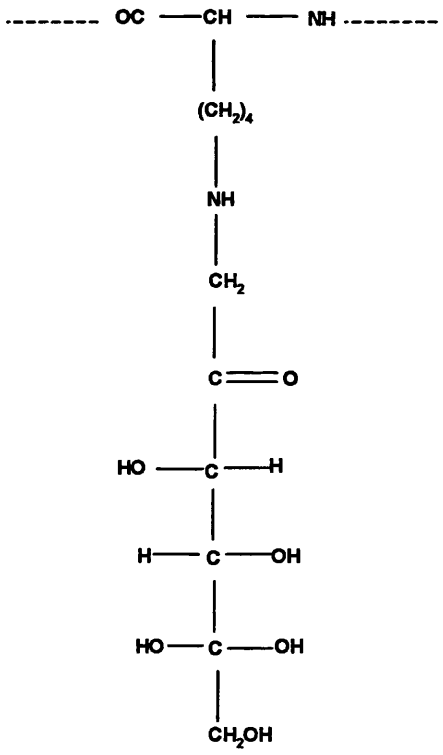

Fructoselysine

Figure 1.29. Reaction between glucose and lysine epsilon amino group

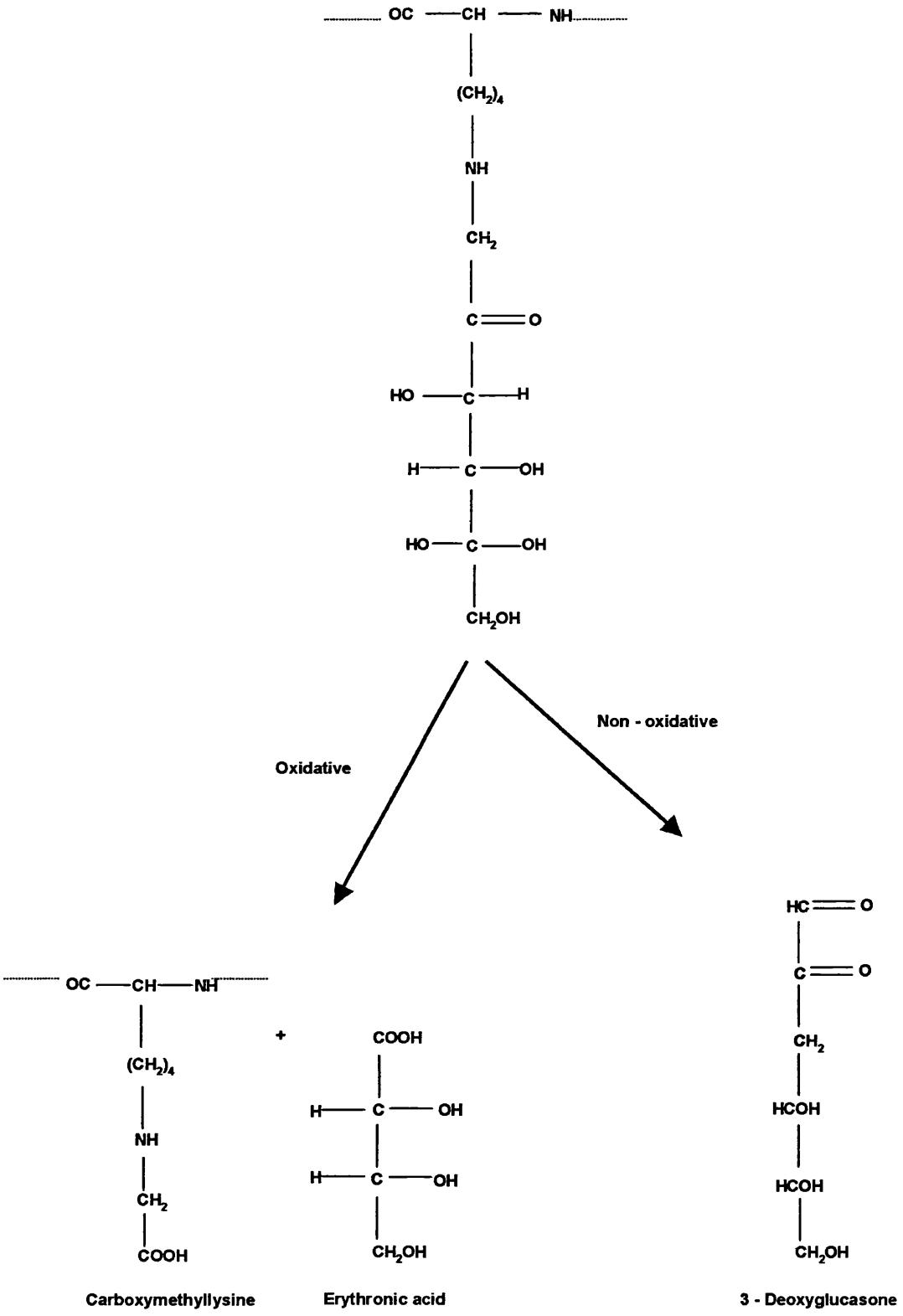

Figure 1.30. Degradation of fructoselysine (furosine)

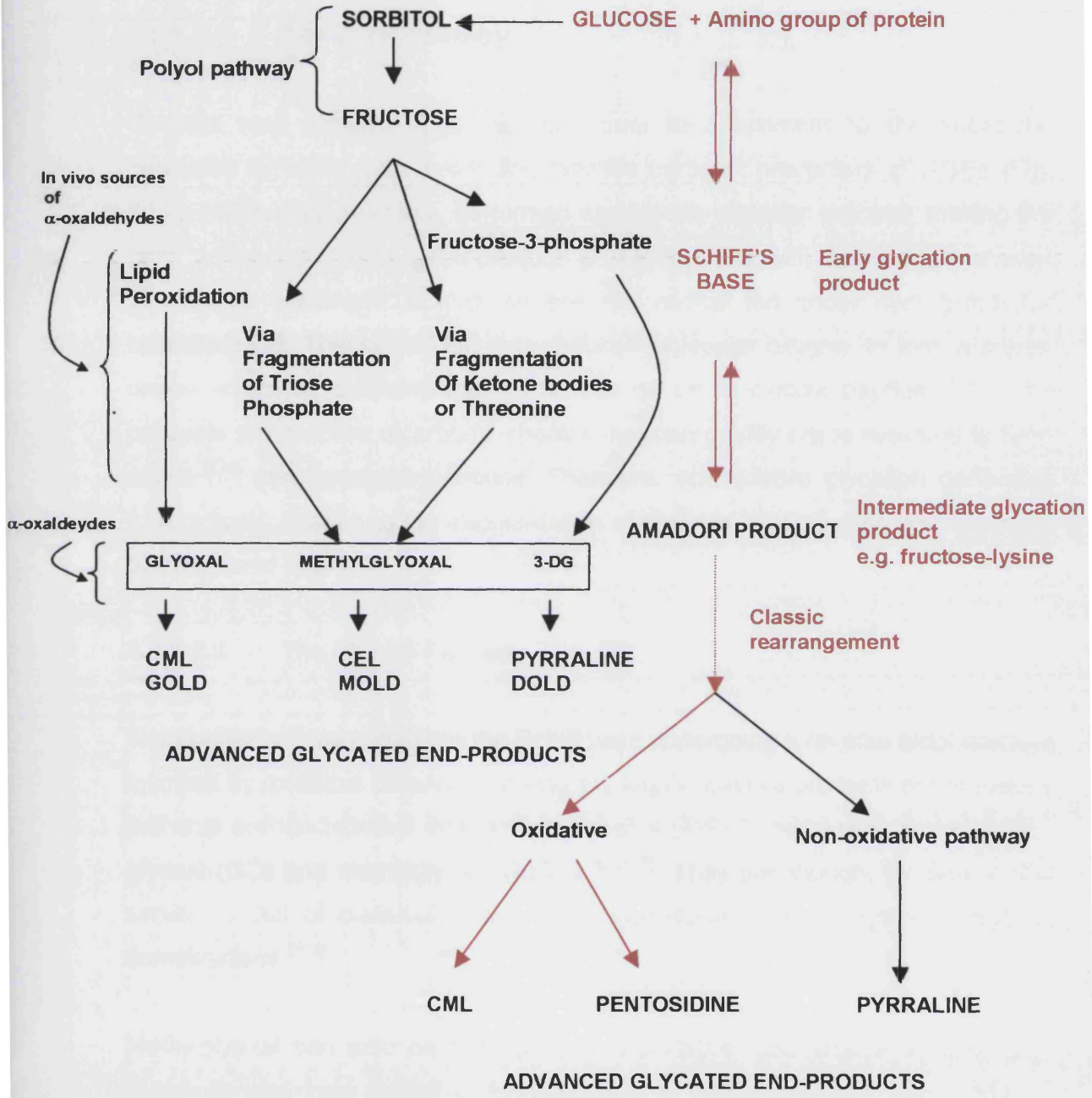

Figure 1.31. A schematic diagram illustrating the known different pathways for the formation of AGEs. The part of the diagram in red font illustrates the pathway of interest in this study.

1.9.1.2 Alternative Pathways

1.9.1.2.1 The Wolff Pathway

Glucose may undergo auto-oxidation, prior to attachment to the substrate, catalysed by metal ions, producing reactive carbonyl precursors of AGEs (Fig. 1.32). AGEs may, therefore, be formed early in the glycation process, making the term "advanced glycation end product" a misnomer; as with the Hodge pathway, glucose is rearranged to form an ene–diol radical ion under hyperglycaemic conditions [114]. This radical ion then reduces molecular oxygen, to form a super-oxide- anion: an oxidizing agent that can go on to oxidize peptides [114]. The products are reactive dicarbonyl species that can modify lysine residues to form AGEs [114] and hydrogen peroxide. Therefore, autoxidative glycation generates free radicals, leading to the fragmentation of proteins, cross-linking and oxidation of associated lipids.

1.9.1.2.2 The Namiki Pathway

The Namiki pathway, involves the Schiff base undergoing a reverse aldol reaction followed by oxidative cleavage. Among the highly reactive products of the Namiki pathway are the reactive intermediate species (RIS) 3–deoxyglucasone (3-DG), glyoxal (GO) and methylglyoxal (MGO) [91;115]. They are thought to have a role similar to that of classical AGEs in the development of old age and diabetic complications [104].

Methylglyoxal can also be formed by non-oxidative mechanisms in anaerobic glycolysis and from oxidative decomposition of polyunsaturated fatty acids. In addition, MGO can be derived from fructose by fragmentation of triose phosphate (whose intracellular concentration is increased in diabetes mellitus) or the catabolism of ketone bodies and threonine [104]. Methylglyoxal is a physiological α-oxaldehyde that can bind to modify arginine, lysine and cysteine residues in proteins (Fig. 1.33). It is formed from glyceraldehydes-3-phosphate and dihydroacetone phosphate, metabolites of the Embden Meyerhof pathway that are generated from glucose or from fructose, a product of the polyol pathway.

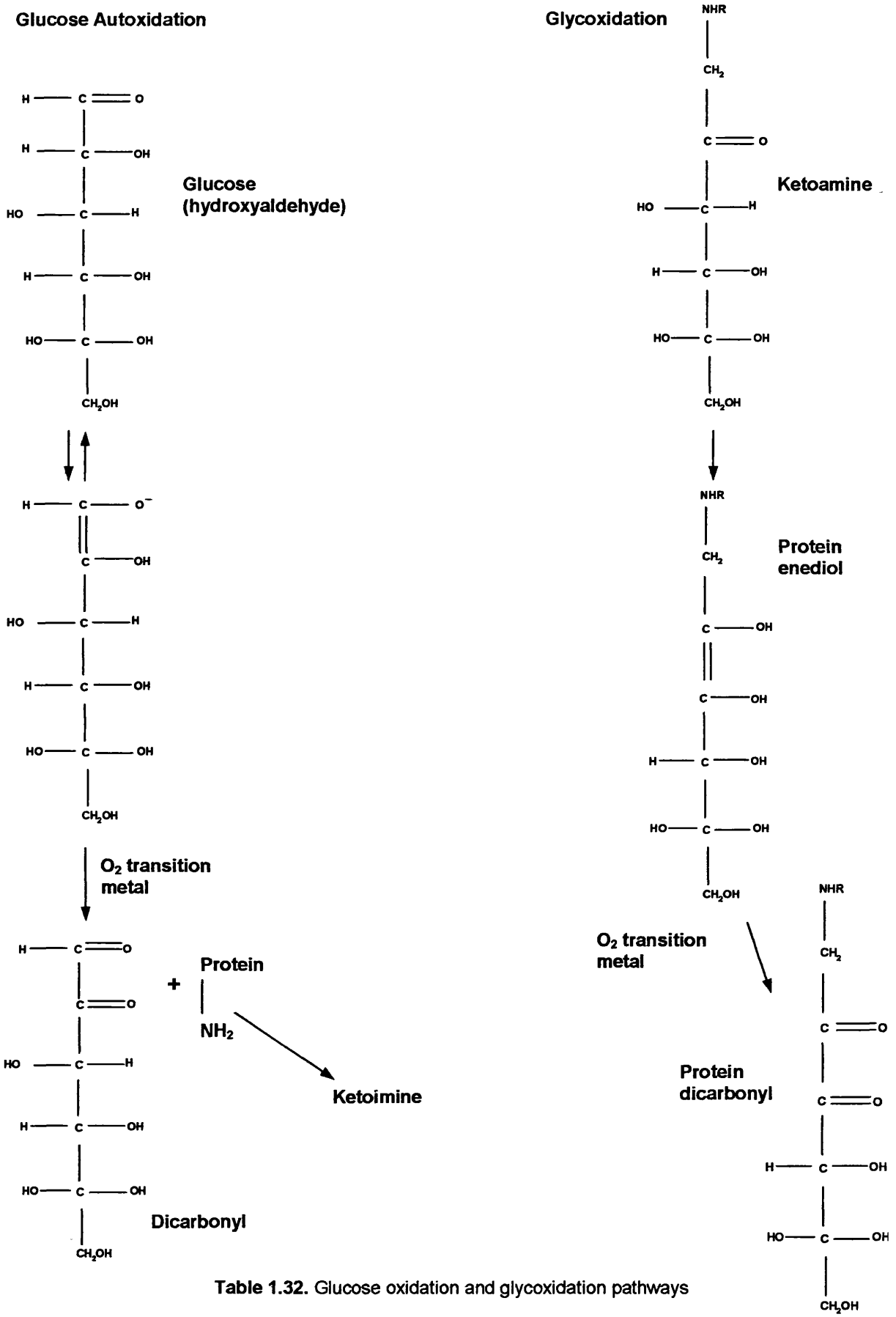

Table 1.32. Glucose oxidation and glycoxidation pathways

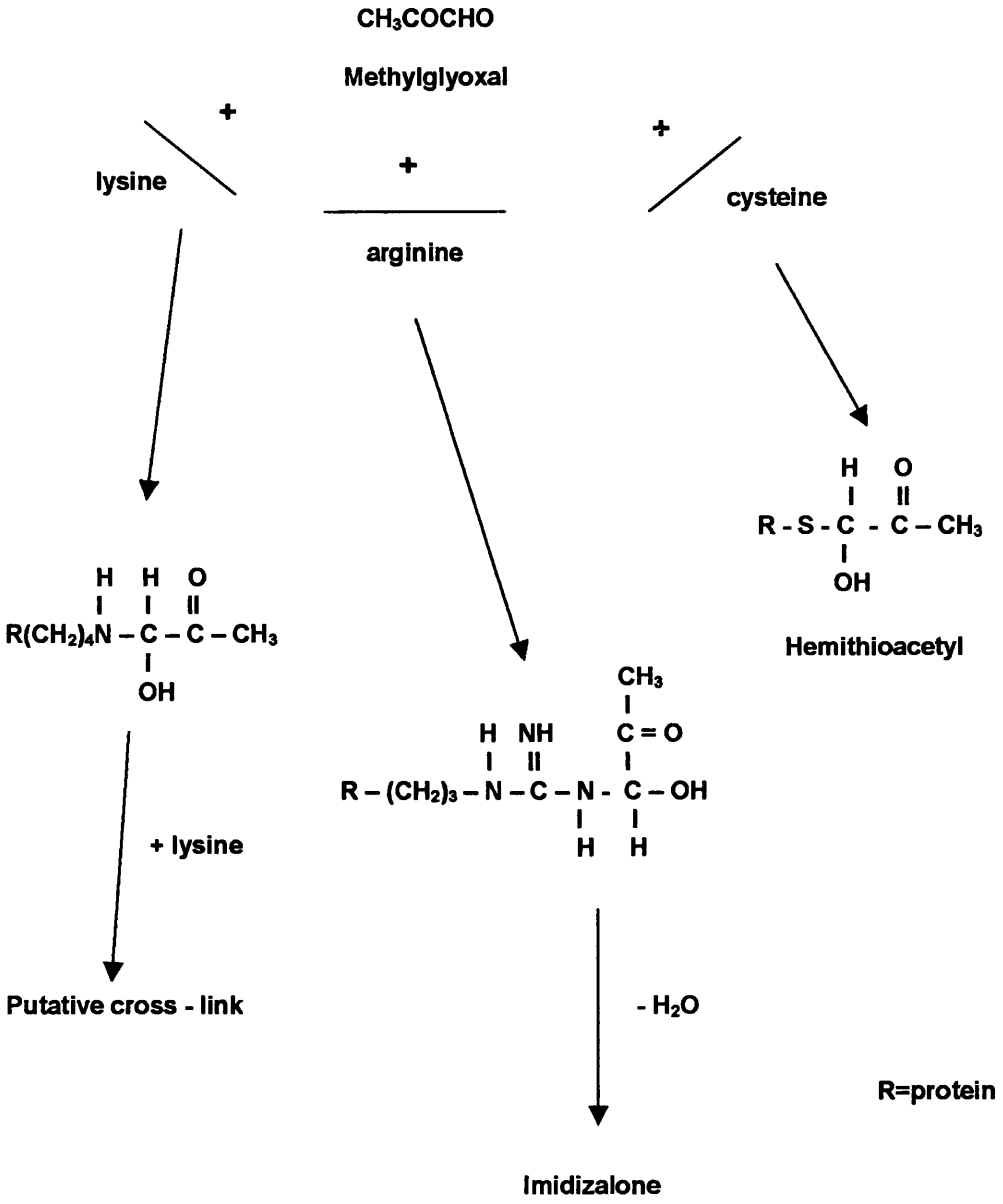

Figure 1.33. Modification of protein amino groups by MGO

Methylglyoxal is usually inactivated by conversion to D–lactate by the glutathione –dependent glyoxalase pathway. However, glyoxalase activity is decreased and blood levels of MGO and D–lactate are increased in diabetes, suggesting deficiencies in glutathione metabolism in diabetes [126]. Glyoxal is a precursor of CML, and is also formed by the degradation of ascorbate (Vitamin C). Because of the disorders in ascorbate homeostasis in diabetes mellitus, ascorbate may be a major source of glycoxidation products in some tissues.

1.9.2 Conditions of Glycation

Contributory factors to the different rates of AGE accumulation apart from sugar concentration include environmental pH, temperature, accessibility of the lysine residues and the half-life of the protein [116]. The resulting structures can possess chromophoric, fluorophoric and cross-linking properties.

In a clinical setting the key saccharides and saccharide derivatives, involved in glycation, are glucose and the reactive α-oxaldehydes - GO, MGO and 3–DG respectively. Consequently, in conditions of elevated blood sugar levels such as diabetic hyperglycemia, glycation rates are increased [117;118]. This results from the fact that AGE formation proceeds through RIS binding indiscriminately to amino groups present on diverse "bystanding" proteins [119]. In fact, AGE levels are increased as early as three months from the development of hyperglycaemia[94]. The levels of AGEs do not return to normal once hyperglycaemia is corrected: instead the products accumulate over the lifetime of the tissue [120].

1.9.3 Glycation Kinetics

The full process of glycation takes place over a period of weeks, and is therefore thought to affect mostly stable, long-lived proteins [91], such as the connective tissue matrix, basement membrane collagen, cartilage collagen, and myelin[119;121-123]. But, AGEs are also found in short–lived proteins as well, such as lipid constituents and nucleic acids - more apparent in diabetes and renal failure [119]. Cellular proteins are less affected by AGEs, due to their high turnover

and fairly short lives, while extra-cellular long-lived proteins are more severely affected [104]. Glycated, peptides of low molecular weights are considered more toxic than larger, heavier proteins. The reason for this is the ability of smaller fragments of glycated proteins to act as 'second generation glycating agents', and glycate other proteins at higher rate than glucose.

1.9.4 Alternative Reducing Agents

Glucose is a relatively slow glycating agent, in comparison to other reducing monosaccharides. The reactivity of the sugar increases as follows: e.g., glucose<mannose<galactose<xylose<fructose<arabinose<ribose [87].

Phosphorylated sugars are much more reactive than their unphosphorylated counterparts [124]. It follows, therefore, that sugars such as fructose and the intracellular glucose-6-phosphate are known to have a faster AGE formation rate, approximately ten times faster [91;125]. This is theoretically explained by fructose's different, possibly preferable, pathway for the formation of the highly reactive α-oxoaldehydes. In addition, the fructose-protein early glycation product is a Heyns product (the parallel to Amadori Product), a significantly more reactive compound.

1.9.5 The Clinical Effects of AGEs

Animal models have shown that AGE concentrations increase within a few weeks after the animal is rendered diabetic and that this increase is systemic, occurring in the kidneys, skin and vascular tissue.

Human studies, such as the Diabetes Control and Complications Trial (1993), confirm that, patients with high blood glucose levels have a higher prevalence of diabetic complications. Glycated haemoglobin, sampled from diabetic patients is an indicator of glycaemic control and is the best studied Amadori product [126]. AGEs are formed irreversibly and are expected to have longer half–lives than early glycation adducts. Given this expectation, the measurement of AGEs may reflect changes in glycaemic control, AGE formation and could therefore be

diagnostic indicators of disease management, or risk indicators of development of disease. The importance of a risk indicator may depend on the type of AGE measured, since AGEs have different functional activities: some are protein cross–linkers, some are agonists at AGE receptors and some have no defined activity. AGE content (CML and pentosidine) of skin collagen has been shown to be a risk maker for microvascular complications of diabetes [105].

1.9.6 Receptors for AGEs (RAGE)

Prior to the discovery of AGE binding proteins, the main biological effects of AGEs were considered to be extracellular and related to cross-linking of long-lived proteins such as collagen [119]. Surface AGE receptors such as RAGE have been identified on a wide range of cells [127;128] the discovery of which raised the possibility that these receptors may modulate the biological effects of AGEs by activating the cellular expression of growth factors and cytokines. These receptors can be activated by a variety of AGEs, which can stimulate inappropriate cellular activity. For example, monocytes bearing RAGEs on their surface can be activated by chemotaxic signals and move towards sites of AGE accumulation where they penetrate the sub-endothelium and form foam cells, leading to the development of arteriosclerosis [129]. The binding of AGEs to receptors on endothelial cells also increases the generation of reactive oxygen species.

1.9.7 Exogenous Sources of AGEs

Tobacco smoke contains high concentrations of GO and MGO and other AGEs from the thermal combustion of saccharides [91]. These AGEs have been observed in coronary artery walls, providing further suggestive evidence of tobaccos contribution to cardiovascular disease.

Because of the heterogeneous nature of the AGEs, the lack of sensitive measurement techniques and the inability to measure the endogenous flux of glycation adducts, the contribution of food derived AGEs has been difficult to determine [130]. For example, the metabolic flux of MGO of a 70 kg human subject

is estimated to be 8.4 mmol/day. This is the same amount as 24 kg of toast or 1440 litres of coffee! [131]. Normal dietry intake of MGO, therefore, may represent a minor contribution to the total body pool of this metabolite. The situation may be different in the case of CML, for example: rats have been fed CML – rich diets and excreted it in urine without any reported ill effect. Normal dietry AGEs may be within limits but excess overwhelms the system.

The physiological significance of dietry α-oxaldehydes and glycation adducts depends on: the contribution to the dietry component makes to the total body pool of metabolite; the detoxification capacity of the host and the functional activity of the particular glycation adduct concerned.

Another suggested source or catalyst of AGE formation is sun [132]. Levels of AGEs in elastic fibres in the upper dermis are significantly higher in skin chronically exposed to sunlight. Ultraviolet light could stimulate oxidation by activating free-radical intermediates.

1.9.8 Physiological Defence against Glycation

There are 2 chief natural defense processes against glycation. Firstly, metabolism has evolved to use glucose as the most prevalent monosaccharide, a monosaccharide that has a relatively low reactivity towards glycation. Secondly, there is a risk of rapid formation of MGO ih Embden-Meherhof glycolysis, this is minimised by evolving glycolytic energetics to maintain very low steady state levels of triosephosphate and triosephosphate isomerase (Fig. 1.34).

Frutoseamine is the glycation adduct found in highest concentration in proteins and phospholipids. Since it may degrade to form reactive β,α-dicarbonyl precursors of AGEs, either directly or via the Schiff's base, the removal of fructoseamines from proteins may be a protective endogenous anti-glycation response.

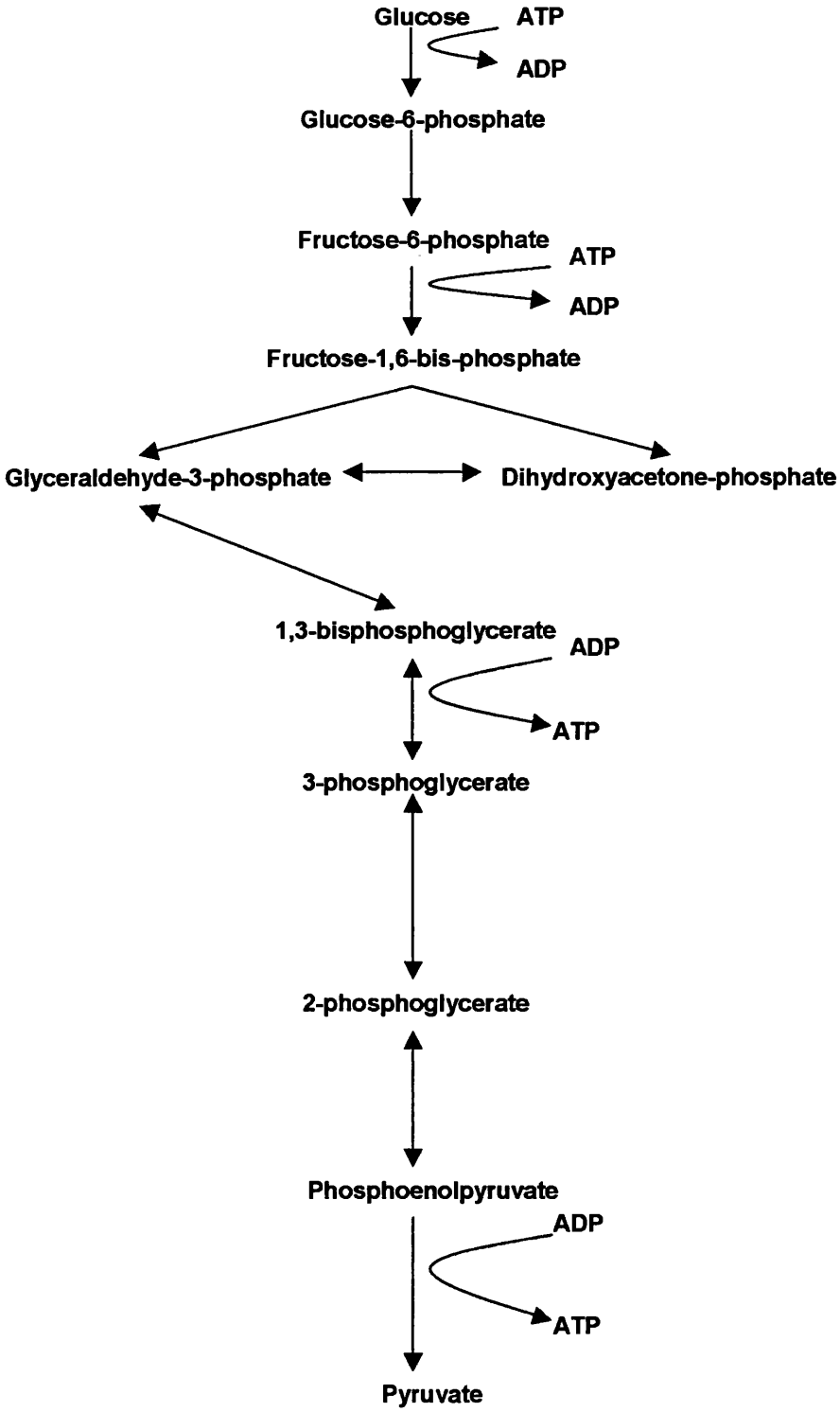

Figure 1.34. A schematic diagram illustrating Embden–Meherhof glycolysis

Inside cells, the impact of glycation is countered by the high turnover of cellular proteins, phopholipids and RNA, and mechanisms of DNA repair. Degradation of the extracellular AGE–modified proteins requires specific recognition by receptors, internalization of the AGE ligand–receptor complex and proteolytic processing of the AGE–ligand.

1.9.9 Cross-Link Formation

AGEs form covalent cross-links with adjacent protein strands. This cross-linking stiffens tissues, which were formally flexible and elastic. The process happens gradually, so that cross-links accumulate over the years on the longest lived proteins that do not get recycled very often. The clearest evidence of this is found in the extracellular collagen and elastin. In non-pathological states, collagen is involved in cross-linking, between the N and C terminal groups of each collagen strand. Abnormalities in collagen cross-linking lead to increased stiffness of the protein matrix and reduced digestibility of the proteins by enzymes [98;116;122], seen in advanced aging and in diabetes [105;133]. The chemistry of AGE cross-linking involves the lysine and arginine residues of the protein [134]. The principle of cross-linking could be applied to keratin filaments in the epidermis. In addition, cross linking is thought to be the reason for the trapping of serum proteins, such as albumin, low density lipoprotein (LDL), and immunoglobulin G (IgG), causing luminal narrowing - a major feature in blood vessels in diabetes.

1.9.10 Inhibition of AGE Formation

The realization that the progression from the Amadori product to protein cross–links requires slow rearrangement reactions, suggests possible pharmacological strategic interventions. In addition to the treatment of hyperglycaemia, there are 2 routes for the inhibition of the Maillard reaction *in vivo*: (1) Trapping of reactive intermediates in non–enzymatic reactions between carbohydrates and proteins; and (2) Inhibiting the rate of formation of AGEs by the reduction of oxidative stress.

1.9.10.1 Route 1

Therapeutic modalities include the development of compounds designed to break apart cross–linked macromolecules [135], AGE inhibitors, such as aminoguanidine[101;136], aspirin [137-140] arginine, arginine–lysine, tetracylcline, uboquinone, and RAGE blockers [141-143].

Aminoguanidine (AG) is a hydrazine-like, small, nucleophilic compound that is thought to interact with Amadori-derived products, thereby blocking the formation of AGEs [144]. It is a potent and specific inhibitor of glucose mediated cross–linking *in vivo* [101]. The terminal amino group of the aminoguanidine reacts specifically with glucose derived reactive intermediates and prevents protein–protein or protein lipid cross–links from forming. Its activity is concentration dependent [145].

It is pharmacologically effective at plasma concentrations of less than 100 µmol/L, while much higher doses are typically required for inhibition of the Maillard reaction *in vitro*. The main disadvantage of aminoguandine is that in low doses it also inhibits some enzymatic activity in the nitric oxide acid pathway, therefore affecting vascular tone [146]. There are questions related to the toxicity of aminoguanidine in high doses, which may compromise its use as therapy in humans. ALT-946 is a more potent compound with a limited effect on the nitric acid pathway, making it a preferable inhibitor particularly in kidney tissue [147]. Pyridoxamine (PM) inhibits lipoxidative modification of proteins by trapping intermediates of the pathway [148].

At present the development of these compounds is in its infancy, and the full medical benefits that may accrue from the use aminoguanidine–like compounds are under investigation by way of clinical trials.

1.9.10.2 Route 2

Antioxidants like ascorbic acid, vitamin E, uric acid and glutathione are all decreased in diabetes. In particular, the glutathione levels are depressed both in the plasma of diabetic patients and at the edges of foot ulcers [149].

Exogenous vitamin C and E are reported to inhibit glycation [150], although it is difficult to explain as the early stages of glycation do not involve oxidative reactions. Vitamin E inhibits glycation *in vitro* and *vivo* in a dose dependent manner [151].

Because of the complex nature of the Maillard reaction and its role in the initiation of lipid peroxidation, it is unlikely that any single drug therapy will be sufficient to inhibit the formation of AGEs and the subsequent pathologies. However, any effort to decrease the oxidative stress is likely to be beneficial. In the holistic treatment of diabetes mellitus and age–related diseases, patients are frequently advised to stop smoking and to limit their alcohol intake.

1.9.11 Processes Related to Aging

There is a close relationship between glycation and three other metabolic processes: free radical damage, mitochondrial defects and calcium dyshomeostasis (Fig. 1.34). All four processes play crucial roles in cellular and organism senescence [152]. Other modifications besides that of glycation include carbamylation, racemization and deamination. This post–translational modifications result in altered stability of the protein and decreased digestibility[153]. Aging is also associated with decreased protein synthesis - 70% of total protein synthesis may be reduced in aged animals.

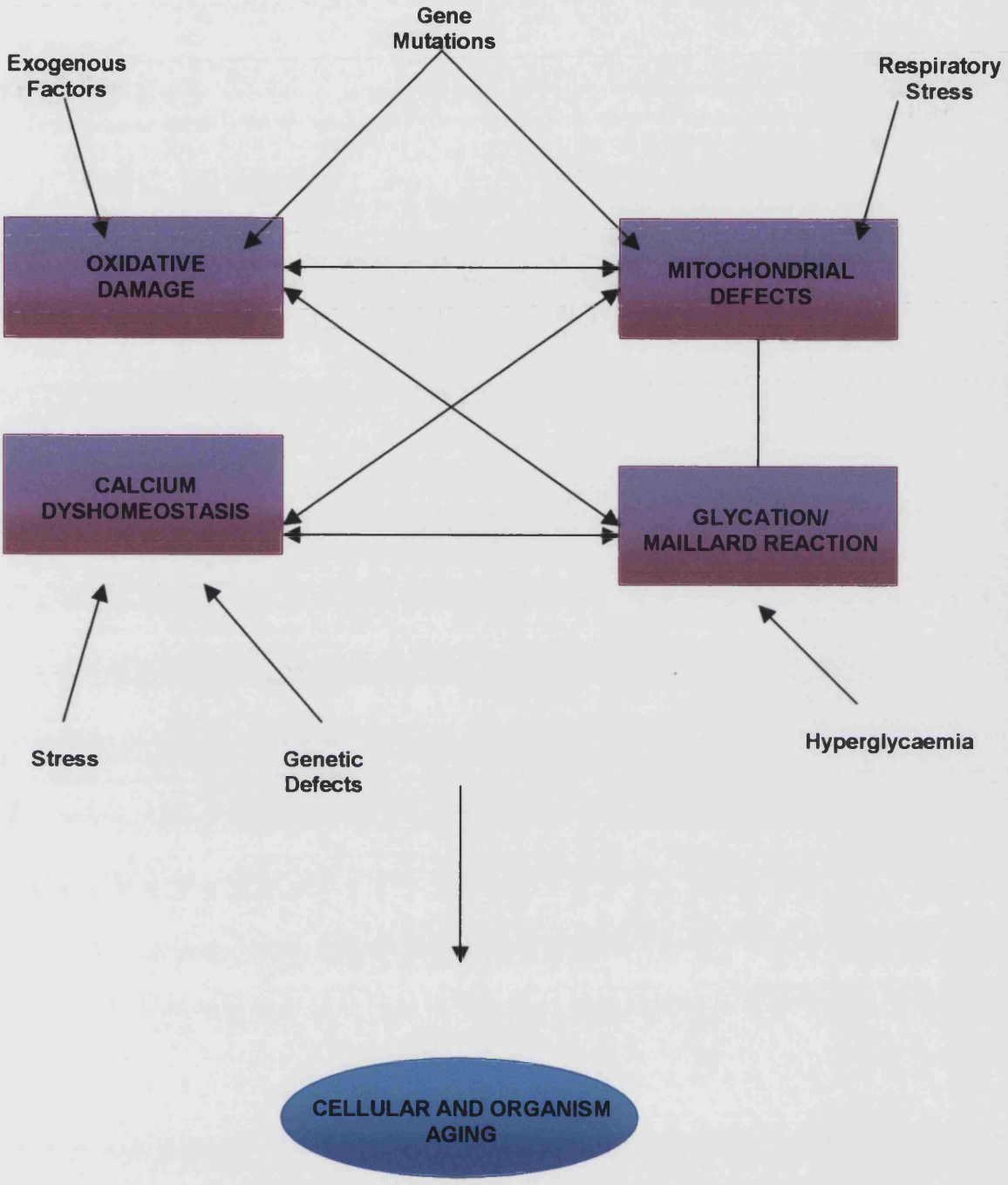

Figure 1.35. Diagrammatic presentation of the hypothesis of glycation aging

1.9.12 Non-enzymatic Glycation and Collagen

Alterations in collagen synthesis and turnover in diabetes [45] are accompanied by structural and functional changes related to cross–linking [125], such as decreased joint and skin mobility [37], impaired wound healing, decreased solubility [154;155] and increased resistance to enzymatic digestion [36;156] (Table 1.8)

Table 1.8. Chemical and physical changes in collagen in diabetes.

Chemical	Physical
Increased glycation	Increased browning
Increased pentosidine	Increased fluorescence
Increased carboxymethylation	Increased mechanical strength
Increased cross – linking	Increase thermal stability
Maturation of reducible cross – links	Decreased solubility and elasticity
Resistance to enzymatic digestion	Resistance to denaturants.

The rate of glycation may not be gradual as the tissue accumulates with time, but immediate, therefore the point at which tissues become glycated could be of significance. For example, it is interesting that older Type II diabetics do not have more glycated tendon collagen than their age matched controls [155;156]. Therefore, it could be possible that in the postmature collagen tendon there are a limited number of sites available for glycation and that these sites are occupied early during the course of hyperglycaemia. An alternative hypothesis could be that abnormal collagen is synthesized by diabetics and that this abnormality leads to changes that appear to represent accelerated aging. This is a feasible argument, insinuating that one or more properties of collagen are altered in ways that stimulate accelerated aging.

1.9.12.1 Skin Collagen and Glycation

Skin has collagen present in abundance and is the site for a number of age related changes. Both biochemical and biomechanical studies of diabetic palmar skin *in vitro* have revealed many pertinent findings [57]. Melling and associates (2000) [57] noted that in general the palmar skin from diabetics was brown/ yellow

in colour and thicker than that from non–diabetics, with reduced pepsin digestion. There was also a higher concentration of fluorescent compounds in the diabetic skin samples than in the non–diabetic ones [57]. Vishwanath *et al* (1986) [157] duplicated these findings along with measuring increased skin collagen content in diabetics. These observations did not correlate with age, diabetes duration, severity of nephropathy, retinopathy, arterial stiffness, and joint stiffness in the hands although there was, a weak but positive correlation between blood HbA1c levels [157]. Therefore, Amadori products alone cannot explain the pathogenesis of diabetic skin complications. Animal studies carried out on streptozotocin diabetic rats revealed similar findings, demonstrating an increase in skin collagen stiffness with an additional interesting observation of a reduction in collagen content with increase in duration of diabetes [158].

1.9.12.2 AGE Measurement in the Skin Collagen

In accordance with the concept that the quantification of AGEs could provide a tissue measure of the integrated glycaemia over several years and an estimate of the consequent risk of the development of the complications, several studies have investigated the relationship between AGE content in skin and diabetic complications [92]. Skin collagen levels of specific and non-specific AGEs (pentosidine and CML) were found to correlate positively with the duration of diabetes and to varying degrees with the severity of retinopathy and nephropathy in patients with Type I diabetes [92;105]. In one study, intensive treatment of glycaemia in Type I diabetic subjects, over a period of 4 months, resulted in a decrease in skin collagen glycation but had no effect on the glycoxidation products [159]. Similar results were observed in Type II diabetics followed over five years of therapy [160]. One study has been carried out on a larger cohort (n=216 Type I diabetics) of diabetic individuals assessing all of these factors mentioned[145]. In this study the relationship between long–term intensive control of glycaemia and indicators of skin collagen glycation (furosine), glycoxidation (pentosidine and CML), and cross–linking (acid and pepsin solubility) were measured. The results showed that 5 years of intensive treatment was associated with lower furosine, pentosidine and CML levels and higher acid–soluble and pepsin–soluble collagen. Also the study revealed a correlation

between secondary complications of diabetes and all of the full set of measured variables.

1.9.13 Epidermal Proteins and Glycation

Increased glycation of proteins of the plantar epidermis, as well as those of hair and nails [161-165] may contribute considerably to the stiffness and other changes seen in the skin of the hands and feet of diabetics. Delbridge *et al* (1985) [166] showed that epidermal proteins from the plantar aspect of the foot undergo increased glycation, which relate to diabetic control and possible neuropathic ulceration. Márová *et al* (1995) [167] confirmed these results and suggested that the glycation of proteins of the stratum corneum can serve as a variable for long term monitoring of glycaemia. Márová also suggested that by monitoring the course of glycation in specific dermal tissues, one could predict the development of dermatological complications seen in diabetes. This study also established a good correlation between glycated proteins and age. These two studies demonstrate that the glycation of plantar stratum corneum proteins is subject to certain laws applicable to proteins of other tissues i.e. the glucose binds to the proteins at the same rate and follows a first order reaction with respect to the concentration of the glucose. Although Nozaki *et al* (1988) [163] revealed some years earlier no significant correlation between increased glycation of SC proteins and the prevalence of cutaneous manifestations. None of these studies pursued what the effects of glycation on epidermal proteins would have on the biomechanical properties of the skin. Aspirin can block this glycation process, be it in relatively large doses, in SC tissue, which adds to the evidence that the process of glycation of keratins may follow the same pathways as that of glycation of other tissues in the body [166].

1.9.13.1 Methods of Analysis of Glycated Epidermal Proteins

The first point of discussion, with regards to quantification techniques, is the assay procedure for NEG. Most studies on keratin-based tissues have used the TBA method of measurements of glycation [164;166]. The principle of this method is the reaction of 2–thiobarbituric acid and 5–hydroxymethylfurfuraldehyde (HMF)

produced after the hydrolysis of glycated protein from oxalic acid. Therefore, various other substances with aldehyde groups may be measured simultaneously[168]. Brevity seems to be an advantage of this method even though it is a semi–quantitative technique [164;166]. The furosine assay used for the measurement of NEG of nail and SC proteins [58;162], is superior to the thiobarbituric acid assay with respect to specificity, because furosine is the hydrolysed product of fructose–lysine linkages present only in glycated proteins. The measurement of furosine by high performance liquid chromatography (HPLC) had been described as specific and sensitive [168].

The second point of discussion is the relationship between furosine content in the epidermis and blood glucose levels. Sueki *et al* (1989) [162] revealed a close correlation between HbA1c and furosine (%) of SC and nail. Glycation of many other proteins has been shown to be a function of the duration of exposure and concentration of glucose in the environment. Therefore, if the stratum corneum is turned over more rapidly than nail and hair tissue and collagen in the dermis, the opportunity for the former to become glycated will be diminished. The mean turnover time for the entire epidermis is estimated to be 40 days [69]. Therefore, the furosine value of the corneal layer of skin may reflect the blood glucose of the last 4–7 weeks similar to that reflected by HbA1c levels. Furosine values obtained from the free edge of the nail reflect the blood glucose of the previous 4 months before. This could be amore valuable indicator for the evaluation of long-term control of diabetic patients than is HbA1c. This suggests that the prolonged retention of the SC and nail may accelerate the formation AGEs. Although Paisey *et al* (1984) [164], found a significant correlation between the glycation of the proximal 4cm of hair and the simultaneously measured HbA1c value, there was a considerable scatter in the results. This scatter may be due, in part, to the variation in the rate of growth or the hair proteins being glycated *in vivo* with different dynamics than that of haemoglobin, an important factor when considering the dynamics of SC proteins.

Since glucose diffuses freely into epidermal cells, NEG of keratin formed during epidermal differentiation should, like all other proteins studied so far, be related to glucose levels over that period. From this information it is reasonable to propose

that in skin conditions where the rate of cell turnover and desquamation is affected, there may be an effect on the accumulation of glycated proteins within that tissue site.

1.10 Summary

It is recognised that the aetiologies of callus formation in diabetes are complex, each of which would have to be considered separately before a clear-cut difference in any one factor can be demonstrated. Clearly, the literature shows that further investigations into diabetic plantar thick skin are needed. Glycation of proteins occurs in the diabetic population, but a direct connection between glycation of keratins and ulceration in diabetes has not been elucidated, though this relationship is implicated. It seems reasonable to hypothesise that alterations in the NEG of keratins may contribute to the changes in the biomechanical properties of the epidermis, therefore accelerating the development of callus. Thus, changes in keratin may be an additional factor contributing to ulceration in diabetics in whom all the factors are present. If such a relationship exists therapeutic options could be targeted at preventing this progression.

The practical clinical question is whether measurement of plantar keratin variables would yield additional useful information to that provided by HbA1c, as the individual's risk of developing ulcers. If a reliable epidermal keratin predictor emerges, it would identify subjects who are particularly in need of intensive glycaemic control or anticomplication therapy, and those at very low risk of complications could be spared the rigors and risks of intensive therapy of Type I diabetes.

This study aimed to measure the accumulation of the early glycation adduct, furosine, and the AGEs, pentosidine and CML, in plantar epidermal keratins, along with the measurement of plantar epidermal thickness and flexibility. The glycated proteins were quantified by the adaptation and development of existing analytical techniques, mainly HPLC, mass spectroscopy and immunoassays. Before collecting this data from a group of 190 volunteers (103 Types II diabetics and 87 non–diabetics), all the methods were tested for sensitivity and specificity.

1.11 Hypotheses

The following hypotheses were tested:

1. There is an increase of glycation of plantar epidermal proteins in Type II diabetes.
2. There is a decrease in flexibility of pedal epidermis in Type II diabetes.
3. There is an increase in the thickness of pedal epidermis in Type II diabetes.

1.12 Statistical Analysis

All data analyses were preformed on a personal computer. Mathematical functions, graphical representation of data and curve fitting were all performed using Kaleidagraph™, for Windows, version 3.5 (Synergy Software (PCS Inc.)) and Microsoft® Excel 2000, version 5.0 (Microsoft Corporation). . Power tests were calculated using Sample Power™ (SPSS Inc.).

All statistical analyses were carried out by SPSS for Windows (SPSS Inc. 1989 – 2001). The median, interquartile range, minimum and maximum values of the grouped data were illustrated by box plots. Values in the text were quoted as the arithmetic mean ± one standard deviation (mean ± SD). The standard deviation is a measure of the variability of the individual values around the mean in a data set. The distribution of the data was plotted as histograms and Q-Q plots. This was done for continuous outcomes inorder to see whether the data was normally distributed. This showed that the data had a skewed distribution, therefore standard parametric techniques were considered as being inappropriate when comparing outcomes between two groups. The Mann-Whitney test was used to test for the significance between the data sets. This is a non-parametric test that does not rely on the data following a normal distribution. It was decided apriori to use a 5% two-sided significance level to decide whether to reject the null hypothesis ($p \leq 0.05$). When investigating the association between two continuous variables a non-parametric form of the correlation co-efficient was used, the Spearman correlation analysis.

2.0 Chapter 2 – Extraction and Purification of Keratin Proteins from Human Plantar Callus Samples

2.1 Review of Methods of Keratin Extraction and Identification from Epidermal Tissues

The process of normal keratinisation is characterised by a series of morphological and biological changes, as cells progress from the germinative basal layer through to the outer cornified layer [169]. One key change is the formation of disulphide bonds between keratin intermediate filaments during terminal differentiation, providing stability, strength and chemical inertness to the keratin fibres [65]. The origins of these bonds lie in the free sulphydryl groups (-SH from cysteine) in the living layers of the epidermis, which gradually convert to disulphide bonds (-S–S-) in the SC (Fig. 2.1). The disulphide bonds are a characteristic feature of mature epidermal cells, rendering them relatively insoluble and resistant to keratinolytic agents [65;170] .

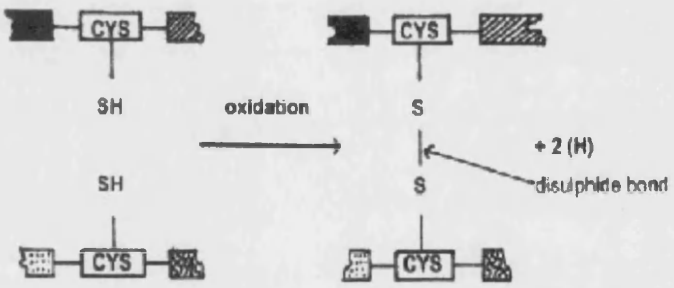

Figure 2.1. Schematic diagram illustrating disulphide bond formation.

In view of the insolubility of keratin proteins, investigatiors have used degradative solvents (sodium hydroxide and methanoic acid), denaturants (aqueous urea and lithium bromide), reducing agents (ß–mercaptoethanol) and surfactants (sodium dodecyl sulfate-SDS), to successfully extract proteins from epidermal cell [171].

Water in-soluble proteins from normal human epidermis can be sequentially extracted with increasing concentrations of urea [170], and when the same tissues

are incubated with additional SDS and ß–mercaptoethanol more keratins are extracted. The procedure disrupts the cell membranes and releases the keratin filaments in the form of their constituent polypepetide subunits and offers quantitative extraction. In the case of human epidermis [78], these subunits represent up to two thirds of the total dry weight mass of the epidermis. Yamauchi and associates (1976) [172] also used a mixture of urea, ß–mercaptoethanol and SDS to extract keratins from wool. They demonstrated that SDS is essential to produce a high yield of keratin proteins (40–50 wt%). They also demonstrated that above a temperature of 100°C and in alkaline conditions the keratins decompose. The ideal extraction conditions were a temperature between 50-70°C and a pH around 7 and 8. The same reagents and conditions have been used to extract keratins from human epidermal cells, including the SC[78].

Baden *et al* [173] confirmed that only trace amounts of keratins are extracted if SDS is not used and that ß–mercaptoethanol is essential for the selective extraction of keratin from tissues. For example, nails contain epidermal and hair keratin - with 50mM 2–mercaptoethanol, only epidermal types are extracted and hair keratins are extracted with 200nM 2–mercaptoethanol [174]. This adds to the suggestion that different keratins have different structural features despite their co-existence.

Once the aqueous solution of keratins is obtained, classic methods of protein identification and quantification can be employed. The proteins can be separated by one dimensional sodium dodecyl sulphate polyacrylamide gel electrophoresis (SDS–PAGE) giving protein bands of different molecular weights, identified by the use of known molecular weight markers. In order to identify the presence of specific keratins, immunoblot techniques can be employed using monoclonal antibodies. The specificity of these antibodies is crucial to the identification of keratins in the protein extract.

2.1.1 Existing knowledge of Molecular Weights of Keratins after Protein Extraction

Gel electrophoresis and immunoblotting techniques demonstrate isoelectric variants of keratins, depicted as many bands covering a broad range of molecular weights [175]. This variation applies to cultured keratinocytes and human epidermal cells (Table 2.1) from different body sites and disease states [78].

Table 2.1. Molecular weights of keratins extracted from different keratinised tissue types

Tissue type	Molecular weight (kDa)	References
Cultured epidermal cells	10 – 200	[78]
Keratinocytes	45 – 58	[78]
Human epidermis	40 – 70	[78]
Glycated human foreskin keratin	53	[176]

This apparent heterogeneity is due to post–translational modifications, such as phosphorylation [78]. The functional significance of these post–translational changes is uncertain but may play a role in modulating the interactions of the cytoskeleton with other intracellular structures. In view of the accumulating evidence that sugar moieties on proteins are involved in the intracellular adaptation of proteins, it is possible that glycated keratins are synthesised in the epidermis. One study shows that human keratinocytes (cultured from foreskin) synthesise a glycated keratin of mass 53 kDa [176]. Further investigations into this keratin have not been pursued.

2.1.2 Keratins Identified in the Stratum Corneum

Over 20 different human keratin polypeptides have been identified in various epithelia, hair and nails and are classified as members of an acidic subfamily (Type I) or a relatively basic subfamily (Type II). The co-existence of these two types of keratins in the filament correlate with specific phenotypic features of epithelial differentiation [170].

Normal human epidermis contains four major keratins (molecular masses 67, 58, 56.5, and 50 kDa, corresponding to keratins K1, K5, K10/11, and K14,

respectively), as well as lesser amounts of K2 (65 kDa) and K15 (50 kDa). The major keratin polypeptides are sequentially expressed during the course of epidermal differentiation. Keratin K5 (Type II) and keratin K14 (Type I) are co-expressed in basal cells, whereas keratins K1 and K10/11 (types II and I, respectively) are synthesised in the suprabasal cells (Table 2.2). Using a combination of biological and immunological techniques, Woodcock–Mitchell *et al*[169] confirmed that a 50 kDa (K14 and K15) and a 58 kDa (K5) keratin were present in all living layers including the relatively undifferentiated basal cell layer, whereas a 56 kDa (K10/11) keratin and 65- 67 kDa (K2, K1 and K5) keratins were associated only with more differentiated cells above the basal layer. The latter keratins are therefore regarded as molecular markers of keratinisation (Table 2.3). In keeping with these concepts, studies of epidermal keratin polypeptide interactions *in vitro* have demonstrated that filaments reconstituted from keratins K5 and K14 form filaments similar to those seen in living (and dividing) basal cells, whereas reconstituted filaments containing keratins K1 and K10/11 have a propensity to aggregate, as occurs in formation of the SC.

Table 2.2. Predominant keratins present in the viable layers of normal human epidermis

Keratin	Type of Keratin	Molecular weight (kDa)
K1*	II	67
K5*	II	58
K10/K11*	I	56.5
K14*	I	50
K2¤	II	65
K15¤	I	50

* Main keratin bands.
¤ Keratins present in lesser amounts
Sun and Green 1978[78].

Table 2.3. The presence of specific keratins in different layers of the epidermis

Layer of epidermis	Keratin	References
Basal layer	K5	
	K14	[78]
	K15	
Suprabasal cells	K1*	
	K10/11*	
	K5*	
	K14	[169]
	K15	
	K2*	
All living layers	K14	
	K15	
	K5	

*** Molecular markers of keratinisation**

2.2 Aims of this Thesis

- The extraction of keratin proteins, with minimal contamination by other proteins, in aqueous solution.
- Identification and quantification of keratins within the extracts.
- Comparisons between keratins extracted from diabetic and non-diabetic callus specimens.

2.3 Introduction

Three methods of extraction were employed to confirm previous findings and develop an efficient method of producing pure solution of keratins of a high yield. The first method involved sequential extraction using different concentrations of urea (in a Tris buffer). The second involved a series of sequential extractions using a Tris buffer, Tris and urea buffer and Tris, urea and ß–mercaptoethanol buffer. The third method was an adaptation of methods 1 and 2 combined, resulting in a speedy and efficient extraction procedure. Each extract was examined by one-dimensional SDS-PAGE to ascertain the molecular weights of all proteins present in solution followed by, immunoblot (Western blot) analysis, using monoclonal and polyclonal antibodies to identify specific keratins.

2.4 Method 1 – Extraction and Identification of Keratins using Different Concentrations of Urea Solution

2.4.1 Reagents and Buffers*

Buffer 1	Tris/HCl (25 mM, pH 7.4), KCl (1.5M) in d.H_2O (100 ml)
Buffer 2	EDTA (5 mM), EGTA (1 mM), Pepstatin A (5 µg/ml) and Antipain (10 µg/ml) in dH_2O (50 ml)
Buffer 3	*Buffers 1 and 2* in a 1:1 ratio and Triton-X 100 (0.5 ml)
Buffer 4	Same as stock solution 3 but without Triton X-100
Urea solutions	2, 4, 6 and 9.5M urea in buffer 4.

Plantar callus samples taken from subject 6N (see Chapter 4, Table 4.2).

2.4.2 Extraction Procedure

The sample of human plantar callus (0.25 g) was minced using a blade to 1 to $2mm^3$ and subjected to a series of sequential extractions in urea solutions of differing concentrations (2, 4, 6 and 9.5 M urea) and one direct extraction in 9.5M urea solution as follows. *Buffer 3* (10 ml) was added to a callus sample, incubated over night and homogenized (30 min). The sample was centrifuged (4000 rpm, 15 min) at 4°C and the supernatant discarded. The pellet was washed with *buffer 4*, centrifuged as described above and the solvent discarded, leaving a solid pellet ready for lyophilising.

Direct extraction procedure - The dry pellet was incubated for 3h at room temperature (RT) in urea solution (4 ml, 9.5 M), followed by centrifuging (4000 rpm, 15 min). The supernatant was removed and stored at +4°C and labelled – *9.5M urea direct extract.*

Sequential extraction procedure - The remaining sample was incubated at 4°C in urea solution (2 ml, 2 M) for 3h, shaking occasionally. The sample was

* All chemicals are bought from Sigma Chemicals, Poole, Dorset – unless otherwise stated.

centrifuged (4000 rpm, 15 min) and the supernatant stored in a glass vial (labelled *2 M urea sequential extract*). This procedure was repeated on the remaining protein pellet using 4 M, 6 M and 9.5 M urea solutions (at room temperature). The extracts were stored in glass vials at +4°C. The protein content of each extract was measured using the Lowry protein assay (Appendix I).

2.4.3 Identification of Proteins in Extracts using One – Dimensional SDS – PAGE and Immunoblot (Western Blot) Techniques.

The method protocols are described in full in Appendices II and III. In summary, samples containing 50 µg of proteins were heated at 100°C for 4 min in 150 µl of sample buffer. The upper stacking gel contained 5% acrylamide and the lower separating gel contained 12.5% acrylamide. The samples were run alongside markers of known molecular weight. All samples were treated with ß–mercaptoethanol prior to separation. A constant current of 200 mV was applied to the gel slab (18 cm x 17 cm x 1.5 mm) for approximately 3 h until the dye front approached to within 1cm of the end. The gel was then stained in fresh Coomasie blue staining solution for 1–2 h and the stain removed by incubating the gel in destaining solution. A gel light transilluminator and appropriate software were used to analyse the gel. The relative molecular weights of each protein band were calculated from the retardation factor compared to the standard protein mixture.

To better understand the polypeptides extracted at each urea concentration, unstained gels of the extracts were blotted onto nitrocellulose and then probed according to the Western ligand blot protocol described in Appendix III. Two monoclonal antibodies (AE1 and AE3, 1mg/ ml concentration) and one polyclonal antibody (SIGMA antikeratin, 1/1000 concentration) against epidermal keratins were used to identify specific keratins. Anti-mouse/anti-guinea pig IgG horseradish peroxidase antibody (10 µl) was added to the blocking buffer (20 ml).

2.4.4 Results

2.4.4.1 Protein concentration of keratin extracts

The table and graph below (Table 2.4 & Fig. 2.2) report the concentration of protein measured in each extract.

Table 2.4. Protein concentration of keratin extracts.

Extract	Concentration of Protein (mg/ml)
9.5M urea direct extract	0.655
2M urea sequential extract	0.501
4M urea sequential extract	0.431
6M urea sequential extract	0.980
9.5M urea sequential extract	0.745

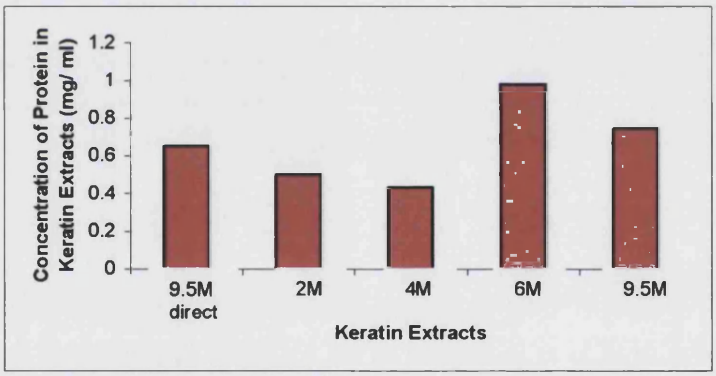

Figure 2.2. Protein concentration of keratin extracts

2.4.4.2 Detection of Keratin Proteins Extracted from different Urea Solutions using One-Dimensional SDS-PAGE and Immunoblot Analysis

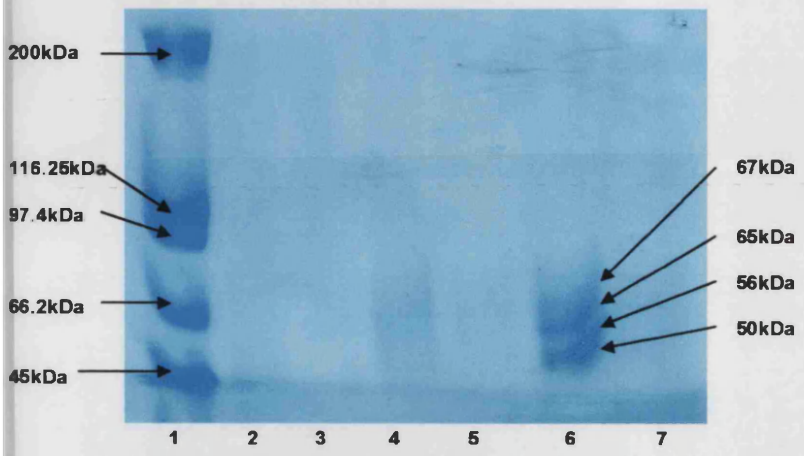

1 Molecular weight markers
2 Keratin standard (Sigma)
3 Direct keratin extract using 9.5M urea solution
4 Sequential keratin extract using 2M urea solution
5 Sequential keratin extract using 4M urea solution
6 Sequential keratin extract using 6M urea solution
7 Sequential keratin extract using 9.5m urea solution

Figure 2.3. Direct and sequential keratin extracts from human plantar callus (method 1)

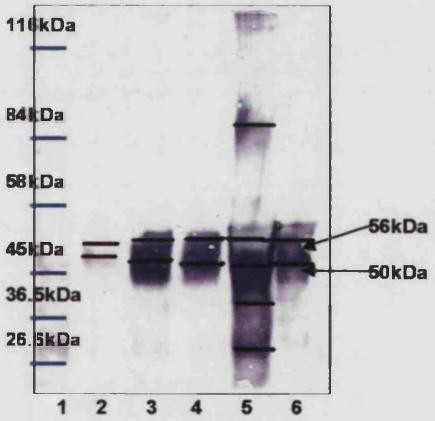

Figure 2.4. Western blot analysis using AE1 monoclonal anti-keratin antibody. *

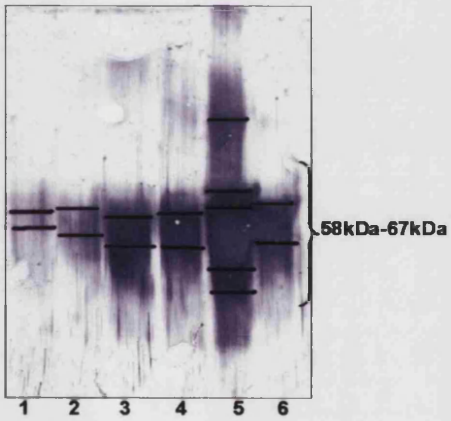

Figure 2.5. Western blot analysis using AE3 monoclonal anti-keratin antibody. *

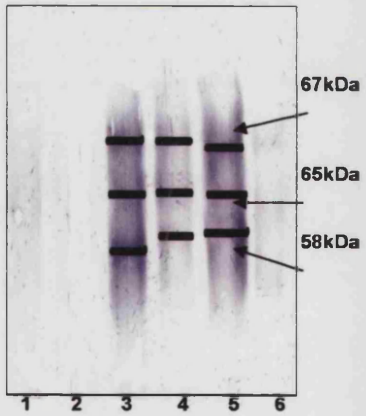

Figure 2.6. Western blot analysis using a polyclonal anti-keratin antibody. *

1 Keratin standard (Sigma)
2 Direct keratin extract using 9.5 M urea solution
3 Sequential keratin extract using 2 M urea solution
4 Sequential keratin extract using 4 M urea solution
5 Sequential keratin extract using 6 M urea solution
6 Sequential keratin extract using 9.5 M urea solution

* **The main bands are marked in, as the photographs do not show them clearly**

Coomassie Blue staining of the SDS–PAGE gels showed bands on the range of 50–65 kDa (67, 65, 58, 56.5 and 50 kDa – representing keratins K1, K2, K5, K10/11 and K14/15, respectively) in all 4 sequential extracts and the direct extract (Fig. 2.3). The 2 M urea extract contained relatively small amounts of numerous proteins, so that faint polypeptide bands were distributed over a molecular weight range of 50 – 70 kDa (Fig 2.3). In the 4 M urea extract the keratin bands were more pronounced. The majority of keratins were extracted by the 6 M urea solution, this was confirmed by the highest protein concentration measured by the Lowry protein assay (Table 2.2 & Fig.2.2). Although, one additional high molecular weight band (~85 kDa) was noticeable in the 6M extract, the keratin bands were dominant (Fig. 2.3-lane 6, Fig. 2.4–lane 5, Fig. 2.5–lane 5). Higher molecular weight keratins are synthesised in progressively more differentiated cell layers, suggesting that the increase in molecular weight may be a signal for cell death, producing the stratum corneum [177]. The same reasoning can be applied to regions of diseased skin, for example in psoriasis the amount of keratin filament subunits of high molecular weight are substantially diminished in comparison to normal skin, with an increase in the amount of lower molecular weight subunits [171].

Keratins were identified by reacting the electroblots with monoclonal anti–keratin antibodies AE3 and AE1. AE3 antibodies bind to K1, K2 and K5 and AE1 antibodies bind to keratins K10/ K11, K14 and K15 so that together the antibodies recognise all major epidermal proteins [178]. In the 9.5 M urea direct extract, AE1 antibodies identify a light band at 50 kDa (K14 and K15) and the AE3 antibodies bond to K1, K2 and K5 (67, 65 and 58 kDa, respectively). Immunoblot analysis of the sequential extracts showed that all the major epidermal proteins were present in increasing amounts as the urea concentrations used for extraction increased (Fig. 2.4–2.6). The most prominent bands were noted from the 6 M urea extract.

The experiment was repeated twice using a range of concentrations of urea between 6 M and 9.5 M. The 7 M urea extracts had the same keratins as those found in the 6 M extracts but were of a higher concentration. The urea concentrations higher than 7M were less effective in extracting proteins.

2.5 Method 2 – Sequential Extraction of Keratins using different Extraction Buffers.

2.5.1 Introduction

This method involved sequential extraction of keratins using a Tris only buffer, a Tris and urea buffer, and a Tris, urea and reducing agent buffer. This experiment aims to confirm that reducing agents (ß–mercaptoethanol) and denaturants (urea) work together to extract more keratin proteins from callus specimens, than denaturant on its own.

2.5.2 Reagents

Buffer 1 - Tris/HCl (20mM, pH 7.4), ***Buffer 2*** - Tris/HCl (20mM, pH 7.4) containing urea (7M), Buffer 3-Tris/HCl (20mM) containing urea (7M) and β-mercaptoethanol (0.1M).

2.5.3 Method

The callus tissue (0.25 g) was minced using a scalpel to 1 to 2 mm^3 pieces. The extraction procedure was carried out in 3 steps using the different buffers described. The callus was placed in a plastic vial, *Buffer1* (2 ml) was added and the mixture was homogenised (6000 rpm, 10 min) and incubated at room temperature for 16 h. The supernatant was decanted and stored at 4°C after centrifuging (13000 rpm, 15 min). The remaining callus sample was resuspended in *Buffer 1* (2 ml) and homogenised (6000rpm, 10 min) and incubated at room temperature for another 16 h. The supernatant was decanted and stored at 4°C and the procedure was repeated for a third time. The extraction procedure was repeated using *Buffer 2* (extracts collected every 16 h for 48 h) and again with *Buffer 3* (extracts collected every 16 h for 88 h). The protein content of each extract was measured using the Lowry method of protein detection (Appendix I). All the extracts were examined by one–dimensional SDS-PAGE and immunoblot techniques.

2.5.4 Results

2.5.4.1 Protein Concentration of each Extract

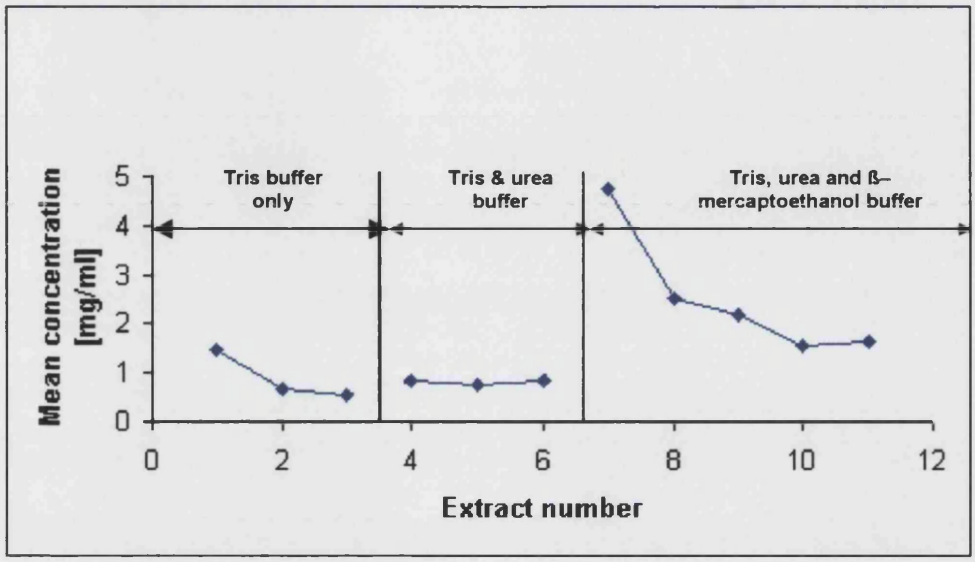

Figure 2.7. Graph illustrating the protein concentration of each extract

2.5.4.2 Detection of Keratin Proteins from each Extract using One-Dimensional SDS - PAGE and Immunoblot Analysis

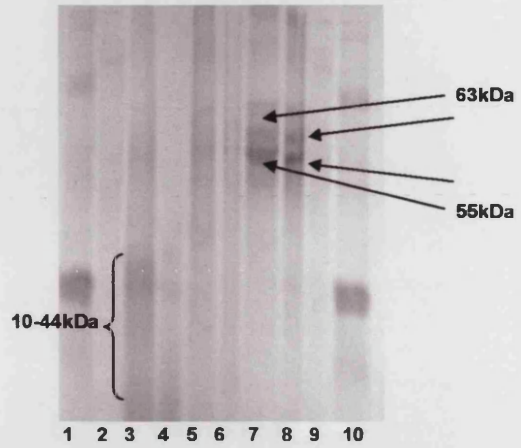

1	Molecular weight marker
2	Keratin standard (SIGMA)
3	Tris/HCl buffer extract
4	Tris/HCl buffer extract
5	7M urea and Tris/HCl buffer extract
6	7M urea and Tris/HCl buffer extract
7	7M urea, Tris/HCl and β-mercaptoethanol buffer extract
8	7M urea, Tris/HCl and β-mercaptoethanol buffer extract
9	Keratin standard (SIGMA)
10	Molecular weight marker

Figure 2.8: Keratin extracts from human plantar callus (method 3)

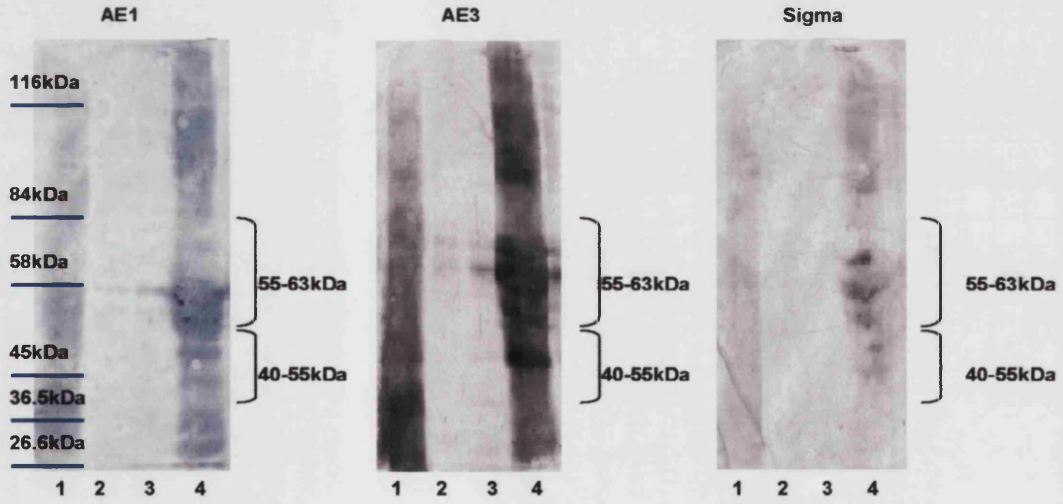

Figure 2.9: Western blot analysis using AE1, AE3 and Sigma anti-keratin antibodies.

1	Keratin standard [SIGMA]
2	Tris/HCl buffer extract
3	7M urea and Tris/HCl buffer extract
4	7M urea, Tris/HCl and β-mercaptoethanol buffer extract

2.5.4.3 Microscopic Examination of the Extracted Keratin Cells-The Effect of Reducing Agent on Human Stratum Corneum Cells

Photographs of the suspensions in 7 M urea and β-mercaptoethanol and urea alone were taken (Plate 2.1-2.3). The cells from the urea suspension alone were intact, whereas the cells from the reduced extract were macerated and appeared to have no cell structure.

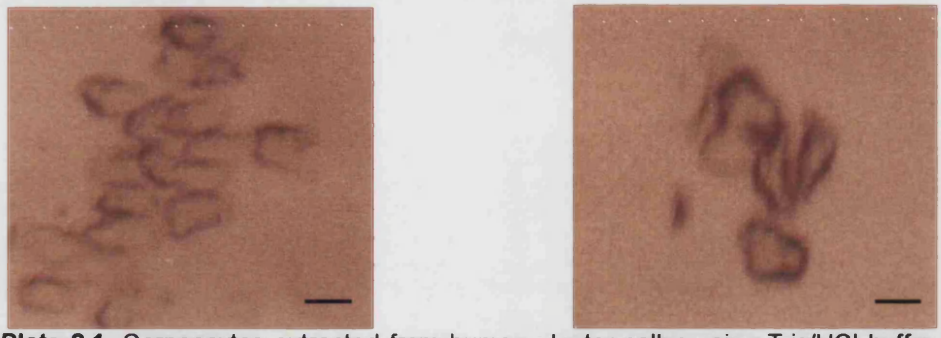

Plate 2.1. Corneocytes extracted from human plantar callus using Tris/HCl buffer and 7 M urea only. Photograph taken from a light (phase) microscope. —— Represents 25 μm

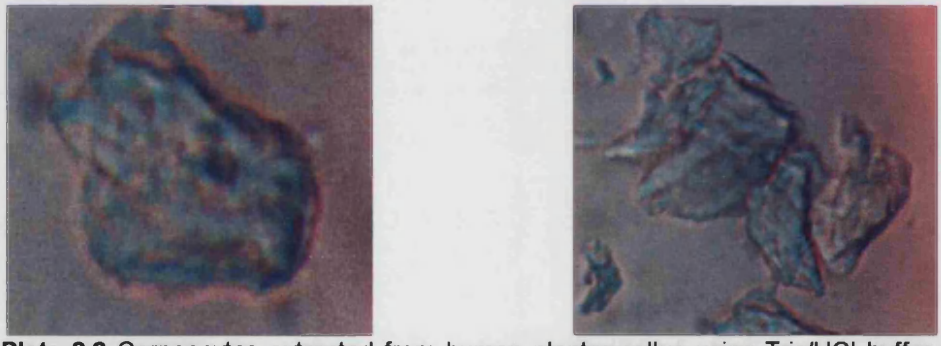

Plate 2.2 Corneocytes extracted from human plantar callus using Tris/HCl buffer and 7 M urea only. Photograph taken from a light (phase) microscope.

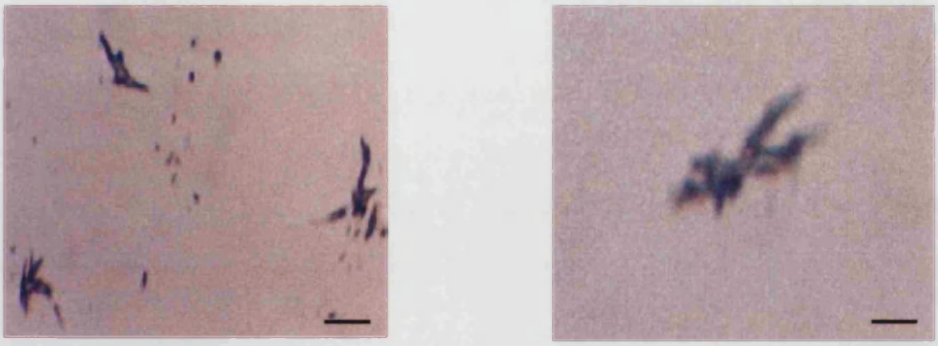

Plate 2.3 Corneocytes extracted from human plantar callus using Tris/HCl buffer, 7 M urea and β-mercaptoethanol. Photograph taken from a light (phase) microscope.

2.5.5 Discussion

The identity of the patterns on the immunoblots showed that almost all keratins proteins were insoluble in Tris buffer (Fig. 2.8, lanes 2). The proteins from the other extracts were resolved into two major bands of molecular weight 55 and 63 kDa. These proteins are in the same molecular weights as those described for the epidermal keratins in a number of mammalian species [78] .

The SDS–PAGE gels (Fig. 2.8) showed the Tris buffer extract to have a number of non–keratin bands with a molecular weight range of 10 to 48kDa (presumably serum albumin). The urea extracts contained traces of keratins, as shown in the immunoblot (Fig. 2.9, lanes 3). The extracts containing urea and reducing agent contained all the epidermal keratins recognised by AE1 and AE3 antibodies (Fig. 2.9, lanes 4). Other studies have produced similar gel patterns from samples taken from the SC on the forearm [78]. Sun and Green (1978) [78] showed that Tris extracted cultured keratinocytes contained many water soluble proteins; but in contrast to the corresponding extract of SC, the urea fraction contained over 80% of the extracted keratins, the reducing agent being necessary for release a small proportion of the total protein. The reducing agent was essential for the extraction of significant amounts of protein, this is consistent with earlier observations [173], and is supported by microscopic examination of the cells (Plates 2.1–2.3).

2.6 Method 3 – Preparation of a Stable Aqueous Solution of Keratins using Denaturant (Urea), a Reducing Agent (ß–mercaptoethanol) and Surfactant (SDS) as the Extraction Buffer

2.6.1 Introduction

The previous two methods confirm that for the successful extraction of epidermal keratins a combination of denaturant and reducing agent as the extraction buffer is needed. Yamauchi *et al* (1988) [179] recommended the addition of a surfactant (SDS) to prevent the reconstitution of keratin fibres post extraction. The following method was adapted from the Yamauchi method, using all three compounds for the direct extraction of keratins.

2.6.2 Reagents

Urea (7M), Sodium dodecyl sulphate (SDS), β-mercaptoethanol, cellulose dialysis tubing (diameter 2.5cm diameter, molecular cut off of 8000-10,000D).

2.6.3 Method

A mixture of callus (0.25 g), urea (4.5 ml, 7 M), SDS (0.15 g) and β-mercaptoethanol the (0.375 ml) was placed in a sealed glass vial and dry heated for 12 h at 50°C[∞]. The mixture was filtered through a stainless steel mesh and the filtrate was dialyzed against degassed water until a clear, colourless solution remained in the dialysis tube. The aqueous solution was stored in a plastic vial at -70°C. The extract was analysed using one-dimensional SDS–PAGE and immunoblot techniques as described previously.

[∞] As the keratin is not extracted in acidic pH (<5) and undergoes decomposition at alkaline pH, the aqueous phase was maintained at a neutral pH

[170]

2.6.4 Results

2.6.4.1 Detection of Keratin Proteins by One-Dimensional SDS-PAGE and Immunoblot Analysis

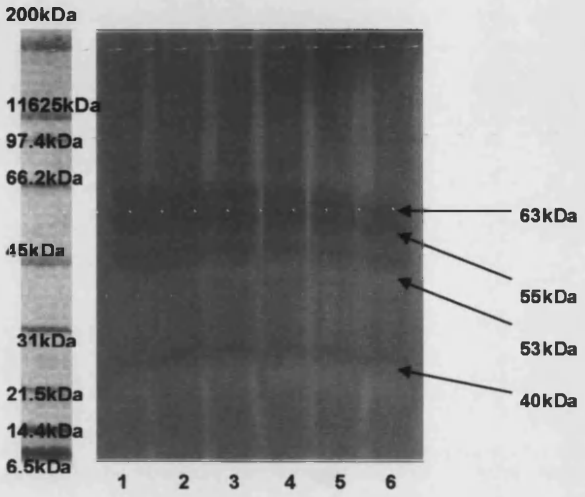

Figure 2.10. Keratin extracts from human callus (method 2)

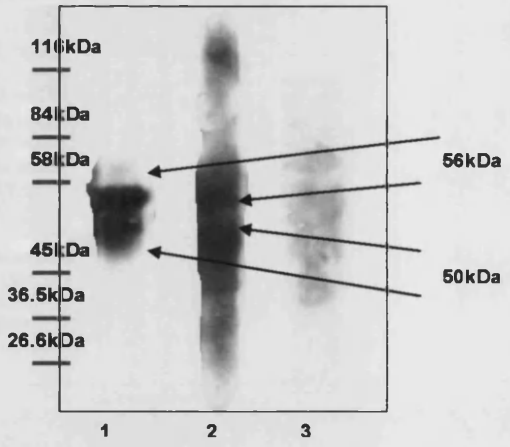

Figure 2.11. Western blot analysis using AE1, AE3 and Sigma keratin antibodies.
(On separate blots – brought together for comparison.)

1 Keratin extract immunoblot using AE1 primary antibody
2 Keratin extract immunoblot using AE3 primary antibody
3 Keratin extract immunoblot using Sigma primary antibody

The protein bands were well defined, in comparison to the gels from previous experiments, where the bands appeared blurred. These streaks could have occurred as a result of the urea and SDS in the solution, causing the proteins to 'drag' along the gel. Purification of the extracts using gel filtration made little difference to the clarity of the protein bands and had disadvantages, mainly that of dilution and loss of proteins during the procedure. It was therefore decided that desalting of the extracts would introduce too many errors. The prolonged, repeated dialysis of the extracts reduced the presence of contaminants.

The direct method of extraction using the key compounds–urea, SDS and ß–mercaptoethanol produced solutions containing all the epidermal keratins recognised by monoclonal and polyclonal antibodies. The SDS–PAGE gels stained with Coomassie blue showed additional bands of molecular weight 40, 53 and 63 kDa (Fig. 2.10). The 53 kDa protein, by virtue of its size, corresponds to glycated keratin [176]. However, it also corresponds to keratin K13, which is found in cultured keratinocytes but is a characteristic keratin of non–stratified epithelial cells.

This procedure was less time consuming than the first two methods and had the same outcomes with regards to specific keratin content. It was clear from the immunoblot analysis that the majority of the proteins in the solutions are keratins, with trace amounts of non–keratin proteins.

The reproducibility of the extraction procedure was confirmed by repeating the method on 14 randomly selected callus samples (Appendix IV). All the sample extracts showed the 2 main bands at molecular weights 55 and 63 kDa. The immunoblot analyses showed similar results to the immunoblots from section 2.6.4.1.

2.7 Summary

It is evident from these results that the proteins of human plantar callus have varying degrees of solubility i.e. they are only partially soluble in the absence of reducing agents, even after excessive physical cell disruption, which suggests that a small proportion of the keratin chains are not cross–linked by disulphide bonds. However, for the successful extraction of all major epidermal keratins, cleavage of disulphide cross–links, by a reducing agent is needed.

The keratins are extracted via the following processes: 1) the microfibrilla of the cortical cells are loosened by the hydrogen bond breaking effect of urea and depolymerised by reduction (by β-mercaptoethanol) of the inter- and intra molecular S–S bonds (to –SH groups), and 2) the resulting reduced keratins are introduced into water forming large micelles with surfactant (SDS) molecules (Fig. 2.12). Although no full explanation of the stability of the keratin solution can be given, it is speculated that the micelles are separated from each other by electrostatic repulsion, thereby retarding the aggregation of the protein molecules and oxidation of the nearby -SH groups, to form S–S bonds [172].

When observing the repeatability of the gel patterns between different individuals, although the same bands appeared on the gels, they differed in amounts from person to person (Appendix IV). However, duplicate samples from the same individual were identical. Baden *et al* (1978) [175] showed that in two individuals the electrophoretic pattern of keratin from normal epidermis was compared to that with seborrheic keratosis. Although the same major components were present there was a variation in the amounts. It is possible that the differences in the polypeptide composition of different body areas are responsible for the variations observed. Baden and associates were unable to test this further due to the lack of samples from different body areas from the same subject. Whether these differences in modalities actually reflect the changes in size as a result of some modification, such as the addition of carbohydrate component, has not been determined. Phosphorylation of the proteins is among the causes of the charged heterogeneity. Phosphorylation of keratinocytes *in vitro* can be readily achieved and analysed by using labeled 32P and 2–dimensional electrophoresis.

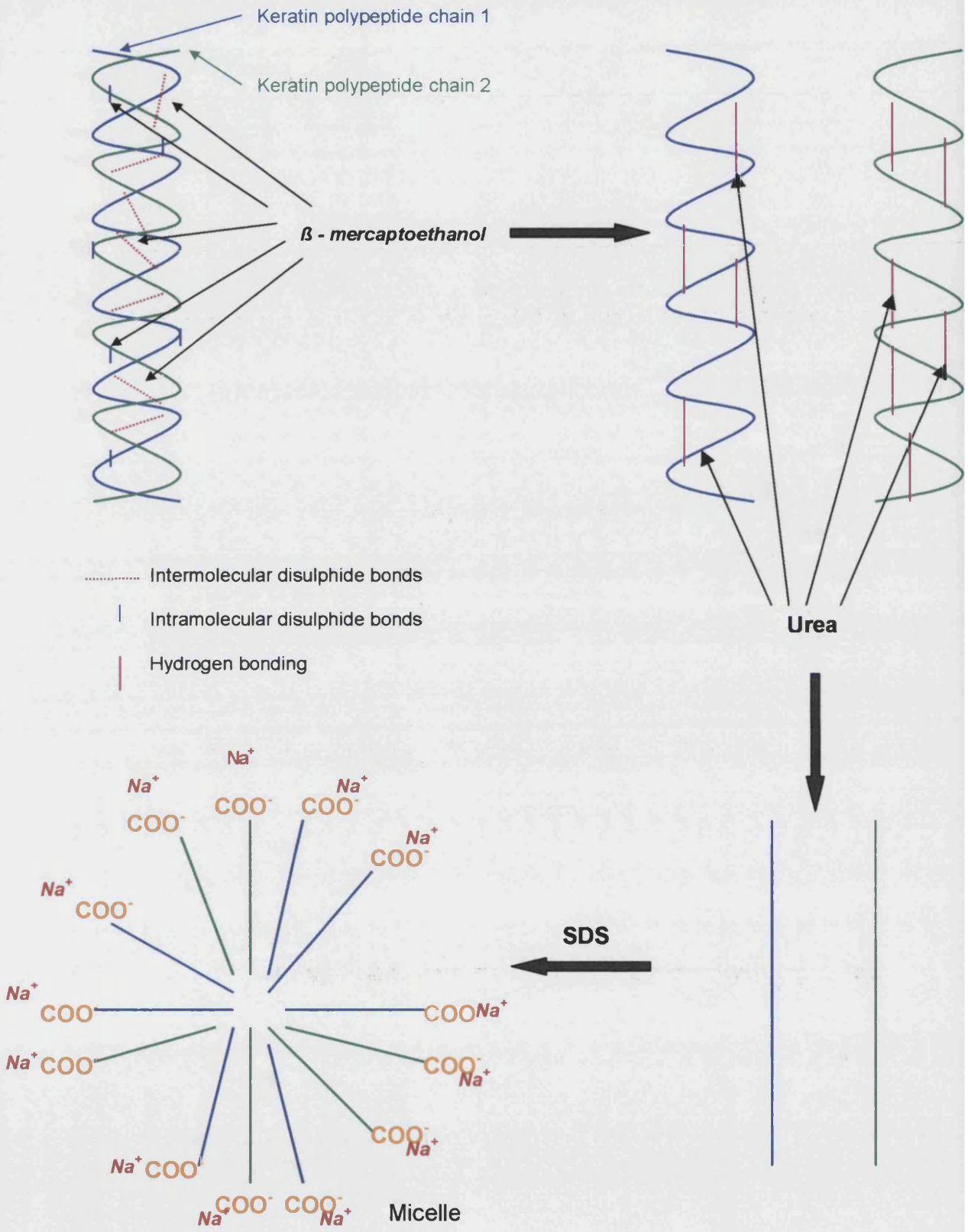

Figure 2.12. Schematic diagram illustrating the actions of urea, SDS and ß–mercaptoethanol on keratin proteins.

Testing for glycation using a similar technique is less simple as all the sugars involved with glycation are organic themselves, therefore radioactive labeling would be an inappropriate technique.

Polyclonal probes on all the blots agreed with the monoclonal probes, suggesting the differences in keratin composition of the sequential extracts were not due to post–translational modifications. Therefore, it is unclear as to what causes the heterogeneity of keratin filaments.

The protein analyses of plantar callus samples revealed the presence of all the main keratins present in the living and cornified layers of normal epidermis, with additional keratins unique to plantar specimens. As described in sections 1.8.3 & 1.84, keratins K2, K9, K6, K16, K1 and K10 are the most prevalent keratins in palmar and plantar epidermis (Table 2.5). All the protein bands from the extracts in these experiments lie in the region of 40–70 kDa. Due to their close proximity, the resolution of the bands is not clear enough (e.g. K10 MW=56.5 and K6 MW=56) to be able to identify lone keratins, but the presence of these keratins as a collective is clear. Future work would benefit from the isolation and quantification of specific keratins from plantar sites from different individuals, to assess whether these keratins are common in particular groups of people, for example diabetics or people who develop pathological callus. The keratins that would be of use to study are K1 and K10 (markers of keratinisation) and K6 and K16 (markers of proliferation in response to trauma), including analysis of their glycated states.

Despite attempts to alter the concentrations of protein solutions applied to the SDS-PAGE gels, the protein resolution was poor. Any concentration of solution below 50 μg produced poorly visible bands on the gels, which in turn did not transfer well onto the immunoblots. This problem of 'smearing' of the protein bands is a common problem, which has not yet been resolved by protein chemists [61].

Table 2.5. Keratins common in plantar and palmar epidermis.

Keratin	Type	Observed molecular weight–kDa (SDS–PAGE human)	Distribution
K1	II	67	Co–expressed with K10 in the post–mitotic differentiating cells of the epidermis
K10	I	56.5	
K6	II	56	Occur in a number of complex epithelia, but there is as yet no obvious relationship between their expression and a particular program of terminal differentiation or epithelial function. Expression is strongly induced after acute challenge (e.g. injury), and in the context of diseases featuring aberrant epithelial differentiation.
K16	I	48	Co–expressed with keratin K6 in a number of complex epithelia. Expression is induced after acute injury.
K2	II	65	Expressed late in the differentiating process. It is not co–expressed with a partner keratin
K9	I	64	Expressed in post–mitotic differentiating layers of palmar and plantar epidermis. It is co–expressed with K1 and is not present in normal interfollicular epidermis of trunk skin.

All the keratins common to plantar epidermal tissues (K1, K10, K6, K16, K2, K9, molecular weight 48-64 kDa) were identified in the extracts generated from six diabetic and six non-diabetic plantar callus samples, and agreed with the work of other investigators [180]. The individual bands of protein varied in density of colour within each extract and between extracts. This would imply that the concentration of certain keratins differed. However, the extracts were comprised of different classes of keratins, which differ in sulphur content, and the Coomassie Blue stain is taken up by proteins high in sulphur content and less so in the low sulphur compounds [61]. An improvement in the resolution of the keratin mixtures is only slightly achieved by running the protein mixture on a two-dimensional SDS-PAGE gel [61]. Therefore, the calculations of the concentrations of keratins in the extracts, using SDS-PAGE gels, would have been unreliable, hence the use of the Lowry protein assay to quantify the concentration of the proteins in the extracts.

In addition to the keratin protein bands on the SDS-PAGE gels, there were two faint bands, in the 40 and 53 kDa regions that were not identified as being keratins by consequent immunoblot analysis. The 40 kDa protein occurred less frequently than the 53 kDa protein that was visible in all the samples and is a known glycated keratin [176]. The 40 kDa protein has been identified as a glycoprotein from human epidermis [67]. Due to the unavoidable smearing of the protein bands of the gels, it could be possible that glycated proteins may be present amongst the identified keratin bands.

The collection of studies in this thesis concentrates on the extraction of plantar epidermal keratins as a group (using method 3), followed by the measurement of glycated adducts within this group. Chapter 9 describes the measurement of furosine, pentosidine and CML in the extracts of 103 diabetic and 87 non–diabetic callus samples. The glycated protein content will be expressed in terms of AGE per mg of protein. The quantity of keratins will be measured by using the Lowry method of protein detection. The selective analysis of specific keratins is an area that should be addressed in the future.

Chapter 3.0 Synthesis of AGE Standards – Carboxymethyllysine (CML) and Pentosidine

3.1 Aims

- Synthesis of a high yield of pure CML and pentosidine.

There is currently no commercial source of CML and pentosidine.

3.2 Synthesis of CML

CML is an acid stable, colourless, non–UV active molecule (Fig. 3.1). Its formation requires oxidative conditions, and it can be formed from a broad range of reducing agents, including glucose [181].

In this chapter several different methods of CML synthesis are described. Each method produced different products. Only one produced pure CML of an adequate yield.

3.2.1 Method 1 – The Synthesis of CML – An Adaptation of the Snyder and Angelici (1973) Procedure[182]

The procedure involves the reaction between iodoacetic acid and L–lysine (Fig. 3.2)

3.2.1.1 Reagents*

Iodoacetic acid (50 mM), L–lysine (50 mM), sodium hydroxide (5 M), HCl (6 M), ammonia (0.5 M), ethanol, Dowex 50W–X4 (100 – 200 mesh) cation exchange resin (NH_4^+).

*Unless otherwise indicated, reagents were the highest quality obtainable from Sigma or Aldrich Chemicals Co.

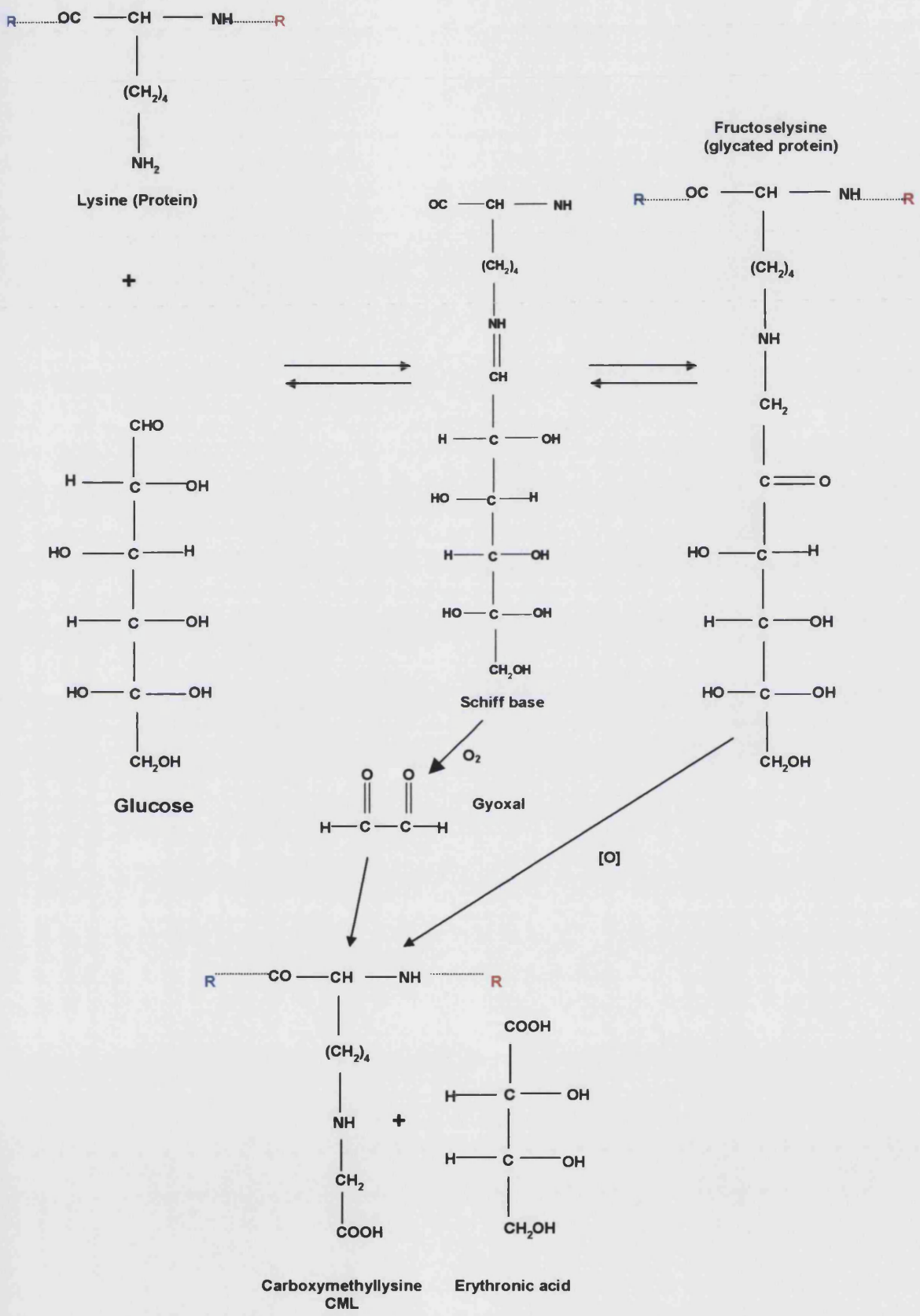

Figure 3.1. Illustration of the glycation of proteins and the routes of formation of CML

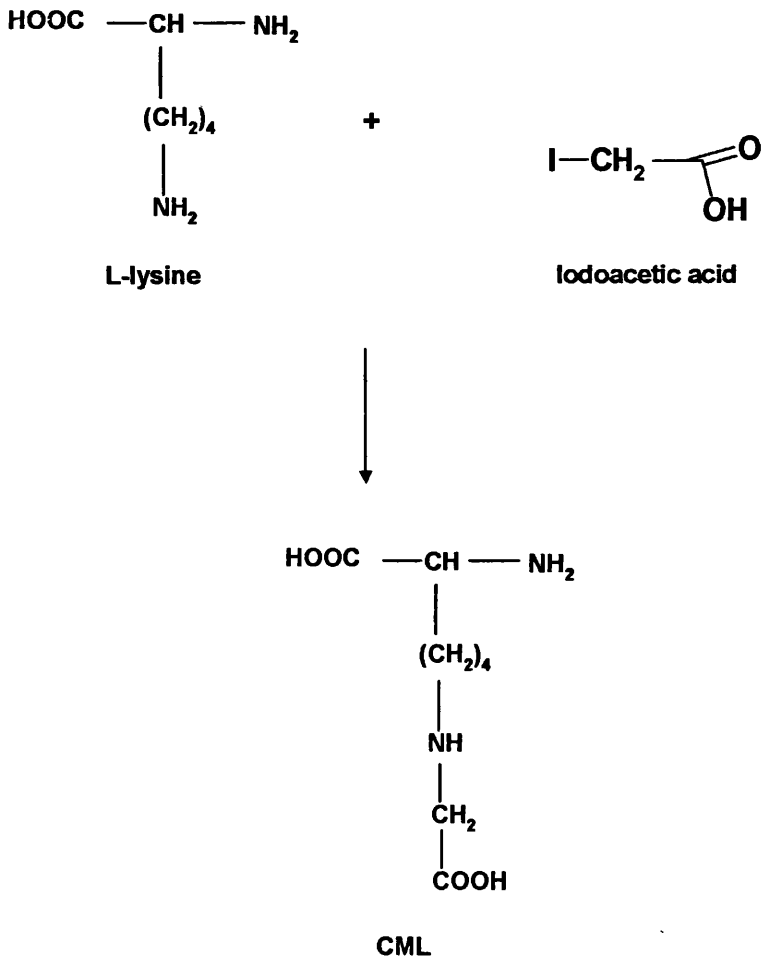

Figure 3.2. The reaction between iodoacetic and L–lysine.

3.2.1.2 Method

Iodoacetic acid (50 mM) and L–lysine (50 mM) were separately adjusted to a pH of 11 with sodium hydroxide (NaOH). The iodoacetic acid was maintained at 0°C by placing the container in ice. The 2 solutions were stirred together at a temperature of 50°C and maintained at a pH of 11. After 90 min the pH remained at a steady pH of 11, without addition of NaOH, indicating that the reaction had ceased. At this point enough HCl (6M) was added to reduce the pH to 2. The solution was loaded onto a 2 x 80cm column of Dowex 50W–X4 (100–200 mesh) cation exchange resin in the H^+ form and eluted with 160 ml water (one column volume) followed by ammonia (0.5 M).

The bulk of the CML was displaced from the column by ammonia. Fractions containing the CML had a pH between 2 and 4 (fractions 1–4). These were pooled and reduced in volume at 50°C under rotary evaporation until white crystals were visible. The addition of ethanol, equal to 3 times the solution volume, encouraged further precipitation. After filtering, the precipitate was washed with ethanol and dried under vacuum.

Characterisation of the products was accomplished by nuclear magnetic resonance (NMR) spectroscopy and gas chromatography/ mass spectroscopy (GC/ MS).

3.2.1.3 Results

Approximately 2.5 mg of product was derivatised in preparation for GC/MS analysis (see Appendix V & VI for a full description of the derivatisation procedure and GC/MS conditions). CML was eluted at a retention time of ~35 min, along with several other peaks between 40 and 50min (Appendix VII, Fig. VII.ii) NMR spectroscopy confirmed the presence of CML with additional impurities, possibly CML salts (Appendix VII, Fig. VII.i). Yield = 6.3 mg.

The significant flaw in this method was the use of lysine without protection of the α-NH_2 group, thus both the -NH_2 groups were open to attack by acetic acid (Fig. 3.3). In theory, an alkaline pH during the reaction procedure makes the ε-NH_2 more susceptible to the reaction with iodoacetic acid than the α-NH_2. Therefore, the close monitoring of pH during the reaction is important. The presence of lysine and CML in the analytical spectra confirms that the reaction was not complete due to an insufficient amount of iodoacetic acid.

The next point of error was the inadequate separation of the mixture of lysine, CML and CML salts, using ion exchange chromatography (Fig. 3.4). Miyazawa (1980) [183] suggested ways of improving the separation by using water instead of ammonia as the eluent and passing the mixture through a shorter cation exchange column.

3.2.1.4 Conclusion

The experiment was repeated, bearing in mind the suggestions made by Miyizawa (1980) [183], i.e. the reaction was allowed to continue until the mixture was positive to the ninhydrin test (confirming the completion of the reaction), followed by elution with water on a shorter cation-exchange column. With these corrections applied pure CML was still not harvested.

Although this method produced the desired product the difficulties in isolating pure CML were profound. The next attempt involved using lysine with a protected α-NH_2 group as the starting material, with close monitoring of the pH of the reaction mixture. This attempt was a method proposed by Prof. Baynes, University of South Carolina.

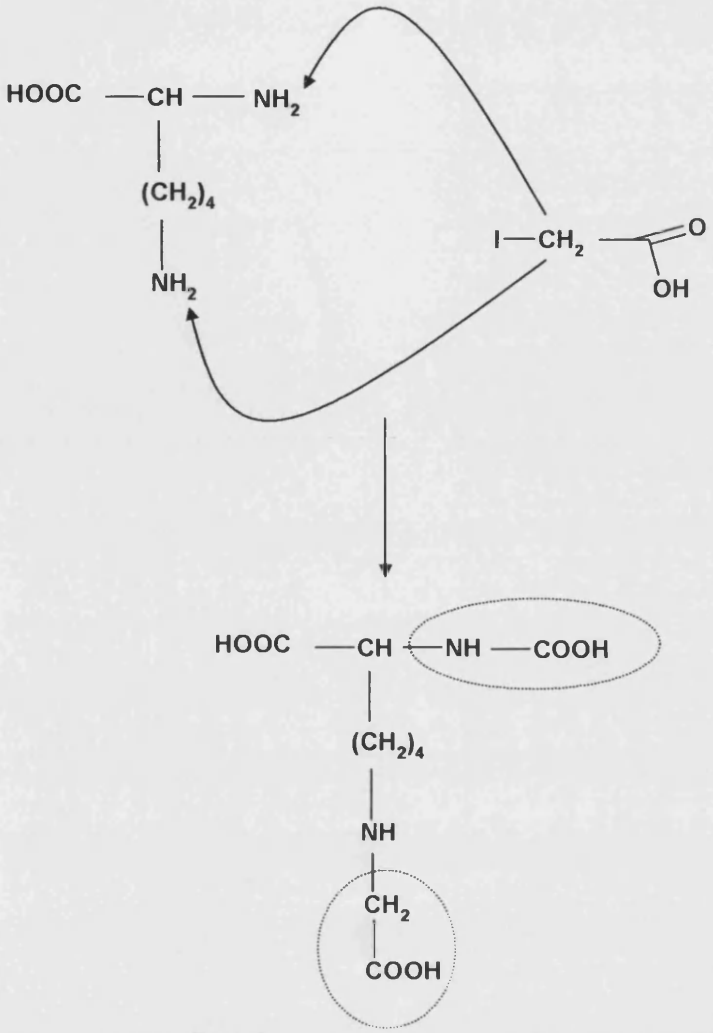

Figure 3.3. Schematic diagram illustrating the two possible points of acetylation of lysine by iodoacetic acid. This explains the relative speedy completion of the reaction, as 2 iodoacetic acid molecules are used for every one lysine molecule

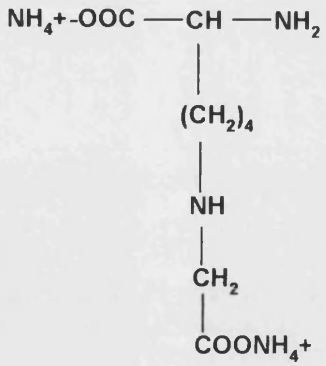

Figure 3.4: Figure illustrating the suggested CML ammonium salt structure formed during cation exchange chromatography.

3.2.2 Method 2 – The Synthesis of CML – Method provided Courtesy of Prof. Baynes (University of South Carolina, USA).

3.2.2.1 Reagents

N^{α}-acetyl-lysine (75 mM), glyoxylic acid (75 mM), sodium cyanoborohydride (225mM), potassium phosphate buffer (0.2 M), sodium hydroxide (1 M), hydrochloric acid (1 M, 2 M and 6 M), Dowex-50 (NH^{+}_{4} form).

3.2.2.2 Method

The reagents N^{α}–acetyllysine, glyoxylic acid and sodium cyanoborohydride were mixed in a ratio of 1:1:3, respectively, in potassium phosphate buffer (0.2 M, pH 7.4), and incubated at room temperature for 24 hours in a screw cap glass vial (Fig. 3.5). The pH was checked at 1-2 hour intervals and re-adjusted to 7.4 with sodium hydroxide (1 M), as required. After 24 hours at room temperature, the solution was adjusted to pH 2 with HCl (6 M) in order to discharge the residual sodium cyanoborohydride. After the effervescence ceased (release of hydrogen gas), which took approximately 6 hours, the solution was dried by rotary evaporation. The resulting white, crystalline solid (labelled crude/protected CML) was dissolved in HCl (10 ml, 2 M) and heated for 2 hours at 50°C (to remove the acetyl group). Water (15 ml) was added to the mixture and lyophilised overnight to dryness.

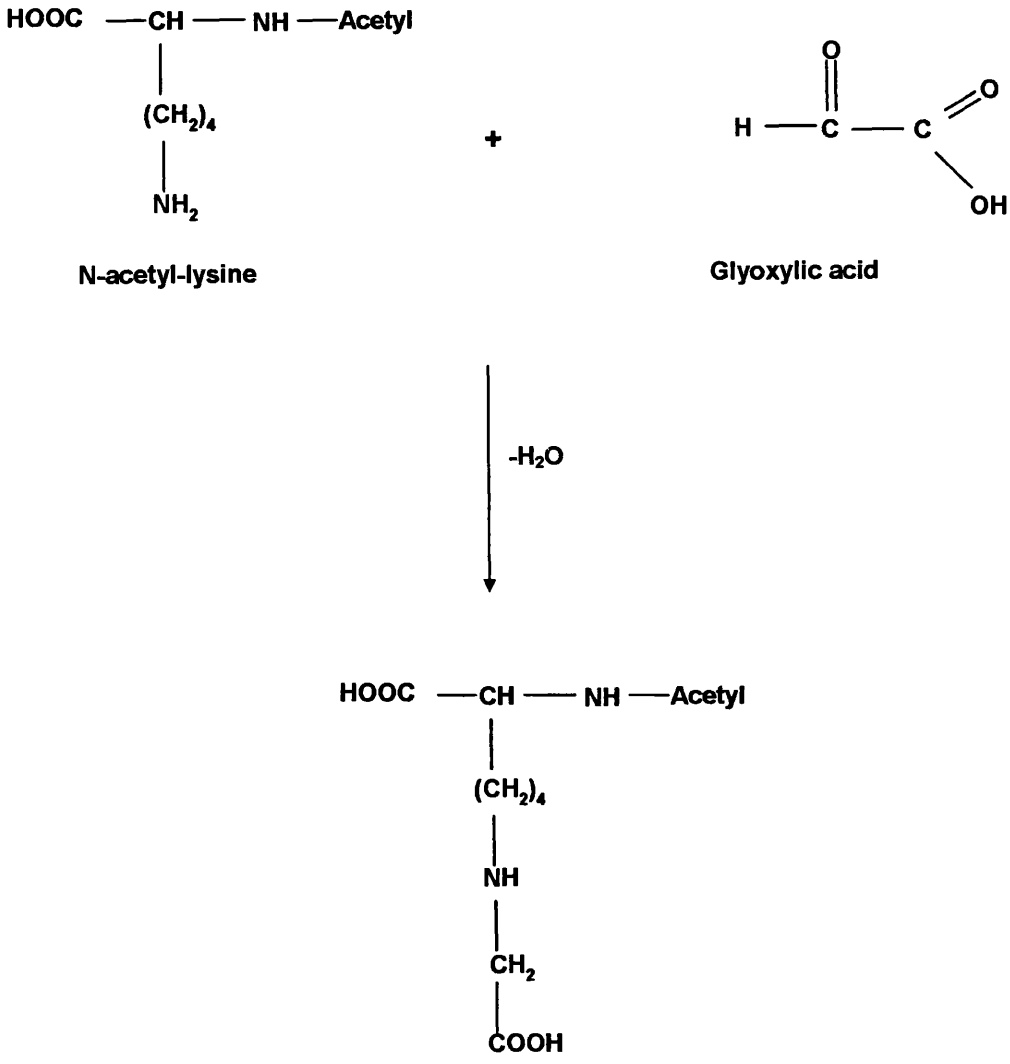

Figure 3.5. Illustration of the reaction between glyoxylic acid and N^{α}–acetyllysine producing CML.

The sample was dissolved in dH_2O (50 ml) and the pH was adjusted to 7 using sodium hydroxide (1 M). The solution was applied to a 2 x 8 cm column of Dowex-50 in NH^+_4 form*. The CML eluted from the column in dH_2O (1-2 column volumes). The eluent was lyophilised to dryness and the resulting white solid (labeled: pure CML) was analysed by NMR spectroscopy.

3.2.2.3 Results

The NMR spectra showed that most of the εCH_2 (>80%) was still present in the non-carboxymethylated form (i.e. it is a doublet rather than a multiplet). The αCH move upfield due to the *N*-acetyl group. No CML was present (Appendix VII, Fig. VII.iii).

3.2.2.4 Conclusions

This experiment was repeated and produced the same results. Advice was sought from Prof. Thornalley and associates (Department of Biochemistry, University of Essex, UK) who suggested 3 adjustments to the existing method: (1) the use α-t-BOC–lysine as the starting amino acid, this is a better protecting group than the acetyl group; (2) reducing the molarity of the phosphate buffer from 1 M to 1 mM (this was discovered by one of the chemists at Essex University by chance) and (3) close monitoring of the pH of the reaction mixture at 7.4 through out the reaction, as changes in pH have a profound effect on the progression of the reaction.

* Dowex-50 H^+ was cleaned by boiling for 30mins in 10 volumes of sodium hydroxide (1M), washed with dH_2O, then cleaned again by boiling for 30mins in 10 volumes of HCl (1M). The resin was washed with water until near neutral and then placed in the column and washed with NaOH (1M) until converted to NH^+_4 form (pH of elution solution >10. The column was then washed with water until neutral and then used for the purification of CML.

3.2.3 Method 3 – The Synthesis of CML using a Method Recommended by Prof. Thornalley (Department of Biochemistry, University of Essex, UK).

3.2.3.1 Reagents

α-t-BOC-lysine, glyoxylic acid, sodium phosphate buffer, pH 7.4 (1 mM), sodium hydroxide (3 M), sodium cyanoborohydride (4 mM), hydrochloric acid (1 M and 0.5M), trifluoracetic acid (TFA), methanol.

3.2.3.2 Method

Sodium phosphate buffer, pH 7.4 (1 mM, 40 ml), α-t-BOC-lysine (98.4 mg, 0.4mmol) and glyoxylic acid monohydrate (148 mg, 2 mmol) were mixed together in a plastic vial and the pH adjusted to 7.4 with sodium hydroxide (5 M). Sodium cyanoborohydride (252 mg, 4 mmol) was added to the mixture and the pH of the solution was adjusted to 7.4 using hydrochloric acid (1 M). The reaction mixture was incubated at 37°C for 24 hours. During this time, the pH of the solution was monitored and maintained at 7.4 at the following incubation times: 15 min, 30 min, 1 hour, 2 hours, 4 hours, 6 hours*.

After the 24 hours incubation period was complete the sample was placed in a round-bottomed flask and lyophilised over night, resulting in a dry, white, solid. The solid was reconstituted in 0.1% TFA in water (2 ml). The pH of the solution was immediately adjusted to pH 2 using HCl (1 M) whilst continuously stirring (monitoring every half hour). The solution was spin filtered using 0.2 μm cellulose acetate, microspin filter tubes (Alltech) for 5 min at 4000 rpm. The crude CML was then ready for preparative HPLC (Column:25 x 10mm Waters RCM, detection wavelength: 230 nm, mobile phase flow rate: 9.9 ml/min, mobile phase: 0.1% TFA(aq)).

---

* It was noted that the pH of the solution was high in the first hour of the reaction and by the 4 to 6 hours incubation time, the pH had stabilized to 7.4. Therefore, it is recommended to monitor the pH of the mixture over the first 2 hours of the reaction.

A solution of α-t-BOC-lysine (5 m/gml) was injected into the system (RT: 10 min). The crude CML (0.5 ml) was injected into the system and one single broad peak was detected, spanning a retention time of approximately 9 to 11 mins. The remainder of the solution was injected into the system and the relevant fractions collected pooled together and lyophilised over night. A portion of the dried, white solid was submitted for NMR spectroscopy confirming the solid to be pure protected CML (Appendix VII, Fig. VII.iva).

The CML was deprotected by dissolving the crude CML in 0.5M HCl (0.1ml used for every 10mg of sample) and incubating overnight at room temperature. The sample was lyophilised and NMR, carbon and mass spectroscopy achieved confirmation of successful deprotection (Appendix VII, Fig. VII.ivb – VII.vi).

The NMR spectrum VII.ivb shows 1:1 ratios of the β, γ, δ, ε, where β, γ and δ are 1.4, 1.2 and 0.9 ppm. The CH_2CO_2 of the carboxymethyl group is at 2.5ppm in this spectrum. The loss of the tBOC signals are shown in VII.ivb.

The pure CML was stored at -20°C. The total yield of pure CML was 39.3mg.

3.2.2.3 Conclusions

This method produced a pure batch of CML of a substantial yield and confirmed that the BOC protected lysine was more desirable than the acetyl protected lysine. The pure CML was used as the external standard for the identification of CML in human plantar callus (Chapter 5).

3.3 Synthesis of Pentosidine

Pentosidine is an acid stable, highly fluorescent AGE and cross–link, derived from one molecule of arginine, one of lysine and a pentose sugar (e.g. ribose) bridged in to an imidozo-pyridinium structure (Fig 3.6). Dyer *et al* (1991) [110]

have also described its formation from glucose, by a slower rate and probably through oxidation of glucose to arabinose. Since its formation from either glucose or ribose requires oxidation, pentosidine is both an AGE and a glycoxidation product [111].

It is present in small amounts in many long-lived human tissues, including skin collagen [108;110;184], and is a biological marker of protein glycoxidation. Due to its biochemical structure, pentosidine cannot be derivatised in preparation for GC/MS analysis. Detection and quantification is achieved by acid hydrolysis followed by fluorescent HPLC detection (Chapter 4).

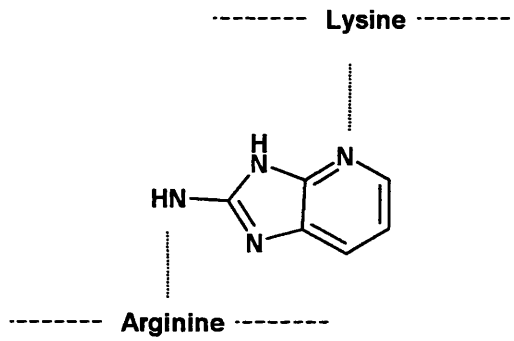

Figure 3.6. Structure of Pentosidine

3.3.1 Reagents

Sodium phosphate buffer (0.2 M, pH 9), sodium hydroxide (5 M), N^{α}-acetyl-L-lysine, N^{α}-acetyl-L-arginine, D-ribose, hydrochloric acid (6 M, 12 M), ninhydrin, Dowex AG5050W-X8 (200-400 mesh, H+ form).

3.3.2 Method

N^{α}-acetyl-L-arginine (3.243 g, 15 mmol) and N^{α}-acetyl-L-arginine (941 mg, 5 mmol) were dissolved in 100 ml 0.2 M phosphate buffer, pH=9. The solution was heated in a water bath at 65°C for 48 hours under continuous stirring. During

incubation, 10 portions (75 mg each) of D-ribose were periodically added to the reaction mixture (Fig. 3.7). After each addition of ribose, the pH was adjusted to 9 using NaOH. The mixture was hydrolysed in four vacuum-sealed glass vials using HCl (30 ml, 12 M) at 110°C for 2 hours. The resulting solution was reduced under low pressure at 60°C and the dried brown residue was dissolved in dH_2O (20 ml) and applied to a chromatography column (16x120 mm), filled with cation exchange resin (Dowex 50W-X8) H+ form (flow rate: 1 ml/min, wavelength: 254nm). The column was eluted with water (~250 ml) followed by HCl (400 ml, 2.6 M). Pentosidine was eluted with HCl (150 ml, 6 M) at a flow rate of 1 ml/min and fractions (10 ml) were collected and tested for the ninhydrin reaction. Ninhydrin positive fractions (5-16) were pooled and dried under reduced pressure at 60°C. The sample was then dissolved in dH_2O (4 ml) and filtered through a syringe filter (0.2 μm). Of this solution, 200 μl portions were injected into the same preparative HPLC system as that used for the CML preparation in section 3.2.3.2. Pentosidine was eluted (RT: 4 min at wavelength 230 nm) from aqueous acetic acid (50 mM).

3.3.3 Results and Conclusions

Fractions were pooled together, lyophilized to dryness and pure pentosidine was identified by NMR spectroscopy (Appendix VII, Fig. VII.v). The total yield of pure pentosidine was 22.5mg.

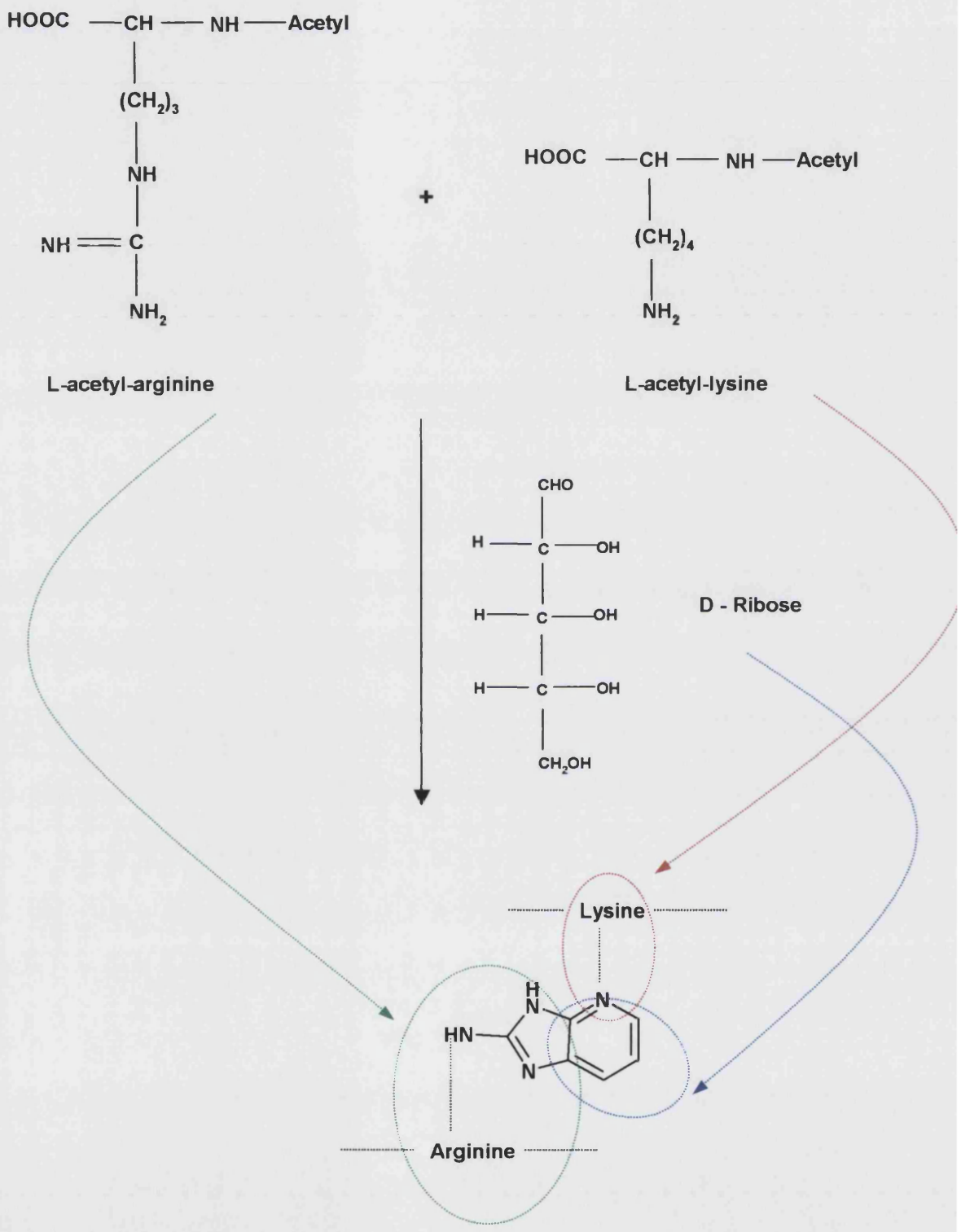

Figure3.7. Diagram illustrating the synthesis of pentosidine

4.0 CHAPTER 4 - Quantification of Furosine and Pentosidine in Human Plantar Callus using HPLC.

4.1 Introduction – Measurement of Glucose, Early Glycation Adducts and AGEs

To date the measurement of AGEs has been confined to investigative laboratories. Currently there is no universally established method of detection of AGEs, units of measurement, nor any commercially available assay kits. This makes it hard to evaluate and compare results from different studies. Currently, the most common forms of detection of AGEs are HPLC, GC-MS, enzyme-linked immunosorbent assay (ELISA) [185] immunohistochemistry.

There are no reports to date on the correlation between the degree of glycation of plantar epidermal keratins and pedal skin complications in diabetes. Glucose in the epidermal cells, intercellular spaces, microcirculation of the skin, passive diffusion rate of the glucose and carbohydrate metabolism all contribute to the overall epidermal glucose concentration in diabetes [162].

With the discovery of glycation in foods [186], and later in human tissues, the proteins that were extensively investigated were from blood plasma [187], urine[188], skin collagen [189] and dialysate proteins [190]. Studies on skin collagen directed further investigations into glycation of keratins in epidermis, nails and hair.

The most frequently used techniques for the determination of NEG of proteins in the 1980s were colorimetric methods, primarily the TBA assay [121] . The technique was also used to measure the glycation of hair and epidermal keratins[161;163;164]. The key problem with this procedure was the high non–specific background absorbance, leading to a loss of sensitivity [168]. The use of the TBA reaction for the measurement of glycated haemoglobin and glycated serum proteins has largely been replaced by newer, more specific techniques tailored to the particular analyte and to the needs of the clinical laboratory. Keratinised tissues were investigated by adapting these methods, principally the detection of furosine [162;191], but no attempts to detect AGEs in these tissues were made.

4.1.1 Reaction with TBA

The TBA method is one of the oldest chemical assays for glycated proteins [192]. It is a colorimetric procedure based on the formation of a chromogen upon the reaction between TBA and HMF. HMF is generated from the dehydration of hexose sugars by boiling in oxalic acid [193].

The technique remains useful for the estimation of glycation of proteins [194]. Its advantages include simplicity, lack of the need for sophisticated equipment, and absence of interference by Schiff base intermediates. Its disadvantages include a low sensitivity due to a low yield of HMF and susceptibility of interference by free glucose, other sugars and glycoproteins [195]. Some of these problems can be partially avoided by modifications of the technique [161], but avoidance of interference by glycoproteins cannot be completely achieved, making the TBA method more suitable for relative and not absolute measurements of glycated proteins. In this regard the method has been used successfully to demonstrate increased glycation of collagen [156] and keratin [166].

4.1.2 Borohydride Reduction

Sodium borohydride or sodium cyanoborohydride will reduce the aldimine and ketoamine products of NEG, converting them to aminohexitols. The aminohexitols can then be identified with amino acid analysis [195]. Reduction with tritiated borohydride is often used to enhance sensitivity when the amounts of protein available for analysis are small. Simultaneous reduction of peptide bonds can limit specificity, but separation and identification of the tritiated aminohexitols by amino acid analysis or by affinity chromatography of the labeled borohydride-reduced peptides helps address this problem.

4.1.3 Amino Acid Analysis

Glycated amino acid derivatives in acid hydrolysates of proteins can be detected and measured by HPLC and modifications of conventional amino acid analysis. Since acid hydrolysis of the ketoamine produces some racemization at the

second carbon atom, mannitol as well as glucitol derivatives are formed. Partial degradation further complicate identification of different amino acid derivatives.

4.1.4 Furosine Detection

Fructoseamine (1 amino-1-deoxyfructose) is the stable ketoamine derivative formed after the condensation of glucose with protein. Since non-enzymatic glycation largely involves ε-amino groups of lysine, ε-D-fructose-lysine is the principle fructoseamine formed. Acid hydrolysis of this compound leads to the formation furosine [168]. Furosine can be separated on HPLC and quantified by reference to furosine standard, allowing the development of a sensitive and specific method for the quantitative determination of the overall level of non-enzymatic glycation in proteins [168]. The method has been successfully applied for specific measurement of glycation of serum and tissue proteins, in which the only source of furosine is the glycated amino groups of lysine residues [195].

The disadvantages of the HPLC assay, with regards to routine clinical studies, are: the long assay time due to the use of the gradient elution; the high acidity of the sample which can damage the chromatographic injector and column and the use of very expensive furosine dedicated chromatographic columns [187]. The studies in this thesis succeed in adapting the protocols so as to overcome these hindrances.

Other analytical methods used for furosine quantification, in different biological samples, include ion–exchange chromatography with amino acid analysis and post–column ninhydrin derivatisation [89] and gas–liquid chromatography [118]. The sensitivity, accuracy and precision of these methods differ and they are often time consuming, expensive and not sufficiently free of interference.

4.1.5 HPLC Methods of Detection and Quantification of Furosine and Pentosidine

In order to be able to assay for glycation adducts, the polypeptide chain of the protein being analysed is split into smaller peptide subunits. Hydrolysis is successfully conducted by acid (HCl) or peptidases (Fig. 4.1). The peptidases are residue specific and will only hydrolyse peptide bonds where those residues occur. Therefore, by using specific proteolytic enzymes, predetermined fragments can be formed prior to analysis, specificity being the advantage of this method. Acid hydrolysis is a well used method of analysis, resulting in the complete breakdown of the peptide chain into its constituent amino acid residues. This method is widely used when preparing a protein for HPLC detection of furosine in human serum and keratin containing tissues [162;168;168;191].

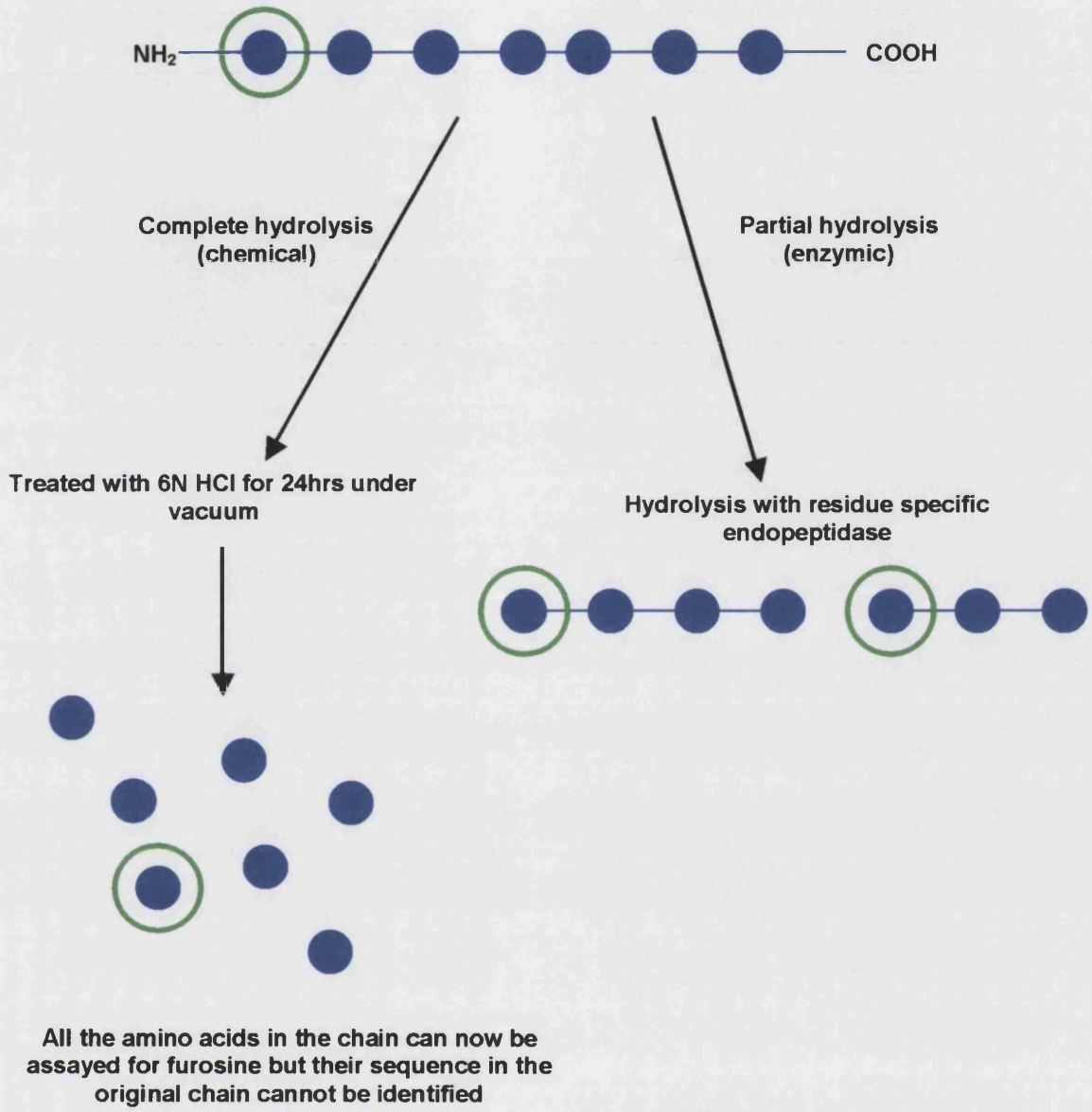

Figure 4.1. Schematic representation of the use of hydrolytic procedures in preparation for furosine HPLC analysis. The presence of a free amino group , with which a reagent can react, enables the amino acid to be identified.

4.1.5.2 HPLC Analysis of Acid Hydrolysates for Furosine

After the acid hydrolysis of the test protein has been carried out, a portion of the sample is dissolved in an appropriate buffer and injected into an HPLC system. Different laboratories have used different HPLC set-ups that have suited them and have provided an adequate resolution of the furosine peak (Table 4.1).

Table 4.1. Description of the variations of HPLC protocol for the identification and quantification of furosine.

Column type	Column size [mm]	Particle size [µm]	Mobile phase 1	Mobile phase 2	Retention time for Furosine [min]	Reference
C_{18}	4x200	10	H_3PO_4 (7mM)	H_3PO_4 (5.6mM)	3	[195]6]
C_8	4.6x200	unknown	Acetic acid (0.4%	Acetic acid (0.4%) & KCl (0.27%)	28	[190;196]7]
C_{18}	4.6x200	unknown	Sodium acetate (0.4%)	Acetonitrile (6%)	13	[187]8]
C_{18}	4x300	5	H_3PO_4 (7mM)	Not used	4.6	[58]0]
C_{18}	4.6x150	5	NaH_3PO_4 (50mM)	Not used	3.79	[162;191]2]

Furosine was detected at absorption 280nm and the flow rate was 1ml/min.
The details in blue font indicate the protocols used for measuring furosine in keratinised tissues.

4.1.5.2 HPLC Analysis of Acid Hydrolysates for Pentosidine

Pentosidine has excitation-emission maxima at 335/385nm and is assayed by HPLC. Acid hydrolysates of human tissues have a pentosidine concentration ranging from 30-250 pmol/mg protein have been found in dura mater, skin, and glomerular basement membranes [108;197].

Initial attempts to quantitate pentosidine in blood and other proteins have highlighted interference by fluorescent artifacts, generate during acid hydrolysis. This lead to a detailed study that achieved an accurate chromatographic method for quantification of low levels of pentosidine in blood and tissue proteins [198]. Pentosidine was determined by applying acid-hydrolysed samples (under hypoxic conditions) to HPLC. Borohydride reduction before acid hydrolysis had no

significant effect on the accumulation of artifacts. Separations were made with a 25x0.46cm C-18 column (10um) column with a linear gradient program of 10-17% acetonitrile from 0 to 35min containing water and 0.1% heptafluorobutyric acid (HFBA). The eluent was monitored by fluorescent detection at an excitation-emission wavelength of 335/385nm (attenuation: 4, gain:x100). A similar method was used in this thesis.

According to Baynes and associates (Department of Chemistry and Biochemistry, University of South Carolina), reduction of the sample before acid hydrolysis prevents interference from products of decomposition, Amadori products and reactive AGEs on proteins. This step together with hydrolysis under nitrogen generally reduces the complexity of the chromatograms.

4.1.6 Summary

This chapter reports the development of an HPLC protocol for reliable furosine and pentosidine determination in human plantar epidermal tissues. The method for furosine detection involved the integration and adaptation of several methods previously developed to quantitate furosine in both food products and human tissues. The pentosidine assay also deviated slightly from the conventional protocol. Both methods were suited to the tissue being analysed and the laboratory set-up. The experiments concentrated on the reproducibility of the methods and compared the results from callus tissues and keratin extracts. It also challenged the method of acid hydrolysis of the proteins, suggesting that the glycation adducts may be lost during the process. An enzymatic hydrolysis method was tested to see whether there was less destruction of furosine and pentosidine in comparison to acid hydrolysis.

4.2 Development of a Furosine and Pentosidine HPLC Assay for Human Plantar Keratin Proteins

4.2.1 Aims

- Measurement of inter- and intra-assay variation of furosine and pentosidine standards including day-to-day variance, recovery, stability and precision.
- To test that hydrolysis of tissues under hypoxic conditions is optimal for quantification.
- A comparison of furosine and pentosidine content from acid hydrolysed plantar callus tissue and keratin extracts.
- A comparison of furosine and pentosidine content from enzyme hydrolysed plantar callus tissue and keratin extracts.
- To determine the optimal hydrolysis time for keratins.
- To determine the recovery, stability and precision of the chosen method of analysis.

4.2.2 Sample Collection and Subject Details

Specimens of callus were obtained from a random sample of 6 diabetics attending the London Foot Hospital. The same number of control patients was taken as a random sample from the non-diabetic subjects attending the London Foot Hospital for chiropody treatment. These subjects did not suffer from any saccharide metabolism disorder. Each group comprised of males and females aged between 30 and 80yr. Both groups were age matched (Table 4.2). The callus specimens were taken from the plantar metatarsal area using a scalpel. Areas involved with sepsis and specimens contaminated with blood were avoided. Each specimen was stored at -70°C[⊗].

⊗ Furosine assay by HPLC as been used to demonstrate an increase in glycated lysine over time with storage of serum samples at -20°C, perhaps due to the ongoing reaction between glucose and lysine ε-amino groups in the frozen serum. Storage at -70°C eliminates this problem (Cohen 1996).

Table 4.2. Details of the subjects used for the study

Identification of Normal Subjects	Age of Normal Subjects [years]	Identification of Diabetic Subjects	Type of Diabetes	Type of Therapy	Number of Years of Diagnosis
1N	65	1D	II	Insulin	30
2N	55	2D	II	Insulin	9
3N	60	3D∞	II	Insulin	10
4N	55	4D	II	Oral	13
5N	78	5D	II	Insulin	26
6N	37	6D *	II	Insulin	32

∞ Plantar callus was taken from the periphery of a long standing neuropathic ulcer.
* Poorly controlled diabetes with continuous ulceration
All subjects were male.

4.2.3 Inter- and Intra-Assay Variance of Furosine and Pentosidine Standard Measurement

4.2.3.1 Reagents

Furosine standard (Neosystem, Groupe SNPE, Strasbourg), pentosidine (synthesised in Chapter 3), trifluoracetic acid (TFA), HPLC grade water.

4.2.3.2 HPLC conditions

Table 4.3. HPLC conditions for furosine detection.

Mobile Phase Gradient	Time [min]	%A	%B
	0	100	0
	10	75	25
	15	75	25
	20	100	0
	35	100	0

Automated injector system (Waters 712 WISP), pump system (Varian), UV monitor (Waters 486), software (Prostar, Varian), column (Hypersil C18 100mx4.6mm, particle size 7μm), mobile phase A (0.1% TFA in HPLC grade water), mobile phase B (0.1% TFA in HPLC grade acetonitrile), flow rate 1ml/min and absorbance 280nm.

Table 4.4. HPLC conditions for pentosidine detection.

Mobile Phase Gradient	Time [min]	%A	%B
	0	100	0
	5	90	10
	10	90	10
	15	100	0
	25	100	0

Automated injector system (Waters 712 WISP), pump system (Varian), UV monitor (Waters 486), software (Prostar, Varian), column (Hypersil, BDS C18 250mmx4.6mm, particle size 5μm), mobile phase A (0.1% TFA in HPLC grade water), mobile phase B (0.1% TFA in HPLC grade acetonitrile), flow rate 1ml/min, excitation wavelength: 335nm, emission wavelength: 385nm.

4.2.3.3 Methods

Each standard was dissolved in 0.1% TFA (aq) and a set of serial dilutions made up (furosine: 15.6, 7.8, 3.9 and 1.95 µg/ml; pentosidine: 200, 100, 50, 25 and 12.5 ng/ml) and stored at -80°C. These ranges were chosen as the furosine and pentosidine content in the test samples fell within these concentrations and lower concentrations produced poor chromatograms. To minimise variability in the results, through solvent evaporation, the vials were sealed before being placed in the HPLC machine.

4.2.3.4 Results

4.2.3.4.1 External Standard Curves

There was a linear relationship between standard peak area and varying concentrations of each standard (Fig. 4.2-4.5). Injections of all the dilutions of standard were carried out three times and on two different days to monitor inter-assay and day-to-day repeatability, respectively (Table 4.5).

Table 4.5. Day-to-day and interassay repeatability of HPLC standard injections (raw data in Appendix VIII, .Tables VIII.i-VIII.iv).

		Furosine	Pentosidine
Interassay RT [min]	Mean	8.13 – 8.37	10.25 – 10.44
	Standard deviation	0.03 – 0.09	0.008 – 0.03
	Standard error	0.002 – 0.04	0.005 – 0.02
Day-to-day repeatability RT [min]	Mean	8.19 – 8.35	10.28 – 10.39
	Standard deviation	0.02 – 0.06	0.01 – 0.05
	Standard error	0.01 – 0.13	0.01 – 0.03
Peak area CV [counts]		<10	<10

a

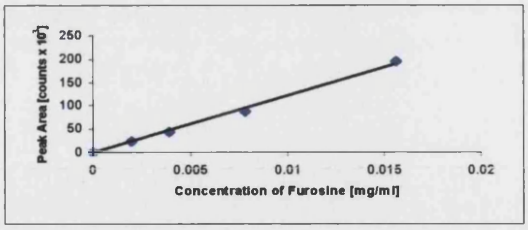

b

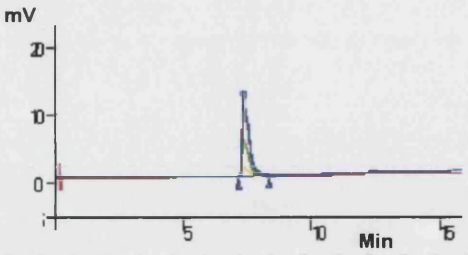

Figure 4.2.
Day one a. Standard curve of furosine analysed by HPLC. **b.** Chromatograms of furosine peaks (retention times 8.18.4 min) Absorption peaks at 280 nm

a

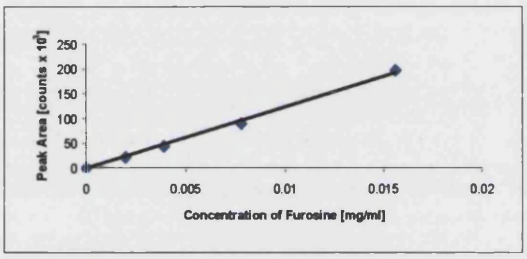

b

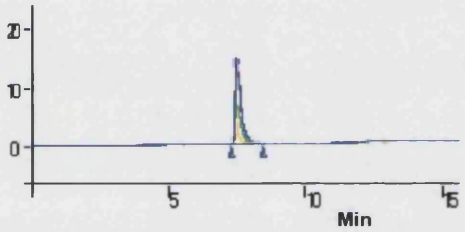

Figure 4.3.
Day two a. Standard curve of furosine analysed by HPLC. **b.** Chromatograms of furosine peaks (retentions time 8.1-8.2 min)

a

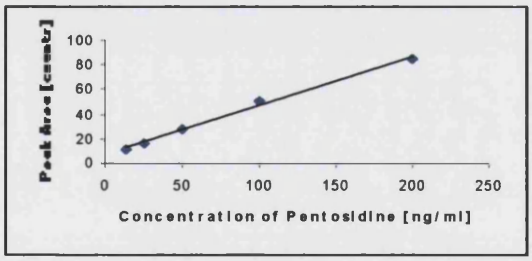

b

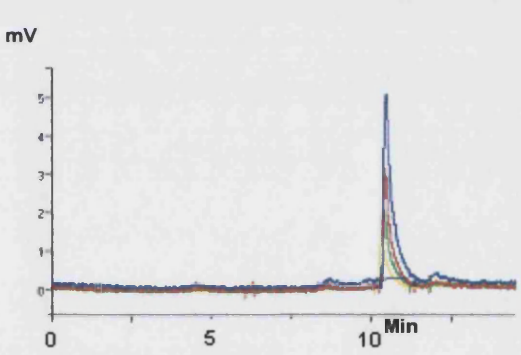

Figure 4.4. Day one
a. Standard curve of pentosidine analysed by HPLC. Absorption peaks at ex: 335nm em: 385 nm
b. Chromatograms of pentosidine standard peaks (retention times 10.3-10.44min)

a

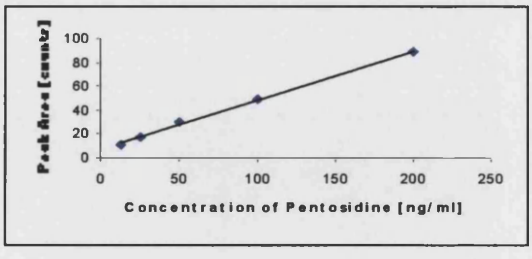

b

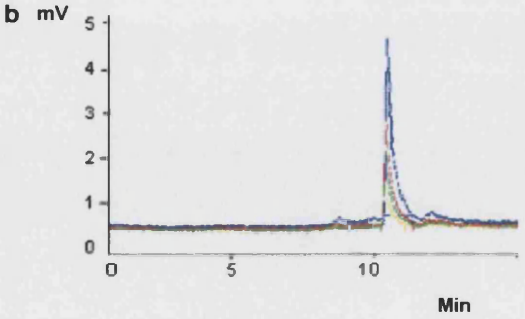

Figure 4.5. Day two
a. Standard curve of pentosidine analysed by HPLC. Absorption peaks at ex: 335nm em: 385 nm
b. Chromatograms of pentosidine standard peaks (retention times 10.3-10.44min)

4.2.4 Freeze-Thaw Study of Furosine and Pentosidine Standards

4.2.3.3 Aims

- To assess whether repeated freezing and thawing of standard solutions changes the quality of the chromatograms.

4.2.3.4 Methods

Aliquots (0.5 ml) of furosine and pentosidine standards (15.6 µg/ml and 200ng/ml, respectively) were respectively placed in plastic vials and thawed and refrozen for up to six cycles. The experiments were repeated twice and the mean peak area (counts x 10^3) was plotted against freeze-thaw cycle number (Figs. 4.6 & 4.7)

4.2.3.5 Results

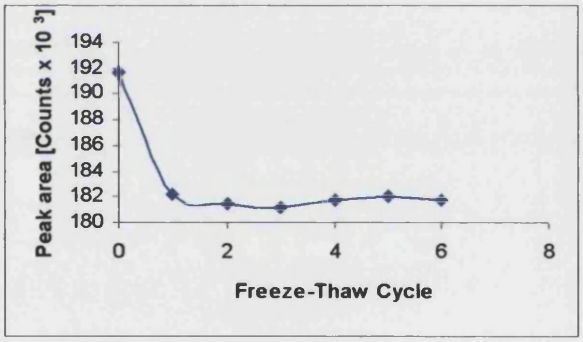

Figure 4.6. The effect of successive freeze-thaw cycles on levels of furosine standard (0.0156 mg/ml)

There was a decrease in peak area after the first freeze thaw cycle, from 191.7x10^3 to 182.2x10^3counts. The area of this peak lies outside the 95% confidence limit interval of the mean (mean: 195.02x10^3, upper limit: 201.11x10^3, lower limit: 188.93x10^3). Raw data in Appendix VIII, Table VIII.v

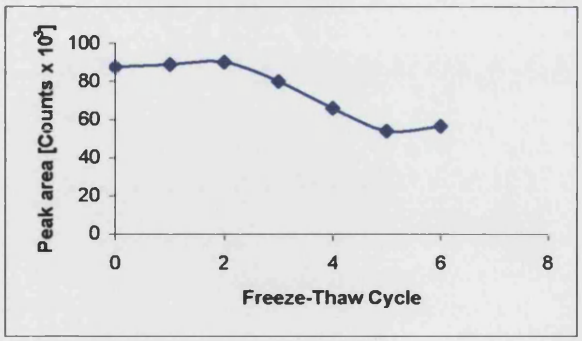

Figure 4.7. The effect of successive freeze-thaw cycles on levels of pentosidine standard (200 ng/ml)

There was a decrease in peak area after the third freeze thaw cycle, from 80.0 x 10^3 to 66.1 x 10^3 counts which continues to decrease in subsequent freeze/thaw cycles. The area of this peak lies within the 95% confidence limit interval of the mean (mean: 73.406, upper limit: 91.191x10^3, lower limit: 54.082x10^3). Raw Data in Appendix VIII Table VIII.vi

A similar observation was made when hydrolysates were freeze-thawed and assayed for furosine and pentosidine. Therefore, the repeated freeze-thawing of the standards was avoided when measuring of glycation adducts in tissue samples in future experiments (Chapter 9).

4.2.4 Acid Hydrolysis of Human Plantar Callus Samples under Hypoxic and Non-Hypoxic Conditions

4.2.4.1 Aims

- To assess the effects of oxygen, nitrogen and air during hydrolysis on the measurement of furosine and pentosidine in callus samples.

4.2.4.2 Reagents

Hydrochloric acid (6 M), trifluoracetic acid (TFA), ethanol, acetonitrile (HPLC grade)

4.2.4.3 Methods

Callus tissue (5 mg) was washed with absolute ethanol followed by water, 3 times, cut into small pieces using a blade and placed in a glass vial. An aliquot of HCl (0.2 ml, 6 M) was added to the sample, flushed with nitrogen gas and sealed with a Teflon lined cap. The sample was heated for 18 h at 110°C, shaking occasionally to allow dispersion on the callus tissue in the solution. This was carried out on all the callus samples (1–6 diabetics and controls). The procedure was then repeated with oxygen and air in place of nitrogen to see if there is a difference in the amount of furosine and pentosidine measured. The hydrolysates were lyophilised over night to dryness and redissolved in TFA (200 µl, 0.1% aqueous). The solutions were filtered, if necessary, using a syringe filter (0.2 µm Millipore). The protein content of each hydrolysate was measured using the Lowry method of protein detection (Appendix I) and all samples were subsequently adjusted to a 1 mg/ml solution in preparation for HPLC analysis.

4.2.4.4 Results

There was a higher yield of furosine and pentosidine from samples hydrolised in the presence of nitrogen (Fig. 4.8 & 4.11). Therefore, all future hydrolysis procedures were carried out under hypoxic conditions. While there was no significant difference in furosine content between the diabetic and non-diabetic groups (Fig 4.9) there were greater inter-individual differences in furosine levels in diabetic callus compared to non-diabetic controls (diabetic mean furosine: 354.5 ± 268.6 ng/mg protein; non-diabetic mean furosine:224.6±75.3 ng/mg protein). However, in the case of pentosidine content (Fig. 4.12), the opposite was the case (diabetic mean pentosidine:153.9±106.6 ng/mg protein; non-diabetic mean pentosidine: 325.5±172.8 ng/mg protein). The diabetic subjects, 2D (55 yr) and 6D (37 yr), showed high levels of furosine in comparison to their matched controls (Fig. 4.10). The diabetic subject 6D, had relatively high levels of furosine, although, he was the youngest of the group (37 yr). Both of these subjects were the only patients with plantar ulcers (see Appendix VIII Tables VIII.vii. & VIII.viii).

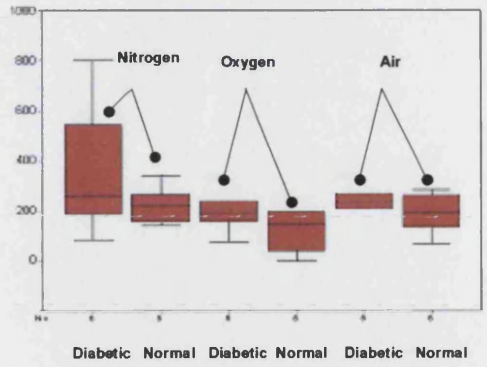

Figure 4.8. Box plot comparing the amount of furosine in diabetic and non-diabetic callus samples hydrolysed in the presence of nitrogen, oxygen and air.

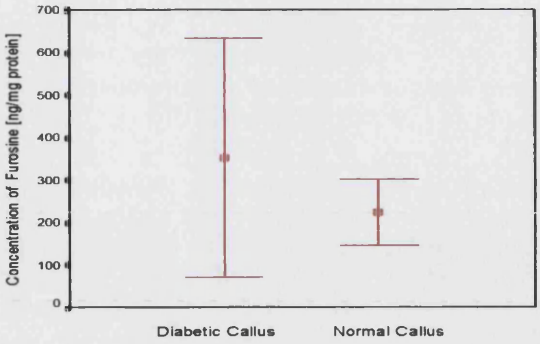

Figure 4.9. Plot of furosine data from diabetic and non-diabetic callus samples hydrolysed under hypoxic conditions

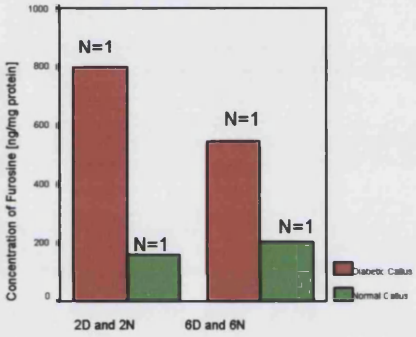

Figure 4.10: Bar chart comparing the concentration of furosine in callus taken from diabetic ulcers and normal callus

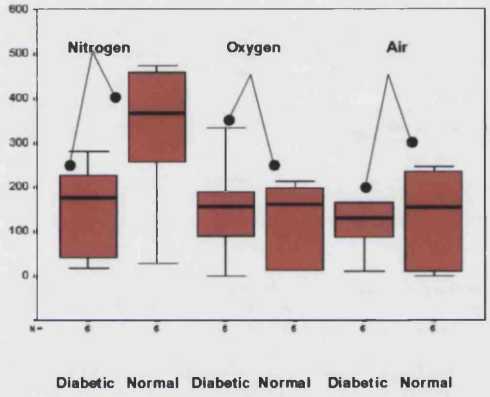

Figure 4.11. Box plot comparing the amount of pentosidine in diabetic and non-diabetic callus samples hydrolysed in the presence of nitrogen, oxygen and air.

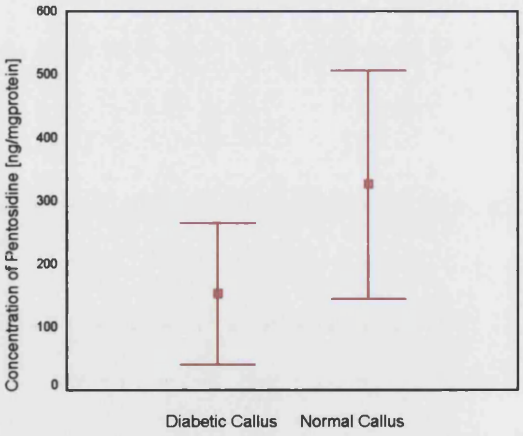

Figure 4.12. Data from diabetic and non-diabetic callus samples hydrolysed under hypoxic conditions

4.2.5 Acid Hydrolysis of Human Plantar Epidermal Keratin Extracts

4.2.5.1 Aims

- To measure the furosine and pentosidine content in plantar keratin.
- To compare the amount of glycation adducts measured from callus and keratin hydrolysates.

4.2.5.2 Reagents

Hydrochloric acid (6 M), trifluoracetic acid (TFA), acetontrile (HPLC grade), keratin extracts from Chapter 2

4.2.5.3 Methods

Keratin extracts were lyophilised to dryness and approximately 0.2 mg was hydrolysed in HCl (200 μl, 6 M) as described in the previous section, under nitrogen gas. The hydrolysates were dissolved in 0.1% TFA (aq) and adjusted to a 1mg/ml protein concentration in preparation for HPLC analysis.

4.2.5.4 Results

There was a higher yield of furosine from the keratin extracts, than that of callus tissue (Fig. 4.13) and a lower yield of pentosidine from extracts than callus (Fig. 4.14). As with the callus hydrolysates, there is no significant difference in furosine content between diabetic and non-diabetic keratin hydrolysates – p=0.368 (Fig. 4.15). The pentosidine concentration was greater in diabetic keratin extracts than controls – p=0.048 (Fig. 4.16). There were greater inter-individual differences in the amount of furosine measured from diabetic samples (diabetic mean furosine: 151.3 ± 354.1 ng/mg protein; non-diabetic mean furosine: 146.9 ± 300.8 ng/mg protein; diabetic mean pentosidine: 42. 3± 53.6 ng/mg protein; non-diabetic mean pentosidine: 10.7 ± 6.8 ng/mg protein).

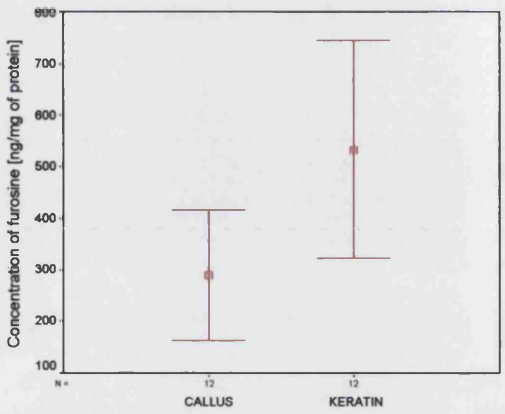

Figure 4.13. Graph illustrating the difference in furosine content between callus and keratin extracts hydrolysed in acid

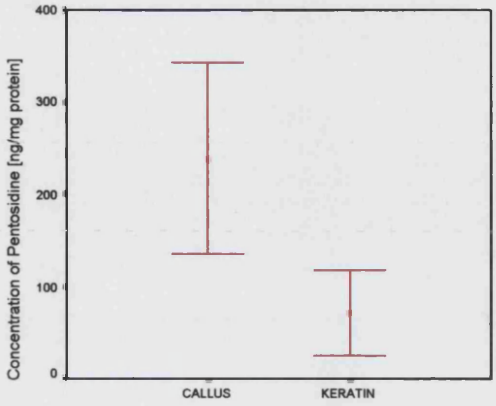

Figure 4.14. Graph illustrating the difference in pentosidine content between callus and keratin extracts hydrolysed in acid

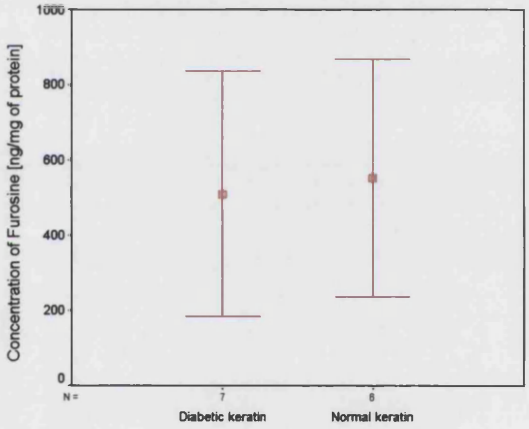

Figure 4.15. Graph illustrating the difference in furosine content between diabetic and normal keratin extracts

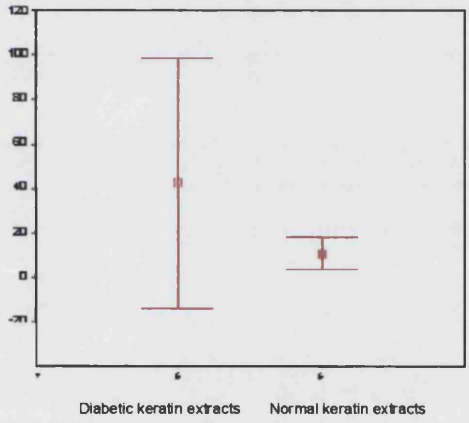

Figure 4.16. Graph illustrating the difference in pentosidine content between diabetic and normal keratin extracts

The results show that the nature of the tissue used for acid hydrolysis is relevant when measuring furosine and pentosidine. There is a significantly higher amount of furosine measured from keratin extracts than that of corresponding callus samples. A possible explanation for this is the keratin extraction procedure produces free polypeptide chains that are readily hydrolysed by acid, and in callus tissue the keratin filaments are tightly bound together by disulphide bonds, which are not adequately hydrolysed by HCl, and hence limiting the amount of

free furosine and pentosidine in the hydrolysate. Alternatively, the glycation adducts could be destroyed during acid hydrolysis.

All the chromatograms of the callus hydrolysates show the presence of tyrosine in abundance, which suggests that there is a degree of successful hydrolysis of the protein chains. However, is possible that the acid may disrupt the glycated side chains of the amino acids. This may be the case for both the callus tissue samples and the keratin extracts. In view of this, the next investigation involved the hydrolysis of callus and keratin extracts using enzymes to see if a higher amount of furosine and pentosidine could be measured.

4.2.6 Enzyme Hydrolysis of Human Plantar Callus Samples[P]

4.2.6.1 Aims

- To investigate if there is a difference between acid and enzyme hydrolysis on the amount of furosine and pentosidine measured.

4.2.7.2 Reagents

Pepsin, pronase E, aminopeptidase, hydrochloric acid, potassium phosphate (0.5 M), potassium hydroxide

Samples
Callus samples (1 mg), keratin extracts (100 μg)

4.2.7.3 Methods

To each sample (callus 5 mg, keratin 200 μg) dH_2O (25 μl), HCl (25 μl, 4 mM) and pepsin solution (5 μg/ml, 2 mg/ml in 20 mM HCl) were added and incubated at 37°C for 24 h. The samples were neutralised to 7.4 pH by adding potassium

[P] Dr N Ahmed, Department of Biochemistry, Essex University, has developed the protocol for enzymolysis. The procedure is unpublished. Dr Ahmed has kindly given permission for this method to be tested in this study.

phosphate buffer (25 µl, 0.5 M, pH 7.4) and potassium hydroxide (5 µl, 260 mM). Pronase E (5 µl, 2 mg/ml in 10 mM potassium phosphate, pH 7.4) was added to each sample and incubated at 37°C for 24 h. Aminopeptidase solution (5 µl, 2 mg/ml in 10 mM potassium phosphate, pH 7.4) was added and the samples were incubated for a further 48 h at 37°C. The hydrolysis was carried out under nitrogen gas. The resulting hydrolysates were centrifuged, before use to afford a clear solution. The samples were adjusted to 1mg/ml protein concentrations.

4.2.7.4 Results

The acid hydrolysis of keratins produced the highest yield of furosine and pentosidine in comparison to enzyme hydrolysates of both callus and keratin extracts (Fig. 4.17 & 4.18). Therefore, the acid hydrolysis of keratin extracts was the standard procedure used in the future. The next stage involved refining the method for accuracy and efficiency.

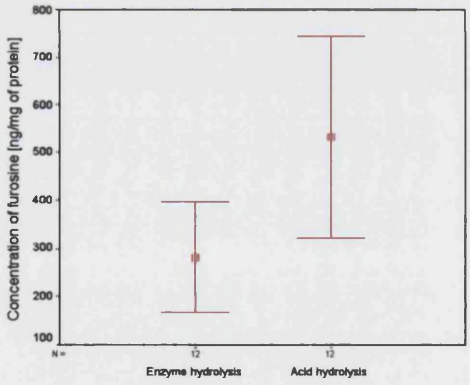

Figure 4.17. Graph comparing the furosine content of acid and enzyme hydrolysates.

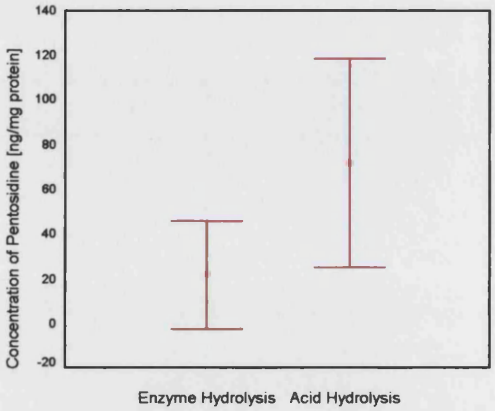

Figure 4.18. Graph comparing results from acid and enzyme hydrolysis of keratin extracts

4.2.8 Time Course Acid Hydrolysis of Callus and Keratin Extracts

4.2.8.3 Aims

- To find the optimal hydrolysis conditions for keratin extracts.

4.2.8.2 Methods

Keratin extracts were hydrolysed for different time periods (2, 4, 6, 18, 24 and 30 h) and assayed for furosine and pentosidine content. The experiments were carried out in triplicate and the mean concentrations plotted in the graphs below.

4.2.8.3 Results

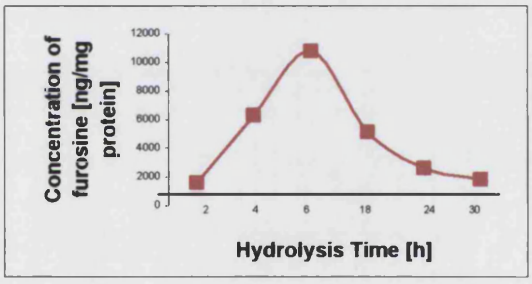

Figure 4.19. Keratin extracts hydrolysed for different periods of time and assayed for furosine (see Appendix VIII Fig. VIII.xi for data)

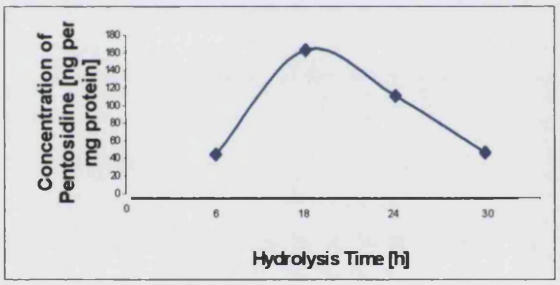

Figure 4.20. Keratin extracts hydrolysed for different periods of time and assayed for pentosidine (see Appendix VIII Table VIII.xi for data)

The optimum hydrolysis times for furosine and pentosidine assays were 6 and 18h, respectively (Figs. 4.19 & 4.20). These conditions differ from those of optimal furosine detection in other tissues, such as urine, where the hydrolysis time is 24 h [188].

4.2.9 Recovery, Stability and Precision of Assays using Acid Hydrolysates of Keratin Extracts

4.2.9.1 Methods

Threes keratin extracts were selected at random for the measurement of furosine and pentosidine recovery. Known amounts of standard were added (1, 0.1, 0.01 and 0.001 mg/ml) to the keratin (0.2 mg) before acid hydrolysis and assayed for furosine and pentosidine. At the same time, furosine and pentosidine standards were hydrolysed without test samples and assayed. The experiments were carried out in triplicate and the mean percentage recovery of the glycation adducts were calculated.

The hydrolysates were stored at -70°C and a random selection of the samples assayed every month to assess for any deterioration in furosine and pentosidine content. The within run precision and day-to-day precision was assessed on all sample hydrolysates.

4.2.9.2 Results

4.2.9.2.1 Recovery

Table 4.6. Recovery of furosine from keratin extract hydrolysed in acid for 6h (data in Appendix VIII, Table VIII.xii).

Samples	Mean % Recovery of Furosine
minus furosine	
1 mg/ml furosine	79.97
0.1 mg/ml furosine	77.36
0.01 mg/ml furosine	76.60
0.001 mg/ml furosine	75.00

Table 4.7. Recover of pentosidine from keratin extracts hydrolysed in acid for 18h (data in Appendix VIII, Table VIII.xiii).

Samples	Mean % Recovery of Pentosidine
minus pentosidine	
1 mg/ml pentosidine	69.97
0.1 mg/ml pentosidine	57.36
0.01 mg/ml pentosidine	56.60
0.001 mg/ml pentosidine	45.00

4.2.9.2.2 Stability

All hydrolysates were stored at -70°C and showed no change in furosine and pentosidine content for up to three months. After a period of six months the samples had deteriorated.

4.2.9.2.3 Precision

The precision of furosine and pentosidine determination was carried out on all keratin hydrolysates. The within run precision and day-to-day repeatability of the measurement of furosine and pentosidine concentration was adequate (CV<10).

4.2.9.3 Discussion

This section was successful in completing the assay design for furosine and pentosidine detection. The results allowed the confident measurement of the glycation adducts in the 12 samples collected for this section and for the callus samples in the larger sample groups in Chapter 9.

4.2.10 Acid Hydrolysis of Keratin Extracts

4.2.10.1 Aims

- Acid hydrolysis of keratin extracts 6 and 18 h and assayed furosine and pentosidine, respectively.

4.2.10.2 Methods

The keratin extracts (0.2 mg) from all the callus samples were hydrolysed in HCl (200 µl, 6 M), for 6 and 18 h. Evaporation and reconstitution in buffer was the same as described in previous methods. The protein concentrations of the hydrolysates were standardised to 1mg/ml before injection into the HPLC systems.

4.2.10.3 Results

The concentration of furosine and pentosidine measured from the diabetic samples covered a wider range than non-diabetic samples (Table 4.7, Figs. 4.21 & 4.22). A difference in the distribution of the glycation adducts between groups was suggested. This was tested further in Chapter 9, where more samples were assayed for furosine and pentosidine (103 diabetics and 87 non-diabetics) and statistically analysed.

Table 4.8. Comparison of furosine and pentosidine concentrations between diabetic and non-diabetic subjects (data in Appendix VIII.xiv & VIII.xv).

	Furosine		Pentosidine	
	Diabetic Keratin n = 6	**Non-diabetic Keratin n = 6**	**Diabetic Keratin n = 6**	**Non-diabetic Keratin n = 6**
Concentration range (µg/mg protein	1.69-240	1.46-15.29	40.46-210.63	2.56-156.10
Mean	48.4	5.2	104.7	39.6
±SD	94.3	5.8	75.9	60.7

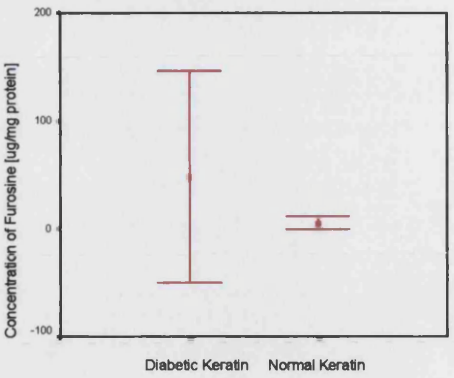

Figure 4.21. Graph comparing the furosine content from diabetic and non-diabetic keratin extracts hydrolysed for 6h in acid.

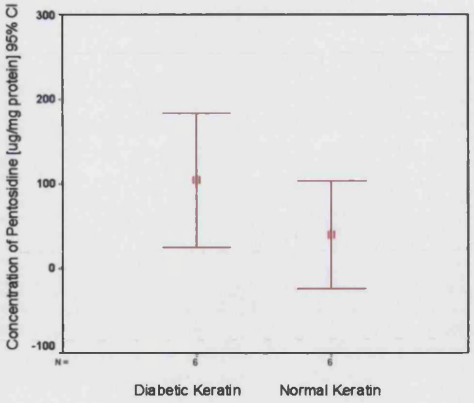

Figure 4.22: Graph comparing the pentosidine content from diabetic and non-diabetic keratin extracts hydrolysed for 18h in acid.

4.3 Discussion

This chapter illustrated the problems associated with the accurate quantification of furosine, in particular, in callus tissue. Due to the biochemical nature of callus, it is probable that the keratin extraction procedure frees the polypeptide chains from their hydrogen and disulphide bonds, thus leaving the proteins exposed for hydrolysis. The next step involved the collection of more callus tissue samples from diabetics and non-diabetics to see if there is an association between increased glycation and diabetes (Chapter 9).

4.4 Measurement of Glycohaemoglobin (HbA1c) and Glycated Serum Proteins in the Blood of Non-Diabetic Subjects

4.4.1 Aims

- Record HbA1c levels from blood samples taken from volunteers.
- To measure glycated adducts in the serum of blood samples taken from volunteers.
- To compare the results with the glycation adducts measured in keratin proteins.

4.4.2 Introduction

Recent advances in biochemical research have strengthened the argument in favour of "tight" control of diabetes as a means of preventing the long–term complications of the disease. The evidence in favour of this hypothesis is quite compelling, and it is reasonable to recommend good long–term control of diabetes to patients in an attempt to prevent the late complications [199]. Good long–term monitoring cannot be easily achieved without frequent home self–monitoring of either blood or urine glucose. Home self–monitoring of blood glucose has become possible over the past 15 years and has made a major impact on the, management of diabetes.

Neuropathy and vascular disease, both likely contributory factors in the development of foot lesions, are two of the late complications of diabetes. An overall glycaemic control since diagnosis may be more relevant to the development of foot pathologies than recording the degree of current glycaemic control [200]. There are also some theoretical reasons to recommend good blood glucose control in the presence of an acute foot lesion. Inadequate control probably interferes with white–cell function, which is important in combating infection. Also, wound healing might be impaired in the setting of very poor diabetes control, perhaps because of the glycation of structural proteins.

4.4.2.1 The Chemistry of Glycohaemoglobin

In 1966 Holmquist and Schroeder [201] demonstrated the presence of an N–terminal blocking group involving a Schiff base in haemoglobin A_{1c}. By the 1970s it was confirmed that this blocking group was glucose, which is added non-enzymatically and then undergoes an Amadori rearrangement to form a stable ketoamine linkage to the valine residue. The aldimine intermediate is often referred to as labile HbA_{1c} and the rate of its reaction to the ketoamine is some 60 times slower than the reverse reaction to glucose and haemoglobin. It is an indicator of glycaemia from the preceding 6–12 weeks, in comparison to advanced glycation, which reflects a process that can occur over a longer period of time. Haemoglobin glycated at other positions on the polypeptide subunit is

referred to as non–A_{1c} glycohaemoglobin or glycated haemoglobin. In the case of non–A_{1c} haemoglobin the glucose is linked to an ε–amino group or lysine residues in the α or β chains. The A_{1c} and the non-A_{1c} configurations together constitute the total glycohaemoglobin and their formation is increased in diabetic patients with ambient hyperglycaemia. The normal range of HbA_{1c} is 4%-6% of total haemoglobin.

Many methods are available to measure glycohaemoglobin species. In general these fall into two categories; tests such as ion exchange chromatography and electrophoresis, that rely on charge differences to separate the glucose–modified from the unmodified haemoglobin; and tests such as affinity chromatography, immunoassay and colorimetric procedures that exploit the presence of carbohydrate to distinguish glycohaemoglobin from non–glycated haemoglobin species. Each different test has its advantages and disadvantages and the costs are different per test. There is a reasonable correlation of values between methods but each laboratory should establish and stipulate the non-diabetic reference range for the method it has selected. It is worth noting that when the glycohaemoglobin is high, a change of 1% may reflect greater changes in glycaemia (in mg/dL) than it does in the lower ranges of glycohaemoglobin values.

Ion exchange chromatography is the most commonly employed method for the measurement of HbA_{1c}. This method relies on the change in charge of the haemoglobin molecules conferred by N–terminal modification with glucose. Haemoglobins glycated at the amino terminus of the β–chains elute from the cation-exchange resin ahead of the main HbA_0 peak, and are named according to the elution order as HbA_{1a}, HbA_{1b} and HbA_{1c}. Haemoglobin glycated at other sites than the β–chain amino terminus elute in the leading edge of the main HbA_0 peak. This portion may represent some 50% of the total glycated haemoglobin and may be measured by glycation specific methods such as the TBA method, or by boronate affinity chromatography.

4.4.2.2 The Chemistry and Measurement of Non-Enzymatically Glycated Serum Proteins

Albumin and other serum proteins may be non-enzymatically glycated *in vitro* and *in vivo*. Chromatographic and colormetric measurement of these non-enzymatically glycated proteins shows that levels are approximately two to three times higher in diabetic than non-diabetic subjects. Because serum and plasma proteins have shorter half-lives than haemoglobin, glycated proteins are altered more rapidly than glycated haemoglobin in response to prolonged decreases or increases in blood glucose levels.

There are several techniques for demonstrating the presence and extent of glycation of serum proteins. Serum albumin can be separated chromatographically into glycated and non-glycated fractions, by application onto a carboxymethylcellulose column and elution with sodium acetate. The main drawback of this procedure is that it is laborious and time–consuming, involving chromatography on several columns and using multiple buffers. This inevitably limits its clinical application.

An alternative approach is to measure directly the amount of adducted glucose. This is achieved by the weak acid hydrolysis of the haemoglobin resulting in the release of HMF, which can be quantitated by a colour reaction with TBA. A similar technique has been applied to albumin, resulting in a strongly positive test with the glycated and not the non–glycated albumin. This method has a strong correlation with the chromatographic technique. The necessity to purify and then concentrate albumin also makes this technique laborious for routine clinic work.

4.4.3 Method for the Measurement of HbA1c and Glycated Plasma Proteins used in this Study

4.4.3.1 Low Pressure Cation Exchange Chromatography for the Measurement of HbA1c

The Hb-GOLD analyser and associated reagent kit (Drew Scientific Ltd, Cumdria, UK) is an automated instrument intended for *in vitro* estimation of human glycated haemoglobin fractions. The reagent kit is capable of a range of assays including routine measurement of HbA1c in whole blood in the care of diabetes.

The Hb-GOLD analyser uses low pressure cation exchange chromatography in conjunction with gradient elution to separate human haemoglobin subtypes and variants from haemolysed blood. The separated haemoglobin fractions are monitored by means of absorption of light at 415nm. The chromatogram obtained is recorded and a software program performs the analysis of the chromatogram and generates a results report. This method of HbA1c measurement was used for this study. Samples were sent to the haematology department at the Whittington Hospital for analysis (Table 4.8).

Table 4.9. Ranges used for HbA1c levels using the Hb-GOLD analyser

Haematology Normal Ranges		
Non Diabetic		3.6 - 6.0
Diabetic	Well controlled	<7.0
	Average Control	7.0 - 10.0
	Poor Control	>10.0

4.4.3.2 The Measurement of Glycated Serum Proteins using HPLC

4.4.3.2.1 Extraction of Plasma Proteins

Venous blood (5 ml) was collected in heparinised tubes and immediately centrifuged for 10 min at +4°C and 3000 rpm to allow for the serum to separate. Unless immediately analysed, the serum samples were stored at -70°C. An aliquot of serum (0.25 ml) was placed in a vial in ice. Trichloracetic acid (2.25 ml, 6%w/v), that had been allowed to cool in ice for 15mins, was added to the sample and allowed to sit in the ice for 5min. A light yellow precipitate was formed as the trichloracetic acid was added. The mixture was centrifuged for 15min at +4°C and 3000rpm, allowing the protein pellet to settle at the bottom of the vial.

4.4.3.2.2 Acid Hydrolysis of Plasma Proteins

The protein pellet was placed in a glass vial and HCl (200 µl, 6 M) was added. The vials were flushed with nitrogen gas for 5 min and sealed with Teflon® lined lids. The sample was then heated at 110°C for 24 h. Once the hydrolysis was complete dH20 (4 ml) was added to the sample, mixed thoroughly and passed through a syringe filter (0.2 µm, Millipore). The sample was lyophilised over night and then reconstituted in 0.1% TFA (aq) to a concentration of 1 mg/ml protein content in preparation for injection into the HPLC system for the detection of furosine and pentosidine. The HPLC conditions were the same as those used for the detection of furosine and pentosidine in keratin extract hydrolysates in section 4.2.3.2.

4.5 Statistical Analysis of Data Collected from Non-Diabetic Keratin Extracts and Serum Proteins

This section concentrates on the data collected from the non-diabetic group. A full explanation of the recruitment of patients is described in detail in Chapter 9, along with the comparison of data between the diabetic and non-diabetic groups.

4.5.1 Distribution of the Ages

Table 4.10. Information regarding non-diabetic subjects.

Total Number	Mean Age [yrs]	Number of Males	Mean Age of Males [yrs]	Age Range of Males [yrs]	Number of Females	Mean Age of Females [yrs]	Age Range of Females [yrs]
87	57.0±10.9	38	55.6 ± 6.8	43 - 69	49	58.1 ± 13.1	35 - 81

Fig. 4.23 illustrates the distribution of the age data. A histogram and Q-Q plot of the different ages confirms a normal distribution. The distributions of the furosine and pentosidine data collected from keratin extracts and serum of non-diabetic individuals were all skewed, therefore non-parametric statistical tests were used (see Appendix IX for distribution plots).

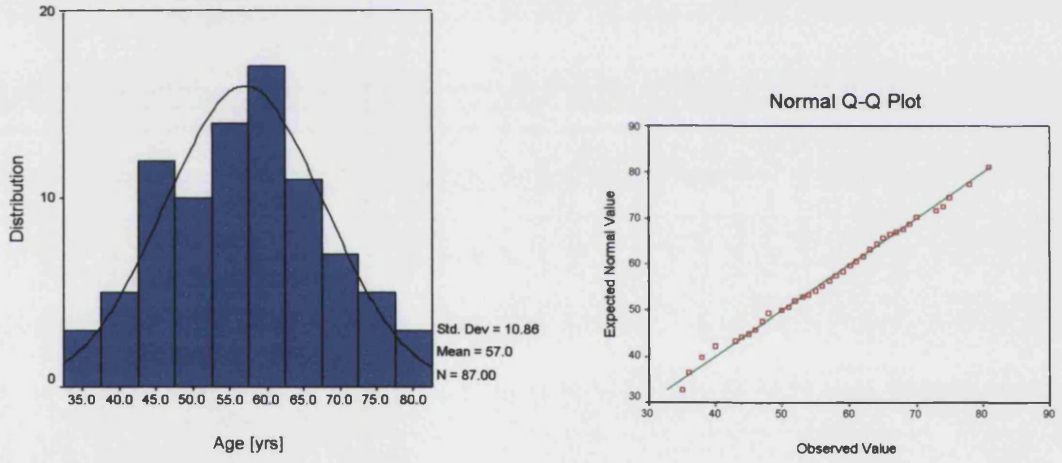

Figure 4.23. Histogram and Q-Q plot illustrating the distribution of ages in a group of 87 non-diabetic subjects

4.5.2 Data Analysis

Samples of callus and venous blood were collected at the same time from all the volunteers so that a comparison of the furosine and the pentosidine content from both types of proteins could be made. As the process of glycation, and the accumulation of AGEs increases with age in many human tissues, a comparison of the quantities of glycated keratin adducts with age was conducted.

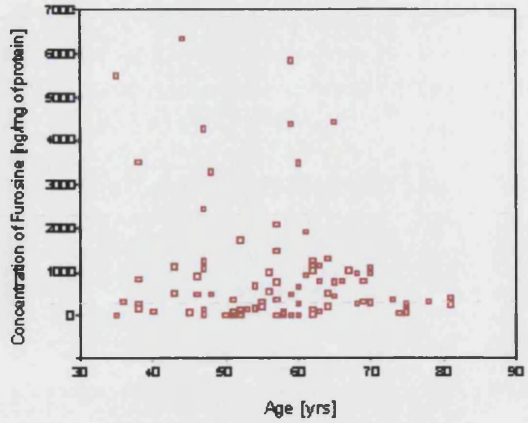

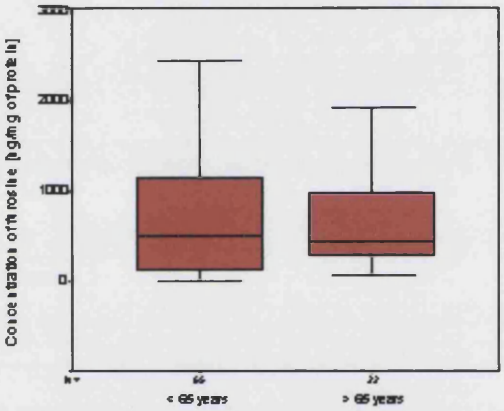

Spearman Correlation
r=-0.193

Age group <65 years n=67
Median: 495.5 ng/mg of protein.
Interquartile range: 1114.6 ng/mg of protein.
Minimum: 0. ng/mg of protein
Maximum: 6331.6 ng/mg of protein

Age group ≥65 years n=20
Median: 376.1 ng/mg of protein.
Interquartile range: 660.2 ng/mg of protein.
Minimum: 0.0 ng/mg of protein
Maximum: 4443.0 ng/mg of protein

Mann-Whitney Test
p=0.888

Figure 4.24. The relationship between age and furosine measured in plantar keratin extracts.

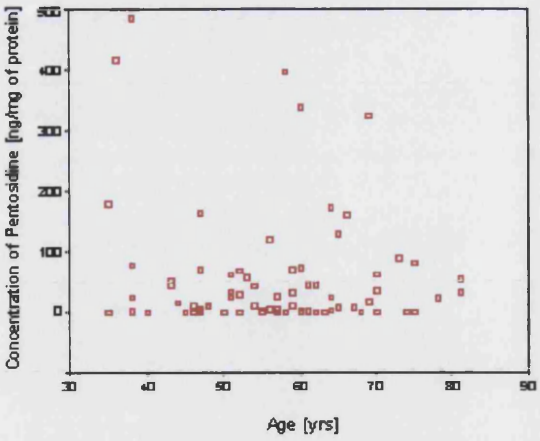

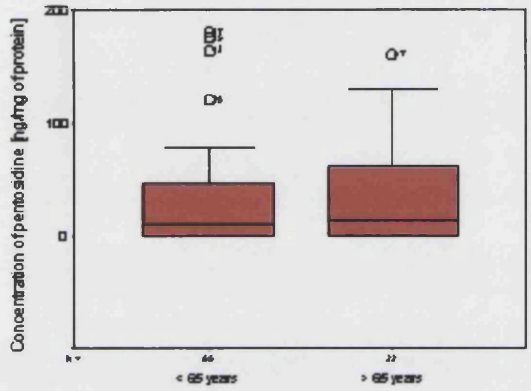

Spearman's Correlation
r=-0.143

Age group <65 years n=67
Median: 8.8 ng/mg of protein.
Interquartile range: 45.9 ng/mg of protein.
Minimum: 0.0 ng/mg of protein
Maximum: 485.4 ng/mg of protein

Age group ≥65 years n=20
Median: 20.5 ng/mg of protein.
Interquartile range: 76.7 ng/mg of protein.
Minimum: 0.0 ng/mg of protein
Maximum: 324.4 ng/mg of protein

Mann-Whitney Test
p=0.416

Figure 4.25. The relationship between age and pentosidine measured in plantar keratin extracts.

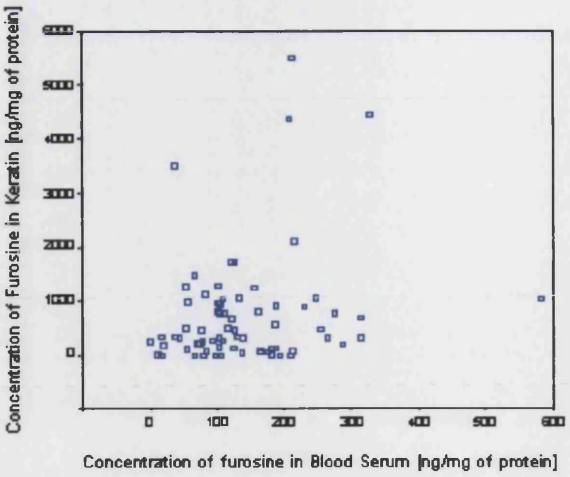

Spearman's Correlation
r=0.084

Furosine in Keratin Extracts
Median: 471.1 ng/mg of protein
Interquartile range: 903.1 ng/mg of protein
Minimum: 0.0 ng/mg of protein
Maximum: 6331.6 ng/mg of protein

Furosine in Blood Serum
Median: 122.7 ng/mg of protein
Interquartile range: 110.2 ng/mg of protein
Minimum: 0.0 ng/mg of protein
Maximum: 580.5 ng/mg of protein

Mann-Whitney Test
p=0.001

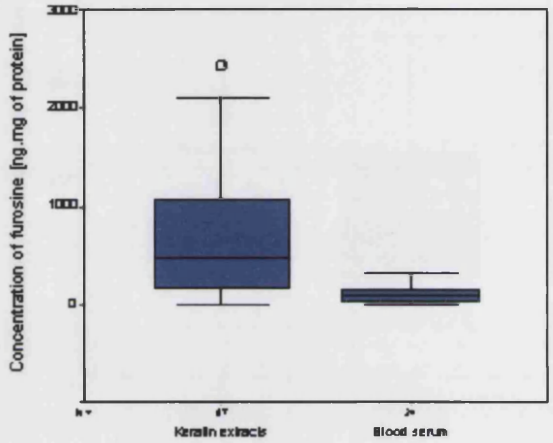

Figure 4.26. The relationship between the concentration of furosine in keratin extracts and serum proteins.

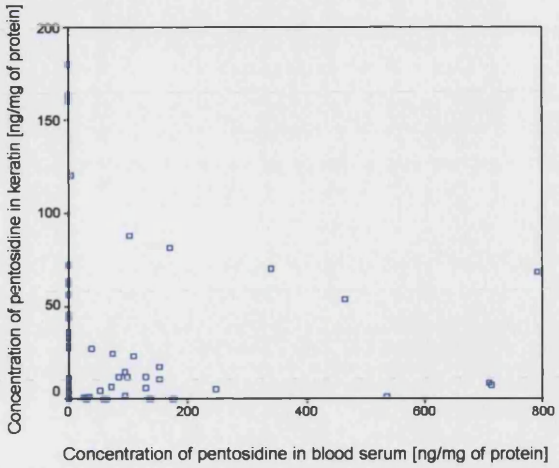

Spearman's Correlation
r=0.136

Pentosidine in Keratin Extracts
Median: 10.5 ng/mg of protein
Interquartile range: 54.1 ng/mg of protein
Minimum: 0.0 ng/mg of protein
Maximum: 485.4 ng/mg of protein

Pentosidine in Blood Serum
Median: 25.6 ng/mg of protein
Interquartile range: 134.5 ng/mg of protein
Minimum: 0.0 ng/mg of protein
Maximum: 1569.4 ng/mg of protein

Mann-Whitney Test
p=0.437

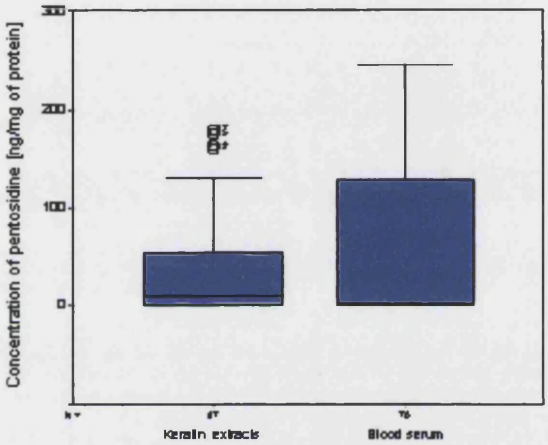

Figure 4.27. The relationship between the concentration of pentosidine in keratin extracts and serum proteins.

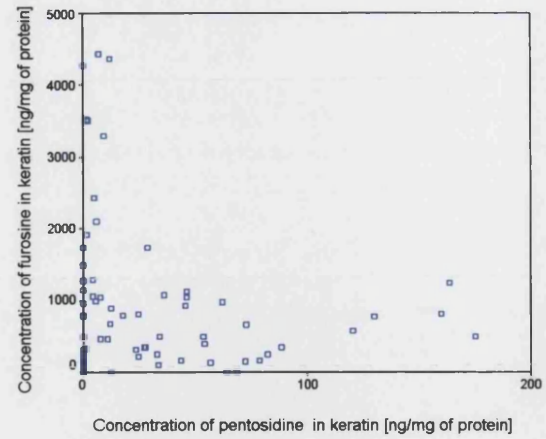

Spearman's Correlation
r=0.112

Furosine in Keratin Extracts
Median: 471.2 ng/mg of protein
Interquartile range: 903.1 ng/mg of protein
Minimum: 0.0 ng/mg of protein
Maximum: 6331.6 ng/mg of protein

Pensosidine in Keratin Extracts
Median: 10.6 ng/mg of protein
Interquartile range: 54.1 ng/mg of protein
Minimum: 0.0 ng/mg of protein
Maximum: 485.4 ng/mg of protein

Mann-Whitney Test
p=0.001

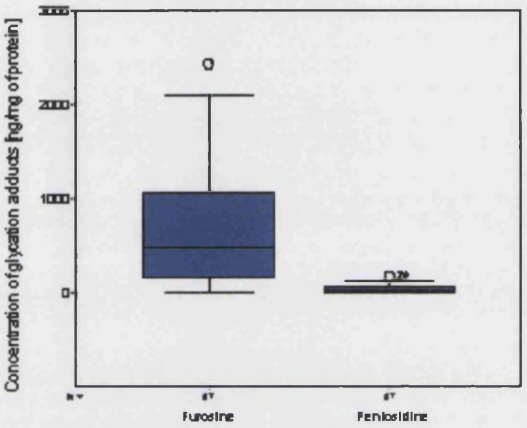

Figure 4.28. The relationship between the concentration of furosine and pentosidine in keratin extracts.

4.5.4 Discussion

The first point of discussion is the measurement of the amount of glycation adducts present in the plantar callus protein extracts. The HPLC methods of detection of both furosine and pentosidine in this study have been specific, sensitive and reproducible. Several research groups [162;163;191] have demonstrated the HPLC quantitative analysis furosine in plantar callus tissue. In these studies the quantity of furosine was expressed as a percentage of the tyrosine present in the acid hydrolysates, therefore a comparison between this data and previous studies was not possible. The measurement of pentosidine had to be in the same units as the furosine, but tyrosine was not visible on the fluorescence chromatograms of the pentosidine assays. Therefore, the

concentrations of the glycation adducts were expressed as ng/mg of protein, using external standard curves. As the assays were carried out over a prolonged period of time, quality control measures were put into place to ensure that the standard curves did not deviate from assay to assay. The assays for furosine and pentosidine in these series of experiments were accurate and reproducible.

The second point was the relationship between furosine and pentosidine in the keratin extracts, and the age of the subjects. There was no correlation between furosine ($r=0.21$) and pentosidine ($r=0.04$) in keratin and the ages of the subjects. Although the median and range of furosine and pentosidine concentrations was higher in the older age group than that of the younger group, the difference between the groups was not statistically significant (furosine: $p=0.888$, $n=87$, pentosidine: $p=0.416$, $n=87$).

The relationship between the glycation adducts in keratin and in the blood serum from the same subjects was tested. There was no correlation between furosine and pentosidine in keratin extracts and furosine and pentosidine measured in blood serum (furosine: $r=0.084$, pentosidine $r=0.136$). There is a wider interquartile range of concentration readings for furosine in keratin extracts (903.1 ng/mg of protein) than the concentration found in the blood serum samples (110.2 ng/mg of protein). The opposite was the case for the pentosidine in keratin (54.1 ng/mg of protein) and in the blood serum (134.5 ng/mg of protein).

There was no correlation between the HbA1c levels and furosine ($r=0.145$) and pentosidine ($r=-0.105$) in the keratin extracts.

5.0 Chapter 5 - The Detection of CML using GC-MS.

5.1 Methods of Measuring CML

The two main methods of detection of CML (UV inactive) are GC-MS [117;118;188] and HPLC, after derivatisation with *o*-phthaldialdehyde (OPA) [202]. These methods have their advantages, but GC-MS is the most common technique used for CML detection

5.1.1 Carboxymethyllysine Assay by HPLC with Post-Column Detection

Post-column detection of CML using OPA involves a sequential dual column system or a single column system [196]. Samples are injected into a C-18 reverse-phase column and the fractions containing CML are collected, dried and reinjected into a different C-18 column for clear CML detection. Although the method is very sensitive, it is time consuming and the high sensitivity of the procedure makes it prone to interference by contaminants.

5.1.2 GC-MS Assay for the Detection of CML

Gas chromatography-mass spectroscopy is a technique often used for the detection of CML and furosine in protein hydrolysates. It comprises of two techniques: gas chromatography (used to separate the components of a mixture of compounds) and mass spectroscopy (used to characterise each individual component). The principle of GC-MS is based on the production and analysis of ions formed from neutral compounds, a process known as fragmentation. The resulting spectra present the masses of each ion in the form of a mass: charge ratio (*m/z*), therefore giving information about the mass of the ion, although not its exact structure. The advantage of the MS system is that only a trace amount (a few nanograms) of test sample is required for successful identification, however, the sample is not recoverable.

In order for a compound to be suitable for GC-MS analysis it must be volatile to allow for breakdown and rearrangement in the gaseous state. Proteins and peptides need to be reacted with compounds that render them more volatile prior to GC-MS analysis. In the case of CML, this process of derivatisation conventionally involves acylation at the unprotected N-terminus and esterification of the carboxylic acid functional groups (Fig. 5.1).

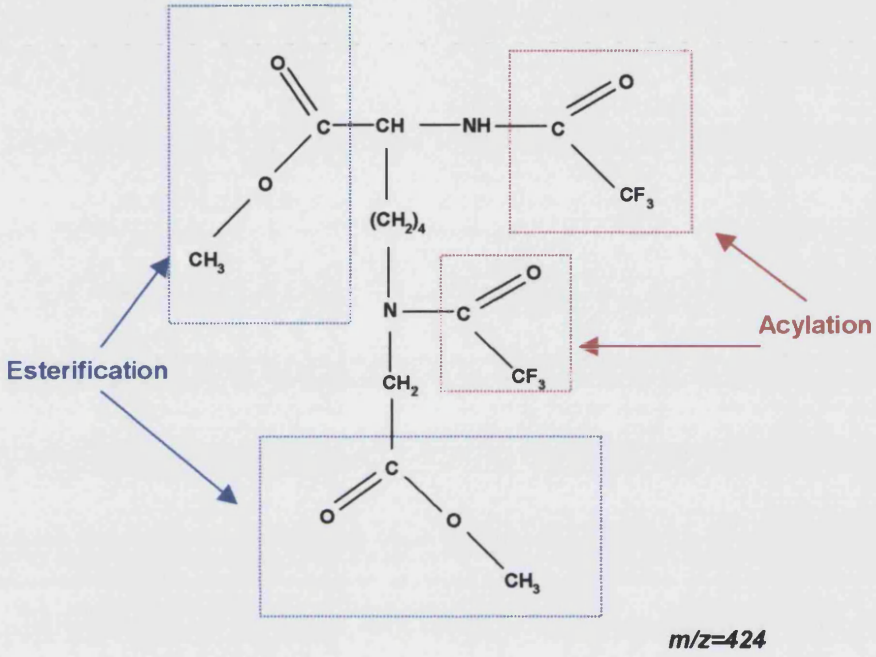

Figure 5.1: The chemical structure of CML after esterification by methanolic acid and acylation by trifluoracetic acid (TFAA)

5.1.3 Summary

Before the test samples of plantar epidermal keratins were analysed for CML content, a series of experiments were carried out to test the GC-MS method of analysis for efficiency using a pure synthetic CML standard. The suitability of the derivatisation procedure was also tested, with regards to the acylation procedure and the use of a suitable injection solvent was also investigated.

5.2 Carboxymethyllysine as a GC-MS Analyte

5.2.1 Aims

- To validate the sample derivatisation procedure prior to GC-MS.
- To detect CML from acid and enzyme hydrolysates using GC-MS.
- To quantify the presence of CML in plantar epidermal keratins.

5.2.2 Reagents

Methanolic acid (0.5 M), dichloromethane, TFAA, methanol, lysine, CML (synthesised in Chapter 3).

5.2.3 Experiment 1 – GC-MS Spectrum of Pure CML

5.2.3.1 Aims

- To produce a mass spectrum of pure synthetic CML that compares to spectra in previous literature.

5.2.3.2 Methods

Pure CML (1 mg) was placed in a glass vial and methanolic acid (0.5 ml, 0.5 M) was added and heated for 1 h at 70°C. The acid was removed by rotary evaporation and dichloromethane (0.5 ml) was added and mixed. Trifluoracetic anhydride (1 ml) was added to the solution and mixed and the reaction mixture was allowed to stand at room temperature for 1 h. All solvent was removed under rotary evaporation, until the sample was dry. The samples were dissolved in 100 µl of dichloromethane, mixed thoroughly and 1 µl of the solution was injected into the GC-MS system (see Appendix VI for the GC-MS equipment conditions). Different concentrations of the derivatised CML were injected into the system, until a clear, peak was achieved.

5.2.3.3 Results

The chromatogram for pure CML had one major peak at the retention time of ~34 min (Fig. 5.2). The mass spectrum of this peak (Fig. 5.3) compares well to the spectra seen in previous literature in this field (Fig 5.4). The ion *m/z* 392 confirmed the detection of CML. This *m/z* value was chosen because it provides good reproducibility and sensitivity [117], although the molecular ion for CML is *m/z* 424 (Fig. 5.1).

There were two additional small peaks noted at the paling end of the main CML peak (Fig. 5.2). These peaks suggest that a small portion of the CML has a slightly different stereochemistry. In view of these results, the CML spectrum was compared with a spectrum of lysine in the next experiment.

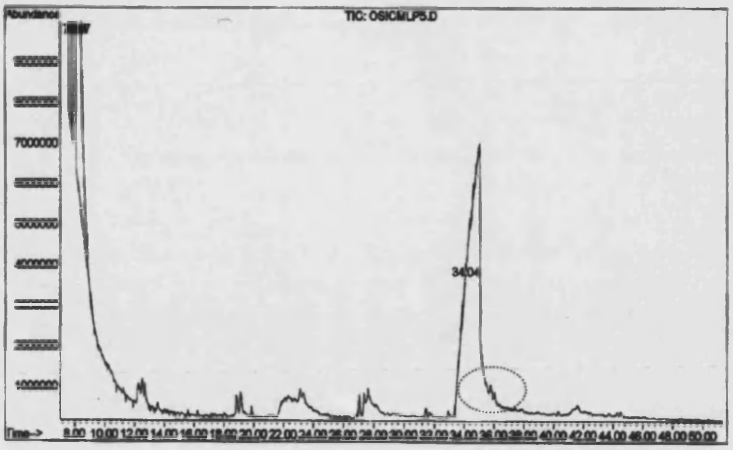

Figure 5.2. Chromatogram of synthesised CML

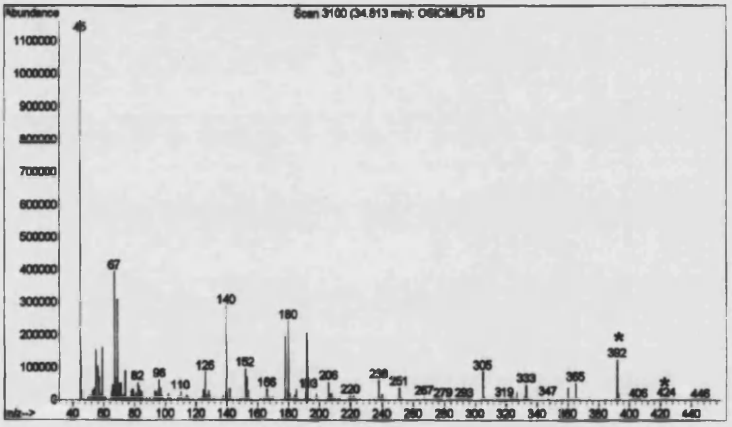

Figure 5.3. Mass spectrum at 34 min of synthesised CML

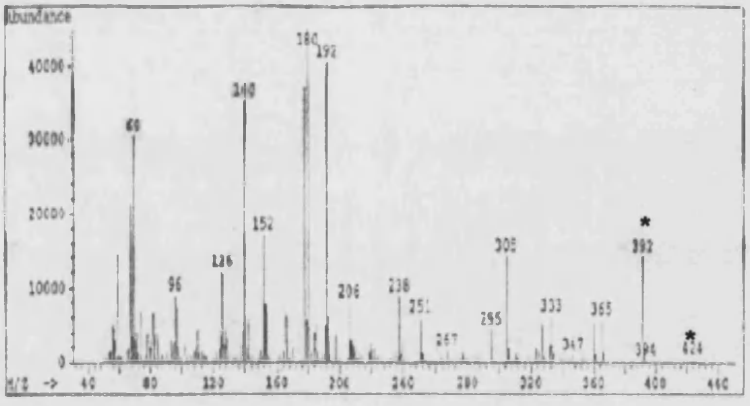

Figure 5.4. Mass spectrum of synthesised CML taken from reference [203]

5.2.4 Experiment 2 – A Comparison of Lysine and Synthetic CML Mass Spectra

5.2.4.1 Aims

- To assess whether there are fragments that are common to both lysine and CML.
- To differentiate between lysine and CML spectra.

5.2.4.2 Methods

The amino acid lysine and pure CML were derivatised according to the protocol described in section 5.2.3.2 and injected into the mass spectrometer.

5.2.4.3 Results

The ion *m/z* 320 is used to identify lysine [117]. There are fragments that are common to both lysine and CML spectra: *m/z* 126, 180, 251, and 293 (Figs. 5.6-5.8). These fragments are common to lysine and lysine based compounds. The chromatogram of lysine had a major peak at 22 min with 2 minor peaks at the paling end of the peak (Fig. 5.5). This was similar to the CML chromatogram, suggesting that the stereochemical changes observed in CML originates from lysine at an early stage of synthesis, and probably not as a result of deterioration of CML with time. This concept was tested in the next experiment.

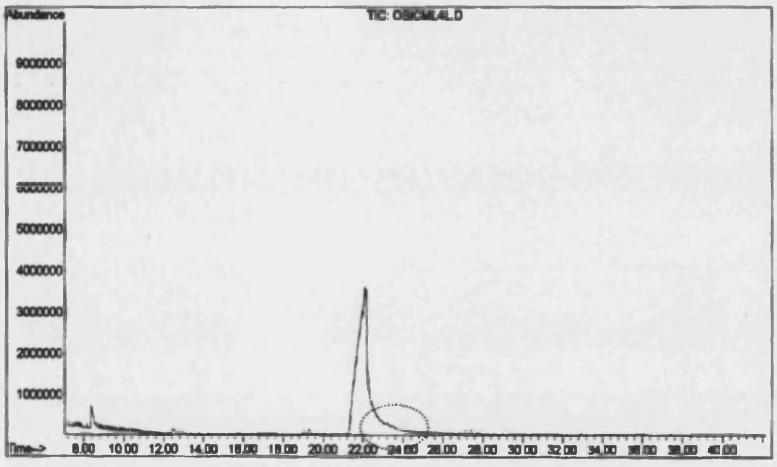

Figure 5.5. Chromatogram of lysine

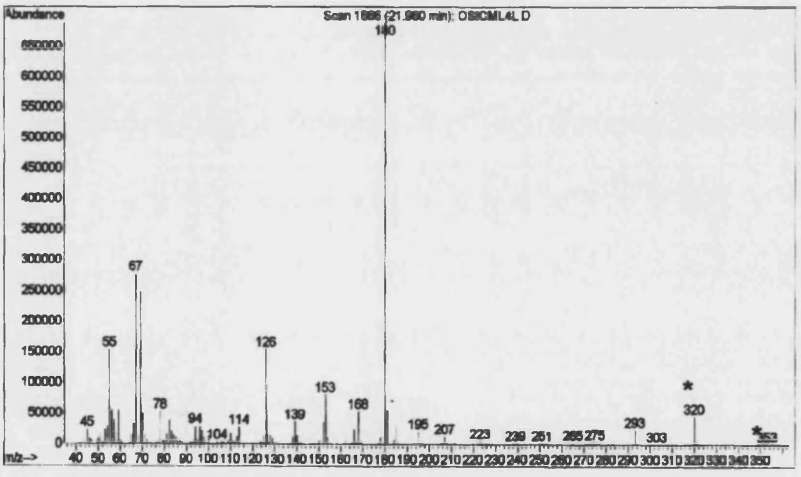

Figure 5.6: Mass spectrum of lysine at 22 min

5.2.4.4 Fragmentation Patterns of CML and Lysine

The fragments used to identify CML and lysine are illustrated in Figs. 5.7 and 5.8, respectively.

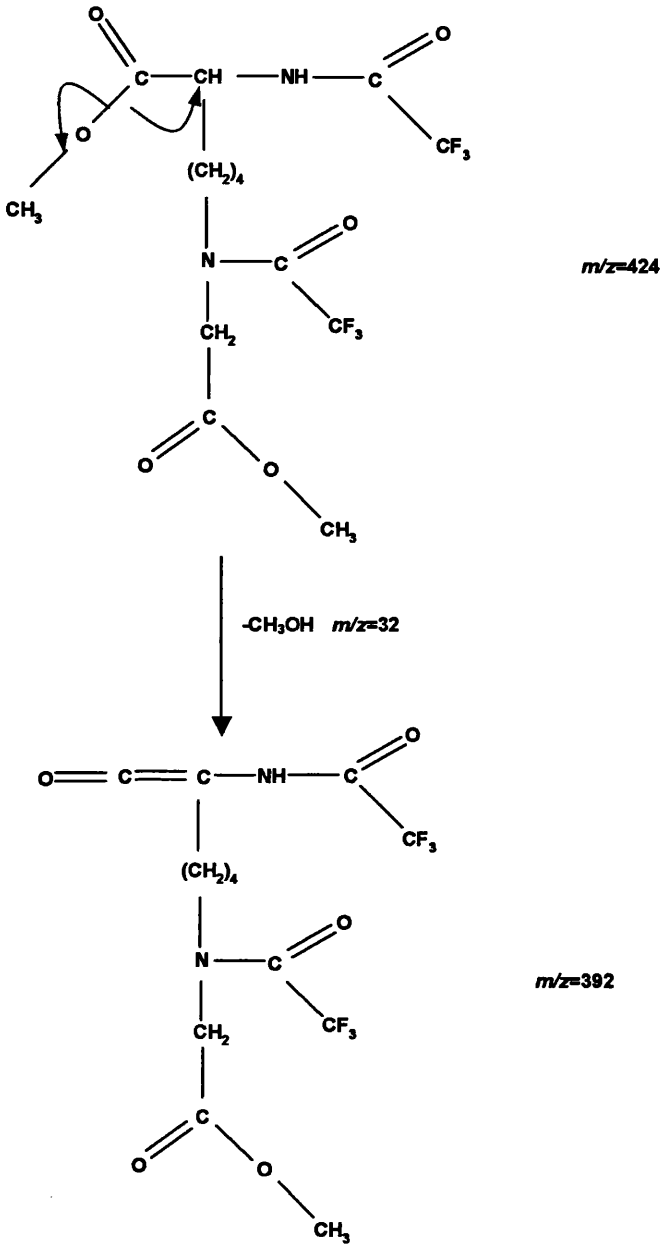

Figure 5.7. Main fragments of CML

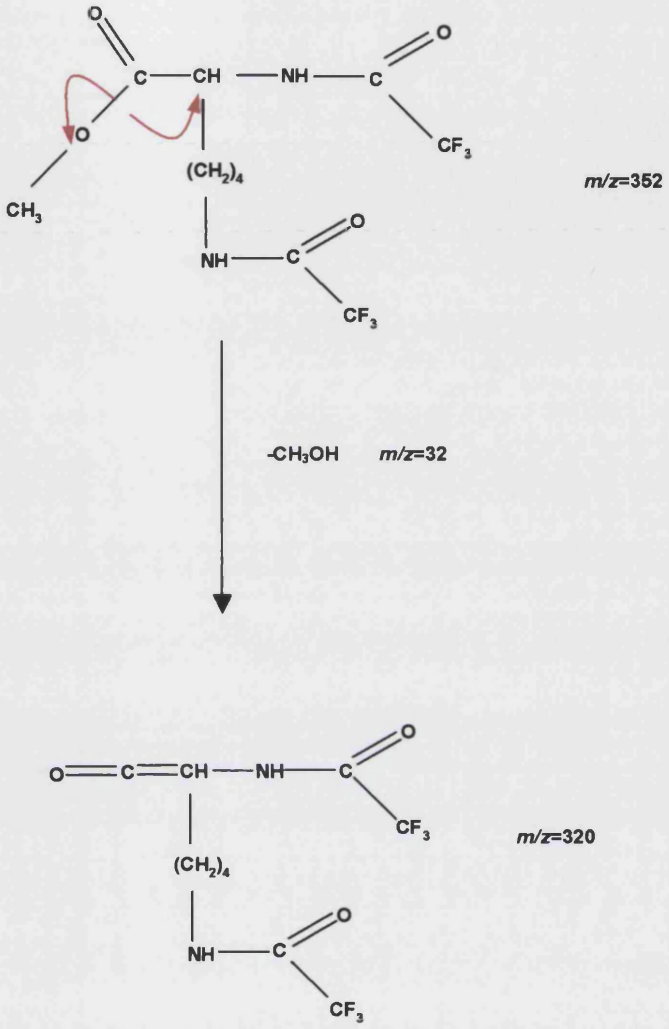

Figure 5.8. Main fragments of lysine

5.2.5 Experiment 3 – The Stability of Synthetic CML

5.2.5.1 Aims

- To assess whether CML deteriorates with time.
- To assess whether CML deteriorates during the acid hydrolysis procedure

5.2.5.2 Methods

A sample of CML was derivatised according to the protocol described in section 5.2.3.2 and injected into the GC-MS system. The sample was stored in methanol at +4°C and after a period of 2 months was rederivatised and injected into the system. The mass spectrum was compared to that of the fresh CML sample.

A known amount of CML (40 µg) was added to a known amount of keratin extract (1 mg). Another vial containing pure CML alone (40 µg) was prepared. Both mixtures were then hydrolysed in HCl (200 µl, 6M) under nitrogen for 18 h at 110°C and the resulting hydrolysates were lyophilised to dryness. The hydrolysates were derivatised and injected into the system according to the protocol.

5.2.5.3 Results

The chromatograms of fresh CML and 2 month old CML were identical.

The chromatograms of CML alone and CML plus keratin were also identical. This confirms that CML is relatively stable with time and is not damaged during acid hydrolysis.

5.2.6 Experiment 4 – Testing the Efficiency of Acylation as part of the Derivatisation Procedure

5.2.6.1 Aims

- To identify the optimal incubation time for the acylation procedure using TFAA.

5.2.6.2 Methods

Three aliquots of keratin hydrolysate (0.3 mg) were incubated with TFAA for 20, 40 and 60 min, respectively. The remainder of the derivatisation procedure was carried out as previously described and injected into the GC-MS system. CML was isolated from the spectra and the abundance of the key fragments were compared.

5.2.6.3 Results

The abundance of the CML fragments increased as the incubation time increased (Fig. 5.9). The 60 min incubation time for the acylation procedure produced chromatograms with the greatest abundance of CML fragments. This agrees with the incubation times used by Dunn *et al* (1989) [117].

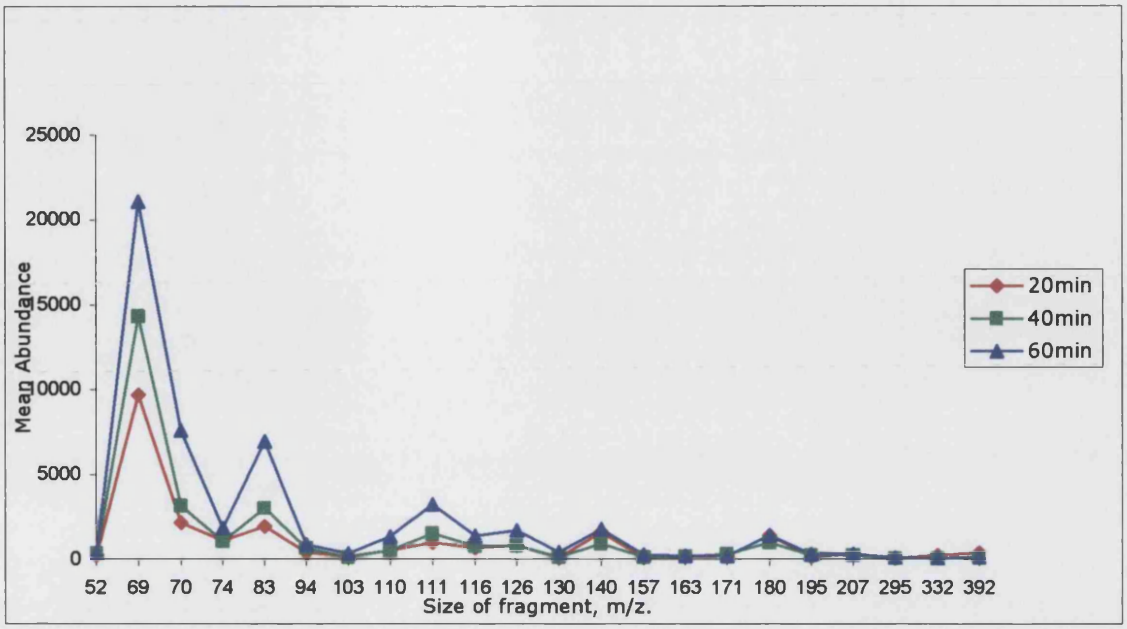

Figure 5.9. The abundance of CML fragments following different incubation times with TFAA

5.2.7 Experiment 5 – Testing the Suitability of the Solvent used for Injection into the GC-MS System

5.2.7.1 Aims

- To compare the effect of two different injection solvents on the quality of the mass spectra of CML.

5.2.7.2 Methods

Two separate samples of CML were derivatised according to the existing protocol. One sample was dissolved in dichloromethane and another in a mixture of methanol and dichloromethane (ratio-1:2) prior to injection into the system.

5.2.7.3 Results

The two spectra were different from each other (Figs. 5.10–5.11). The peak obtained from the dichloromethane injection solvent was a sharp, well-resolved

peak (RT=33.7 min), akin to spectra observed in the previous experiments. The mixture of methanol and dichloromethane produced a poor CML peak, with an additional peak at 43.1 min. The peak was considerably smaller, than that produced when dichloromethane alone was used, suggesting poor delivery of the test compound and possible destruction of CML. The peak is relatively broad, with the methanol solvent, indicating that methanol is a slower carrier of CML than dichloromethane. It is clear from looking at the quality of the chromatograms, that dichloromethane was a suitable delivery solvent for the analysis of CML.

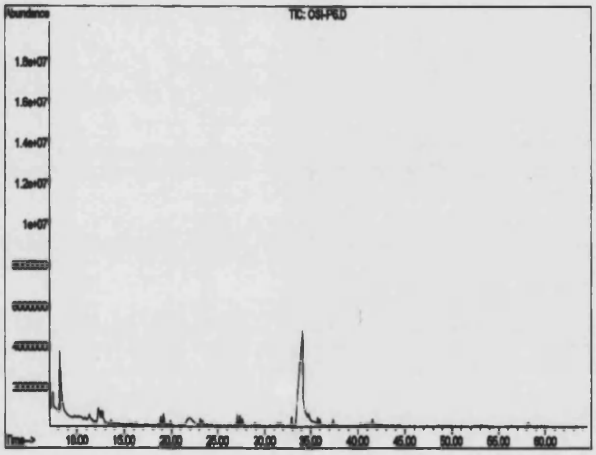

Figure 5.10. Chromatogram of CML injected with dichloromethane

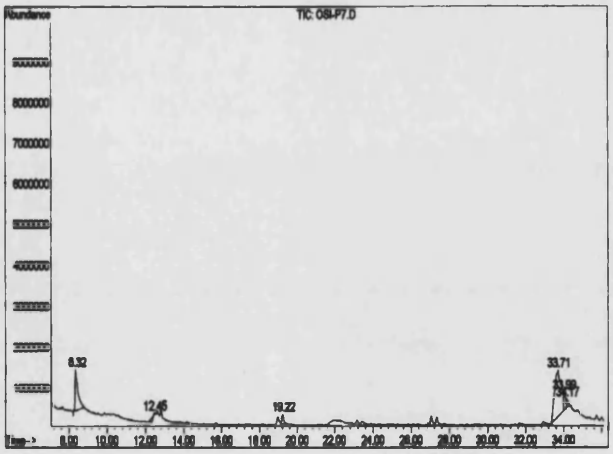

Figure 5.11: Chromatogram of CML injected with dichloromethane:methanol (2:1)

5.3 Detection of CML in Human Plantar Epidermal Keratin Hydrolysates

5.3.1 Aims

- To detect the presence of CML in diabetic and non-diabetic plantar epidermal keratin samples.
- To investigate whether the conditions of hydrolysis influence the detection of CML within keratin samples.

5.3.2 The Detection of CML in Acid Hydrolysates of Callus and Keratin Extracts

5.3.2.1 Aims

- To assess if there is a difference in the detection of CML between callus tissue and keratin extracts.

5.3.2.2 Methods

A set of 6 diabetic and 6 non-diabetic callus and keratin extracts was selected randomly from 100 samples. Equal amounts of the samples (callus-5 mg, keratin-0.2 mg) were hydrolysed in acid as described in Chapter 4. Hydrolysis was carried out in the presence of sodium borohydride solution, to prevent the formation of artifactual CML, and derivatised according to the protocol, prior to injection into the GC-MS system. An aliquot of pure CML standard was also injected into the system to obtain a reference retention time for CML. The investigator was not told what the samples were to prevent any bias.

5.3.2.3 Results

The retention time for the standard CML was approximately 32 min. All the samples showed no trace of CML. The same results were also produced when the samples were hydrolysed without borohydride reduction.

These results suggest that the GC-MS method is not sensitive enough to detect small amounts of CML in the samples. They also suggest the possibility that acid hydrolysis may destroy any CML present in the samples. However, the acid hydrolysis of the synthetic CML does not have a destructive effect. Therefore, the next step involved the analysis of enzyme hydrolysates.

5.3.3 The Detection of CML in Enzyme Hydrolysates of Extracted Keratins

5.3.3.1 Aims

- To detect the presence of CML in diabetic and non-diabetic keratin samples hydrolysed by enzymes.

5.3.3.2 Methods

Two samples of callus and two of keratin extracts were hydrolysed using enzymes, according to the methods described in Chapter 4 and injected into the GC-MS system. The investigator did not know what the samples were until after all the spectra were collected.

5.3.3.3 Results

All four hydrolysates showed traces of CML, but the chromatograms presented with poor peaks, making quantification difficult (Figs. 5.12-5.15). Although the peaks were not quantifiable, the method could be used for a qualitative investigation of the samples. As the presence of the AGE, CML has never been detected in plantar keratin tissues, it was pertinent to test this. Therefore, 12 keratin samples (6 diabetic and 6 non-diabetic) were hydrolysed using the same procedure and given to another investigator to carry out the GC-MS procedure. CML was not detected in all the samples, even though two of the samples were used earlier on by the first investigator, where CML was detected.

a.

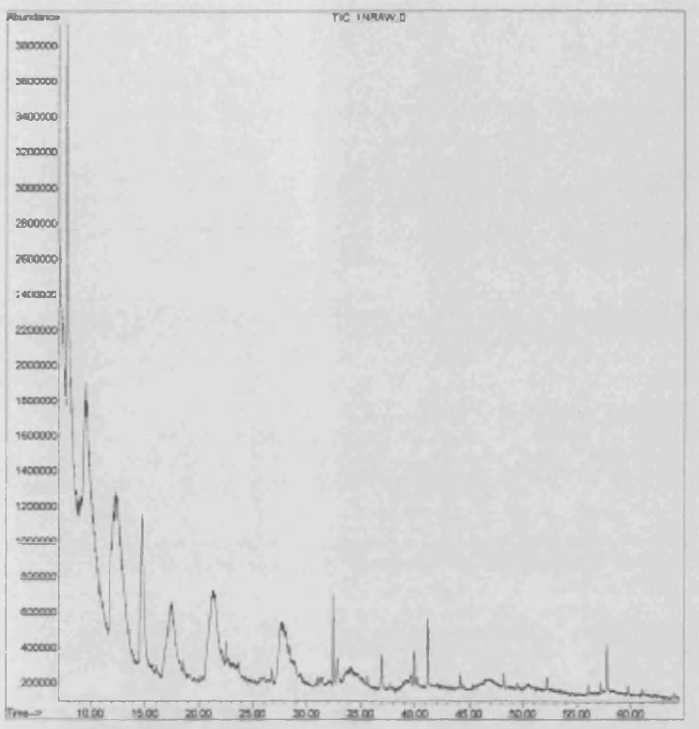

a.

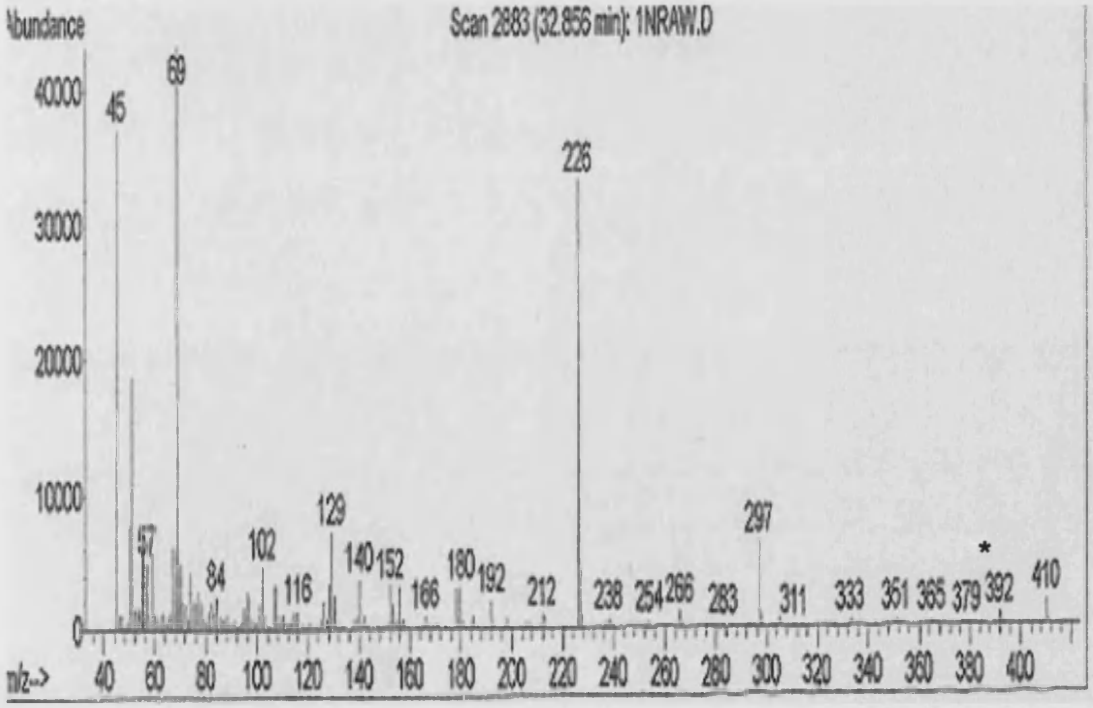

Figure 5.12. a. Chromatogram of an enzyme hydrolysate of non-diabetic callus sample.
b. Mass spectrum of CML peak at ~33 min

a.

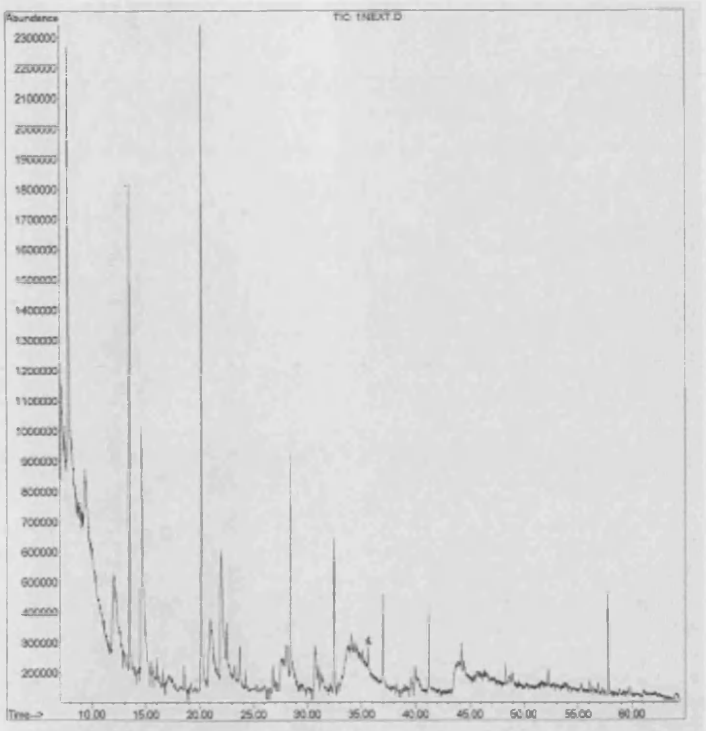

b.

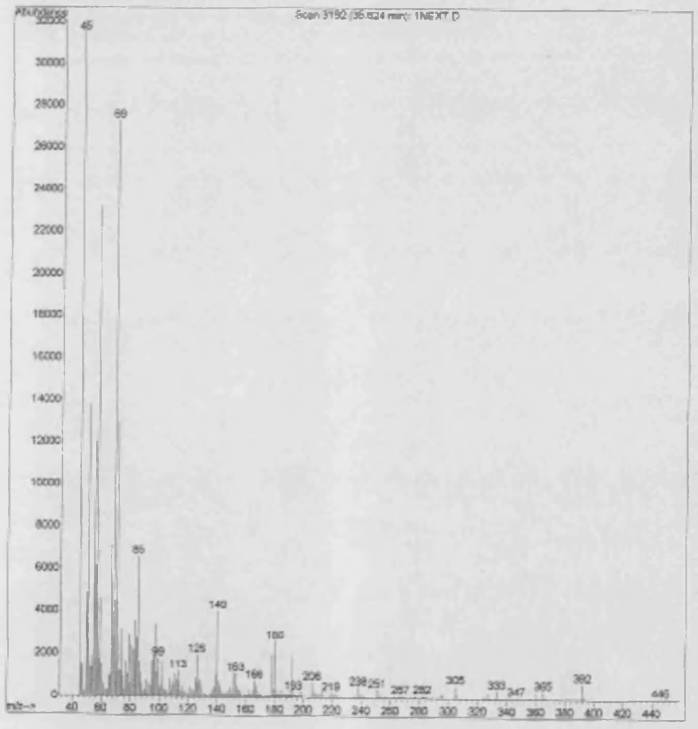

Figure 5.13: a. Chromatogram of an enzyme hydrolysate of non-diabetic keratin extract.
b. Mass spectrum of CML peak at ~34 min

a.

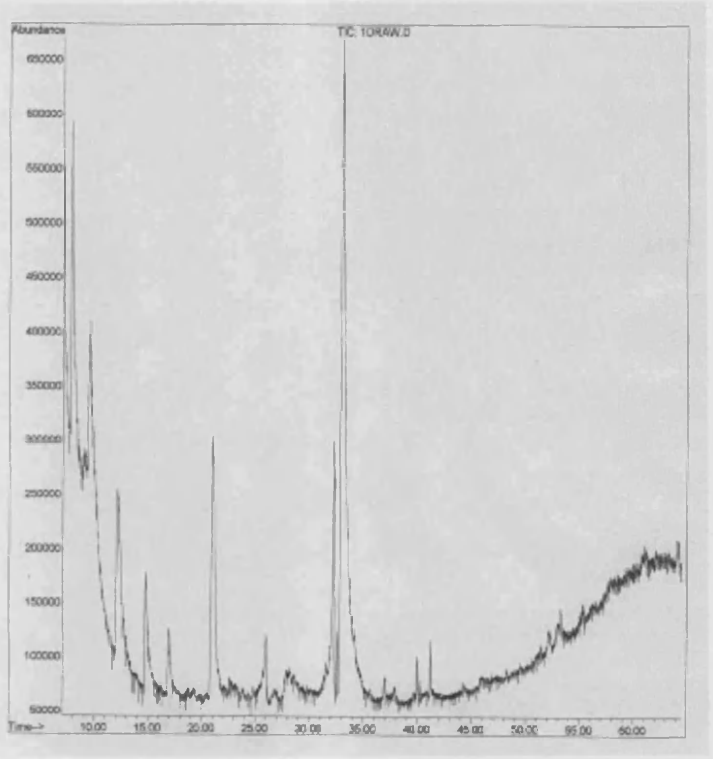

b.

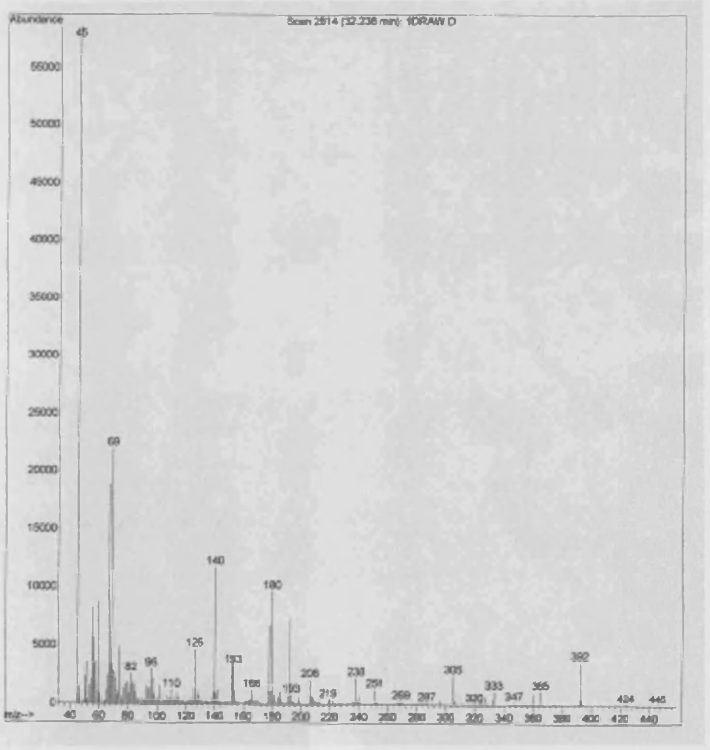

Figure 5.14. a. Chromatogram of an enzyme hydrolysate of a diabetic callus sample.
b. Mass spectrum of CML peak at ~32 min

a.

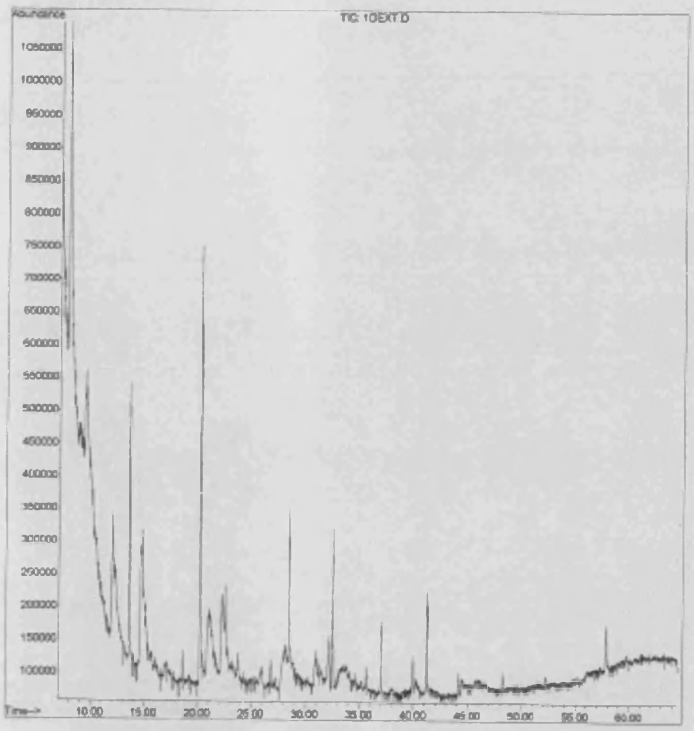

b.

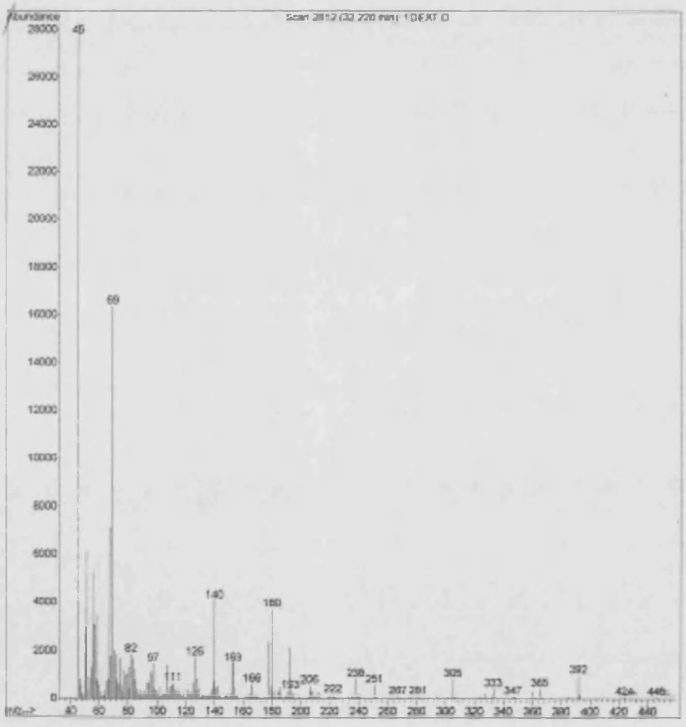

Figure 5.15: a. Chromatogram of an enzyme hydrolysate of a diabetic keratin extract.
b. Mass spectrum of CML peak at ~32min

After prolonged close monitoring of both the investigator conducting the derivatisation and injection procedures, an error could not be identified, although there was no anomaly when both investigators processed synthetic CML. Therefore, although the method was shown to be successful for repeated identification of synthetic CML, it was not sufficient for detecting CML in the test samples, as it was susceptible to inter-investigator error or chemical instability.

5.4 Discussion

The ultimate aim of these series of studies was to develop an efficient and accurate technique for the quantification of CML in plantar epidermal keratin proteins, so that the hypothesis that CML levels are higher in diabetics than non-diabetics could be tested.

The outcomes of these experiments have shown that CML was not reliably detected from hydrolysates of plantar keratin proteins. The method of CML detection was tested and refined using synthetic CML, which concurred with previous work in this area [118] . These results suggest 2 possible outcomes: firstly, there was no CML present in the samples, and secondly, the amount of CML in the tissue samples was too small for detection by this method, i.e. the GC-MS method of detection lacks sensitivity. It would be logical to presume that the former reason is unlikely to be the case, as both furosine and pentosidine were detected in the same samples. Pentosidine and CML are glycoxidation products and therefore it is correct to presume that they both form under oxidative conditions within proteins. However, the origins of these AGEs are different, pentosidine is formed from cross-links between lysine and arginine residues and CML forms by utilising lysine from proteins and lipids. The question of the speed with which these AGEs form is also put forward, especially in epidermal proteins, as the skin has a relatively short turnover time in comparison to other tissues. Therefore, further investigations into the lipid-sugar interactions and general protein kinetics of epidermal tissues are needed.

If, however, CML is present in the samples, the options of using more sensitive methods of detection need to be considered. This study has shown the GC-MS method to be a qualitative one, which has been reflected by other investigators [117;118]. It has been used purely for the detection, not quantification, of CML in blood and collagen and little attention has been paid to the nature of the CML mass spectrum and its fragmentation patterns. This study has been helpful in understanding the spectrum of CML and hence improving our understanding of its structure. A full understanding of the chemistry of the compound is essential before any quantification is attempted. This is still unknown due to its possible heterogeneous nature in tissues. A more specific method would be helpful to identify exact structures.

One method that could prove to be beneficial in this endeavor is selective ion monitoring spectroscopy (SIM-GC/MS). The advantage of this method is that it focuses on a selected target ion and does not monitor the rest of the spectrum, therefore being less time-consuming than GC-MS. The development of this method would also be useful, for the simultaneous detection of furosine and CML.

Recently, there has been a popular shift to the use of competitive ELISA techniques for the detection of CML. The monoclonal antibodies used for these assays produced controversial results, questioning their specificity. This will be discussed in the next chapter.

Chapter 6.0-Production and Characterisation of Antibodies against Furosine and CML

6.1 Introduction

In clinical research, immunological approaches have been used to examine the presence of immunoreactive AGE proteins in human tissues [185;204] such as blood vessels, kidney tissue and skin [134] using antibodies of unknown specificity [185] in the competitive ELISA format [185;205].

Immunoreactive AGEs were first developed by Makita and associates (1992)[185], involving the incubation of a protein (e.g. BSA) with glucose in preparation for immunisation. These anti-AGE antibodies recognised CML as the major determinant [206] as well as other minor epitopes. It has been assumed that the anti-AGE antibodies are equivalent to anti-CML antibodies for most ELISAs, but immunochemical differences emerge *in situ*. The main problem of the design of antibodies to AGE modified proteins is the affinity of the antibody for the AGE-protein versus the affinity of the antibody for the free compound. This is important as, pentosidine and CML present in serum exist as more than 95% bound to circulating albumin, with less than 2% in low molecular weight free forms [207]. The antibodies raised have a high affinity against AGE-protein or CML-protein, but have a 1000-fold lower affinity against free CML. This leads to the false negative result that CML is not the epitope recognised by the antibody [185]. Therefore, this type of antibody is not suitable for the determination of free CML. Schleicher E *et al* (1997) [208] showed a 50-fold loss in affinity for free CML when KLH-CML was used as an immunogen. Also, the serum concentrations of CML determined by ELISA, using the polyclonal antibodies raised, were 50-100 times lower than by HPLC, thus illustrating the problem of standardising ELISAs. In contrast, anti-pentosidine antibodies against hapten-modified protein have a high affinity for the free molecule but a low affinity against the protein modified *in vivo* or during the Maillard reaction *in vitro* due to steric hindrance [209]. Immunoassays using such antibodies can be used when the AGE is released from the protein via acid or enzyme hydrolysis [209].

Immunological approaches have been attempted to determine the major AGE structures expressed *in vivo*. Using AGE-BSA as an antigen, a monoclonal anti-AGE antibody (6D12) and polyclonal anti-AGE antibodies have been raised [210]. Studies examining the immunoreactivity of these antibodies have demonstrated that both antibodies react with AGE samples obtained from proteins, peptides, lysine derivatives, and monoaminocarboxylic acids, suggesting the presence of a common AGE structure(s) in these AGE preparations. Subsequent immunological studies using 6D12 have disclosed the presence of AGE in several tissues and their potential involvement in disease processes [206].

In spite of these immunological studies, the epitope structure recognised by 6D12 is still not known. Determination of the structure is crucial to the uncovering of the chemical structure of AGEs. It is thought that the chemical structure differs from pyrraline and pentosidine since neither of them is recognised by 6D12 [210]. Ikeda *et al* (1996) showed that the epitope of 6D12 is a CML-protein adduct with a carbonyl group important for immunological recognition of AGE proteins. They also detected a major epitope other than the CML-protein adduct.

The development of immunoassays with the ability to quantify accurately AGE levels would be advantageous, primarily because other quantification techniques are time consuming, costly and insensitive. This chapter describes attempts to produce specific antibodies to furosine and CML, concentrating on achieving adequate affinity and a sufficient quantity of the antibodies to make the development of an immunoassay feasible. A number of established strategies were applied in the production of the antibodies to manipulate the hosts' immune response with a view to optimising the antibody production.

6.1.1 The Principles of Antibody Production Techniques

Antibodies are raised by exploiting the B-cell mediated, immune response of a host animal. This response relies on the ability of the host to register the foreign material (immunogen) as non-self and raise antibodies which are complimentary to the molecule of interest and consequently be harvested and purified. The ability of the immunogen to produce a suitable immune response in the host

animal is referred to as immunogenicity. Immunogenicity is defined by the chemical structure of the immunogen.

Antibodies are synthesized by specialised lymphocyte cells (plasma cells), which are in the terminal stage of B-cell differentiation. The production of a strong immune response is governed by the induction and regulation of the differentiation of B-cells into plasma cells. During differentiation, B-cells transform from immature B-cells, that bear cell surface receptors but do not secrete antibodies, to the activated form which secrete antibodies, but have no cellular surface receptors. This process is controlled by the presence of the antigen and the cell-cell communication between the B-cells and the helper T-cells and a number of cytokines.

Immunogens can be naturally occurring or synthetic substances. For an immunogen to be effective, it must have some key features: it must have an epitope recognised by the cell surface receptor on the virgin B-cell; it must have one site that can be recognised simultaneously by a T-cell receptor and it must be degradable

Even with these properties, it is often necessary to encourage the host animal to produce an adequate immune response. This can be achieved through alterations to the dosage and the form of the antigen; the use of adjuvants or the modification of the antigen.

It is essential that the immunogen is pure so as to prevent any inappropriate immune responses. Following initial exposure, there is a primary humoural response against the immunogen. This response is characterised by the presence of predominantly IgM molecules in the serum after approximately 7 days. These rise to a peak concentration at about 12 days after exposure and then diminish. Subsequent booster injections result in the production of predominantly IgG classes of antibody. These form after a short lag phase due to the rearrangement of the B-cell genes. This is referred to as affinity maturation. The subsequent exposures to the immunogen result in an increase in the logarithmic phase of antibody production with expected plateau antibody titre of

some 10-100 times higher, and with an extended decay phase, than by primary immunisation alone.

Failure of an animal to respond to an immunogen may be due to the elimination of the appropriate B and/or T-cell populations during the development of self-tolerance. Consequently, molecules with a high degree of similarity to the host's isoform will be ignored by the immune system.

Animals are usually chosen for immunisation according to the following criteria: how much serum is required; from which species is the antigen isolated from and how much antigen is available.

Antibody production relies on two distinct methods: polyclonal antiserum and monoclonal antibody production.

6.1.2 Polyclonal Antibodies

Polyclonal antisera are routinely used for purification protocols such as ELISA and radioimmunoassay (RIA), where the aim is to capture the antigen.

Polyclonal antibodies are heterogeneous in nature. These antibodies recognise all possible epitopes on the surface of the immunogen. Each antibody group may vary with respect to affinity, titre and avidity (the force of attraction for the whole complement). These antibodies have their advantages, particularly if they are put through procedures that could potentially alter the structure of the antibody. An example of this is the conjugation of the antibody to enzymes or carrier proteins. However, there are disadvantages to this technology such as: the potential for a high degree of cross-reactivity with proteins sharing similar surface epitopes and the potential inter-batch variation in the affinity and specificity of antiserum.

During the production of polyclonal antiserum, animals which show a positive response to the immunogen are maintained in a state of globinaemia by repeated booster injections following the initial immunisation and then bled at suitable intervals to harvest the immunoglobulins. The choice of animal is dependent on a

number of factors including its size, which will influence the amount of serum that can be harvested, and the ease of husbandry. Also, the immunogen used must be sufficiently disparate from the host's endogenous isoform so as to be recognised as non-self and promote an immune response.

6.1.3 Monoclonal Antibody Production

In contrast to polyclonal antibodies, monoclonal antibodies are homogenous in nature and recognise one desired epitope on the target molecule. Fusion of B-cells result in the production of these antibodies and a suitable myeloma cell. These cells are termed hybridomas and they inherit selective characteristics from each of their constituent cell types; immortality from the myeloma cells and the ability to produce the required antibodies from the B-cells. The advantages of adopting this method of antibody production are: the hybridoma cell lines can be frozen and stored to ensure a constant supply of antibodies and the specific epitopic recognition sites of the antibody. Following subcutaneous injection and subsequent boosters, spleens are harvested from the animals that demonstrate a positive response, as determined by tail bleeds.

6.1.3.1 Fusion

Fusion of B–cells obtained from the spleens of immunised animals with constantly dividing, immortal plasmacytoma cell–lines is usually accomplished using polyethylene glycol (PEG). PEG causes the exchange of lipids on adjacent cells and in turn leads to the integrated cell membranes. Choice of plasmacytoma cells from the same species is preferable due to the decreased chromosome stability of inter–species fusions and potential loss of non–rodent genetic material during cell division [211]. Due to the limited number of myeloma cell lines from other species, rodent cell lines are favoured. Myeloma cells must be in the log phase of growth at the time of fusion and from a cell lineage with a proven record of successful fusions.

6.1.3.2 Selection of Hybridomas

Fusion of the B–cells with the plasmacytoma results in a mixed population of hybridoma cells: B–cell–B–cell, plasmacytoma–plasmacytoma and B–cell–plasmacytoma hybrids. Additionally, the media will contain unfused plasmacytoma and B–cells. From this mixture of cell types, only the immortal, antibody producing plasmacytoma–B–cell hybrids are selected (Fig. 6.1). The most common selection method involves the use of hypoxanthine aminpterin thymidine (HAT) medium [205;212].

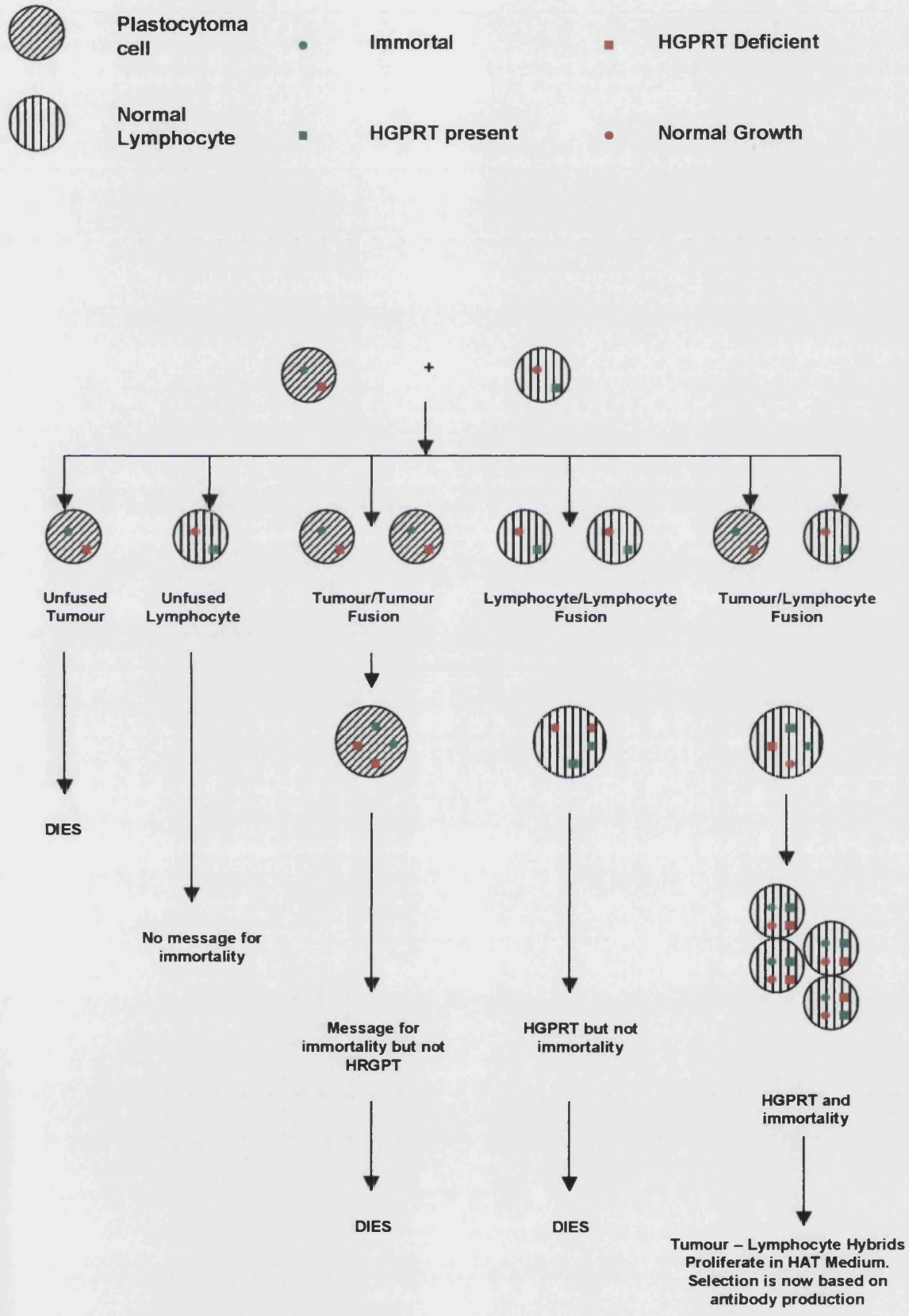

Figure 6.1. Cell Selection in HAT Medium

6.1.3.3 Isolation of Single Cells and Colony Development

As a result of fusion and HAT selection there is a heterogeneous mixture of immortalised antibody secreting cells. As the cells stabilise their chromosome number, the ability to produce viable antibodies may be lost allowing non–secreting cells to predominate. Isolation and initiation of a cell line from a single progenitor ensures homogeneity of the antibody produced. This is achieved by using the limited dilution technique. This involves the sequential dilution of cells demonstrating a positive response, at reduced densities over a period of a few weeks to allow for environmental adjustment. Eventually, cell densities will reach 1–2 cells per well allowing individual colonies to be chosen for continued proliferation.

6.1.3.4 Scale up of Antibody Production *in vivo*

The production of monoclonal antibodies on a large scale has been achieved, in the past, through *in vivo* intraperitoneal injection of hybridoma cells into a synergenic host. The cells proliferate in the peritoneal cavity of the animal and secrete the antibody in a fluid akin to plasma called ascites. This is drained from the animal approximately 2–3 times. However, due to the advances in *in vitro* protocols, and more stringent regulations governing the use of animals in scientific experiments, the *in vivo* approach to antibody production has been prohibited by the Animals Act 1984.

6.1.3.5 Scale up of Antibody Production *in vitro*

With this approach, cells are maintained in continuous culture, secreting the antibody product into the culture medium. Typical yields are within the region of 5–25 mg antibody per litre of culture medium. The disadvantage of this procedure is the risk of the introduction of contaminants into the culture medium. Such contaminants would have to be rigorously removed before use in therapeutic interventions and would have implications for infection in long–term cultures. Another disadvantage of this type of antibody production is the slow growth rate of the animal cells.

6.1.4 Furosine and CML as Immunogens

Furosine and CML are relatively small molecules (molecular weight 255 & 204, respectively), which is a disadvantage if they are to behave as effective immunogens. The conjugation of the furosine and CML with appropriate carrier molecules, is necessary before being introduced into the host. The heterogeneity of CML, in particular, could also be a problem when attempting to design specific antibodies.

6.1.5 Site of Immunisation and the Manipulation of the Immune Response

The route by which the antigen enters the host can have implications on the immunogenic potential of the molecule. The route of immunisation determines the site at which the immunogen is presented to the host animal. Generally, intramuscular and subcutaneous injections present the immunogen at the secondary lymphoid tissue immediately draining the site of the injection. Intravascular immunisation results in filtering in the spleen and ingestion results in an immune response in the mucosal lining. The route of administration and the distribution of the antigen will determine the microenvironment in which the antigen interacts with the antigen presenting cells [213]. T-and B–cells have the preferred microenvironments where the majority of the immune response occurs prior to migration to the primary lymphoid tissue. Augmentation and enrichment of the B–cells sensitised to the immunogen may occur at one site in preference to another resulting in site dependent differences in the efficacy of antibody production.

6.2 Aims

- Production of polyclonal antiserum against furosine in a rabbit host using synthetic furosine as the immunogen.
- Production of monoclonal antibodies derived from spleenic B–cells of mice immunised with synthetic furosine and CML.

- Screening for the above antibodies to assess their ability to bind to furosine and CML in the solid phase and in the free solution phase.

6.3 Immunisation Methods

6.3.1 Antigens

Furosine was obtained commercially (Neosystem, Groupe SNPE, Strasbourg) and CML was synthesised in the laboratories at Essex University, Department of Biochemistry (Chapter 3). The purity of these antigens was essential. These were conjugated to both thyroglobulin (Tg) and bovine serum albumin (BSA), respectively ready for immunisation.

6.3.2 Conjugation of the Antigens to Carrier Molecule (Carried out by ISL, Paignton, Devon)

Conjugation of the antigens to BSA and thyroglobulin was carried out in a two-step process employing an activator to link the free amine groups of the antigens to the carboxyl groups on the carrier protein. Each of the respective peptides were incubated in the presence of BSA at a molar ratio of 1:1.5 and with the thyroglobulin at a molar ratio of 1:2, in the presence of 1ml 0.8 M gluteraldehyde with constant agitation, at room temperature for 4 h. Excess gluteraldehyde was removed by a PD –10 column and peptide containing fractions were stored at -70°C.

The furosine and CML were conjugated to keyhole limpet haemocyanin (KLH) in two steps. An activator was employed to link the free amine groups of the furosine to carboxyl groups on the carrier protein. The target ratio was 50 hapten:1 carrier. Following the reaction, the conjugate was separated from any excess unbound hapten by use of a desalting column.

6.3.3 Rabbit Immunisation for Polyclonal Antibody Production (Carried out by ISL, Paignton, Devon)

One female New Zealand white rabbit (less than 6 mth old) was immunised with furosine, subcutaneously in Freunds complete adjuvant (1 mg of carrier hapten conjugate), on two occasions. Ear bleeds were taken on the day of the first immunisation (prebleed, 10 ml), on day 12 after immunisation (1st test–bleed, 10 ml) and 22 days after initial immunisation (2nd test–bleed, 10 ml). At this 22 day stage, the serum was tested for immune response using furosine bound to the solid phase. The rabbit was given a series of booster injections in Freunds incomplete adjuvant over the next four weeks. Further ear bleeds were taken and screened as before. Finally, a terminal bleed (20 ml) was taken to confirm antibody production and aliquots of the antiserum (0.5 ml) were stored at -70°C.

6.3.4 Mouse Immunisation for Monoclonal Antibody Production (carried out by T Jowett, Department of Medicine, UCL).

A total of two mice, aged 6 to 8 weeks old were used. The mice were injected subcutaneously with the peptide conjugate conformations (of furosine and CML). Each injection consisted of 50 µg conjugate in 100 µl RiBi adjuvant^{r} (Sigma Chemicals, Poole, Dorset, UK). An intraperitoneal booster was administered four weeks later comprising 50µg of each respective conjugate in RiBi (200 µl). Eleven days later, earbleeds were taken for antibody response using peptide–BSA conjugate coated microtitre plates. The test bleed at a dilution of 1/100 was positive for a mixture of IgG and IgM. Therefore, a second booster of 50 µg was administered intraperitoneally 15 days later. Further test bleeds were taken 12 days after the second boost and both mice sera were screened positive at 1/1000 dilution. Both had a strong IgG component and a weak IgM component. In order to reduce the Tg response and enhance the furosine and CML response, an intravenous furosine–BSA and CML–BSA conjugate (100 µg) in saline solution was administered after the second boost. The following day an identical mixture was injected intraperitoneally in saline solution and 3 days later the spleens were

removed. One spleen was stored at -70°C and the other was used for the fusion with plasmacytoma cells (Appendix X).

6.3.5 Summary

The mice injected with CML did not produce an adequate response to CML *in vitro*, even following booster injections. The mice injected with furosine produced a response to furosine, enough to warrant further investigations into the specificity of the antibodies.

6.4 Polyclonal Antibodies to Furosine - Titration of Antiserum with Furosine in the Solid Phase

The following series of assays were repeated, changing certain aspects of the experiment each time to improve the results. Therefore, the assay technique will be stated once (termed "template assay") and any subsequent modifications will only state the changes to the assay, to avoid repetition.

6.4.1 "Template" Assay

96-well microtitre plates (Immulon 4, Dynatech, UK), were coated with intact furosine (2 μg/ml, 200 μl) in Tris/NaCl coating buffer (pH 9) and incubated over night at +4°C, in a humidity chamber. A series of wells with no furosine (control wells) were also prepared. Each well was washed 5 times with phosphate buffered saline solution with 0.05% Tween (PBST, 200 μl) and all non-specific sites were blocked using BSA in PBST (200 μl, pH 7.4) and incubating at +37°C in a humidity chamber. After the incubation the wells were washed again with PBST (200 μl) and dried thoroughly in between washes. Rabbit anti-serum was prepared in diluting buffer, BSA in PBST (200 μl), applied to the wells and incubated at +37°C in a humidity chamber. The plates were aspirated, washed 5 times with PBST (200 μl) and dried thoroughly between each wash. Anti-rabbit-

[t] This adjuvant system is a stable oil in water emulsion which is recommended for use in mice and guinea pigs and is an alternative to conventional Freunds water–in–oil emulsion.

IgG-peroxidase conjugate (Sigma Chemical Co., Poole, UK), in diluting buffer (200 µl) was added to the wells and incubated in a humidity chamber at +37°C for 1 h. The plates were washed as described previously. Freshly made working substrate solution, containing 75 ml substrate buffer (500 ml of 2.5 g citric acid and 3.372 Na_2HPO_4 pH 5), 40mg 0-phenylenediamine (OPD) and 25 µl of 30% hydrogen peroxide (H_2O_2), was added to each well (150 µl). The wells were incubated at room temperature in the dark. After 30 min the reaction was stopped with 50 µl of 2 M sulphuric acid and the plate was mixed for 2 min. The optical density at 490 nm recorded.

6.4.2 Assay 1 - Titration of Pre-Bleed Versus Test-Bleed with Furosine in the Solid Phase

6.4.2.1 Reagents

Blocking buffer (1% BSA in PBST, 2hr incubation), diluting buffer (1% BSA in PBST), pre-bleed and test-bleed (1/10, 1/100, 1/1000, $1/1x10^4$, $1/1x10^5$, $1/1x10^6$, $1/1x10^7$, $1/1x10^8$, 5hr incubation), secondary antibody (1/10000).

6.4.2.2 Results

Results from antiserum dilutions of 1/10 to 1/100 are only shown as subsequent dilutions showed no visible absorbance readings.

Table 6.1. Results from assay 1

∞	Test reading $OD_{(490)}$	Control reading $OD_{(490)}$	Signal/background ratio
1/10 pre-bleed	0.285	0.350	0.814
1/10 test-bleed	0.417	0.360	1.158
1/100 pre-bleed	0.103	0.125	0.824
1/100 test-bleed	0.188	0.122	1.541

The control wells presented with high absorbance readings, suggesting a lack of specific binding by the antibodies in the test bleeds. A relatively small amount of

binding to the furosine coated plates was observed. To improve these results the effect of a high concentration of coating of furosine on binding was tested.

6.4.3 Assay 2 - Titration of Pre-Bleed Versus Test-Bleed with Different Concentrations of Furosine in the Solid Phase (incubation overnight and for 3 nights at +4°C)

6.4.3.1 Reagents

Antigen (2, 5, 10 μg/ml, overnight and 3 night incubations at 4°C), pre-bleed and test-bleed (1/10, 1/100, 1/1000, $1/1x10^4$)

6.4.3.2 Results

Table 6.2. Titration of pre-bleed versus test-bleed with different concentrations of furosine in the solid phase (incubation overnight)

Antigen coating concentration [μg/ml]	Bleed samples 1/10dilution	Absorbance $OD_{(490)}$	Control reading $OD_{(490)}$	Signal/noise ratio
2	Pre-bleed	0.198	0.217	0.912
	Test-bleed	0.244	0.243	1.004
5	Pre-bleed	0.212	0.304	0.697
	Test-bleed	0.260	0.325	0.800
10	Pre-bleed	0.207	0.258	0.802
	Test-bleed	0.239	0.281	0.851

Readings from the wells coated in 2 μg/ml antigen were not similar to the results from assay 1, even though the conditions of the assay were identical.

Table 6.3. Titration of pre-bleed versus test-bleed with different concentrations of furosine in the solid phase (incubation for 3 nights at +4°C)

Antigen coating concentration [μg/ml]	Bleed samples 1/10 dilution	Absorbance $OD_{(490)}$	Control reading $OD_{(490)}$	Signal/noise ratio
2	Pre-bleed	0.225	0.248	0.907
	Test-bleed	0.238	0.224	1.063
5	Pre-bleed	0.250	0.251	0.996
	Test-bleed	0.256	0.253	1.012
10	Pre-bleed	0.268	0.256	1.017
	Test-bleed	0.215	0.185	1.162

The readings from the majority of the control wells were higher than the test readings. This made the comparison between different assay conditions difficult. However, the absorbance readings taken after 3 nights of coating were higher than those after 1 night in the case of 5 and 10 μg/ml antigen concentration.

6.4.4 Assay 3 - Titration of 1st Test-Bleed Versus 2nd Test-Bleed with Furosine (10 μg/ml) in the Solid Phase

6.4.4.1 Reagents

Antigen (10μg/ml, overnight incubation), coating buffer (0.1% bovine serum albumin in Tris/NaCl pH 9), test-bleed 1and 2 (1/10, 1/100, 1/1000, 1/10000, $1/1x10^5$, $1/1x10^6$, $1/1x10^7$, $1/1x10^8$)

6.4.4.1 Results

Table 6.4 Results from assay 3

	Dilution	Absorbance $OD_{(490)}$	Control reading $OD_{(490)}$	Signal/noise ratio
1st test-bleed	1/10	0.590	0.579	1.019
	1/100	0.158	0.112	1.411
	1/1000	0.075	0.071	1.056
2nd test-bleed	1/10	0.541	0.338	1.600
	1/100	0.155	0.098	1.582
	1/1000	0.071	0.064	1.109

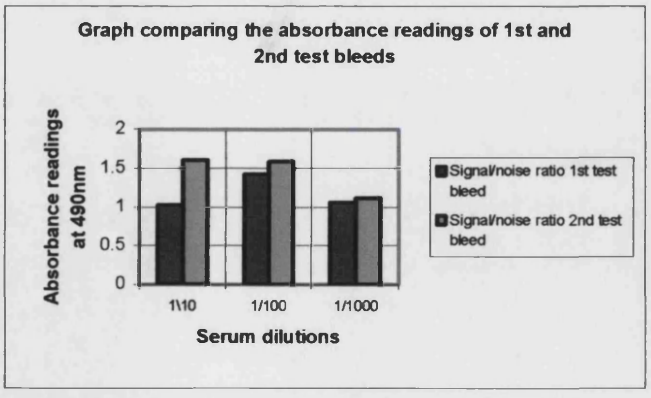

Figure 6.2. Results from assay 3

There was difference between the 1st and 2nd test-bleeds at a concentration of 1/10 (CV>10). All subsequant dilutions showed a minimal difference between the test bleeds. As with previous assays the control absorbance reading were high and there was an inconsistancy between readings taken from assay 2 and 3 where the assay conditions were identical (assay 2: $OD_{(490)}$ = 0.239, S/N = 0.851, assay 3: $OD_{(490)}$ = 0.590, S/N = 1.019).

Assays 1 to 3 indicated that there was some binding of the antibody to the antigen. To test for specificity and affinity, the antibody was purified before further titrations against furosine were carried out.

6.5 Titration of Purified Anti-Furosine Antibody with Furosine in the Solid Phase

The rabbit anti-serum was purified using affinity chromatography (Appendix XI and XII). The antibody was titrated with furosine in the solid phase, bound to microtitre plates. The same template assay was used as in section 6.4.1

6.5.1 Assay 1 - Titration of Purified Versus Terminal Bleed Antiserum with Furosine in the Solid Phase (range of concentrations of furosine coating)

6.5.1.1 Reagents

Antigen (0, 2, 5, 10 μg/ml, 2hr incubation at 37°C), anti-furosine antibody (0.1, 0.01, 0.001, 0.0001 mg/ml), terminal bleed (1/10, 1/100, 1/1000, 1/10000)

6.6.1.2 Results

Table 6.5. Results from assay 1

Conc of purified antibody [mg/ml]	2μg/ml furosine coating mean absorbance $OD_{(490)}$	2μg/ml furosine coating signal/noise ratio	5μg/ml furosine coating mean absorbance $OD_{(490)}$	5μg/ml furosine coating signal/noise ratio	10μg/ml furosine coating mean absorbance $OD_{(490)}$	10μg/ml furosine coating signal/noise ratio
0.1	0.085	1.417	0.088	1.467	0.078	1.300
0.01	0.072	1.200	0.068	1.133	0.065	1.083
0.001	0.064	1.067	0.062	1.033	0.063	1.050
0.0001	0.066	1.100	0.066	1.100	0.066	1.100
Conc of terminal bleed						
1/10	0.142	2.784	0.153	3.000	0.137	2.686
1/100	0.077	1.510	0.075	1.471	0.073	1.422
1/1000	0.070	1.373	0.069	1.353	0.066	1.294
1/10000	0.061	1.196	0.062	1.216	0.060	1.176

Mean control $OD_{(490)}$ = 0.056 (± 0.006)

There was no difference between wells with different amounts of furosine coating (CVs<10). The absorbance readings decreased as the concentrations of the antibody and anti - serum decreased. The control readings were relatively lower than previous assays.

The control readings from all the assays decreased as the concentrations of the primary antibody decreased. This suggests that there is a degree of non-specific binding. The size of the furosine antigen coated on the wells (molecular weight 255) may be too small for adequate *in vitro* binding between the antigen and furosine to occur. Therefore, the free furosine antigen (2.5 mg) was conjugated (carried out by ISL, Paignton, Devon) to bovine BSA (5 mg) and used to coat the wells in the next assay.

6.5.2 Assay 2 - Titration of Purified Antiserum with Furosine Conjugated to BSA in the Solid Phase

6.5.2.1 Reagents

Furosine-BSA conjugate (2 μg/ml, overnight incubation at 4°C), blocking buffer (1% BSA in PBST), diluting buffer (1% BSA in PBST), anti-furosine antibody (0.1, 0.01, 0.001 mg/ml).

6.6.2.2 Results

Table 6.6. Results from assay 2

Concentration of antibody [mg/ml]	Mean absorbance $OD_{(490)}$	Control reading $OD_{(490)}$	Signal/noise ratio
0.1	0.546	0.184	2.965
0.01	0.152	0.073	2.329
0.001	0.069	0.047	1.266

The absorbance readings are higher and the control readings lower than those seen with free furosine coating (CV>10). The control readings still increased with corresponding increases of antibody.

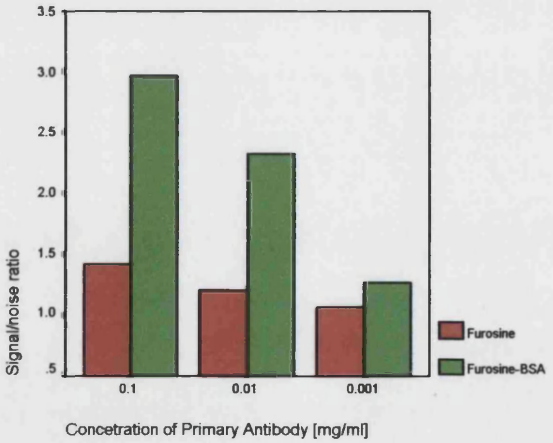

Figure 6.3. Graph comparing results from free furosine and conjugated furosine coated wells.

This assay was repeated with the aim of duplicating the results. There was, once again, a difference in the absorbance readings between the assays and the control wells had higher readings.

6.6 Discussion

These results show minimal non-specific binding of the polyclonal antibody to the antigen, *in* vitro. In view of this, it was decided that the polyclonal antibodies raised were not satisfactory and that the production of monoclonal antibodies by hybridoma technology would prove to be advantageous. The advantages of monoclonal antibodies over polyclonal antibodies are that they are homogenous (i.e. every antibody molecule is identical in antigen binding properties) and also, the hybridoma cell lines secreting the antibodies are immortal, hence there is an inexhaustible supply of the antibody.

6.7 Screening of Monoclonal Antibodies to Furosine (Carried out by T Jowett, Department of Medicine, UCL).

6.7.1 Preliminary Screening Assays of 2C3 and 6B11 Antibody Substrates

The antibodies were screened against BSA-conjugate and free BSA. Out of 8 microtitre plates, 11 wells recognised the furosine conjugate and not the free BSA. The cells relating to these wells were grown. Two of the cell lines were IgG and the others IgM types. The IgG cell lines were named 2C3 and 6B11. The cells lines were cloned by limiting dilution. Two clones of each cell line were cloned and named 2C3/C4, 2C3/C6, 6B11/A7 and 6B11/H12.

The substrates for 2C3 and 6B11 were tested with different free AGEs and AGEs conjugated with proteins. Both substrates recognized furosine-BSA, furosine-Tg CML-Tg conjugates and Tg, but not CML-BSA and BSA. There antibodies recognize both AGEs and free Tg, suggesting lack of specificity.

Following on from these results, displacement assays were carried out, which involved the coating of wells (10 µg/ml, 100 µl) with the Tg and BSA conjugates

of furosine and adding the antibody substrate (1/50 dilution, 50 µl) with the conjugates (1.25 µg/ml, 50 µl) added to that. No displacement was noted. The same procedure was repeated using two keratin proteins acid hydrolysates and the competitive agent and no displacement was observed in this case either.

6.7.2 Concentration and Purification of Immunoglobulins from Substrates 2C3 and 6B11

6.7.2.1 Reagents

Solid ammonium sulphate, NaOH (1 M), HCl (1 M), substrates 2C3 and 6B11 (10 ml), PBS.

6.7.2.2 Methods

The substrates (10 ml) were placed in labeled Universal containers (20 ml capacity). Each substrate pH was adjusted to 5.5 using HCl (1 M). This pH aided maximum precipitation. Solid ammonium sulphate (5.75 g) was slowly added to the substrates whilst stirring. This amount of ammonium sulphate in 10 ml of substrate formed a 75% saturated solution. When all the salt was added, each mixture was stirred (1 h, RT) to allow the mixture to equilibrate. The mixtures were then centrifuged (15 min, 3000 rpm) and the supernatant was discarded. The precipitate was redissolved in 1 ml of PBS and stored at +4°C in preparation for purification.

The immunoglobulin concentrate was purified using affinity chromatography (Appendix XI and XII).

6.7.3 Titration of Antibodies 2C3/C4 and 6B11/A7 with Furosine and CML Conjugates in the Solid Phase

6.7.3.1 Methods

96-well microtitre plates (Immulon 4, Dynatech, UK), were coated with furosine, furosine-BSA, furosine-Tg, BSA, CML, CML-BSA, CML-Tg, arginine and lysine (2 μg/ml, 200 μl) in Tris/NaCl coating buffer (pH 9) and incubated for 2 h at 37°C and then over night at +4°C, in a humidity chamber. A series of wells with no furosine (control wells) were also prepared. Each well was washed 5 times with phosphate buffered saline solution with 0.05% Tween (PBST, 200 μl) and all non-specific sites were blocked using bovine serum albumin (BSA) in PBST (200 μl, pH 7.4) and incubated at +37°C for 2 h in a humidity chamber. After the incubation the wells were washed 5 times with PBST (200 μl) and dried thoroughly in between washes. The antibody was prepared in diluting buffer, 1% BSA in PBST (200 μl), applied to the wells (200 μl) and incubated at +37°C in a humidity chamber for 5 h. The plates were aspirated, washed 5 times with PBST (200 μl) and dried thoroughly between each wash. Anti-rabbit-IgG-peroxidase conjugate (Sigma Chemical Co., Poole, UK), in diluting buffer (200 μl) was added to the wells and incubated in a humidity chamber at +37°C for 1 h. The plates were washed as described previously. Freshly made working substrate solution, containing 75 ml substrate buffer (500 ml of 2.5 g citric acid and 3.372 Na_2HPO_4 pH 5), 40 mg OPD and 25μl of 30% H_2O_2, was added to each well (150 μl). The wells were incubated at room temperature in the dark. After 30 min the reaction was stopped with 50 μl of 2 M sulphuric acid and the plate was mixed for 2 minutes. The optical density at 490 nm recorded.

6.7.3.2 Results

The sound/noise ratios were calculated for each titration and compared (Appendix XIII).

Table 6.7. Table illustrating the highest absorption readings observed from the monoclonal antibodies.

Conc of 2C3/C4 antibody [mg/ml]	2 μg/ml F-BSA coating noise/sound ratio	2 μg/ml F-Tg coating noise/sound ratio	2 μg/ml CML-Tg coating noise/sound ratio
0.1	4.725	17.104	10.000
0.01	3.786	11.673	5.000
0.001	1.200	5.618	2.327
0.0001	0.926	6.098	2.805
Conc of 6B11/A7 antibody [mg/ml]			
0.1	6.612	7.209	9.786
0.01	3.687	14.212	7.419
0.001	2.181	8.627	3.157
0.0001	1.071	7.667	2.240

Antibody binding is noted in all of the wells by both monoclonal antibodies. Binding is significantly higher in the wells coated with furosine-BSA, furosine-Tg and CML-Tg conjugates, in particular the Tg conjugates (Fig. 6.4 & Table 6.7). The molecular weight of Tg and BSA is 330,000 and 67,000, respectively. This could explain the increased binding of the antibodies to the larger Tg conjugates. The antibodies bind to all the wells in varying degrees confirming, therefore, their non-specific binding.

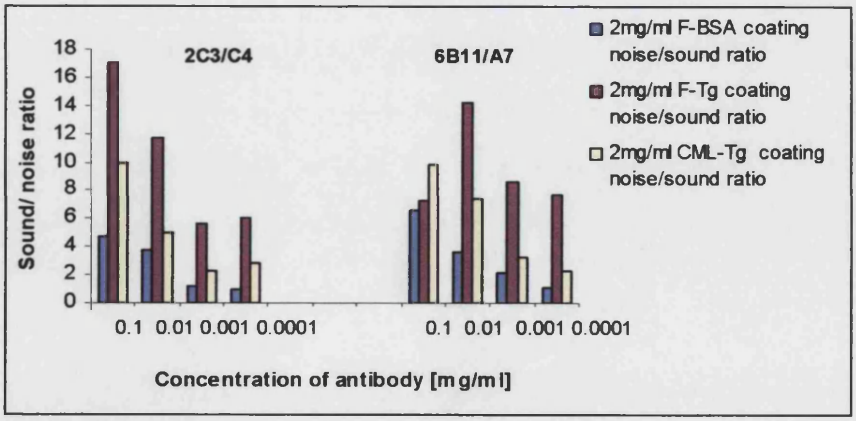

Figure 6.4. Titration of Antibodies 2C3/C4 and 6B11/A7 with Furosine and CML Conjugates in the Solid Phase

6.8 Discussion

These set of experiments have demonstrated the non-specific binding of polyclonal and monoclonal anti-furosine antibodies. Antibodies against CML were not raised successfully, suggesting a degree of similarity of CML to the hosts' isoform, hence being ignored by the hosts' immune system. There are several explanations as to why it is difficult to raise specific monoclonal antibodies to certain glycation adducts.

The immunogen used in this study contrasted to those used in previous studies in that the carrier protein was directly attached to furosine and CML prior to injection into the host. Other groups have shown that AGE modified KLH or BSA can be used as immunogens to prepare polyclonal [210;213] and monoclonal [210] antisera that recognize a spectrum of AGE epitopes in addition to CML, pentosidine and possibly early glycation adducts [214;215].This use of *in vitro* AGE immunogens produced a range of AGEs, not all of which have been structurally defined [204;210] and including ones that may be less abundant in tissues [216]. Thus, these types of antibodies might find their best use in surveys of age-dependent accumulation of a larger number of epitopes that might not be revealed by antibodies with narrower epitope reactivity, such as pentosidine and CML.

The use of pure glycation adducts conjugated with appropriate carrier proteins was adopted in this study in an attempt to reduce the generation of heterogeneous, unknown AGE compounds and therefore increase the specificity of the resulting antibodies. This technique was not successful and supports the literature further by confirming the need for further structural studies of the advanced glycation pathways as they occur *in vivo*, under native conditions.

7.0 Chapter 7 - Investigation of the Mechanical Properties of Pedal Skin, *in vivo,* using a Vertical Negative Pressure Technique

7.1 Introduction

The anisotropic nature of the skin introduces complexities in its mechanical nature, mainly that it exhibits non-linear stress-strain properties, and viscoelastic (time-dependent) behaviour [217]. Because of this complexity, almost all significant work that has been carried out on the skin has been *in vitro* [218]. The main problems with *in vitro* studies are the deterioration of skin after it has been removed from the host, causing marked alterations in the mechanical properties [219]. *In vivo*, the viscoelastic properties of the skin prove to be difficult to analyse due to the behaviour of the collagen and elastin in association with tissue fluids. The search for an accurate, non-invasive technique of measuring the mechanical behaviour of the skin, *in vivo* would be useful for observing the progression of skin pathologies and for testing the efficacy of skin treatments.

The ways in which various groups in this field have carried out their experiments are very different, producing indecisive and conflicting results. Some investigations of the mechanical properties of human skin, *in vivo*, use equipment that measures the deformation of skin after the application of uniaxial, biaxial or multiaxial forces [220]. Devices that apply these forces have been developed in research laboratories for experimental purposes, but only a few are available commercially. As the skin is a three-dimensional tissue, the application of multiaxial forces is more realistic than uni- and bi- axial forces [219]. The vertical suction technique is an example of this type of method. The two types of commercial, vertical suction devices available are the Dermaflex® (Cortex Technology, Denmark) and the Cutometer® (580 MPA, Courage and Khazaka Electronic UK Ltd). The Cutometer® has mainly been used in the cosmetics industry for monitoring the effects of topical emollients on the biomechanical properties of facial and forearm skin [221]. It has recently been used for research purposes on assessing the elasticity of diabetic skin on different points on the body excluding the feet [222]. For this study the Cutometer® was used to

characterise and measure the viscoelastic properties of the epidermis on the feet of diabetic and non-diabetic individuals.

7.2 Techniques used to Measure Skin Mechanics *in vivo*

There are four directions of loads that can be applied to the skin: vertical pressure i.e. ballistrometry [223] and indentation [224;225] techniques; vertical suction [221;223;223;226-229], linear horizontal, uniaxial traction [230;231] and torsion in the horizontal plane [232-234].

7.2.1 Vacuum Suction Devices

As explained in Chapter 1, the majority of the studies investigating the flexibility of diabetic skin have involved qualitative clinical observations. More recently there has been the development of devices, which either indent or draw up the skin[226;228;232;233;235]. Nikkels–Tassoudji *et al* (1996) [222] have shown that the mechanical properties of diabetic skin differ according to the type of diabetes, the test site and the age group. The authors identified the potential advantages of such techniques, correlating the physical changes in the skin to the duration of diabetes, the degree of metabolic control and the prevalence of complications related to diabetes. The relationship between these variables has been inconsistent from study to study [39-41].

The main advantage of the vacuum suction technique is that it reduces the likelihood of underlying tissues interfering with the measurements. This has been clearly demonstrated [222;229] by measuring skin flexibility on different body sites, but not plantar skin. Skin thickness and flexibility analysis, using ultrasonography and vacuum suction, respectively, on pedal skin would provide an insight into its biomechanical nature.

The decision to use the suction method for this study was influenced by the nature of the skin on the foot, particularly plantar skin. Although the plantar skin may be thicker than other sites on the body, it is in close proximity to underlying bones and joints. A method such as indentation would not portray properties

unique to the skin but would also include the structures lying beneath the skin. The torsion method could overcome these problems, but as the relatively thick plantar skin is tightly tethered to subcutaneous tissues via fibrous attachments, these attachments would be included in the measurements. The vertical suction method minimises interference from tissues other than the skin. This will be discussed in more detail later on in this section. Only one published study has investigated the physical properties of plantar diabetic skin by using an indentation method [234].

7.3 Physical Nature of Skin in Relation to Structure

The physical nature of skin incorporates elastic and viscous properties of solids[217]. This viscoelastic mechanical model is different in different structural components of the skin. For example, the physical behaviour of the stratum corneum and the upper layers of the epidermis are influenced by fluctuations in the water content, as a result of changes in the environmental humidity [221]. The internal portion of the epidermis, where the basement membrane, desmosomes, and elastic fibres are housed, anchors the epidermis to the deeper tissues. The papillary dermis has relatively loose connective tissue in contrast to the reticular dermis, where the connective tissue is packed tightly and the subcutaneous region attaches to the deeper fascia. Each of these tissue types have different viscoelastic properties, which in combination give the skin its overall flexibility.

The elastic fibres, the architecture of which is important in the dermis, are principally responsible for the elastic properties of the skin under minor loads. The elastic fibres in the immediate subepidermal area form a delicate framework perpendicular to the epidermal surface. These fibres are attached to the epidermal-dermal junction from one side, and to the layers of elastic fibres that run parallel to the surface of the skin from the other. Thus, the structure and the shape of the epidermal-dermal junction may influence the elasticity of the skin and any clinical conditions affecting this fibre framework of skin are likely to alter its biomechanical properties.

The load extension properties of *in vivo* human skin are found to be dependent upon both static and dynamic tensions. The static tensions are the natural tensions existing in normal skin and vary between different anatomical sites [227;235]. The dynamic tensions are caused by a combination of forces, which are associated with joint movement, voluntary muscle activity, and gravity [236]. Dynamic forces have an important influence on the magnitude of skin tensions, i.e. as joints move, the magnitude and direction of tensions within the skin change markedly [230].

7.4 Mechanical Properties of Normal Skin

7.4.1 Introduction to Terminology

The mechanical properties of the skin are defined in terms of the deformation produced by a given force over a period of time. The following is a list of terms that are commonly used when referring to skin mechanics:

- *Stress* is a system of forces in equilibrium producing strain in a material or part of a material. The stresses may be regarded as the forces applied to deform the material or as equal or opposite forces with which the body resists. In all cases the stress is measured as a force per unit area.
- *Strain* is the change in volume (*volume strain*) and/ or a change in shape of a material, as a result of applied stresses. Linear *strain* is the extension per unit length due to an applied stress.
- An *elastic* material is a material that undergoes changes in the relative positions of its components that disappears as the deforming stress is removed. A purely elastic material resumes its original size and shape after being subjected to deforming stresses
- *Elastic hysteresis* is a phenomenon that occurs when a stress is applied in steps to an elastic body, and removed in equal steps. The strain on unloading is greater than at the corresponding stress when loading. This hysteresis is very small for materials such as steel and very large for imperfectly elastic materials such as rubber. On a graph of stress against

strain, the area within the *hysteresis loop* represents the energy dissipation per unit volume in a cycle of loading and unloading.

- An *elastic modulus* is the ratio of stress to strain, within the limit of proportionality.
- *Young modulus* is the ratio of stress to strain for a homogenous material that obeys *Hooke's law.*
- *Hooke's law* in its most general form, states that, for a certain range of stresses, the *strain* produced is proportional to the *stress* applied (independent of time), and disappears completely on removal of the *stress.* This law is the basis of the theory of elasticity.
- A *viscoelastic* material has the properties of elastic solid when a deforming stress is applied and continues to stretch, with time, under a constant *stress* (viscous fluid behaviour). The latter phenomenon is called *creep.*
- A *plastic* material deforms in response to the application of stress and does not return to its original shape once this stress has been removed. It is the opposite case when the material is purely elastic. A material can possess both elastic and plastic qualities, that are governed by the magnitude of the stress applied.
- An *isotropic* material possesses properties, such as elastic constants, that do not vary in direction.
- An *anisotropic* material possesses physical properties that vary with direction.

The skin exhibits viscoelastic behaviour [219], and the typical properties are non-linear stress-strain with hysteresis. The deformation of the skin is time-dependent, with a phenomenon of creep associated with it.

7.4.2 Factors Influencing the Mechanical Properties of the Skin

The mechanical properties of the skin depend on the anatomical site [235]. For example the skin, is more distensible, under suction, around acral areas such as

the malleoli and forearms, in comparison to proximal areas such as the thigh, trunk and arm.

Female skin appears to be more distensible in acral areas in comparison to male skin. No correlation has been found between gender and skin elasticity [227], although female hormones may have a role in the modulation of skin mechanical properties, since skin elasticity in women changes throughout the menstrual cycle [227;235].

Age also has an effect on the mechanical properties of the skin, although the evidence is confusing [223]. Scientists using the Cutometer® 580 MPA have demonstrated that the indices of elasticity diminish with age [223;227;235]. This could be due to the damage, disintegration, or changes of the structure of the elastic fibres that appear in both intrinsic and solar aging.

Some studies have shown that skin elasticity fluctuates during the day [237]. This may be due to an adaptation to the standing position and that the accumulation of fluid within the dermis and the restoration of previous shape is associated with fluid removal. Skin elastic forces contribute to the recovery of skin shape after stretch and thus enhance the clearance of intercellular fluid. Hence, the evening increase of elasticity of acral skin is advantageous because strong recoil forces assist in the removal of oedematous fluid that accumulates in the extremities during the day. The viscoelastic properties of the skin are impaired by inflammatory skin conditions where oedema and interstitial fluid exists e.g. systemic sclerosis [228;231;238].

Another factor, which can affect measurements, is the state of hydration of the stratum corneum. While it represents approximately two-thirds of the epidermal thickness, its influences cannot be neglected: its Young's modulus is 1000 times higher than that of skin–10^8 N/m^2 for a water content of 13% [233].

7.5 Determination of Skin Mechanical Properties using Vertical Suction

The principle of the suction method is the measurement of skin elevation caused by the suction force exerted, over a defined area of skin. Measuring the skin elevation as a function of time enables the examiner to calculate particular variables reflecting the skin's mechanical properties.

The two most popular commercial devices used for the measurement of skin flexibility are the Dermaflex A® (Cortex Technology, Hadsund, Denmark) and the Cutometer® 580 MPA (Courage and Khazaka, Cologne, Germany) [235].

7.5.1 Cutometer® 580 MPA

The Cutometer® 580 MPA consists of a generator for the vacuum; a sensor of skin elevation within the probe and a data software package. The suction probe has a steel ring, 2 mm in diameter (the Dermaflex® has an aperture diameter of 10 mm) that demarcates the area of skin where the suction is applied. A double adhesive ring is placed on the metal ring so as to prevent the influence of skin creeping during the suction. The instrument is designed so that the vacuum strength, length of suction and number of suction cycles can be adjusted.

The Cutometer® 580 MPA differs from the Dermaflex A® in that the diameter of the aperture on the suction chamber is much smaller, making the measurements exclusive to the epidermis and papillary dermis and involves the deeper layers of the dermis and the subcutaneous tissues in part only [235]. As plantar epidermis is relatively thicker than other parts of the body, interference by the dermis should be even less likely.

The main difference between the two devices, that influenced the selection of the Cutometer® 580 MPA for this study, was the format in which the data could be collected. The Cutometer® 580 MPA not only provided a set of skin displacement readings with time, but also provided pressure readings in the time that the displacement data was gathered. This was not part of the original software

package and was kindly provided by Courage and Khazaka on request. The relevance of this data will be explained later on in this chapter.

7.5.1.1 Description of the Measuring Probe[♦]

The handheld measuring probe is attached to the main apparatus via an electric cable and air tube (Fig. 7.1). The machine is designed so that a variable vacuum pressure is applied to the surface of the skin, ranging from 50 to 500 mbar. The relative accuracy of the vacuum varies from 10% for vacuum values between 20 and 100 mbar to 5% for higher vacuum values of 100 to 500 mbar. The vacuum is drawn through the aperture and pulls the surface of the skin up into the aperture of the probe. Inside the probe, the penetration depth is determined by an optical system, which consists of a light source and a light receptor, a long with two prisms facing each other, which project the light from the transmitter to the receptor. The light intensity varies according to the penetration depth of the skin. This information is then converted to the time-displacement curves outputted by the computer software. The skin adjacent to the probe aperture is maintained in position by an external guard ring attached to the probe shield (external diameter of 2.5cm). The measuring probe weighs approximately 90g. The function of the springs, inside the probe, is to maintain a constant force of $2x10^3$ N/m^2 when it is applied vertically on the skin surface. The absolute accuracy of the skin deformation measurement is 0.010 mm. The diameter of the probe aperture is 2 mm.

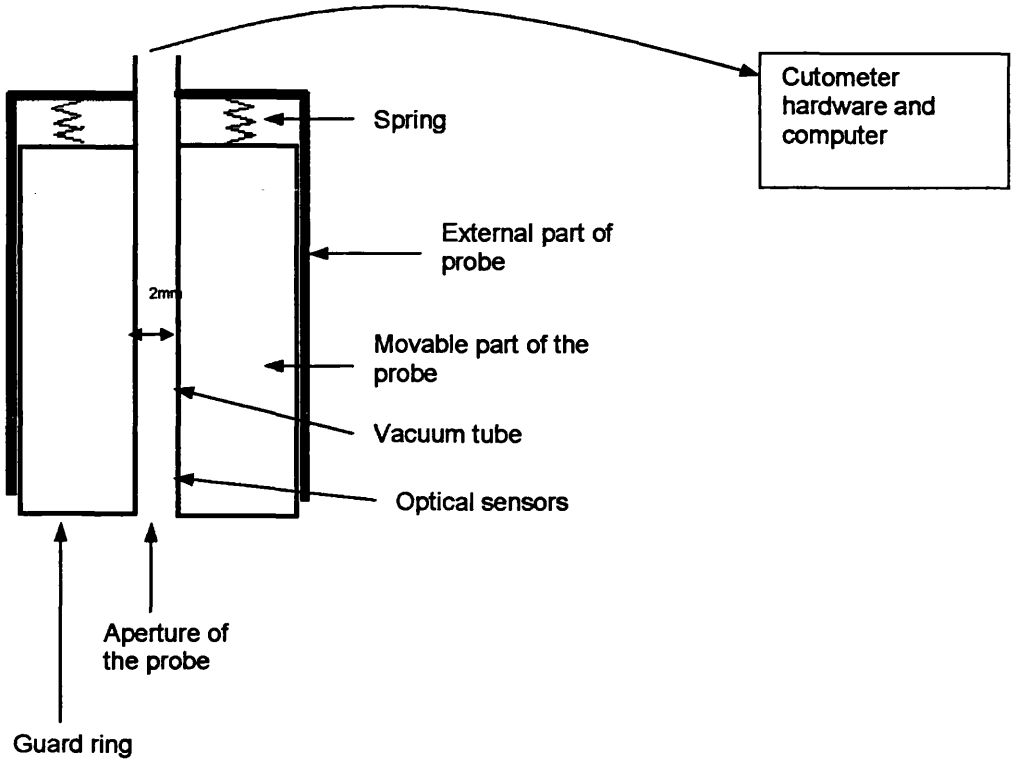

Figure 7.1. Schematic diagram of the measuring probe of the Cutometer® 580 MPA. Aperture size 2mm.

* Courage and Khazaka provided all information in this section.

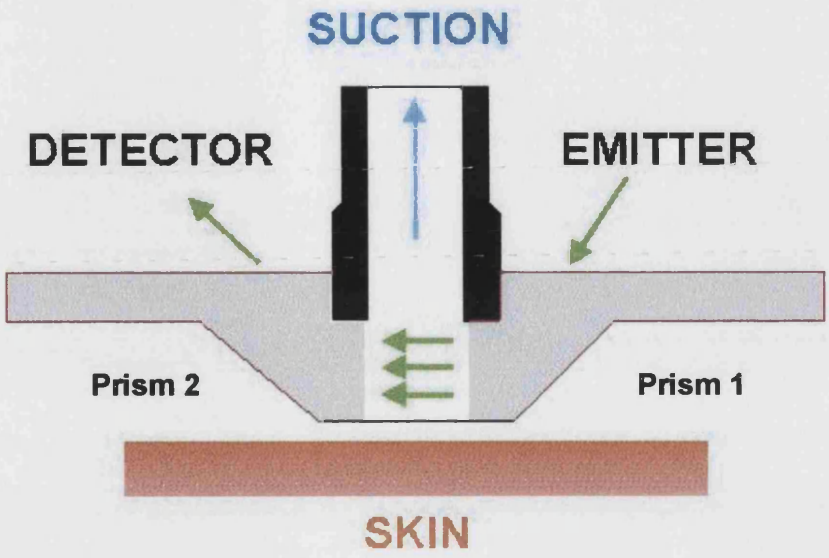

Figure 7.2. Schematic diagram illustrating the optical detection system within the probe

The head of the probe houses two prisms (Fig. 7.2). One prism emits green light (565 nm) of constant intensity along its entire length. The second prism receives the light, therefore as the skin moves up into the aperture the intensity of the light received by the second prism is decreased. The mathematical function between the decreasing light intensity and the position of the skin entering the aperture is linear when measuring displacements between 0 and 900 μm, but is not linear at displacement distances between 900 and 1700 μm (Fig. 7.3). As a result of this curved data, the probe is calibrated by a tool designed by the company that allows for a pin to enter the aperture step by step at known intervals and the light intensity readings as a result of these different distances are stored. As the prisms are not identical for every probe that is made, the calibration procedures must be carried out for each probe. The results of the calibration are stored in the fixed memory of the probe and also on the factory calibration database.

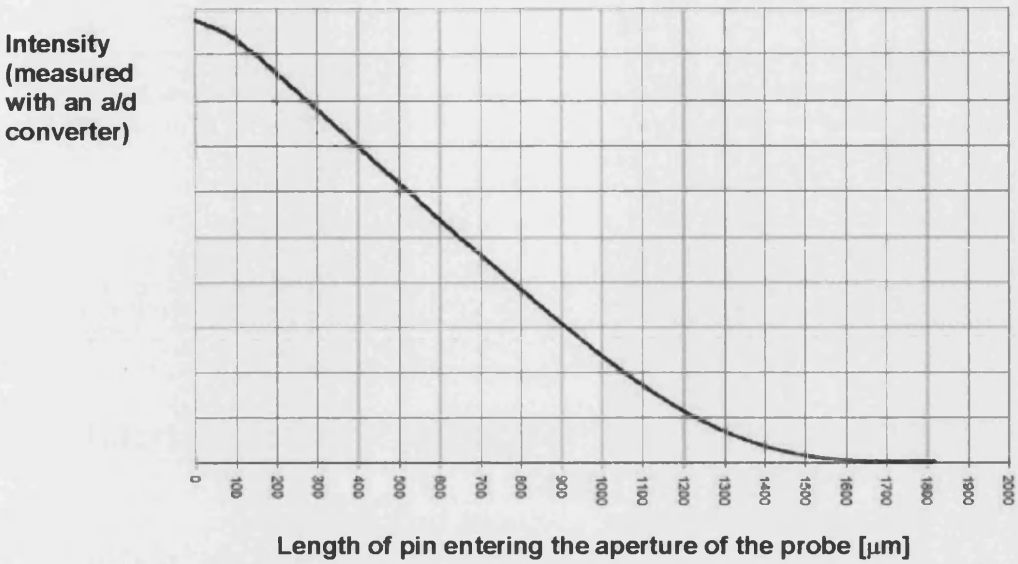

Figure 7.3. Curve of light intensity absorbed by prism two as the emitted light from prism one is blocked at different depths. Graph supplied by Courage and Khazaka.

The device was linked to an IBM compatible personal computer. Standard control software, directing the Cutometer® 580 MPA, was provided by the company. The software allowed the storage of data such as date and time of the experiment, skin site, external temperature, relative humidity and the mode of measuring technique. In addition, the graphic display provided a curve of displacement and pressure versus time, along with the numerical data.

7.5.1.2 Handling the Measuring Probe

The correct handling of the probe is essential for exact and reproducible measurements. The measurements should always be made under the same room conditions i.e. the relative humidity and external temperature have to be constant. Only in this case can measurements over a long period of time be compared. The ideal conditions are an external temperature of 20°C and a relative humidity of 40–60%. The test subjects need at least 10 minutes to acclimatise. Blood circulation has to return to normal after possible physical strain. The probe must be applied at right angles to the skin and pressed down until the guard ring is level with the external casing of the probe, and maintained in this position to ensure a constant application of pressure. If the skin site has hair it is advisable to shave the area as it may touch the optical sensors when the

suction is applied. The probe must be held as steady as possible during the measurement time. This is achieved by applying a double-sided tape to the probe and the skin surface to avoid slipping.

7.5.1.3 Description of the Measuring Modes

The Cutometer® 580 MPA offers 4 different measuring modes for different scientific requirements (Table 7.1).

Table 7.1. Description of the different modes provided by the Cutometer® 580 MPA

Mode	Description	Illustration of Description
1	Measurement with constant negative pressure	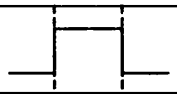
2	Measurement with linear rising and falling negative pressure	
3	Measurement with first constant then linear falling negative pressure	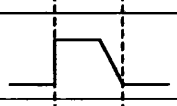
4	Measurement with linear rising negative pressure and then abrupt cessation of the negative pressure	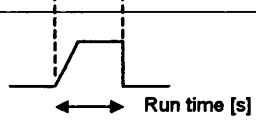

Mode 1 was used in this study, where the skin was drawn into the aperture of the probe during an allotted measuring time with a constant negative pressure, after which the pressure was abruptly switched off and the skin released.

7.5.2 Variables and Prerequisites to be Considered when Taking Skin Elasticity Measurements

7.5.2.1 Biological and Environmental Variables

The biological variables that need to be considered before taking skin elasticity measurements are: sex, age, race, anatomical site, endocrine factors (e.g. hormonal cycle, hormonal treatment); water balance (including treatment with diuretics), general and localised diseases and diurnal variation of water

accumulation in the dependent parts of the body. The environmental factors include: sun exposure (e.g. photodamage, psoralens ultraviolet A (PUVA) photosclerosis); seasonal variations in the humidity of the stratum corneum; previous physical stress to the skin (the skin has a "stress memory" that can last for at least 1h) and topical treatments.

7.5.2.2 Standardisation for Measurements

The probe is very sensitive to movement [236] therefore both the probe and the skin should be static when the readings are taken. The body and foot should be in a standard position. This is crucial, as the pronation or supination of the foot could have a significant effect on the movement of skin over the joints. The site to be measured should be carefully marked and adjacent sites should be measured and a mean value calculated. The placement of the probe should be perpendicular to the skin surface throughout the process of data collection. Repeated measurements in the same area should be avoided for at least 1h, as the initial recording will temporarily modify the viscoelastic behaviour of the tissue within that region.

7.5.2.3 Pretension of the Skin

As described previously, the skin immediately adjacent to the aperture of the measuring probe is held in position by a guard ring. However, even with this in place there is a degree of lateral displacement of the skin next to the opening when the suction is applied. The purpose of this instrument is to only measure the vertical displacement of the skin during suction and not any lateral displacement. In order to minimise the lateral skin displacement the skin should undergo pretension before the measurement is carried out. Pretension of the skin is achieved by applying a preliminary suction on the surface of the skin for a short period of time (0.1 s). With this implemented the maximum skin deformation readings taken show minimal variability [221].

7.5.3 Viscoelastic Qualities of the Skin

Because of the viscoelastic nature of human skin, a simple stress strain relationship is an insufficient description of the tissue, i.e. Young's Modulus is not applicable.

The viscoelastic components of skin are highlighted in Fig. 7.4. The curve is described in two parts in the suction phase, and two in the relaxation phase. In the first half of the suction phase the slope of the curve is almost perpendicular, this is the series elastic component or immediate stretch (Ue). The second part of the curve flattens more and more until it reaches a maximum at the end of the suction phase. This is the viscoelastic component or delayed stretch (Uv_1). After the suction phase (e.g. 60s at 500 mbar) the suction is switched off. In a highly elastic material the curve returns to the starting point immediately and perpendicularly after removal of suction. In a viscoelastic material, such as the skin, there are two parts to the curve: the falling perpendicular, series elastic component (Ur) and the viscoelastic component (Uv_2), which flattens out to zero.

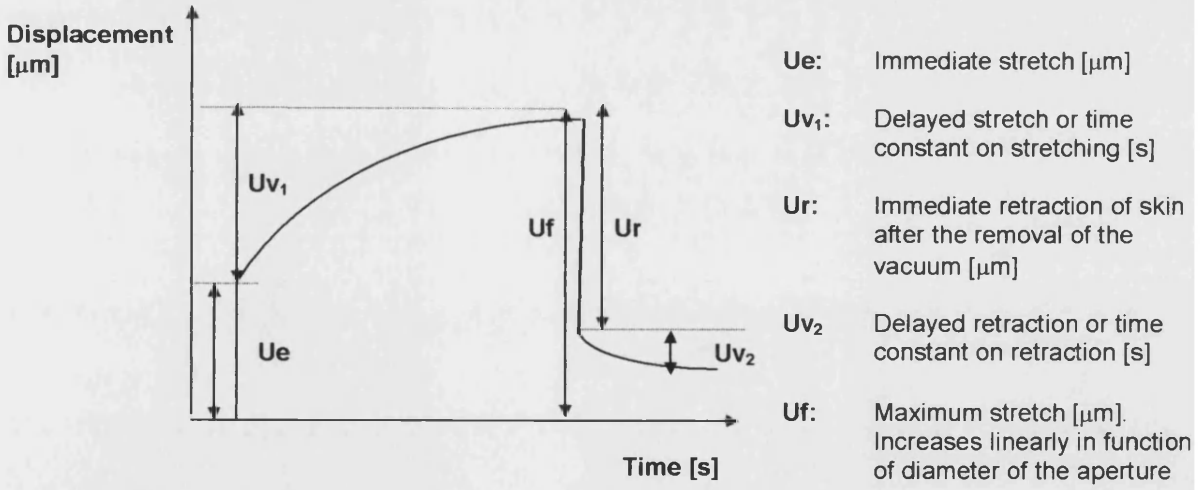

Figure 7.4. Curve illustrating the viscoelastic properties of the skin using vertical suction

This curve is characteristic of skin as a whole, therefore suggesting that the epidermis has a role in this viscoelastic behaviour, but what significance does the epidermis alone have on the overall mechanics of the skin? This may be explained by the knowledge that palmar tissue exhibits parameters of viscoelasticity [223]. Palmar skin has a similar structure to plantar skin in terms of the preponderance of the stratum corneum; therefore, it could be possible that a viscoelastic model may describe mechanics of plantar epidermis. Keratin fibres in the epidermis may follow similar mechanics as collagen fibres in the dermis that of reorientation of the fibre network, allowing the extension of the epidermis as a non-linear stress-strain curve. This study attempts to concentrate on the possible viscoelastic components of the epidermis on three sites on the foot (see section 7.7.1).

7.5.4 Mechanical Models of Viscoelastic Behaviour

Based on Hooke's law, models of viscoelastic behaviour are a combination of a linear spring with a Young's modulus (E) and a dashpot with a viscosity (η). The elastic spring produces a deformation directly proportional to the load; the dashpot (likened to a shock-absorber) produces a velocity of deformation proportional to the load. These two components may be combined in different ways to describe the viscoelastic behaviour of materials [219]. The two simplest combinations are the Maxwell and Voight models (Fig. 7.5 & 7.6).

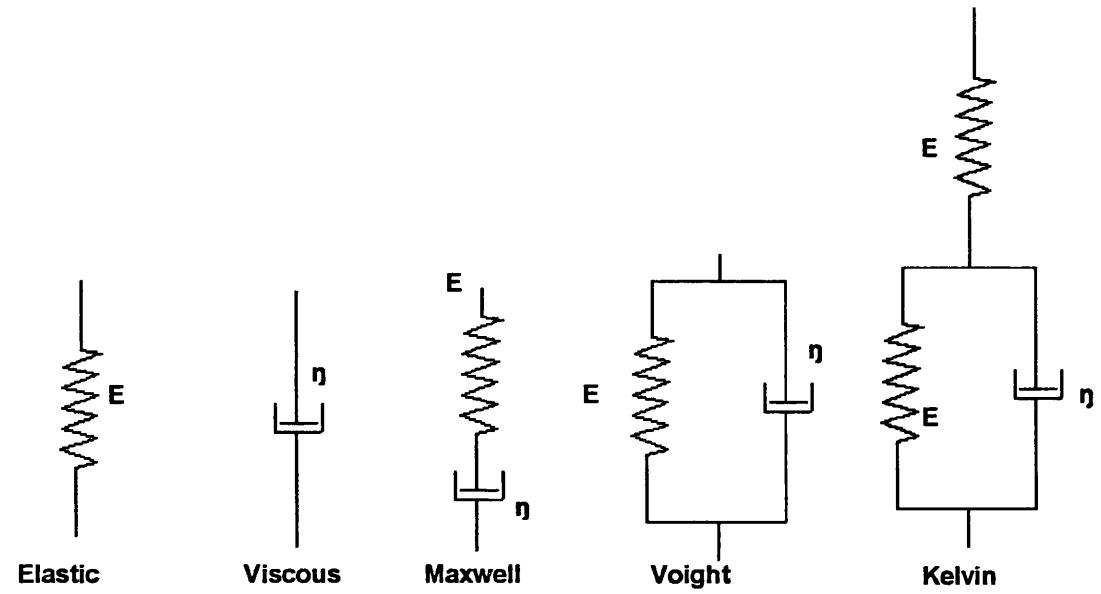

Figure 7.5. Diagrams illustrating viscoelastic models of behaviour of materials.

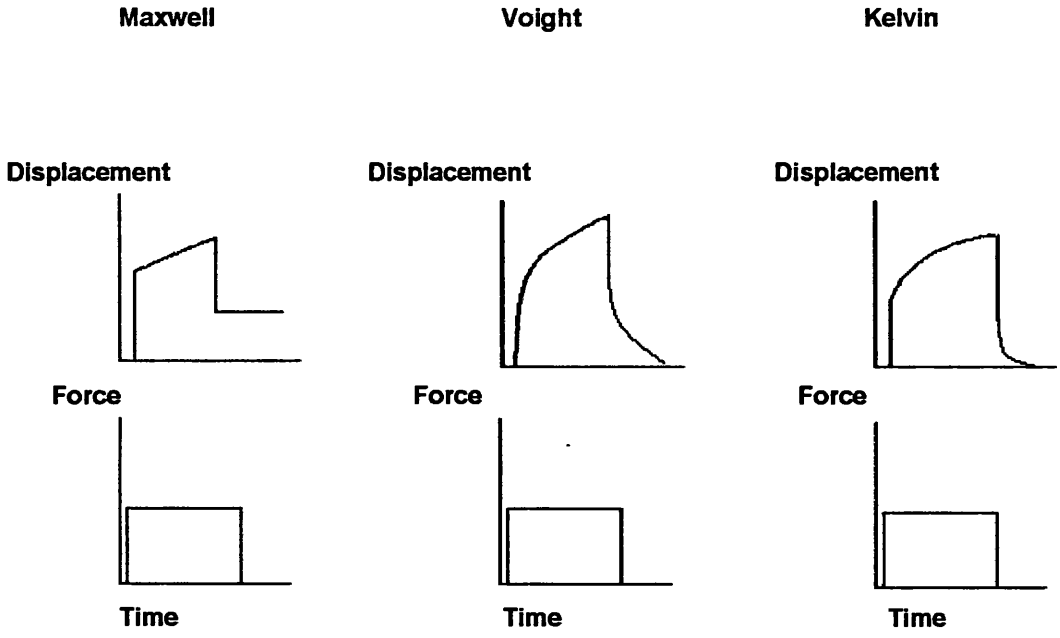

Figure 7.6. Graphs of viscoelastic models of behaviour of materials.

7.6 Summary

The Cutometer® 580 MPA, has the ability to measure the viscoelastic properties of the skin *in vivo*. Under well-controlled experimental conditions, reproducible, accurate stress-strain and strain-time curves can be obtained, which give quantitative information concerning the elastic and viscoelastic properties of the skin.

In this study similar conditions were adopted to study the viscoelastic properties of the epidermis on three different sites on the feet using a 2mm diameter aperture. The reproducibility and accuracy of the measurements were confirmed. The influence of physiological parameters such as age, sex and race were analysed. Data collected from non-diabetic subjects were compared to that of diabetic subjects in Chapter 9.

7.7 The Suitability of the Cutometer® 580 MPA for Measurement of the Physical Properties of Pedal Epidermis

7.7.1 Sites of Measurement

Measurements were taken from three sites on the left foot of each volunteer: the medial longitudinal arch (MLA); the plantar aspect of the 3rd metatarsophalangeal joint (MTPJ) and the dorsal aspect of the 3rd MTPJ (Fig. 7.7).

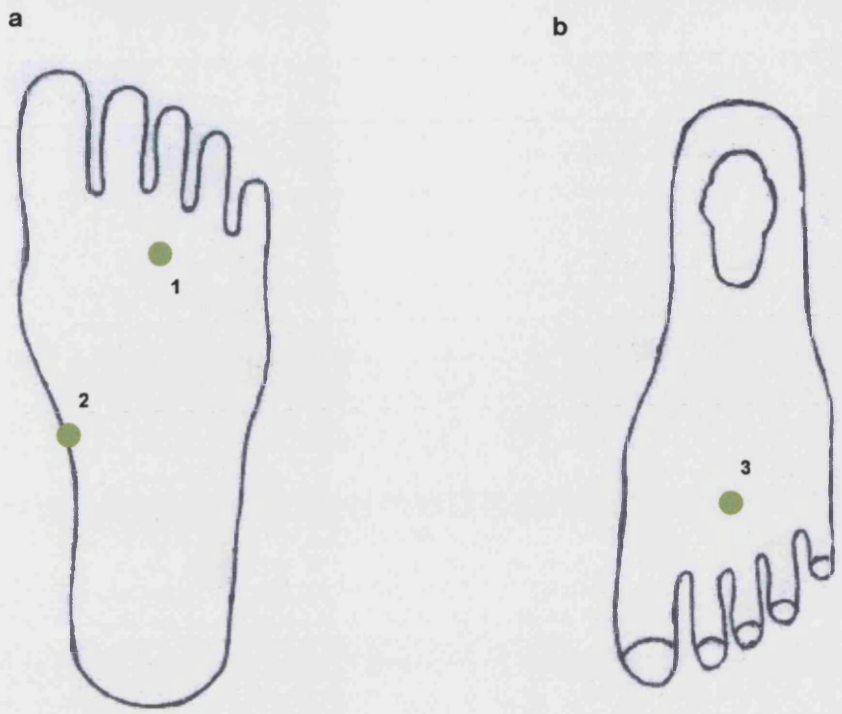

Figure 7.7. Diagram illustrating the sites used for collecting data. **a:** Plantar view of the foot **b:** Dorsal view of the foot. **1** – PMA, **2** – MLA, **3** - dorsum

7.7.2 Assessment of Equipment for a Square Wave Pressure Application

7.7.2.1 Methods

The accuracy of the epidermal displacement readings depends on the consistency of the vacuum suction pressure (square wave form). Any delays in achieving an immediate, maximum, vacuum suction will also cause a delay in the displacement readings. Pressure and displacement readings were observed on each of the three sites on 10 diabetic subjects and 10 age and sex matched controls.

Cutometer® 580 MPA settings, Mode 1:

Pressure 500 mbar
Rate 20 mbar/s
On–time 60s
Off–time 60s

7.7.2.2 Results

Two types of pressure curves were obtained. The pressure showed either an increasing or decreasing exponential 'creep' after an instantaneous change, until a new steady state of approximately 500 mbar was achieved (Fig. 7.8).

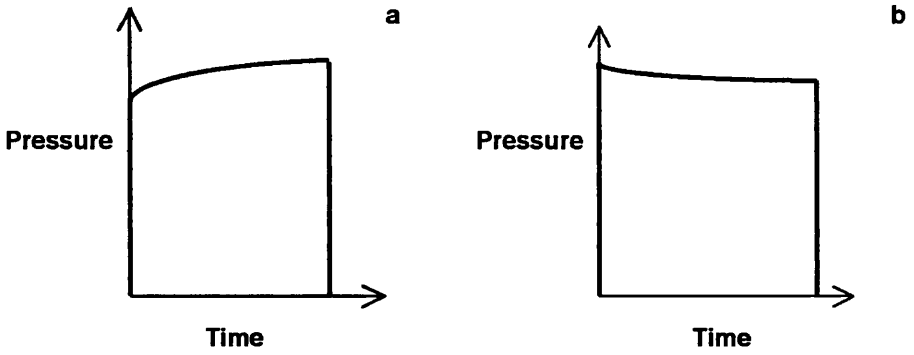

Figure 7.8: Illustration of the pressure curves. **a:** Ascending pressure curve, **b:** Descending pressure curve

Although these anomalies in the applied pressures seemed minimal it was necessary, to confirm whether they influenced significantly the displacement readings. The pressure curves were analysed as follows:

7.7.2.2.1 Ascending Pressure Curve Analysis

In this case there was an increasing creep of pressure, which would have increased the displacement values over that expected from an instantaneous extension, A_1. The pressure curve was described as:

$$P = A_1 + A_2 * (1 - \exp(-t/\tau)) \qquad 1$$

Where:

P = Pressure

A_1 = Initial pressure reading

A_2 = Pressure difference from initial reading to 60s reading

t = time

τ = time constant

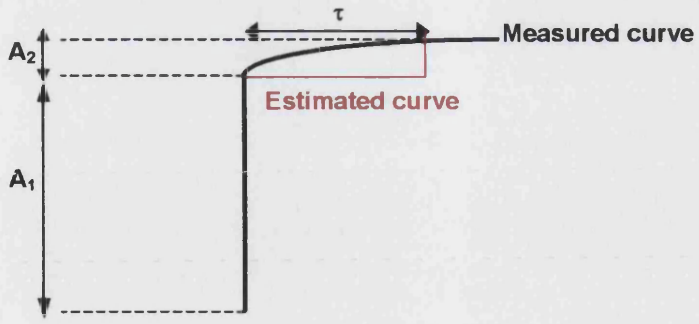

Figure 7.9. Ascending pressure curve correction

In this case displacement curve data were reduced by a factor:

$$(A_2*(1- \exp(-t/\tau)))/ A_2 \qquad 2$$

to a square wave of pressure, A_1.

7.7.2.2.2 Descending Pressure Curve

In this case there was a decreasing creep of pressure which would have decreased the displacement values over that expected from an instantaneous extension, $A_1 + A_2$. The pressure curve was described as (Fig. 7.10).

$$P = A_1 + A_2 *(\exp(-t/\tau)) \qquad 3$$

Where:

P = Pressure
A_1 = Initial pressure reading
A_2 = Pressure difference from initial reading to 60s reading
t = time
τ = time constant

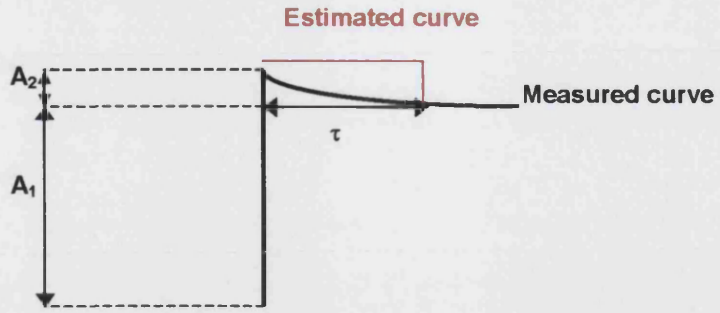

Figure 7.10. Descending pressure curve correction

In this case displacement curve data were increased by a factor:

$$(A_2 * (\exp(-t/\tau)))/(A_1 + A_2) \qquad 4$$

to a square wave of pressure $(A_1 + A_2)$.

7.7.2.2.3 Calculations and Results

Table 7.2. Percentage error for the corrected displacement curve data from the dorsal site

	Measured Displacement (μm)	Corrected Displacement (μm)	% Error
Non-diabetic subjects			
1	171	167	-2.34
2	176	173	-1.71
3	80	77	-3.75
4	152	150	-1.32
5	200	196	-2.00
6	154	153	-0.65
7	82	79	-3.66
8	109	107	-1.84
9	146	144	-1.37
10	114	111	-2.63
Diabetic subjects			
1	152	149	-1.98
2	136	132	-2.94
3	104	104	0.00
4	253	250	-1.19
5	128	126	-1.57
6	162	160	-1.24
7	270	269	-0.37
8	320	317	-0.94
9	211	207	-1.90
10	245	243	-0.82

Table 7.3. Percentage error for the corrected displacement curve data from the MLA

	Measured Displacement (μm)	Corrected Displacement (μm)	% Error
Non-diabetic subjects			
1	94	92	-2.13
2	90	87	-3.35
3	80	75	-6.25
4	16	14	-12.4
5	71	69	-2.88
6	91	87	-4.4
7	83	80	-3.61
8	95	93	-2.11
9	94	91	-3.19
10	101	99	-1.98
Diabetic subjects			
1	52	53	+1.98
2	99	97	-2.02
3	104	104	0.00
4	104	103	-0.96
5	76	74	-2.63
6	160	158	-1.25
7	200	198	-1.00
8	310	309	-0.33
9	162	162	0.00
10	213	211	-0.94

Table 7.4. Percentage error for the corrected displacement curve data from the PMA

	Measured Displacement (μm)	Corrected Displacement (μm)	% Error
Non-diabetic subjects			
1	99	96	-3.03
2	96	95	-1.04
3	132	129	-2.27
4	2	2	0.00
5	94	92	-2.13
6	25	24	-4.00
7	38	36	-5.26
8	27	25	-7.41
9	5	3	-40.00
10	39	38	-2.56
Diabetic subjects			
1	4	4	0.00
2	1	1	0.00
3	81	86	+6.17
4	4	4	0.00
5	28	31	+9.68
6	63	62	-1.59
7	80	78	-2.5
8	270	268	-0.74
9	167	166	-0.60
10	142	142	0.00

In general the magnitudes of the creeps were proportionately small compared to the instantaneous changes in pressure. Of the 60 pressure curves, 57 demonstrated ascending creeps and 3 had descending creeps after the instantaneous pressure changes. In the determinations of the ascending creeps the proportion of A1/A2 was 0.03 ± 0.06 (n=57) and for descending creeps was 0.06 ± 0.04 (n=3). The percentage error between the measured displacement data and the corrected data were calculated as being 1.71 ± 1.00 for the dorsal site; 2.47 ± 2.95 for the MLA and 2.86 ± 3.73 for the PMA (Tables 7.2-7.4).

7.7.3 Assessment of the Elastic Behaviour of the Epidermis

A Hookian elastic solid is a solid that obeys Hooke's Law, which states that the stress is linearly proportional to the strain. The following experiments examined the elastic behaviour of the epidermis on the foot. Stress–strain curves were compiled to confirm or refute the tissues elastic behaviour.

7.7.3.1 Methods

Data were collected from each of the three sites from 10 subjects. At each site a series of displacement curves were generated at pressures of 100, 200, 300, 400 and 500 mbar.

Stress–strain curves were generated by plotting the maximum displacement readings against pressure.

7.7.3.2 Results

The stress-strain curves for all 10 subjects were linear (Tables 7.5-77, Figs. 7.11-7.13), with r values between 0.29 and 0.98, mean r=0.85 0.15. The values for the displacement at 500 mbar were calculated from the slope of the graphs and compared to the measured displacement readings at 500 mbar (Tables 7.7-7.10).

Table 7.5. Displacement readings from the dorsum of the foot at different pressure settings.

Subject	Displacement @ 100mbar (µm)	Displacement @ 200mbar (µm)	Displacement @ 300mbar (µm)	Displacement @ 400mbar (µm)	Displacement @ 500mbar (µm)
1	31	30	69	62	90
2	46	55	103	95	90
3	10	30	40	60	142
4	20	40	60	90	86
5	20	40	60	90	86
6	30	70	90	120	113
7	32	79	122	102	104
8	100	175	198	205	254
9	25	50	60	120	150
10	46	50	78	100	201

Table 7.6. Displacement readings from the MLA of the foot at different pressure settings.

Subject	Displacement @ 100mbar (µm)	Displacement @ 200mbar (µm)	Displacement @ 300mbar (µm)	Displacement @ 400mbar (µm)	Displacement @ 500mbar (µm)
1	25	31	64	48	50
2	20	30	30	30	58
3	10	0	10	20	27
4	10	20	40	40	39
5	10	20	40	40	39
6	10	20	90	90	70
7	50	20	40	40	88
8	75	100	150	220	240
9	43	60	76	80	110
10	41	72	70	72	85

Table 7.7. Displacement readings from the PMA of the foot at different pressure settings.

Subject	Displacement @ 100mbar (µm)	Displacement @ 200mbar (µm)	Displacement @ 300mbar (µm)	Displacement @ 400mbar (µm)	Displacement @ 500mbar (µm)
1	10	45	87	89	93
2	20	50	90	90	81
3	7	13	14	29	13
4	10	47	60	41	59
5	10	47	60	41	59
6	10	47	60	41	59
7	20	40	40	60	81
8	53	55	60	80	82
9	18	32	30	60	70
10	0	0	10	10	20

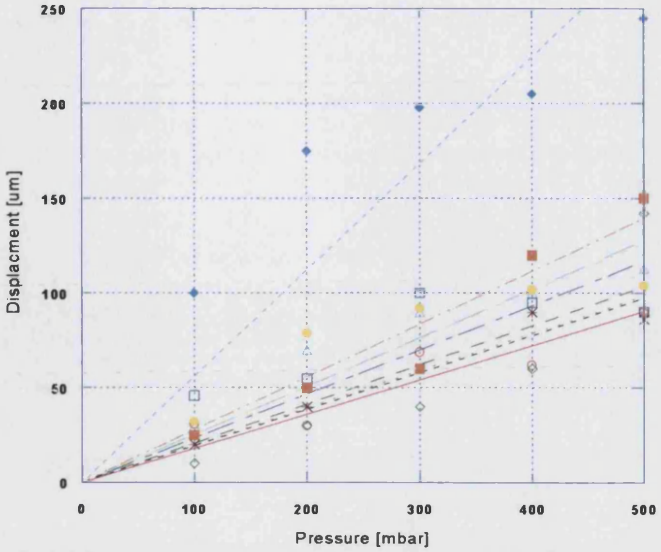

Figure 7.11. Maximum displacement readings from the dorsum of the foot at different pressure settings.

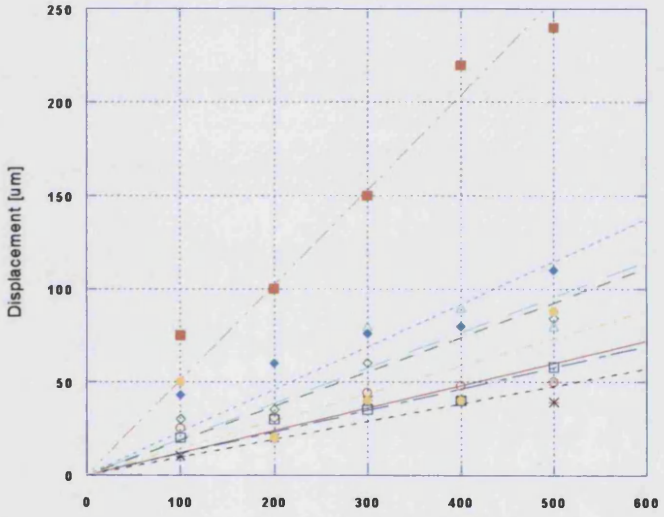

Figure 7.12. Maximum displacement readings from the PMA of the foot at different pressure settings.

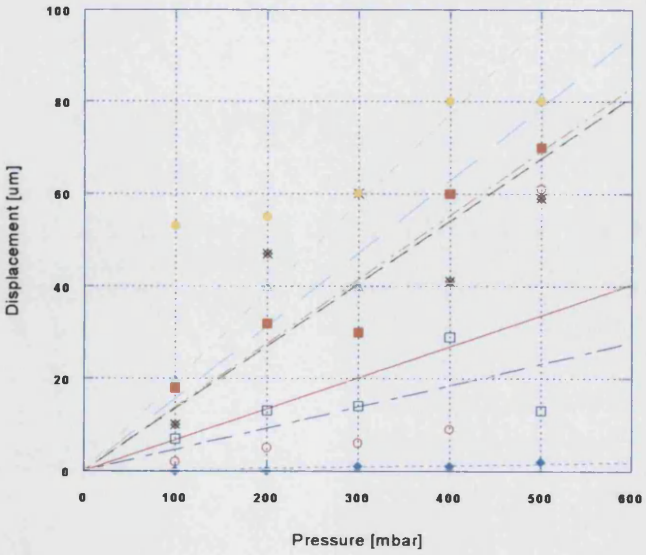

Figure 7.13. Maximum displacement readings from the PMA of the foot at different pressure settings.

These single values calculated at 500 mbar were representative of the stress-strain portion of the curves, therefore any deviation of the measured reading at 500 mbar from the line curve, is representative of the deviation from elastic behaviour. The difference between the measured reading and estimated displacement at 500 mbar was minimal (Tables 7.8-7.10).

Table 7.8. Values calculated for the gradient of the slope taken from the dorsum of the foot.

Subject	Estimated displacement reading at 500 mbar	R value	Displacement reading at 500 mbar
1	0.09	0.92	0.09
2	0.12	0.86	0.09
3	0.10	0.91	0.14
4	0.10	0.96	0.09
5	0.10	0.97	0.09
6	0.14	0.96	0.11
7	0.14	0.89	0.10
8	0.29	0.94	0.25
9	0.14	0.97	0.15
10	0.16	0.91	0.20
	Mean±SD = 0.14±0.06		**Mean±SD = 0.13±0.06**

Table 7.9. Values calculated for the gradient of the slope taken from the MLA of the foot.

Subject	Estimated displacement reading at 500 mbar	R value	Displacement reading at 500 mbar
1	0.05	0.96	0.06
2	0.07	0.84	0.05
3	0.09	0.97	0.08
4	0.05	0.88	0.04
5	0.05	0.88	0.04
6	0.09	0.87	0.07
7	0.07	0.61	0.09
8	0.26	0.98	0.24
9	0.11	0.98	0.11
10	0.10	0.88	0.09
	Mean±SD = 0.09±0.06		Mean±SD = 0.09±0.06

Table 7.10 Values calculated for the gradient of the slope taken from the PMA of the foot.

Subject	Estimated displacement reading at 500 mbar	R value	Displacement reading at 500 mbar
1	0.05	0.77	0.06
2	0.04	0.54	0.06
3	0.02	0.72	0.01
4	0.07	0.72	0.06
5	0.07	0.72	0.06
6	0.07	0.97	0.06
7	0.08	0.93	0.08
8	0.10	0.29	0.24
9	0.07	0.94	0.07
10	0.002	0.89	0.002
	Mean±SD = 0.06±0.03		Mean±SD =0.07±0.06

7.7.4 Standardisation of Methods

7.7.4.1 Aims

- To determine the appropriate body and foot position that the volunteer should be placed in with minimal variation in readings.
- To test the machine for repeatability of data collection at the same site of skin.
- To test the effects of pretension on the epidermis on the data.

7.7.4.2 Methods

Three healthy (non-diabetic) volunteers with no foot or skin pathologies were used for this set of experiments. The three sites on the foot were marked carefully and the volunteer lay in a supine position on the bed for 15 min before readings were taken. The probe was applied perpendicular to the skin for every reading and care was taken not to apply any external pressure. Double-sided tape was used to keep the probe in position. The room temperature and humidity was noted at the time the readings were taken.

7.7.4.2.1 Standardisation of Body and Foot Position

Ranges of different body and foot positions, in different combinations, were selected (Table 7.11) and readings were taken from the three sites in each position.

Table 7.11. Description of the body positions when taking measurements.

Body Position	Foot Position
Sitting	Relaxed position
	Sub-talar joint neutral
Lying supine	Relaxed position
	Sub-talar joint neutral
Lying prone knee extended	Relaxed position
	Sub-talar joint neutral

7.7.4.2.1.1 Results

Table 7.12. Relationship between body position and skin displacement in specific sites on the foot. Subject 1.

		Maximum Displacement of Epidermis (μm) using negative pressure of 500 mbar		
Body Position	**Foot Position**	**PMA**	**MLA**	**Dorsum**
Sitting	Relaxed position	40	90	230
	Sub-talar joint neutral	40	80	200
Lying supine	Relaxed position	20	80	260
	Sub-talar joint neutral	20	70	190
Lying prone knee extended	Relaxed position	10	70	100
	Sub-talar joint neutral	10	60	720
	Mean ± SD	**23.3 ± 13.7**	**75±10.5**	**283.3 ± 220.6**

Table 7.13. Relationship between body position and skin displacement in specific sites on the foot. Subject 2.

		Maximum Displacement of Epidermis (μm) using negative pressure of 500 mbar		
Body Position	**Foot Position**	**PMA**	**MLA**	**Dorsum**
Sitting	Relaxed position	12	24	52
	Sub-talar joint neutral	10	23	41
Lying supine	Relaxed position	10	21	70
	Sub-talar joint neutral	10	20	40
Lying prone knee extended	Relaxed position	10	25	30
	Sub-talar joint neutral	10	20	80
	Mean ± SD	**10.3± 0.8**	**22.2 ±2.1**	**52.2± 19.3**

Table 7.14. Relationship between body position and skin displacement in specific sites on the foot. Subject 3

		Maximum Displacement of Epidermis (μm) using a negative pressure of 500 mbar		
Body Position	**Foot Position**	**PMA**	**MLA**	**Dorsum**
Sitting	Relaxed position	130	80	60
	Sub-talar joint neutral	120	80	80
Lying supine	Relaxed position	120	85	120
	Sub-talar joint neutral	110	70	75
Lying prone knee extended	Relaxed position	100	70	50
	Sub-talar joint neutral	100	60	120
	Mean ± SD	**113.3±12.1**	**74.2±9.2**	**84.2± 29.7**

Table 7.15. The comparison of data collected in different body positions using independent t-test, p values quoted.

	Subject	**PMA**	**MLA**	**Dorsum**
Sitting v lying	1	0.004	0.094	0.647
	2	0.178	0.331	0.664
	3	0.088	0.321	0.472
Prone v supine	1	-	0.293	0.613
	2	-	0.515	-
	3	0.095	0.30	0.792
STJ neutral v STJ relaxed	1	-	0.288	0.394
	2	0.374	0.210	0.872
	3	0.561	0.365	0.596

There was no statistical significant difference in the data between subjects 1 and 2 ($p>0.05$). However, the data from subject 3 was significantly different from subjects 1 and 2. Therefore, the data could not be grouped together for analysis.

To test for difference in the data as a result of different body positions, independent t tests were performed (Table 7.15). There was no significant difference between readings taken when the volunteers were sitting and lying. There were also no marked differences between prone and supine positions in each of the subjects. The sitting body position was chosen, as many of the potential volunteers for the main study would be elderly. This position did prove to be the most comfortable for the patients. There was no statistically significant difference between the relaxed and sub-talar joint neutral positions when the subjects were lying or sitting. However, the standard deviation from the mean of

the data from the dorsal site when the two different positions were adopted was high (Tables 7.12 – 7.14). Clinical biomechanical observations show that, when the foot is placed in a relaxed position on a surface, the shape and positioning of the foot differs greatly from person to person. When the foot is placed in a standard sub-talar joint neutral position, this variation is minimal. Therefore, a standard, neutral foot position for all volunteers was chosen.

7.7.4.2.2 Assessing the Variability in Readings between Sites

Once standard body and foot positions were identified, the next step was to test the variation in readings from different sections of skin on the same site. Three readings were taking on different sections of skin and compared (Fig. 7.14).

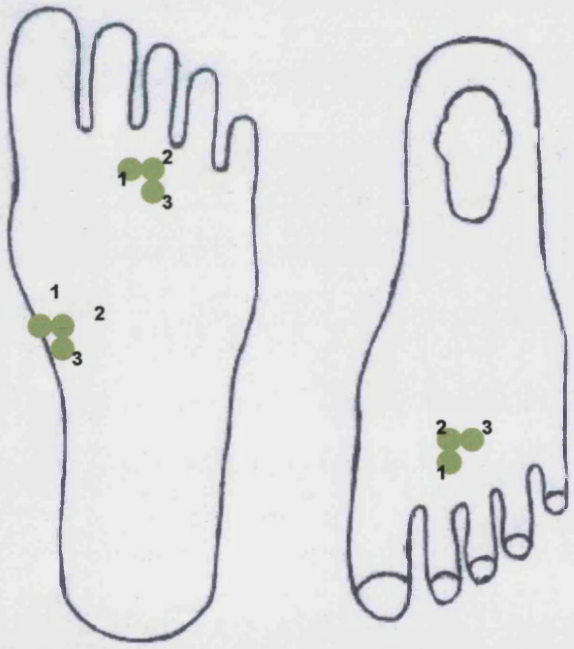

Figure 7.14. Illustration of the points measured on each site of the foot.

7.7.4.2.2.1 Results

The results showed minimal differences between adjacent regions on a particular site of the skin (Table 7.16-7.18). In the main study the three sites were marked according to specific anatomical positions. These results allow the measurements to be taken with confidence even if the probe deviates slightly from the marked position.

Table 7.16. Variability between sites when subject is in the sitting position with the foot in STJ neutral position. Subject 1

		Displacement of Epidermis (µm)	Coefficient of Variation (%)
PMA	**Site 1**	15	6.3
	Site 2	20	
	Site 3	18	
MLA	**Site 1**	98	12.3
	Site 2	102	
	Site 3	105	
Dorsum	**Site 1**	200	33.3
	Site 2	200	
	Site 3	210	

Table 7.17. Variability between sites when subject is in the sitting position with the foot in STJ neutral position. Subject 2

		Displacement of Epidermis (µm)	Coefficient of Variation (%)
PMA	**Site 1**	10	0
	Site 2	10	
	Site 3	10	
MLA	**Site 1**	23	0.3
	Site 2	24	
	Site 3	23	
Dorsum	**Site 1**	42	1.3
	Site 2	44	
	Site 3	44	

Table 7.18. Variability between sites when subject is in the sitting position with the foot in STJ neutral position. Subject 3

		Displacement of Epidermis (µm)	Coefficient of Variation (%)
PMA	**Site 1**	117	6.3
	Site 2	120	
	Site 3	115	
MLA	**Site 1**	98	6.3
	Site 2	100	
	Site 3	95	
Dorsum	**Site 1**	83	6.3
	Site 2	85	
	Site 3	80	

7.7.4.2.3 Testing the Effect of Pretension of Skin

In this case two points adjacent to each other were marked on the measurement site. The first area was not subjected to skin pretension and the second was (0.1s). Three consecutive readings were taken from each point and the results were compared.

7.7.4.2.3.1 Result

These results showed that pretension did not have a significant effect on the data collection, therefore in future experiments pretension was not used (Table 7.9-7.11).

Table 7.19. Comparing epidermal displacement with and without pretension. Subject 1

		Displacement of Epidermis without pretension (μm)	Displacement of Epidermis with pretension (μm)	Paired t-test p value
PMA	**Site 1**	15	15	0.423
	Site 2	20	21	
	Site 3	18	18	
MLA	**Site 1**	98	98	0.423
	Site 2	102	105	
	Site 3	105	105	
Dorsum	**Site 1**	200	200	-
	Site 2	200	200	
	Site 3	210	210	

Table 7.20. Comparing epidermal displacement with and without pretension. Subject 2

		Displacement of Epidermis without pretension(μm)	Displacement of Epidermis with pretension(μm)	Paired t-test p value
PMA	**Site 1**	10	10	-
	Site 2	10	10	
	Site 3	10	10	
MLA	**Site 1**	23	20	0.184
	Site 2	24	21	
	Site 3	23	23	
Dorsum	**Site 1**	42	42	0.423
	Site 2	44	40	
	Site 3	44	44	

Table 7.21. Comparing epidermal displacement with and without pretension. Subject 3

		Displacement of Epidermis without pretension(μm)	Displacement of Epidermis with pretension(μm)	Paired t-test p value
PMA	**Site 1**	117	110	0.423
	Site 2	120	120	
	Site 3	115	115	
MLA	**Site 1**	98	98	0.423
	Site 2	100	99	
	Site 3	95	95	
Dorsum	**Site 1**	83	84	0.225
	Site 2	85	87	
	Site 3	80	80	

7.7.4.2.4 Testing whether 1hr is enough for the Skin to lose its "Elastic Memory"

This was carried out on each of the three sites on the foot. Three consecutive readings were taken from each site and then the subject was asked to lie in a resting position (prone). After 1hr readings were taken from each site and the data was compared to that of the initial data set.

7.7.4.2.4.1 Results

Table 7.22. Subject 1

		Initial Displacement of Epidermis (μm)	Displacement of Epidermis after 1hr (μm)	p value
PMA	**Site 1**	16	16	0.423
	Site 2	19	18	
	Site 3	18	18	
MLA	**Site 1**	98	97	0.074
	Site 2	102	100	
	Site 3	103	100	
Dorsum	**Site 1**	200	200	
	Site 2	200	200	
	Site 3	210	210	

Table 7.23. Subject 2

		Initial Displacement of Epidermis (μm)	Displacement of Epidermis after 1hr (μm)	p value
PMA	**Site 1**	10	10	0.423
	Site 2	9	10	
	Site 3	10	10	
MLA	**Site 1**	23	20	0.423
	Site 2	24	24	
	Site 3	23	23	
Dorsum	**Site 1**	42	42	0.184
	Site 2	44	40	
	Site 3	44	40	

Table 7.24. Subject 3

		Initial Displacement of Epidermis (μm)	Displacement of Epidermis after 1hr (μm)	p value
PMA	**Site 1**	117	110	0.195
	Site 2	120	120	
	Site 3	115	110	
MLA	**Site 1**	98	90	0.204
	Site 2	100	100	
	Site 3	95	90	
Dorsum	**Site 1**	83	80	0.208
	Site 2	85	80	
	Site 3	80	80	

These results confirm that the skin on the foot did not remain distended 1 h after measurements were taken. When repeated measurements were to be taken in the main experiment, 1 h was left between taking the readings.

7.8 Analysis of the Viscoelastic Properties of Pedal Epidermis

Graphical representation of all the data favoured the Kelvin model of viscoelasticity (Fig. 7.15). The first section of each graph describes the series elastic component (a instantaneous function) on stretching of the tissue. The second section depicts an exponential function, which describes the viscous properties and the parallel elastic element. The time constant of this curve describes the viscoelasticity properties. The third section describes the series elastic component on retraction and the final portion of the graph the exponential viscoelastic component of retraction. The tissue studied also exhibited plasticity, i.e. the displacement did not return to zero when the displacing force is removed.

To test that the curves fitted the Kelvin model, a sub group of data were selected, from 15 subjects, and the curves fitted to an exponential curve only (Voight model) and a step plus exponential (Kelvin model) and the curves were compared (Equation 5 and 6).

$$y = A_1 + A_2*(1 - \exp -t/\tau) \qquad 5$$

Kelvin Model

$$y = A_2*(1 - \exp -t/\tau) \qquad 6$$

Voight Model

A_1 = Instantaneous displacement reading

A_2 = Amplitude of the time-dependent (viscoelastic) component

t = time

τ = time constant

All the curves that were fitted using equation 5 (Kelvin model) demonstrated a better fit. Therefore, the Kelvin model of analysis was appropriate for the analysis of epidermal viscoelasticity for all future data analyses.

The series elastic element of the rising and declining portion of the displacement-time curves was expressed as magnitude of the stretch (μm). At the end of the series elastic phase, the time constants of the viscoelastic components of the curves were calculated (Fig. 7.16 & 7.17). The majority of the curves did not return to zero by the end of the run time, suggesting plastic behaviour of the skin. The plasticity was expressed as the ratio of final displacement at 120s to maximum displacement at 60s (Fig. 718).

a.

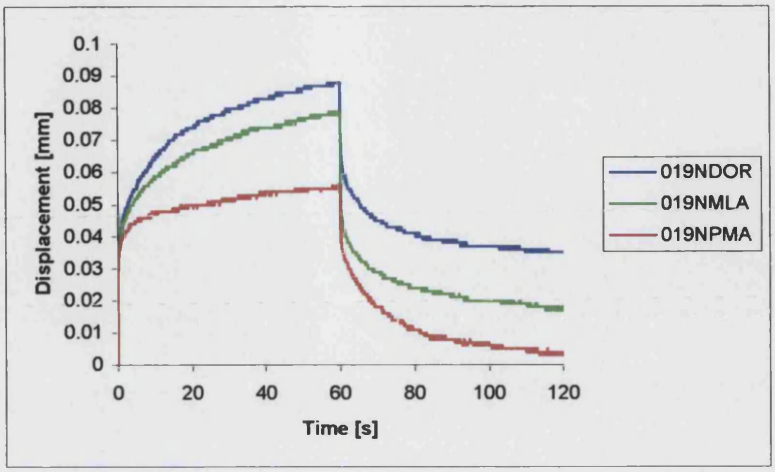

b.

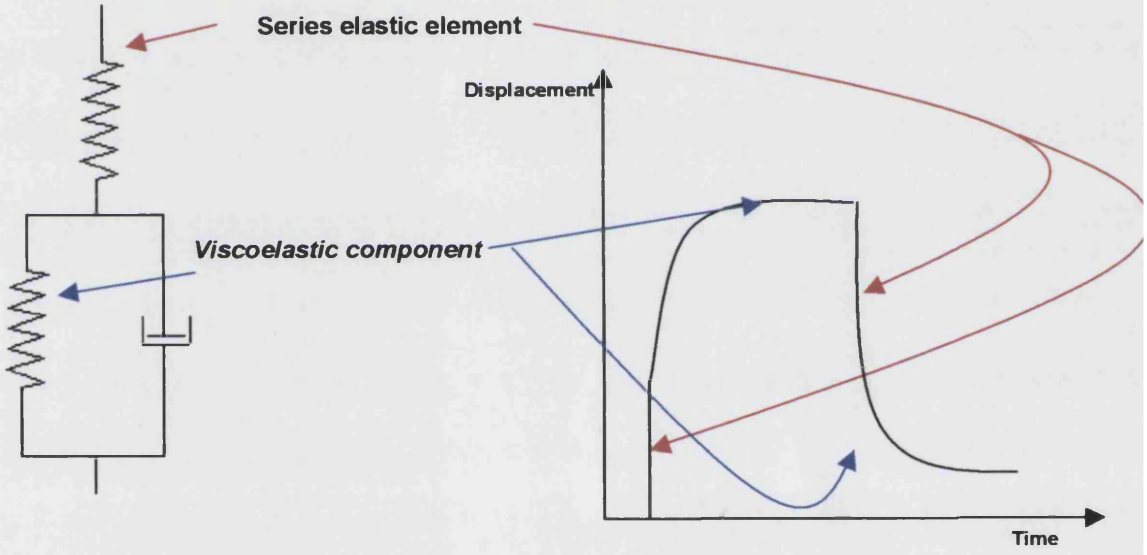

Figure 7.15. a. Examples of the curves obtained from the dorsum, MLA and PMA sites of the foot from a non-diabetic subject. **b.** Illustration of the Kelvin model of viscoelasticity

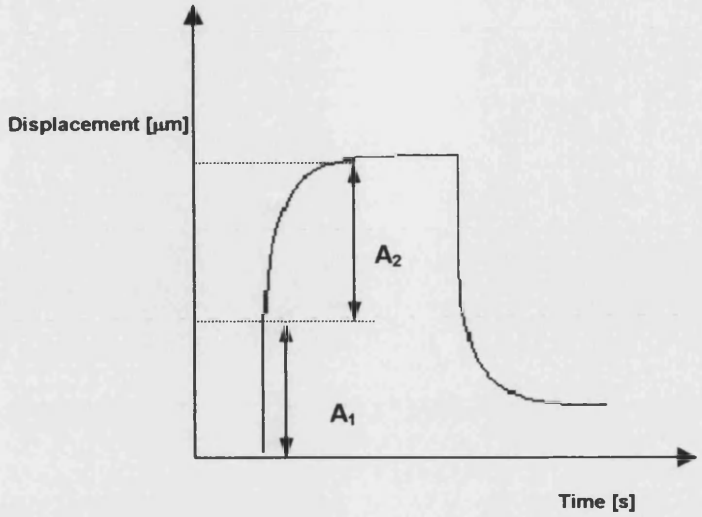

Figure 7.16. Diagram explaining the calculation of the series elastic element and the time constant on the rising portion of the displacement-time curves.

Series elastic element for the rising phase of the curve: A_1

Time constant calculation for the rising phase of the curve:

$$y = A_2 (1 - (\exp -t/\tau)) \qquad 6$$

Where: A_2=distance between the end of the elastic stretch and the displacement at 60s, t=time and τ=time constant.

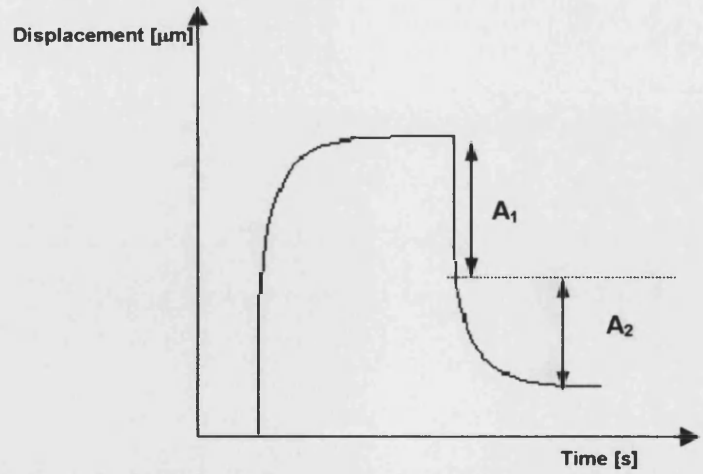

Figure 7.17. Diagram explaining the calculation of the series elastic element and the time constant on the falling portion of the displacement-time curves.

Series elastic element for the rising phase of the curve: A_1

Time constant for the declining phase of the curve:

$$y = A_2 * (\exp(-t/\tau)) \qquad 7$$

Where: A_2=distance between the end of the elastic stretch and the displacement at 60s, t=time and τ=time constant).

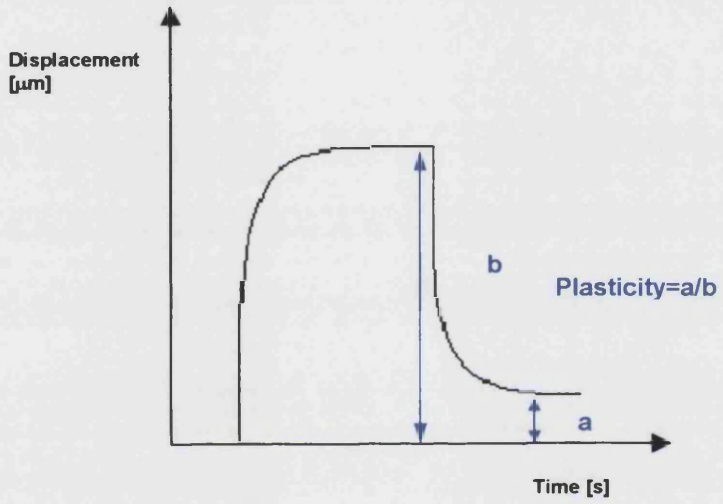

Figure 7.18. Diagram explaining the plasticity calculation. The higher the ratio, the more plastic the tissue.

Plasticity: = a/b

Where a = displacement at 120s
b = displacement at 60s

7.8.1 Closer Analysis of the Descending Portion of the Displacement -Time Curves

There were two possible explanations for the difference in appearance of the first and second portions of the graphs: (1) the tissue was permanently deformed as a direct result of the application of pressure, or (2) the tissue exhibited plastic behaviour. The former is not the case. The plasticity of the tissue is demonstrated

by the gradual return to its original position. The energy required for stretching the tissue (kinetic energy) is stored in the elastic elements (potential energy) and released (kinetic energy) gradually during retraction, as the structural components of the tissue realign with each other. The device had its limitations, as the maximum time for data collection was 120 s, which was not sufficient for monitoring the return of the tissue to its original state.

There was no significant difference between the magnitudes of immediate stretch and immediate retraction (Table 7.25).

Table 7.25. Comparisons between the immediate stretch and immediate retraction data from the three sites on the foot (n=10).

Dorsum Elastic Portion (µm)			MLA Elastic Portion (µm)			PMA Elastic Portion (µm)		
Rising	**Falling**	**p value**	**Rising**	**Falling**	**p value**	**Rising**	**Falling**	**p value**
52.5±21.5	49.0± 15.2	0.578	43.0± 39.5	4.0 ± 25.4	0.616	26.0± 17.8	24.5± 20.6	0.678

7.8 Summary

This set of experiments have shown that the Cutometer® 580 MPA is an appropriate device for the initial investigation of the elastic and the viscoelastic properties of pedal epidermis, *in vivo*[ℵ]. The device is not free of error, however, when taking displacement readings. These errors in the pressure application and subsequent displacement readings, although minimal, were acknowledged when analysing the data in the main study (section 7.11 and chapter 10). This resulted in the delay in the suction readings by a fraction of a second. The environmental conditions, the positioning of the skin site and the use of the measuring probe were all essential features that were standardised.

The following is a presentation of data collected from the three foot sites of 87 healthy volunteers. The time-displacement curves were generated and the elastic and viscoelastic qualities of the epidermis were analysed.

[ℵ] *In vitro* two-dimensional analysis of the mechanical properties plantar callus tissue was attempted, but was not successful (Appendix X).

7.10 Analysis of the Elastic and Viscoelastic Properties of the Epidermis from Different Sites of the Foot in Healthy Volunteers

7.10.1 Aims

- To generate and compare data from all three sites of the feet of 87 healthy volunteers.
- To compare the data between different sites, sexes, ages and races

7.10.2 Methods

The data were collected from the left foot of each of 87 healthy volunteers, in a sitting position, with the foot in subtalar joint neutral (the recruitment process is described in detail in Chapter 9). Before the readings were taken the volunteer lay in a supine position on the bed for approximately 15min. All volunteers were seen in the morning between 9am and 12noon. Readings were collected from the three sites, already identified. The probe was applied perpendicular to the skin for every reading and care was taken not to apply any external pressure. The room temperature and humidity was noted for every set of readings taken.

7.10.3 Results

The room temperature ranged between 21-25°C and the humidity of the environment was between 31-50%. The elasticity of the series elastic element; the time constant and plasticity (explained in section 7.8) were calculated for the three foot sites from all the volunteers.

7.10.4 Statistical Analysis of Data Collected from 87 Non-Diabetic Subjects

A full explanation of the recruitment of patients is described in detail in Chapter 9, along with the comparison of data between the diabetic and non-diabetic groups.

7.10.4.1 Distribution of Data

The distribution of the data was skewed and covered a broad range of readings (Appendix XIV). All the data was analysed using non-parametric statistical analyses, mainly the Mann-Whitney test and the Spearman correlation.

7.10.4.2 Data Analysis

7.10.4.2.1 The Series Elastic Element and the Time Constant (Viscoelastic Component) on Stretching and Retraction of the Epidermis on all Three Sites of the Foot.

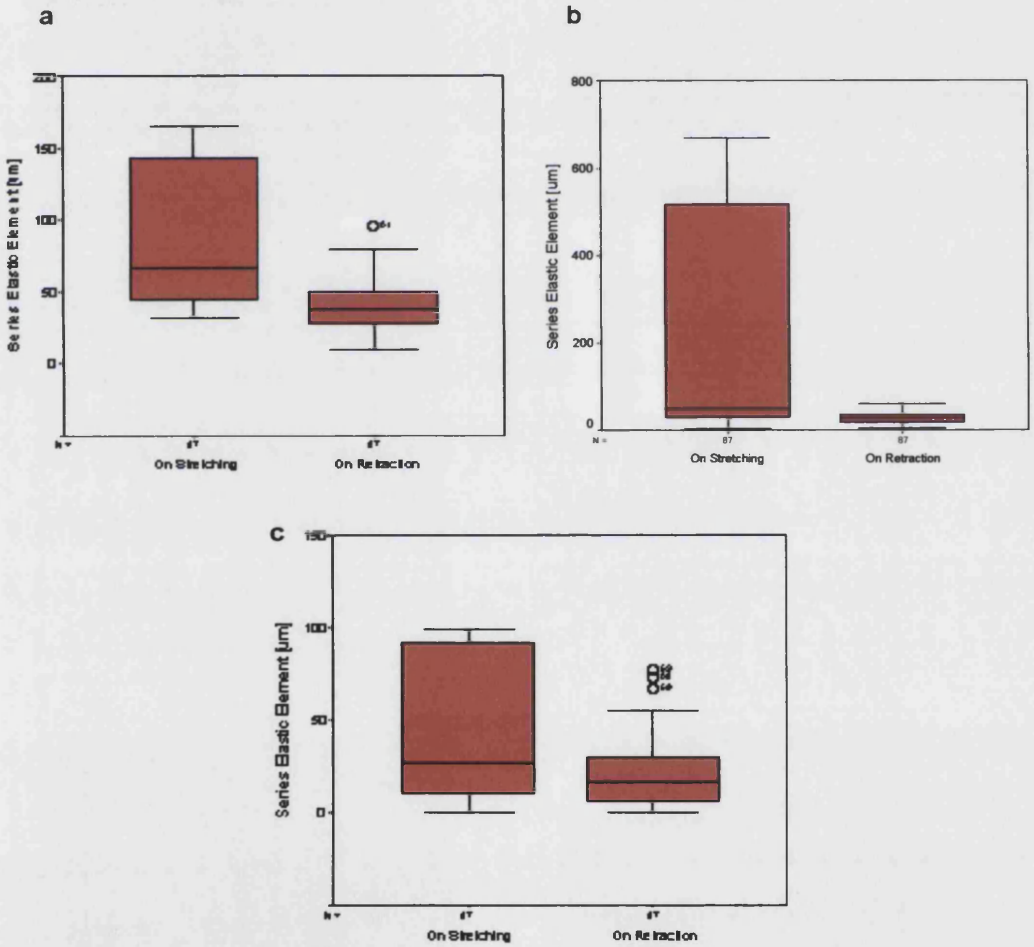

Figure 7.19. A comparison between the series elastic element data on stretching and on retraction. **a.** Dorsum **b.** MLA **c.** PMA

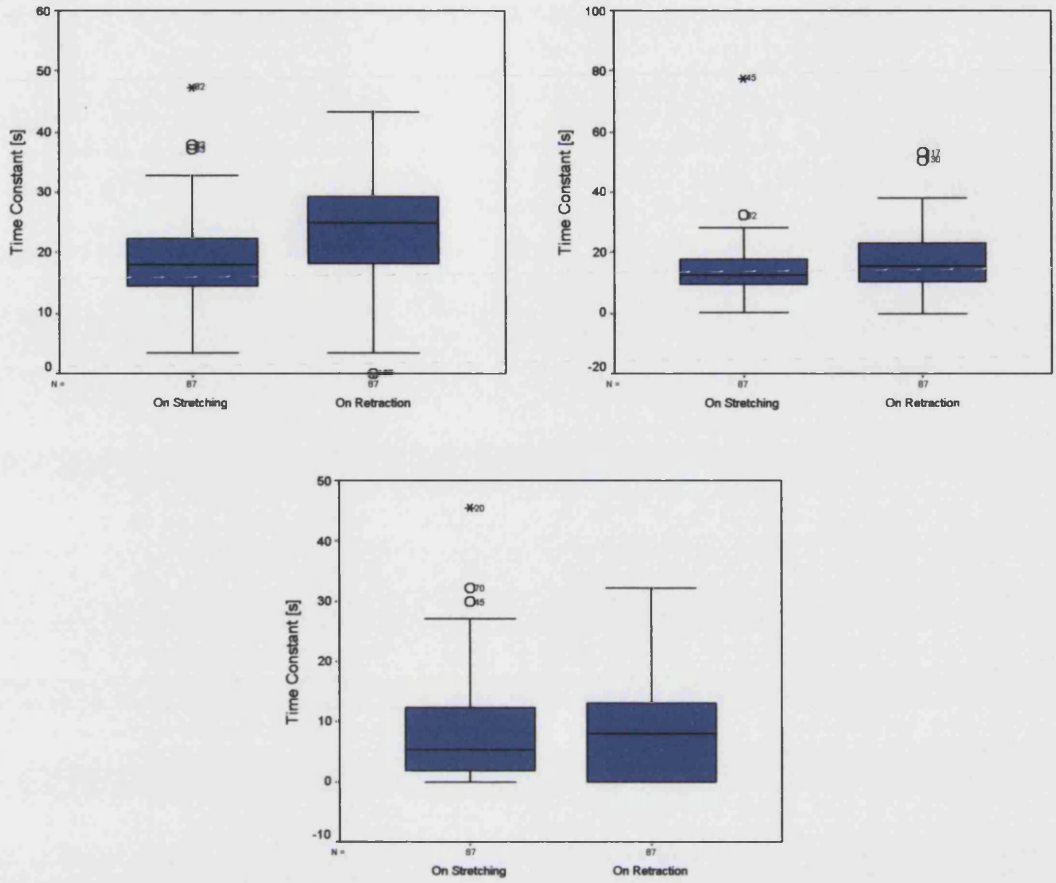

Figure 7.20. A comparison between the time constant data on stretching and on retraction. **a.** Dorsum **b.** MLA **c.** PMA

There was a significant difference between the series elastic element of stretching and on retraction of the epidermis on all sites on the foot (p=0.001). There was a significant difference in the time constants on stretching and retraction on the dorsal epidermis (p=0.001) only and not on the MLA and PMA skin sites.

Table 7.26. Descriptive data for the Series elastic element and time constant data collected from three sites on the feet.

		Dorsum	MLA	PMA
Series Elastic Element on Stretching [μm]	Median	67	47	26
	Interquartile Range	121	489	89
	Minimum	31	2	0
	Maximum	671	671	607
Series Elastic Element of Retraction [μm]	Median	38	27	17
	Interquartile Range	22	20	24
	Minimum	10	4	0
	Maximum	120	61	319
Time constant on Stretching [s]	Median	18.1	12.5	5.3
	Interquartile Range	8.1	8.4	10.9
	Minimum	3.3	0.2	0.0
	Maximum	47.3	77.5	45.4
Time Constant on Retraction [s]	Median	24.9	15.6	7.9
	Interquartile Range	11.1	13.1	13.1
	Minimum	0.0	0.0	0.0
	Maximum	43.4	53.0	32.2

All the indices of elasticity were significantly different from site to site on the feet (p=0.01). The series elastic components, time constants and plasticity (Fig. 7.21) were the greatest on the dorsal site, followed by the MLA and then the PMA.

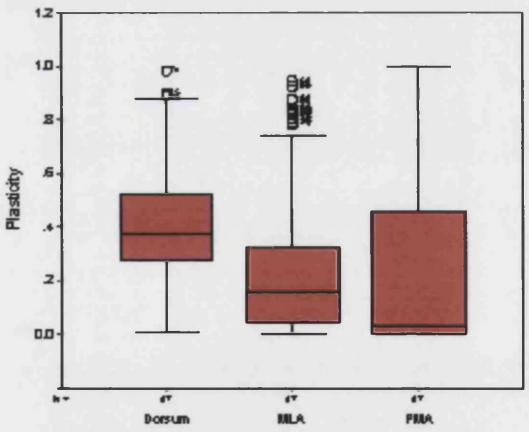

Dorsum
Median: 0.374
Interquartile range: 0.264
Minimum: 0.012
Maximum: 0.979

MLA
Median: 0.191
Interquartile range: 0.282
Minimum: 0.000
Maximum: 0.94

PMA
Median: 0.031
Interquartile range: 0.500
Minimum: 0.000
Maximum: 1.000

Mann-Whitney Test

Dorsum v MLA: p = 0.001

Dorsum V PMA: p = 0.001

MLA v PMA: p = 0.001

Figure 7.21. The relationship between the three sites of the foot and the plasticity of the epidermis.

7.10.4.2.2 The Relationship between Age and the Mechanical Properties of the Pedal Epidermis.

7.10.4.2.2.1.1 The Series Elastic Element on Stretching

There was no correlation between the age of the subjects and the elasticity. No significant difference was noted between the 2 age groups on all three sites (Figs. 7.22-7.24).

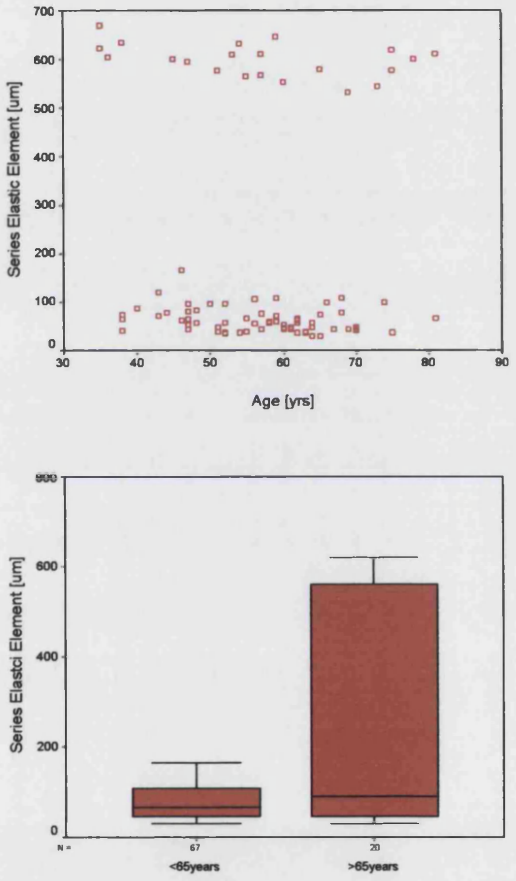

Spearman Correlation
r=0.124

Age group <65 years n=67
Median: 64.0 µm
Interquartile range: 64.0 µm
Minimum: 31.0 µm
Maximum: 671.0 µm

Age group ≥65 years n=20
Median: 89.5 µm
Interquartile range: 523.8 µm
Minimum: 31.0 µm
Maximum: 620 µm

Mann-Whitney Test
p=0.414

Figure 7.22. The relationship between age and the series elastic element on stretching of the epidermis on the dorsum.

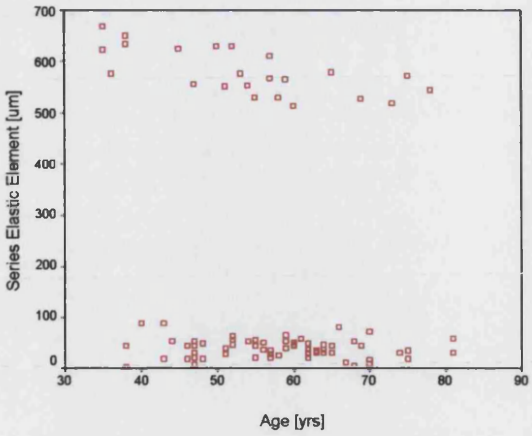

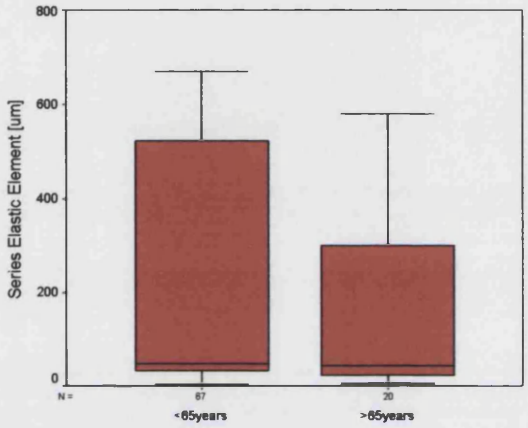

Spearman Correlation
r=-0.042

Age group <65 years n=67
Median: 48.0 µm
Interquartile range: 499.0 µm
Minimum: 2.0 µm
Maximum: 671.0 µm

Age group ≥65 years n=20
Median: 43.0 µm
Interquartile range: 338.5 µm
Minimum: 4.0 µm
Maximum: 580.0 µm

Mann-Whitney Test
p=0.315

Figure 7.23. The relationship between age and the series elastic element on stretching of the epidermis of the MLA.

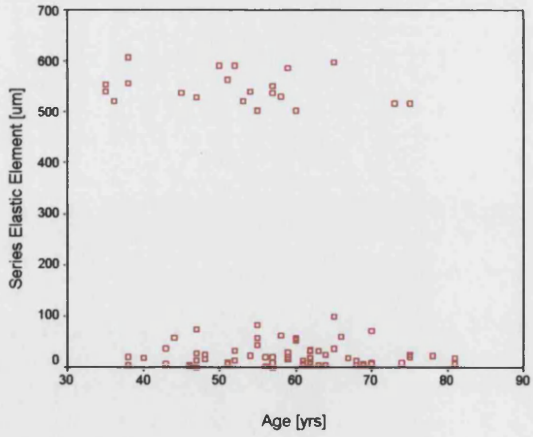

Spearman Correlation
r=-0.114

Age group <65 years n=67
Median: 30.0 µm
Interquartile range: 493.0 µm
Minimum: 0.0 µm
Maximum: 607.0 µm

Age group ≥65 years n=20
Median: 20.0 µm
Interquartile range: 59.8 µm
Minimum: 4.0 µm
Maximum: 597.0 µm

Mann-Whitney Test
p=0.440

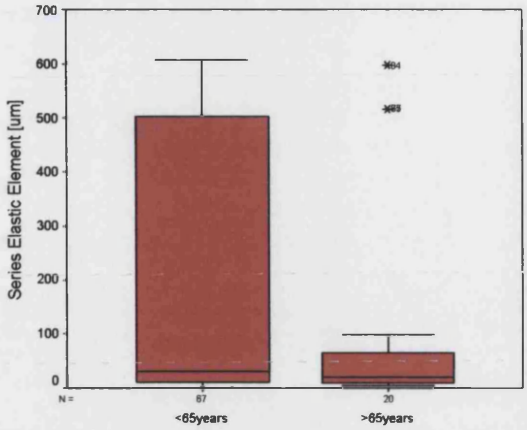

Figure 7.24. The relationship between age and the series elastic element on stretching of the epidermis on the PMA.

7.10.4.2.2.2 Series Elastic Element on Retraction

There was a correlation between age and the rate of retraction on the dorsal site. No such correlation was noted with the MLA and PMA sites, however, a significant difference was noted between the two age groups and the epidermal retraction on the dorsum and MLA. Subjects aged 65 and over had smaller magnitudes of epidermal retraction than compared to the younger age group.

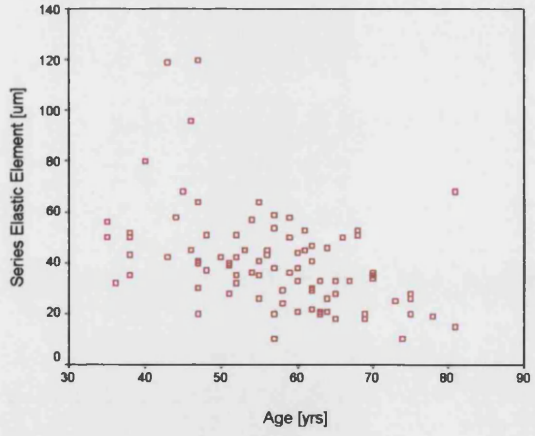

Spearman Correlation
r=-0.274
This correlation is significant at the 0.05 level (2-tailed)

Age group <65 years n=67
Median: 41.0 µm
Interquartile range: 19.0 µm
Minimum: 10.0 µm
Maximum: 120.0 µm

Age group ≥65 years n=20
Median: 28.0 µm
Interquartile range: 16.5 µm
Minimum: 10.0 µm
Maximum: 68.0 µm

Mann-Whitney Test
p=0.002

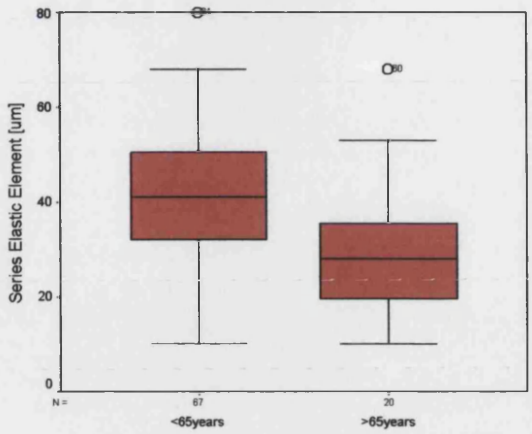

Figure 7.25. The relationship between age and the series elastic element on retraction of the epidermis on the dorsum.

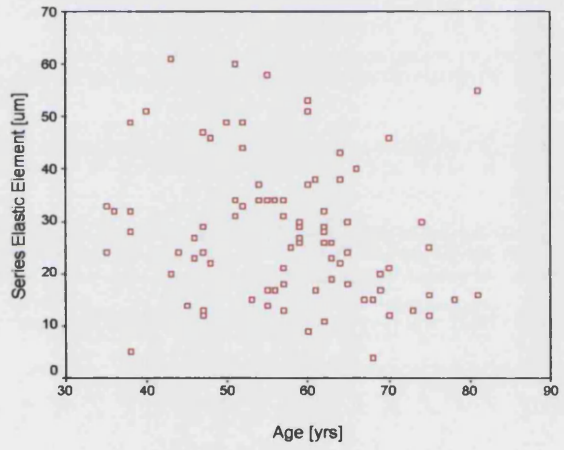

Spearman Correlation
r=-0.265
This correlation is significant at the 0.05 level (2-tailed)

Age group <65 years n=67
Median: 29.0µm
Interquartile range: 16.0µm
Minimum: 5.0µm
Maximum: 61.0µm

Age group ≥65 years n=20
Median: 17.5µm
Interquartile range: 13.8µm
Minimum: 4.0µm
Maximum: 55.0µm

Mann-Whitney Test
p=0.006

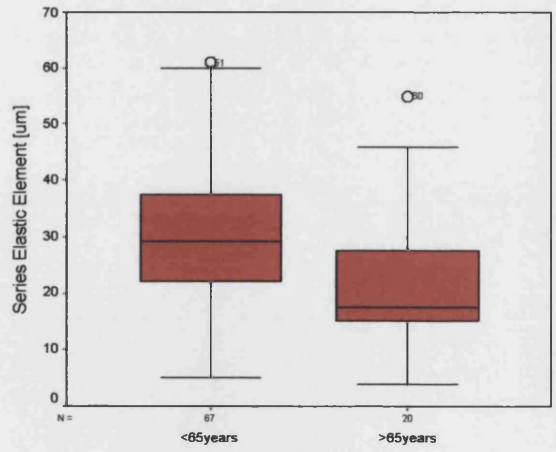

Figure 7.26. The relationship between age and the series elastic element on retraction of the epidermis on the MLA.

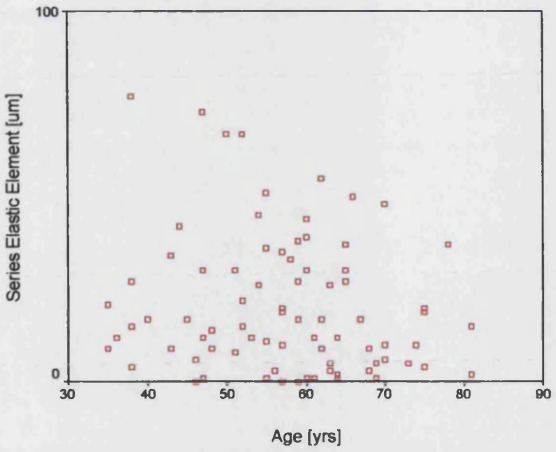

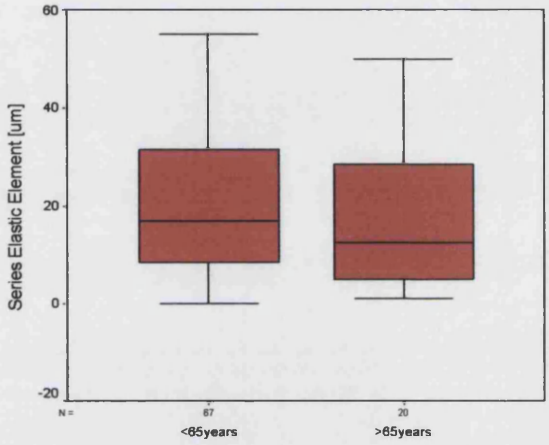

Spearman Correlation
r=-0.090

Age group <65 years n=67
Median: 17.0 µm
Interquartile range: 25.0 µm
Minimum: 0.0 µm
Maximum: 319.0 µm

Age group ≥65 years n=20
Median: 12.5 µm
Interquartile range: 24.25 µm
Minimum: 1.0 µm
Maximum: 50.0 µm

Mann-Whitney Test
p=0.586

Figure 7.27. The relationship between age and the series elastic element on retraction of the epidermis on the PMA.

7.11.4.2.1.3 Time Constants on Stretching

There was no correlation between age and viscoelasticity (time constant).

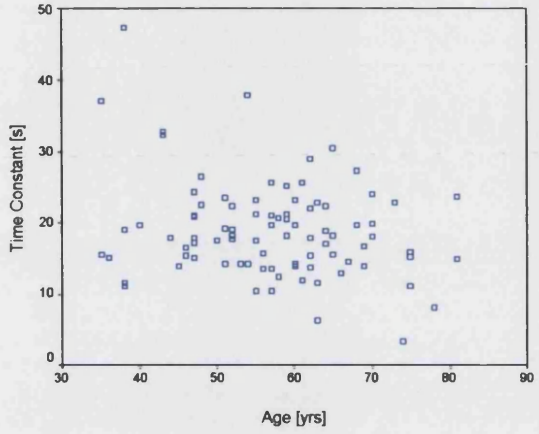

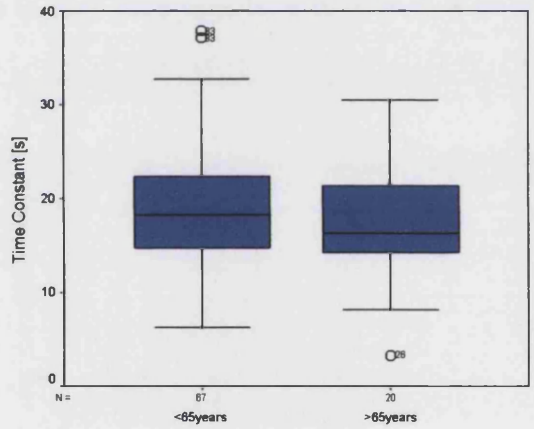

Spearman Correlation
r=-0.131

Age group <65 years n=67
Median: 18.2 s
Interquartile range: 8.1 s
Minimum: 6.3 s
Maximum: 47.3 s

Age group ≥65 years n=20
Median: 16.3 s
Interquartile range: 8.0 s
Minimum: 3.3 s
Maximum: 30.5 s

Mann-Whitney Test
p=0.348

Figure 7.28. The relationship between age and the time constants on stretching of the dorsal epidermis.

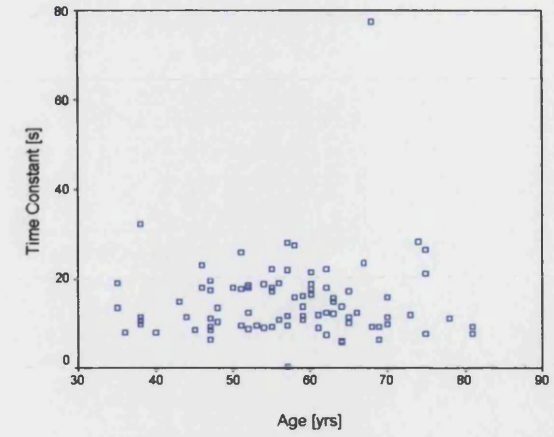

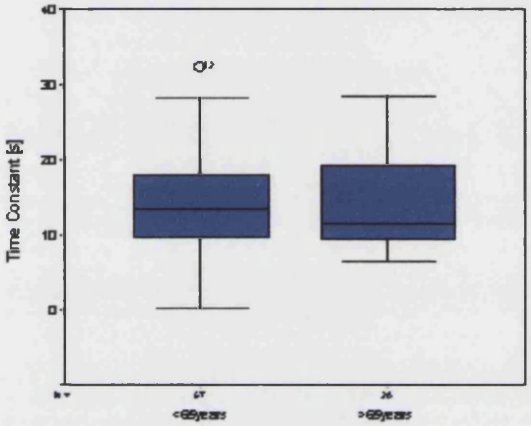

Spearman Correlation
r=-0.023

Age group <65 years n=67
Median: 13.7 s
Interquartile range: 8.4 s
Minimum: 0.2 s
Maximum: 32.4 s

Age group ≥65 years n=20
Median: 11.4 s
Interquartile range: 11.0 s
Minimum: 6.5 s
Maximum: 77.5 s

Mann-Whitney Test
p=0.539

Figure 7.29. The relationship between age and the time constants on stretching the epidermis on the MLA.

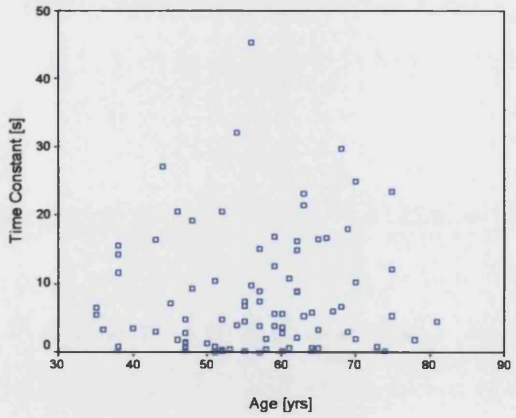

Spearman Correlation
r=-0.069

Age group <65 years n=67
Median: 5.3 s
Interquartile range: 10.4 s
Minimum: 0.0 s
Maximum: 45.4 s

Age group ≥65 years n=20
Median: 5.6 s
Interquartile range: 14.5 s
Minimum: 0.2 s
Maximum: 29.9 s

Mann-Whitney Test
p=0.380

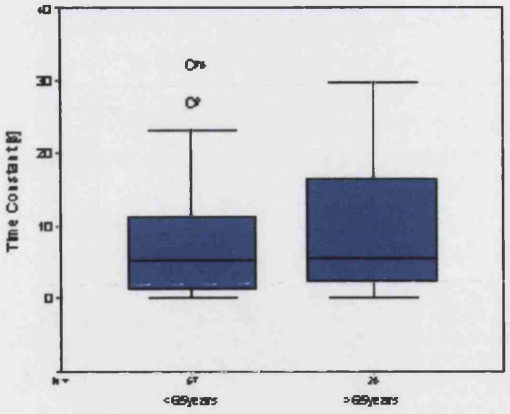

Figure 7.30. The relationship between age and the time constants on stretching of the epidermis on PMA.

7.10.4.2.2.5 Time Constants on Retraction

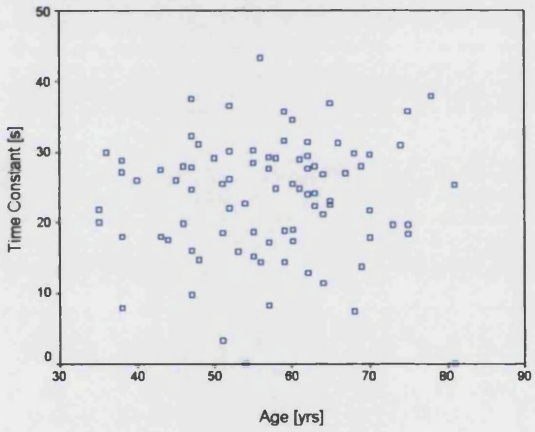

Spearman Correlation
r=0.027

Age group <65 years n=67
Median: 24.9 s
Interquartile range: 10.9 s
Minimum: 0.0 s
Maximum: 43.4 s

Age group ≥65 years n=20
Median: 24.2 s
Interquartile range: 12.0 s
Minimum: 0.0 s
Maximum: 37.8 s

Mann-Whitney Test
p=0.661

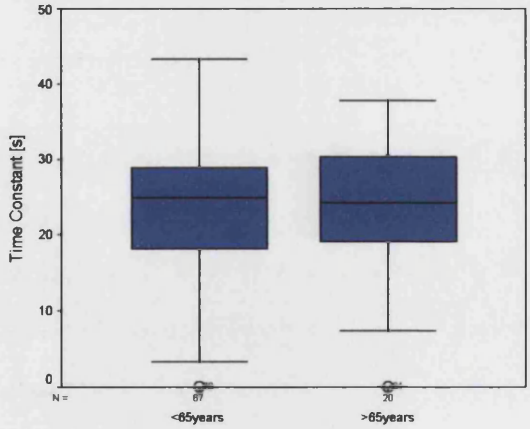

Figure 7.31. The relationship between age and the time constants on retraction of the dorsal epidermis.

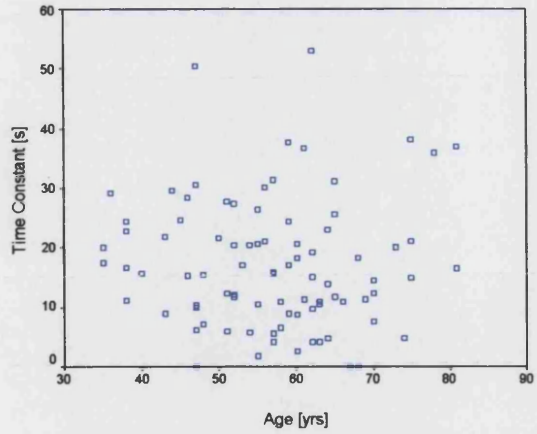

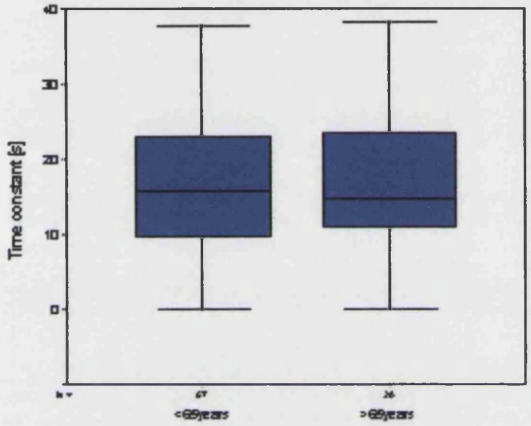

Spearman Correlation
r=-0.31

Age group <65 years n=67
Median: 15.6 s
Interquartile range: 13.5 s
Minimum: 0.0 s
Maximum: 53.1 s

Age group ≥65 years n=20
Median: 14.6 s
Interquartile range: 13.5 s
Minimum: 0.0 s
Maximum: 38.2 s

Mann-Whitney Test
p=0.976

Figure 7.32. The relationship between age and the time constants on retraction of the epidermis on the MLA.

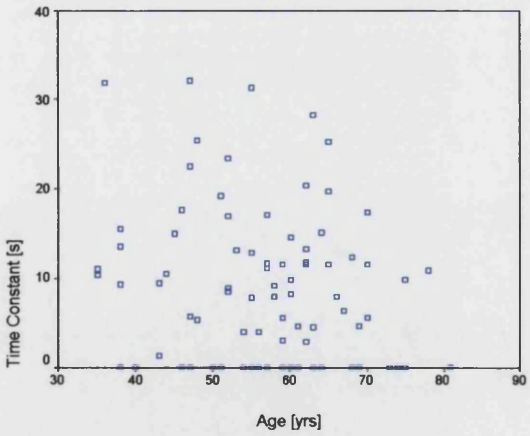

Spearman Correlation
r=-0.200

Age group <65 years n=67
Median: 8.5 s
Interquartile range: 13.5 s
Minimum: 0.0 s
Maximum: 32.2 s

Age group ≥65 years n=20
Median: 5.9 s
Interquartile range: 11.5 s
Minimum: 0.0 s
Maximum: 25.4 s

Mann-Whitney Test
p=0.418

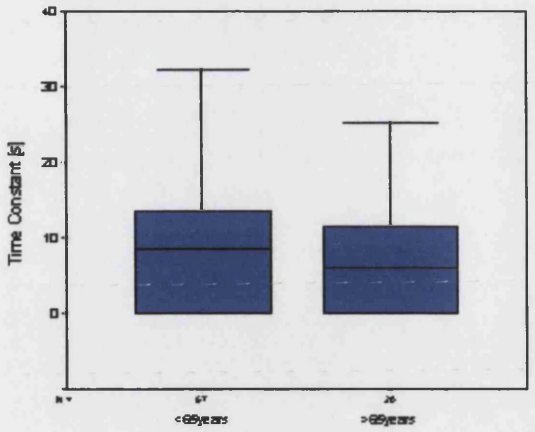

Figure 7.33. The relationship between age and the time constants on retraction of the epidermis on the PMA.

7.10.4.2.2.5 Epidermal Plasticity

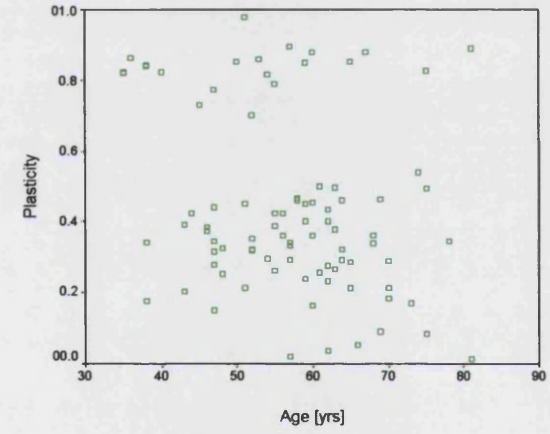

Spearman Correlation
r=-0.261

Age group <65 years n=67
Median: 0.387
Interquartile range: 0.411
Minimum: 0.020
Maximum: 0.979

Age group >65 years n=20
Median: 312
Interquartile range: 0.355
Minimum: 0.012
Maximum: 0.890

Mann-Whitney Test
p=0.164

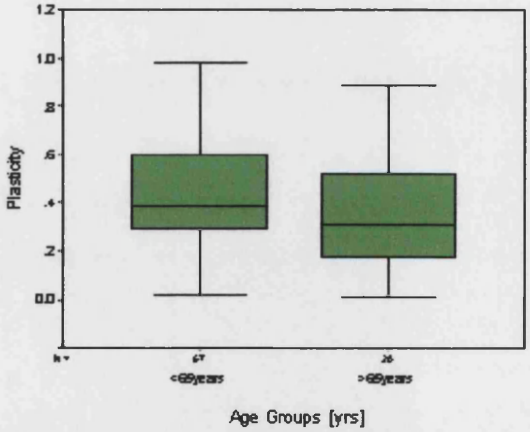

Figure 7.34. The relationship between age and plasticity of dorsal epidermis.

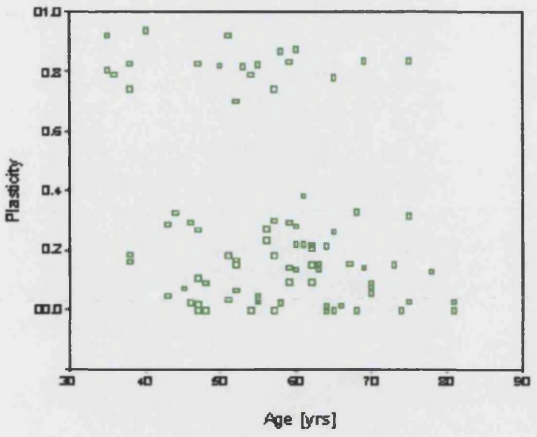

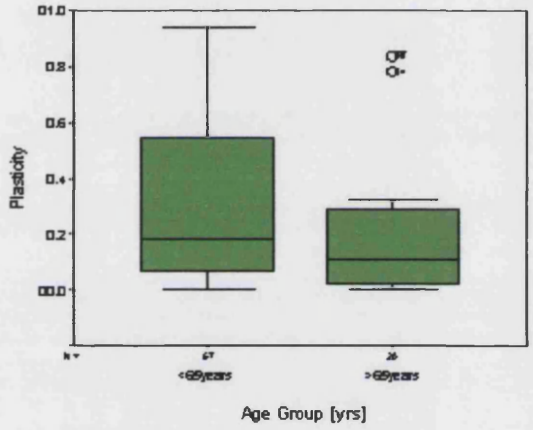

Spearman Correlation
r=-0.294

Age group <65 years n=67
Median: 0.184
Interquartile range: 0.634
Minimum: 0.000
Maximum: 0.940

Age group >65 years n=20
Median: 0.111
Interquartile range: 0.284
Minimum: 0.000
Maximum: 0.839

Mann-Whitney Test
p=0.116

Figure 7.35. The relationship between age and epidermal plasticity on the MLA.

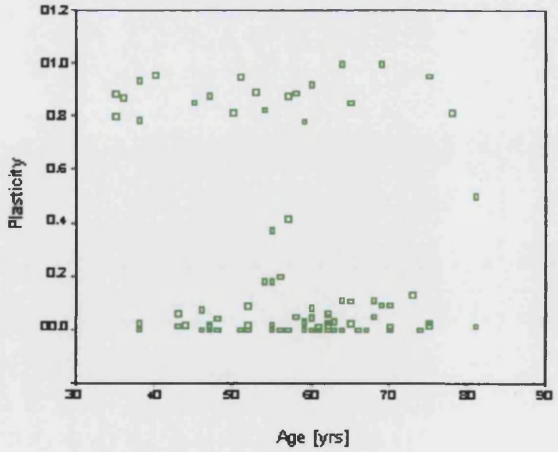

Spearman Correlation
r=-0.171

Age group <65 years n=67
Median: 0.030
Interquartile range: 0.781
Minimum: 0.000
Maximum: 1.000

Age group >65 years n=20
Median: 0.072
Interquartile range: 0.397
Minimum: 0.000
Maximum: 1.000

Mann-Whitney Test
p=0.557
The level of significance is 0.05 (2-tailed)

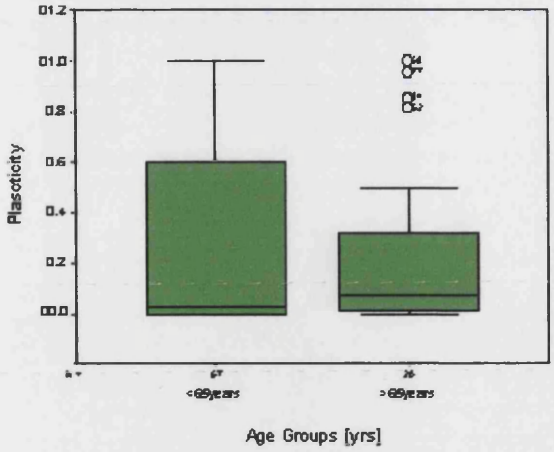

Figure 7.36. The relationship between age and epidermal plasticity on the PMA.

7.10.4.2.3 The Relationship between the Sexes and the Mechanical Properties of Pedal Epidermis

There was a marked difference in the series elastic element between the males and the females (males: n=38, females: n=49) on all foot sites ($p<0.05$). There was a significant difference between the sexes with regards to the time constants on the MLA and dorsal sites ($p<0.05$), but not the PMA site.

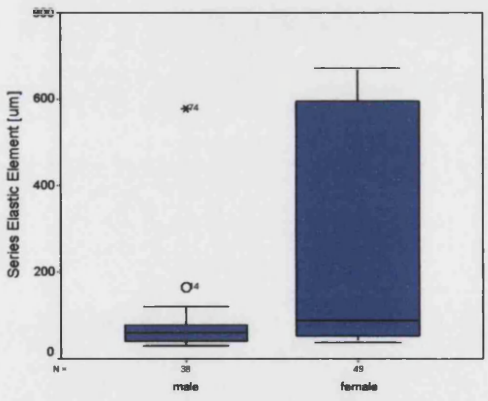

Male n=38
Median: 59.50 µm
Interquartile range: 39.0 µm
Minimum: 31.0 µm
Maximum: 578.0 µm

Female n=49
Median: 87.0 µm
Interquartile range: 546.5 µm
Minimum: 37 µm
Maximum: 671 µm

Mann-Whitney Test
p=0.001

Figure 7.37. The relationship between the sexes and the series elastic element on stretching of the dorsal epidermis.

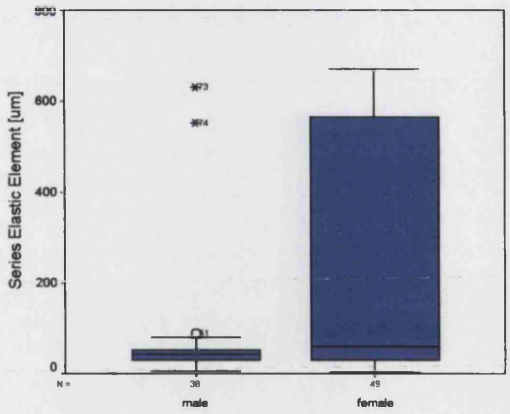

Male n=38
Median: 43.0 µm
Interquartile range: 22.5 µm
Minimum: 6.0 µm
Maximum: 630.0 µm

Female n=49
Median: 59.0 µm
Interquartile range: 538.0 µm
Minimum: 2.0 µm
Maximum: 671.0 µm

Mann-Whitney Test
p=0.028

Figure 7.38. The relationship between the sexes and the series elastic element on stretching of the epidermis on the MLA.

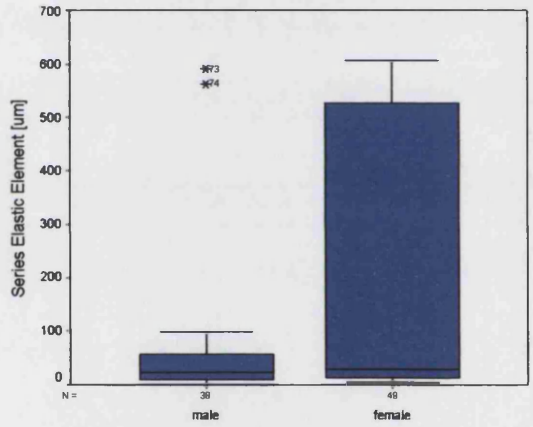

Male n=38
Median: 22.0 µm
Interquartile range: 49.3 µm
Minimum: 0.0 µm
Maximum: 590.0 µm

Female n=49
Median: 28.0 µm
Interquartile range: 517.5 µm
Minimum: 4.0 µm
Maximum: 607.0 µm

Mann-Whitney Test
p=0.039

Figure 7.39. The relationship between the sexes and the series elastic element on stretching of the epidermis on PMA.

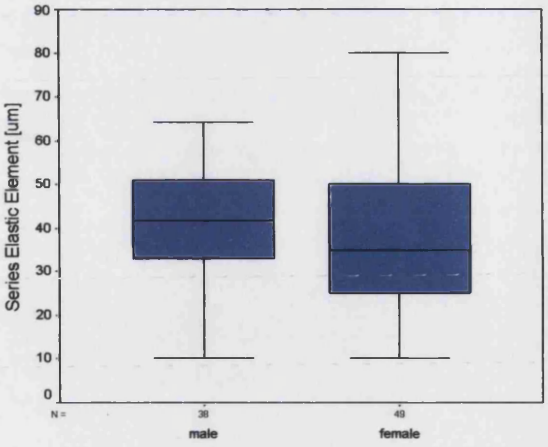

Male n=38
Median: 41.5 µm
Interquartile range: 18.25 µm
Minimum: 10.0 µm
Maximum: 120.0 µm

Female n=49
Median: 35.0 µm
Interquartile range: 25.5 µm
Minimum: 10.0 µm
Maximum: 80.0 µm

Mann-Whitney Test
p=0.084

Figure 7.40. The relationship between the sexes and the series elastic element on retraction of the dorsal epidermis.

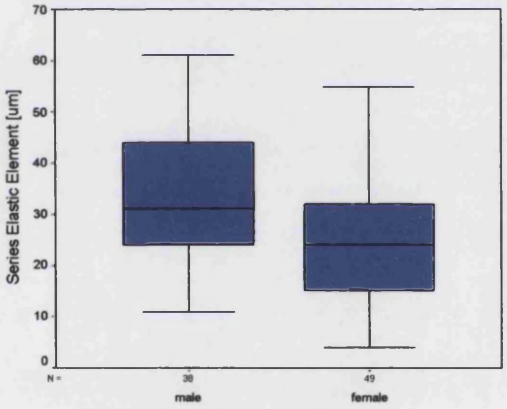

Male n=38
Median: 31.0 µm
Interquartile range: 20.3 µm
Minimum: 11.0 µm
Maximum: 61.0 µm

Female n=49
Median: 24.0 µm
Interquartile range: 17.5 µm
Minimum: 4.0 µm
Maximum: 55.0 µm

Mann-Whitney Test
p=0.006

Figure 7.41. The relationship between the sexes and the series elastic element on retraction of the epidermis on the MLA.

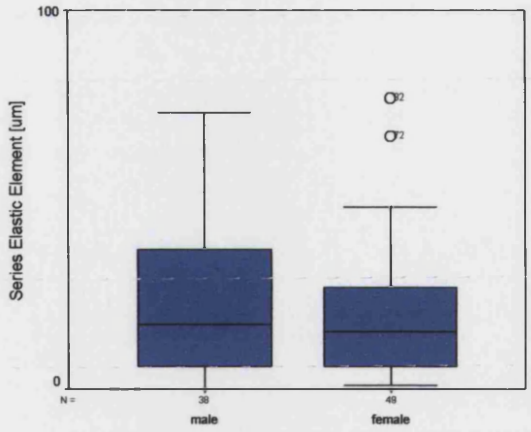

Male n=38
Median: 17.0 µm
Interquartile range: 31.5 µm
Minimum: 0.0 µm
Maximum: 319.0 µm

Female n=49
Median: 15.0 µm
Interquartile range: 21.5 µm
Minimum: 1.0 µm
Maximum: 77.0 µm

Mann-Whitney Test
p=0.006

Figure 7.42. The relationship between the sexes and the series elastic element on retraction of the epidermis on the PMA.

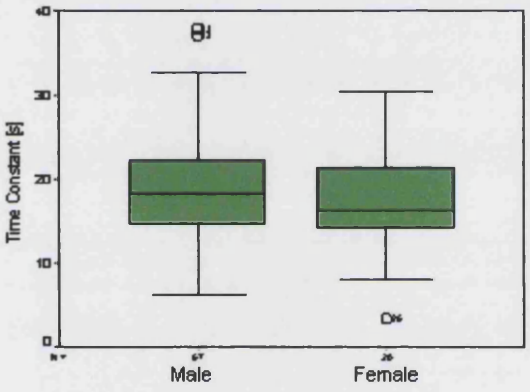

Male n=38
Median: 19.1 s
Interquartile range: 6.6 s
Minimum: 12.0 s
Maximum: 37.9 s

Female n=49
Median: 17.1 s
Interquartile range: 7.4 s
Minimum: 3.3 s
Maximum: 47.3 s

Mann-Whitney Test
p=0.050

Figure 7.43. The relationship between the sexes and the time constant stretching of the dorsal epidermis.

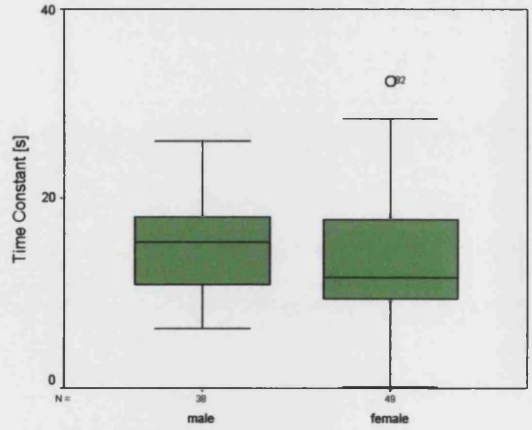

Male n=38
Median: 15.4 s
Interquartile range: 7.2 s
Minimum: 6.2 s
Maximum: 26.1 s

Female n=49
Median: 11.6 s
Interquartile range: 8.9 s
Minimum: 0.2 s
Maximum: 77.5 s

Mann-Whitney Test
p=0.050

Figure 7.44. The relationship between the sexes and the time constants on stretching of the epidermis on the MLA.

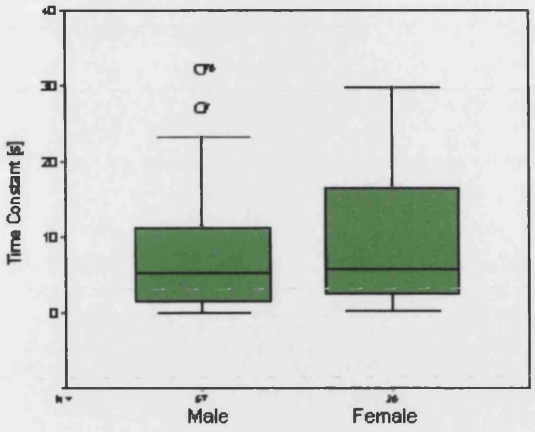

Male n=38
Median: 6.3 s
Interquartile range: 14.0 s
Minimum: 0.0 s
Maximum: 45.4 s

Female n=49
Median: 4.5 s
Interquartile range: 9.1 s
Minimum: 0.1 s
Maximum: 32.2 s

Mann-Whitney Test
p=0.457

Figure 7.45 The relationship between the sexes and the time constants on stretching of the epidermis on the PMA.

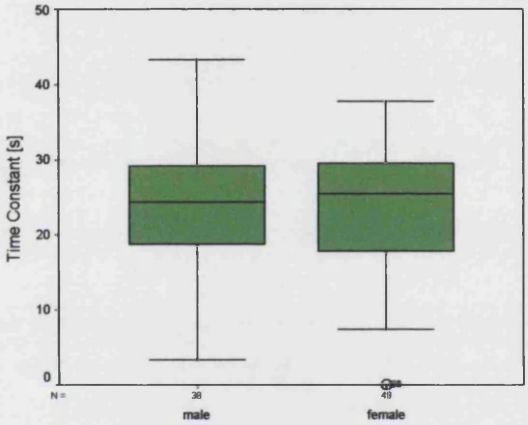

Male n=38
Median: 24.4 s
Interquartile range: 10.5 s
Minimum: 3.3 s
Maximum: 43.4 s

Female n=49
Median: 25.4 s
Interquartile range: 12.1 s
Minimum: 0.0 s
Maximum: 37.8 s

Mann-Whitney Test
p=0.001

Figure 7.46 The relationship between the sexes and the time constants on retraction of the dorsal epidermis.

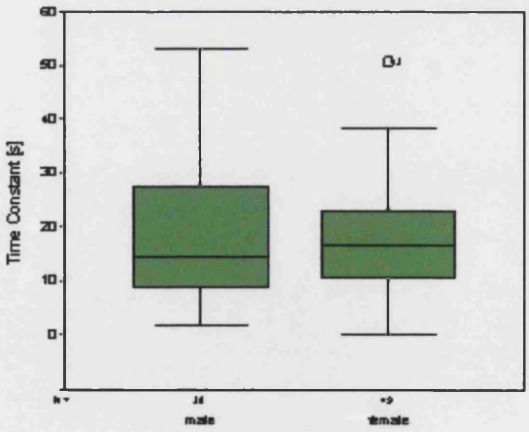

Male n=38
Median: 14.4 s
Interquartile range: 19.3 s
Minimum: 1.7 s
Maximum: 53.0 s

Female n=49
Median: 16.7 s
Interquartile range: 12.3 s
Minimum: 0.0 s
Maximum: 50.5 s

Mann-Whitney Test
p=0. 006

Figure 7.47. The relationship between sexes the time constants on retraction of the epidermis on the MLA.

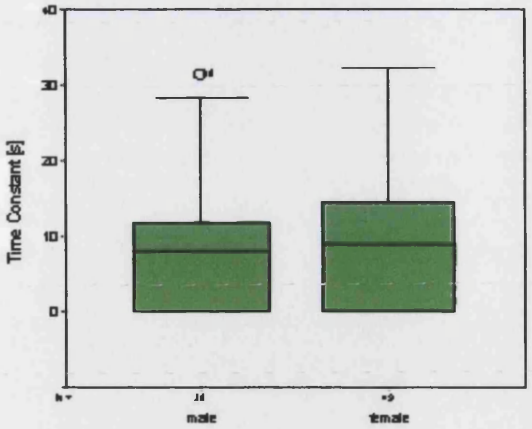

Male n=38
Median: 7.9 s
Interquartile range: 11.7 s
Minimum: 0.0 s
Maximum: 31.5 s

Female n=49
Median: 9.1 s
Interquartile range: 14.8 s
Minimum: 0.0 s
Maximum: 32.2 s

Mann-Whitney Test
p=0.415

Figure 7.48. The relationship between the sexes and the time constants on retraction of the epidermis on the PMA

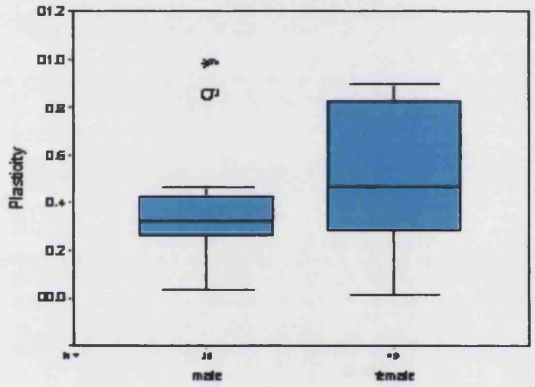

Male n=38
Median: 0.323
Interquartile range: 0.600
Minimum: 0.380
Maximum: 0.979

Female n=49
Median: 0.462
Interquartile range: 0.542
Minimum: 0.012
Maximum: 0.897

Mann-Whitney Test
p=0.013

Figure 7.49. The relationship between the sexes and dorsal epidermal plasticity

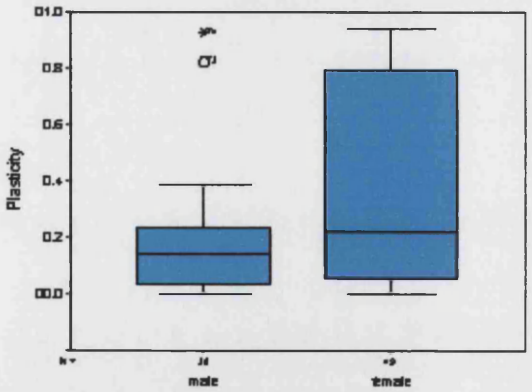

Male n=38
Median: 0.142
Interquartile range: 0.207
Minimum: 0.000
Maximum: 0.926

Female n=49
Median: 0.218
Interquartile range: 0.746
Minimum: 0.000
Maximum: 0.940

Mann-Whitney Test
p=0.054

Figure 7.50. The relationship between the sexes and epidermal plasticity on the MLA.

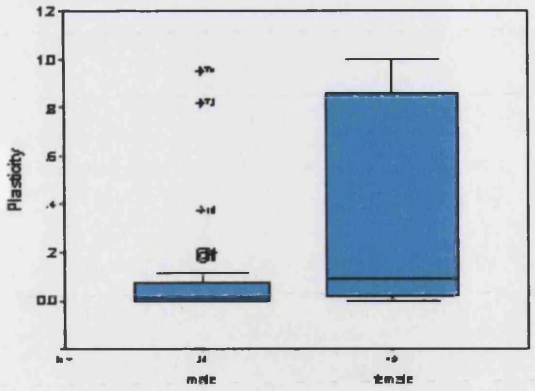

Male n=38
Median: 0.016
Interquartile range: 0.076
Minimum: 0.000
Maximum: 0.951

Female n=49
Median: 0.087
Interquartile range: 0.848
Minimum: 0.000
Maximum: 1.000

Mann-Whitney Test
p=0.001

Figure 7.51. The relationship between the sexes and epidermal plasticity on the PMA.

7.10.4.2.4 The Relationship between Ethnicity and the Mechanical Properties of the Epidermis on the Foot

The subjects were divided into two groups (caucasian: n=69 and non-caucasian: n=18). The numbers in the groups differed greatly; therefore further investigations should be carried out to gain a more realistic association.

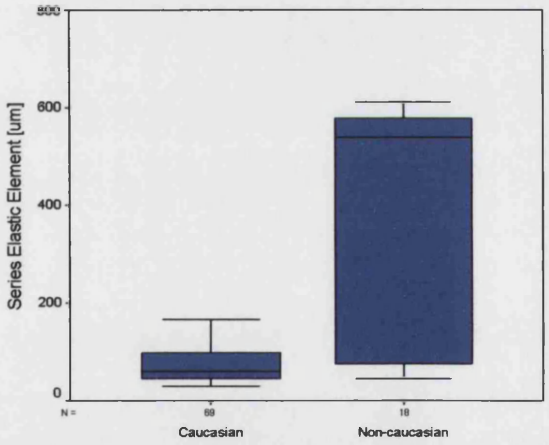

Caucasian n=69
Median: 61.0 µm
Interquartile range: 55.5 µm
Minimum: 31.0 µm
Maximum: 671.0 µm

Non-caucasian n=18
Median: 538.5 µm
Interquartile range: 508.0 µm
Minimum: 44.0 µm
Maximum: 611.0 µm

Mann-Whitney Test
p=0.003

Figure 7.52. The relationship between ethnicity and the series elastic element on stretching of the dorsal epidermis.

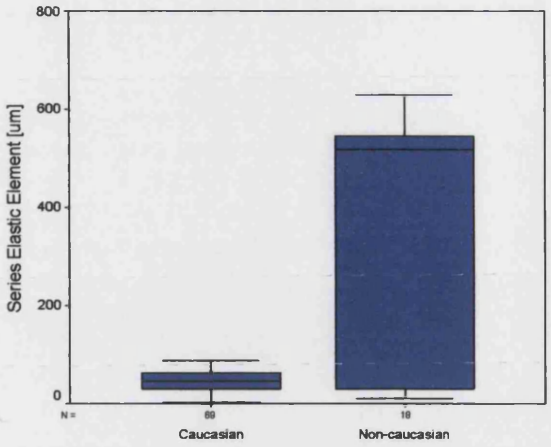

Caucasian n=69
Median: 46.0 µm
Interquartile range: 32.0 µm
Minimum: 2.0 µm
Maximum: 671.0 µm

Non-caucasian n=18
Median: 516.5 µm
Interquartile range: 520.3 µm
Minimum: 9.0 µm
Maximum: 630.0 µm

Mann-Whitney Test
p=0.438

Figure 7.53. The relationship between ethnicity and the series elastic element on stretching of the epidermis of the MLA.

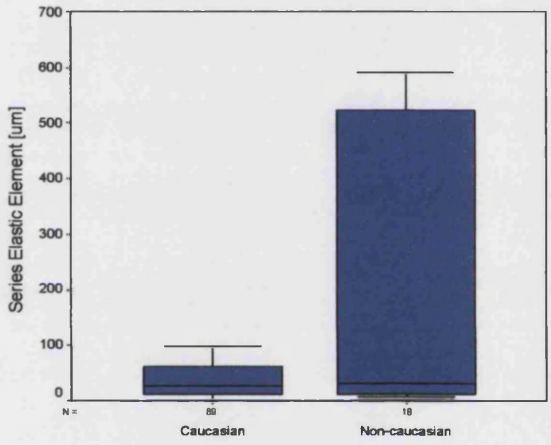

Caucasian n=69
Median: 26.0 µm
Interquartile range: 57.0 µm
Minimum: 0.0 µm
Maximum: 607.0 µm

Non-caucasian n=18
Median: 30.0 µm
Interquartile range: 514.0 µm
Minimum: 7.0 µm
Maximum: 590.0 µm

Mann-Whitney Test
p=0.393

Figure 7.54. The relationship between ethnicity and the series elastic element on stretching of the epidermis of the PMA.

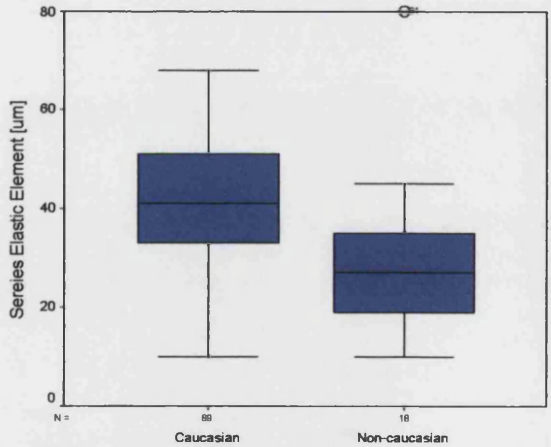

Caucasian n=69
Median: 41.0 µm
Interquartile range: 18.5 µm
Minimum: 10.0 µm
Maximum: 120.0 µm

Non-caucasian n=18
Median: 27.0 µm
Interquartile range: 18.0 µm
Minimum: 10.0 µm
Maximum: 80.0 µm

Mann-Whitney Test
p=0.001

Figure 7.55. The relationship between ethnicity and the series elastic element on retraction of the dorsal epidermis.

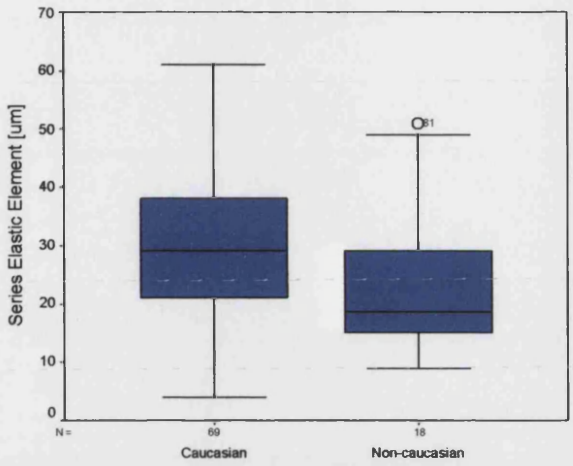

Caucasian n=69
Median: 29.0 µm
Interquartile range: 17.5 µm
Minimum: 4.0 µm
Maximum: 61.0 µm

Non-caucasian n=18
Median: 18.5 µm
Interquartile range: 14.25 µm
Minimum: 9.0 µm
Maximum: 51.0 µm

Mann-Whitney Test
p=0.024

Figure 7.56. The relationship between ethnicity and the series elastic element on retraction of the epidermis of the MLA.

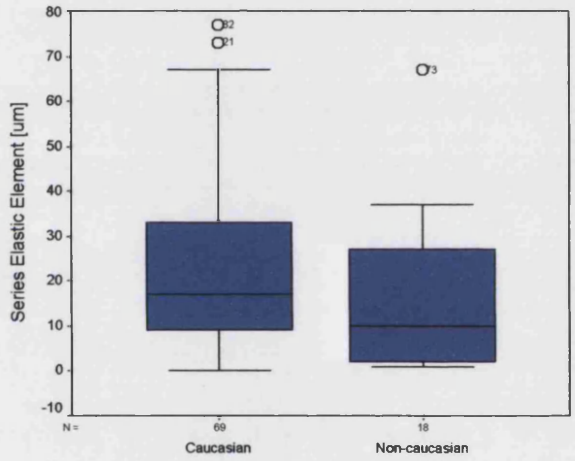

Caucasian n=69
Median: 17.0 µm
Interquartile range: 25.0 µm
Minimum: 0.0 µm
Maximum: 319.0 µm

Non-caucasian n=18
Median: 10.0 µm
Interquartile range: 26.0 µm
Minimum: 1.0 µm
Maximum: 67.0 µm

Mann-Whitney Test
p=0.160

Figure 7.57. The relationship between ethnicity and the series elastic element on retraction of the epidermis of the PMA.

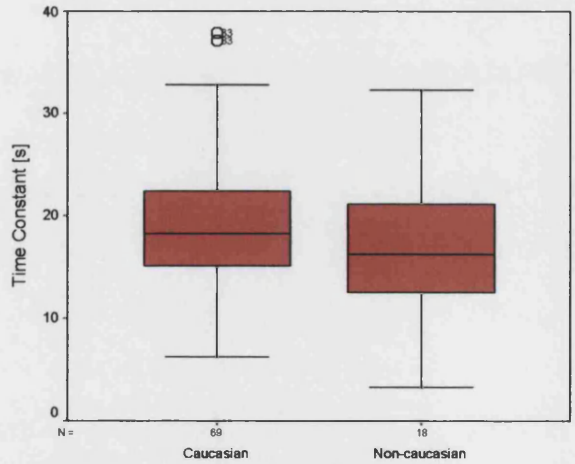

Caucasian n=69
Median: 18.2 s
Interquartile range: 7.3 s
Minimum: 6.3 s
Maximum: 47.3 s

Non-caucasian n=18
Median: 16.3 s
Interquartile range: 9.4 s
Minimum: 3.3 s
Maximum: 32.3 s

Mann-Whitney Test
p=0.224

Figure 7.58. The relationship between ethnicity and the time constants on stretching of the dorsal epidermis.

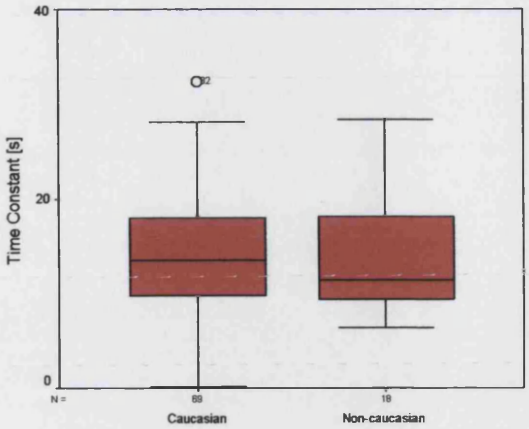

Caucasian n=69
Median: 13.5 s
Interquartile range: 8.3 s
Minimum: 0.2 s
Maximum: 77.5 s

Non-caucasian n=18
Median: 11.4 s
Interquartile range: 9.3 s
Minimum: 6.4 s
Maximum: 28.4 s

Mann-Whitney Test
p=0.438

Figure 7.59. The relationship between ethnicity and the time constants on stretching of the epidermis of the MLA.

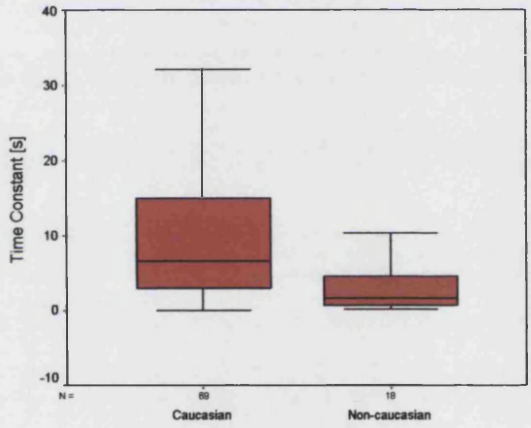

Caucasian n=69
Median: 6.5 s
Interquartile range: 12.1 s
Minimum: 0.0 s
Maximum: 45.4 s

Non-caucasian n=19
Median: 1.6 s
Interquartile range: 4.1 s
Minimum: 0.1 s
Maximum: 25.1 s

Mann-Whitney Test
p=0.003

Figure 7.60. The relationship between ethnicity and the time constants on stretching of the epidermis of the PMA.

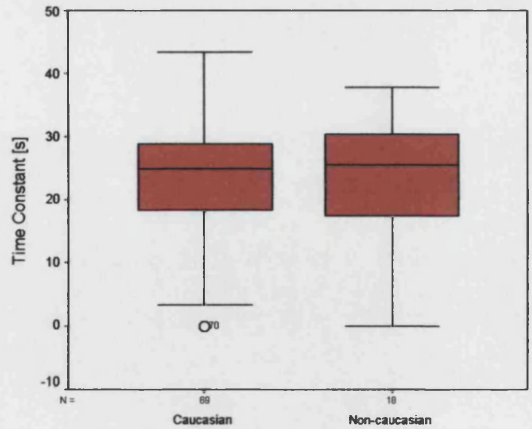

Caucasian n=69
Median: 24.9 s
Interquartile range: 10.6 s
Minimum: 0.0 s
Maximum: 43.4 s

Non-caucasian n=19
Median: 25.4 s
Interquartile range: 13.5 s
Minimum: 0.0 s
Maximum: 37.8 s

Mann-Whitney Test
p=0.001

Figure 7.61. The relationship between ethnicity and the time constants on retraction of the dorsal epidermis.

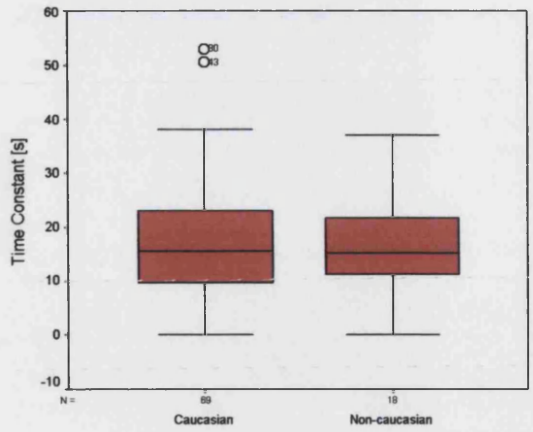

Caucasian n=69
Median: 15.6 s
Interquartile range: 14.4 s
Minimum: 0.0 s
Maximum: 53.0 s

Non-caucasian n=19
Median: 15.2 s
Interquartile range: 11.7 s
Minimum: 0.0 s
Maximum: 37.0 s

Mann-Whitney Test
p=0.081

Figure 7.62. The relationship between ethnicity and the time constants on retraction of the epidermis of the MLA.

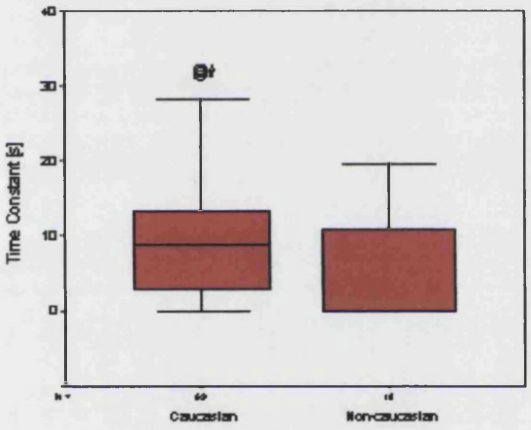

Caucasian n=69
Median: 8.9 s
Interquartile range: 12.6 s
Minimum: 0.0 s
Maximum: 32.2 s

Non-caucasian n=19
Median: 0.0 s
Interquartile range: 11.0 s
Minimum: 0.0 s
Maximum: 19.7 s

Mann-Whitney Test
p=0.159

Figure 7.63. The relationship between ethnicity and the time constants on retraction of the epidermis of the PMA.

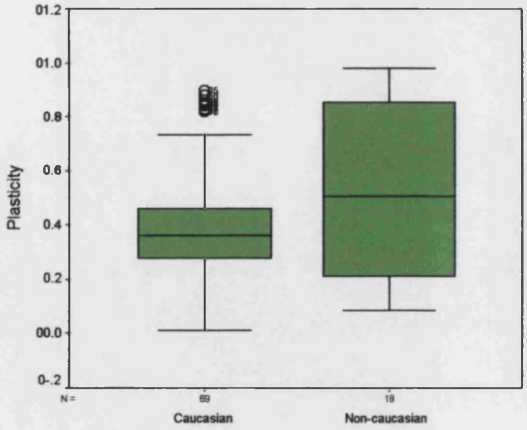

Caucasian n=69
Median: 0.362
Interquartile range: 0.187
Minimum: 0.012
Maximum: 0.897

Non-caucasian n=19
Median: 0.503
Interquartile range: 0.644
Minimum: 0.083
Maximum: 0.979

Mann-Whitney Test
p=0.197

Figure 7.64. The relationship between ethnicity and dorsal epidermal plasticity

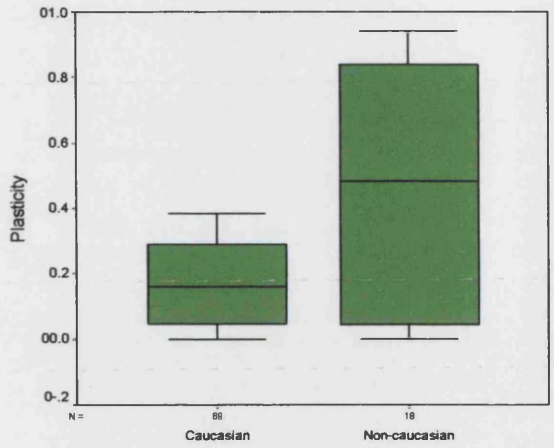

Caucasian n=69
Median: 0.161
Interquartile range: 0.251
Minimum: 0.000
Maximum: 0.926

Non-caucasian n=19
Median: 0.483
Interquartile range: 0.806
Minimum: 0.000
Maximum: 0.940

Mann-Whitney Test
p=0.224

Figure 7.65. The relationship between ethnicity and epidermal plasticity on the MLA.

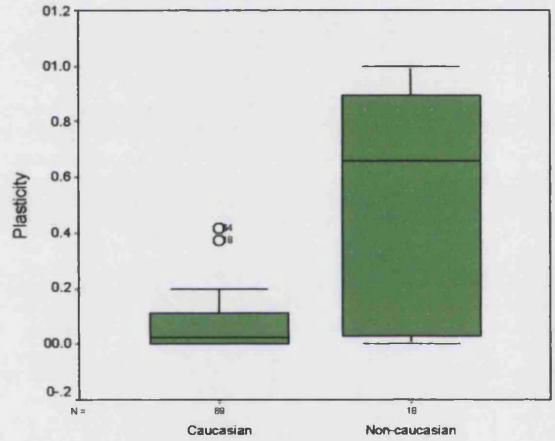

Caucasian n=69
Median: 0.024
Interquartile range: 0.146
Minimum: 0.000
Maximum: 1.000

Non-caucasian n=19
Median: 0.657
Interquartile range: 0.877
Minimum: 0.000
Maximum: 1.000

Mann-Whitney Test
p=0.003

Figure 7.66. The relationship between ethnicity and epidermal plasticity on the PMA.

7.11 Summary

The series elastic element on stretching was significantly higher than on retraction of the epidermis, on all sites of the foot (Fig. 7.19, p=0.001). There was a correlation between the age of the volunteers and the series elastic element on retraction of the dorsal epidermis (Fig. 7.25, r= -0.274), suggesting that as age increases, the epidermal dorsal elasticity decreases. This was not noted on the MLA and PMA sites. The viscoelasticity on stretching of the tissue was significantly lower than the viscoelasticity when the displacing force was removed

on the dorsal site only (Fig. 7.20, p=0.001). The viscoelasticity and plasticity on all three sites did not relate to age.

When comparing the mechanical properties between genders and ethnicity the linear elasticity elements on stretching were significantly higher in females than males. The time constants on stretching were lower in females than males, but they were higher on retraction of the skin on the dorsal and MLA sites only. Plasticity was significantly greater on all sites in the female group.

7.12 Discussion

The evaluation of the mechanical properties of the epidermis of the foot has been successfully conducted with a vertical suction device. In the past, one of the limitations of such devices has been a lack of detail in the data collected, hence imposing limitations on the analysis. An additional hindrance has been the inability of devices to make sufficient measurements of rigid areas of skin [239].

In this study the suppliers of the Cutometer® 580 MPA adapted the software to provide pressure-time and displacement-time profiles, simultaneously. With these data, the machine was successfully tested for accuracy and repeatability. The time taken for the pressure to rise from the initial 0mbar reading to 500mbar was a fraction of a second (~0.1 s). The pressure theoretically should have remained constant (500 mbar) throughout the 120 s of data collection as the force application in the Kelvin model must follow a square wave pattern. In practice, the pressure was seen to deviate above or below 500 mbar. This error was measured and all the displacement data were adjusted to fit the corrected (square wave) pressure.

In order to minimise variations in data between individuals, the position of the body and feet of each volunteer were standardised. The environmental conditions were maintained as constant as possible and the readings were taken at the same time of day for each volunteer. The room temperature (21-25°C) and humidity (31-50%) did not deviate from the recommended levels.

Although the measurements were referred to in terms of the elastic and viscoelastic components of the epidermis, the influence of the underlying dermal tissues cannot be ignored. Because of the size of the aperture in the probe, the dermal involvement was probably minimal. A possible way of testing for the extent of dermal involvement would be to take an ultrasound image of the skin during the application of the displacing force. The development of such a device would not only identify the structures involved during deformation, but could also provide details of the accumulation of fluids in the area and any other underlying anomalies in the skin structure. The two techniques when used in synchrony, may be useful in monitoring the change in the physical properties of skin during the progression of disease and also in assessing the local beneficial effects of particular treatments. The next chapter investigates ultrasound images of normal pedal skin and the appearance of different structures (e.g. collagen, fat and fluids) within the skin expressed in terms of echogenicity.

Application of fixed stress induced a tissue change that followed a viscoelastic path. That the instrument is known to sample the epidermis disproportionately to the dermis supports the view that the epidermis is a viscoelastic tissue, just as the same properties are exhibited by the dermis.

The linear elastic constant of the epidermis on stretching was higher than on retraction on all three sites on the foot, i.e. the rate of stretch exceeded the rate of retraction. This was expected, as an external energy force fuels the process of stretching the tissue. Once the displacing force is released, the speed with which the skin retracts is energised by the recoil of the tissue and not aided by an external source of energy (Fig. 7.67).

Due to the limited work conducted on pedal skin, there is no standard to compare any changes in the mechanical properties of this area of skin in response to disease. Before speculating on the pathological changes in the epidermis on the feet, the need to understand the mechanical behaviour of this type of skin in the absence of disease is fundamental. The three different sites on the foot in this study were chosen in relation to the compression, shear and torsion pressures that they are subjected to during gait. The dorsal skin is least involved with

mechanical trauma of this kind (although footwear is a common source of friction) and the PMA is subjected to relatively high pressures. The common protective physiological response of skin, particularly that of the PMA is the development of hyperkeratosis, which may lead to the formation of pathological callus.

Other factors that should be considered when looking at these different sites are what relationship they have with the underlying structures, such as bones and joints. The movement of these structures may impose an intrinsic adaptive response by the dermal and epidermal tissues, i.e. just as the skin adapts to external forces by thickening, it must be flexible enough to accommodate the movement of joints such as the metatarsophalangeal joints, during gait. The blood and nerve supplies to these areas may also have an input, more so in peripheral vascular disease and peripheral neuropathy. The mechanical behaviour at a cellular level in relation to the glycation of the epidermal proteins and cell-cell adherence proteins, as well as the physical behaviour of the skin on a macro level are discussed in the final chapter when the data from the diabetic population is considered.

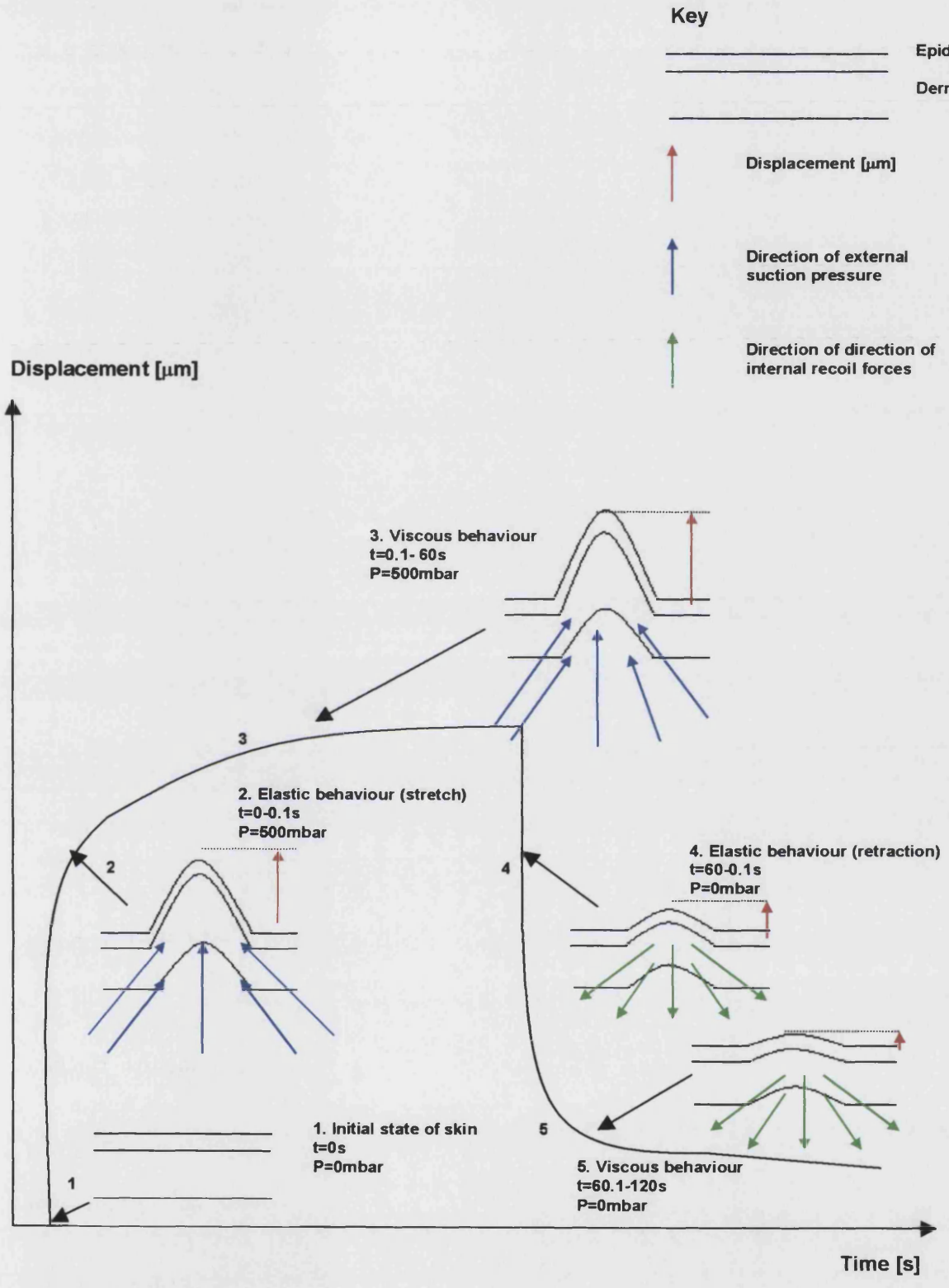

Figure 7.67. Diagram illustrating the viscoelastic behaviour of the skin when subjected to vertical suction pressure.

The dorsal skin had the greatest plasticity, linear elasticity constant and time constant of viscoelasticity both on stretching and retraction. The lowest values of all the indices of elasticity were measured on the PMA. Therefore, the epidermal tissue on the PMA area is less elastic, viscous and plastic than the skin on other, less weight bearing areas. This sets a standard to which the data collected from the diabetic subjects can be compared.

An interesting result was the decrease in the linear elasticity element, on retraction, with an increase in age on dorsal site only. This suggests that, effects of aging limit the ability for the elastic recoil of dorsal skin. This correlation was not seen on the MLA and PMA sites. It could be reasoned that the equilibrium state of the epidermis (before any displacing force is applied) on all three sites possesses different quantities of internal bonding (and therefore energy) between the cells and between the cell constituents. Therefore, when the suction force is applied to the surface of the skin, the adhesion between the cells and the intermolecular bonds that maintain the structure of the epidermis, are challenged and the tissue stretches. If the bonds are stronger or more abundant in the PMA site than the dorsal epidermis, then higher forces would be needed to stretch the tissue to the extent of the dorsal epidermis. It follows that these high/ abundant energies holding the tissue together remain within the tissue when under stress and not released during the viscoelastic and eventually the series elastic element on retraction. In brief, the skin is less flexible on the PMA than the dorsum of the foot. Ishikawa T *et* al (1995) [227] found that the elastic properties of palmar skin (the finger) were not correlated with ageing. It is possible that fingers are exposed to various exogenous stimuli that profoundly affect the nature of the skin, this masking of chronological changes may also be occurring in plantar skin.

The next chapter focuses on the application of high frequency ultrasound imaging for the measurement of epidermal thickness. One of the observations made in Chapter 8, is the epidermis is thinner on the dorsum than the PMA. Therefore, under suction pressure, it is likely that a higher proportion of the highly elastic dermis on the dorsum will be drawn up into the aperture than on the PMA and will contribute to the elasticity readings.

8.0 Chapter 8 – The Investigation of Pedal Skin, *in vivo*, using High Frequency Ultrasound Imaging

8.1 Introduction

Until the advent of high-resolution ultrasound imaging of skin, methods such as skin pinching and weighing of skin biopsies [37;240] had attempted to describe semi–quantitatively the consequences of disease on dermal tissues. High-frequency B-mode ultrasonography provides a method for two–dimensional *in vivo* imaging of the skin. Although examination of this kind does not have the resolution of histology, the advantages of ultrasound are that it is non-invasive and the results are immediate [220]. Reflected ultrasound waves are detected and processed by the instrument to produce a real-time image, as a one-dimensional amplitude modulated display (A scan) or a 2-dimensional brightness modulated display (B scan). Ultrasound has been used in a variety of dermal applications, such as measuring full skin thickness [241], dermal odema [242;243], skin tumours [244] and wounds [245]. This is especially relevant to skin sites such as the sole of the foot, where full skin thickness removal for histological analysis, particularly from neuroischaemic diabetic patients, is not feasible.

The preferred instrument for skin imaging is the Dermascan C®, 20 MHz ultrasound scanner (Cortex Technology, Hadsund, Denmark). The majority of the studies carried out using the Dermascan C® have concentrated only on the skin of the arms and legs. The authors described thick skin on the palms and the soles, but did not discuss the results in detail, and no quantitative data were reported [220;241;246;247].

8.2 Techniques used to Measure Skin Mechanics *in vivo*

Over the past 30 years there has been extensive development and refinement of equipment and techniques involved with high-frequency ultrasonography. This has led to three types of scanning techniques: A-mode scanners (unidirectional in principle and suitable for measuring the skin thickness and the distances

between easily identifiable interfaces); B-mode scanners (bi-directional and allowing cross-sectional imaging of the skin); C-mode scanners (depicting a number of automatic and parallel B–scans forming a three-dimensional image of skin); M-mode scanners (recording moving interfaces such as the wall of a large artery) and Doppler (measuring fluid flow such as blood). At the moment A–, B– and C–mode ultrasonography are directly relevant to skin research.

8.3 Ultrasound Examination of Normal Skin

Although the basic organisation of the skin is the same throughout the body, the skin on the plantar aspect of the foot is unique [241], in that it is thick (approximately 10 times thicker than epidermis on other parts of the body) and hairless. The stratum corneum is the thickest layer in plantar epidermis. Even in the foetus it is appreciably thicker than the skin over other areas. During life, the plantar skin adapts to continuous pressure and friction by further thickening. The dermis in the sole is about 3mm or more thick and is composed of vascular, dense connective tissue.

The acoustic density of components of the skin, determines the clarity of an ultrasound image. The ultrasonic wave penetrating through the skin is partially reflected at the boundaries of the adjacent structures, and echoes of various amplitudes are generated. The average amplitude of the echoes in a defined area of the image is termed "echogenicity". The epidermis and dermis reflect ultrasound variably, but both have well-defined interface echoes, excluding the interface between the dermis the subcutaneous fat, which is far from smooth due to the attachments of the subcutaneous retinacula. These factors are subject to regional variation, with thinner skin on the arms and legs in comparison to the acoustically dense truncal skin [241]. A well-organised fibre network in the dermis allows for high reflectance of ultrasound, consequently producing clear images. A disturbance of this network, such as odema causing a subepidermal increase in interstitial fluid, results in low reflectance. Echoes may be disturbed by air contained within epidermal scales, which cause heavy reflections and shadows on the images, thus making the epidermis a low–reflectant. Dermal echoes are also influenced by the distensibility state of the skin, which can alter according to

the positioning of the joints. In the palms and the soles the fibre orientation is variable, and the ultrasound reflectancy is consequently disturbed. However, the epidermal thickness is easily measured on palms and soles, where the interface to the low–reflectant dermis of these regions can be reliably defined.

8.4 Ultrasound Versus Histology as Comparative Techniques

Histological examination, with its long tradition, is regarded as a gold standard for the investigation of skin. This makes the use of ultrasonography, as a new alternative, difficult. The main limitation of the histological technique, in terms of comparative studies, is the skin undergoes retraction and gross change of dimensions on cutting and removal.

Although, *in vivo* 20 MHz ultrasound examination does not have the resolution of histology, the layers of the skin are identifiable (Table 8.1).

Table 8.1. Ultrasound characteristics of normal human skin

Skin components		Ultrasound (20MHz) characteristics
Epidermis	**Stratum Corneum**	Strong entry echo, dependent upon the thickness of the stratum corneum.
	Cellular layer	Thin echolucent band, not usually possible to measure, unless from an area that has a characteristically thick epidermis.
Dermis	**Papillary dermis**	Generally an echo–poor region, but interspersed with areas of high echogenicity.
	Reticular dermis	An echo–rich region, the majority of the echogenicity originating from collagen fibres within the tissue. Collagen is identified as bundles aligned parallel to the surface of the skin on the scans.
	Hypodermis	Generally an echo poor region, but the fine collagen network that lies within the tissue can also be identified as bands of higher echogenicity.
Muscle layer	**Muscle tissue** **Connective tissue**	These areas can be identified as echo–rich bands, with a regular alignment of fibres within the bands themselves, although it is thought that the muscle tissue itself is echo–poor.

8.5 Ultrasound Technology and Ultrasound Equipment

Acoustic impedance is defined as the product of the density of the tissue and the velocity of sound in the tissue. The elasticity and density of the tissue determine the velocity of longitudinal sound waves in a tissue. It is the difference in acoustic impedance between two adjacent media, which determines echogenicity. Ultrasound follows optical laws where the character of a tissue interface and the incident angle of the ultrasound beam are prerequisites for an echo to be apparent.

The centre of frequency of any ultrasound equipment gives only limited information about the resolution of the system. There is a popular but incorrect idea that high frequency is automatically followed by high resolution, and it is often forgotten that, with high frequency, the viewing field in depth becomes smaller. General experience has confirmed that 20 MHz provides a good compromise between resolution and viewing depth.

8.5.1 Technical Specifications for Good Resolution

Resolution and appropriateness of an ultrasound system can be deduced only partly from certain technical specifications, and the skill of the operator. To avoid biased evaluations, the principles of objective and blinded comparison should be employed whenever possible. Some main variables to consider are: bandwidth and centre frequency; resolution (axial and lateral); scan speed; swept gain (fixed or adjustable); viewing field in depth (fixed and adjustable); scan modes (A/B/C/M); measuring and storage facilities and image analysis; and a selection of probes.

8.6 Skin Ultrasonography using the Dermascan® C

For this study the images of skin were obtained by the Dermascan® C Ver, 3, ultrasound scanner (Dermascan C®, Cortex Technology, Hadsund, Denmark). The instrument comprises of 3 main parts: the ceramic transducer (centre frequency 20MHz), the visualisation and analysis system and the data storage

facility. The probe is housed in water bath, and sealed at the point of contact with a thin plastic membrane. The scanning field is 22.4 x 2.4 mm. The maximum width of the field of view is 13mm and may be scrolled down to 30 mm in depth. A minimal amount of conventional coupling gel is used on the surface of the skin.

Each B-mode picture is composed of 224 A-scans (12 images per second). Swept gain is fully operator adjustable with respect to slope, level and profile and can be saved for standardisation of the method. The gain and viewing fields can also be adjusted on the live image.

With computer assisted image analysis systems (IBM–compatible), it is possible to quantify the amplitude of single echoes, and thus to measure echogenicity. The density of the tissue determines the velocity of the longitudinal waves in a tissue. The intensity of the reflected echoes is evaluated by the microprocessor, and visualised as a coloured two-dimensional image. Care must be taken to maintain the probe perpendicular to the skin surface during scanning and to minimise the pressure of the transducer on the skin surface to ensure a satisfactory scan [246].

8.6.1 Validation of the Dermascan C® - Carried out by Cortex Technology

Protocols documenting the accurate capture of images and measurements were validated by the makers of the device.

8.6.1.1 Image Capture Validation Procedures

A plastic test specimen with a known thickness and sound velocity is scanned. As the material used is homogenous, two distinct echoes are achieved from which the thickness can be measured using the predetermined sound velocity of the material. The thickness measurement procedure follows an in-depth measurement along the horizontal axis. The accuracy of the horizontal scaling of the captured images was also documented. Similarly the accuracy of the vertical

scaling was documented by scanning a wire set-up within the material with a known inter-wire distances.

8.6.1.2 Measurement Functions Validation Procedures

Once the scaling is found to be correct, measurements of distances are validated by drawing triangles, with predefined corner co-ordinates, on the captured image and measuring the length of the sides. This process ensures that the captured image is correctly scaled both in the horizontal and vertical axes. Once the image is shown to be correct, the next stage is to show that any (software) calculations, which derive results from the image, are also correct, i.e. the sides, areas and line lengths drawn on the B-scan images are calculated theoretically and compared to the results obtained from the scanner. This is then compared with the results on the Dermascan C® software and the measurement functions. In short, the validation procedure confirms the accuracy of the image and the accuracy of the derived results.

All measurements were repeated for the three different zoom levels and an error of +/- 1% was accepted. The validation procedure was checked and accepted by the American Food and Drug Administration (USA).

8.7 Ultrasound Velocity of Skin

Ultrasound velocity in skin can depend on the body region. Estimates of ultrasound velocity are: 1550 m/s in the stratum corneum; 1540 m/s in the epidermis [246]; 1580 m/s in the dermis and 1440 m/s in subcutaneous fat. Ultrasound velocity 1580 m/s is commonly used for the imaging and measurement of total skin thickness. However, in the stratum corneum the velocity is higher and will probably approach the velocity of ultrasound in the nail plate, 2459 m/s. From a practical point of view, a minor deviation of ultrasound velocity from the true value of a particular location will not influence significantly the full skin thickness measurement, but may influence measurements of the epidermis.

8.8 Ultrasound Examination of Skin Pathologies

8.8.1 A-Mode Scanning

A-mode scanning is useful for measuring nail-plate and epidermal thickness and has also been used in the past for the quantification of different skin diseases, e.g. psoriasis, sclerotic lesions, tumours and inflammatory odema in contact and atopic dermatitis. A-mode skin thickness measurements can contribute to diagnosis, and it is a useful tool to follow-up and assess the effect of treatments, e.g. corticosteroids. It is common to find that skin thickening and thinning, as a result of the pathological conditions, including endocrine disorders, is more pronounced in the extremities than on the trunk. Thus, as a quantitative tool, A-mode ultrasound measurements of skin thickness have a wide field of application in experimental as well as clinical dermatology. A-mode measurements do not bear the obvious risk of bias of B-mode measurements, when the scan line can be selected from the image. In measurement of skin thickness with A-mode it is recommended that the mean of 3 readings be taken in order to minimise biological local site variation and selection of a less appropriate echo. However, with the Dermascan C® scanner, used in this study, an average skin thickness measurement is made based on 224 A-mode scans and a 22.3 mm piece of skin can be measured relatively quickly.

8.8.2 B-Mode and C-Mode

These types of scanning can be used when the images do not necessarily have to provide quantitative data. The natural field of study using these modes is that of analysis of tumours. Other areas of qualitative analysis using this type of scanning are: wounds [245;247;248] inflammatory lesions; subepidermal odema, scleroderma and psoriasis [249]. Recent data suggests that B mode assessment is more reproducible, although its execution requires more time and attention [250]. Different results are obtained by performing these measurements at the same skin site employing different swept gain curves. By using a gain curve at a higher level a higher measurement is recorded. This explains why a fixed gain curve must be adopted when taking measurements from different subjects.

8.9 Ultrasound Imaging of Skin from the Foot

The echographic images of thick, ridged skin are very different from images taken from thin skin. The epidermis in the images of the very thick ridged skin (at least 100 μm) is very well defined, whereas in the thin skin it is too thin to be resolved [246;249]. However, the separation between the dermis and the subcutaneous layer in thick, ridged skin is ill defined, in contrast to thin skin. This could be due to the fact that in the palms and soles the fibre orientation in the dermis is variable and therefore the ultrasound reflectancy is less. Also, some of the ultrasound waves will not penetrate through the thick epidermis and papillary dermis. In some of the images there is a low echogenic layer just deep to the epidermis. This subepidermal low echogenic band has been described in aged skin on sun-exposed sites, in the legs of persons with venous disease, and is a frequent finding in ultrasonic images.

The most striking characteristics of images of plantar and palmar skin are the very echogenic structures within the epidermis, parallel to the entrance echo. These structures are visible in images of the skin on the heel, the metatarsal heads and the fingertips, although in images of older persons they are less pronounced.

The histopathological pattern of the sole of the foot confirms the thick epidermis measured by ultrasonography along with clearly visible layers of the epidermis. When methylene blue stain is used, the thickening of the epidermis is seen at the sites where the eccrine sweat glands penetrate through the epidermis into the dermis. This thickening of the epidermis could explain the echogenic structures in the images made by the ultrasound scanner. The thickening of the epidermis around the eccrine gland at the point where they penetrate through the epidermis into the dermis is probably a mechanism to protect the eccrine sweat glands from shearing stresses. Alternatively this low echogenic internal epidermal echo may represent the stratum corneum of the epidermis, the water barrier zone of the skin. It has been suggested that the skin on the sole of the foot needs water to preserve its resilience [53]. There is some evidence that water content of the skin will increase after the application of pressure [251].

8.9.1 Plantar Pressures and Ultrasound Imaging

The pathophysiology of pressure ulcers on the foot is not completely understood. In recent years it has been realised that simple ischaemia alone is an inadequate explanation of pressure ulcer pathogenesis. It is suggested that the skin needs water to maintain its resilience and its resistance to external injury and will therefore increase in its water content after being subjected to increased pressure [251].

The plantar surface of the foot is frequently exposed to external pressures, the magnitude of which depends on the type of activity and peak pressure values under the calcaneus and the metatarsal heads. These pressures result in the compression of the skin and the underlying tissue and the skin blood supply. Thoolen (1999) [251] reported that ultrasound images of the plantar aspect of the foot after a period of application of external pressure showed a reduction in the echogenicity of the skin. This could correlate with an increase in water content, but could also correlate with the alteration in the organisation of the collagen fibres.

8.10 Summary

This study aimed to define the characteristics of normal plantar skin using high frequency, diagnostic ultrasound A&B-mode scanning. Measurements of epidermal thickness at specific sites on the foot were made and compared. The effects of capturing images at different acoustic velocities, on the measurement of epidermal thickness, were also tested.

8.11 Measurement of Epidermal Thickness on the Feet

8.11.1 Aims

- Examining ultrasound images taken from different sites on the foot and identifying relevant skin structures.
- To compare the thickness of the epidermis from different sites on the foot.

8.11.2 Methods

Images of the skin were taken from each volunteer, from the same sites as described in Chapter 7: PMA, MLA and dorsal aspect of the left foot. Each volunteer was sitting with the foot in a subtalar joint neutral position. Images were captured with the ultrasound machine set at an acoustic velocity 1580 m/s (recommended value for full skin thickness imaging). The epidermal thickness was measured using the A- and B-scan images. The outer and inner boundary lines, representing the epidermis, were used to take measurements. The software generated an average reading in mm. The same swept gain setting was used for every image taken (Fig. 8.1). Care was taken to maintain the ultrasound beam perpendicular to the skin surface and to minimise the pressure of the transducer on the skin surface to ensure a satisfactory scan.

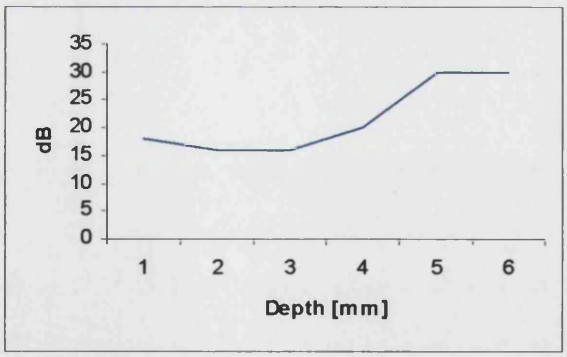

Figure 8.1. Illustration of the swept gain setting used for ultrasound images

The images were taken from all the volunteers recruited for the study:103 diabetic and 87 non-diabetic individuals. The data collected from the non-diabetic subjects were analysed in this section and the data taken from diabetic individuals was analysed and discussed in Chapter 9 and 10.

8.11.3 Results

8.11.3.1 Examination of the Ultrasound Images

The ultrasound scans were presented in a linear rainbow scale such that areas of tissue that had a high acoustic impedance (e.g. collagen) appeared as white, red or yellow areas. Tissue areas with low acoustic impedance (e.g. cellular or fluid filled) were represented as blue or black areas (Fig. 8.2).

The ultrasound scan (Fig. 8.2) demonstrates an echogenic (high acoustic impedance) entry echo in the surface of the tissue (yellow and white band) below which a thin area of echolucency was poorly defined and difficult to measure accurately. This measuring difficulty may have been due to the undulating nature of the rete ridges and papillae of the epidermal-dermal junction causing refraction of the ultrasound signal, thus complicating the signal reflection. Alternatively, there may have been partial masking of the epidermis entry echo by the echogenic characteristics of the stratum corneum, thus attenuating the ultrasound signal. This was supported by data showing that areas with very hyperkeratotic horny plaques cause a marked reflectance of signal, whereas with thin or hydrated epidermis virtually no entry echo signal is identifiable [249].

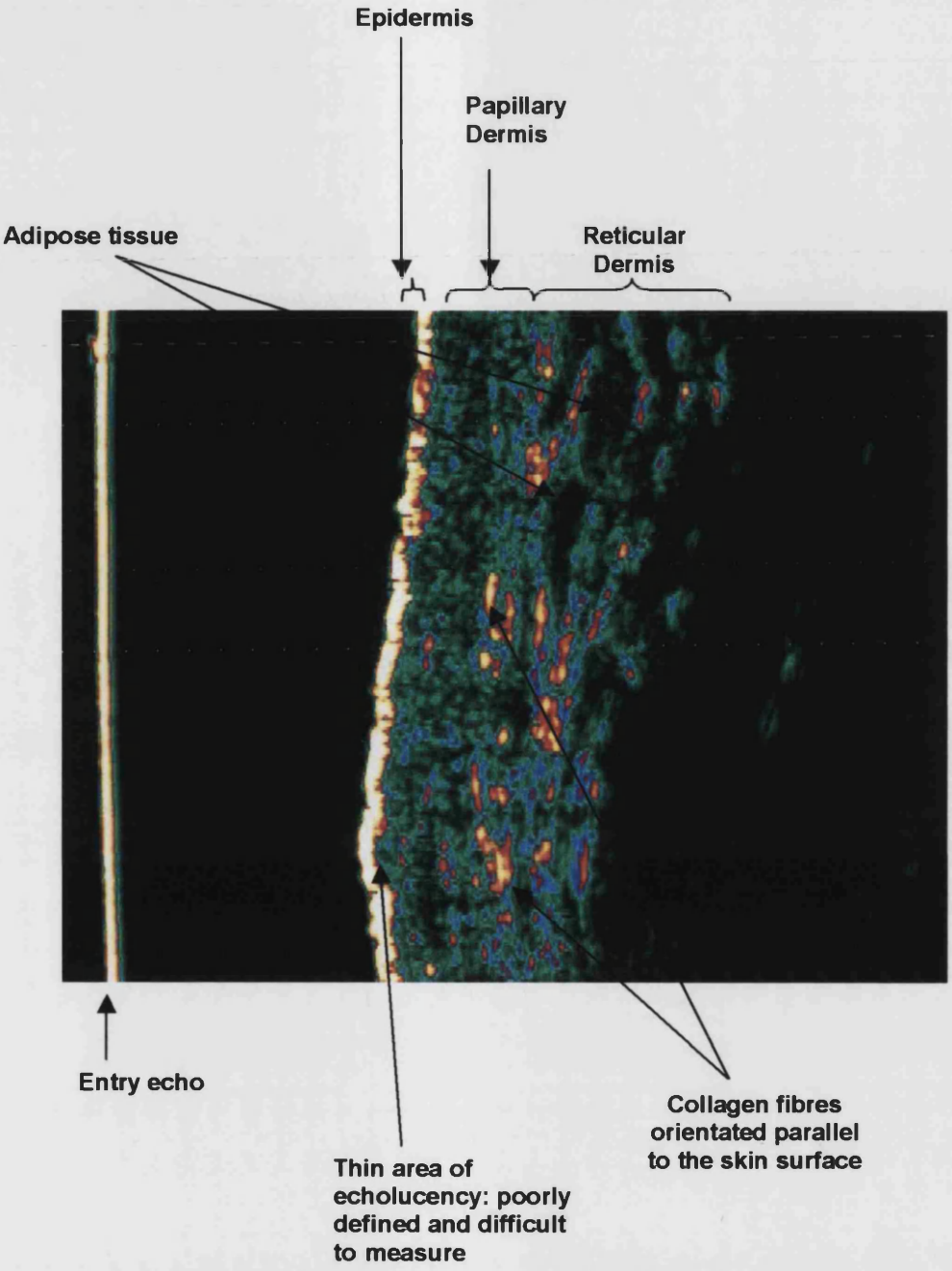

Figure 8.2. A typical ultrasound image of skin taken from the dorsum of the foot.

The dermis is divided into 3 regions, the papillary dermis that contains hillock like projections of fine collagen, reticulin and elastin fibres, blood vessels, terminal nerves and fibrils that anchor the epidermis to the dermis. The deeper reticular dermis is composed of thicker and coarser bundles of type I and type III collagen interwoven with elastin fibres. Below this lies the hypodermis, a thin layer of loose connective tissue and adipose cells. Collagen fibres are orientated in a criss-cross network, the long axis of the fibres tending to lie parallel to the skin's surface. Subcutaneous fat may extend into parts if the reticular dermis where coils of the sweat glands are often found.

The ultrasound scan of the dermis could be divided into an upper band consisting of echolucent areas, interspersed with echo-rich areas. This latter feature found throughout the tissue corresponded to areas of the papillary dermis containing adipose tissue, which could be identified as specific nodular echolucent areas on the scans. Deeper in the tissue highly regular echo-dense regions (yellow and red) were attributed to collagen fibres orientated parallel to the skin surface within the reticular dermis.

8.11.3.2 Comparison between Different Skin Sites

a.

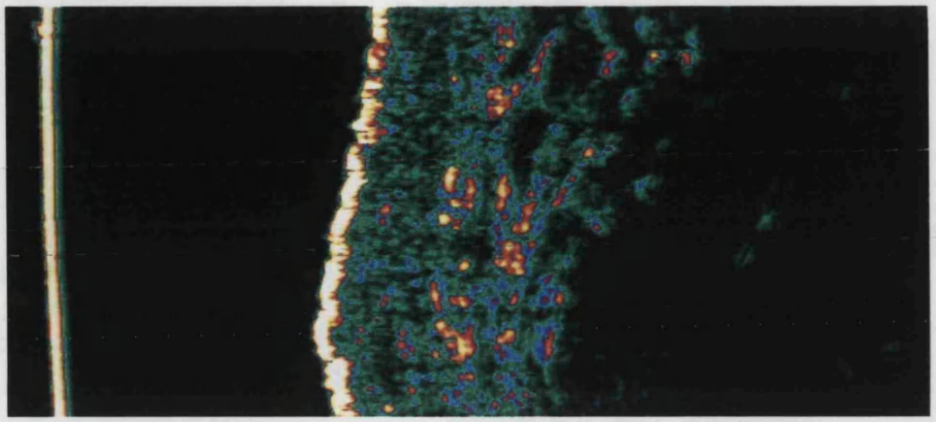

b.

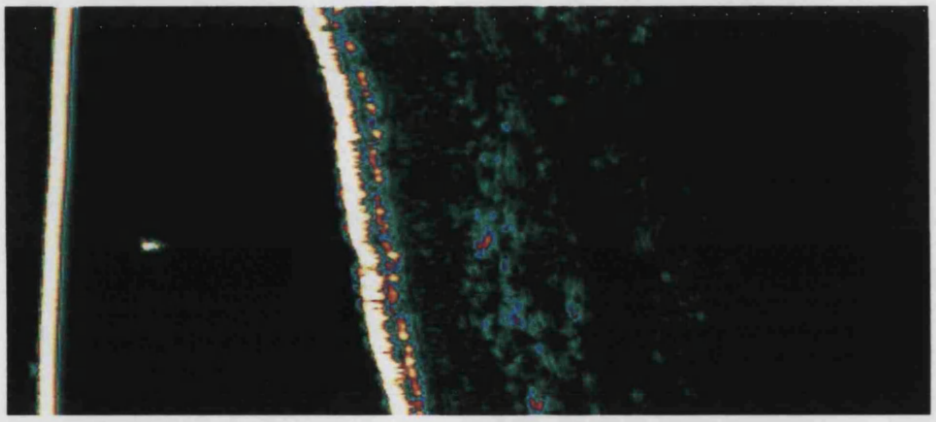

c.

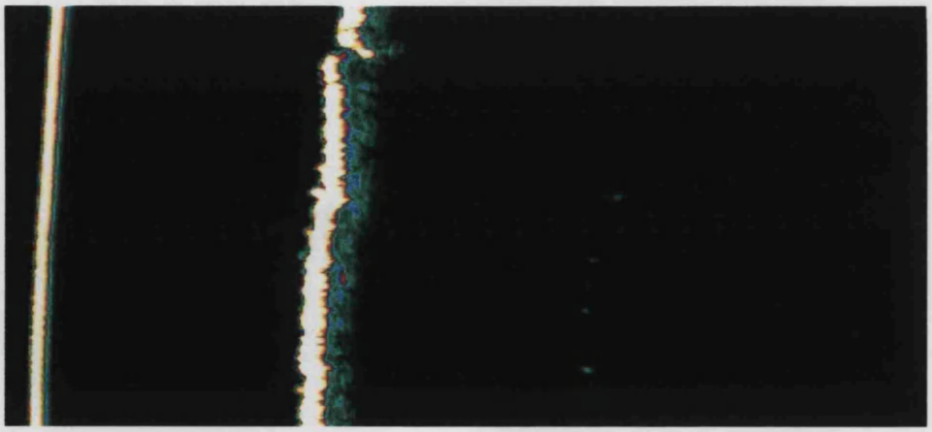

Figure 8.3. Examples of ultrasound images taken from the **a.** dorsum, **b.** medial longitudinal arch and **c.** plantar metatarsal area on the feet.

All the images of dorsal skin presented with the characteristics of skin found elsewhere on the body, that of clearly defined identifiable regions in dermis, represented by orange and red areas and the epidermis, represented by the bright yellow regions (Fig. 8.3a). All the images generated from the three different foot sites clearly illustrated the yellow epidermal bands in varying degrees of thickness. The PMA and MLA images, particularly the latter, often had a band of low echolucency immediately beneath the yellow epidermal band (Fig. 8.3b), which could be as a result of the high echolucency of the stratum corneum portion of the epidermis. Therefore, the measurements of the yellow bands were representative of the epidermal stratum corneum. There were also observed differences in the dermal images between the different sites. The plantar arch and metatarsal images had a higher distribution of black and blue areas. The PMA site, almost always, had no visible dermal structures in the images (Fig. 8.3 c). This can be explained by the presence of a higher amount of stratum corneum tissue on the PMA sites in relation to the other two sites. Hence, the relatively thick epidermis may mask parts of the entry echo and attenuate the ultrasound signal.

The quantitative analyses of epidermal (stratum corneum) thickness on the three sites on the foot are examined in detail in the following sections.

8.11.3.3 Measurements of the Epidermis taken at an Acoustic Velocity of 1580m/s

8.11.3.3.1 Distribution of Data

This section concentrates on the data collected from non-diabetic subjects. A full explanation of the recruitment of patients is described in detail in Chapter 9, along with the comparison of data between the diabetic and non-diabetic groups.

The distribution of the data was skewed; therefore non-parametric statistical analyses were used (Appendix XV).

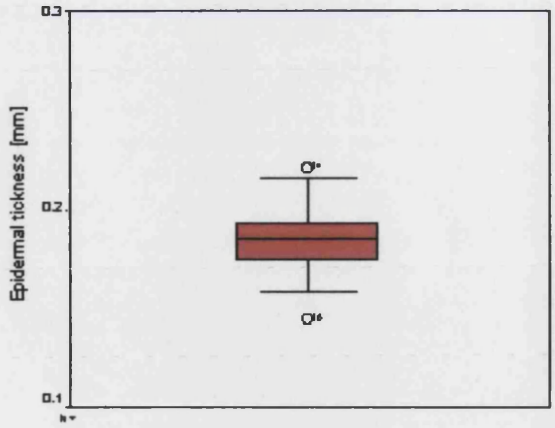

Velocity 1580 m/s
Median: 0.18 mm
Interquartile range: 0.02 mm
Minimum: 0.14 mm
Maximum: 0.22 mm

Figure 8.4. Epidermal thickness measurements taken from the dorsum of the foot at a velocity of 1580 m/s.

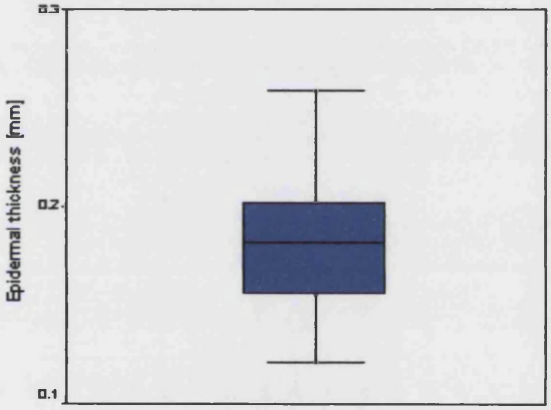

Velocity 1580 m/s
Median: 0.18 mm
Interquartile range: 0.05 mm
Minimum: 0.12 mm
Maximum: 0.30 mm

Figure 8.5. Epidermal thickness measurements taken from the MLA of the foot at a velocity of 1580 m/s.

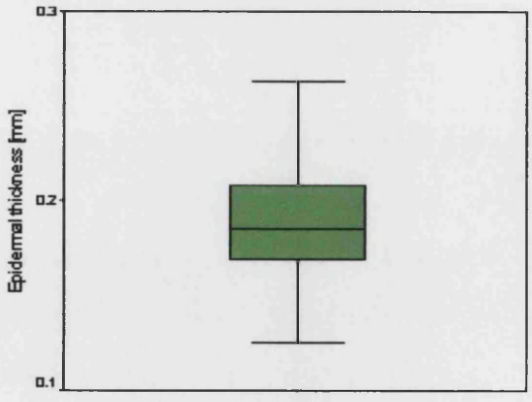

Velocity 1580 m/s
Median: 0.18 mm
Interquartile range: 0.04 mm
Minimum: 0.09 mm
Maximum: 0.27 mm

Figure 8.6. Epidermal thickness measurements taken from the PMA of the foot at velocity of 1580 m/s.

8.11.3.4 The Difference in Epidermal Thickness between the Three Different Sites on the Foot

No statistically significant difference was noted in the thickness of the epidermis between the three different sites on the foot. The range of values were greater from the data collected from the PMA and MLA sites, in comparison to the dorsal skin (Fig. 8.7).

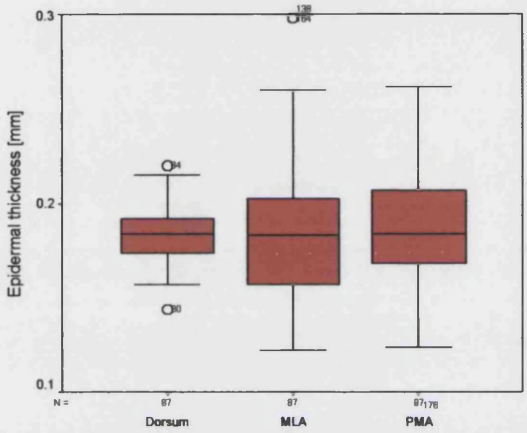

Dorsum
Median: 0.18 mm
Interquartile range: 0.02 mm
Minimum: 0.14 mm
Maximum: 0.22 mm

MLA
Median: 0.18 mm
Interquartile range: 0.05 mm
Minimum: 0.12 mm
Maximum: 0.30 mm

PMA
Median: 0.18 mm
Interquartile range: 0.04 mm
Minimum: 0.09 mm
Maximum: 0.26 mm

Mann-Whitney Test

Dorsum v MLA	p = 0.409
Dorsum v PMA	p = 0.523
MLA v PMA	p = 0.241

Figure 8.7. The relationship between epidermal thickness measurements taken from the dorsum, MLA and PMA regions of the foot at a velocity of 1580 m/s.

8.11.3.5 The Relationship between Age and Thickness of Pedal Epidermis.

The epidermal thickness data from all three foot sites did not correlate with the age of the subjects (Figs. 8.8-8.10).

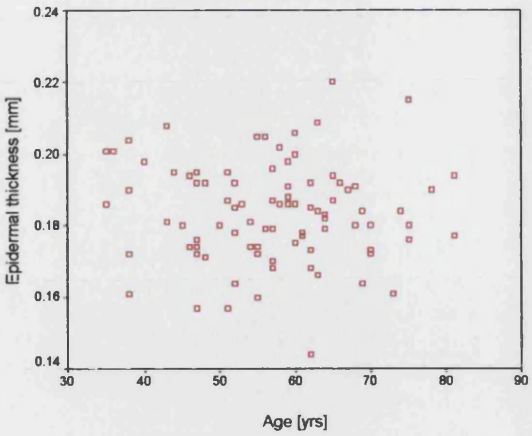

Spearman Correlation
r=-0.046

Age group <65 years n=67
Median: 0.18 mm
Interquartile range: 0.02 mm
Minimum: 0.14 mm
Maximum: 0.21 mm

Age group ≥65 years n=20
Median: 0.18 mm
Interquartile range: 0.02 mm
Minimum: 0.16 mm
Maximum: 0.22 mm

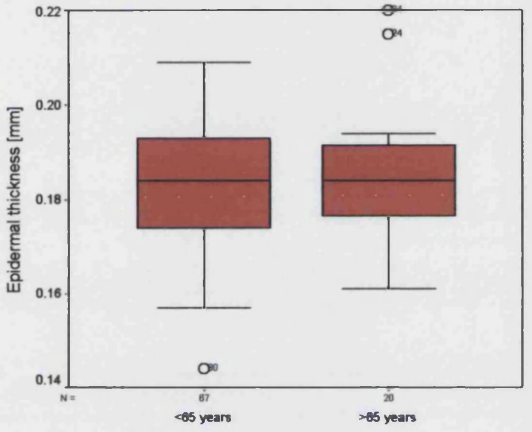

Mann-Whitney Test
p=0.844

Figure 8.8. The relationship between age and epidermal thickness measurements taken from the dorsum of the foot at a velocity of 1580 m/s.

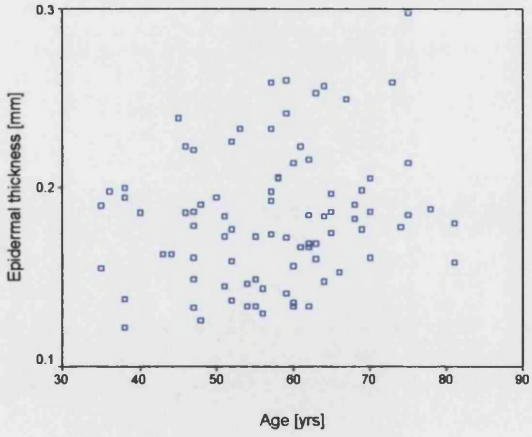

Spearman Correlation
r=0.149

Age group <65 years n=67
Median: 0.17 mm
Interquartile range: 0.06 mm
Minimum: 0.12 mm
Maximum: 0.30 mm

Age group ≥65 years n=20
Median: 0.19 mm
Interquartile range: 0.03 mm
Minimum: 0.15 mm
Maximum: 0.30 mm

Mann-Whitney Test
p=0.091

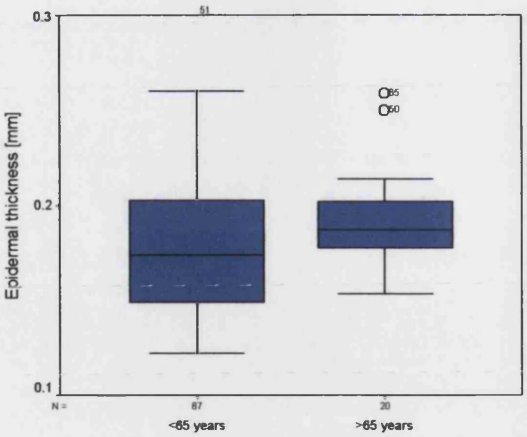

Figure 8.9. The relationship between age and epidermal thickness measurements taken from the MLA of the foot at a velocity of 1580m/s.

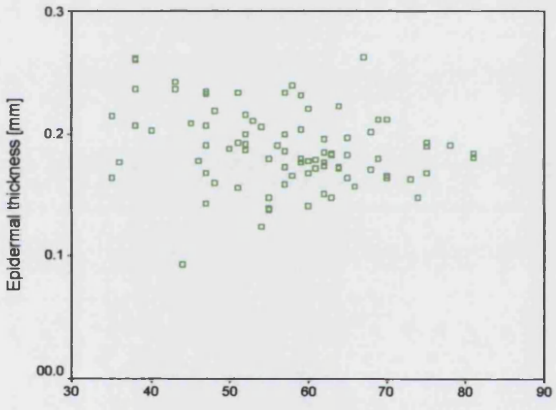

Spearman Correlation
r=-0.65

Age group <65 years n=67
Median: 0.19 mm
Interquartile range: 0.04 mm
Minimum: 0.09 mm
Maximum: 0.26 mm

Age group ≥65 years n=20
Median: 0.18 mm
Interquartile range: 0.32 mm
Minimum: 0.15 mm
Maximum: 0.26 mm

Mann-Whitney Test
p=0.411

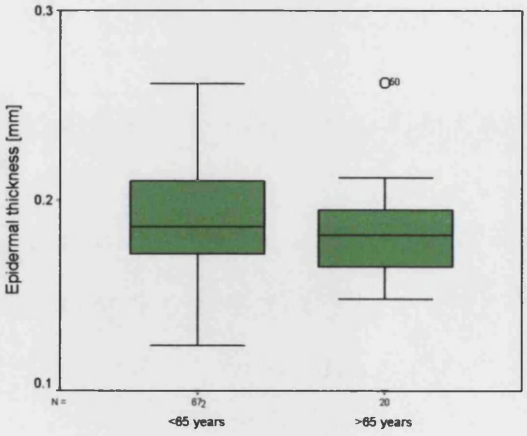

Figure 8.10. The relationship between age and epidermal thickness measurements taken from the PMA of the foot at a velocity of 1580m/s.

8.11.3.6 The Relationship between the Sexes and the Thickness of Pedal Epidermis

There was a significant difference in the epidermal thickness data, collected from all three foot sites, between males and the females (dorsum: p=0.042, MLA: p=0.036, and PMA: p=0.002). Women demonstrated greater epidermal thickness.

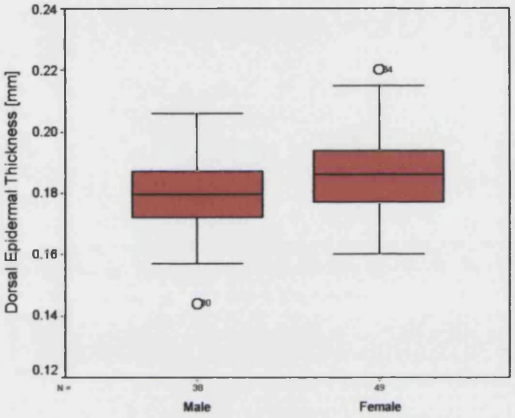

Male n=38
Median: 0.18 mm
Interquartile range: 0.02 mm
Minimum: 0.14 mm
Maximum: 0.21 mm

Female n=49
Median: 0.19 mm
Interquartile range: 0.02 mm
Minimum: 0.16 mm
Maximum: 0.22 mm

Mann-Whitney Test
p=0.042

Figure 8.11. The relationship between the sexes and epidermal thickness measurements taken from the dorsum of the foot at a velocity of 1580 m/s.

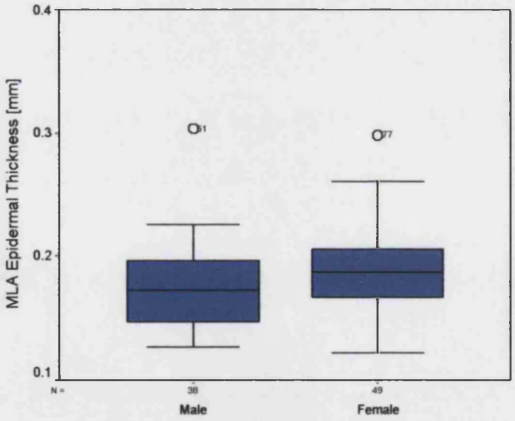

Male n=38
Median: 0.17 mm
Interquartile range: 0.05 mm
Minimum: 0.13 mm
Maximum: 0.30 mm

Female n=49
Median: 0.19 mm
Interquartile range: 0.05 mm
Minimum: 0.12 mm
Maximum: 0.30 mm

Mann-Whitney Test
p=0.036

Figure 8.12. The relationship between the sexes and epidermal thickness measurements taken from the MLA of the foot at a velocity of 1580 m/s.

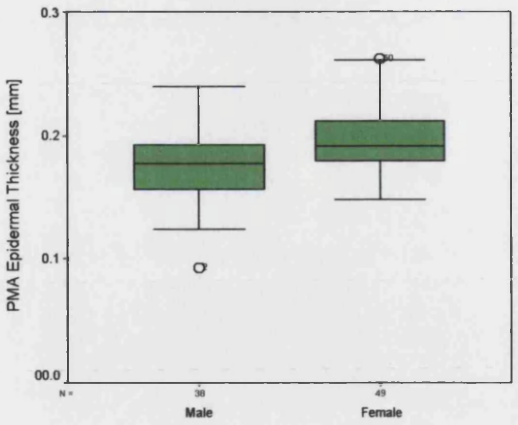

Male n=38
Median: 0.18 mm
Interquartile range: 0.04 mm
Minimum: 0.09 mm
Maximum: 0.24 mm

Female n=49
Median: 0.19 mm
Interquartile range: 0.04 mm
Minimum: 0.15 mm
Maximum: 0.26 mm

Mann-Whitney Test
p=0.002

Figure 8.13. The relationship between the sexes and epidermal thickness measurements from the PMA of the foot at a velocity of 1580 m/s.

8.11.3.7 The Relationship between Ethnicity and the Epidermal Thickness on the Foot

The subjects were divided into two groups (caucasian: n=69 and non-caucasian: n=18) and the two variables compared. No difference was noted between the two groups. The numbers in the groups differed greatly; therefore further investigations should be carried out if a more realistic association is to be made.

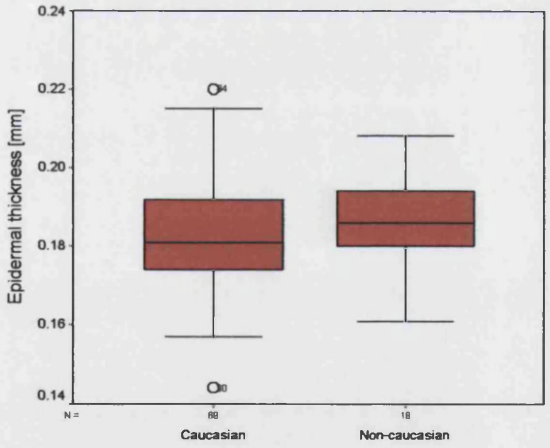

Caucasian n = 69
Median: 0.18 mm
Interquartile range: 0.02 mm
Minimum: 0.14 mm
Maximum: 0.22 mm

Non-caucasian n = 18
Median: 0.19 mm
Interquartile range: 0.01 mm
Minimum: 0.16 mm
Maximum: 0.21 mm

Mann-Whitney Test
p=0.222

Figure 8.14. The relationship between ethnicity and epidermal thickness measurements taken from the dorsum of the foot at a velocity of 1580 m/s.

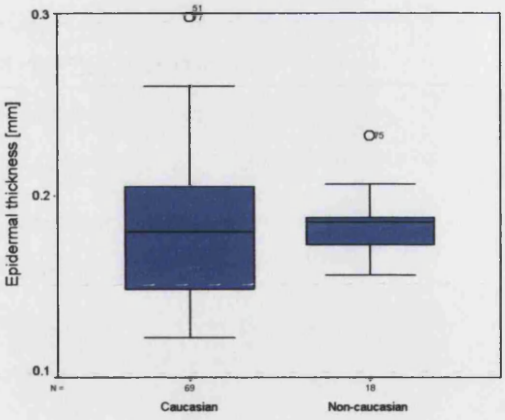

Caucasian n = 69
Median: 0.18 mm
Interquartile range: 0.06 mm
Minimum: 0.12 mm
Maximum: 0.30 mm

Non-caucasian n= =19
Median: 0.19 mm
Interquartile range: 0.02 mm
Minimum: 0.16 mm
Maximum: 0.26 mm

Mann-Whitney Test
p=0.571

Figure 8.15. The relationship between ethnicity and epidermal thickness measurements taken from the MLA of the foot at a velocity of 1580 m/s.

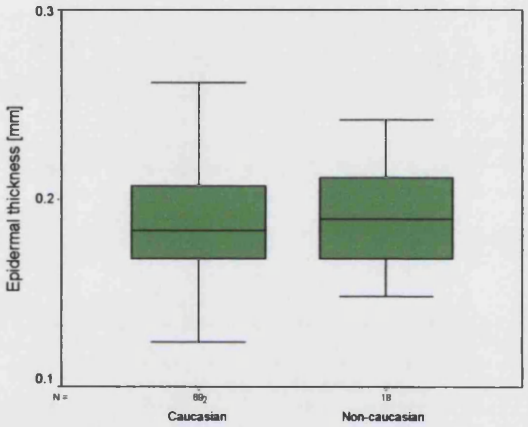

Caucasian n = 69
Median: 0.18 mm
Interquartile range: 0.39 mm
Minimum: 0.09 mm
Maximum: 0.26 mm

Non-caucasian
Median: 0.19 mm
Interquartile range: 0.04 mm
Minimum: 0.15 mm
Maximum: 0.24 mm

Mann-Whitney Test
p=0.597

Figure 8.16. The comparison between ethnicity and epidermal thickness measurements taken from the PMA of the foot at a velocity of 1580m/s.

8.11.4 Summary of Results

The measurements of epidermal thickness, taken from 87 healthy volunteers, showed no differences from site to site. There was a statistically significant difference between the thickness of epidermis on all sites on the foot between the sexes. Female epidermis was thicker than male epidermis.

This study has allowed for the comprehensive analysis of skin images on the foot, leading to the measurement of the epidermis on elected areas on the foot. The accuracy of the measurement technique and the relationship between the different areas will be discussed in more detail in the final chapter, after a comparison of this data is made with the diabetic patient data.

9.0 Chapter 9 – Patient Recruitment, Data Collection and Data Analysis

9.1 Introduction

This section outlines the patient recruitment process for the study, followed by a systematic collection of information from the volunteers regarding their diabetes status, therapy, secondary complications and general health. The health of the lower limbs was determined by extensive examination, enabling the investigator to categorise their physiological and structural condition e.g. peripheral ischaemia, peripheral sensory polyneuropathy, pes cavus, pes planus etc. Such categorisation enabled the ease of data assessment, particularly in the correlation analysis between data sets.

9.2 Patient Recruitment

9.2.1 Inclusion Criteria

- ***Test group - diabetic patients with plantar callus:*** All adults diagnosed with Type II diabetes, according to the WHO criteria [252] (Appendix XVI), were targeted in one health care district of North London (Barnet, Enfield, Harringay and Camden and Islington). Patients over the age of 18 years were invited to take part in the study from two main groups: the podiatry department and the Diabetic Eye Screening Service, Whittington hospital. Of the individuals that showed an interest in the study, the volunteers with callus on PMA were accepted.

- ***Control group - non–diabetic subjects with plantar callus:*** This group consisted of non-diabetic individuals age and sex matched to the diabetic test group. These patients were recruited from a poster and leaflet campaign in a number of Whittington Hospital Outpatient units.

- Subjects able to understand the research question.

9.2.2 Exclusion Criteria

- The presence of diffuse peripheral neuropathy other than diabetic neuropathy e.g. malignancy, alcohol abuse, drug abuse, anaemia, vitamin B_{12} deficiency or untreated hypothyroidism.
- Significant neurological disorders other than diabetic polyneuropathy e.g. stroke with significant neurological deficit, transient ischaemic attacks, multiple sclerosis, epilepsy, dementia and paraplegia.
- Previous or present treatment with cytotoxic drugs and/;or radiotherapy.
- Drug medications that may affect the autonomic nervous system and epidermal keratin metabolism.
- Individuals with systemic disorders likely to effect epidermal cell kinetics e.g. eczema, psoriasis and scleroderma.

The local hospital advisory ethical committee approved the protocol and ethics committees from all other participating centres approved the study. Written and verbal informed consent was obtained from every subject studied. One investigator carried out all the physical examinations. Examinations of the lower limb extremity were carried out on both legs.

9.2.3 Medical History

9.2.3.1 General Medical History

Details of medical conditions, drug therapies, skin and connective tissue disorders, social factors and ethnicity were noted. Duration and treatment of diabetes, blood or urine sugar levels and patients' social history, including details of smoking history were also collected. It was determined whether patients were registered blind or had impaired vision by questioning them. They were also asked if they had ever been treated for protein in their urine, were having ongoing haemodialysis, continuous ambulatory peritoneal dialysis, or previous kidney transplant.

9.2.3.2 Podiatric History

Patients were questioned as to whether they had previously attended a podiatrist for a routine visit for treatment and/or for foot care advice. Details of past foot ulceration were documented via questioning and/or accessing the podiatry/ medical notes. All diabetic patients were given diabetic foot care advice.

Patients were assigned a footwear risk category, dependent on which type of shoe and/or insole was worn by the patient when attending the research clinic: low risk e.g. trainers, lace–ups, boots (with a low heel), extra depth (bespoke and semi-bespoke) shoes, and high risk e.g. 'slip–ons', slippers; sandals, high–heeled shoes and flip–flops. The style of orthoses worn by the patient was also recorded.

9.2.4 Sample Collection

9.2.4.1 Venous Blood

Aliquots of venous blood (2 x 5 ml and 1 x 2 ml) were collected in heparinised tubes for HbA1c, glycation adduct and random glucose analysis, respectively. The HbA1c and random glucose were conducted at the haematology laboratories in the hospital. The glycation adducts in the serum were prepared and analysed in the research laboratory by the investigator, according to the protocols already described in Chapter 4 (section 4.4.3.2).

9.2.4.2 Plantar Callus

The site, approximate size and aesthetic nature of the callus were recorded. For the quantification of glycation adducts (furosine and pentosidine) in the callus, tissue specimens were collected from the PMA, immediately weighed and stored at -70°C. Before HPLC analysis, keratins were extracted from the callus tissue according to the protocol described in Chapter 2 (section 2.6) and acid hydrolysed as described in Chapter 4 (section 4.2.10).

9.2.5 Lower Limb Examinations

9.2.5.1 Assessment of Foot and Hand Structure

Structural deformities in the feet were assessed by noting: small muscle wasting♦, hammer and claw toes, 1st MTPJ deformities (hallux valgus and hallux limitus), prominent metatarsal heads, Charcot arthropathy and the range of motion of the STJ, MTJ and 1st MTPJs. Excessive subtalar joint pronation and supination (i.e. pes cavus and pes planus) were determined during stance and gait. Limited range of motion in the hands was examined by noting if there was lack of contact between any of the metacarpalphalangeal joints whilst attempting the 'prayer position' [47]. The presence of yellow nails♣ and skin♠ were also noted on both the hands and the feet along with any other nail pathologies were noted.

9.2.5.2 Assessment for Peripheral Neuropathy

Prior to the physical examination, patients were asked "Do you think you have good sensation or feeling in your feet?". After responding, they were asked if they had symptoms of burning, tingling, or shooting pains in their feet, including the duration of the symptoms, indicating positive clinical symptoms of neuropathy.

Peripheral neuropathy was assessed by a number of well-established clinical techniques [22;253]. Abnormalities of pain sensation were determined using a Neurotip™; vibration sensation was tested on the tip of the hallux, malleoli and tibial tuberosities, using a 128–Hz tuning fork; dorsal temperature sensation was carried out using warm and cool rods; and Achilles tendon and patella tendon reflexes were also assessed. Cutaneous pressure perception was tested using a 1 g, 10 g and 75 g Semmes Weinstein monofilament at six sites (1st and 5th plantar metatarsal area, heel, arch, apices of toes and dorsum) on each foot.

♦ Wasting of the inerossi results in 'troughing' between the dorsal tendons [25].

♣ Yellow nails were defined as smooth, slightly thickened nails of a yellow of yellowish green hue. They were often noted on the hallux nail only and in general on the proximal edge of the nails.

♠ The palms of the hands and soles of the feet were checked for a yellow hue in the skin.

With the eyes closed, the patients were required to elicit a 'yes/ no' response to monofilament pressure and correctly identify the site of contact. The filament was placed on the foot perpendicular to the surface of the skin to ensure that the filament flexed with a constant force, commencing with the 1 g filament. If the 1 g filament was not felt at any one site the 10 g filament was then tested at that position. Furthermore, if the 10 g filament was not felt, the 75 g monofilament was similarly applied. For statistical analysis, insensitivity to at least the 10 g filament at any one site on either foot was indicated as abnormal sensation.

Each sensory test was scored (Appendix XVII). According to this system a score of up to 19 represented people with no peripheral neuropathy; a score of 20-22 represented moderate neuropathy and a score of between 23-37 represented severe neuropathy.

9.2.5.3 Assessment of Peripheral Circulation

Peripheral vascular status was assessed by palpation of the dorsalis pedis and posterior tibial pulses on both feet. Presence of two or less of the four pedal pulses, either with or without the presence of odema, and/ or an ankle–brachial index (ABI) of < 0.9 [254]*, indicated PVD [255]. In the case of arteriosclerosis and atheroma the ABI is less than 0.9. However, in cases where there is median arterial calcification, there is as an artificially elevated systolic pressure in the ankle, giving an ABI reading of above 0.9. Doppler analysis was used to clarify the type of blood flow in the periphery e.g. triphasic, biphasic or monophasic. Patients were classified as having intermittent claudication (IC) if they experienced calf pain on exertion within 100 yards or less. Claudication is often absent because of concomitant neuropathy. In addition the patients were questioned about any previous peripheral angioplasty or peripheral bypass surgery they had undergone to determine a comprehensive peripheral vascular history.

9.2.6 Physical Measurements if Pedal Skin

9.2.6.1 Ultrasonography

Ultrasound images (frequency 1580 m/s) were taken of the skin from the three sites: plantar metatarsal area immediately adjacent to the callus, medial longitudinal arch and the dorsal aspect of the foot, avoiding areas with prominent tendons and bony protuberances.

The images were all taken with the same gain parameters and saved for measurement of epidermal thickness using A-mode, as detailed in Chapter 8 (section 8.11.2).

9.2.6.2 Epidermal Mechanics

The epidermal mechanics were measured on the same three sites used for the ultrasound imaging. The humidity and temperature within the room was noted.

9.2.7 Outcomes Measures

The following data were recorded from each diabetic (n=103) and non-diabetic (n=87) subject.

- Concentration of furosine and pentosidine (ng/mg of protein) in plantar callus.
- Concentration of furosine and pentosidine (ng/mg of protein) in blood serum.
- HbA1c
- Random glucose
- Epidermal thickness on the PMA, MLA and dorsum of the left foot.
- Epidermal viscoelasticity on the PMA, MLA and dorsum of the left foot.

---

* Ankle-Brachial index is calculated as the higher of the DP or PT arterial systolic Doppler blood

9.3 Results

9.3.1 Patient Details

A total of 103 Types II diabetic patients and 87 non-diabetic subjects were invited to take part in the study (Table 9.1).

Table 9.1. Patient groups used in the study.

Subject Group	Total Number	Number of Males	Mean Age [yrs]	Age Range [yrs]	Number of Females	Mean Age [yrs]	Age Range [yrs]
Type II Diabetics	103	58	64.9 ± 11.0	37 - 86	45	62.0 ± 8.9	36 - 82
Non-Diabetics	87	38	55.6 ± 6.8	43 - 69	49	58.1 ± 13.1	35 - 81

9.3.1.1 Diabetic Patient Details

The duration of diabetes was calculated from the date of diagnosis, and ranged from 0.1 to 32.0 yrs (mean: 6.4 ± 7.0 yrs).

The Body Mass Index (BMI)[∞] ranged from 20.0 to 61.3. On average, the subjects were overweight (mean BMI: 25.0 ± 1.7).

The majority of the volunteers (65%) were taking regular oral hypoglycaemic drugs; 27% were controlling their diabetes through diet; 6% were on insulin therapy alone and 2% were on a combination of oral hypoglycaemic and insulin therapies.

Only 28% of patients reported the presence of complications secondary to diabetes. Retinopathy was reported by 16% of the subjects; 8% had renal problems and 4% reported peripheral neuropathy. The incidence of vascular complications was: poor peripheral circulation (3%); hypertension (49%); myocardial infarction (7%) and angina (19%).

---

pressure divided by the higher brachial arterial Doppler blood pressure in both arms

[∞] BMI - <18.5: underweight; 18.5–24.9: normal; 25.0-29.9: overweight and >30.0: obese.

Generally, 6% of subjects reported foot pathologies, 7% had Tinea Pedis and only 3% reported poor peripheral circulation problems.

A positive smoking history was elicited from 16% of the patients.

9.3.1.2 Non-Diabetic Subject Details

The BMI of the non-diabetic group ranged from 19.8 to 39.3. On average the volunteers were overweight, with a mean BMI of 27.0 ± 4.3.

Reports of problems with the feet came from 43% of the volunteers, 16% of which presented with Tinea Pedis as a skin complaint. Only one person complained of problems with peripheral circulation (Raynauds syndrome). Other vascular pathologies included: hypertension (23%), myocardial infarction (3%) and angina (2%).

A positive history of smoking was elicited from 23% of the patients.

9.3.2 Questioning and Examinations

All the volunteers (diabetics and non-diabetics) were asked the same questions and subjected to the same examinations.

9.3.2.1 Description of Callus

Pathological callus formation was present in 52% and 77% of the diabetic and non-diabetic volunteers, respectively.

A majority of the diabetic group presented with minimal stratum corneum thickening, whereas the non-diabetic group had an almost equal presentation of the three callus groups (Table 9.2). Both groups presented with predominantly diffuse callus covering an area of less than 1 cm^2 of plantar skin, with a texture that was either glassy or flaky. Only a small portion of the patients had discrete

round or oval callus plaques. The association of the callus with corns was 15% and 25% in the diabetic and non-diabetic groups, respectively.

Close examination of the footwear revealed an approximate ratio of 1:2 of high risk to low risk categories (Table 9.3).

Table 9.2. Description of plantar callus in diabetic and control volunteers

Description of Callus		Diabetics (%)	Non-Diabetics (%)
Thickness	Discrete area with minimal thickening of keratin layer	64	39
	Moderate Thickening	26	37
	Marked Thickening	10	24
Shape	Diffuse	55	69
	Oval	37	22
	Round	8	5
Texture	Spongy	1	2
	Glassy	48	49
	Flaky	51	48
Associated with Corns	Yes	15	26
	No	85	62
Area	< 1cm	68	68
	1 – 3cm	24	31
	3 – 5 cm	8	1
Chiropody Treatment/ Callus Removal	1 – 3 mths	38	5
	3 – 6 mths	8	0
	6 – 9 mths	0	0
	9 – 12 mths	12	0
	No treatment	43	95

Table 9.3. Description footwear.

		Diabetic (%)	Non-diabetic (%)
Low risk footwear	**Bespoke**	3	0
	Semis-bespoke	1	1
	Well-fitted shoes	62	67
High risk footwear	**Ill-fitted shoes**	34	32

Table 9.4. Description of insoles and orthoses.

	Diabetic (%)	Non-diabetic (%)
Simple insole	6	3
Casted orthotic	2	3
Diabetic insole	2	0
No orthoses	90	93

Diabetic volunteers with moderate and marked peripheral neuropathy had corns associated with callus (Table 9.5).

Table 9.5. The incidence of callus formation in neuropathic patients

Type of Neuropathy	Number of Patients with Thick Plantar Callus	Incidence of Thick Plantar Callus (%)	Number of Patients with Discrete Plantar Callus Lesions	Incidence of Discrete Plantar Callus Lesions (%)	Number of Patient with Corns Associated with Callus	Incidence of Corns Associated with Callus (%)
None (n=19)	44	90	19	39	1	11
Moderate (n=35)	29	83	18	51	7	20
Severe (n=19)	18	95	5	26	7	37

9.3.2.2 Structure of the Foot and Cutaneous Pathologies

Diabetics had a higher incidence of anhydrosis than non-diabetics, as well as a large percentage of yellow nails in both the feet and the hands (Table 9.6). The structures of the toes were similar in both groups. Diabetics presented with a higher occurrence of pronated foot than the controls. A cavoid type foot presented in the diabetic group was of the same incidence as non-diabetic pes cavus. The presentation of one pes cavus foot and one pes planus foot was only seen in the non-diabetics group.

Table 9.6. Results from the physical examination of the feet of 190 patient.

Structural Pathology		Diabetics	Non–Diabetics
Skin Pathologies	Fissures	4	2
	Tinea Pedis	7	7
	Anhydrosis	72	48
	Hyperhydrosis	9	14
	Absence of Hair	27	22
Nail Pathologies	O/C	0	0
	O/M	14	16
	O/X	5	0
	Yellow Nail	63	39
	Normal	22	43
Lesser Toe Structure	Hammertoes	8	3
	Claw	27	32
	Mallet	0	2
	Normal	65	66
Hallux Structure	HAV	21	34
	Trigger	4	6
	Hyperextended	1	1
	Normal	46	56
General Foot Structure	Pes Planus	61	48
	Pes Cavus	17	18
	Pes Cavus & Pes Planus	0	6
	Normal	21	28
Limited ROM in Feet	STJ	23	15
	MTJ	7	2
	1st MTPJ	27	23
	Charcot Foot	0	0
	Normal ROM	46	62
History of Ulceration	Yes	7	0
	No	93	0
Hands	Limited ROM	47	22
	Normal ROM	53	97
	Yellow skin	18	2
	Yellow nail	7	1

Of the marked neuropathy group, 63% (12 out of 19) presented with limited range of motion (ROM) in the feet. Patients with moderate no signs of peripheral neuropathy also had a high incidence of limited ROM in the joints of the foot, of 51% (25 out of 49). The same incidence of limited ROM was noted in volunteers with moderate neuropathy. The limited ROM was noted to be significantly higher in the older age group ($p=0.003$). Cheiroarthropathy in conjunction with limited ROM in the feet was noted in 33% (34 out of 103) of the diabetic subjects.

9.3.2.3 Peripheral Neurological Examination

The prevalence of symptomatic neuropathy was 33%, of which 52% was of a chronic nature; 25% of patients had symptoms of chronic pain and 15% had acute pain. A history of foot ulceration was described by 7% of the patients; 72% presented with autonomic symptoms (Table 9.7).

Table 9.7. Information regarding the symptoms of neuropathy

		Number of Subjects
Symptoms	Present	33
	Absent	70
Nature of Symptoms	Positive symptoms	34
	Negative symptoms	69
Duration of symptoms	<1yr	17
	1-3yrs	5
	>3yrs	12
Chronic pain	Yes	26
	No	77
Acute pain	Neuropathic pain	15
	Contact hyperaesthesia	2
	No	86
History of ulceration	Yes	7
	No	96
Autonomic symptoms	Yes	74
	No	29

According to the scoring system 48% of the patients had no neuropathy, 33% presented with mild neuropathy and 19% showed signs of severe neuropathy. All the non-diabetics subjects scored 19 (Table 9.8).

Figure 9.8. Neuropathic examinations and scoring system.

Neurological Examination		Score	Number of Subjects
Pin Prick	Painful	**1**	73
	Unclear	**2**	6
	Not painful	**3**	24
Light touch	Yes	**1**	86
	Unclear	**2**	9
	No	**3**	8
Vibration	Yes	**1**	16
	No	**2**	87
Pressure perception	Yes	**1**	90
	Unclear	**2**	5
	No	**3**	8
Ankle reflex	L/F yes	**1**	97
	R/F yes	**2**	97
	L/F no	**3**	6
	R/F no	**4**	6
Knee reflex	L/F yes	**1**	103
	R/F yes	**2**	103
	L/F no	**3**	0
	R/F no	**4**	0
Muscular atrophy	No bilateral	**1 2**	0
	Yes unilateral	**2 3**	6
	Yes bilateral	**3 4**	97
Proprioception	Yes	**1**	103
	No	**2**	0
Two point discrimination	Yes	**1**	93
	No	**2**	10

9.3.2.4 Peripheral Vascular Examination

Measurement of the ankle brachial index revealed 24% of diabetics and 2% of non-diabetics to have an index of less than 0.9. Diabetic patients (22%) and non-diabetic patients (2%) complained of intermittent claudication IC. Of the diabetic patients with IC: 75% had an ABI greater than 0.9 and the remaining 25% had an ABI of less than or equal to 0.9. There were no patients with an ABI of less than 0.5.

Therefore, there was a higher incidence of PVD in the diabetics than the non-diabetics. Only 10% (2 out of 19) of diabetics with severe neuropathy had PVD. Out of the patients with no peripheral neuropathy 47% (23 out of 49) had PVD and of the moderate neuropaths 37% (13 Out of 35) had peripheral ischaemia (Table 9.9).

Table 9.9. Results of the peripheral vascular examinations.

Vascular Examination		Diabetic	Non-diabetic
Skin colour	**Normal**	65	92
	Hyperaemic	28	7
	Pallor	7	1
Skin texture	**Hyperhydrotic**	7	17
	Anhydrotic	79	46
	Trophic changes	18	2
	Normal	13	34
Skin temperature	**Normal**	55	80
	Cold	35	18
	Warm	10	1
Varicose veins	**Yes**	21	14
	No	79	86
Odema	**Yes**	23	7
	No	77	93
History of DVT	**Yes**	3	3
	No	97	97
Vascular surgery	**Yes**	11	5
	No	89	95
Intermittent claudication	**Yes**	22	2
	No	78	98
Heart conditions	**Myocardial infarction**	7	2
	Angina	17	2
	Hypertension	49	23
Capillary refill time	**Immediate**	14	57
	1sec	29	22
	2sec	30	14
	3sec	21	7
	>3sec	6	0
Palpable pedal pulses	**R/F Dorsalis Pedis only**	25	24
	L/F Dorsalis Pedis only	25	24
	R/F Posterior Tibial only	3	0
	L/F Posterior Tibial only	3	0
	All pedal pulses	71	76
	No	1	0
Doppler analysis	**Triphasic**	50	86
	Biphasic	45	11
	Monophasic	24	2
AB index	**<0.9**	24	2
	>0.9	76	98

9.4 Statistical Analysis of Data

9.4.1 Distribution of Data

The data was not normally distributed (Appendix XVIII). Non-parametric methods of analysis were used.

9.4.2 Analysis of Furosine Data

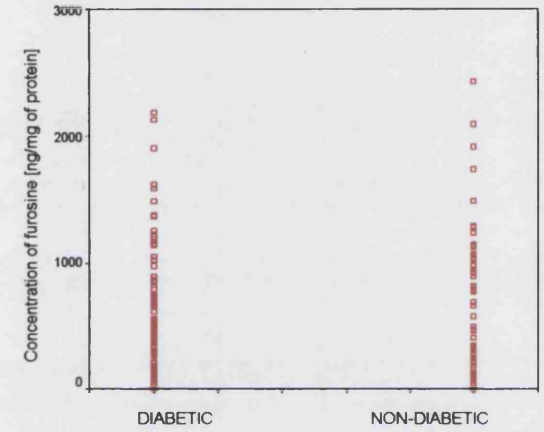

Diabetics n=103
Median: 507.3 ng/mg of protein
Interquartile range: 589.1 ng/mg of protein
Minimum: 0.0 ng/mg of protein
Maximum: 1590.5 ng/mg of protein

Non-diabetics n=87
Median: 471.2 ng/mg of protein
Interquartile range: 903.1 ng/mg of protein
Minimum: 0.0 ng/mg of protein
Maximum: 6331.6 ng/mg of protein

Mann-Whitney Test
p=0.503

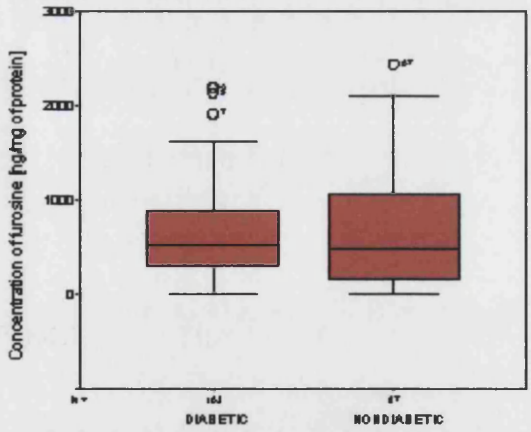

Figure 9.1. The comparison of furosine concentrations in the plantar callus of diabetic and non-diabetic individuals

There was no significant difference in the concentration of furosine between the diabetic and non-diabetic individuals.

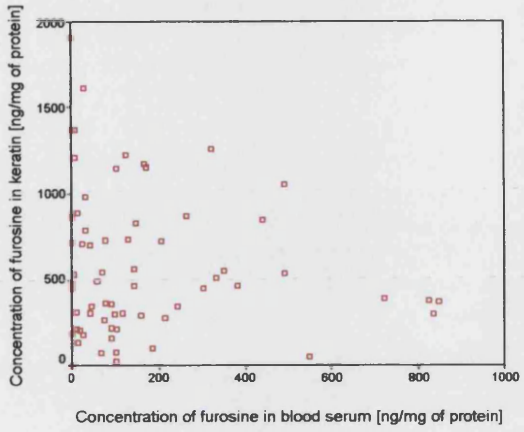

Spearman's Correlation
r=-0.115

Furosine in Keratin Extracts n=103
Median: 507.3 ng/mg of protein
Interquartile range: 589.1 ng/mg of protein
Minimum: 0.0 ng/mg of protein
Maximum: 1590.5 ng/mg of protein

Furosine in Blood Serum n=80
Median: 99.2 ng/mg of protein
Interquartile range: 268.6 ng/mg of protein
Minimum: 0.0 ng/mg of protein
Maximum: 2526.1 ng/mg of protein

Mann-Whitney Test
p=0.001

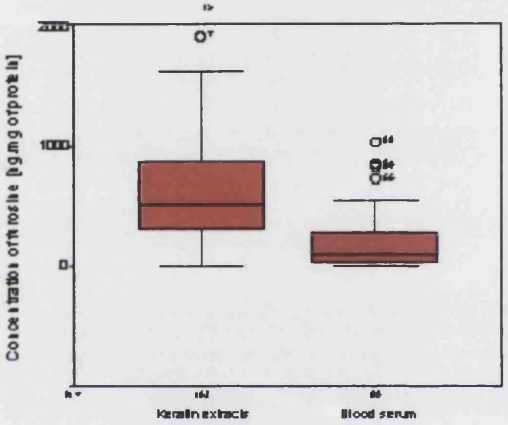

Figure 9.2. The comparison of furosine concentrations in diabetic plantar callus and blood serum.

There was no correlation between the concentration of furosine in plantar callus and furosine in the blood serum of diabetic individuals (Fig. 9.2). A significant difference was noted between the two groups.

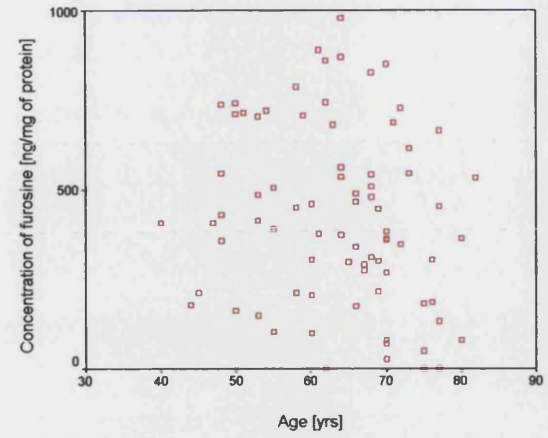

Spearman Correlation
r=0.088

Age group <65 years n=50
Median: 621.9 ng/mg of protein.
Interquartile range: 535.3 ng/mg of protein.
Minimum: 0.0 ng/mg of protein
Maximum: 4757.8 ng/mg of protein

Age group ≥65 years n=53
Median: 452.5 ng/mg of protein.
Interquartile range: 728.2 ng/mg of protein.
Minimum: 0.0 ng/mg of protein
Maximum: 1590.5 ng/mg of protein

Mann-Whitney Test
p=0.180

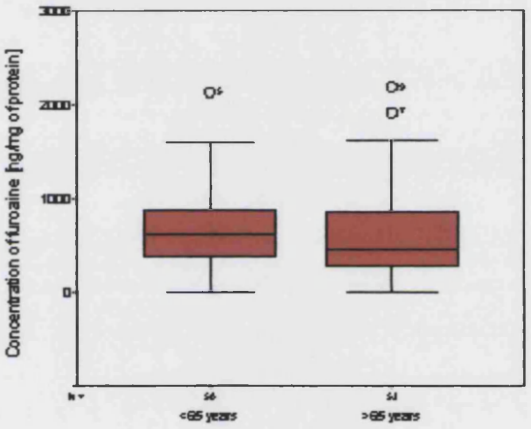

Figure 9.3. The comparison of furosine concentrations in diabetic plantar callus and the age of the subjects.

There was no correlation between the concentration of furosine in diabetic plantar callus and the age of the volunteers (Fig. 9.3). There was no significant difference found between the two age groups in terms of furosine concentration (Fig. 9.3).

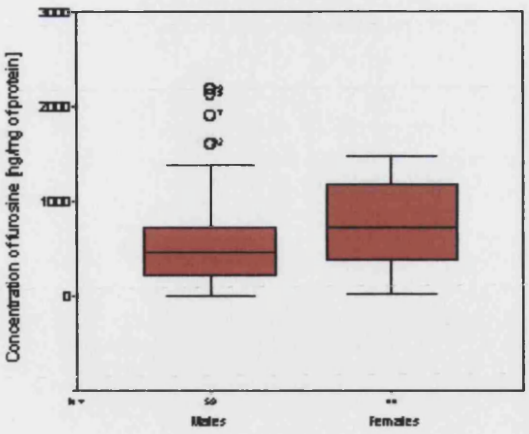

Male n=59
Median: 447.2 ng/mg of protein
Interquartile range: 502.6 ng/mg of protein
Minimum: 0.0 ng/mg of protein
Maximum: 3368.7 ng/mg of protein
Mean: 615.2 ng/mg of protein

Female n=44
Median: 729.9 ng/mg of protein
Interquartile range: 825.7 ng/mg of protein
Minimum: 26.6 ng/mg of protein
Maximum: 1590.5 ng/mg of protein
Mean: 1549.7 ng/mg of protein

Mann-Whitney Test
p=0.01

Figure 9.4. The comparison of furosine concentrations in diabetic plantar callus in males and females.

There was a significant difference in the concentration of furosine in diabetic plantar callus between males and females (p=0.01). The concentration of furosine in the female diabetic callus samples was significantly higher than that measured in male diabetic callus.

9.4.3 Analysis of Pentosidine Data

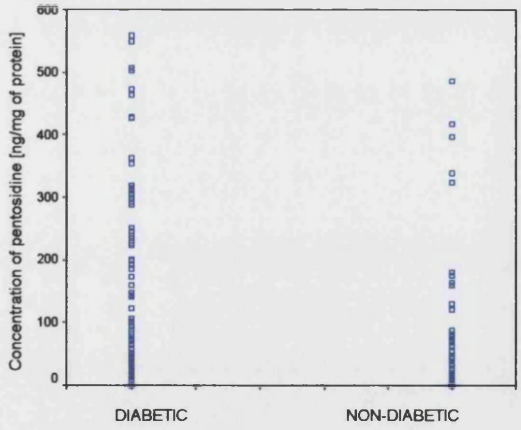

Diabetics n=103
Median: 72.8 ng/mg of protein
Interquartile range: 171.3 ng/mg of protein
Minimum: 0.0 ng/mg of protein
Maximum: 848.3 ng/mg of protein
Mean: 136.9 ng/mg of protein

Non-diabetics n=87
Median: 10.5 ng/mg of protein
Interquartile range: 54.1 ng/mg of protein
Minimum: 0.0 ng/mg of protein
Maximum: 485.4 ng/mg of protein
Mean: 49.8 ng/mg of protein

Mann-Whitney Test
p=0.001

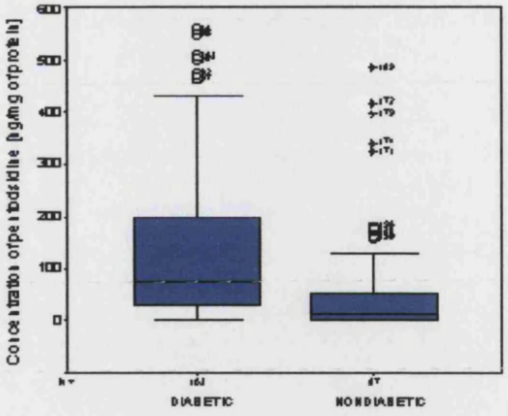

Figure 9.5. The comparison of the concentrations of pentosidine in the plantar callus of diabetic and non-diabetic individuals.

A significant difference was found between the test and control groups when comparing the concentration of pentosidine in plantar callus tissue (p=0.001). The power of this result was 99% (where; n = 190 and positive proportion = 35%).

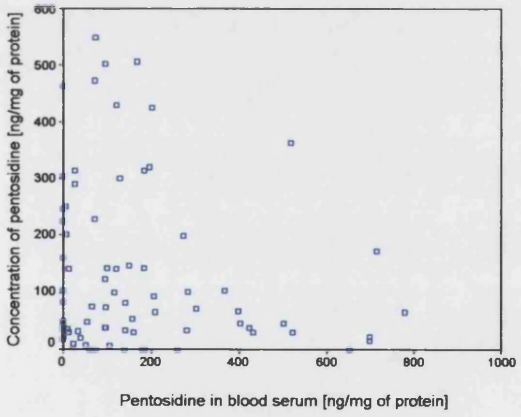

Spearman's Correlation
r=-0.023

Pentosidine in Keratin Extracts n=103
Median: 72.3 ng/mg of protein
Interquartile range: 171.3 ng/mg of protein
Minimum: 0.0 ng/mg of protein
Maximum: 848.3 ng/mg of protein

Pentosidine in Blood Serum n=90
Median: 119.6 ng/mg of protein
Interquartile range: 260.2 ng/mg of protein
Minimum: 0.0 ng/mg of protein
Maximum: 1780.2 ng/mg of protein

Mann-Whitney Test
p=0.149

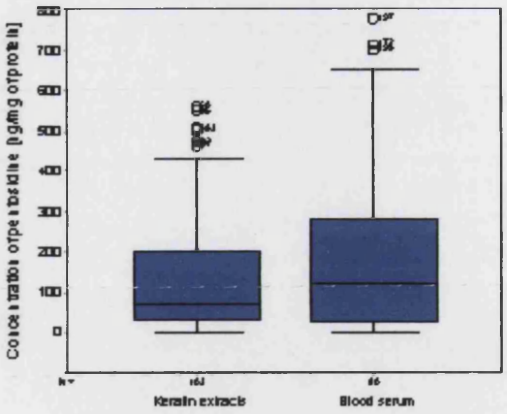

Figure 9.6. The comparison of pentosidine concentrations in diabetic plantar callus and blood serum.

There was no correlation between the concentration of pentosidine in diabetic plantar callus and the blood serum concentration of pentosidine (Fig. 9.6).

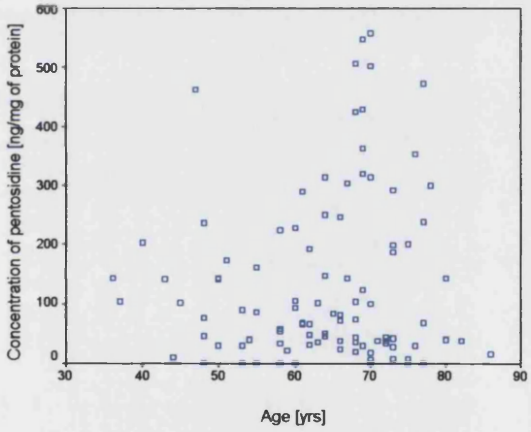

Spearman Correlation
r=0.095

Age group <65 years n=50
Median: 71.0 ng/mg of protein.
Interquartile range: 119.5 ng/mg of protein.
Minimum: 0.0 ng/mg of protein
Maximum: 848.3 ng/mg of protein

Age group ≥65 years n=53
Median: 72.8 ng/mg of protein.
Interquartile range: 266.3 ng/mg of protein.
Minimum: 0.0 ng/mg of protein
Maximum: 558.2 ng/mg of protein

Mann-Whitney Test
p=0.456

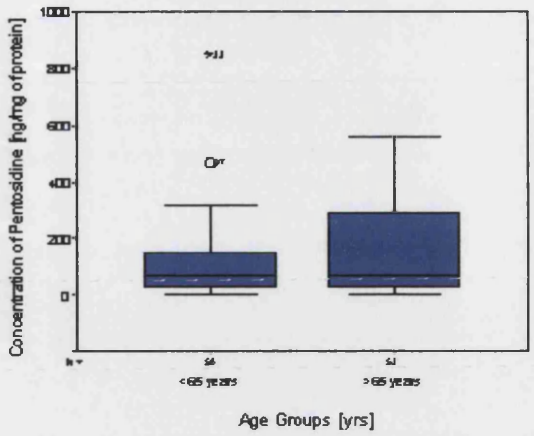

Figure 9.7. The comparison of pentosidine concentrations in diabetic plantar callus and the age of the subjects.

No positive correlation was found between the concentration of pentosidine in diabetic plantar callus and the age of the volunteers (Fig. 9.7). There was no significant difference found between the two age groups.

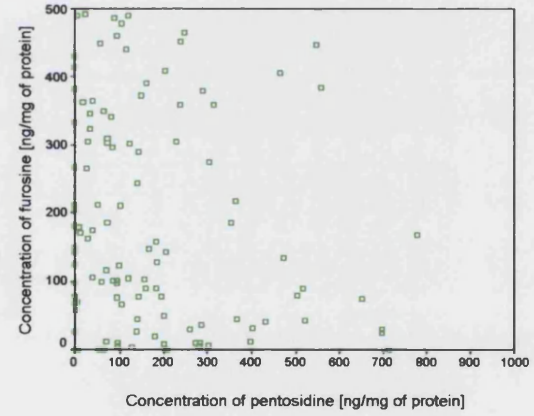

Spearman's Correlation
r=0.144

Furosine in Keratin Extracts n=103
Median: 507.3 ng/mg of protein
Interquartile range: 589.1 ng/mg of protein
Minimum: 0.0 ng/mg of protein
Maximum: 15904.9 ng/mg of protein

Pentosidine in Keratin Extracts n=103
Median: 73.9 ng/mg of protein
Interquartile range: 170.0 ng/mg of protein
Minimum: 0.0 ng/mg of protein
Maximum: 848.3 ng/mg of protein

Mann-Whitney Test
p=0.001

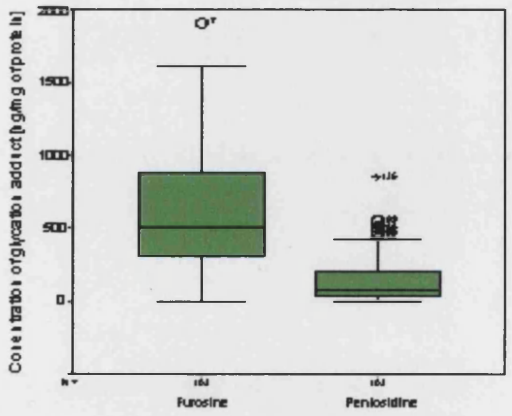

Figure 9.8. The comparison of pentosidine and furosine concentrations in the plantar diabetic callus samples.

There was no correlation between the concentration of furosine and pentosidine in the diabetic plantar callus samples (Fig. 9.8). The amount of furosine measured in the samples was significantly higher (~ 7-times) than pentosidine in the same set of callus samples.

9.4.4 Mechanical Properties of the Epidermis

9.4.4.1 The Series Elastic Elements and the Time Constants on Stretching and on Retraction of the Epidermis on all Three Sites of the Foot

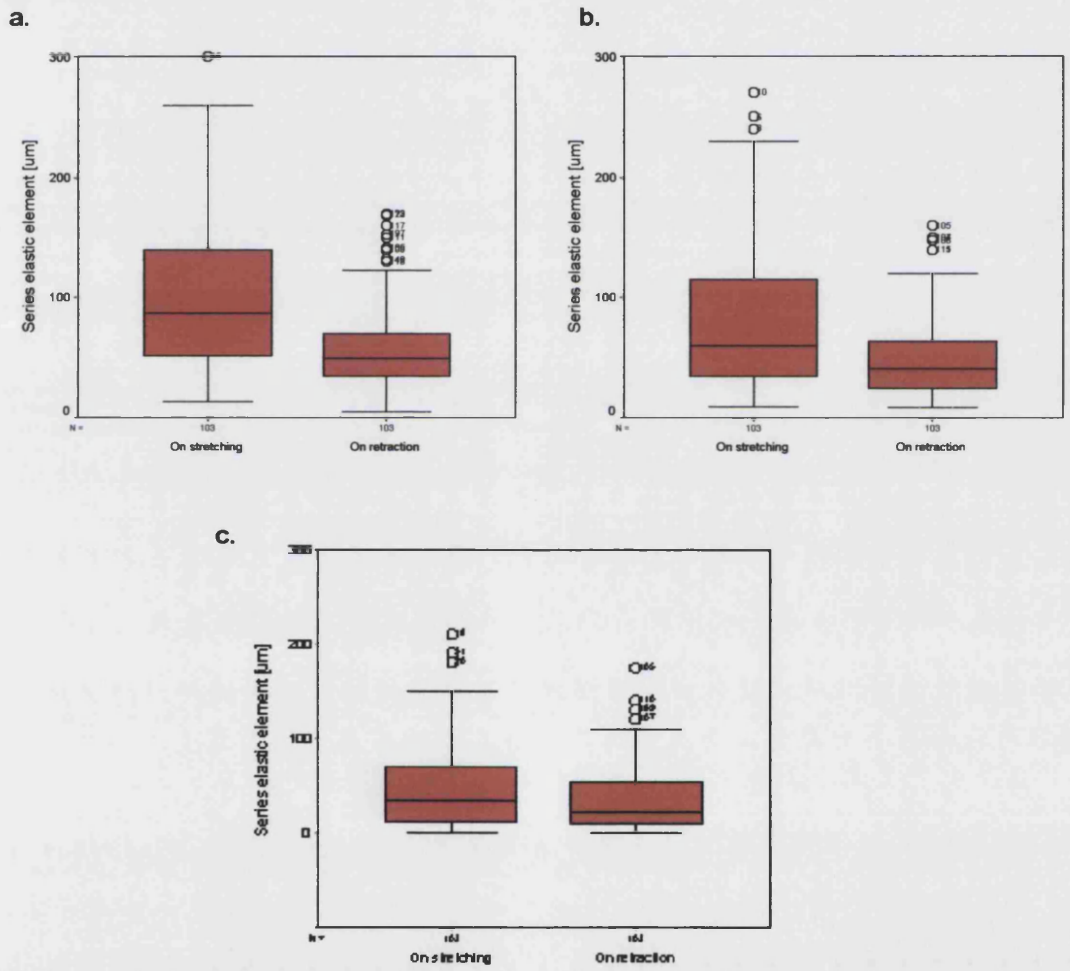

Fig. 9.9. A comparison between the series elastic element data in stretching and on retraction. **a.** Dorsum **b.** MLA **c.** PMA

There was a significant difference between the series elastic element data on stretching and retraction on all sites on the foot ($p<0.01$).

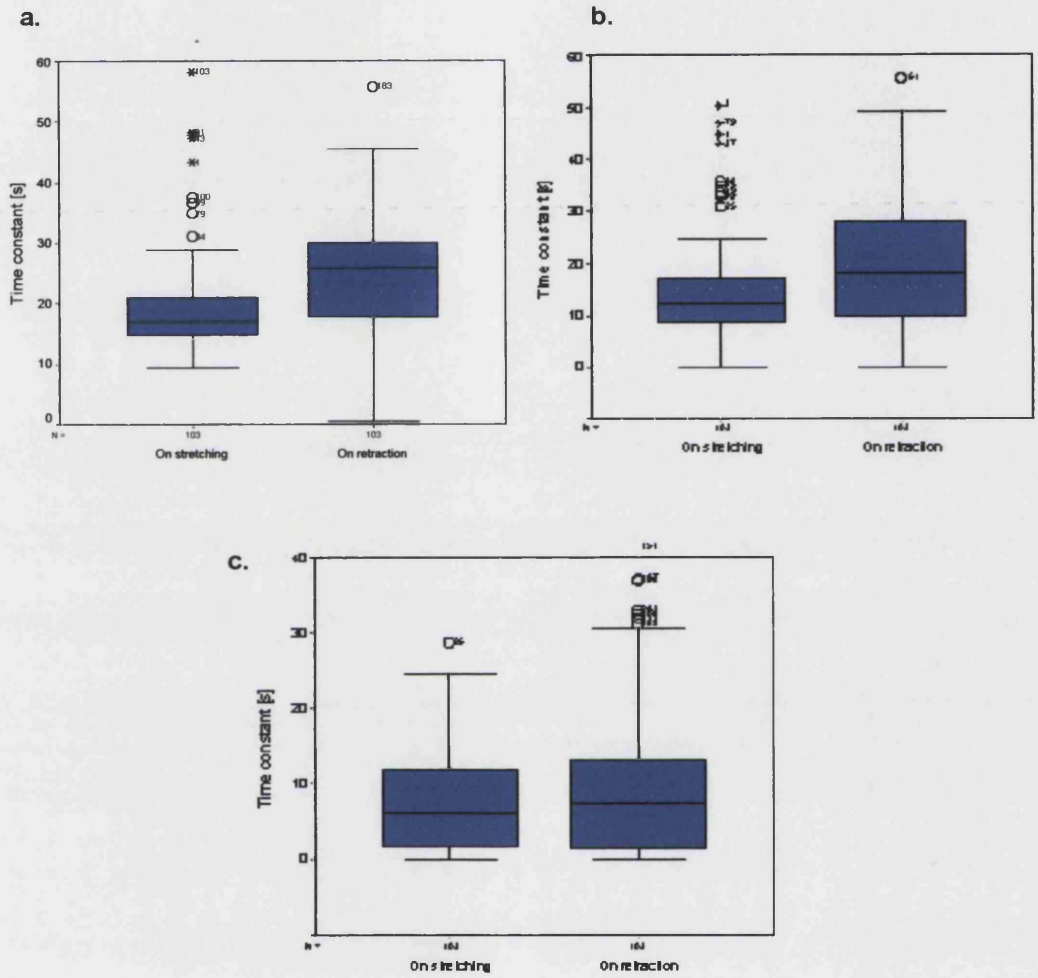

Fig. 9.10. A comparison between the time constant data in stretching and on retraction. **a.** Dorsum **b.** MLA **c.** PMA

There was a significant difference between the time constants on stretching and retraction of the dorsal skin ($p<0.01$), but not on the MLA and PMA ($p>0.05$).

Table 9.10: Descriptive data for the series elastic element and time constant data collected from three sites on diabetic feet.

		Dorsum	MLA	PMA
Series Elastic Element on Stretching [μm]	Median	87	60	34
	Interquartile Range	90	85	59
	Minimum	13	9	0
	Maximum	300	270	280
Series Elastic Element of Retraction [μm]	Median	50	41	21
	Interquartile Range	36	40	48
	Minimum	5	8	0
	Maximum	192	220	250
Time constant on Stretching [s]	Median	17.1	12.4	6.2
	Interquartile Range	6.3	8.7	10.4
	Minimum	9.4	0.0	0.0
	Maximum	6307	65.0	61.3
Time Constant on Retraction [s]	Median	25.8	18.3	7.3
	Interquartile Range	12.5	18.5	12.0
	Minimum	0.5	0.0	0.0
	Maximum	55.8	55.6	41.3

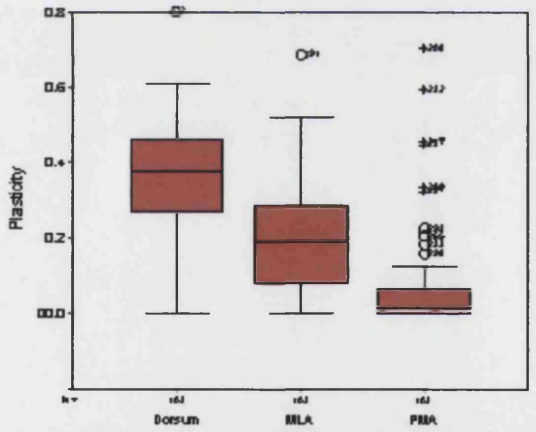

Dorsum
Median: 0.38
Interquartile range: 0.19
Minimum: 0.00
Maximum: 0.98

MLA
Median: 0.19
Interquartile range: 0.21
Minimum: 0.00
Maximum: 0.97

PMA
Median: 0.02
Interquartile range: 0.07
Minimum: 0.00
Maximum: 1.00

Mann-Whitney Test

Dorsum v MLA: p = 0.001

Dorsum V PMA: p = 0.001

MLA v PMA: p = 0.001

Fig. 9.11. A comparison of plasticity data between the three sites on the foot.

9.4.4.2 The Series Elastic Element Data

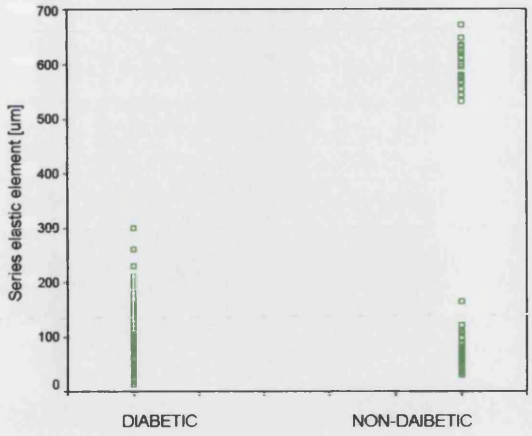

Diabetics n=103
Median: 87.0 µm
Interquartile range: 90.0 µm
Minimum: 13.0 µm
Maximum: 300.0 µm

Non-diabetic n=87
Median: 67.0 µm
Interquartile range: 121.0 µm
Minimum: 31.0 µm
Maximum: 671.0 µm

Mann-Whitney Test
p=0.756

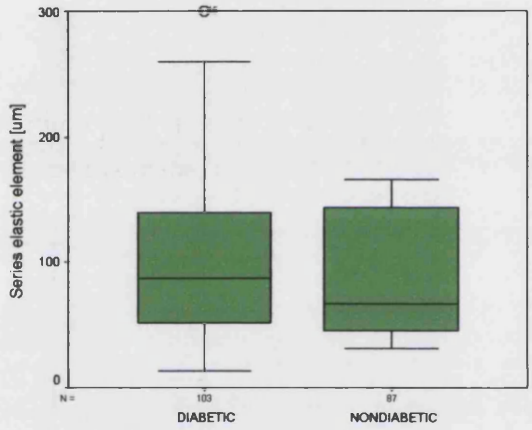

Figure 9.12. Diabetic and non-diabetic series elastic elements on stretching of the dorsal epidermis.

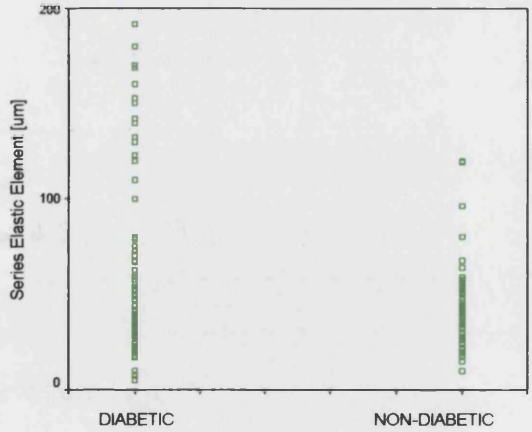

Diabetics n=103
Median: 50.0 µm
Interquartile range: 36.0 µm
Minimum: 5.0 µm
Maximum: 192.0 µm

Non-diabetic n=87
Median: 38.0 µm
Interquartile range: 22.0 µm
Minimum: 10.0 µm
Maximum: 120.0 µm

Mann-Whitney Test
p=0.001

Sample Power
99%
n = 190
Positive proportion = 35%

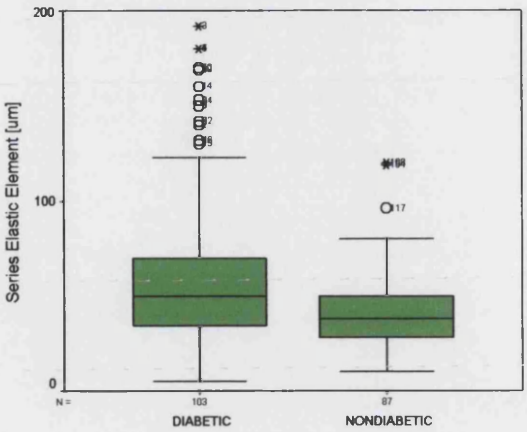

Figure 9.13. Diabetic and non-diabetic series elastic elements on retraction of the dorsal epidermis.

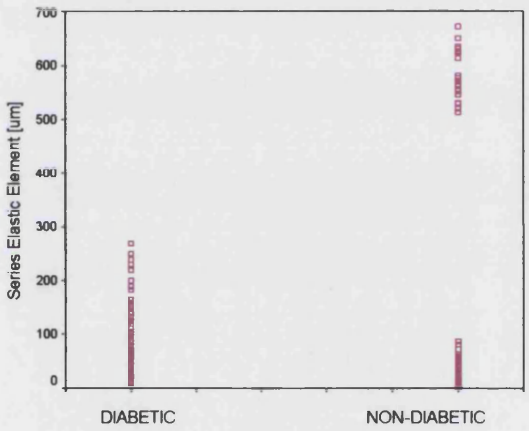

Diabetics n=103
Median: 60.0 µm
Interquartile range: 85.0 µm
Minimum: 9.0 µm
Maximum: 270.0 µm

Non-diabetic n=87
Median: 47.0 µm
Interquartile range: 489.0 µm
Minimum: 2.0 µm
Maximum: 671.0 µm

Mann-Whitney Test
p=0.497

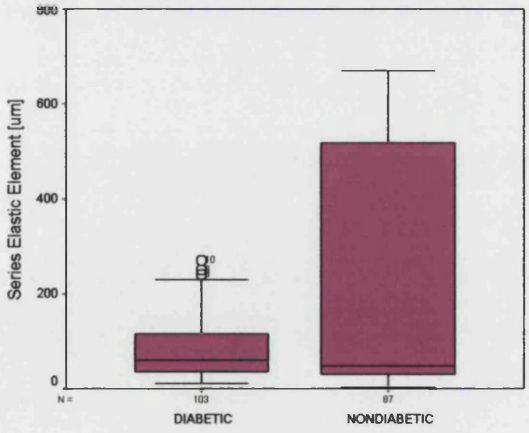

Figure 9.14. Diabetic and non-diabetic series elastic elements on stretching of the epidermis on the MLA.

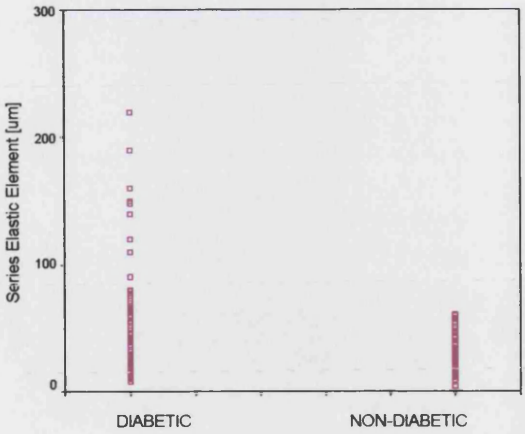

Diabetics n=103
Median: 41.0 µm
Interquartile range: 40.0 µm
Minimum: 8.0 µm
Maximum: 220.0 µm

Non-diabetic n=87
Median: 27.0 µm
Interquartile range: 20.0 µm
Minimum: 4.0 µm
Maximum: 61.0 µm

Mann-Whitney Test
p=0.001

Sample Power
97%
n = 190
Positive proportion = 36%

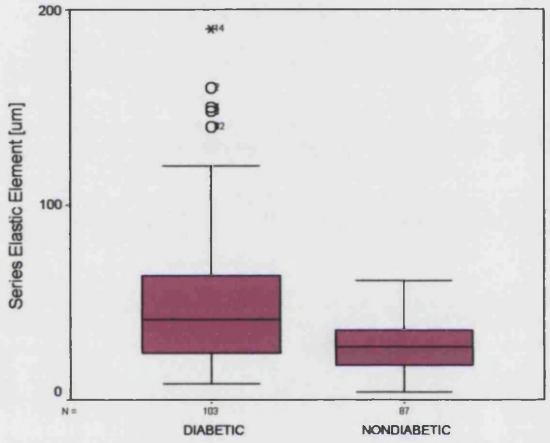

Figure 9.15. Diabetic and non-diabetic series elastic elements on retraction of the epidermis on the MLA.

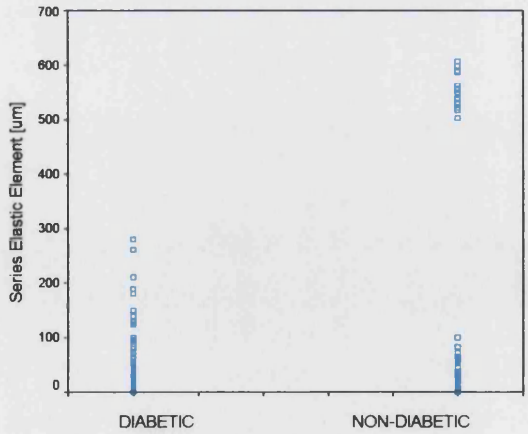

Diabetics n=103
Median: 34.0 µm
Interquartile range: 59.0 µm
Minimum: 0.0 µm
Maximum: 280.0 µm

Non-diabetic n=87
Median: 26.0 µm
Interquartile range: 89.0 µm
Minimum: 0.0 µm
Maximum: 607.0 µm

Mann-Whitney Test
p=0.996

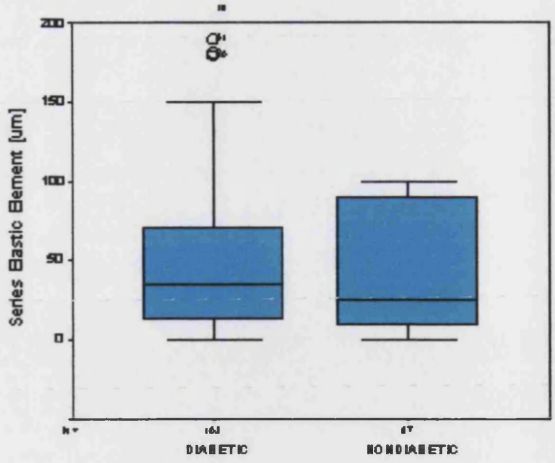

Figure 9.16. Diabetic and non-diabetic series elastic elements on stretching of the epidermis on the PMA.

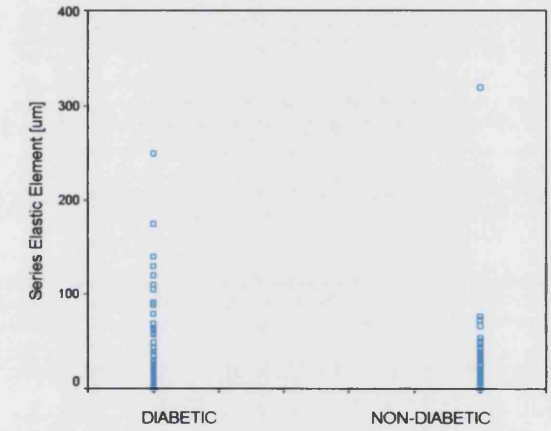

Diabetics n=103
Median: 21.0 µm
Interquartile range: 48.0 µm
Minimum: 0.0 µm
Maximum: 250.0 µm

Non-diabetic n=87
Median: 17.0 µm
Interquartile range: 24.0 µm
Minimum: 0.0 µm
Maximum: 3197.0 µm

Mann-Whitney Test
p=0.004

Sample Power
100%
n = 190
Positive proportion = 19%

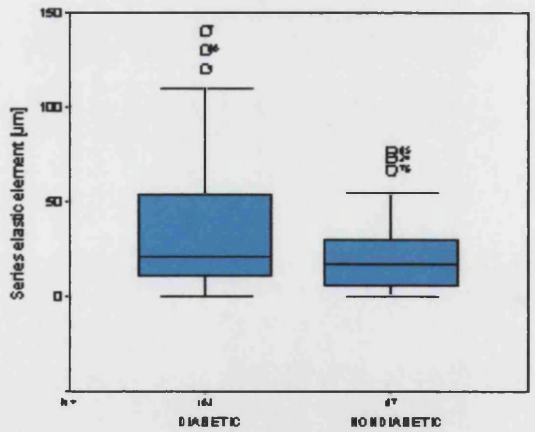

Figure 9.17. Diabetic and non-diabetic series elastic element on retraction of the epidermis on the PMA.

For all three foot sites, there was a significant difference in the series elastic elements on retraction of the epidermis between the diabetic and non-diabetic groups (Fig. 9.12 – 9.17).

There was no difference in the series elastic elements between males and females, on all sites on the foot (Fig. 9.18-9.23).

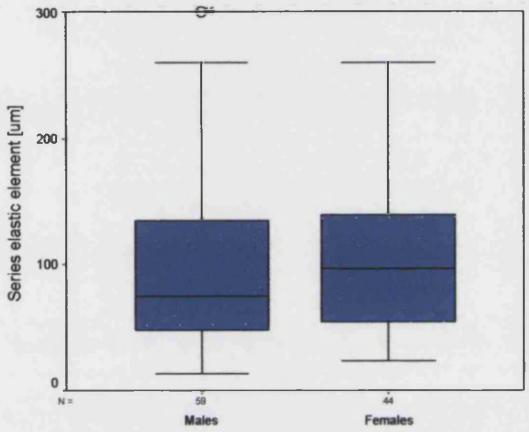

Male n=59
Median: 75.0 µm
Interquartile range: 93.0 µm
Minimum: 13.0 µm
Maximum: 300.0 µm

Female n=44
Median: 96.5 µm
Interquartile range: 86.5 µm
Minimum: 23.0µm
Maximum: 260.0 µm

Mann-Whitney Test
p=0.271

Figure 9.18. The relationship between the sexes and the series elastic element on stretching of the dorsal epidermis.

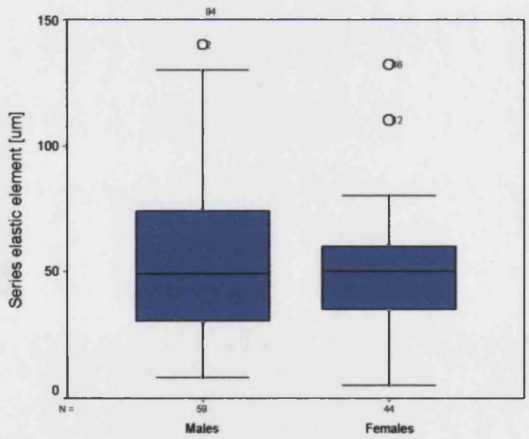

Male n=59
Median: 49.0 µm
Interquartile range: 45.0 µm
Minimum: 8.0 µm
Maximum: 192.0 µm

Female n=44
Median: 50.0 µm
Interquartile range: 25.0 µm
Minimum: 5.0 µm
Maximum: 170.0 µm

Mann-Whitney Test
p=0.997

Figure 9.19. The relationship between the sexes and the series elastics element on retraction of the dorsal epidermis.

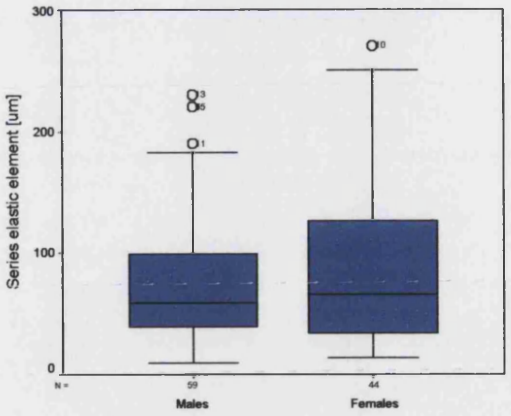

Male n-59
Median: 59.0 µm
Interquartile range: 65.0 µm
Minimum: 9 µm
Maximum: 230 µm

Female n=44
Median: 66.0 µm
Interquartile range: 94.5 µm
Minimum: 14.0 µm
Maximum: 270.0 µm

Mann-Whitney Test
p=0.535
The level of significance is 0.05 (2-tailed)

Figure 9.20. The relationship between the sexes and the series elastic elements on the stretching of the epidermis on the MLA

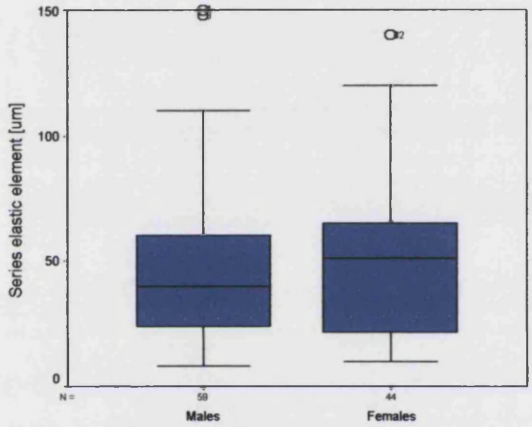

Male n=59
Median: 40.0 µm
Interquartile range: 37.0 µm
Minimum: 8.0 µm
Maximum: 220 µm

Female n=44
Median: 51.0 µm
Interquartile range: 44.75 µm
Minimum: 10.0 µm
Maximum: 190.0 µm

Mann-Whitney Test
p=0.577

Figure 9.21. The relationship between the sexes and the series elastic elements on the retraction of the epidermis on the MLA

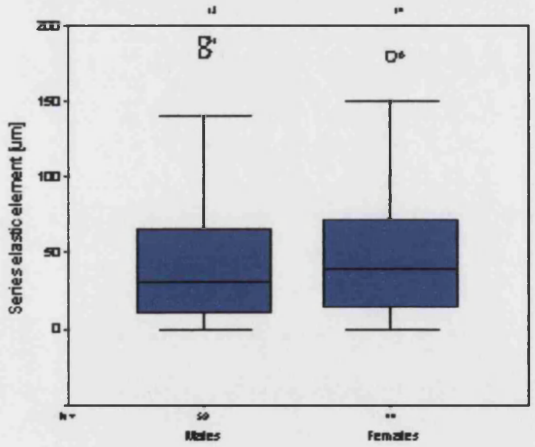

Male n=59
Median: 31.0 µm
Interquartile range: 60.0µm
Minimum: 0.0 µm
Maximum: 260.0 µm

Female n=44
Median: 40.0µm
Interquartile range: 57.5µm
Minimum: 0.0µm
Maximum: 280.0 µm

Mann-Whitney Test
p=0.356

Figure 9.22. The relationship between the sexes and the series elastic elements on stretching of the epidermis on the PMA

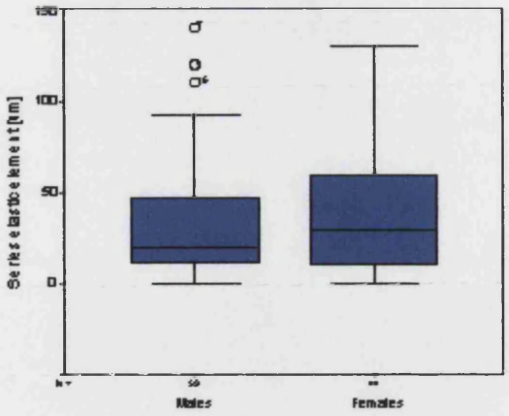

Male n=59
Median: 20.0 µm
Interquartile range: 39.0 µm
Minimum: 0.0µm
Maximum: 250.0 µm

Female n=44
Median: 29.5 µm
Interquartile range: 49.75 µm
Minimum: 0.0 µm
Maximum: 130.0 µm

Mann-Whitney Test
p=0.518

Figure 9.23. The relationship between the sexes and the series elastic elements on retraction of the epidermis on the PMA.

The same set of readings was divided into different ethnic origins, Caucasian and non-caucasian and the indices of elasticity compared (Fig. 9.24-9.29). No significant difference between the two groups was recorded, in terms of elasticity of the skin.

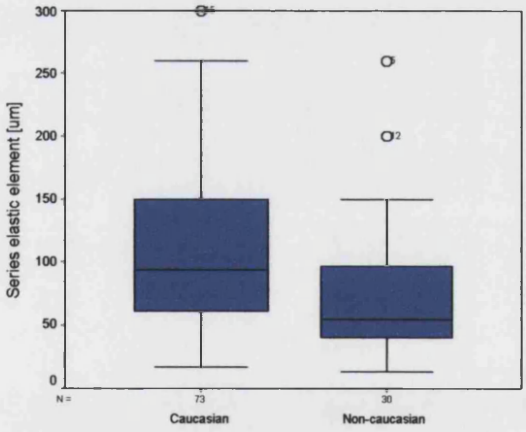

Caucasian n=73
Median: 94.0 µm
Interquartile range: 89.5 µm
Minimum: 17.0 µm
Maximum: 300.0 µm

Non-caucasian n=30
Median: 54.0 µm
Interquartile range: 60.5 µm
Minimum: 13.0 µm
Maximum: 260.0 µm

Mann-Whitney Test
p=0.271

Figure 9.24. The relationship between ethnicity and the series elastic element on stretching of dorsal epidermis.

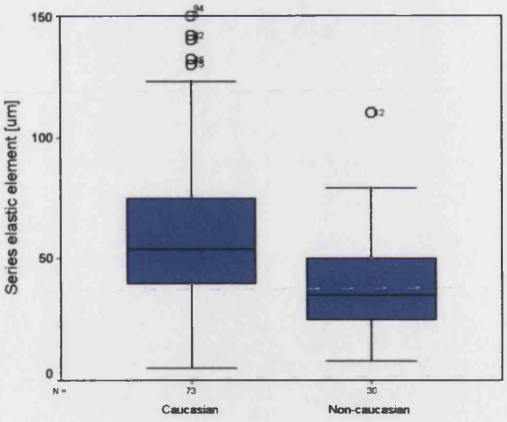

Caucasian n=73
Median: 54.0 µm
Interquartile range: 38.0 µm
Minimum: 5.0 µm
Maximum: 192.0 µm

Non-caucasian n=30
Median: 35.0 µm
Interquartile range: 27.3 µm
Minimum: 8.0 µm
Maximum: 180.0 µm

Mann-Whitney Test
p=0.997

Figure 9.25. The relationship between ethnicity and the series elastic elements on retraction of dorsal epidermis.

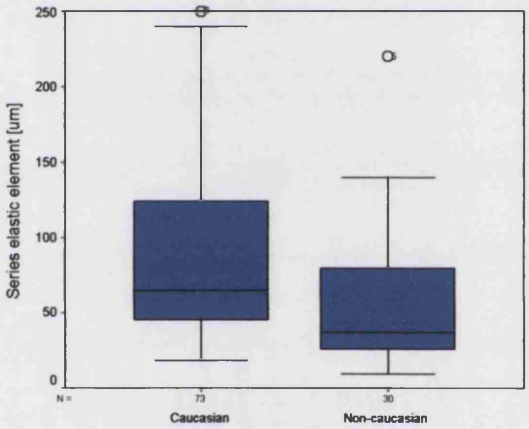

Caucasian n=73
Median: 65.0 µm
Interquartile range: 80.5 µm
Minimum: 18.0 µm
Maximum: 250.0 µm

Non-caucasian n=30
Median: 37.0 µm
Interquartile range: 62.25 µm
Minimum: 9.0 µm
Maximum: 270.0 µm

Mann-Whitney Test
p=0.535

Figure 9.26. The relationship between the ethnicity and the series elastic element on stretching of the epidermis of the MLA.

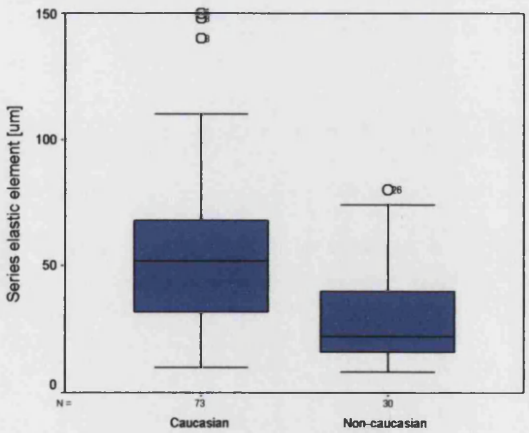

Caucasian n=73
Median: 52.0 µm
Interquartile range: 38.0 µm
Minimum: 10.0 µm
Maximum: 220.0 µm

Non-caucasian n=30
Median: 52.0 µm
Interquartile range: 38.0 µm
Minimum: 10.0 µm
Maximum: 220 µm

Mann-Whitney Test
p=0.577

Figure 9.27. The relationship between the ethnicity and the series elastic elements on retraction of the epidermis of the MLA.

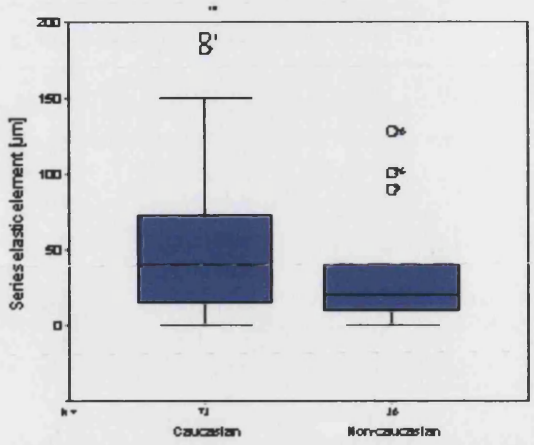

Caucasian n=73
Median: 40.0 µm
Interquartile range: 57.5 µm
Minimum: 0.0 µm
Maximum: 280.0 µm

Non-caucasian n=30
Median: 20.0 µm
Interquartile range: 30.0 µm
Minimum: 0.0 µm
Maximum: 190.0 µm

Mann-Whitney Test
p=0.356

Figure 9.28. The relationship between ethnicity and the series elastic elements on stretching of the epidermis of the PMA

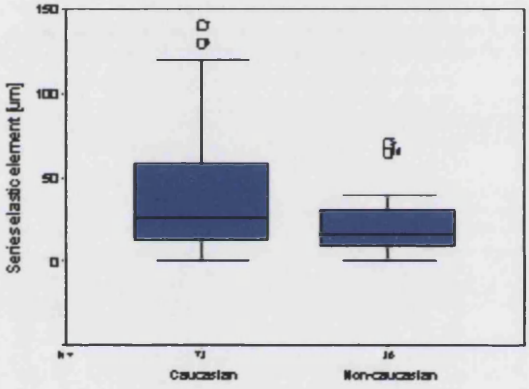

Caucasian n=73
Median: 26.0 µm
Interquartile range: 46.5 µm
Minimum: 0.0µm
Maximum: 250.0 µm

Non-caucasian n=30
Median: 26.0 µm
Interquartile range: 46.5 µm
Minimum: 0.0 µm
Maximum: 250.0 µm

Mann-Whitney Test
p=0.518

Figure 9.29. The relationship between ethnicity and the series elastic elements on retraction of the epidermis of the PMA.

9.4.4.3 The Time Constant Data

There was no difference in the viscoelastic time constants of the epidermis between the two groups of patients on all three sites on the feet (Fig. 9.30-9.35).

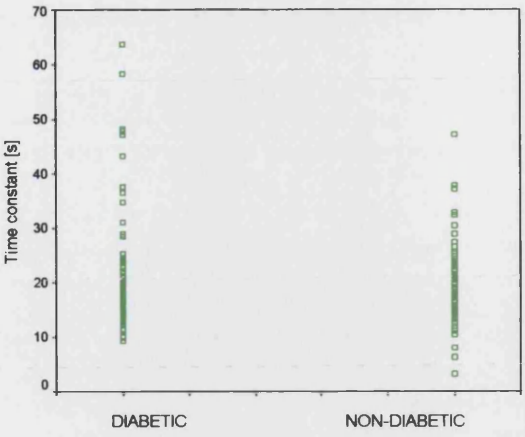

Diabetics n=103
Median: 17.1s
Interquartile range: 6.3s
Minimum: 9.4s
Maximum: 63.7s

Non-diabetics n=87
Median: 18.1s
Interquartile range: 8.1s
Minimum: 3.3s
Maximum: 47.3s

Mann-Whitney Test
p=0.714

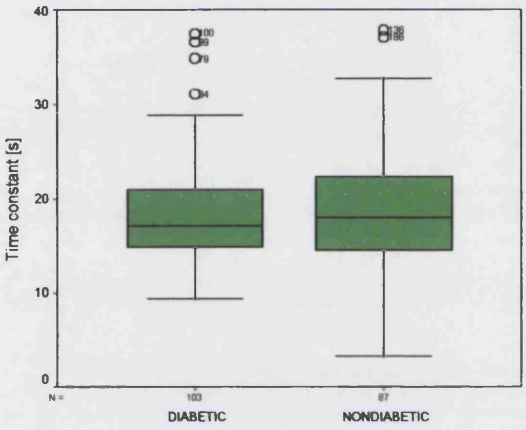

Figure 9.30: Diabetic and non-diabetic time constants on stretching of the dorsal epidermis.

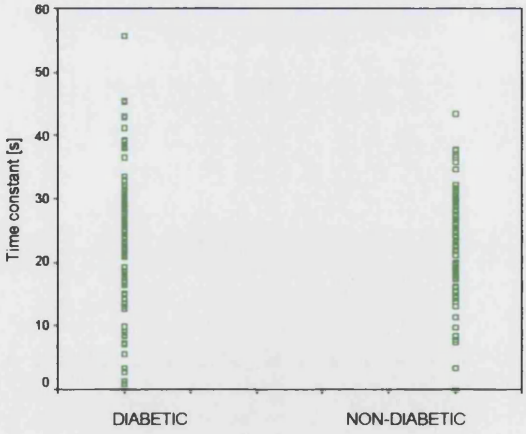

Diabetics n=103
Median: 25.8s
Interquartile range: 12.5s
Minimum: 0.5s
Maximum: 55.8s

Non-diabetics n=87
Median: 24.9s
Interquartile range: 11.1s
Minimum: 0.0s
Maximum: 43.4s

Mann-Whitney Test
p=0.632

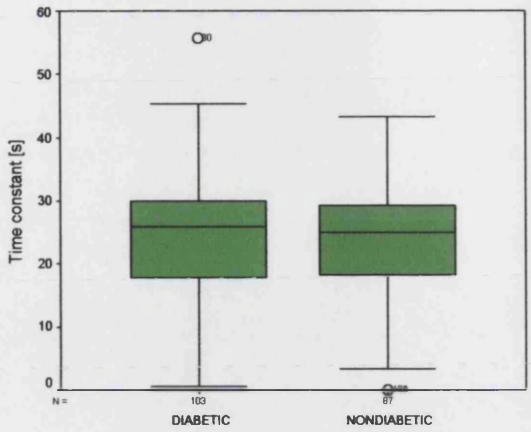

Figure 9.31. Diabetic and non-diabetic time constants on retraction of the dorsal epidermis.

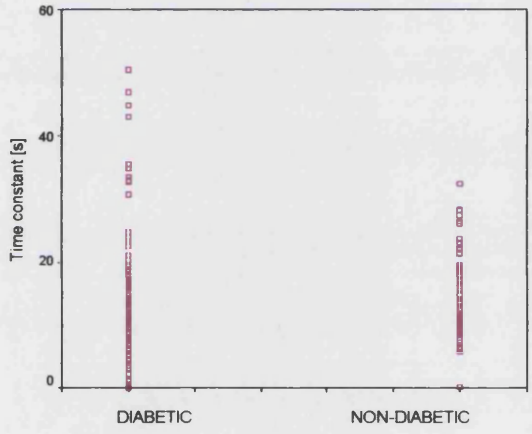

Diabetics n=103
Median: 12.4s
Interquartile range: 8.7s
Minimum: 0.0s
Maximum: 65.4s

Non-diabetics n=87
Median: 12.5s
Interquartile range: 8.4s
Minimum: 0.2s
Maximum: 77.3s

Mann-Whitney Test
p=0.353

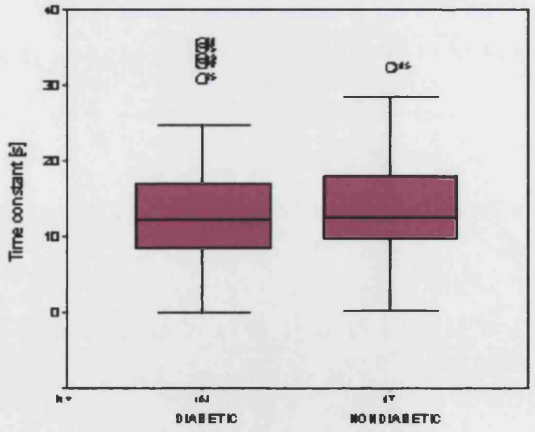

Figure 9.32. Diabetic and non-diabetic time constants on stretching of the epidermis on the MLA

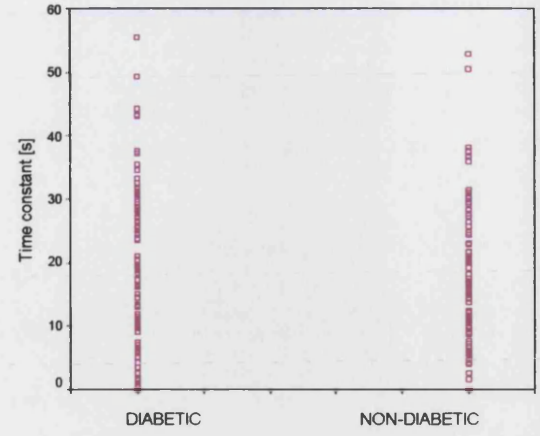

Diabetics n=103
Median: 18.3s
Interquartile range: 18.5s
Minimum: 0.0s
Maximum: 55.6s

Non-diabetics n=87
Median: 15.6s
Interquartile range: 13.1s
Minimum: 0.0s
Maximum: 53.0s

Mann-Whitney Test
p=0.335

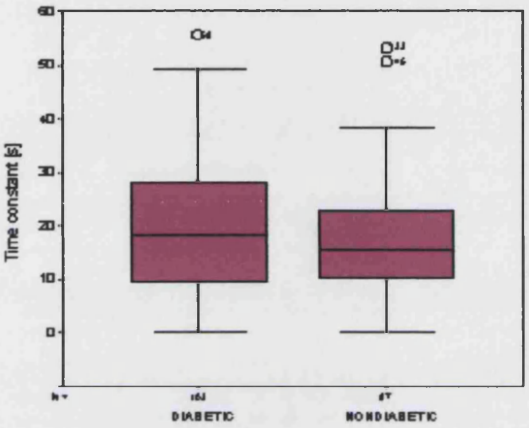

Figure 9.33. Diabetic and non-diabetic time constants on retraction of the epidermis on the MLA

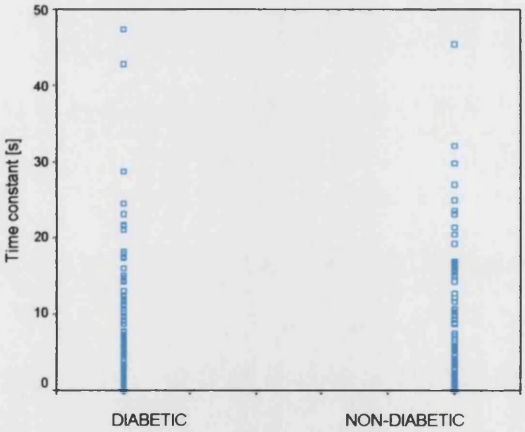

Diabetics n=103
Median: 98.3s
Interquartile range: 10.4s
Minimum: 0.0s
Maximum: 61.3s

Non-diabetics n=87
Median: 5.4s
Interquartile range: 10.9s
Minimum: 0.0s
Maximum: 45.4s

Mann-Whitney Test
p=0.800

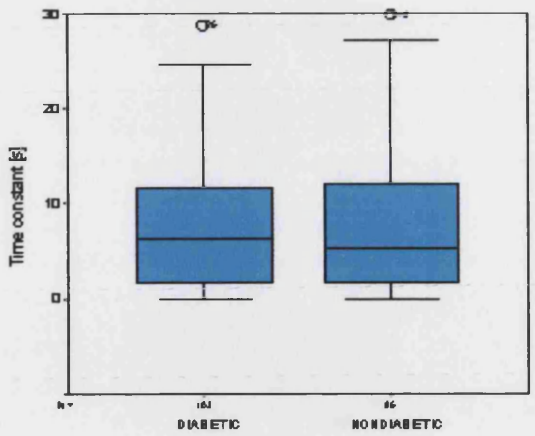

Figure 9.34. Diabetic and non-diabetic time constants on stretching of the epidermis on the PMA

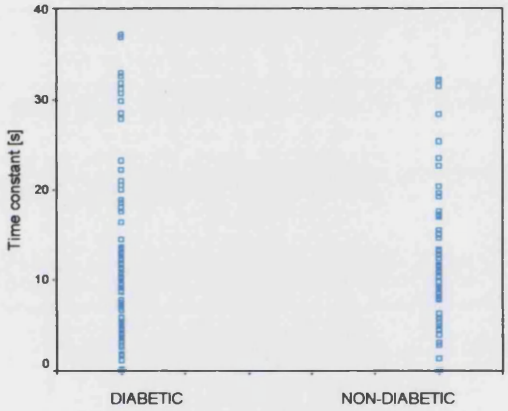

Diabetics n=103
Median: 7.3s
Interquartile range: 12.0s
Minimum: 0.0s
Maximum: 41.3s

Non-diabetics n=87
Median: 7.9s
Interquartile range: 13.1s
Minimum: 0.0s
Maximum: 32.2s

Mann-Whitney Test
p=0.547

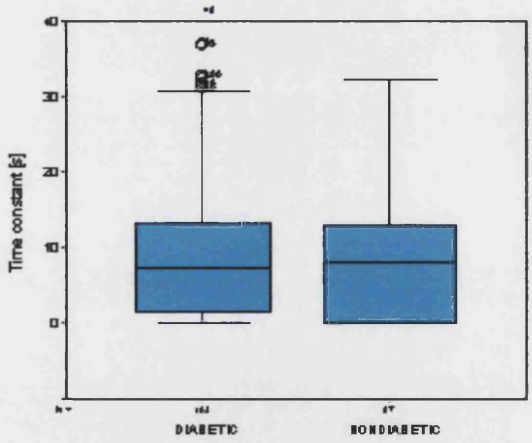

Figure 9.35. Diabetic and non-diabetic time constants on retraction of the epidermis on the PMA

There was a significant difference in epidermal viscoelasticity between the three different sites on the feet (Fig.9.36).

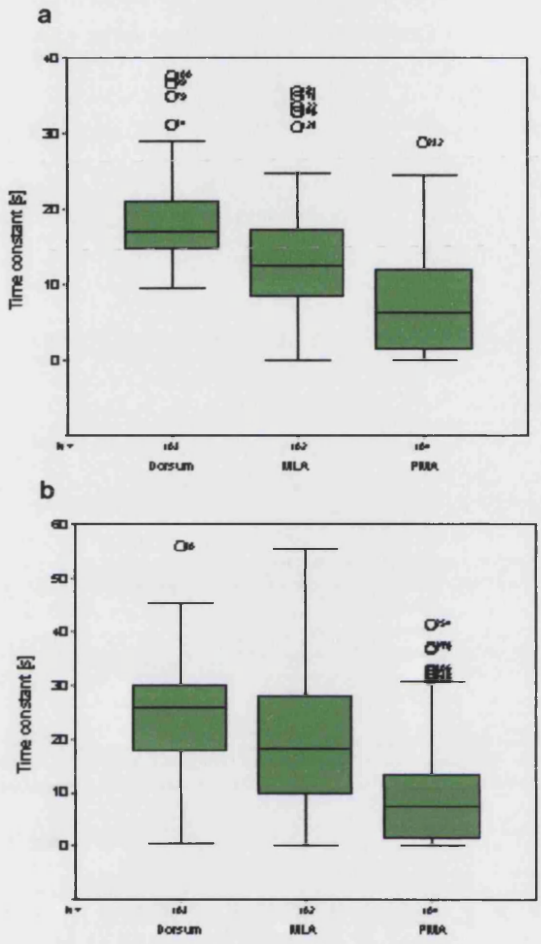

Mann-Whitney Test for a. and b.

Dorsum v MLA	p = 0.001
MLA v PMA	p = 0.001
Dorsum v PMA	p = 0.001

Figure 9.36: A comparison of the time constant data between different sites on the foot **a.** on stretching and **b.** retraction.

No statistical difference was noted in the time constant measurements between the sexes (Figs. 9.37-9.42).

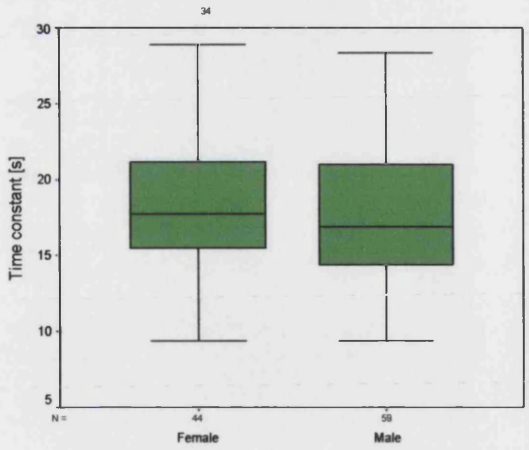

Male n=59
Median: 16.9s
Interquartile range: 6.6s
Minimum: 9.4s
Maximum: 63.7s

Female n=44
Median: 17.7s
Interquartile range: 5.8s
Minimum: 9.4s
Maximum: 31.1s

Mann-Whitney Test
p=0.445

Figure 9.37. The relationship between the sexes and the time constants on stretching of the dorsal epidermis.

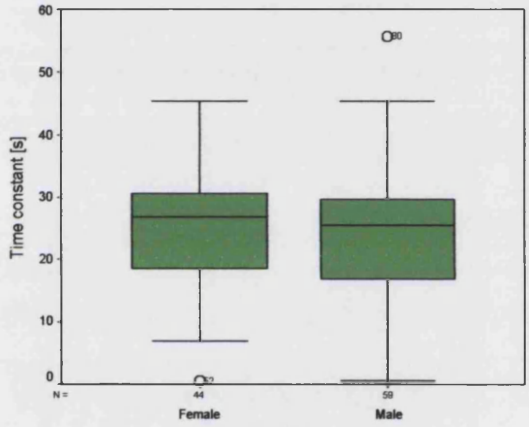

Male n=59
Median: 25.5s
Interquartile range: 13.2s
Minimum: 0.6s
Maximum: 55.8s

Female n=44
Median: 26.9s
Interquartile range: 12.0s
Minimum: 0.5s
Maximum: 45.4s

Mann-Whitney Test
p=0.358

Figure 9.38. The relationship between the sexes and time constant on retraction of the dorsal epidermis.

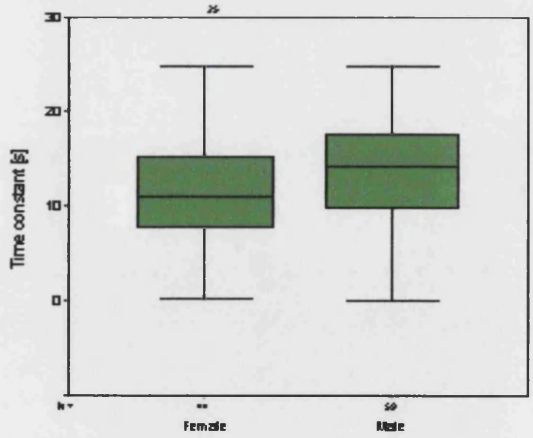

Male n=59
Median: 14.1s
Interquartile range: 8.6s
Minimum: 0.0s
Maximum: 65.4s

Female n=44
Median: 11.0s
Interquartile range: 7.9s
Minimum: 0.2s
Maximum: 43.1s

Mann-Whitney Test
p=0.057

Figure 9.39. The relationship between the sexes and time constants on stretching of the epidermis9on the MLA.

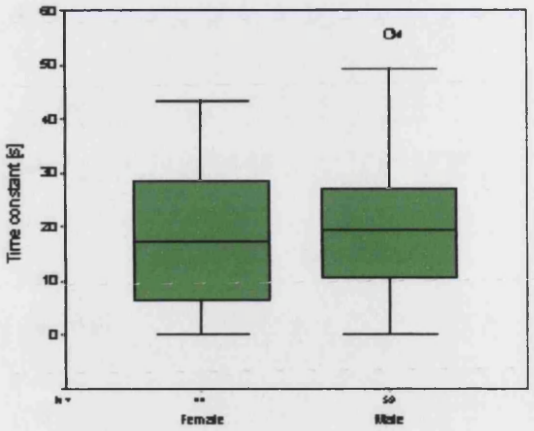

Male n=59
Median: 19.3s
Interquartile range: 16.6s
Minimum: 0.0s
Maximum: 55.6s

Female n=44
Median: 6.9s
Interquartile range: 11.4s
Minimum: 0.0s
Maximum: 41.3s

Mann-Whitney Test
p=0.451

Figure 9.40. The relationship between the sexes and time constant on retraction of the epidermis on the MLA.

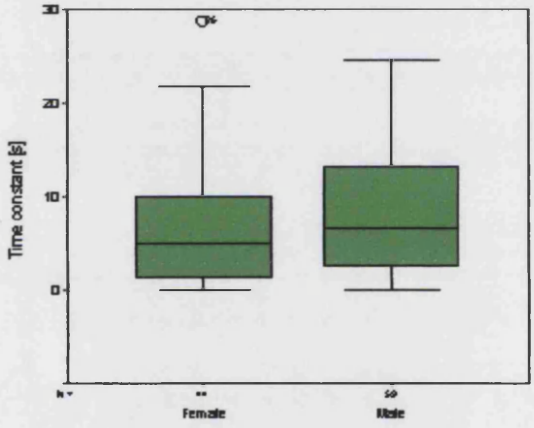

Male n=59
Median: 6.5s
Interquartile range: 10.9s
Minimum: 0.0s
Maximum: 61.3s

Female n=44
Median: 5.0s
Interquartile range: 8.8s
Minimum: 0.0s
Maximum: 28.7s

Mann-Whitney Test
p=0.270

Figure 9.41. The relationship between the sexes and time constants on stretching of the epidermis on the PMA.

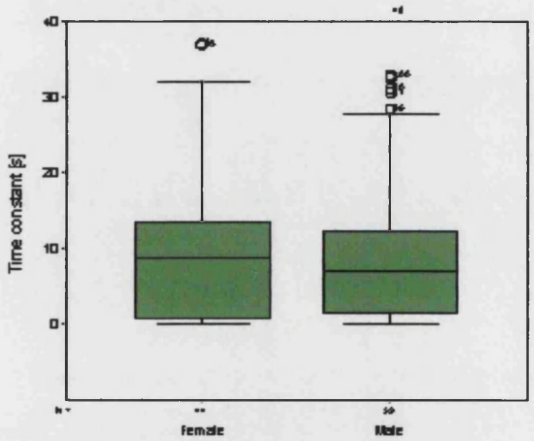

Male n=59
Median: 6.9s
Interquartile range: 11.4s
Minimum: 0.0s
Maximum: 41.3s

Female n=44
Median: 8.8s
Interquartile range: 13.1s
Minimum: 0.0s
Maximum: 37.1s

Mann-Whitney Test
p=0.708

Figure 9.42. The relationship between the sexes and time constants on retraction of the epidermis on the PMA.

There was a significant difference in the time constants on stretching of the epidermis between the two ethnic groups on the dorsal and MLA sights, but not on the PMA site (Figs. 9.43-9.46). These results were approached with caution as the patient numbers in each group differed.

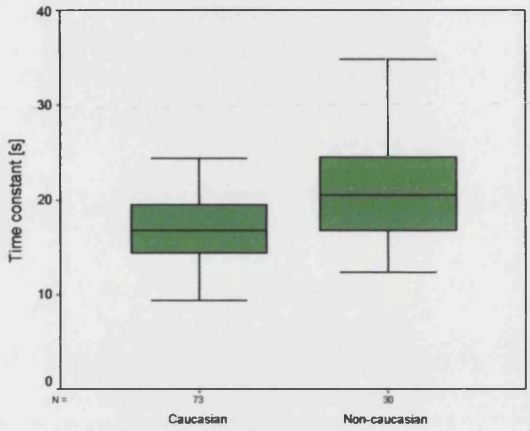

Caucasian n=73
Median: 16.7s
Interquartile range: 5.2s
Minimum: 9.4s
Maximum: 63.7s

Non-caucasian n=30
Median: 20.6s
Interquartile range: 8.3s
Minimum: 12.3s
Maximum: 48.2s

Mann-Whitney Test
p=0.006

Figure 9.43. The relationship between ethnicity and time constants on stretching of the dorsal epidermis.

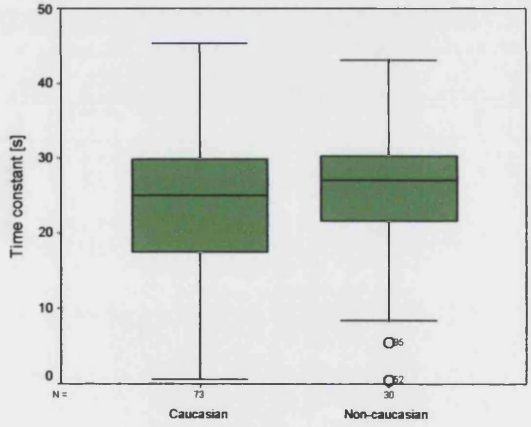

Caucasian n=73
Median: 25.0s
Interquartile range: 12.8s
Minimum: 0.6s
Maximum: 45.4s

Non-caucasian n=30
Median: 27.0s
Interquartile range: 9.1s
Minimum: 0.5s
Maximum: 55.8s

Mann-Whitney Test
p=0.234

Figure 9.44. The relationship between ethnicity and time constants on retraction of the dorsal epidermis.

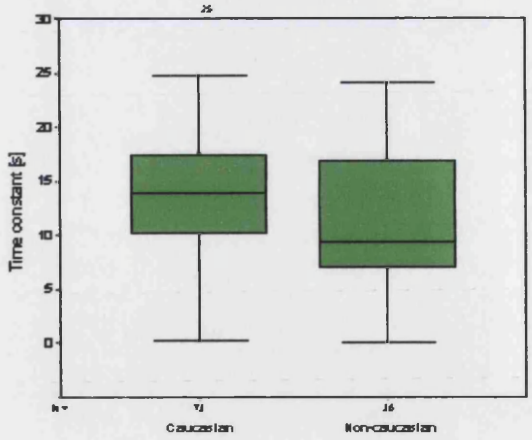

Caucasian n=73
Median: 13.8s
Interquartile range: 7.7s
Minimum: 0.3s
Maximum: 65.4s

Non-caucasian n=30
Median: 9.4s
Interquartile range: 10.6s
Minimum: 0.0s
Maximum: 46.9s

Mann-Whitney Test
p=0.035

Figure 9.45. The relationship between ethnicity and time constants on stretching of the epidermis on the MLA.

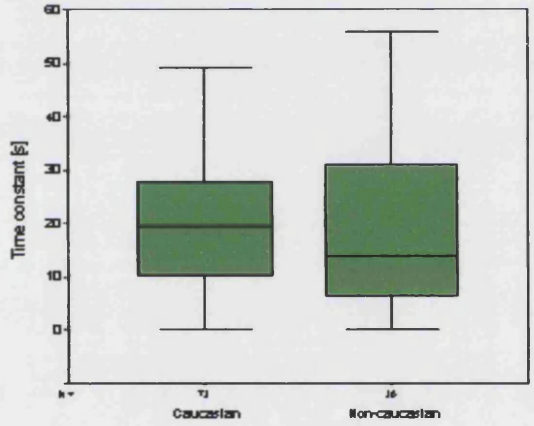

Caucasian n=73
Median: 19.3s
Interquartile range: 17.8s
Minimum: 0.0s
Maximum: 49.3s

Non-caucasian n=30
Median: 13.8s
Interquartile range: 24.7s
Minimum: 0.0s
Maximum: 55.6s

Mann-Whitney Test
p=0.463

Figure 9.46. The relationship between ethnicity and time constants on retraction of the epidermis on the MLA.

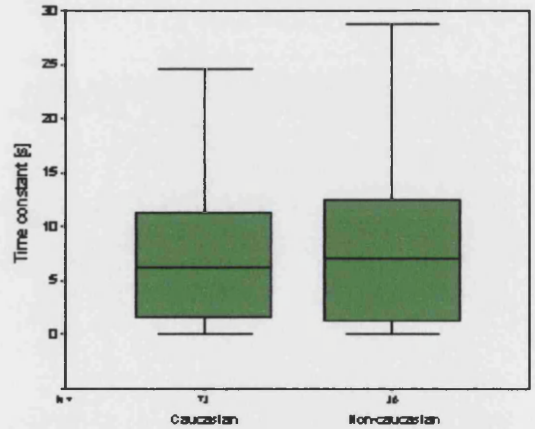

Caucasian n=73
Median: 6.1s
Interquartile range: 10.0s
Minimum: 0.0s
Maximum: 61.3s

Non-caucasian n=30
Median: 7.1s
Interquartile range: 11.4s
Minimum: 0.0s
Maximum: 28.7s

Mann-Whitney Test
p=0.783

Figure 9.47. The relationship between ethnicity and time constants on stretching of the epidermis on the PMA.

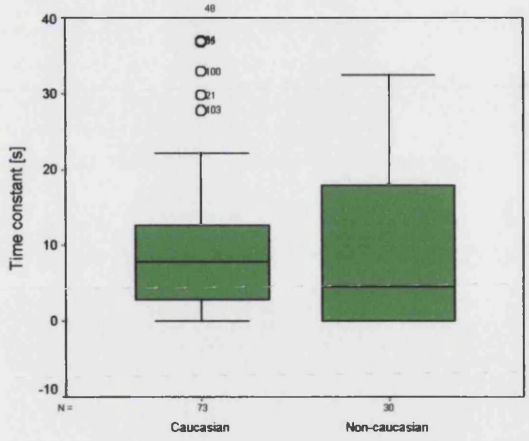

Caucasian n=73
Median: 7.9s
Interquartile range: 10.1s
Minimum: 0.0s
Maximum: 41.3s

Non-caucasian n=30
Median: 4.5s
Interquartile range: 18.5s
Minimum: 0.0s
Maximum: 32.5s

Mann-Whitney Test
p=0.329

Figure 9.48. The relationship between ethnicity and time constant on retraction of the epidermis on the PMA.

9.4.4.4 Epidermal Plasticity

The plasticity of the epidermis on the PMA of non-diabetics was significantly greater than diabetic epidermis on a similar skin site (Fig. 9.51).

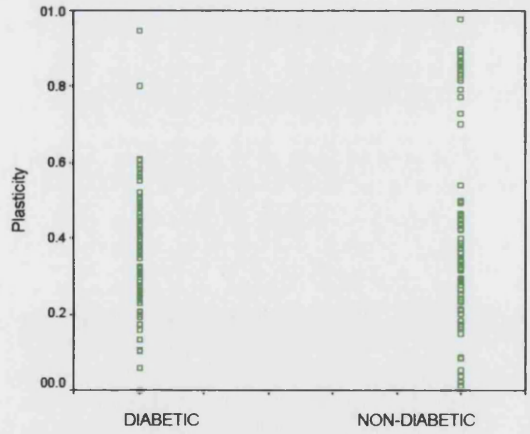

Diabetics n=103
Median: 0.38
Interquartile range: 0.19
Minimum: 0.00
Maximum: 0.45

Non-diabetics n=87
Median: 0.38
Interquartile range: 0.26
Minimum: 0.01
Maximum: 0.98

Mann-Whitney Test
p=0.436

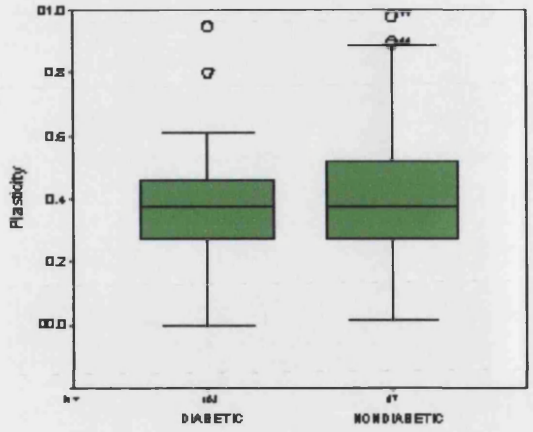

Figure 9.49. Diabetic and non-diabetic plasticity of dorsal epidermis.

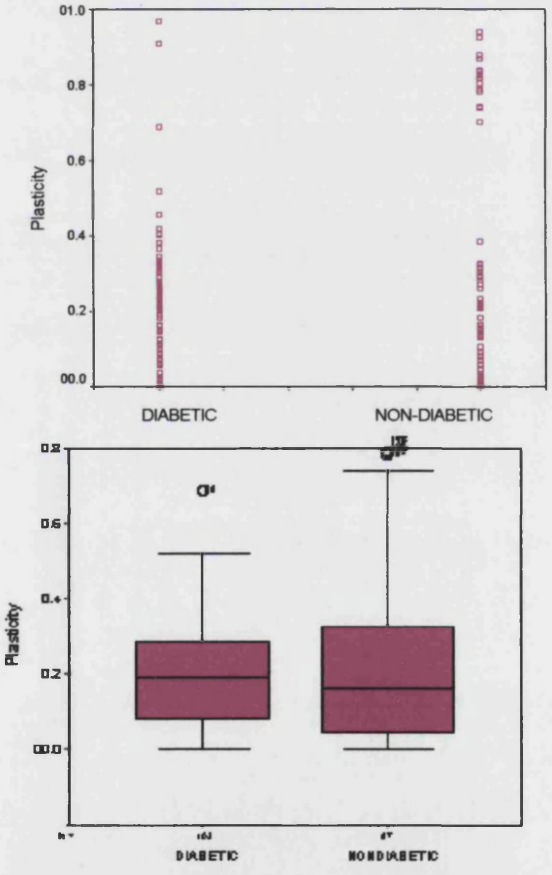

Diabetics n=103
Median: 0.19
Interquartile range: 0.21
Minimum: 0.00
Maximum: 0.97

Non-diabetics n=87
Median: 0.16
Interquartile range: 0.28
Minimum: 0.00
Maximum: 0.94

Mann-Whitney Test
p=0.854

Figure 9.50. Diabetic and non-diabetic plasticity of epidermis on the MLA

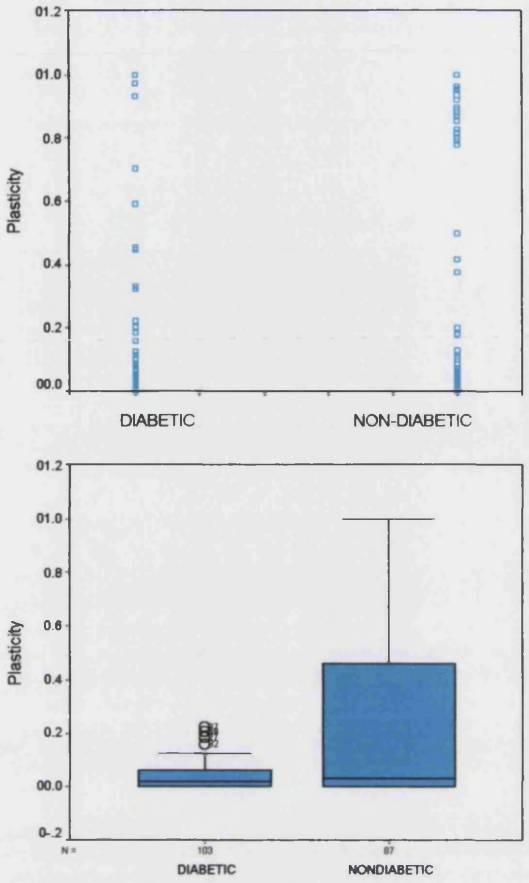

Diabetics n=103
Median: 0.02
Interquartile range: 0.07
Minimum: 0.00
Maximum: 1.00

Non-diabetics n=87
Median: 0.03
Interquartile range: 0.050
Minimum: 0.00
Maximum: 1.00

Mann-Whitney Test
p=0.007

Figure 9.51. Diabetic and non-diabetic plasticity of epidermis on the PMA.

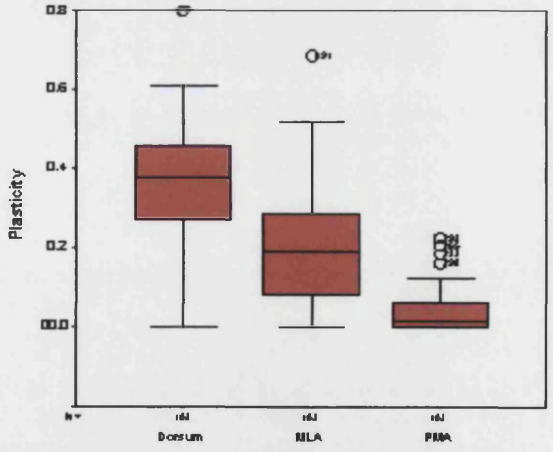

Mann-Whitney Test

Dorsum v MLA	p = 0.001
MLA v PMA	p = 0.001
Dorsum v PMA	p = 0.001

Figure 9.52. The epidermal plasticity on different sites of in the foot.

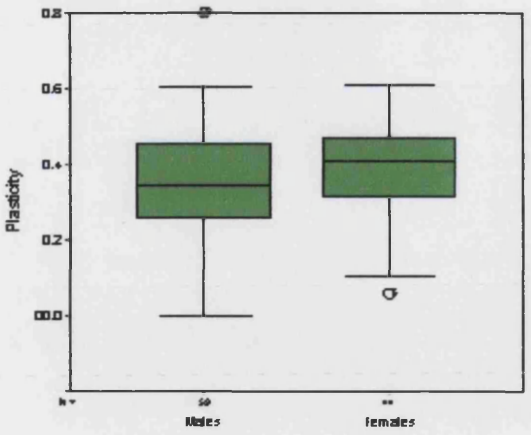

Male n=59
Median: 0.35
Interquartile range: 0.21
Minimum: 0.0
Maximum: 0.95

Female n=44
Median: 0.41
Interquartile range: 0.16
Minimum: 0.06
Maximum: 0.61

Mann-Whitney Test
p=0.266

Figure 9.53. The relationship between the sexes and epidermal plasticity on the dorsum.

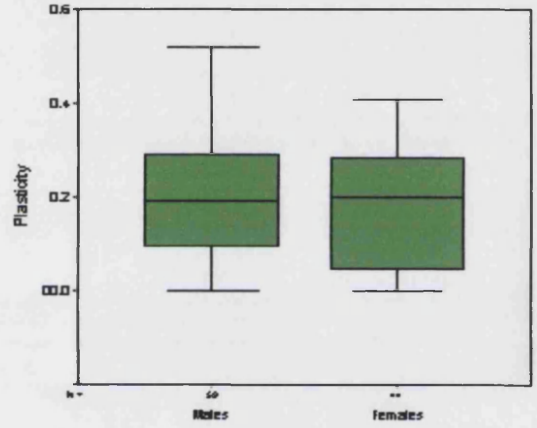

Male n=59
Median: 0.19
Interquartile range: 0.2
Minimum: 0.00
Maximum: 0.91

Female n=44
Median: 0.20
Interquartile range: 0.24
Minimum: 0.00
Maximum: 0.97

Mann-Whitney Test
p=0.414

Figure 9.54. The relationship between the sexes and epidermal plasticity on the MLA.

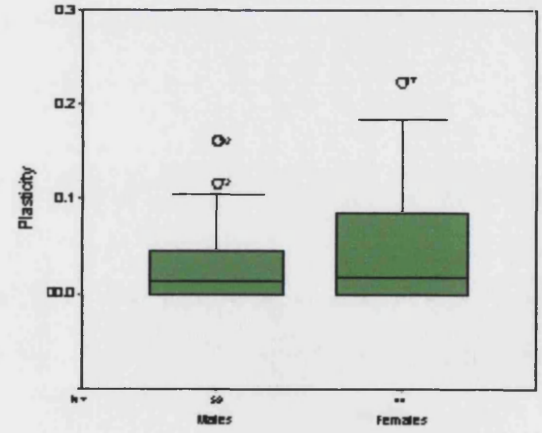

Male n=59
Median: 0.01
Interquartile range: 0.05
Minimum: 0.00
Maximum: 1.00

Female n=44
Median: 0.02
Interquartile range: 0.08
Minimum: 0.00
Maximum: 0.97

Mann-Whitney Test
p=0.534

Figure 9.55. The relationship between the sexes and epidermal plasticity on the PMA.

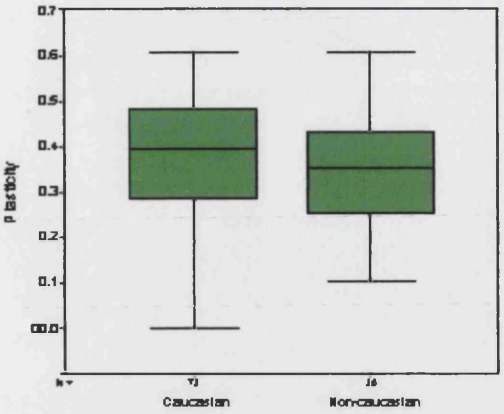

Caucasian n=73
Median: 0.39
Interquartile range: 0.20
Minimum: 0.00
Maximum: 0.95

Non-caucasian n=30
Median: 0.35
Interquartile range: 0.18
Minimum: 0.10
Maximum: 0.61

Mann-Whitney Test
p=0.084

Figure 9.56. The relationship between ethnicity and epidermal plasticity on the dorsum.

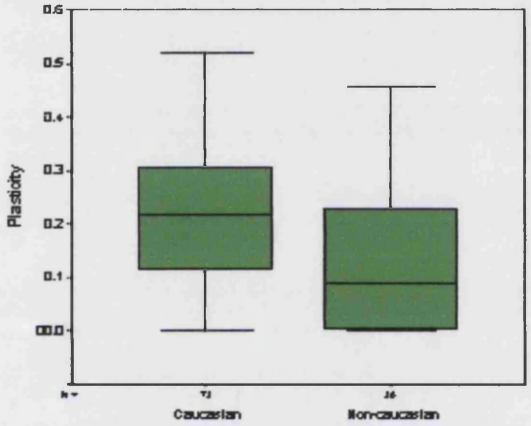

Caucasian n=73
Median: 0.22
Interquartile range: 0.19
Minimum: 0.00
Maximum: 0.91

Non-caucasian n=30
Median: 0.09
Interquartile range: 0.23
Minimum: 0.00
Maximum: 0.97

Mann-Whitney Test
p=0.002

Figure 9.57. The relationship between ethnicity and epidermal plasticity on the MLA.

The plasticity of the epidermis on the MLA and PMA sites was significantly greater in the Caucasian group than the non-caucasian group (Figs. 9.57 & 9.58).

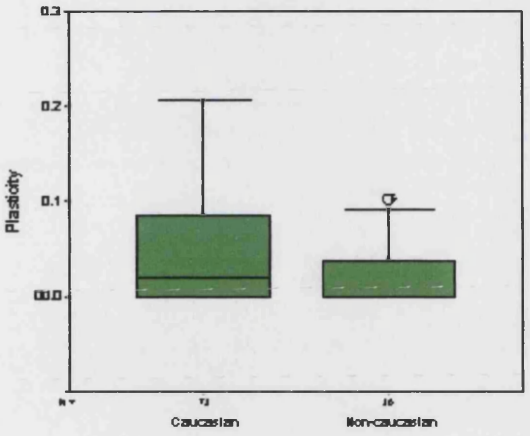

Caucasian n=73
Median: 0.02
Interquartile range: 0.08
Minimum: 0.00
Maximum: 1.00

Non-caucasian n=30
Median: 0.00
Interquartile range: 0.04
Minimum: 0.00
Maximum: 0.59

Mann-Whitney Test
p=0.016

Figure 9.58. The relationship between ethnicity and epidermal plasticity on the PMA.

9.4.5 Epidermal Thickness Data

There was a statistical significant difference in the thickness of the epidermis between the diabetic and non-diabetic groups on the PMA site only (Fig. 9.61). The power of this result was 70% (where: n = 190 and positive proportion = 41%)

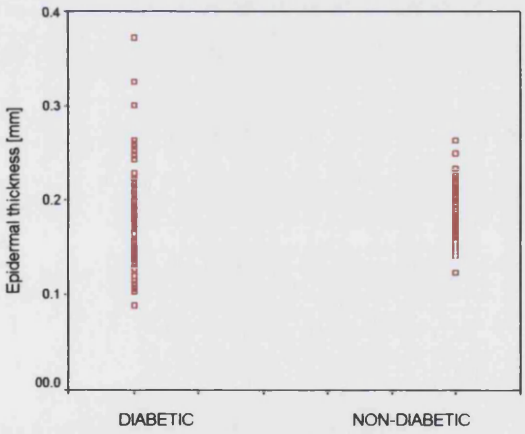

Diabetics n=103
Median: 0.18mm
Interquartile range: 0.05mm
Minimum: 0.09mm
Maximum: 0.44mm

Non-diabetics n=87
Median: 0.18mm
Interquartile range: 0.02mm
Minimum: 0.14mm
Maximum: 0.22mm

Mann-Whitney Test
p=0.996

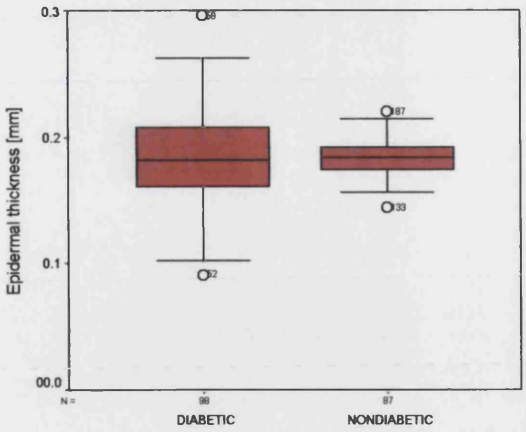

Figure 9.59. Diabetic and non-diabetic dorsal epidermal thickness.

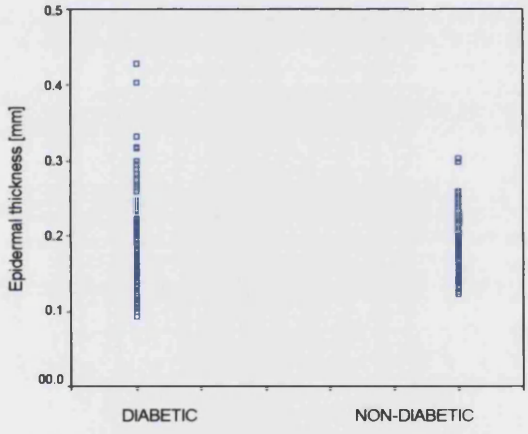

Diabetics n=103
Median: 0.19mm
Interquartile range: 0.08mm
Minimum: 0.09mm
Maximum: 0.43mm

Non-diabetics n=87
Median: 0.18mm
Interquartile range: 0.05mm
Minimum: 0.12mm
Maximum: 0.30mm

Mann-Whitney Test
p=0.336

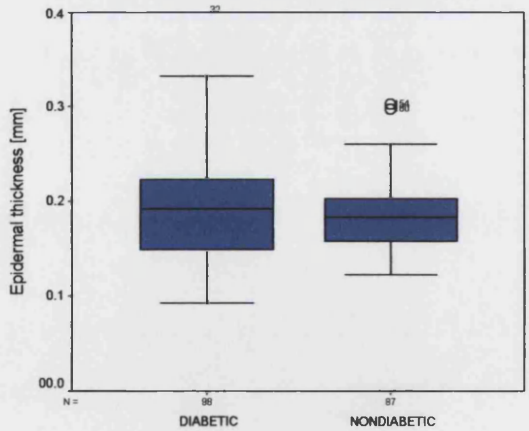

Figure 9.60. Diabetic and non-diabetic epidermal thickness on the MLA

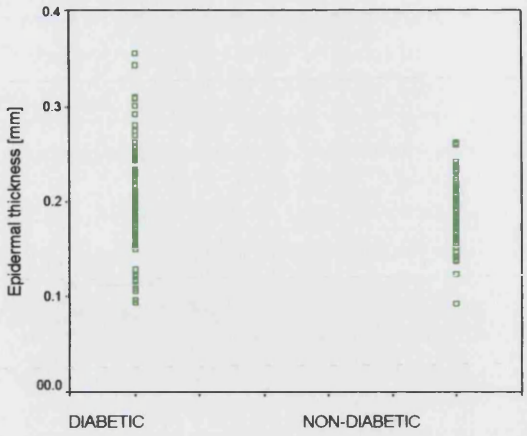

Diabetics n=103
Median: 0.20mm
Interquartile range: 0.07mm
Minimum: 0.09mm
Maximum: 0.26mm

Non-diabetics n=87
Median: 0.18mm
Interquartile range: 0.04mm
Minimum: 0.09mm
Maximum: 0.26mm

Mann-WhitneyTest
p=0.017

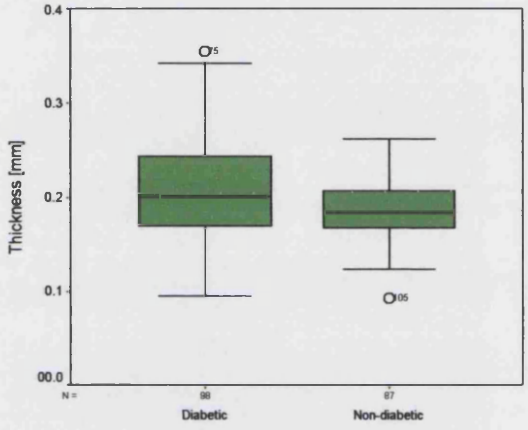

Figure 9.61. Diabetic and non-diabetic epidermal thickness on the PMA.

As would be expected, the epidermal thickness was the highest on the PMA site, followed by the MLA and then the dorsal sites (Fig. 9.62).

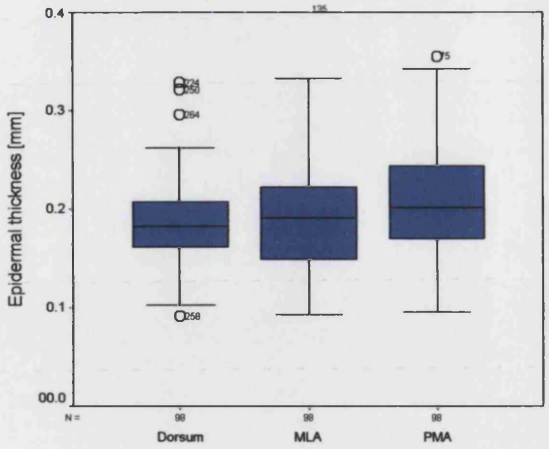

Mann-Whitney Test

Dorsum v MLA	p = 0.477
MLA v PMA	p = 0.147
Dorsum v PMA	p = 0.009

Figure 9.62. Epidermal thickness on different sites on the foot.

The epidermal thickness data did not differ between the sexes or the ethnic groups on all three sites on the feet of diabetic individuals (Figs. 9.63-9.68).

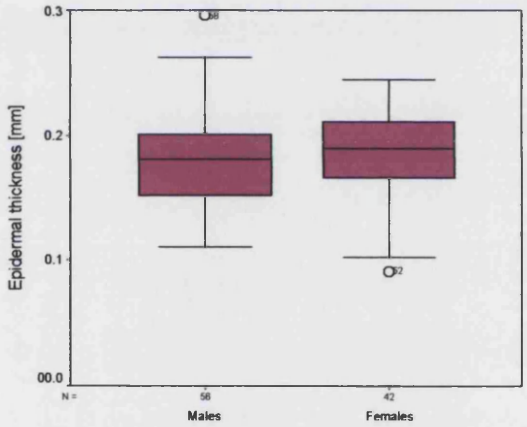

Male n=59
Median: 0.18mm
Interquartile range: 0.05mm
Minimum: 0.11mm
Maximum: 0.32mm

Female n=44
Median: 0.19mm
Interquartile range: 0.05mm
Minimum: 0.09mm
Maximum: 0.44mm

Mann-Whitney Test
p=0.311

Figure 9.63. The relationship between the sexes and dorsal epidermal thickness

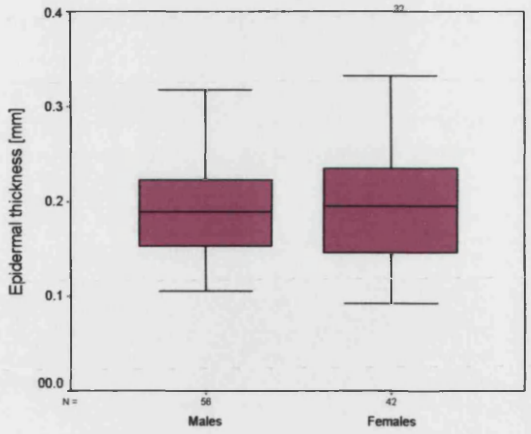

Male n=59
Median: 0.19mm
Interquartile range: 0.07mm
Minimum: 0.11mm
Maximum: 0.43mm

Female n=44
Median: 0.20mm
Interquartile range: 0.09mm
Minimum: 0.09mm
Maximum: 0.40mm

Mann-Whitney Test
p=0.963

Figure 9.64. The relationship between the sexes and epidermal thickness on the MLA.

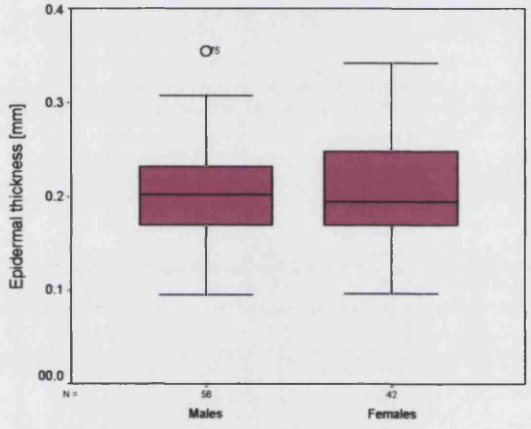

Male n=59
Median: 0.20mm
Interquartile range: 0.06mm
Minimum: 0.09mm
Maximum: 0.36mm

Female n=44
Median: 0.20mm
Interquartile range: 0.08mm
Minimum: 0.10mm
Maximum: 0.34mm

Mann-Whitney Test
p=0.858

Figure 9.65. The relationship between the sexes and epidermal thickness on the PMA.

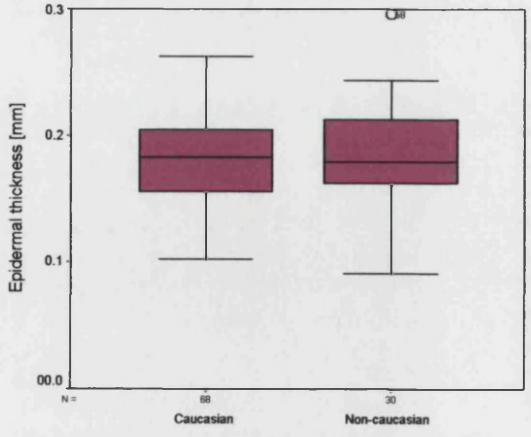

Caucasian n=73
Median: 0.18mm
Interquartile range: 0.05mm
Minimum: 0.10mm
Maximum: 0.44mm

Non-caucasian n=44
Median: 0.18mm
Interquartile range: 0.05mm
Minimum: 0.09mm
Maximum: 0.32mm

Mann-Whitney Test
p=1.000

Figure 9.66. The relationship between ethnicity and dorsal epidermal thickness.

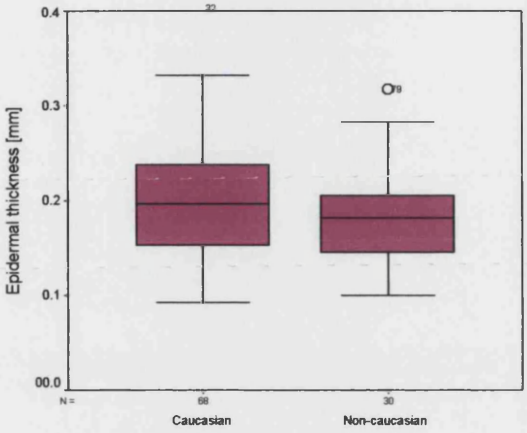

Caucasian n=59
Median: 0.20mm
Interquartile range: 0.09mm
Minimum: 0.09mm
Maximum: 0.43mm

Non-caucasian n=44
Median: 0.18mm
Interquartile range: 0.06mm
Minimum: 0.10mm
Maximum: 0.32mm

Mann-Whitney Test
p=0.277

Figure 9.67. The relationship between ethnicity and epidermal thickness on the MLA.

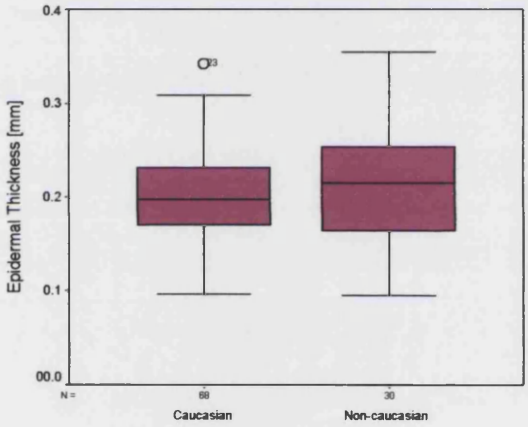

Caucasian n=59
Median: 0.20mm
Interquartile range: 0.06mm
Minimum: 0.10mm
Maximum: 0.34mm

Non-caucasian n=44
Median: 0.21mm
Interquartile range: 0.09mm
Minimum: 0.09mm
Maximum: 0.36mm

Mann-Whitney Test
p=0.553

Figure 9.68. The relationship between ethnicity and epidermal thickness on the PMA.

9.5 Summary of Results

9.5.1 Callus Incidence and Distribution

Pathological callus formation was present in 52% of the diabetic patient population and 77% of the non-diabetic population. The majority of the diabetic patients presented with minimal stratum corneum thickening and the control group had an equal distribution of the three callus descriptions. The controls also

had more corns associated with callus than the diabetic patients and this was related to an increase in age. There was no relationship between the age of diabetics and callus formation. The area of the callus was relatively small in both the groups (68% had a callus area of $1cm^3$).

Both groups were overweight, although the range of BMI data was greater than that of the non-diabetics (diabetics: 20-61.3, and non-diabetics: 29.8-39.3).

There was a high prevalence of callus formation in the sensitive and insensitive diabetic sub-groups. There was no association between the distribution of callus and the duration of diabetes. There was an association between the formation of corns and diabetic peripheral sensory neuropathy.

9.5.2 Foot and Hand Structures and Cutaneous Pathologies

There was a similar incidence of toes deformities in both groups. The diabetic group had a much higher incidence of *pes planus* in comparison to the controls. There was a difference between the diabetic patients with no neuropathy, moderate neuropathy and marked neuropathy presenting with limited ROM of the feet (51%, 63% and 63%, respectively). The limited ROM in the diabetic groups was greater in the older age group. The combination of cheiroarthropathy and limited ROM in feet was seen in 33% of the diabetic patients.

9.5.3 Glycation Adducts

The significant finding in this study was the amount of pentosidine being higher in the diabetic plantar callus in comparison to the controls (Fig. 9.5, p=0.001). In contrast, the quantity of the early glycation product, furosine, was similar in each of the groups (Fig. 9.1, p=0.503).

There was a higher concentration of furosine in the plantar callus (Fig. 9.8) than pentosidine (Fig. 9.8, p=0.001). Within the diabetic group of subjects, a difference was observed in furosine concentrations between males and females (Fig. 9.4,

p=0.01). The concentration of both furosine and pentosidine was not associated with age.

There was a marked difference between furosine in callus and furosine in blood serum, whereas the same difference was not observed when pentosidine was measured in these tissues (Fig. 9.2 & 9.6). Both compounds did not show a positive association with HbA1c levels.

9.5.4 Mechanical Properties of the Epidermis on the Feet

The epidermis on the three different sites on the foot displayed differences in the elastic, viscoelastic and plastic behaviour. These properties were quantifiably higher on dorsal skin than MLA and PMA skin. The epidermis on the PMA was the least elastic, viscoelastic and plastic of the three sites.

The series elastic element on retraction of the epidermis was significantly greater in diabetes, on all three foot sites ($p < 0.05$). There were no marked differences in the data between males and females. The epidermal plasticity of of diabetic plantar epidermis was significantly lower than non-diabetic plantar epidermis ($p = 0.77$).

9.5.5 Epidermal Thickness

The epidermal thickness on the PMA of the foot was significantly higher in the diabetics than the controls (Fig. 9.61, p=0.017). The range of thickness readings, on three sites, was broader in the diabetics than the non-diabetics (Figs. 9.59 – 9.61). As with the elasticity data, the epidermal thickness differed between the sites, i.e. the epidermis was the thickest on the PMA, followed by the MLA and dorsal sites consecutively (Fig. 9.62). The sex and ethnic origins of the subjects apparently have no effect on the epidermal thickness.

There were no positive correlations between the epidermal thickness and elasticity, or between the quantity of glycation adducts and the physical properties.

10.0 Chapter 10 – Discussion

10.1 Introduction

In this thesis, mechanical and biochemical methods were developed and tested to improve the quantitative evaluation of pedal epidermis in healthy and Type II diabetic populations. The primary aim of this series of investigations was to test for an association between epidermal mechanics and the accumulation of glycation products, principally furosine, pentosidine and carboxymethyllysine, within the superficial layers of the plantar stratum corneum.

Quantitative mechanical measurements were achieved by the use of vertical, negative (suction) pressure, to identify and compare specific indices of elasticity, between the groups. High frequency A- and B-mode ultrasound imaging (20 MHz) was implemented for the quantitative measurement of epidermal thickness and to assess qualitative differences between the skin on different sites of the foot.

The exploration of different keratin extraction methods achieved the aim of designing a protocol that not only produced a broad spectrum of epidermal keratins but also was cost-effective and time-efficient. The latter point was important as the proceeding hydrolysis methods and HPLC and GC/MS analyses would add to the experimental time for each sample. The development of accurate analytical techniques for the identification and quantification of specific glycation adducts from acid hydrolysed keratin extracts was achieved

The need for pure synthetic AGE standards, for accurate quantification of glycated compounds, was highlighted. The purity of the compounds was essential for them to act as immunogens for raising monoclonal antibodies, with the appropriate specificity.

The detection of CML using GC/MS was shown to be appropriate for the qualitative detection of CML but lacked the sensitivity for its quantification. Recent publications have explored electrospray ionisation and matrix assisted laser

desorption/ ionisation time-of-flight (MALDI-TOF) as a method of protein analysis. This technique analyses the protein as a whole therefore eliminating any interference by artefacts liable to be generated during hydrolysis. In theory MALDI-TOF would be advantageous in mapping the exact glycation sites along the keratin protein chain [256], however evidence of this method being an effective tool for CML quantification has not been forthcoming [256].

The preparation and analysis of hydrolysates for CML using GC/MS was time consuming and produced semiquantitative results. Other methods of quantification were sought leading to the production of monoclonal antibodies against CML and furosine. These antibodies did not bind selectively to the glycation products. Other groups have identified the same problems discussed in this study and the search for anti-AGE antibodies to specific AGEs is still in progress in many glycation research centres around the world. In this thesis pure CML and furosine were attached to carrier proteins before injection into the host, as opposed to the injection of a mixture of AGEs formed via incubation of BSA or KLH in glucose prior to immunisation. This deliberate alteration was an attempt to encourage the development of antibodies with specific binding sites for CML and furosine. The injection of glycated BSA/ KLH by other researchers in this field was in effect injecting a mixture of AGEs some of which have not been identified as yet. Therefore a mixture of AGEs could encourage the production of antibodies with non-specific binding activities. These antibodies would have their uses in identifying AGEs as a collective in tissues at the expense of identifying specific AGEs. In view of this knowledge the need for the identification of individual AGEs takes priority above immunoassay development.

A series of clinical observations that are pertinent to the condition of the "diabetic foot" were recorded during the collection of the experimental data to support or refute observations made previously of the foot pathologies commonly seen in diabetes.

This final chapter discusses the evidence that has emerged from several expositions in the analysis of epidermal tissues in Type II diabetes using

knowledge from a diverse range of disciplines particularly that of the biochemical and physical behaviour of the epidermis at a micro and macro level.

The published literature, reviewed in Chapter 1, in the field of diabetes and non-enzymatic glycation of proteins, over the past two decades has made a valid contribution to a clearer understanding of the origins of the secondary complications related to diabetes. As glycation potentially involves any protein, many tissues have been investigated. Blood tissue was used for pioneering studies in this field, for its ease of access and for the dynamic nature of its constituent proteins in relation to glucose during hyperglycaemic and normoglycaemic states. The pursuit of a therapeutic intervention, to inhibit the prevention of the glycation of human proteins, still exists today and is complicated by the multifarious nature of glycation products. The evolution of this area of biochemistry, aided by the acceptance of the heterogeneous nature of these modified proteins, has entered the 21st century with a less blinkered view of the singular influence that glycation adducts have on the progression of tissue pathology in diabetes. During the latter part of the 1990s a shift towards the investigation of reactive oxygen species (ROS) provided a connection between ROS and the four hypotheses that explain cell pathology in diabetes: increased polyol pathway flux; activation of protein kinase C isoforms; increased hexoseamine pathway and increased accumulation of AGEs [257]. This mosaic of interrelated processes explains pathologies not only seen in diabetes, but in rheumatoid arthritis, Alzheimers disease and cardiovascular disease.

For a short period of time, different investigators explored the measurement of furosine, in plantar callus tissue, hair and nails. These groups concentrated their efforts on measuring the amount of furosine in these keratin rich tissues, with a vision of using the concentration of furosine as an index for hyperglycaemia. These published works confirmed the presence of furosine in plantar callus. It seems surprising that further scrutiny for the presence of AGEs in these tissues was not attempted, as the confirmation of the presence of an early glycation product suggests a potential for AGE formation. However, in these studies, the sole aim of measuring furosine in the callus tissues was to see if it could act as an indication of glycaemic control. The local effects of protein glycation on the

physical properties of the skin were not considered. Different investigators recognised the implications that protein glycation may have on the mechanical properties of tissues such as tendon and dermal collagen, but a detailed investigation of skin on the feet was not carried out.

The hypotheses tested in this thesis, originated from the lack of knowledge, in this area of medicine, in terms of diabetic foot pathologies. It attempted to confirm the presence of known early and late glycation products, using accurate analytical techniques and applied these results to the implications they may have on the physical behaviour of plantar skin in diabetes.

10.2 Hypothesis 1: There is an Increase in Glycation of Plantar Epidermal Proteins in Type II Diabetes.

The accumulation of furosine and pentosidine in plantar callus tissues was evident in diabetic and non-diabetic subjects. There was no significant difference in furosine concentration between the two groups. However, the range of concentrations of furosine in diabetic callus was greater than those recorded in the non-diabetic callus.

There was, on average, a greater concentration of furosine than pentosidine in callus collected from both groups.

There was a significantly higher concentration of pentosidine in diabetic callus than controls ($p<0.001$). As with the furosine results, the range of pentosidine concentrations was greater in the diabetic samples than controls.

The paths of non-enzymatic glycation, studied in this thesis, were the formation of furosine, which exclusively involves the terminal amino group of a lysine residue; and pentosidine involving both lysine and arginine residues. From the genesis of the single keratin polypeptide chain through to the complex filament network formation, there are lysine and arginine residues present at all points along the way, which are potentially susceptible to non-enzymatic glycation at all these levels of keratin synthesis.

The glucose that is involved with glycation originates from the circulation, diffuses into the interstitial fluid spaces of the dermis and the epidermis and migrates across the epidermal cell membrane into the interior of the cell [70]. It serves as a fuel for the synthesis of DNA, lipids and proteins. Glucose utilisation is increased with an increase in epidermal cell proliferation, such as in psoriasis and wound healing [61]. Plantar epidermal tissue, as a result of mechanical stimulation has a high cell turnover rate, and the utilisation of glucose, by the keratinocytes is increased commensurately. In a hyperglycaemic environment, a surplus of glucose may be a substrate for glycation of all the proteins expressed by the keratinocyte cells.

The majority of the proteins extracted from the plantar callus specimens were keratins. There is a possibility that trace amounts of unknown proteins, unidentifiable by electrophoresis and immunoblot techniques were present in the extracts. According to the model of callus formation [26], immature keratinocytes enter the stratum corneum, and as a consequence of their lack of appropriate differentiation, desmosomal degradation is incomplete. This contrasts to normal differentiation where the structural integrity of the desmosomes decreases in the superficial layers of the epidermis, allowing for desquamation of the corneocytes [258]. Therefore, it is possible that, the intracellular attachment proteins (desmoplakins and plakoglobins) [62;180;259;260] that reside in the desmosomes may be present in the callus tissues sampled in this thesis. The desmogleins, desmocollins and integrin $\alpha 6\beta 4$, found in hemidesmosomes would be less likely to be present in the superficial layers of the stratum corneum as their purpose is to bind the basal keratinocytes to the basement laminar [261-263].

Although there is a possibility that desmoplakins and plakoglobins may be present in the plantar callus tissue, it is the proteins in the stratum corneum layer that are of more importance. The terminal differentiation programme for human keratinocytes involves the formation of a cell envelope (CE) structure consisting of a thin layer (~15 nm thick) of insoluble, isopeptide bond cross-linked proteins (involucrin, cysteine, and the carboxy termini of desmoplakin and envoplakin) with a thin layer (~5 nm thick) of attached lipids [264]. This structure forms on the

intracellular surface of the plasma membrane and ultimately replaces it and the cytoskeletal connections to the cell periphery are lost, as part of controlled death [265]. The bulk of the terminally differentiated epidermal corneocytes consists of cytoskeletal keratin intermediate filament-filaggrin complex that is retained within the CE structure (Fig. 10.1). The enzyme facilitated *N*–(γ-glutamyl) lysine cross-links between the glutamyl of the involucrin (molecular weight 26 kDa) and the primary amino group of lysine residues from other proteins result in stable macromolecular assemblies incorporated within the CE [264]. Loricim (26 kDa) is rich in cysteine, serine and glycine amino acids and is characteristically insoluble due to disulphide bonding and is, in conjunction with proline rich elafin, subjected to *N*–(γ-glutamyl) lysine isopeptide bonding in the inner cytoplasmic layer of the CE late in the epidermal differentiation phase. It comprises 80% of the CE and provides resilience to the stratum corneum as a result of its flexible character [67;264]. It is involucrin that confers rigidity and insolubility to corneocytes in the stratum corneum. All of the proteins that reside in the CE are linked via isopeptide bonds to keratin filaments (K1, K2, K5 and K6). Although these proteins are less abundant than the keratins within the desquamating layers of the epidermis, they may be present in slightly higher proportions in the deeper layers of the stratum corneum. The samples of plantar callus tissues collected in this study consisted of both the superficial and deep layers of the stratum corneum, therefore a fraction of the CE proteins may also have been present in the extracts generated. Therefore, it is possible that these proteins may also be subject to glycation. Further investigations of these proteins in isolation would be necessary.

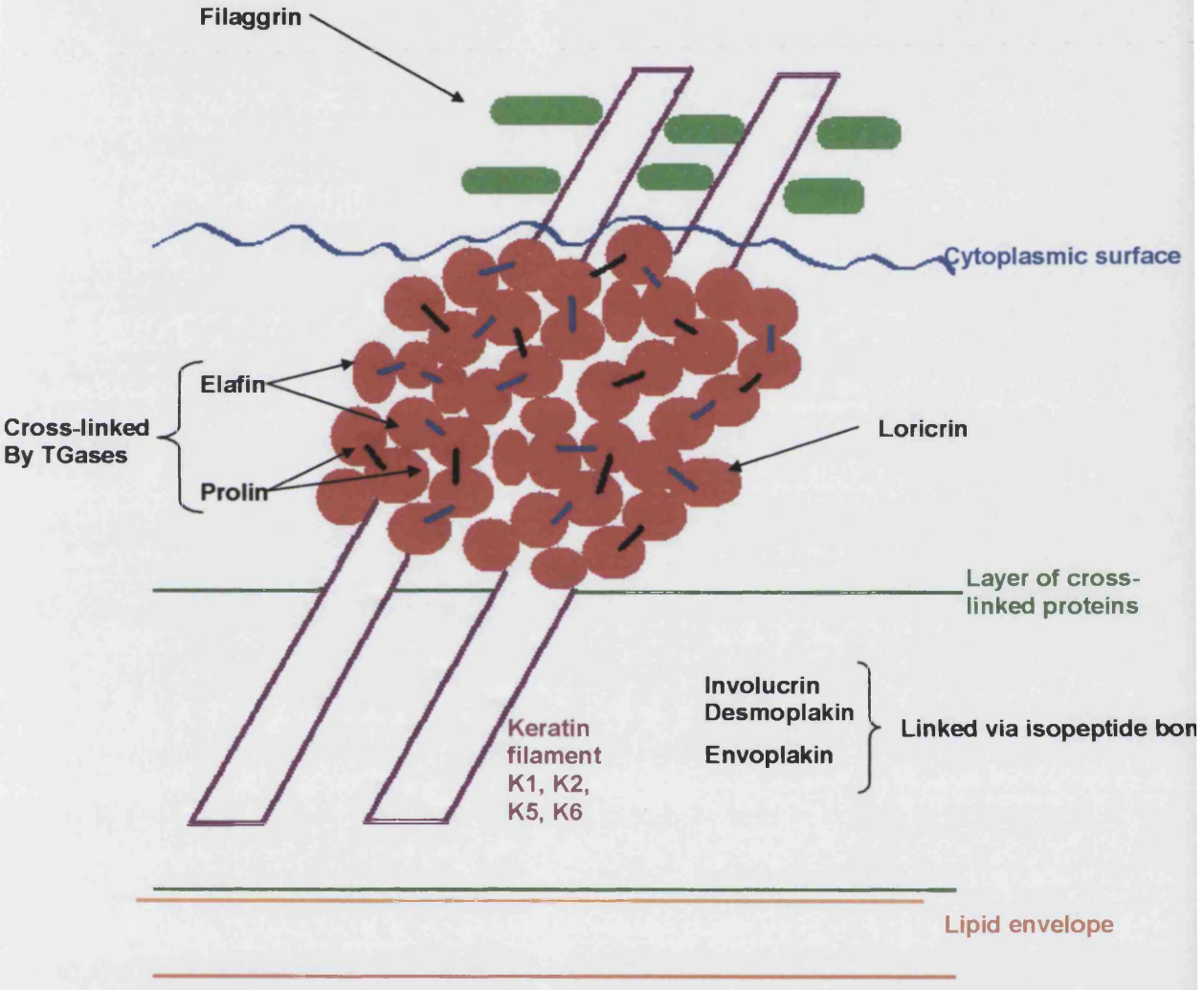

Figure 10.1. Schematic diagram of the cell envelope (CE).
Filaggrin (histidine rich protein) is in abundance in keratinocytes as they approach terminal differentiation in the SC. These are synthesised by the keratohyalin granules within the granular cells from the profilagrin protein. During the transition from the granular layer, the profilagrin is dephosphorylated to filaggrin. This conversion only occurs in tissues, which synthesise high molecular weight keratins. The intracorneocyte filaggrins are short lived in the lower stratum corneum. Filaggrin lies between the keratin filaments and acts by aggregating the keratin filaments. The protein involucrin (molecular weight 80-90kDa), is expressed in association with keratins K1 and K10 in the spinous layer. The protein loricrin is expressed in the granular cells, and its function is to add to the cytoarchitecture of the keratinocytes.

The accumulation of AGEs in human tissue proteins is related to the turnover rate of those tissues: the longer the life span of a tissue the greater the potential of an increased accumulation of AGEs. The average time that keratinocytes take to travel from the basement membrane to the surface of the stratum corneum, in the non-pathological skin is approximately 40 days [69;266]. This value applies to human volar skin and is subject to variation on different sites of the body. The epidermal kinetics of plantar skin are disturbed so as to adapt to the pressures of gait. This perturbation encourages an increased rate of cell renewal and decreased desquamation, hence the thickening of the stratum corneum.

The measurement of a greater concentration of furosine than pentosidine in the callus specimens has several explanations. If the furosine is exclusively converted to pentosidine then the corneocytes desquamate before this process of conversion is allowed to complete. Alternatively, furosine could be the intermediate compound for the conversion to other AGEs in addition to pentosidine. With the existing knowledge that the modifications of proteins into different AGEs originate from furosine, it is reasonable to suggest that a fraction of furosine generated in plantar epidermis is converted to pentosidine and the remainder could generate other AGEs such as CML. The identification of trace amounts of CML described in Chapter 5 supports this hypothesis. There is also a possibility that sugar attachment could be occurring at different times and different points along the keratin chain, therefore at the time of sampling the tissues there could be both furosine and pentosidine formations along the same keratin chain. Finally, the immaturity of the corneocytes entering the callus domain of the stratum corneum could reflect the higher levels of furosine in relation to pentosidine.

It would be pertinent to investigate the dispersion of individual keratins and glycated proteins within epidermal tissues as a consequence of physical damage. Such physical challenges include the response of the plantar epidermis to repetitive low grade trauma during gait, forming callus or, in more extreme cases, ulcers [267].

Is there an association between the concentration of furosine and pentosidine in plantar epidermal proteins and circulating blood serum proteins?

There was no correlation between furosine in plantar callus and furosine in blood serum (diabetic r=-0.115, non-diabetic r=0.084). A similar observation was recorded for pentosidine concentrations (diabetic r=-0.023, non-diabetic r=0.136).

The half-life of haemoglobin tissue (~120 days) is approximately three times longer than the epidermal turnover time, therefore one would expect a greater potential for the accumulation of AGEs in the blood serum protein than plantar epidermal keratins. This was reflected by the pentosidine data, where the ratio of pentosidine concentration in the keratins to that measured in the blood serum was 1:3 and 1:2 in diabetics and controls, respectively. The reverse was recorded with the furosine data where its concentration in keratin was much higher than in blood serum (diabetics 4:1; non-diabetics 7:1).

Is there an association between the concentration of furosine and pentosidine in plantar epidermal proteins and glycaemic control?

There was no correlation between the HbA1c values and the accumulation of furosine and pentosidine in diabetic plantar keratin (furosine r=0.107, pentosidine r=0.158). Therefore, the measurement of furosine and pentosidine in the plantar callus tissues of this study did not reflect glycaemic control.

The presence of increased levels of keratin glycation independent of HbA1c levels, could be due to hyperglycaemic "memory". This phenomenon has been seen in microvasculature, where there is a persistent progression of hyperglycaemia induced alterations during the subsequent periods of normal glucose homeostasis [268]. Animal studies have demonstrated the development of retinopathy long after the glucose levels were normalised and the same effect has been noted in humans in the DCCT, where despite intensive therapy for hyperglycaemia, retinopathy and nephropathy were evident four years after the trial, even though the HbA1c levels were maintained. However, in these studies

the furosine and pentosidine concentrations in dermal collagen were significantly reduced, but the CML content and solubility of collagen increased [189]. The concept of hyperglycaemic memory may be explained by the production of superoxides, in the mitochondria, at physiological concentrations of glucose, with the resulting continued activation of the pathways in the absence of hyperglycaemia. Therefore, the interruption of AGE formation can be achieved by the inhibition of the production of superoxidase [269]. It would be difficult to accomplish this using conventional antioxidants, as their effects are selective according to their stiochiometry. New compounds that have a lower molecular weight than the conventional antioxidants behave as scavengers of superoxides by mimicking the behaviour of enzymes. These compounds normalise diabetes-induced inhibition of aortic prostacylcin synthetase in animals and significantly improve diabetes-induced reduction of nerve conduction and reduced blood flow [270].

Does the concentration of furosine and pentosidine in diabetic and non-diabetic plantar epidermal proteins increase with age?

There was no association between furosine and pentosidine concentrations and age in both groups (diabetic furosine r=0.088; diabetic pentosidine r=0.095; non-diabetic furosine r=-.0.193; non-diabetic pentosidine r=-0.143).

As already mentioned, the accumulation of the glycation products, particularly pentosidine, is influenced by keratinocyte turnover. It could be that this specialised area of skin, with its unique epidermal kinetics, needs the focus of glycation redirected to the age of the tissue and not the age of the person.

The next section addresses the second hypothesis by discussing the protein associations in epidermal tissue that provide the resilience and flexibility that is key to its protective function. The discussion addresses the function of intramolecular bonds and intercellular adhesions that are present in varying combinations throughout the epidermis, and adapts the knowledge obtained in Chapter 7 to the physical properties of plantar epidermal tissues. As these cellular interactions contribute to the physical behaviour of the epidermis at a

macro level, this knowledge is adapted to plantar epidermis in its normal state before the effects of hyperglycaemia are considered.

10.3 Hypothesis 2: There is a Decrease in Flexibility of Pedal Epidermis in Type II Diabetes.

The term flexibility is used to describe the five indices of elasticity measured in this thesis: the series elastic element on stretching and retraction; time constants on stretching and retraction and plasticity.

The series elastic element, retraction of the epidermis was significantly greater in the diabetic group on the three sites on the foot ($p<0.05$) than the controls. For a realistic expression of elasticity these data were corrected according to the epidermal thickness, measured by ultrasonography, giving a time constant or the series elastic element reading per unit thickness of epidermis. The series elastic coefficient/ mm of epidermis was significantly greater in the diabetic population than the controls ($p<0.001$). No other differences were noted when the thickness of the skin was taken into account.

There was no significant difference in the time constants on stretching and retraction between the diabetic and control groups ($p>0.05$). The epidermal plasticity of non - diabetic plantar epidermis was significantly greater than that of diabetic plantar epidermis ($p < 0.007$).

Other than keratins there are specific proteins, unique to keratinocytes that facilitate inter- and intra-cellular adhesions of epidermal keratinocytes. The expression of these proteins changes throughout the keratinisation process. As a collective, the keratinocytes provide the plantar epidermis with the appropriate mechanical properties it requires to withstand mechanical trauma. Increased cross-linking via pentosidine AGE formation may effect the dynamics of the epidermis.

Between the keratin filaments there are the non-helical domains, N- and C-terminal groups, protruding into the cellular matrix. A suggested mechanism for

the elasticity of the stratum corneum is through the reduction of the intermolecular forces between these filaments through non-helical regions, with the help of water extractable materials such as free amino acids (48.3% of water extractable materials). The properties associated with increased elasticity depend on increased intermolecular interaction between the water-extractable materials and the keratin fibres in the non-helical regions in the presence of an appropriate amount of water [271]. Therefore, dehyradation of the tissue would cause a reduction in this interaction and reduce the skins elasticity (Fig. 10.2). The profound change in the mechanical properties of the matrix upon dehydration is evident. In diabetes, autonomic neuropathy results in clinically anhydrotic skin on the foot (72% of diabetics in this thesis), therefore with less water in the stratum corneum the elastic and viscolelastic properties of the epidermai may be affected. To add to this model further, the protruding amino terminal domains may also be subject to glycation, therefore disturbing the dynamics between the keratin filaments even more (Fig. 10.2).

The structures within the cells, other than keratins that contribute to cell adhesion, have been mentioned earlier in this chapter. The mechanical properties of the epidermis result from its geometric form and the intrinsic properties of its constituent materials, mainly linearly elastic, high modulus keratin fibres embedded in a viscoelastic matrix of a lower modulus. The physical properties of keratin filaments are determined by their length (which is much higher than the cross-sectional area and thus provides a high level of flexibility; orientation (parallel arrangement); and packing (influenced by the size of the keratin bundles). Keratin intermediate filaments anchor to the desmoplakins within the desmosomes [258] providing the keratinocytes with a degree of tensile strength. Although the KIFs do not pass through the cell membrane, they are indirectly connected to each other through the desmosomes, forming a continual fibre network and structural continuity throughout the cell system. If glycation occurs at the terminal domains of the keratin filament tetramers, there is a possibility that the length of the filaments may be altered, thus compromising the flexibility.

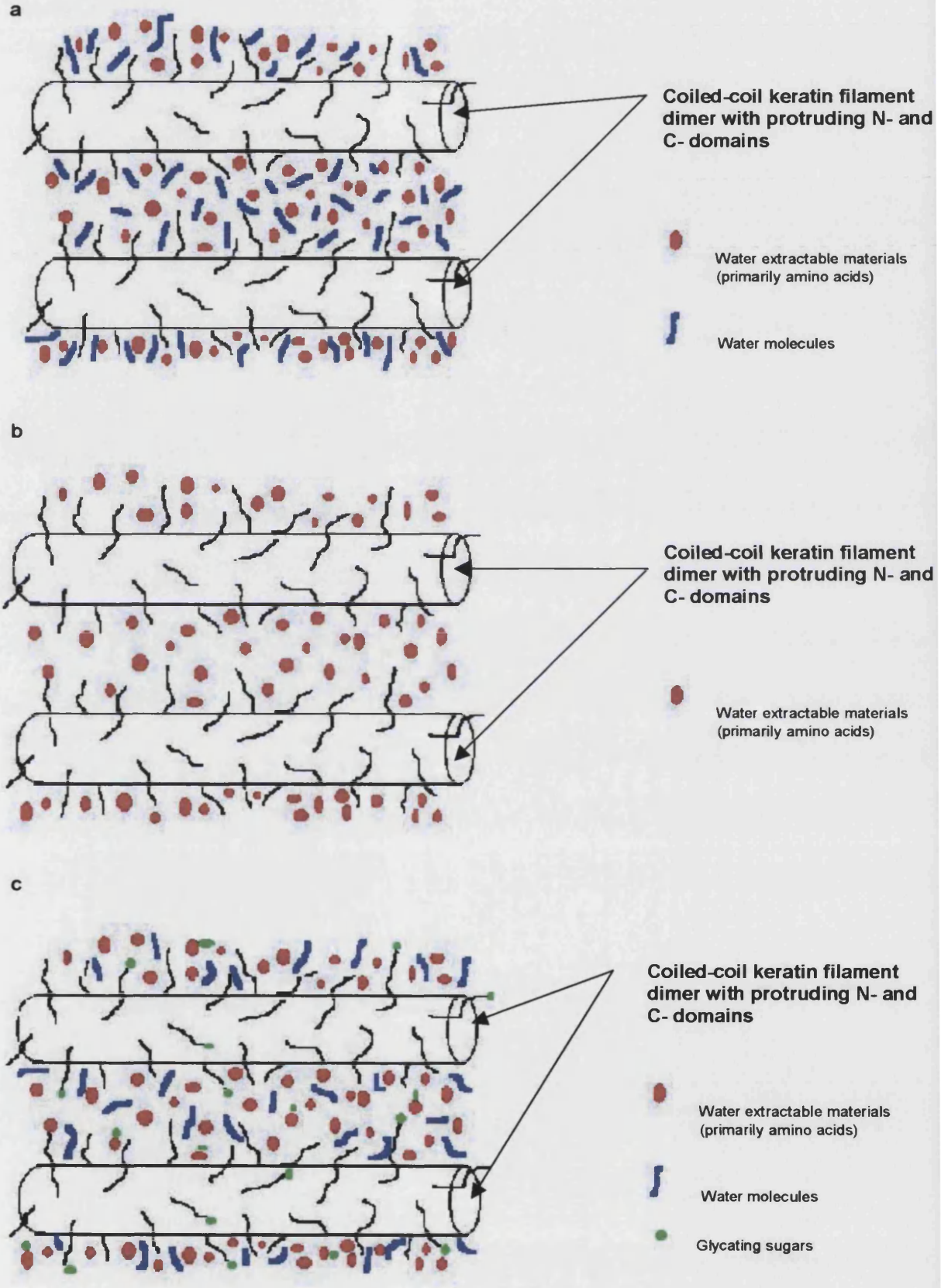

Figure 10.2. Diagram illustrating the possible affects of glycation and on the physical nature of the keratin filaments

When subjected to a deforming force it seems that the keratin filament will essentially behave as a linear elastic tissue and the stress that develops within the filaments will occur as a result of resistance to stretching offered by the α-helices. At larger strains the molecular organisation of the filament is progressively disrupted, as shown by X-ray diffraction studies, but these strains lie outside the normal physiological range encountered [272].

This synopsis of the cohesion inter and extracellular structures of keratinocytes has explained how the keratins in the epidermis provide the skin with the resilience and flexibility that is essential during natural joint and muscle movement. This is of particular importance on the foot, where the skin lies in closely associated with muscle and bone tissue. The plantar epidermis is the first point of contact the skin has with the ground (or shoe) during gait, and is designed to withstand shear, compression and torsion stresses. The function of keratin filaments in epidermal cells is to impart mechanical integrity to the cells, without which they would become fragile and prone to rupturing upon mild physical trauma [62].

In a clinical environment, the measurement of *in vivo* skin flexibility has involved basic devices in the past and observations have been understandably subjective. The evaluation of the viscoelasticity of the epidermis, in relation to vertical negative pressure, on different sites on the foot has been successfully conducted in this thesis using the Cutometer®.

The *in vitro* studies confirmed the difficulties encountered when attempting to simulate an *in vivo* environment for the callus specimens. When the stratum corneum (consisting of live cells) is separated from the skin, mechanical behaviour is grossly altered as a result of the removal of the dermis [273]. The problem of preventing dehydration of callus, which begins immediately after the removal from the foot, still remains.

The macro-structure of human epidermis, it is characterised as a 3-dimensional arrangement of fibres, which when stretched, could eventually change to one with a largely 2-dimensional orientation. In an experimental diabetes model,

Andreassen et al (1981) [158] demonstrated profound alterations in the collagen of diabetic rat skin, leading to an increase in the stiffness and strength. This stiffness is characterised by additional glycated cross-links formed between collagen molecules along with the whole extent of the triple helix, thus reducing the ability to change fibre orientation in this way i.e. reducing the ability to stretch under stress [56;274;275]. This experimental model could is transferable to epidermal tissues, *in vivo.* Therefore, if there is a greater degree of cross-links between keratin filaments, the ability to lengthen when under stress decreases. The results in this thesis show diabetic epidermis to exhibit greater elasticity on retraction of the epidermis than the non-diabetic epidermis. The elasticity on stretching of the epidermis did not differ between the two groups and the plantar epidermal plasticity was lower in the diabetic groups. Therefore, although the epidermis has the ability to retract in diabetes, more readily than non-diabetic epidermis, it is possible that the realignment of the tissues, after the deforming force is released, takes longer in the diabetic epidermis.

10.4 Hypothesis 3: There is an Increase in the Thickness of Pedal Epidermis in Type II Diabetes.

The plantar epidermal thickness was significantly higher in diabetics in comparison to controls ($p<0.05$), implying a denser plantar epidermis in diabetes. This fits the reasoning that the keratinocytes respond to mechanical trauma by increasing cell proliferation [73;276]. Therefore, the density of the tissues is expressed as high echogenicity in the ultrasound images.

Is there an association between the flexibility of pedal epidermis and age, gender and ethnicity?

There was no association between age and epidermal flexibility, with the exception of the linear elastic element on retraction of non-diabetic dorsal epidermis ($r=-0.559$).

There was no difference in all five indices of elasticity between the genders in the diabetic group ($p>0.05$). Differences were noted between the ethnic groups, in

varying degrees, on all three sites of the feet of both diabetics and controls ($p<0.05$). The Black and Asian skin types were overall less plastic and viscoelastic than the Caucasian skin types. The non-diabetic group only reflected this trend on the MLA site in terms of series linear coefficient on stretching the epidermis ($p<0.001$). These results need to be considered with caution, as the patient numbers in the groups were small. To gain a more realistic knowledge of the physical properties of skin in different skin types, further studies, recruiting more patients would increase the power of the results.

Is there an association between the thickness of pedal epidermis and age, gender and ethnicity?

There were no significant differences recorded in the epidermal thickness between the genders and between groups of different ethnic origin ($p>0.05$). In the diabetic population there was no correlation between age and epidermal thickness on all sites of the foot.

The non-diabetic females had thicker epidermis than the males on all three sites of the foot. Previous ultrasound studies have measured the full thickness of skin on other parts of the body as being thinner in the females [241]. As the acoustic density of the epidermis increases it can mask the echoes travelling into the dermis, therefore giving a false representation of the dermal layer of the skin. This could be an explanation for the results recorded in the Olsen study.

The low acoustic density of skin often creates problems when skin thickness measurements are made, as it is often difficult to convincingly identify the interface between the dermis and deeper structures, and there is a risk that the thickness of the dermis is underestimated [241]. The images taken of the pedal skin in this thesis, particularly the PMA, did not show the dermal structures clearly. This is advantageous as it makes the epidermal-dermal boundary definition clearer. The device does not have a sensitive enough resolution to note slight increases in epidermal thickness such as the swelling of the stratum corneum as a result of the ingress of water. This is an important point applicable to all studies that use this equipment for a quantitative analysis tool. However, the

equipment provides images of skin that are the nearest possible to the *in vivo* representation of the skin on different body sites. The images still provide a far more accurate indication of tissue thickness than histological techniques that ultimately result in post-fixation deformities in the structures.

What were the clinical observations made in the feet of diabetic and non-diabetic volunteers?

The genesis of this thesis originated from the detrimental effects that plantar callosities have on a foot at risk of ulceration. Clinical observations of diabetic callus, in particular around a chronic ulcer, question the physical nature of the tissues whilst the healing process is underway. Surveys analysing the distribution of callus in diabetic populations have reported conflicting outcomes. If the theory of glycation having an effect on the epidermal tissues was to be explored, it was imperative that the volunteers recruited for this study were examined for callus distribution and quality, so that an extrapolation callus formation and glycation accumulation could be scrutinised. It was essential that the population being investigated in this study was representative of the population of Type II diabetics. The recruitment of volunteers was based on the random sample of the diabetic population in North London. The overall participation rate was approximately 10%. The age distribution of the diabetic population was not normal, but slightly skewed to the right. This is this would be expected as persons with Type II diabetes usually, but not always, present with the disease above the age of 40; therefore, the occurrence of diabetes would favour the older population. The ages of the control group were of a normal distribution.

Calluses appear to have a mechanical etiology, although not all areas of high pressure develop callus, therefore the exact mechanical stimulus of callus formation is not clear. Calluses can act by distributing the force from an area or can behave in the opposite way by acting as a foreign body on the surface of the skin [33]. In this thesis, pathological callus was present in 52% of the diabetic patient population and 77% of the non-diabetic group, agreeing with previously published data by Holewski *et al* (1989) [8]. The majority of the diabetics presented with minimal stratum corneum thickening whereas the non-diabetics

presented with an even distribution of all three types of callus. In addition, the controls had more corns than the diabetic patients, which was associated with an increase in age.

In the diabetic group a similar prevalence of callus formation was recorded in both neuropathic and non-neuropathic diabetic patients of all ages. Callus formation was independent of duration of diabetes, which agrees with other data [32]. Most of the diabetics with peripheral sensory neuropathy did present with plantar corns.

Both diabetic and non-diabetic groups were overweight (BMI=25 and 27, respectively). The range of BMI was greater in the diabetics (minimum=20 and maximum=61.3) than the non-diabetics (minimum=29.8 and maximum=39.3. The natural progression from this observation would be that as the body mass increases, there is an increase in plantar pressures. This association was tested by Ahroni *et al* (1999) [16], where there was no correlation between body mass and peak plantar pressures. Another study reported that patients with neuropathic ulceration were significantly heavier than diabetic patients without ulceration [277], and also had an uneven plantar pressure distribution.

The diabetic population had a greater incidence of bilateral *pes planus*. From a clinical perspective the connection with Charcot foot is brought to mind, where it is theorised that the arterio-venous shunting, as a consequence of postganglionic autonomic denervation, causes demineralisation of the bones and the resulting collapse of the foot. This phenomenon occurs gradually over time or can present as acute attacks which if not dealt with early enough, will result in gross deformities of the foot. These data demonstrate *pes planus* as a structural deformity of the diabetic foot. With this in mind one would expect the demineralisation of the skin would lead to abnormalities in the connective tissue metabolism and structural changes in the skin. Diabetic A-V shunting is mainly found in the diabetic lower limb and foot, yet the largest difference in skin thickness is found in the thigh and not the foot [41]. In this study, diabetic neuropathy did not relate to epidermal thickening, but the differences in thickness were present between the diabetics and controls in the plantar skin. This

suggests that another aspect of diabetes other than neuropathy may have an effect on epidermal thickness.

Diabetic patients with PVD had thinner epidermis on the PMA and dorsal sites ($p=0.018$ and $p=0.024$, respectively) than diabetic patients without PVD. This agrees with the concept of poor nutrition of the skin, leading to its atrophy and of the associating appendages. A point of discussion with regards to glycation, would be that if there is a limited blood supply to the foot, the amount of glucose that may diffuse into the dermis followed by the epidermal tissues would also be reduced. Therefore, the potential for glycation of tissues is low. The amount of furosine noted in the keratin was far higher than that found in circulating blood, which suggests that free glucose from the circulating tissues may have diffused into tissues elsewhere in the body. Without detailed information about the blood in the immediate vicinity of the foot, only an assumption connecting the two can be made. Other studies using ultrasonography have not found a relationship between microvascular disease and increased thickness of skin in the extremities [40]. Whether changes in capillary blood flow, increase of glycation, polyol accumulation or other metabolic disorders are responsible for these findings remains to be established.

The majority of the patients with marked peripheral neuropathy (63%) and moderate peripheral neuropathy (63%) presented with limited range of motion (ROM) in the feet and 51% of the patients with no signs of neuropathy also presented with limited ROM in the feet. Reduced joint mobility in the feet, in particular the sub-talar joint disrupts the biomechanical function of the foot, therefore compromising plantar pressure distribution [278]. This limited ROM may distribute plantar pressures unevenly due to the resulting lack of shock absorption that the rigid foot will supply. The same phenomenon is seen to occur in diabetics with ulceration, more so than in diabetics without ulceration [279]. An increase in glycation related cross-linking of the collagen in extensor tendons of diabetics subjects, altering the ultrastructure of the associated tendons [125].

This thesis demonstrated no relationship between the epidermal thickness and HbA1c levels. The relationship between the cheiroarthropathy and peripheral

sensory neuropathy was not clear (no neuropathy: 49%; moderate neuropathy: 39% and marked neuropathy: 63%). The results are interesting, as the concept of limited digital range of motion is conventionally seen in Type I diabetes. In this study an association between the limited ROM in the feet and the small joints in the hands was made in some participants.

Although there was a higher incidence of yellow nail in the feet of diabetic patients than the controls, the presence of yellow nails in the controls indicates that the accumulation of AGEs can occur in a non-diabetic state. The non-diabetics with yellow nails did not have PVD. In both groups the presentation of yellow nails on the feet was seen in patients with higher HbA1c readings. Examination of the palmar skin recorded 19 diabetic patients and 2 non-diabetic subjects with a yellow hue on the skin. Those with such a presentation had significantly higher levels of pentosidine in the plantar callus than those without yellow palmar skin ($p<0.05$). The majority of people with chieroarthropathy, limited joint motion in the feet and yellow nails were at least 65 years of age.

Is there an association between clinical pathologies of the feet in diabetes and the physical qualities measured in the feet?

There was no association between epidermal thickness on the feet and the duration of diabetes or glycaemic control.

This thesis did not find a statistical significant difference, between epidermal thickness and neuropathy. There was a significant difference however in epidermal thickness readings taken from the PMA between non-diabetic volunteers and diabetic patients without neuropathy. The former was greater than the latter, which implies that the average thickness PMA of epidermal tissue in diabetic patients to be considerably greater in the neuropathic patients, the PMA data, as a whole, in diabetics is higher than non-diabetic PMA epidermal thickness and therefore may be related to neuropathy. A larger patient group would be needed to confirm this.

10.5 Summary of Conclusion

The following conclusions, based on the present experimental and numerical studies can be drawn:

1. The plantar callus tissues of diabetic and non-diabetic individuals are involved with non-enzymatic glycation. The amount of pentosidine measured is significantly greater in plantar diabetic callus than non-diabetic callus.

2. Keratin is a major determinant of epidermal dynamic stiffness. Site dependent variations, on the feet, in both the dynamic and time-dependent mechanical properties have been recorded in the normal populations. The diabetic pedal epidermis is more elastic on retraction than non-diabetic epidermis and less plastic on the PMA site only. This has allowed for the comparison of data to be made between the diabetic and non-diabetic population. These data can be used for comparative studies in the future regarding the mechanical properties of the epidermis on the periphery of plantar neuropathic ulcers.

3. Regional variations in epidermal thickness were noted between diabetic and non-diabetic populations. Plantar epidermal thickness in the diabetic population was significantly higher than that of the control group.

Reference List

[1] Gould N, Schneider W, Ashikaga T. Epidemiological Survey of Foot Problems in the Continental United States 1978-1979. Foot and Ankle 1980; 1(1):8-10.

[2] Hung LK, Ho YF, Leung PC. Survey of Foot Deformities Among 166 Geriatric Inpatients. Foot and Ankle 1985; 5(4):156-165.

[3] Elton PJ, Sanderson SP. The Chiropodial Survey of Elderly Persons over 65 Years in the Community. Chiropodist 1987; 42:175-178.

[4] White EG, Mulley GP. Footcare for Elderly People: A Community Survey. Age and Ageing 1989; 18:275-278.

[5] Levy LA. Prevalence of Chronic Podiatric Conditions. Journal of the American Podiatric Medical Association 1992; 82(4):221-223.

[6] Benvenuti F, Ferrucci L, Gualnic JM, Gangemi S, Baroni A. Foot Pain and Disability in Older Persons: An Epidemiologic Survey. Journal of the American Geriatric Association 1995; 43(5):479-484.

[7] Bresäter LE, Welin L, Romanus B. Foot Pathology and Risk Factors for Diabetic Foot Disease in Elderly Men. Diabetes Research and Clinical Medicine 1996; 32:103-109.

[8] Holewski JJ, Moss KM, Stess RM, Graf PM, Grunfeld C. Prevalence of Foot Pathology and Lower Extremity Complications in a Diabetic Out Patient Clinic. Journal of Rehabilitation Research and Development 1989; 26(3):35-44.

[9] Rönnemaa T, Kallio V. Prevalence of Foot Problems and need for Foot Care in an Unselected Diabetic Population. Journal of British Podiatric Medicine 1993; 48:185-190.

[10] Working Party of the British Diabetic Association and the Society of Chiropodists. Diabetes and Chiropodial Care. 1-17. 1990. British Diabetic Association.

[11] Murray HJ, Young MJ, Hollis S, Boulton AJM. The Association Between Callus Formation, High Pressures and Neuropathy in Diabetic Foot Ulceration. Diabetic Medicine 1996; 13:979-982.

[12] Reiber GE, Vileikyte L, Boyko EJ, Aguila M, Smith DG, Lavery LA et al. Causal Pathways for Incident Lower - Extremity Ulcers in Patients with Diabetes from Two Settings. Diabetes Care 22[1], 157-162. 1999.

[13] Edmonds ME, Bludell MP, Morris ME, Thomas EM, Cotton LT, Watkins PJ. Improved Survival of the Diabetic Foot: The Role of the Specialized Foot Clinic. Quart J Med 1986; 232:763-771.

[14] Delbridge I, Ctercteko G, Fowler C, Reeve TS, LeQuesne LP. The Aetiology of Diabetic Neuropathic Ulceration of the Foot. Br J Surg 1985; 72(1):1-6.

[15] Edmonds M, Boulton A, Buckenam T, Every N, Foster A, Freeman D et al. Report of the Diabetic Foot and Amputation Group. Diabetic Medicine 1996; 13:S27-S42.

[16] Ahroni JH, Boyko EJ, Forsberg RC. Clinical Correlates of Plantar Pressure Among Diabetic Veterans. Diabetes Care 22[6], 965-972. 1999.

[17] Abouaesha F, Van Schie SHM, Griffiths GD, Young RJ, Boulton AJM. Plantar Tissue Thickness is Related to Peak Plantar Pressure in the High Risk Diabetic Foot. Diabetes Care 24[7], 1270-1274. 2001.

[18] Morris AD, McAlpine R, Steinke D, Boyle DIR, Ebrahim AR, Vasudev N et al. Diabetes and Lower - Limb Amputations in the Community. Diabetes Care 21[5], 738-743. 1998.

[19] Currie CJ, Morgan CL, Peters JR. The Epidemiology and Cost of Inpatient Care for Peripheral Vascular Disease Infection, Neuropathy, and Ulceration in Diabetes. Diabetes Care 1998; 21(1):42-48.

[20] Shin JB, Seong YJ, Lee HJ, Kim SH, Park JR. Foot Screening Technique in a Diabetic Population. J Korean Med Sci 2002; 15:78-82.

[21] Birke JA, Franks BD, Foto JG. First Ray Joint Limitation, Pressure and Ulceration of the First Metatarsal Head in Diabetes. Foot and Ankle 1995; 16(5):277-284.

[22] Boulton AJM, Gries FA, Jervell JA. Guidelines for the Diagnosis and Outpatient Management of Diabetic Peripheral Neuropathy. Diabetic Medicine 1998; 15:508-514.

[23] Sims DS, Cavanagh PR, Ulbrecht JS. Risk Factors in the Diabetic Foot. Recognition and Management. Physical Therapy 1988; 68(12):1887-1901.

[24] Mueller MJ, Minor SD, Diamond JE, Blair VP 3rd. Relationship of Foot Deformity to Ulceration Location in Patients with Diabetes Mellitus. Phys.Ther. 70[6], 356-362. 1990.

[25] Edmonds ME, Foster AVM. Managing the Diabetic Foot. 1 ed. Blackwell Science Ltd, 2000.

[26] Merriman LM, Tollafield DR. Assessment of Skin and Appendages. In: Merriman LM, Tollafield DR, editors. Assessment of the Lower Limb. Churchill Livingston, 1995.

[27] Boulton AJM, Hardisty CA, Betts RP, et al. Dynamic Foot Pressure and other Studies as Diagnostic and Management Aids in Diabetic Neuropathy. Diabetes Care 6, 26-33. 1983.

[28] Booth J, McInnes A. The Aetiology and Management of Plantar Callus Formation. Journalof Wound Care 1997; 6(9):427-430.

[29] Merriman LM, Griffiths C, Tollafield DR. Plantar Lesion Patterns. Chiropodist 1987; 42:145-148.

[30] Bennett PJ, Stocks AE, Whittam DJ. Analysis of Risk Factors for Neuropathic Foot Ulceration in Diabetes Mellitus. Journal of the American Podiatric Medical Association 1996; 86(3):112-116.

[31] Fernando DJS, Masson EA, Veves A, Boulton AJM. Relationship of Limited Joint Mobility to Abnormal Foot Pressures and Diabetic Foot Ulceration. Diabetes Care 1998; 14(1):8-11.

[32] Borssén B, Bergenheim T, Lithner F. The Epidemiology of Foot Lesion in Diabetics Aged 15 - 50 Years. Diabetic Medicine 1990; 7:438-444.

[33] Young MJ, Cavanagh, PR, Thomas G, Johnson MM, Murray H et al. The Effect of Callus Removal on the Dynamic Plantar Foot Pressures in Diabetic Patients. Diabetic Medicine 1992; 9:55-57.

[34] Cavanagh PR, Hennig EM, Rodgers MM, et al. The Measurement of Pressure Distribution on the Plantar Surface of the Diabetic Foot. In: Whittle M, Harris D, editors. Biomechanical Measurement in Orthopaedic Practice. London, England: Oxford University Press, 1985: 159-168.

[35] Schuyler MR, Niewoehner DE, Inkley SC, Kohn R. Abnormal Lung Elasticity in Juvenile Diabetes Mellitus. American Review of Respiratory Disease 113, 3741. 1976.

[36] Hamlin RC, Kohn RR, Luschin JH. Apparent Accelerated Aging of Human Collagen in Diabetes Mellitus. Diabetes 1983; 24(10):902-904.

[37] Grgic A, Rosenbloom AL, Weber FT, Giordano B, Malone JI, Shuster JJ. Joint Contracture - Common Manifestation of Childhood Diabetes Mellitus. The Journal of Pediatrics 1976; 88(4):584-588.

[38] Hanna W, Friesen D, Bombardier C, Gladman D, Hanna A. Pathological Features of Diabetic Thick Skin. Journal of the American Academy of Dermatology 1987; 16(1):546-553.

[39] Collier A, Patrick AW, Bell D, Mathews DM, MacIntyre CCA, Ewing DJ et al. Relationship of Skin Thickness to Duration of Diabetes, Glycemic Control and Diabetic Complications in Male IDDM Patients. Diabetes Care 1989; 12(5):309-312.

[40] Huntley AC, Walter RM Jr. Quantitative Determination of Skin Thickness in Diabetes Mellitus: Relationship between Disease Parameters. Journal of Medicine 1990; 21(5):257-264.

[41] Forst T, Kann P, Pfützner A, Lobmann R, Schäfer H, Beyer J. Association Between "Diabetic Thick Skin Syndrome" and Neurological Disorders in Diabetes Mellitus. Acta Diabetol 1994; 31:73-77.

[42] Jung Y, Hohmann TC, Gerneth JA, Novak J, Wasserman RC, D'Andrea BJ et al. Diabetic Hand Syndrome. Metabolism 1971; 20(11):1008-1015.

[43] Kennedy L, Archer DB, Campbell SL, Beacom R, Johnston PB. Limited Joint Mobility in Type I Diabetes Mellitus. Postgraduate Medical Journal 1982; 58:485-486.

[44] Beacom R, Sawnhey B, Kennedy L. Peripheral Nerve Function in Type I (Insulin Dependent) Diabetic Patients With Limited Joint Mobility. Dermatologia 1983; 25(2):139.

[45] Buckingham B, Reiser KM. Relationship between the Content of lysyl Oxidase-dependent Cross Links in Skin Collagen, Nonenzymatic Glycosylation and Long Term Complications in Type I Diabetes Mellitus. J Clin Invest 86[4], 1046-1054. 1990.

[46] Rosenbloom AL, Frias JI. Diabetes Mellitus, Short Stature and Joint Stiffness - A New Syndrome. Clinical Research 1974; 22(1):92A.

[47] Rosenbloom AL, Siverstein JH, Lezotte DC, Richardson K, McCallum M. Limited Joint Mobility in Childhood Diabetes Mellitus Indicates Increased Risk for Microvascular Disease. The New England Journal of Medicine 1981; 305(4):191-194.

[48] Fitzcharles MA, Duby S, Waddell RW, Banks E, Karsh J. Limitation of Joint Mobility (Cheiroarthropathy) in Adult Non-Insulin - Dependent Diabetic Patients. Ann Rheum Dis 1984; 43(2):251-254.

[49] Seibold JR. Digital Sclerosis in Children with Insulin-Dependent Diabetes Mellitus. Arthritis and Rheumatism 25[11], 1357-1361. 1982.

[50] Collier A, Matthews DM, Kellett HA, Clarke BF. Change in Skin Thickness Associated with Cheiroarthropathy in Insulin Dependent Diabetes Mellitus. British Medical Journal 1986; 292:936.

[51] Lieberman LS, Rosenbloom AL, Riley WJ, Silverstein JH. Reduced Skin Thickness with Pump Administration of Insulin. The New England Journal of Medicine 1980; 303(16):940-941.

[52] Malik RA, Metcalfe J, Sharma AK, Day JL, Rayman G. Skin Epidermal Thickness and Vascular Density in Type I Diabetes. Diabetic Medicine 1992; 9:263-267.

[53] Thoolen M. A Study of the Skin of the Sole of the Foot using High-Frequancy Ultrasonography and Histology. 1999.

[54] Eaton RP, Sibbitt WL, Harsh A. The Effect of Aldose Reductase Inhibiting Agent on Limited Joint Mobility in Diabetic Patients. JAMA 1985; 253(10):1437-1440.

[55] Eaton RP. The Collagen Hydration Hypothesis: A New Paradigm for the Secondary Complications of Diabetes Mellitus. Journal of Chronic Disease 1986; 139(10):763-766.

[56] Kennedy L, Baynes JW. Non-Enzymatic Glycosylation and the Chronic Complications of Diabetes: An Overview. Dermatologia 1984; 26:93-98.

[57] Melling M, Pfeiler W, Karimian-Teherani D, Schnallinger M, Sobal G, Zangerle C et al. Differential Scanning Calorimetry Biochemical, and Biomechanical Analysis of Human Skin from Individuals with Diabetes Mellitus. The Anatomical Record 259, 327-333. 2000.

[58] Oimomi M, Hatanaka H., Ishikawa K, Kubota S, Yoshimura Y, Baba S. Increased Fructose-Lysine of Nail Protein in Diabetic Patients. Klin Wochenschr 1984; 62:477-478.

[59] Birrer RB, Dellacorte PD. Skin and Nail Disorders of the Foot. Emergency Medicine , 27-50. 1993.

[60] Huntley AC. Photoessay: The Skin and Diabetes Mellitus. Dermatology On-line Journal 1[2]. 1995.

[61] Biochemistry and Physiology of the Skin. Oxford University Press, 1983.

[62] Fuchs E. Keratins and the Skin. Annu.Rev.Cell Dev.Biol. 11[123], 153. 1995.

[63] Thomas SE, Dykes PJ, Marks R. Plantar Hyperkeratosis: A Study of Callosities and Normal Plantar Skin. The Journal of Investigative Dermatology 1985; 85:394-397.

[64] Zincazone® Product Information. Internet , http://www.the-boulevard-mall.com/zinc/product.htm. 2004.

[65] Matoltsy AG. Keratinization. The Journal of Investigative Dermatology 67, 20-25. 1976.

[66] Bommannan D, Potts RO, Guy RH. Examination of the Stratum Corneum Barrier Function in vivo by Infrared Spectroscopy. J.Invest.Dermatol. 95, 403-408. 1990.

[67] Brysk MM, Rajaraman S, Penn P, Barlow E, Bell T. Cohesive Properties of Terminally Differentiated Keratinocytes. Expl.Cell.Biol. 57[60], 66. 1989.

[68] Haftek M, Serre G, Mils V, Thivolet J. Immunocytochemical Evidence for the possible Role of Cross - Linked Keratinocyte Envelopes in Stratum Corneum Cohesion. J Histochem Cytochem 39[11], 1531-1538. 1991.

[69] Bergstresser PR, Taylor JR. Epidermal 'Turnover Time' - A New Exmination. British Journal of Dermatology 96, 503-509. 1977.

[70] Halprin KM, Ohkawara A, Adachi K. Glucose Entry into the Human Epidermis: The Concentration of Glucose in the Human Epidermis. The Journal of Investigative Dermatology 1967; 49(6):559-560.

[71] Roberts D, Marks R. The Determination of Regional and Age Variations in the Rate of Desquamation: A Comparison of Four Techniques. J Invest Dermatol 74[1], 13-16. 1980.

[72] Nurse Minerva - Diagrams. Internet , http://www.nurseminerva.co.uk/diagrams.htm. 2004.

[73] MacKenzie IC. The Effects of Frictional Stimulation on Mouse Ear Epidermis. I. Cell Proliferation. The Journal of Investigative Dermatology 62, 80-85. 1974.

[74] Springett K. The Influences of Forces Generated During Gait on the Clinical Appearance and the Physical Properties of Skin Callus. PhD Thesis 1993.

[75] MacKenzie IC. Effects of Frictional Stimulation of the Structure of the Stratum Corneum. In: Marks R, Plewig G, editors. Stratum Corneum. Berlin-Heidelberg: Springer-Verlag, 1983: 146-152.

[76] Plewig G, Scheuber E, Reuter B, Waidelich W. Thickness of Corneocytes. In: Marks R, Plewig G, editors. Stratum Corneum. Berlin-Heidelberg: Springer-Verlag, 1983: 171-173.

[77] McGinley KJ, Marples RR, Plewig G. The Method for Visualising and Quantitating the Desquamating Portion of the Human Stratum Corneum. The Journal of Investigative Dermatology 53[2], 107-111. 1969.

[78] Sun TT, Green H. Keratin Filamments of Cultured Human Epidermal Cells. Formation of Intermolecular Disulfide Bonds during Terminal Differentiation. J Biol Chem 253[6], 2053-2060. 25-3-1978.

[79] Strelkov SV, Herrmann H, Aebi U. Molecular Architecture of Intermediate Filaments. BioEssays 25[3], 243-251. 2003.

[80] Coulombe PA, Fuchs E. Elucidating the Early Stages of Keratin Filament Assembly. The Journal of Cell Biology 111, 153-169. 1990.

[81] Eichner R, Sun TT, Aebi U. The Role of Keratin Subfamilies and Keratin Pairs in the formation of Human Epidermal Intermediate Filaments. J Biol Chem 102[5], 1767-1777. 1986.

[82] Ma L, Yamada S, Wirtz D, Coulombe PA. A 'Hot - Spot' Mutation Alters the Mechanical Properties of Keratins Filament Networks. Nature Cell Biology 3, 503-506. 2001.

[83] Yamaguchi Y, Itami S, Tarutani M, Hosokawa K, Miura H, Yoshikawa K. Regulation of Keratin 9 in Nonpalmoplantar Keratinocytes by Palmopantar Fibroblasts through Epithelial - Mesenchymal Interactions. J Invest Dermatol 112, 483-488. 1999.

[84] Swensson O, Langbein L, McMillan JR, Stevens HP, Leigh IM, McLean WH et al. Specialized Keratin Expression Pattern in Human Ridged Skin as an Adaptation to High Physical Stress. The Journal of Dermatology 139, 767-775. 1998.

[85] Paladini RD, Coulombe PA. The Functional Diversity of Epidermal Keratins Revealed by the Partial Rescue of the Keratin 14 Null Phenotype. The Journal of Cell Biology 146[5], 1185-1201. 6-9-1999.

[86] Wawersik MJ, Mazzalupo S, Nguyen D, Coulombe PA. Increased Levels of Keratin 16 Alter Epithelialization Potential of Mouse Skin Keratinocytes in Vivo and Ex Vivo. Molecular Biology of the Cell 12, 3439-3450. 2001.

[87] Cohen MP. Chemistry. Diabetes and Protein Glycation. Clinical and Pathophysiological Relevance. JC Press Philadelphia, 1996: 5-31.

[88] Cohen MP. Introduction. Diabetes and Protein Glycosylation. Measurement and Biological Relevance. Springer - Verlag, 1986: 1-4.

[89] Finot PA. Nonenzymatic Browning Products: Physiologic Effects and Metabolic Transit in Relation to Chemical Structure. Diabetes 1982; 31 Suppl 3:22-28.

[90] Bucala R, Tracey KJ, Cerami A. Advanced Glycosylation Products Quench Nitric Oxide and Mediate Defective Endothelium-Dependent Vasodilation in Experimental Diabetes. J.Clin.Invest. 87, 432-438. 1991.

[91] Singh R, Barden A, Mori T, Beilin L. Advanced Glycation End Products: A Review. Dermatologia 44, 129-146. 2001.

[92] Monnier VM, Vishwanath V, Frank KE, Elmets CA, Dauchot P, Kohn RR. Relation Between Complications of Type I Diabetes Mellitus and Collagen-Linked Fluorescence. The New England Journal of Medicine 1986; 314:403-408.

[93] Vlassara H, Fuh H, Makita Z, Krungkrai S, Cerami A, Bucala R. Exogenous Advanced Glycosylation End Products Induce Complex Vascular Dysfunction in Normal Animals: A Model for Diabetic and Aging Complications. Proc Natl Acad Sci USA 1992; 89:12043-12047.

[94] Sensi M, et al. Role of Advanced Glycation End-Products (AGE) in Late Diabetic Complications. Diabetes Research and Clinical Practice 1995; 28(1):9-17.

[95] Sugiyama S, Miyata T, Horie K, Iida Y, Tsuyuki M, Tanak H et al. Advanced Glycation End-Products in Diabetic Nephropathy. Nephrol Dial Transplant 11[5], 91-94. 1996.

[96] Takahashi K, Kushida K, Ohishi T, Kawana K, Hoshino H, Uchiyama A et al. Quantitative Analysis of Crosslinks Pyridinoline and Pentosidine in Articular Cartilage of Patients with Bone and Joint Disorders. Arthritis and Rheumatism 37[5], 724-728. 1994.

[97] Münch G, Thome J, Foley P, Schnizel R, Riederer P. Advanced Gylcation End Products in Ageing and Alzheimer's Disease. British Journal of Dermatology 23, 134-143. 1997.

[98] Lee AT, Cerami A. Role of Glycation in Aging. Annals New York Academy of Sciences 1992; 663:63-70.

[99] Brownlee M. Glycation and Diabetic Complications - Lilly Lecture 1993. Diabetes 1993; 43:836-841.

[100] Bucala R, Makita Z, Koschinsky T, Cerami A, Vlassara H. Lipid advanced Glycosylation: Pathway for Lipid Oxidation *In Vivo.* Proc Natl Acad Sci USA 1993; 90:6434-6438.

[101] Brownlee M, Vlassara H, Kooney A, Ulrich P, Cerami A. Aminoguanidine Prevents Diabetes-Induced Arterial Wall Protein Cross-Linking. Science 1986; 232:1629-1632.

[102] Festa A, Schmölzer B, Schernthaner G, Menzel EJ. Differential Expression of Receptors for Advanced Glycation End Products in Monocytes in Patients with IDDM. Diabetologia 41, 674-680. 1998.

[103] Koga K, Yamagishi S, Okamoto T, Inagaki Y, Amano S, Takeuchi M et al. Serum Levels of Glucose-Derived Advanced Glycation End Products are Associated with the Severity of Diabetic Retinopathy in Type 2 Diabetic Patients without Renal Dysfunction. Int J Clin Pharmacol Res 22[1], 13-17. 2002.

[104] Thornalley PJ. The Clnincal Significcance of Glycation. Clin Lab. 45, 263-273. 1999.

[105] McCance DR, Dyer DG, Dunn Ja, Bailie KE, Thorpe SR, Baynes JW et al. Maillard Reaction Products and their Relation to Complications in Insulin-Dependent Diabetes Mellitus. J.Clin.Invest. 91, 2470-2478. 1993.

[106] Miyazaki K, Nagai R, Horiuchi S. Creatine Plays a Direct Role as a Protein Modifier in the Formation of a Novel Advanced Glycation End Product. J.Biochem. 132, 543-550. 2002.

[107] Bierhaus A, Hofmann MA, Ziegler R, Nawroth PP. AGEs and their Interaction with AGE-Receptors in Vascular Disease and Diabetes Mellitus. I. The AGE Concept. Cardovascular Research 37, 586-600. 1998.

[108] Sell DR, Monnier VM. Structure Elucidation of a Scenscence Cross - Link from Human Extracellular Matrix: Implication of Pentoses in the Aging Reaction Process. J.Biol.Chem. 264, 21597-21622. 1989.

[109] Grandhee SK, Monnier VM. Mechanism of the Formation of the Maillard Protein Cross - link, Pentosidine: Glucose, Fructose and Ascorbate as Pentosidine Precursors. J.Biol.Chem. 266, 11649-11653. 1991.

[110] Dyer DG, Blackledge JA, Thorpe SR, Baynes JW. Formation of Pentosidine during Nonenzymatic Browning of Protein by Glucose: Identification of Glucose and other Carbohydrates as possible Precursors of Pentosidine *in vivo*. J.Biol.Chem. 266, 11654-11660. 1991.

[111] Baynes JW. Role of Oxidative Stress in Development of Complications in Diabetes. Diabetes 1991; 40:405-412.

[112] Fu MX, Requena JR, Jenkins AJ, Lyons TJ, Baynes JW, Thorpe SR. The Advanced Glycation End-Product, N^{ε}-(Carboxymethyl)lysine, is a Product of both Lipid and Glycoxidation Reactions. The Journal of Biological Chemistry 271[17], 9982-9986. 1996.

[113] Ando K, Beppu M, Kikugawa K, Nagai R, Horiuchi S. Membrane Proteins of Human Erythrocytes are Modified by Advanced Glycation End Products during Aging in the Circulation. Biochemical and Biophysical Research Communications 258[1], 123-127. 29-4-1999.

[114] Blaton V. Oxidative Stress in Diabetes. eJIFCC 13[5]. 2004.

[115] Wells-Knecht MC, Lyons TJ, McCance DR, Thorpe SR, Baynes JW. Age -Dependent Increase in *Ortho*-tyrosine and Methionine Sulfoxide in Human Skin Collagen is not Accelarated in Diabetes. J.Clin.Invest. 100, 839-846. 1997.

[116] Verzijl N, DeGroot J, Thorpe SR, Shaw JN, Lyons TJ, Bijlsma JWJ et al. Effect of Collagen Turnover on the Accumulation of Advanced Glycation End Products. J.Biol.Chem. 275[50], 39027-39031. 2000.

[117] Dunn JA, Patrick JS, Thorpe SR, Baynes JW. Oxidation and glycated proteins: age-dependent accumulation of N^{ε}-(carboxymethyl)lysine in lens proteins. Biochemistry 28, 9464-9468. 1989.

[118] Dunn JA, McCance DR, Thorpe SR, Llyons TL, Baynes JW. Age-Dependent Accumulation of N- (Carboxymethyl)hydroxylysine in Human skin Collegan. Biochemistry 1991; 30:1205-1210.

[119] Vlassara H. Recent Progress in Advanced Glycation End Products and Diabetic Complications. Diabetes 46[2], S19-S25. 1997.

[120] Brownlee M, Cerami A, Vlassara H. Advanced Glycosylation End Products in Tissue and the Biochemical Basis of Diabetic Complications. N Engl J Med 318[20], 1315-1321. 1988.

[121] Monnier VM, Cerami A. Non-Enzymatic Browning *in vivo:* Possible Process for Aging of Long-Lived Proteins. Science 1981; 211:491-493.

[122] Verzijl N, DeGroot J, Oldhinkel E, Bank RA, Thorpe SR, Baynes JW et al. Age-Related Accumulation of Maillard Reaction Products in Human Articular Cartilage Collagen. Biochem.J 350, 381-387. 2000.

[123] Boel E, Selmer J, Flodgaard HJ, Jensen T. Diabetic Late Complications: Will Aldose Reductase Inhibitors or Inhibitors of Advanced Glycosylation Endproduct Formation hold Promise? Journal of Diabetes and its Complications 9[2], 104-129. 1995.

[124] Monnier VM. Non-Enzymatic Glycosylation, the Maillard Reaction and the Aging Process. Journal of Gerontology 1990; 45(4):B105-B111.

[125] James VJ, Delbridge I, McLennan S, Yue DK. Use of X-Ray Diffraction in Study of Human Diabetic and Aging Collagen. Diabetes 1991; 40(3):391-393.

[126] Cohen MP. Introduction. Diabetes and Protein Glycation. Clinical and Pathophysiological Relevance. JC Press Philadelphia, 1996: 1-4.

[127] Hudson LG, McCawley LJ. Contributions of Epidermal Growth Factor Receptor to Keratinocyte Motility. Microscopy Research and Technique 43, 444-455. 1998.

[128] Hudson BI, Stickland MH, Grant PJ, Futers TS. Characterisation of Allelic and Nucleotide Variation Between the RAGE Gene in Chromosome 6 and a Homologous Pseudogene to its 5' Regulatory Region on the Chromosome. Implications for Polymorphic Studies in Diabetes. Diabetes 50, 2646-2651. 2001.

[129] Hudson BI, Stickland MH, Futers TS, Grant PJ. Study of the 429 T/C and -374/A Receptor for Advanced Gylcation End Products Promotor Polymorphisms in Diabetic and Nondiabetic Subjects with Macrovascular Disease. Diabetes Care 24[11], 2004. 2001.

[130] Koschinsky T, He CJ, Mitsuhashi T, Bucala R, Liu C, Buenting C et al. Orally Absorbed Reactive Glycation Products (Glycotoxins): An Environmental Risk Factor in Diabetic Nephropathy. Proc.Natl.Acad.Sci.USA 94, 6474-6479. 1997.

[131] Thornalley PJ. The Clnincal Significance of Glycation. Clin Lab. 45, 263-273. 1999.

[132] Mizutari K, Ono T, Ikeda K, Kayashima K, Horiuchi S. Photo-Enhanced Modification of Human Skin Elastin in Actinic Elastosis by N^{ε}-(Carboxymethyl)lysine, One of the Glycoxidation Products of the Maillard Reaction. J Invest Dermatol 108, 797-802. 1997.

[133] Paul RG, Bailey AJ. The Effect of Advanced Glycation End-Product Formation Upon Cell Matrix Interactions. The International Journal of Biochemistry and Cell Biology 31, 653-660. 1999.

[134] Monnier VM, Glomb M, Elgawish A, Sell DR. The Mechanism of Collagen Cross-linking in Diabetes A Puzzle Nearing Resolution. Diabetes 1996; 45(SUPPL 3):S67-S72.

[135] Wolffenbuttel BHR, Boulanger CM, Crijns FRL, Huijberts MSP, Poitevin P, Swennen GNM et al. Breakers of Advanced Glycation End Products Restore Large Artery Properties in Experimental Diabetes. Proc.Natl.Acad.Sci.USA 95, 4630-4634. 1998.

[136] Reihsner R, Menzel EJ. Two-Dimensional Stress-Relaxation behaviour of Human Skin as Influenced by Non-Enzymatic Glycation and the Inhibitory Agent Aminoguanidine. Journal of Biomechanics 31, 985-993. 1998.

[137] Azevedo MS, Anguilar Manso CF. Inhibition of NEG of Proteins by Different Compounds. Diabetologia 29[8], 531A. 1986.

[138] Ajiboye R, Harding JJ. The Non-Enzymic Glycosylation of Bovine Lens Proteins by Glucosamine and its Inhibition by Aspirin, Ibuprofen and Glutathione. Exp Eye Res 1989; 49:31-41.

[139] Sensi M, Bruno MR, Pozzilli P. In vitro Inhibition of Non-Enzymatic Glycosylation Induced by Aspirin. Med Sci Res 1987; 15:99-100.

[140] Vinson JA, Howard TB. Inhibition of protein Glycation and Advanced End Products by Ascorbic Acid and Other Vitamins and Nutrients. Nutritional Biochemistry 1996; 7:659-663.

[141] Miyata T, Ishikawa S, Asahi K, Inagi R, Suzuki D, Horie K et al. 2 - Isopropylideneydrozono - 4 - oxo - thiazolidon - 5 - ylacetanilide (OPB - 9195) Treatment Inhibits the Development of Intimal Thickening after Balloon Injury of Rat Carotid Artery: Role of glycoxidation and Lipoxidation Reactions in Vascular Tissue Damage. FEBS Letters 445, 202-206. 1999.

[142] Contreras I, Reiser KM, Martinez N, Giansante E, Lopez T, Suarez N et al. Effects of Aspirin and Basic Amino Acids on Collagen Cross-Links and Complications in NIDDM. Diabetes Care 1997; 20(5):832-835.

[143] Tsuji H, Iehara N, Masegi T, Imura M, Ohkawa J, Arai H et al. Ribozome Targeting of Receptor for Advanced Glycation End Products in Mouse Mesangial Cells. Biochemical and Biophysical Research Communications 245, 583-588. 1998.

[144] Wilkinson-Berka J, Kelly DJ, Koerner SM, Jaworski K, Davis B, Thallas V et al. ALT-946 and Aminguanidine, Inhibitors of Advanced Glycation, Improve Severe Neuropathy in the Diabetic Transgenic (mREN-2)27 Rat. Diabetes 51, 3283-3289. 2002.

[145] Price DL, Rhett PM, Thorpe SR, Baynes JW. Chelating Activity of Advanced Glycation End-Products Inhibitors. The Journal of Biological Chemistry 276[52], 48967-48972. 2001.

[146] Wilkinson-Berka J, Kelly DJ, Koerner SM, Jaworski K, Davis B, Thallas V et al. ALT-946 and Aminguanidine, Inhibitors of Advanced Glycation, Improve Severe Neuropathy in the Diabetic Transgenic (mREN-2)27 Rat. Diabetes 51, 3283-3289. 2002.

[147] Wilkinson-Berka JL, Kelly DJ, Koerner SM, Jaworski K, Davis B, Thallas V et al. ALT-946 and Aminoguanidine,Inhibitors of Advanced Glycation, Improve Severe Nephropathy in the Diabetic Transgenic (mREN-2)27 Rat. Diabetes 51[3283], 3289. 2002.

[148] Metz TO, Alderson NL, Thorpe SR, Baynes JW. Pyridoxamine, an Inhibitor of Advanced Glycation and Lipoxidation Reactions: A Novel Therapy for Treatment of Diabetic Complications. Archives of Biochemstry and Biophysics 419 , 41-49. 2003.

[149] Mudge BP, Harris C, Gilmont RR, Adamson BS, Rees RS. Role of Glutathione Redox Dysfunction in Diabetic Wounds. Wound Re.Reg. 10, 52-58. 2002.

[150] Davie SJ, Gould BJ, Yudkin JS. Effect of Vitamin C on Glycoslyation of Proteins. Diabetes 1992; 41:167-173.

[151] Ceriello A et al. Vitamin E Reduction of Protein Glycosylation in Diabetes. New Prospect for Prevention of Diabetic Complications. Diabetes Care 1991; 14(1):68-72.

[152] W Ying. Deleterious Network Hypothesis of Aging. Medical Hypothesis 48, 143-148. 1997.

[153] Mooradian AD, Wong CW. Molecular Biology of Aging Part II: A Synopsis of Current Research. American Geriatric Society 39[7]. 1991.

[154] Schnider SL, Kohn RR. Effects of Age and Diabetes Mellitus on the Solubility and Nonenzymatic Glucosylation of Human Skin Collagen. Journal of Clinical Investigation 1981; 67:1630-1635.

[155] Kohn RR, Schnider SL. Glycosylation of Human Collagen. Diabetes 1982; 32:680.

[156] Schnider SL, Kohn RR. Glucosylation of Human Collagen in Aging and Diabetes Mellitus. Journal of Clinical Investigation 1980; 66:1179-1181.

[157] Vishwanath V, Frank KE, Elmets CA, Monnier VM. Glycation of Skin Collagen in Type I Diabetes Mellitus. Correlation with Long-Term Complications. Diabetes 1986; 35:916-921.

[158] Andreassen TT, Seyer-Hansen, Oxlund H. Biomechanical changes in Connective Tissues Induced By Experimental Diabetes. Acta Endocrinologica 1981; 98:432-436.

[159] Lyons TJ, Bailie KE, Dyer DG, Dunn JA, Baynes JW. Decease in Skin Collagen Glycation with Improved Glycemic Control in Patients with Insulin-Dependent Diabetes Mellitus. J.Clin.Invest. 87[6], 1910-1915. 1991.

[160] Salmela PI, Oikarinen AI, Ukkola O, Karjalainen A, Linnaluoto M, Puukka R et al. Improved Metabolic Control in Patients with Non-Insulin-Dependent Diabetes Mellitus is Associated with a Slower Accumulation of Glycation Products in Collagen. Eur J Clin Invest 25[7], 494-500. 1995.

[161] Thomas D, Delbridge I, Morris D, Howell M J. Cyclohexanone Extraction: An Improvement in the Thiobarbituric Acid Method for the Determination of Nonenzymatic Glycosylation of Hair and Keratin. Scandinavian Journal of Laboratory and Clinical Investigation 1984; 44(5):457-461.

[162] Sueki H, Shigeyuki N, Fujisawa R, Aoki K, Kuroiwa Y. Glycosylated Proteins of Skin, Nails and Hair: Application as an Index for Long-Term Control of Diabetes Mellitus. The Journal of Dermatology 1989; 16:103-110.

[163] Nozaki S, Sueki H, Fujisawa R, Aoki K, Kuroiwa Y. Glycosylated Proteins of Stratum Corneum, Nail and Hair in Diabetes Mellitus:Correlation with Cutaneous Manifestations. The Journal of Dermatology 1988; 15:320-324.

[164] Paisey RB, Clamp JR, Kent MJC, Light ND, Hopton M, Hartog M. Glycosylation of Hair: Possible Measure of Chronic Hyperglycaemia. British Medical Journal 1984; 288:669-671.

[165] Kobayashi K, Igimi H. Glycation Index of Hair for Non-Invasive Estimation of Diabetic Control. Biol Pharm Bull 1996; 19(4):487-490.

[166] Delbridge I, Ellis CS, Robertson K, Lequesne LP. Non-Enzymatic Glycosylation of Keratin from the Stratum Corneum of the Diabetic Foot. British Journal of Dermatology 1985; 112:547-554.

[167] Márová I, Záhejský J, Sehnolová H. Non-Enzymatic Glycation of Epidermal Proteins of the Stratum Corneum in Diabetic Patients. Acta Diabetol 1995; 32:38-43.

[168] Schleicher E, Wieland OH. Specific Quantitation by HPLC of Protein (Lysine) Bound Glucose in Human Serum Albumin and Other Glycosylated Proteins. J Clin Chem Clin Biochem 1981; 19:81-87.

[169] Woodcock - Mitchell J, Eichner R, Nelson WG, Sun TT. Immunolocalisation of Keratin Polypeptides in Human Epidermis using Monoclonal Antibodies. The Journal of Cell Biology 95, 580-587. 1982.

[170] Eichner R, Kahn M. Differential Extraction off Keratin Subunits and Filaments from Normal Human Epidermis. The Journal of Cell Biology 110, 1149-1158. 1990.

[171] Steinert PM. Structure, Function, and Dynamics of Keratin Intermediate Filaments. J.Invest.Dermatol. 100[6], 729-734. 1993.

[172] Yamauchi K, Yamauchi A, Kusunoki T, Kohda A, Konishi Y. Preparation of Stable Aqueous Solution of Keratins and Physiochemical and Biodegradational Properties of Films. Journal of Biomedical Materials Research 31, 439-444. 1996.

[173] Baden HP, Lee LD, Kubilus J. The Fibrous Proteins of Stratum Corneum. J Invest Dermatol 67[5], 573-576. 1976.

[174] Kitahara T, Ogawa H. The Extraction and Characterisation of Human Nail Keratin. J Dermatol Sci 2[6], 402-406. 1991.

[175] Baden HP, Lee LD. Fibrous Protein of Human Epidermis. The Journal of Investigative Dermatology 71[2], 148-151. 1978.

[176] Roberts P, Brunt J. Biosynthesis of Glycosylated Keratin by Human Keratinocytes. Biochimica et Biophysica Acta 1986; 883:413-419.

[177] Fuchs E, Green H. Changes in Keratin Gene Expression during Terminal Differentiation of the Keratinocyte. Cell 19, 1033-1042. 1980.

[178] Eichner R, Bonitz P, Sun TT. Classification of Epidermal Keratins according to their Immunoreactivity, Isoelectric Point, and Mode of Expression. The Journal of Cell Biology 98, 1388-1396. 1984.

[179] Yamauchi M, Woody DT, Mechanic GL. Aging and Cross-Linking of Skin Collagen. Biochemical and Biophysical Research Communications 1988; 152(2):898-903.

[180] Presland RB, Kuechle MK, Lewis SP, Fleckman P, Dale BA. Regulated Expression of Human Filaggrin in Keratinocytes Results in Cytoskeletal Disruption, loss of Cell -Cell Adhession, and Cell Cycle Arrest. Exp.Cell.Biol. 270, 199-213. 2001.

[181] Reddy S, Bichler J, Wells-Knecht KJ, Thorpe SR, Baynes JW. *N*–(Carboxymethyl)lysine Is a Dominant Advanced Glycation End Product (AGE) Antigen in Tissue Proteins. Biochemistry 1995; 34(10872):10878.

[182] Snyder R, Angelici RJ. Stereoselectivity of N - Carboxymethyl - Amino Acid Complexes of Copper (II) toward Optically Active Amino Acids. J.Inorg.Nucl.Chem. 35, 523-535. 1973.

[183] Miyazwa T. Studies of unusual Amino Acids and their Peptides XII. The Chemistry of N-(carboxymethyl)amino Acids I. The Preparation, Properties and Characterization of N-(carboxymethyl)amino Acids and their Esters. Bul.Chem.Soc.Jpn 53, 2555-2565. 1980.

[185] Makita Z, Vlassara H, Cerami A, Bucala R. Immunochemical Detection of Advanced Glycosylated End Products *In Vivo*. The Journal of Biological Chemistry 1992; 267(8):5133-5138.

[186] Resmini P, Pellegrino L, Battelli G. Accurate Quantification of Furosine in Milk and Dairy Products by a direct HPLC Method. Ital J Food Sci 1990; 3:173-183.

[187] Floridi A, Trizza V, Paolotti P, Lucarelli C, Adachi K. Analytical Strategy for the Assessment of the Protein Glycation Status in Uremic Patients by High Performance Liquid Chromatography. Journal of Chromatography A 846, 65-71. 1999.

[188] Knecht KJ, Dunn Ja, McFarland KF, McCance DR, Lyons TJ, Thorpe SR et al. Effect of Diabetes and Aging on Carboxymethyllysine Levels in Human Urine. Diabetes 40, 190-196. 1991.

[189] Monnier VM, Bautista O, Kenny D, Sell DR, Fogarty JF, Dahms W et al. Skin Collagen Glycation, Glycoxidation and Crosslinknig are Lower in Subjects with Long-Term Intensive Versus Conventional Therapy of Type I Diabetes. Diabetes 48, 870-880. 1999.

[190] Wu YC, Monnier VM, Friedlander M. Reliable Determination of Furosine in Human Serum and Dialysate Proteins by High Performance Liquid Chromatography. Journal of Chromatography B: Biomedical Applications 1995; 667:328-332.

[191] Sueki H, Nozaki S, Numazawa S, Aoki K, Kuroiwa Y, Fujisawa R. Effect of Non-Enzymatic Glycosylation and Heating on Browning of Human Stratum Corneum and Nail. Dermatologia 1991; 183(3):197-202.

[192] Monnier VM, Cerami A. Non-Enzymatic Glycosylation and Browning in Diabetes and Aging Studies on Lens Proteins. Diabetes 1982; 31 Suppl. 3:57-63.

[193] Flückiger R, Gallop PM. Measurement of Nonenzymatic Protein Glycosylation. Methods in Enzymology 1984; 106:77-87.

[194] McMillan DE, Brooks SM. Erythrocyte Spectrum Glycosylation. Diabetes 1982; 31 Suppl. 3:64-69.

[195] Cohen MP. Measurement. Diabetes and Protein Glycation. Clinical and Pathophysiological Relevance. JC Press Philadelphia, 1996: 17-41.

[196] Monnier VM, Fogarty JF, Monnier CS, Sell DR. Glycation, Glycoxidation, and other Maillard Reaction Products. In: Byung Pal Yu, editor. Methods in Aging Research. CRC Press LLC, 1999: 657-681.

[197] Odetti PR, Borgogllio A, Rolandi R. Age-Related Increase of Collagen Fluorescence in Human Subcutaneous Tissue. Metabolism 41[6], 655-658. 1992.

[197] Odetti PR, Borgogllio A, Rolandi R. Age-Related Increase of Collagen Fluorescence in Human Subcutaneous Tissue. Metabolism 41[6], 655-658. 1992.

[198] Odetti PR, Borgogllio A, Rolandi R. Age-Related Increase of Collagen Fluorescence in Human Subcutaneous Tissue. Metabolism 41[6], 655-658. 1992.

[199] Nathan DM, Singer DE, Hurxthal K, Goodson JD. The Clinical Information Value of the Glycosylated Hemoglobin Assay. N Engl J Med 310[6], 341-346. 1984.

[200] Jones EW, Peacock I, McLain S, Fletcher E, Edwards R, Finch RG et al. A Clinico-Pathological Study of Diabetic Foot Ulcers. Diabetic Medicine 1987; 4:475-479.

[201] Holmquist WR, Schroeder WA. A new N-Terminal Blocking Group Involving a Schiff Base in Haemoglobin A_{1c}. Biochemistry 5[8], 2489-2503. 1966.

[202] Monnier VM, Fogarty JF, Monnier CS, Sell DR. Glycation, Glycoxidation, and Other Maillard Reaction Products. In: Byung Pal Yu, editor. Methods in Aging Research. CRC Press, 1999: 657-681.

[203] Glomb MA, Monnier VM. Mechanism of Protein Modification by Glyoxal and Glycoaldehyde, Reactive Intermediates of the Maillard Reaction. The Journal of Biological Chemistry 1995; 270(17 Issue of April):10017-10026.

[204] Nishino T, Horii Y, Shiki H, Yamamoto H, Makita Z, Bucala R et al. Immunohistochemical Detection of Advanced Glycosylation End Products within the Vascular Lesions and Glomeruli in Diabetic Neuropathy. Human Pathology 1995; 26(3):308-313.

[205] Littlefield JW. The Selection of Hybrid Mouse Fibroblasts. Cold Spring Harb Symp Quant Biol. 29, 161-166. 1964.

[206] Ikeda K, Higashi T, Sano H, Jinnouchi Y, Yoshida M, Araki T et al. N^{ε}-(Carboxymethyl)lysine Protein Adduct is a Major Immunological Epitope in Proteins Modified with Advanced Glycation End Products of the Maillard Reaction. Biochemistry 35, 8075-8083. 1996.

[207] Weiss MF, Erhard P, Kader-Attia FA, Wu YC, DeOreo PB, Araki A et al. Mechanisms for the Formation of Glycoxidation Products in End-Stage Renal Disease. Kidney International 57, 2571-2585. 2000.

[208] Schleicher E, Wagner E, Nerlich AG. Increased Accumulation of the Glycoxidation Product N(Epsilon)-(Carboxymethyl)lysine in Human Tissues in Diabetes and Aging. J.Clin.Invest. 99, 457-468. 1997.

[209] Taneda S, Monnier VM. ELISA of Pentosidine, an Advanced Glycation End Product, in Biological Specimens. Endocrinology and Metabolism 40[9], 1766-1773. 1994.

[210] Horiuchi S, Araki N, Morino Y. Immunochemical Approach to Characterize Advanced Glycation End Products of the Maillard Reaction. The Journal of Biological Chemistry 266[12], 7329-7332. 1991.

[211] Weiss MC, Green H. Human-Mouse Hybrid Cell Lines Containing Partial Complements of Human Chromosomes and Functioning Human Genes. Proc.Natl.Acad.Sci. 58, 1104-1111. 1967.

[212] Ephrussi B, Weiss MF. Hybrid Somatic Cells. Sci Am. 220[4], 26-35. 1969.

[213] Nakamura Y, Horii Y, Nishino T, Shiki H, Sakaguchi Y, Kagoshima T et al. Immunohistochemical Localization of Advanced Glycosylated Endproducts in Coronary Atheroma and Cardiac Tissue in Diabetes Mellitus. American Journal of Pathology 1993; 143(6):1649-1656.

[214] Farboud B, Aotaki-Keen A, Miyata T, Hjelmeland LM, Handa JT. Development of a Polyclonal Antibody with Broad Epitope Specificity for Advanced Glycation Endproducts and Localisation of these Epitopes in Bruch's membrane of the Aging Eye. Molecular Vision 5[11], 14-7-1999.

[215] Takeda A, Yasuda T, Miyata T, Mizuno K, Li M, Yoneyama S et al. Immunohistochemical Study of Advanced Glycation End Products in Aging and Alzheimer's Disease Brain. Neuroscience Letters 221, 17-20. 1996.

[216] Farboud B, Aotaki-Keen A, Miyata T, Hjelmeland LM, Handa JT. Development of a Polyclonal Antibody with Broad Epitope Specificity for Advanced Glycation Endproducts and Localisation of these Epitopes in Bruch's membrane of the Aging Eye. Molecular Vision 5[11],14-7-1999.

[217] Khatyr F, Imberdis C, Vescovo P, Varchon D, Lagarde J. Model of Viscoelastic Behaviuor of Skin *in vivo* and Study of Anisotropy. Skin Research and Technology 10, 96-103. 2004.

[218] Reihsner R, Melling M, Pfeiler W, Menzel E. Alterations of Biomechanical and Two-Dimnsional BiomechanicalProperties of Human Skin in Diabetes Mellitus as Compared to Effects of *In Vitro* Non-Enzymatic Glycation. Clinical Biomechanics 15, 379-386. 2000.

[219] Larrabee WF. A Finite Element Model of skin Deformation. I. Biomechanics of Skin and Soft Tissue: A Review. Laryngoscope 1986; 96:399-405.

[220] Serup J, Keiding J, Fullerton A, Ginadecka M, Ginadecka R. Ultrasound Examination of the Skin. In: Serup J, Jemec GBE, editors. Handbook of Non-Invasive Methods and the Skin. CRC Press Inc., 1995: 239-256.

[222] Nikkels-Tassoudji N, Henry F, Letawe C, Piérard-Franchimont C, Lefèbvre P, Piérard GE. Mechanical Properties of Diabetic Waxy Skin. Dermatology 1996; 192:19-22.

[223] Jemec GBE, Selvaag E, Agren M, Wulf HC. Measurement of the Mechanical Properties of Skin with Ballistometer and Suction Cup. Skin Research and Technology 7, 122-126. 2001.

[224] Gefen A, Megido-Ravid M, Azariah M, Itzchack Y, Arcan M. Integration of Plantar Soft Tissue Stiffness Measurements in Routine MRI of the Diabetic Foot. Clinical Biomechanics 16[921], 925. 2001.

[225] Irie T, Oka H, Yamamoto T. Measurement of Hardness of Human Skin with Impact Force. Med and Biol Eng and Comput 1994; 32:231-233.

[226] Takema Y, Yorimoto Y, Kawai M, Imokawa G. Age-Related Changes in the Elastic Properties and Thickness of Human Facial Skin. British Journal of Dermatology 1994; 131:641-648.

[227] Ishikawa T, Ishikawa O, Miyachi Y. Measurement of Skin Elastic Properties with a New Suction Device (I): Relationship to Age Sex and Degree of Obesity in Normal Individuals. The Journal of Dermatology 1995; 22(713):717.

[228] Ishikawa T, Tamura T. Measurement of Skin Elastic Properties with a New Suction Device (II): Systemic Sclerosis. The Journal of Dermatology 1996; 23(165):168.

[229] Diridollou S, Berson M, Vabre V, Black D, Karlsson B, Auriol F et al. An *in vivo* Method for Measuring the Mechanical Properties of the Skin using Ultrasound. Ultrasound in Med Biol 1998; 24(2):215-224.

[230] Thacker JG, Lachitta FA, Allaire PE. *In vivo* Exstensometer for Measurement of the Biomechanical Properties of Human Skin. Rev Sci Instrum 1977; 48(2):181-185.

[231] Ballou SP, Mackiewicz A, Lysikiewicz A, Neuman MR. Direct Quantitation of Skin Elasticity in Systemic Sclerosis. The Journal of Rheumatology 1990; 17(6):790-794.

[232] Agache P, Monneur C, Leveque JL, De Rigal J. Mechanical Properties and Young's Modulus of Human Skin in vivo. Arch Dermatol Res 1980; 269:221-232.

[233] Leveque JL, De Rigal J, Agache P, Monneur C. Influence of Ageing on the in Vivo Extensibility of Human Skin at a Low Stress. Arch Dermatol Res 1980; 269:127-135.

[234] Piaggesi A, Romanelli M, Schipani E, Campi F, Magliaro A, Baccetti F et al. Hardness of Plantar Skin in Diabetic Neuropathis Feet. Journal of Diabetes and its Complications 13, 129-134. 1999.

[235] Cua A B, Wilhelm K P, Maibach H I. Elastic Properties of Human Skin: Relation to Age, Sex and Anatomical Region. Arch Dermatol Res 1990; 282:283-288.

[236] Fong SSL, Hung LK, Cheng JCY. The Cutometer and Ultrasonography in the Assessment of Postburn Hypertrophic Scar - A Preliminary Study. Burns 23[1], S12-S18. 1997.

[237] Tsukahara K, Takema Y, Moriwaki S, Fujimura T, Imokawav G. Dermal Fluid Translocation is an Important Determinant of the Diurnal Variation in Human Skin Thickness. British Journal of Dermatology 145, 590-595. 2001.

[238] Balbir-Gurman A, Denton CP, Nichols B, Knight CJ, Nahir AM, Martin G et al. Non-Invasive Measurement of Biomechanical Skin Properties in Systemic Sclerosis. Ann.Rheum.Dis. 61, 237-241. 2002.

[239] Vexler A, Polyansky I, Gorodetsky R. Evaluation of Skin Viscoelasticity and Anisotrophy by Measurement of Speed of Shear Wave Propagation with Viscoelasticity Skin Analyser. J Invest.Dermatol. 113, 732-739. 1999.

[240] Rodnan GP, Lipinski E, Luksick J. Skin Thickness and Collagen Content in Progressive Systemic Sclerosis and Localized Scleroderma. Arthritis and Rheumatism 1979; 22(2):130-140.

[241] Overgaard Olsen L, Takiwaki H, Serup J. High-Frequency Ultrasound Characterization of Normal Skin. Skin Thickness and Echographic Density of 22 Anatomical Sites. Skin Research and Technology 1995; 1:74-80.

[242] Gniadecka M, Serup J, Sondergaard J. Age-Related Diurnal Changes of Dermal Oedema: Evaluation by High-Frequency Ultrasound. British Journal of Dermatology 131[6], 849-855. 1994.

[243] Diridollou S, Traon AP, Maillet A, Bellossi F, Black D, Patat F et al. Characterisation of Gravity-Induced Facial Skin Oodema using Biophysical Measurement Techniques. Skin Research and Technology 6, 118-127. 2000.

[244] Harland CC, Bamber JC, Gusterson BA, Mortimer PS. High Frequancy, High Resolution B - Scan Ultrasound in the Assessment of Skin Tumours. British Journal of Dermatology 128[5], 525-532. 1993.

[245] Rippon MG, Springett K, Walmsley R, Patrick K, Millson S. Ultrasound Assessment of Skin and Wound Tissue: Comparison with Histology. Skin Research and Technology 1998; 4:147-154.

[246] Fornage B, McGavran MH, Duvic M, Waldron CA. Imaging the Skin with 20MHz US. Radiology 189, 69-76. 1993.

[247] Karim A, Young SR, Lynch JA, Dyson M. A Novel Method of Assessing Skin Ultrasound Scans. Wounds 1994; 6(1):9-15.

[248] Rippon MG, Springett K, Walmsley R. Ultrasound Evaluation of Acute Experimental and Chronic Clinical Wounds. Skin Research and Technology 5, 228-236. 1999.

[249] Vaillant L, Machet L, Callens A, Pourcelot L, Lorette G. Ultrasound Imaging of Psoriatic Skin: Non-Invasive Technique to Evaluate Treatment of Psoriasis. International Journal of Dermatology 33[11], 786-790. 1994.

[250] Seidenari S, Pagnoni A, Di Nardo A, Gianetti A. Echographic Evaluation with: Image Analysis of Normal Skin: Variations According to Age and Sex. Skin Pharmacology 1994; 7:201-209.

[251] Thoolen M. The Effect of Pressure on the Skin of the Sole of the Foot: A High Frequancy Ultrasound Study. Journal . 1999.

[252] World Health Organisation. Definition, Diagnosis and Classification of Diabetes Mellitus and its Complications. 1-27. 1999.

[253] Veves A. Diagnosis of Diabetic Neuropathy. In: Veves A, editor. Contemporary Endocrinology: Clinical Management of Diabetic Neuropathy. Totowa NJ: Human Press Inc., 1998: 61-75.

[254] Vowden KR, Goulding V, Vowden P. Hand-Held Doppler Assessment for Peripheral Arterial Disease. Journal of Wound Care 1996; 5(3):125-128.

[255] Cutajar CL, Marston A, Newcombe JF. Value of Cuff Occlusion Pressures in Assessment of Peripheral Vascular Disease. British Medical Journal 1972; 2:392-395.

[256] Humeny A, Kislinger T, Becker C, Pischetsreider M. Qualitative Determination of Specific Protein Glycation Products by Matrix-Assisted Laser Desorption/ Ionization Mass Spectrometry Peptide Mapping. J.Agric.Food Chem. 50, 2153-2160. 2002.

[257] Brownlee M. Biochemistry and Molecular Cell Biology of Diabetic Complications. Nature 414, 813-820. 13-12-2001.

[258] Candi E, Tarcsa E, Digiovanna JJ, Compton JG, Elias PM, Marekov LN et al. A Highly Concerved Lysine Residue on the Head Domain of Type II Keratins is Essential for the Attachment of Keratin Intermediate Filaments to the Cornified Cell Envelope through Isopeptide Crosslinking by Transglutamases. Proc.Natl.Acad.Sci.USA 95, 2067-2072. 1998.

[259] Arnemann J, Sullivan KH, Magee AI, King IA, Buxton RS. Stratification Related Expression of Isoforms of Desmosomal Cadherins in Human Epidermis. Journal of Cell Science 104, 741-750. 1993.

[260] McGrath JA. Keratinocyte Adhesion and the Missing Link: From Dowling-Meara to Hays-Wells. Clinical and Experimental Dermatology 26, 296-304. 2001.

[261] Alt A, Ohba M, Li L, Gartsbein M, Belanger A, Denning MF et al. Protein Kinase Cδ-Mediated Phosphorylation of α6β4 is Associated with Reduced Integrin Localisation to Hemodesmosomes. Cancer Research 61, 4591-4598. 1-6-2001.

[262] Kaur P, Li A. Adhesive Properties of Human Epidermal Cells: An Analysis of Keratinocyte Stem Cell, Transit Amplifying Cells, and Postmitotic Differentiating Cells. J.Invest.Dermatol. 114, 413-420. 1999.

[263] Levy L, Broad S, Diekmann D, Evans RD, Watt FM. β1 Integrins Regulate Keratinocyte Adhesion and Differentiation by Distinct Mechanisms. Molecular Biology of the Cell 11, 453-466. 2000.

[264] Steinert PM, Marekov LN. The Proteins Elafin, Filaggrin, Keratin Intermediate Filaments, Loricrin and Small Proline Rich Proteins 1 and 2 are Isodipeptide Cross-Linked Components of the Human Epidermal Cornified Cell Envelope. The Journal of Biological Chemistry 230[30], 17702-17711. 28-7-1995.

[265] Hohl D. Cornified Cell Envelope. Dermatologia 180[4], 201-211. 1990.

[266] Halprin KM. Epidermal " Turnover Time" - A Re-Examination. British Journal of Dermatology 86, 14-19. 1972.

[267] Paladini RD, Takahashi K, Bravo NS, Coulombe PA. Onset of Re-Epithelialisation after Skin Injury Correlates with a Reorganisation of Keratin Filaments in Wound Edge Keratinocytes Defining a Potential Role for Keratin 16. The Journal of Cell Biology 132[3], 381-397. 1996.

[268] Brownlee M. Biochemistry and Molecular Cell Biology of Diabetic Complications. Nature 414, 813-820. 13-12-2001.

[269] Brownlee M. Biochemistry and Molecular Cell Biology of Diabetic Complications. Nature 414, 813-820. 13-12-2001.

[270] Brownlee M. Biochemistry and Molecular Cell Biology of Diabetic Complications. Nature 414, 813-820. 13-12-2001.

[271] Jokura Y, Ishikawa K, Tokuda H, Imokawa G. Molecular Analysis of Elastic Properties of the Stratum Corneum by Solid - State ^{13}C - Nuclear Magnetic Resonance Spectroscopy. J Invest Dermatol 104[5], 806-812. 1995.

[272] Feughelman M, Lyman D, Menefee E, Willis B. The Orientation of the α - Helices in α - keratin fibres. International Jounal of Biological Macromolecules 33, 149-152. 2003.

[273] Blank IH. Factors which Influence the Water Content of the Stratum Corneum. J.Invest.Dermatol. 18[6], 433-440. 1952.

[274] Brownlee M, Vlassara H, Cerami A. Non-Enzymatic Glycosylation and the Pathogenesis of Diabetic Complications. Annals of Internal Medicine 101, 527-537. 1984.

[275] Monnier VM, Kohn RR, Cerami A. Accelerated Age-related Browning of Human Collagen in Diabetes Mellitus. Proc.Natl.Acad.Sci.USA 81, 583-587. 1984.

[276] Goldschmidt H, Kligman AM. Exfoliative Cytology of Human Horny Layer. Methods of Cell Removal and Microscopic Tachniques. Arch.Dermatol. 96, 572-576. 1967.

[277] Ctercteko GC, Dhanendran M, Hutton WC, Le Quesne LP. Vertical Forces acting on the Feet of Diabetic Patients with Neuropathic Ulceration. Br.J.Surg. 68[9], 608-614. 1981.

[278] Cavanagh PR, Sims DS, Sanders LJ. Body mass is a poor predictor of peak plantar pressure in diabetic men. Diabetes Care 14[8], 750-755. 1991.

[279] Delbridge I, Perry P, Marr S, Arnold N, Yue DK, Turtle JR et al. Limited Joint Mobility in the Diabetic Foot: Relationship to Neuropathic Ulceration. Diabetic Medicine 5[4], 333-337. 1982.

APPENDICES

Appendix I The Lowry Protein Assay Procedure

Reagents

Reagent A

D_c Protein Assay (Bio-Rad Laboratories). Content: 2% Na_2CO_3 in 0.1N NaOH, 2% NaK Tartrate, 1% $CuSO_4 \cdot 5H_2O$.

Reagent B

D_c Protein Assay/2N Folin reagent (Bio-Rad Laboratories).

Protein Standard

Prepared from bovine serum albumin (BSA)

Instruments

Spectrophotometer which transmits light at 630nm.

Materials

Pipettes, universal plastic vials, Immulon 4 assay wells (Dynex Ltd)

Calibration

BSA protein standards of concentrations 1, 0.75, 0.5, 0.25, 0.1 and 0.00 mg/ml

Method

Each standard (5 μl) was placed in wells in duplicate. Aliquots (5 μl) of each sample were placed in adjacent wells. Reagent A (25 μl) was placed in each of the wells and the mixtures allowed to incubate at room temperature on a shaker for 15 min. Reagent B (200 μl) was added to each well and allowed to incubate for a further 15mins at room temperature on a shaker. The absorbance readings were taken at 630nm.

Appendix II One-Dimensional SDS-PAGE Protocol

Reagents and stock solutions

Acrylamide stock (50% w/v)

Acrylamide (Sigma Chem), 23.38 g and bis-Acrylamide (Sigma Chem), 0.63 g was made up 50 ml in d.H_2O and stored away from light at +4°C.

1M Tris, pH 8.8

Tris (Sigma Chem), 12.1 g was added to 80 ml d.H_2O. The pH adjusted to 8.8 and then made up to 100 ml.

10% Sodium Dodecyl Sulfate (SDS)

SDS (Sigma Chem), 2 g was added to 20 ml d.H_2O.

1% SDS

1 ml of 10% SDS was added to 9 ml d.H_2O.

15% Ammonium Persulphate (APS)

Ammonium persulphate (BioRad), 0.6 g was added to 4 ml d.H_2O. This solution was made up fresh each day before use.

1M Tris pH 6.8

Tris (Sigma Chem), 12.1 g added to 80 ml d.H_2O The pH was adjusted to 6.8 and the solution is then made up to 100 ml .

0.5% Bromophenol Blue

Bromophenol Blue (Sigma Chem), 0.05 g was added to 10 ml d.H_2O.

Gel Assembley

12.5% SDS Acrylamide Separating Gel (makes 2 0ml)

Acrylamide stock	5 ml
1M Tris pH 8.8	7.5 ml
d.H_2O	6.85 ml
10% SDS	0.2 ml
15% APS	0.45 ml

Immediately before pouring the gel, 20 µl TEMED was added.

5% SDS Acrylamide Stacking Gel (makes 5 ml)

Acrylamide stock	0.5 ml
1M Tris pH 6.8	0.62 ml
d.H_2O	3.57 ml
10% SDS	0.05 ml
15% APS	0.25 ml

Immediately before pouring the gel, 10 µl TEMED was added.

The separating gel was poured into the casting apparatus to approximately 1 cm below the bottom of the comb using a syringe and left to set for 30 min, with an overlay of 1% SDS. When set, the SDS was carefully poured off and the comb placed in the apparatus. The stacking gel was poured on top of the separating gel, using a syringe and left to set for approximately 10mins. Once set, the comb was carefully removed and the gel was placed in the electrophoresis tank.

Sample Preparation

Sample Buffer (makes 8 ml)

d.H_2O	4.2 ml
1M Tris, pH 6.8	1.0 ml
Glycerol	0.8 ml
10% SDS	1.6 ml
0.5% Bromophenol Blue	0.4 ml

1 ml of this sample buffer was placed in an Eppendorf vial and 25 μl of β-mercaptoethanol was added immediately prior to addition to the sample under investigation.

5 x Running Buffer

Tris Base (15 g), glycine (72 g) and SDS (5 g) was made up to 1 litre in $d.H_2O$.

For one run, 60 ml of the stock solution was diluted in 240 ml $d.H_2O$; the upper buffer chamber was filled with approximately 115 ml (half way between the long and short plates) and the power tank chamber with approximately 185 ml (enough to cover the anode wire).

Electrophoresis

The samples are loaded onto the gel and run at a constant 100 mV for 60 – 90 mins.

Molecular Weight Markers (Sigma Chem)

Protein	**Molecular Weight (Da)**
Myosin	200,000
β-galactosidase	116,250
Posphorylase	97,400
Serum Albumin	66,200
Oval Albumin	45,000
Carbonic Anhydrase	31,000
Trypsin Inhibitor	21,500
Lysozyme	144,00
Aprotinin	6500

Staining (Coomassie Blue R-250 Staining Solution)

Methanol (Sigma Chem), 400 ml

Glacial Acetic Acid (BDH), 100 ml

d.H_2O, 500 ml

Coomassie Blue (Sigma Chem), 1 g

The gel was carefully placed into the destaining box and enough stain was poured in to cover the gel. This was left on the shaker for 1 to 2 hours.

Destaining (Coomassie Blue Destaining Solution)

Methanol, 400 ml

Glacial Acetic Acid, 100 ml

d.H_2O, 500 ml

The gel was carefully removed from the staining solution and placed in the destain box. Just enough destaining solution was added to cover the gel and this was left on the shaker for 1 hour. The destain was then replaced with fresh solution and left on the shaker over night.

Gel Imaging

An image of the gel was taken using a white light transilluminater and saved using Grabbit - IT© Annotating Grabber (32bit) 2.59 (Ultraviolet Products Limited). The gels were analysed using Gene Tools© Version 2 (Syngene. A division of Synoptics Ltd).

Appendix III Western Blot Analysis Protocol

Reagents and stock solutions

Nitrocellulose membrane

Immun - Blot™ PVDF, membrane for protein blotting 0.2 μm (Bio – Rad, Cat 162 – 0177)

Transfer buffer (x 10)

Tris (hydroxymethyl) aminomethane (Sigma Chem), 15.15 g, glycine (Sigma Chem), 67.3 g and SDS (Sigma, Chem), 5 g were made up in 500 ml d.H_2O (may require warming to aid dissolution). Methanol (BDH), 125 ml was added.

Wash buffer (x 10)

Sodium chloride (8 g), potassium chloride (0.2 g), di-sodium hydrogen orthophosphate (1.15 g) and potassium dihydrogen orthophosphate (0.2 g) were dissolved in 1 litre of d.H_2O and 50 μl of Tween 20 was added.

Blocking buffer

Tris (2.4 g) and bovine serum albumin (9 g) were dissolved in 300 ml d.H_2O (pH should be 7.4)

Primary antibody solution

Anti-keratin antibody (40 μl) was added to the blocking buffer (20 ml).

Secondary antibody

Anti-mouse/ anti-guinea pig IgG HRPO antibody (10 μl) was added to the blocking buffer (20 ml)

Substrate solution a

4-chloro-1-napthol (Sigma Chem), 60mg was added to 20 ml methanol in the dark.

Substrate solution b

Tris (Sigma Chem), 1.21 g and sodium chloride (Sigma, Chem), 14.63 g was dissolved in 400 ml d.H_2O. The pH was adjusted to 7.6 and then the solution was made up to 500 ml.

Working substrate solution

Hydrogen peroxide (60 µl, 30%) was added to 100 ml of substrate b. All of this solution was then added to the substrate and then used immediately.

Protocol

Both the electrodes were soaked in water for 5 min to prevent trapping any air bubbles under the filter paper. The anode was placed in the gel tank and plugged in. Filter paper (9 sheets) were soaked in the transfer buffer and placed on the anode plate. The sheets were placed on the anode one by one and the air bubbles were smoothed out after each sheet was applied. A piece of dialysis membrane was soaked in water for 5 min, then in transfer buffer for 15 min and placed over the filter paper. The nitrocellulose membrane was soaked in methanol for 5 min followed by transfer buffer for 15 min and placed on top of the dialysis membrane. A small piece from the corner of the membrane was cut away in order to orientate the blot. The gel was soaked in water and then in the transfer buffer and then placed on top of the nitrocellulose membrane. Finally, 9 more sheets of filter paper were soaked in transfer buffer and placed over the gel. All air bubbles were gently smoothed away. The cathode plate was placed on top of the assembly and plugged in. The lid was placed on top of the tank and the system set at 80 V and 350 mA for approximately 2 hours. After this time the gel was checked to see whether full transfer of the proteins had occurred. The nitrocellulose membrane was carefully removed from the apparatus and placed in a polyethene bag containing blocking buffer (50 ml). This was incubated at room temperature for 2 hours on a shaker.[∞] The membrane was then placed in a polyethene bag containing wash buffer (50 ml) and incubated at

[∞] The gel was stained and destained according to the protocol described in Appendix I To confirm that complete protein transfer onto the membrane had occurred

room temperature for 20 min on a shaker. The blot was then incubated, on a shaker overnight, in the primary antibody solution (20 ml). The blot was the washed in blocking buffer (50 ml, x 2) and then in wash buffer (50 ml). After this procedure the blot was incubated in the secondary antibody solution for 2 hours at room temperature on the shaker. The blot was finally washed 3 times in was buffer for 15mins each time and then placed in the working substrate solution and gently incubated until grey/black bands were visible. The resulting blot was photographed using the equipment described in Appendix II.

Appendix IV Immunoblots of Keratin Extracts from 14 Callus Specimens using Extraction Method 3 (Chapter 2)

Figure IV.i: Immunoblot using AE1 monoclonal antibody. The 50kDa band is present on the blot but too feint to be visible on this scan.

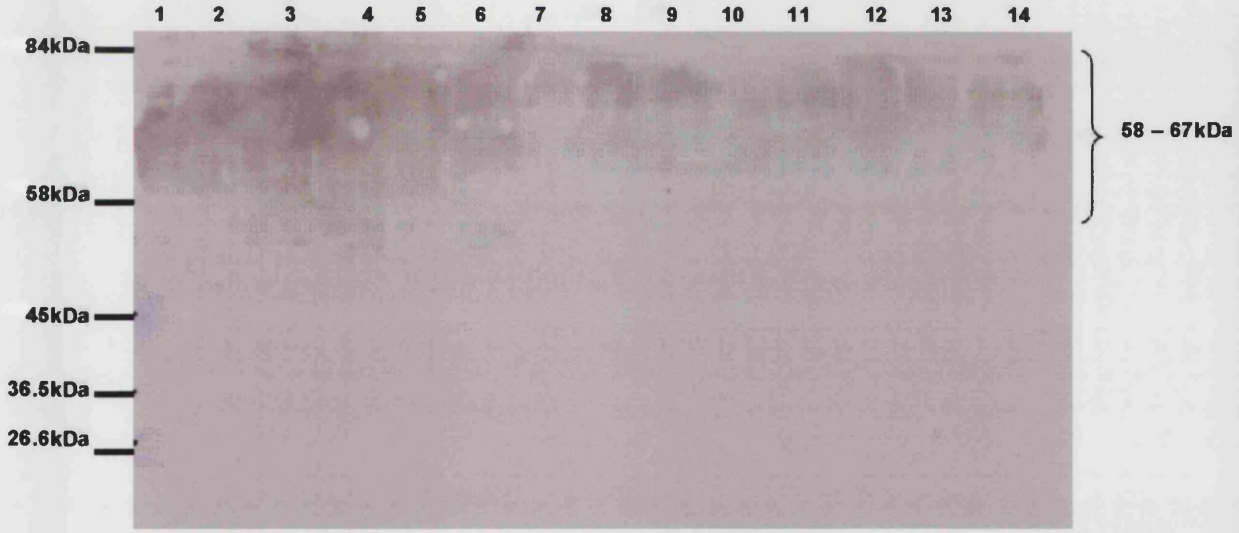

Figure IV.ii: Immunoblot using AE3 monoclonal antibody.

Samples 1–7: Keratin extracts taken from non–diabetic plantar callus samples.

Samples 8–14: Keratin extracts taken from diabetic plantar callus samples

Appendix V Derivatisation Procedure for GC/ MS Analysis of CML

Reagents

Methanolic acid (0.5 M), dichloromethane, TFAA, methanol

Method

The sample (2.5 mg) was placed in a glass vial and methanolic acid (0.5 ml, 0.5 M) was added and heated for 1h at 80°C. The acid was removed by rotary evaporation and dichloromethane (0.5 ml) was added and mixed. Trifluoracetic anhydride (1 ml) was added to the solution and mixed and the reaction mixture was allowed to stand at room temperature for 1h. All solvent was removed under rotary evaporation, until the sample was dry and the vial was sealed and stored at 0°C, ready for GC/MS analysis (see Appendix VI for the GC/MS conditions).

Appendix VI GC/MS Analysis Equipment and Conditions

GC/MS System

Hewlett Packard 5890 Series II Gas Chromatography
HP 5972 Series Mass Selective Detector
HP 7673 Controller

Temperature Program

Initial temperature	50°C for 20 min	
Level 1	Rate	15°C/min
		Final Temperature 130°C
		Time 2 min
Level 2	Rate	2°C/min
		Final Temperature 230°C
		Time 5 min
Level 3	Rate	0°C/min

Total run time = 64.3 min

Appendix VII NMR and GC/MS Spectra from Chapter 3

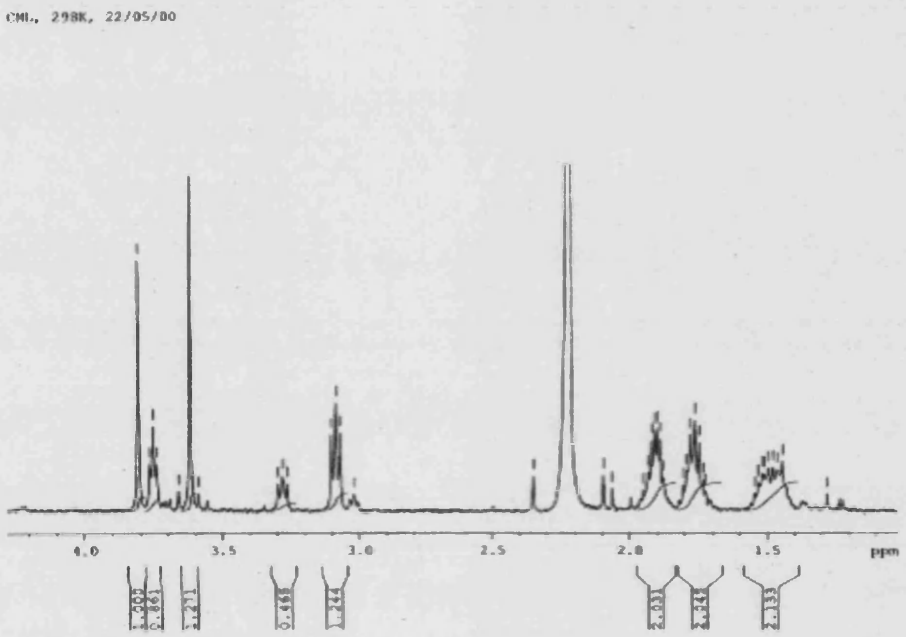

Figure VII.i: NMR spectrum of CML synthesised according to method 1. The spectrum is a mixture of lysine, CML and CML salts.

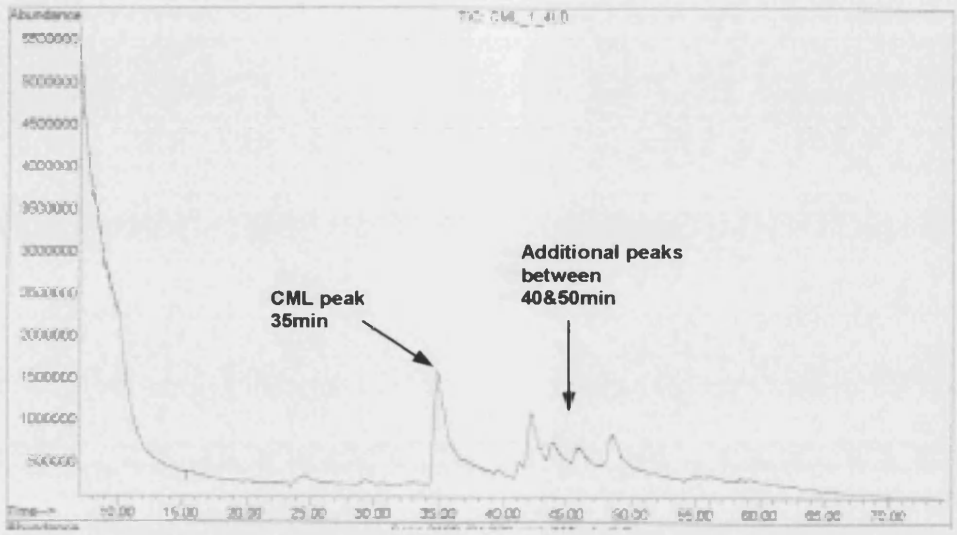

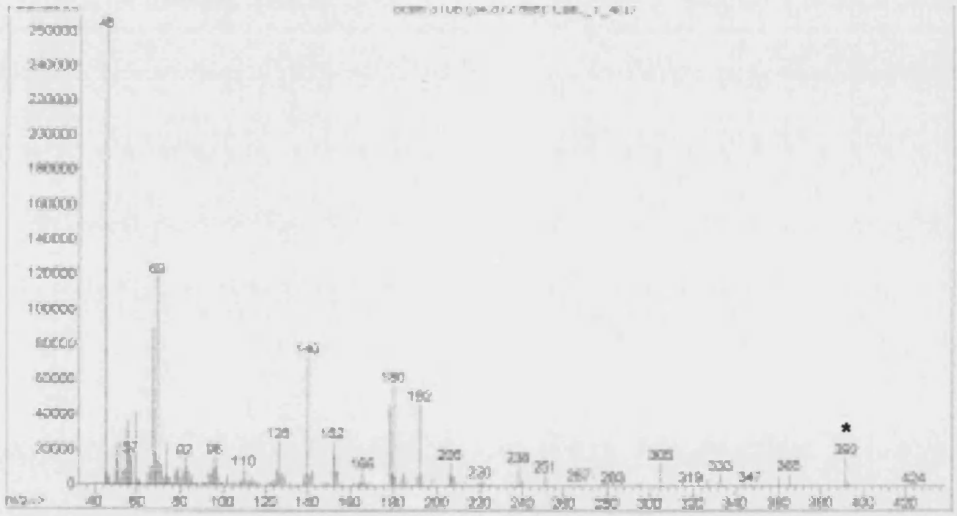

Figure VII.ii: Mass spectrum confirming the presence of CML synthesised according to method 1, with additional impurities.

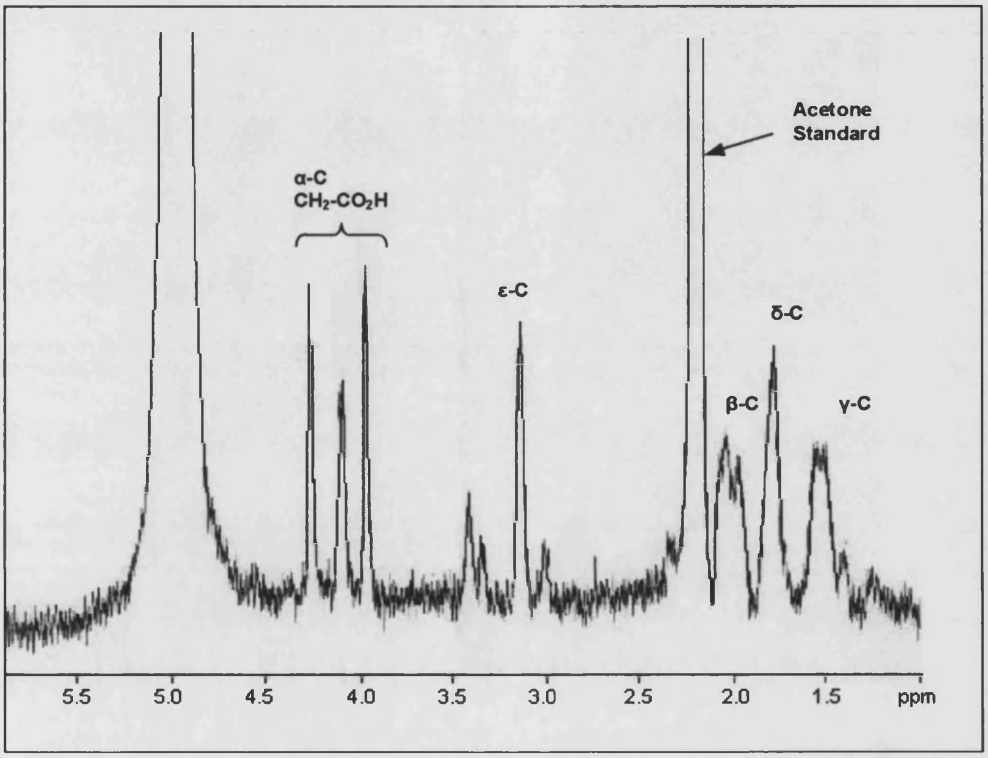

Figure VII.iii: NMR spectrum of the compound formed by method 2. Spectrum indicates the presence of acetyllysine and CML

a

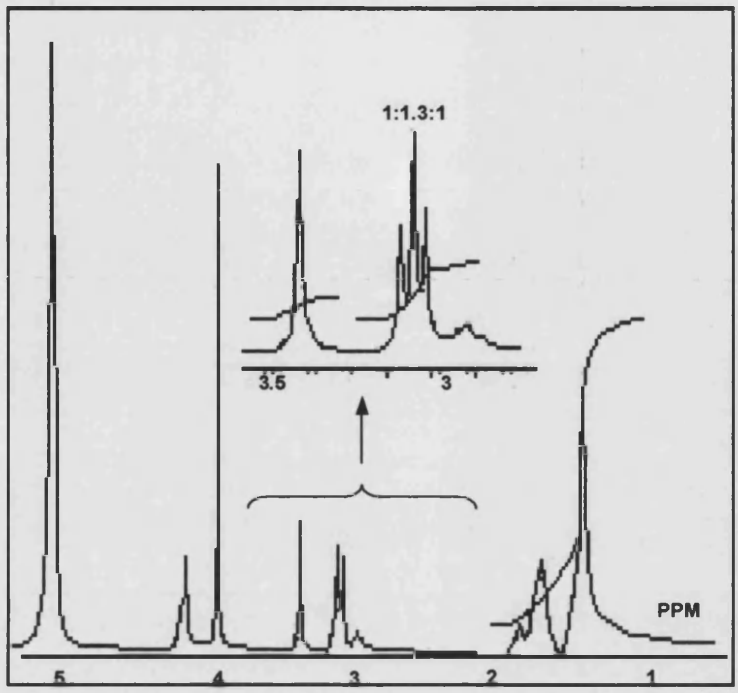

b

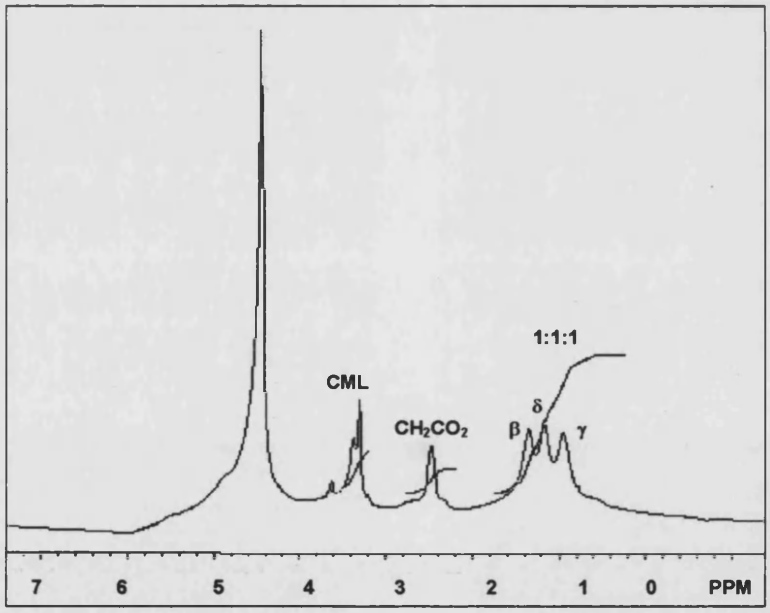

Figure VII.iv: NMR spectra of CML synthesised by method three **a.** protected CML. The product was characterised by ^{1}H NMR (270MHz, CD_3OD) where chemical shift δ_H (ppm) and coupling constant J (Hz) values were: 1.5ppm large singlet 21.650int tBOC, 1.8-1.6ppm multiplet 4 x CH_2, 2.9-3.1ppm triplet 2 int CH_2, 3.3ppm multiplet **b.** deprotected CML

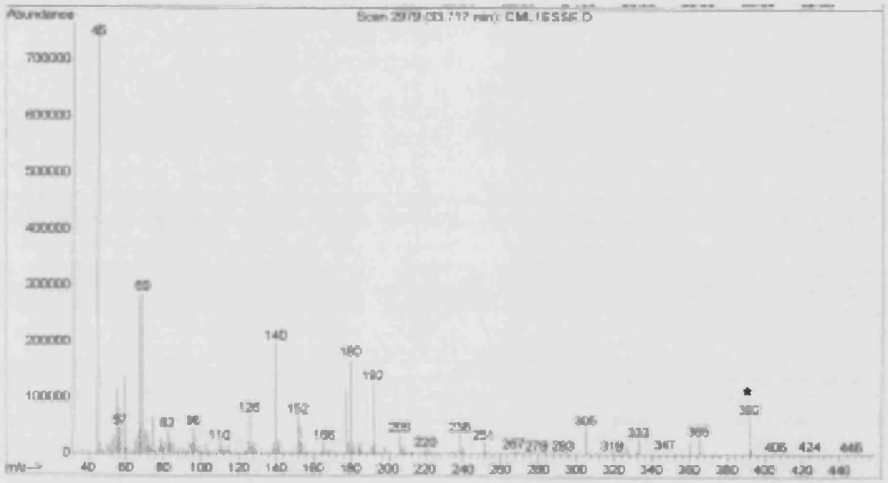

Figure VII.v: Mass spectrum of pure CML synthesised from method 3. CML m/e=392

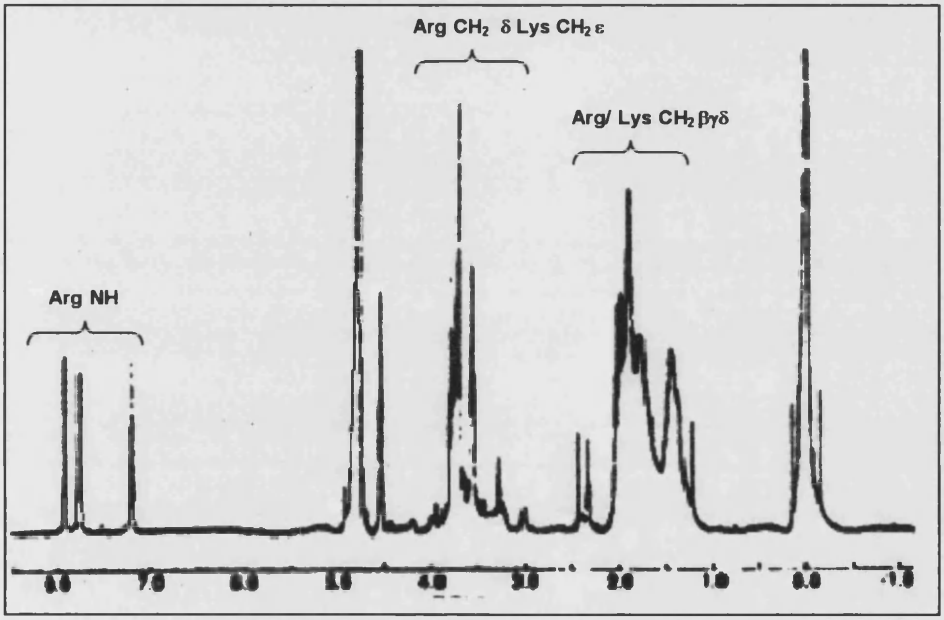

Figure VII.vi: NMR spectrum of pentosidine

Appendix VIII HPLC Data from Chapter 4

Table VIII.i. Furosine standard data from day one and two

0.0156 mg/ml furosine	**RT [min] Day One**	**RT [min] Day Two**	**Area [counts x 10^3] Day one**	**Area [counts X 10^3] Day Two**
1	8.29	8.04	195.43	192.38
2	8.37	8.15	195.27	197.22
3	8.44	8.18	200.85	195.45
Mean	8.37	8.13	197.17	195.02
Standard Deviation	7.41×10^{-2}	7.22×10^{-3}	3.19	2.45
Standard Error	2.27×10^{-2}	4.17×10^{-2}	1.94	1.41
0.0078 mg/ml furosine				
1	8.47	8.23	91.06	87.69
2	8.43	8.23	88.90	87.86
3	8.37	8.21	89.02	87.53
Mean	8.42	8.23	89.66	87.70
Standard Deviation	5.04×10^{-2}	9.81×10^{-2}	2.75	0.17
Standard Error	1.98×10^{-2}	5.67×10^{-3}	1.59	9.68×10^{-2}
0.00390 mg/ml furosine				
1	8.35	8.20	41.25	43.57
2	8.30	8.19	43.30	43.97
3	8.28	8.19	46.69	43.64
Mean	8.31	8.20	43.75	43.73
Standard Deviation	3.43×10^{-2}	6.51×10^{-2}	2.75	0.21
Standard Error	2.91×10^{-2}	2.76×10^{-3}	1.59	0.12
0.00195 mg/ml furosine				
1	8.28	8.20	22.01	22.11
2	8.25	8.19	22.14	22.91
3	8.17	8.20	22.62	24.43
Mean	8.23	8.20	22.26	23.15
Standard Deviation	5.66×10^{-2}	3.06×10^{-2}	0.322	1.18
Standard Error	4.28×10^{-2}	1.76×10^{-3}	0.19	0.68

Table VIII.ii. Data for day-to-day repeatability of furosine standard peaks

0.0156 mg/ml furosine	**RT [min]**	**Peak Area [counts x 10^3]**
Mean Day One	8.37	178.36
Mean Day Two	8.13	197.17
Mean	8.25	187.77
SD	0.17	13.31
CV%	2.07	7.09
0.078 mg/ml furosine	**RT [min]**	**Peak Area [counts x 10^3]**
Mean Day One	8.42	87.69
Mean Day Two	8.23	49.66
Mean	8.33	68.68
SD	0.14	26.90
CV%	1.67	39.16
0.0039 mg/ml furosine	**RT [min]**	**Peak Area [counts x 10^3]**
Mean Day One	8.31	43.73
Mean Day Two	8.20	43.75
Mean	8.26	43.74
SD	0.08	0.015
CV%	0.99	0.03
0.00195 mg/ml furosine	**RT [min]**	**Peak Area [counts x 10^3]**
Mean Day One	8.24	23.15
Mean Day Two	8.20	22.26
Mean	8.22	22.71
SD	0.02	0.63
CV%	0.28	2.77
0.000975mg/ml furosine	**RT [min]**	**Peak Area [counts x 10^3]**
Mean Day One	8.14	10.95
Mean Day Two	8.22	10.96
Mean	8.18	10.95
SD	0.06	0.01
CV%	0.71	0.08

Table VIII.iii. Pentosidine standard data from day one and two

200 ng/ml pentosidine	RT [min] Day One	RT [min] Day Two	Area [counts x 10^3] Day one	Area [counts X 10^3] Day Two
1	10.27	10.44	87.534	88.725
2	10.31	10.42	88.664	88.153
3	10.44	10.30	88.413	88.850
Mean	10.34	10.39	88.204	88.576
Standard Deviation	8.89×10^{-2}	7.57×10^{-3}	0.593	0.372
CV%	0.89	0.87	0.67	0.42
100 ng/ml pentosidine				
1	10.25	10.40	50.490	51.060
2	10.40	10.35	51.898	48.900
3	10.35	10.28	50.491	49.030
Mean	10.33	10.34	50.960	49.670
Standard Deviation	7.64×10^{-2}	6.03×10^{-2}	0.813	1.21
CV%	0.60	0.12	0.19	2.44
50 ng/ml pentosidine				
1	10.26	10.35	30.260	31.250
2	10.30	10.32	31.606	33.307
3	10.28	10.38	31.837	36.698
Mean	10.28	10.35	31.234	33.752
Standard Deviation	0.02	0.300	0.852	2.751
CV%	0.41	0.08	2.73	8.51
25 ng/ml pentosidine				
1	10.30	10.33	21.247	22.015
2	10.34	10.27	22.084	22.145
3	10.28	10.31	23.153	22.627
Mean	10.31	10.30	22.161	22.262
Standard Deoiation	3.055×10^{-2}	3.055×10^{-2}	0.955	0.322
CV%	0.03	0.03	0.96	0.32
12.5 ng/ml pentosidine				
1	10.31	10.32	15.387	15.491
2	10.30	10.34	15.666	15.643
3	10.33	10.30	15.948	15.748
Mean	10.31	10.32	15.667	15.627
Standard Deviation	1.52×10^{-2}	0.02	0.281	0.1292
CV%	0.22	0.18	1.79	0.83

Table VIII.iv. Data for day-to-day repeatability of pentosidine standard peaks

200 ng/ml pentosidine	RT [min]	Peak Area [counts x 10^3]
Mean Day One	10.34	88.204
Mean Day Two	10.39	88.576
Mean	10.37	88.390
SD	0.04	0.186
CV%	0.34	0.21
100 ng/ml pentosidine	**RT [min]**	**Peak Area [counts x 10^3]**
Mean Day One	10.33	50.960
Mean Day Two	10.34	49.670
Mean	10.34	50.315
SD	0.01	0.9122
CV%	0.07	1.81
50 ng/ml pentosidine	**RT [min]**	**Peak Area [counts x 10^3]**
Mean Day One	10.28	31.234
Mean Day Two	10.35	33.752
Mean	10.32	32.493
SD	0.05	1.780
CV%	0.48	5.48
25 ng/ml pentosidine	**RT [min]**	**Peak Area [counts x 10^3]**
Mean Day One	10.31	22.161
Mean Day Two	10.31	22.262
Mean	10.31	22.212
SD	0	0.071
CV%	0	0.32
12.5 ng/ml pentosidine	**RT [min]**	**Peak Area [counts x 10^3]**
Mean Day One	10.31	15.667
Mean Day Two	10.32	15.627
Mean	10.32	15.647
SD	0.01	0.028
CV%	6.86 x 10-5	0.18

Table VIII.v. Furosine data for freeze-thaw study

Freeze/Thaw Cycle	Mean Peak Area [counts x 10^3]
0	191.7
1	182.2
2	181.5
3	181.2
4	181.8
5	184.1
6	181.8

Table VIII.vi. Pentosidine data for freeze-thaw study

Freeze/Thaw Cycle	Mean Peak Area [counts x 10^3]
0	87.7
1	88.9
2	90.2
3	80.0
4	66.1
5	54.1
6	56.4

Table VIII.vii. Hydrolysis of callus samples under hypoxic and non-hypoxic conditions-assayed for furosine

Callus Sample	Concentration of furosine [ng/mg protein] Hydrolysis under nitrogen	Concentration of furosine [ng/mg protein] Hydrolysis under oxygen	Concentration of furosine [ng/mg protein] Hydrolysis under air
1N	343.0	96.8	263.0
2N	156.1	565.9	282.0
3N	263.8	192.2	132.2
4N	141.2	195.8	70.6
5N	245.5	40.9	190.9
6N	198.2	0.0	186.5
1D	293.9	240.5	242.5
2D	801.3	154.7	435.5
3D	217.8	75.9	210.6
4D	184.6	204.0	124.8
5D	83.8	169.3	218.5
6D	545.6	551.8	267.7

Table VIII.viii. Hydrolysis of callus samples under hypoxic and non-hypoxic conditions-assayed for pentosidine

Callus Sample	Concentration of pentosidine [ng/mg protein] Hydrolysis under nitrogen	Concentration of pentosidine [ng/mg protein] Hydrolysis under oxygen	Concentration of pentosidine [ng/mg protein] Hydrolysis under air
1N	458.7	213.8	246.8
2N	257.9	165.2	143.8
3N	447.4	197.9	235.7
4N	285.6	160.1	166.5
5N	474.2	13.8	11.6
6N	28.5	13.8	0.0
1D	138.0	143.3	133.0
2D	18.2	172.0	166.8
3D	41.8	334.6	337.7
4D	226.6	189.4	130.5
5D	281.2	90.2	87.2
6D	217.7	0.0	10.9

Table VIII.ix. Keratin extracts after acid hydrolysis under hypoxic conditions and assayed for furosine and pentosidine

Sample	Concentration of furosine [ng per mg of protein]	Concentration pentosidine [ng per mg of protein]
1N	1234.1	5.2
2N	920.9	22.7
3N	723.7	14.7
4N	279.2	9.3
5N	760.5	5.7
6N	146.9	6.8
1D	498.2	20.4
2D	320.2	34.8
3D	151.3	150.6
4D	281.0	13.0
5D	609.9	18.5
6D	481.4	16.6

Figure VIII.viii

Table VIII.x. Callus and keratin extracts after enzyme hydrolysis-assayed for furosine and pentosidine

Raw SC	Concentration of furosine [ng/mgprotein]	Keratin Extract	Concentration of furosine [ng/mg protein]	Concentration of pentosidine [ng/mg protein]
1N	169.8	**1N**	223.9	6.4
2N	7440.1	**2N**	508.8	10.3
3N	229.1	**3N**	683.2	5.2
4N	366.7	**4N**	205.5	15.2
5N	964.2	**5N**	86.6	11.5
6N	266.0	**6N**	308.6	6.8
1D	223.9	**1D**	213.4	140.5
2D	974.3	**2D**	77.4	6.6
3D	355.6	**3D**	109.7	25.7
4D	146.6	**4D**	243.0	21.7
5D	117.6	**5D**	388.6	5.6
6D	293.0	**6D**	342.3	6.2

Table VIII.xi. Hydrolysis of keratin extracts for different lengths of time

Hydrolysis Time [Hours]	Mean Concentration of Furosine [ng/mg per protein]	Mean Concentration of Pentosidine [ng/mg per protein]
2	1606.4	
4	6340.2	
6	10853.6	44.751
18	5171.4	163.196
24	2610.6	111.172
30	1807.2	46.926

Table VIII.xii. Furosine recovery data for keratin extract after 6h acid hydrolysis

Samples	Percentage Recovery
minus furosine	
1mg/ml furosine	79.97
0.1mg/ml furosine	77.36
0.01mg/ml furosine	76.6
0.001mg/ml furosine	75.00

Table VIII.xiii. Pentosidine recovery data for keratin extract after 18h acid hydrolysis

Samples	Percentage Recovery
minus pentosidine	
1mg/ml pentosidine	69.97
0.1mg/ml pentosidine	57.36
0.01mg/ml pentosidine	56.60
0.001mg/ml pentosidine	45.00

Table VIII.xiv. Concentration of furosine in keratin extracts hydrolysed for 6h in acid

Samples	Peak Area [counts x 10^3]	Concentration of Furosine [μg/mg protein]
1N	9.16	1.76
2N	2.52	1.46
3N	0.27	15.29
4N	2.32	9.23
5N	4.29	2.43
6N	0.55	1.22
1D	4.31	9.40
2D	3.13	1.69
3D	2.53	2.16
4D	4.69	240.00
5D	4.32	25.88
6D	12.54	11.20

Table VIII.xv. Concentration of pentosidine in keratin extracts hydrolysed for 18h in acid

Samples	Peak Area [counts x 10^3]	Concentration of Pentosidine [μg/mg protein]
1N	1.311	2.56
2N	5.899	11.69
3N	28.327	57.28
4N	77.190	156.10
5N	1.628	3.29
6N	3.236	6.54
1D	1041.55	210.63
2D	82.641	167.63
3D	15.162	30.661
4D	64.938	131.321
5D	23.352	47.223
6D	20.005	40.455

Appendix IX The Distribution of the Furosine and Pentosidine Measured in Keratin and Serum Proteins from Non-diabetics individuals

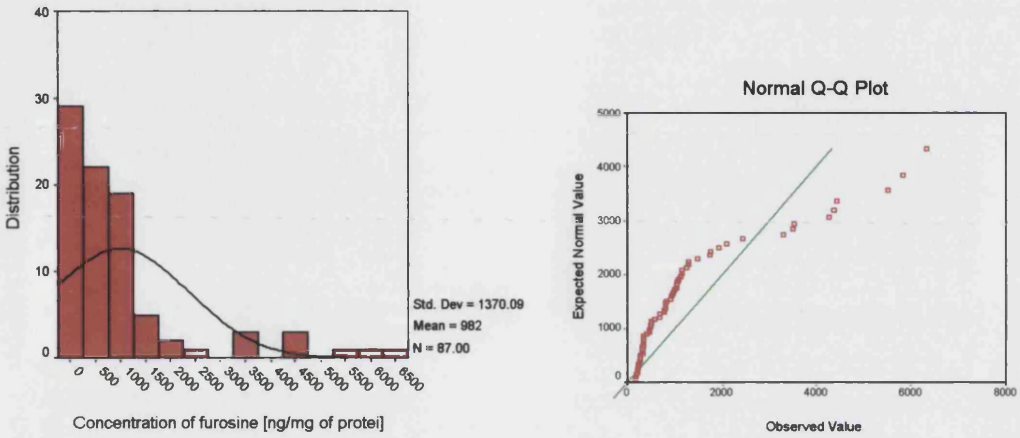

Figure IX.i: The distribution of furosine measured in keratin extracts from 87 non-diabetic subjects

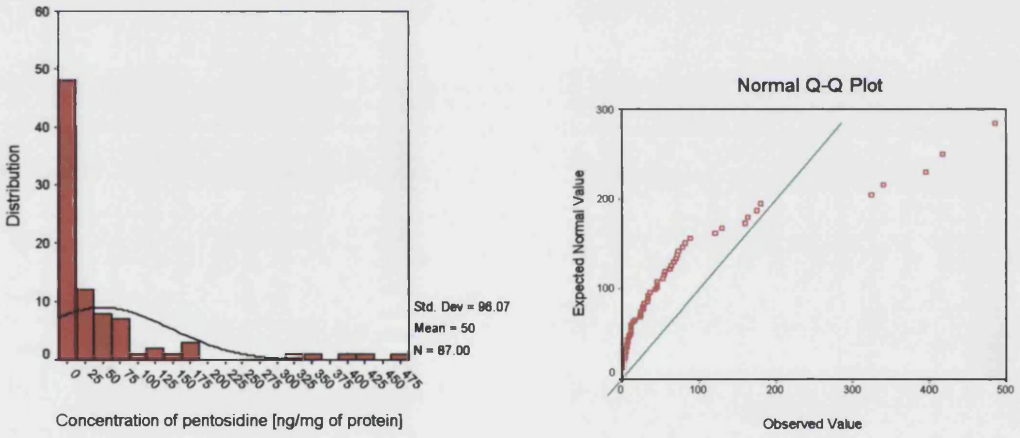

Figure IX.ii: The distribution of pentosidine measured in keratin extracts from 87 non-diabetic subjects

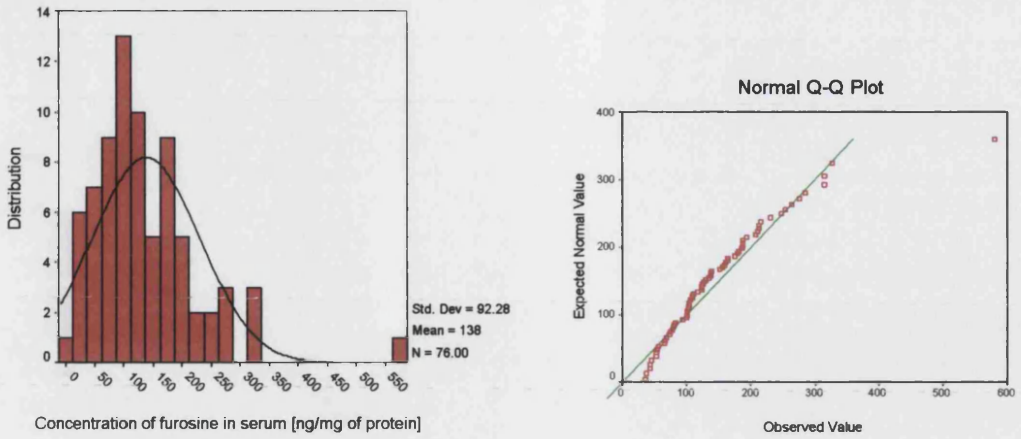

Figure IX.iii: The distribution of furosine measured in the serum of 76 non-diabetic subjects

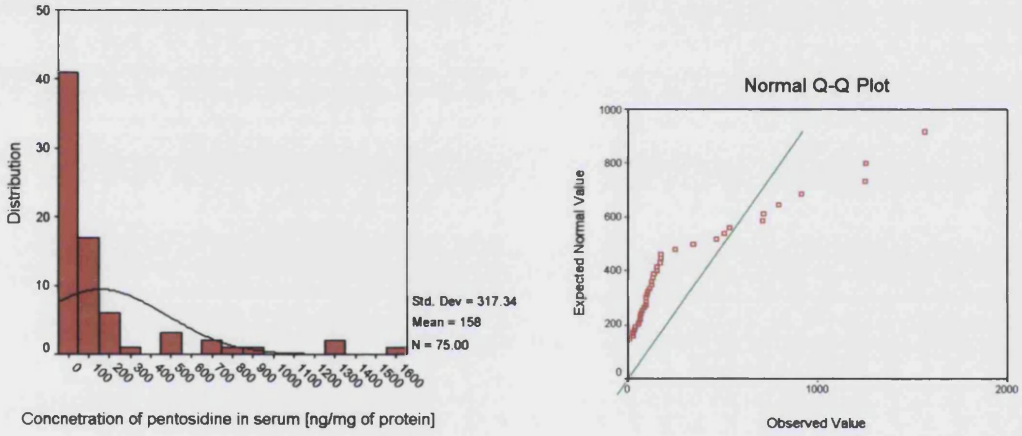

Figure IX.iv: The distribution of pentosidine measured in the serum of 87 non-diabetic subjects

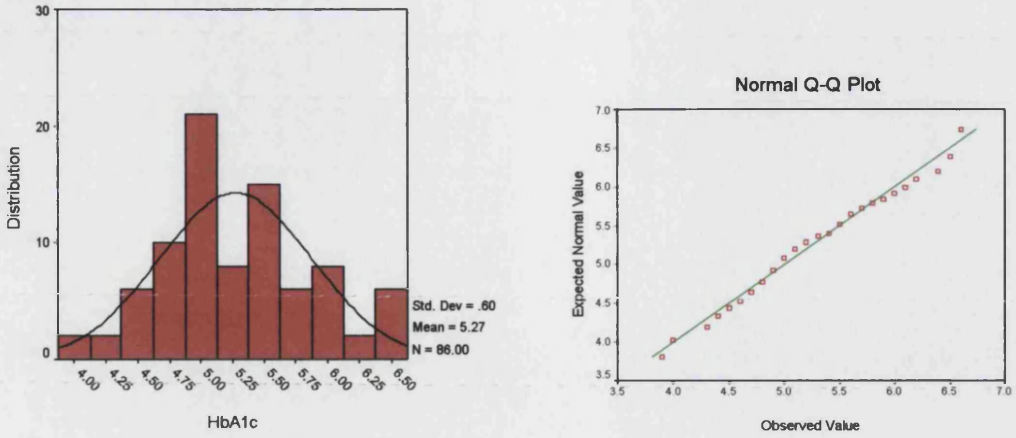

Figure IX.v: The distribution of HbA1c levels in the blood of 87 non-diabetic subjects.

The removal of the outlying data from all of these distributions did not have an effect on the distribution curves, i.e. they remain skewed.

Appendix X Spleen Fusion Protocol – Carried out by T. Jowett, Department of Medicine, UCL

Reagents

3 X 20 ml RPMI
1 X 1 ml RPMI in a Bijou
1 X 1 ml 50% PEG (Sigma, P7181)

Method

The spleen was teased apart using forceps in an aliquot of RPMI (2 ml) in a petri-dish. The mixture was layered onto RPMI (20 ml) in a Universal and decanted using a Pasteur pipette into a second Universal, leaving any clumps behind. The solution was centrifuged at 1000 rpm for 10 min, aspirated and tapped loose. An aliquot of RBCLB (1 ml) was gently mixed in the pipette for 1 min and pipetted into RPMI (20 ml) in a Universal and mixed well. The mixture was centrifuged at 1000 rpm[σ] for 10 min, aspirated and tapped loose again. Whilst swirling RPMI (10 ml) was slowly added to the Universal and any clumps present were removed using a Pasteur pipette. The amount of spleen cells at this point was counted (approximately 10^8 cells/ml). The mixture was allowed to stand until needed. A volume equivalent to 10:1 (spleen: myeloma cells) was used for the next few steps in the procedure.

The mixture was centrifuged for 10 min at 1000 rpm, aspirated and tapped loose. An aliquot of RPMI (20 ml) was added, mixed carefully and centrifuged as described previously. Another aliquot of RPMI (10 ml) was added, mixed thoroughly with a pipette, transferred to the spleen cell universal and mixed thoroughly. The mixture was centrifuged at 1000 rpm for 10 min, aspirated and tapped loose. An aliquot of PEG (1 ml, 50%) was added dropwise with gentle shaking over 2 min, followed by RPMI (1 ml) and shaking gently over 1 min. Over

[σ] Whilst spinning, the number of myeloma cells were counted (0 cells/ml)

a 4 min period RPMI (20 ml) was added under continuous shaking. The Universal was sealed and gently inverted 3 times and centrifuged at 800 rpm for 8 min. The final mixture was aspirated (not tapped loose), Cell medium (CM) (10 ml) was added and swirled gently whilst breaking up any clumps with a Pasteur pipette. The cells were incubated at 37°C for 3-4 h.

An aliquot of hybridoma enhancing supplement (10%, 100 µl) was placed in each well of 8, 96 well plates and incubated at 37°C for a few hours. This is referred to as the "feeder layer". A mixture of fusion products (10 ml), CM (30 ml), CM plus 2 x HAT (40 ml) was place in a sterile bottle and 100µl of this was pipetted into each well onto the feeder layer. After, approximately 4 days the myelomas were mostly dead and the hybridomas were visible. After 14 days they were tested for specific antibodies.

Appendix XI Purification Of Monoclonal and Polyclonal Antisera using Affinity Chromatography – Protein-A- Sepheraose*

Reagents

Protein-A-sepharose CL-4B (Pharmacia, Milton Keynes), Tris/HCl (0.1M, pH 7.0), glycine (0.1 M, pH 3.0), Tris (1 M, pH 9.0)

Method

The protein-A-sepharose gel (1 g) was swollen and washed with 20 ml, 0.1 M Tris/HCl, pH 7.0. The mixture was then centrifuged (10 min, 3000 rpm) and the solvent was decanted off the gel. This wash procedure was repeated 2 more times. An aliquot of the serum (1 ml) was diluted with the starting buffer (4 ml) and added to the gel. The mixture was then incubated at room temperature, under rotation, for 1 h. The gel was placed into a 5 ml column and the breakthrough was collected. It was then washed with 0.1 M Tris, pH 7.0 (20 ml) and the wash was collected. The gel was washed to remove any unwanted contaminants and they were both collected to check for and loss of IgG. The column was then eluted with 0.1M glycine buffer, pH 3.0 (10 ml). Since the elution conditions are quite harsh, it was necessary to collect the fractions in a few drops of 1 M Tris/HCl, pH 9.0 (50 μl), so that the final pH of the fractions was neutral. All fractions were measured for protein content using the Lowry procedure Appendix I) and those containing the antibodies were pooled and stored at -70°C. The pooled fractions were then applied to one dimensional SDS-PAGE to confirm the presence of pure antibodies (Appendix XII).

Protein A–Sepherose CL–4B (Pharmacia, Milton Keynes) is a protein A covalently bonded to a cross-linked matrix, Sepherose CL-4B, by the cyanogen bromide method. This matrix exhibits high chemical and mechanical stability and the protein A-Sepherose CL-4B is stable over the pH range 2-11. It also tolerates high concentrations of denaturants, such as urea and quanidine, commonly used for eluting bound molecules from immunoadsorbants.

Appendix XII Protein A-Sepherose Purification of Polyclonal and Monoclonal Antibodies to Furosine

Antibodies	Concentration of Fractions kept [mg/ml]
Polyclonal	3.21
	7.03
	2.95
Monoclonal 2C3/C4	4.23
	4.30
	3.92
Monoclonal 6B11/A7	5.75
	5.02
	4.70

There are 2 main bands of molecular weights 50 and 25-30 kDa that represent the heavy and the light portions of the antibody. These 2 bands on their own confirm the presence of pure antibody in the fractions collected (Figs. XII.i.a and XII.ib). The breakthroughs and washes were also applied to the gels for comparison (Figs. XII.ii.a and XII.ii.b).

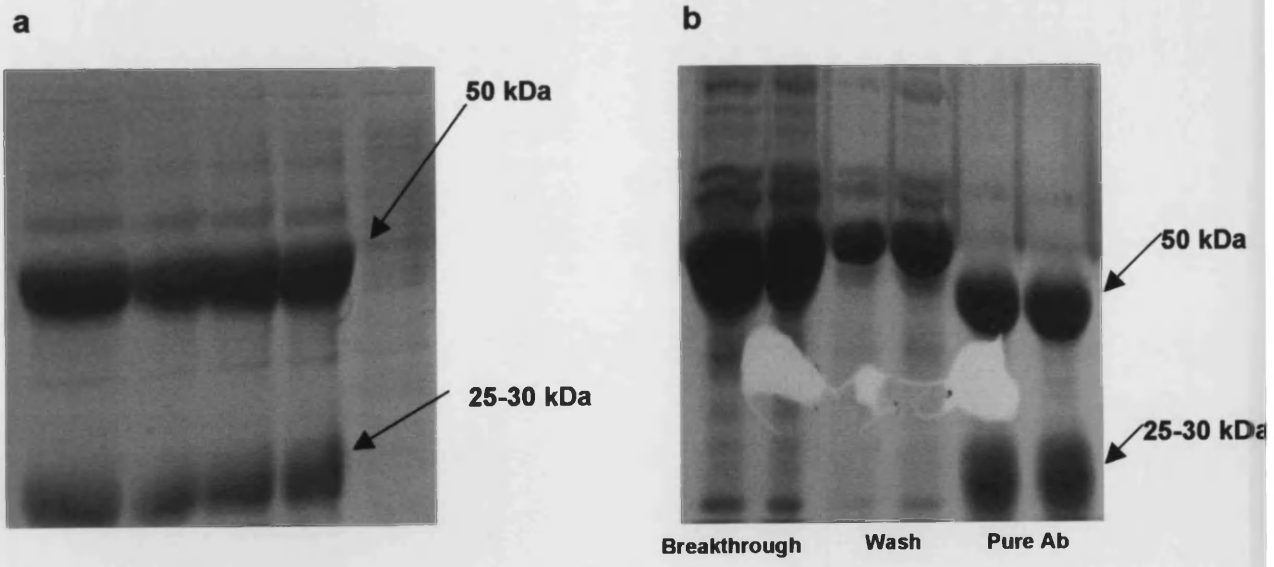

Figure XII.i.a: SDS-PAGE of pure polyclonal antibodies; **b:** SDS-PAGE of pure polyclonal antibodies, breakthrough and wash from purification procedure.

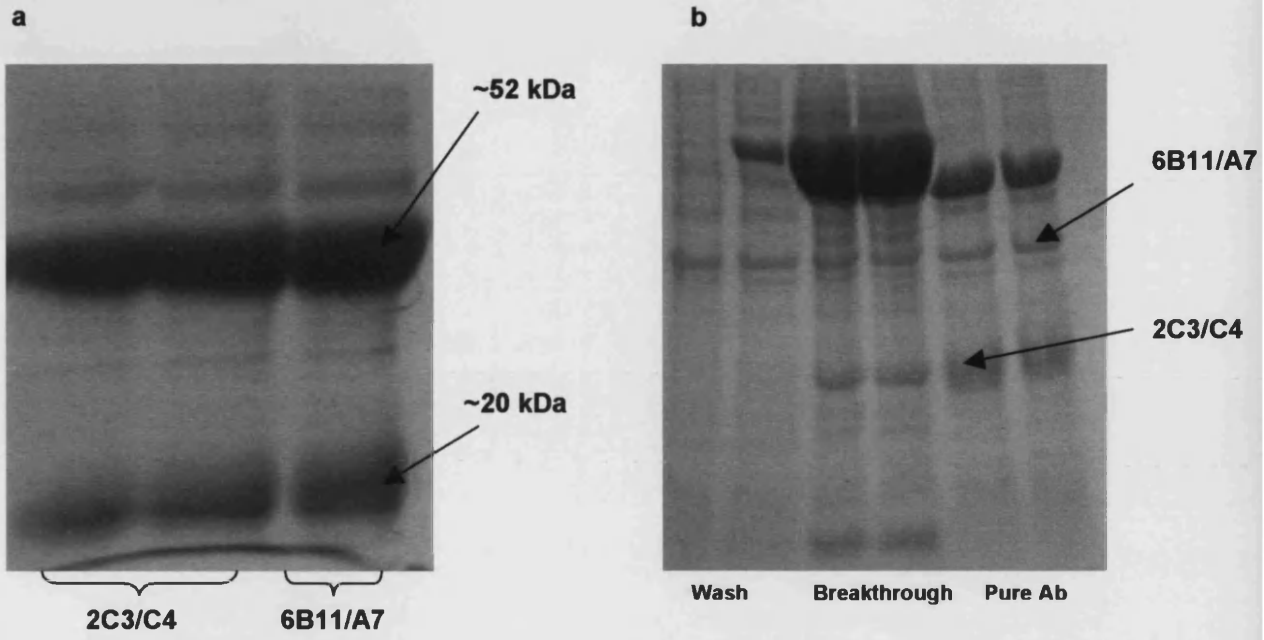

Figure XII.ii.a: SDS-PAGE of pure monoclonal antibodies; **b:** SDS-PAGE of pure monoclonal antibodies, breakthrough and wash from purification procedure.

Appendix XIII Results from Titrations using Monoclonal Antibodies

Conc of polyclonal antibody [mg/ml]	2 µg/ml F coating mean abs $OD_{(490)}$	2 µg/ml F-BSA coating mean abs $OD_{(490)}$	2 µg/ml F-Tg coating mean abs $OD_{(490)}$	2 µg/ml BSA coating mean abs $OD_{(490)}$	2 µg/ml CML coating mean abs $OD_{(490)}$	2 µg/ml CML-BSA coating mean abs $OD_{(490)}$	2 µg/ml CML-Tg coating mean abs $OD_{(490)}$	2 µg/ml Tg coating mean abs $OD_{(490)}$	2 µg/ml arginine coating mean abs $OD_{(490)}$	2 µg/ml lysine coating mean abs $OD_{(490)}$
0.1	0.536	0.499	0.474	0.365	0.116	0.155	0.185	0.257	0.453	0.533
0.01	0.136	0.099	0.100	0.082	0.042	0.068	0.067	0.081	0.091	0.097
0.001	0.059	0.051	0.061	0.066	0.037	0.047	0.093	0.061	0.088	0.046
0.0001	0.075	0.051	0.059	0.050	0.055	0.051	0.048	0.039	0.038	0.041
Conc of 2C3/C4 antibody [mg/ml]										
0.1	0.062	0.430	0.821	0.052	0.049	0.050	0.380	0.044	0.058	0.067
0.01	0.068	0.212	0.642	0.062	0.044	0.041	0.190	0.047	0.043	0.051
0.001	0.052	0.060	0.309	0.060	0.047	0.041	0.114	0.061	0.048	0.054
0.0001	0.490	0.050	0.311	0.052	0.045	0.043	0.115	0.052	0.049	0.066
Conc of 6B11/A7 antibody [mg/ml]										
0.1	0.074	0.562	0.793	0.067	0.050	0.053	0.411	0.036	0.057	0.067
0.01	0.080	0.365	0.739	0.050	0.045	0.044	0.319	0.045	0.055	0.055
0.001	0.079	0.133	0.440	0.055	0.048	0.046	0.161	0.045	0.070	0.046
0.0001	0.074	0.060	0.391	0.049	0.048	0.036	0.112	0.042	0.051	0.061

Conc of polyclonal antibody [mg/ml]	2 μg/ml F coating noise/sound ratio	2 μg/ml F-BSA coating noise/sound ratio	2 μg/ml F-Tg coating noise/sound ratio	2 μg/ml BSA coating noise/sound ratio	2 μg/ml CML coating noise/sound ratio	2 μg/ml CML-BSA coating noise/sound ratio	2 μg/ml CML-Tg coating noise/sound ratio	2 μg/ml Tg coating noise/sound ratio	2 μg/ml arginine coating noise/sound ratio	2 μg/ml lysine coating noise/sound ratio
0.1	1.229	1.002	0.983	0.658	0.892	0.708	0.701	1.019	1.037	1.039
0.01	1.236	0.934	0.736	0.621	0.300	1.115	1.031	1.556	0.813	0.907
0.001	0.957	0.785	0.735	0.805	0.822	0.904	1.788	1.299	1.660	0.730
0.0001	1.230	0.927	0.694	1.000	1.170	1.202	0.842	0.830	0.745	0.820
Conc of 2C3/C4 antibody [mg/ml]										
0.1	0.805	4.725	17.104	0.839	1.140	0.568	10.000	1.128	1.055	1.156
0.01	0.782	3.786	11.673	0.290	0.936	0.784	5.000	0.839	0.683	1.041
0.001	1.000	1.200	5.618	0.780	0.959	0.911	2.327	1.298	1.043	1.109
0.0001	0.925	0.926	6.098	0.505	0.568	0.935	2.805	0.945	0.980	1.269
Conc of 6B11/A7 antibody [mg/ml]										
0.1	1.088	6.612	7.209	1.175	1.163	0.981	9.786	0.782	1.000	0.957
0.01	1.096	3.687	14.212	0.833	1.000	1.023	7.419	1.000	1.100	0.917
0.001	1.411	2.181	8.627	1.078	0.941	1.179	3.157	0.738	1.373	0.767
0.0001	0.824	1.071	7.667	0.961	1.067	0.923	2.240	2.240	0.850	1.245

Appendix XIV Distribution of Data from Chapter 7

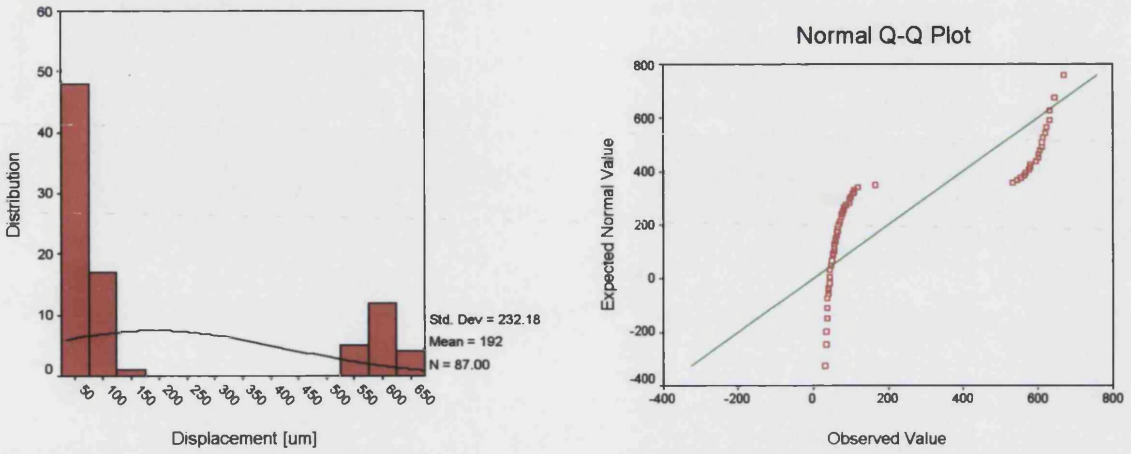

Figure XIV.i: The distribution of the series elastic element data on stretching of dorsal epidermis.

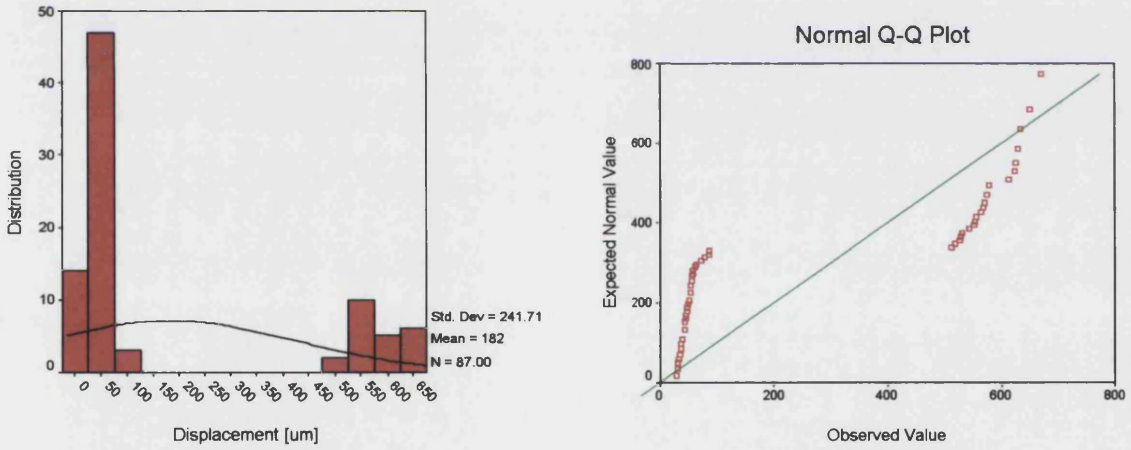

Figure XIV.ii: The distribution of the series elastic element on stretching of the epidermis on the MLA/ .

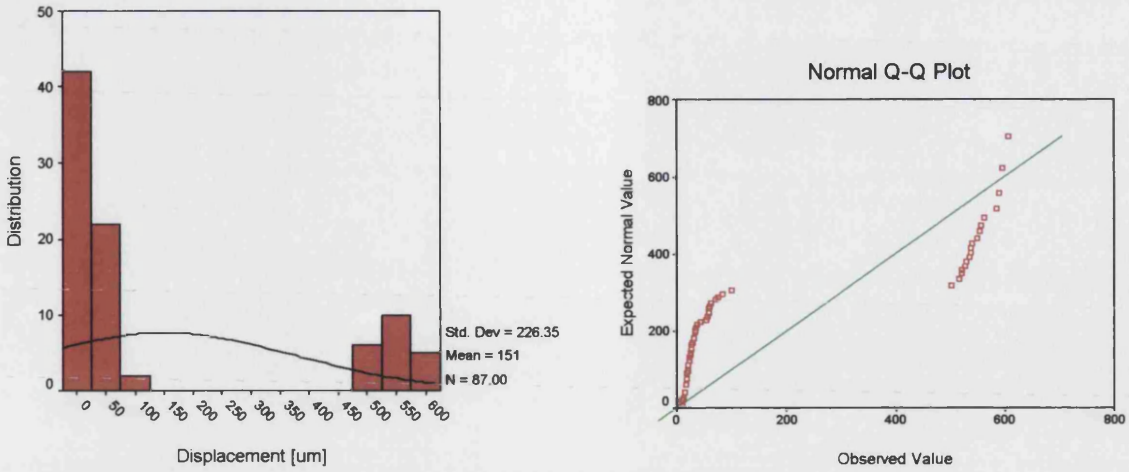

Figure XIV.iii: The distribution of the series elastic element data on stretching of the epidermis on the PMA.

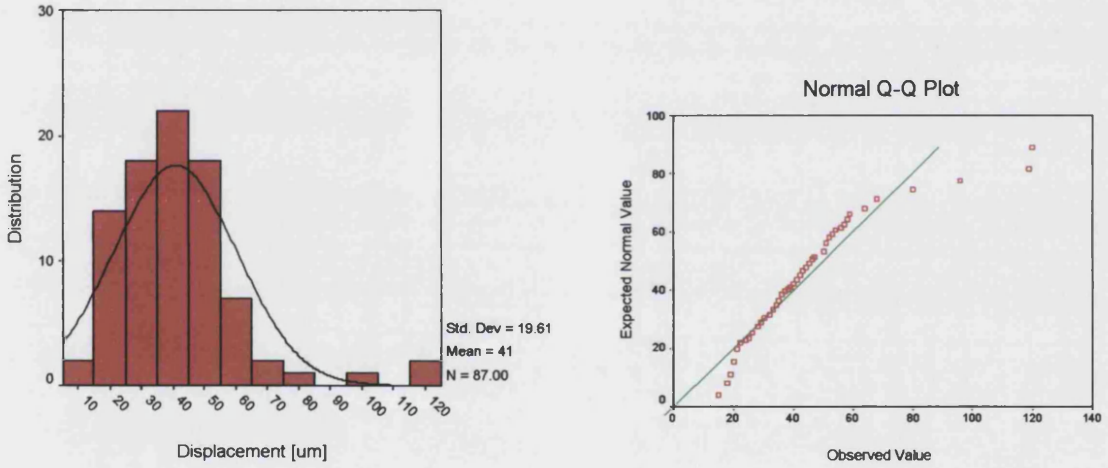

Figure XIV.iv: The distribution of the series elastic element data on retraction of the dorsal epidermis.

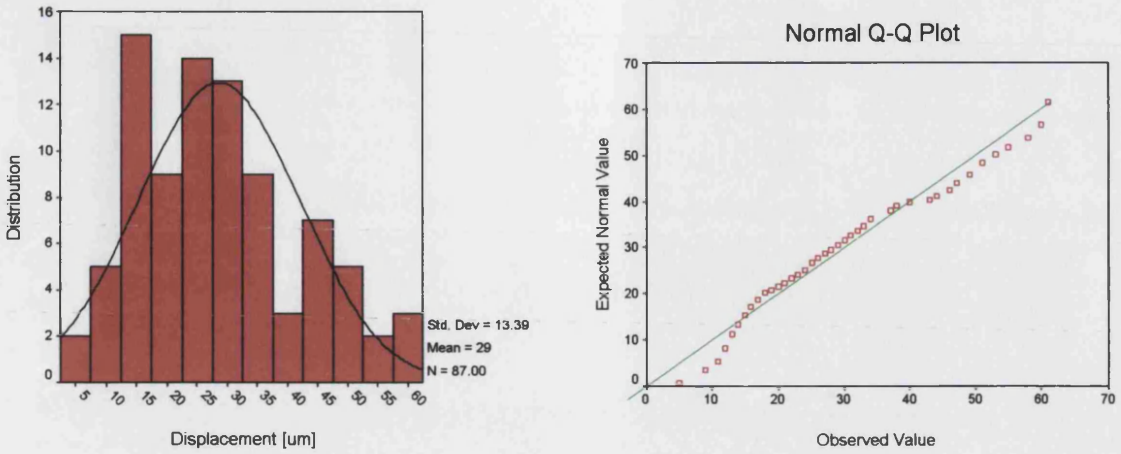

Figure XIV.v: The distribution of the series elastic element data on retraction of the epidermis on the MLA.

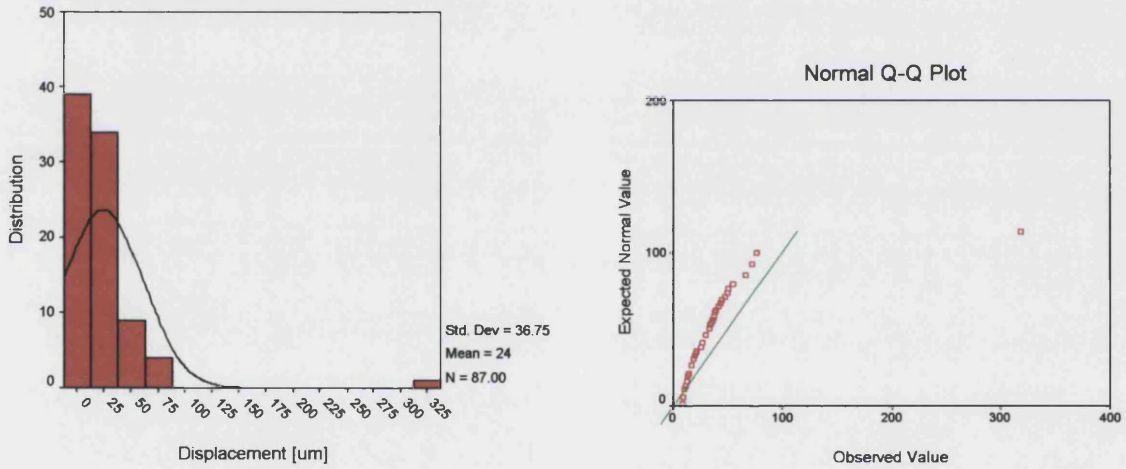

Figure XIV.vi: The distribution of the series elastic element data on retraction of the epidermis on the PMA.

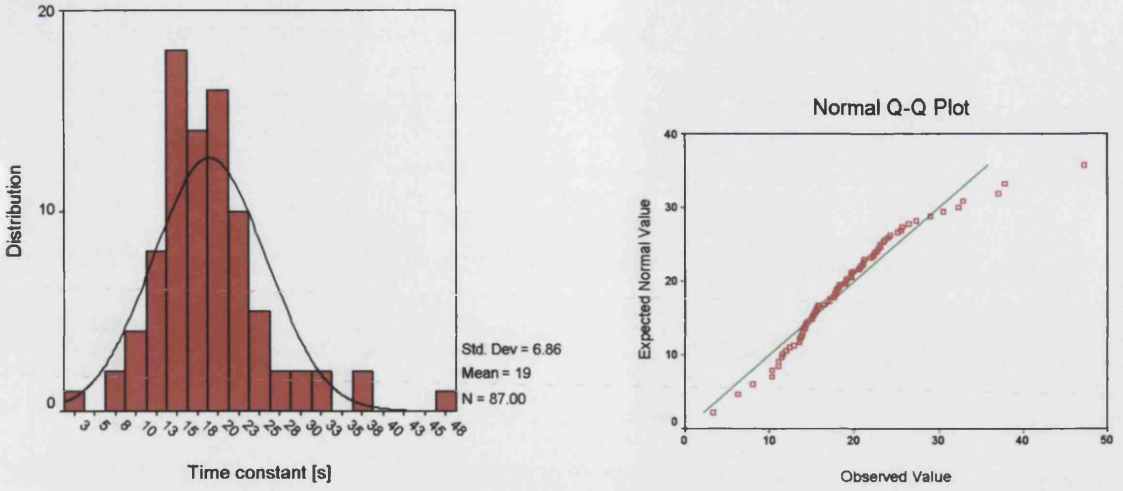

Figure XIV.vii: The distribution of the time constant data on stretching of the dorsal epidermis.

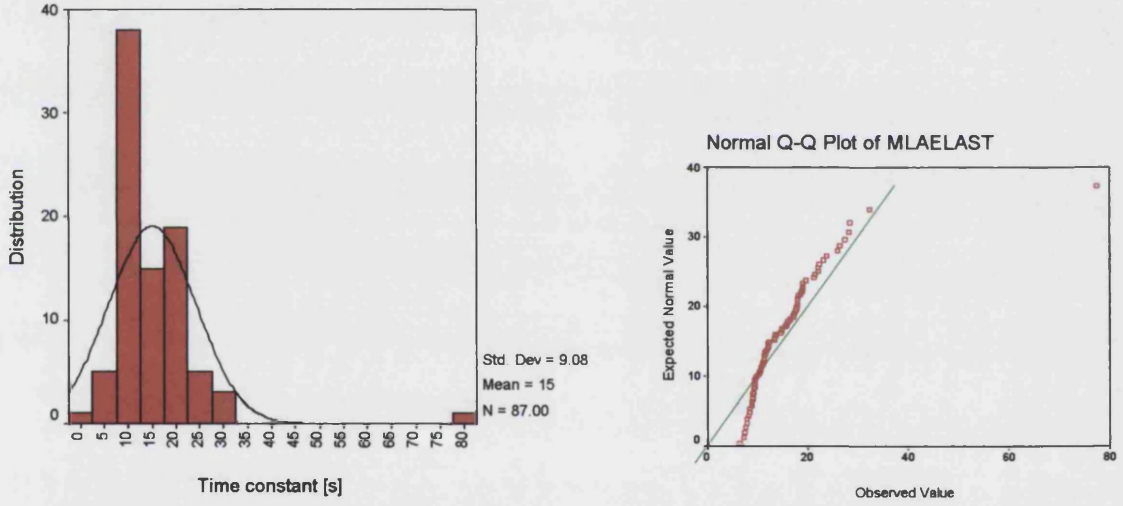

Figure XIV.viii: The distribution of the time constant data on stretching of the epidermis on the MLA.

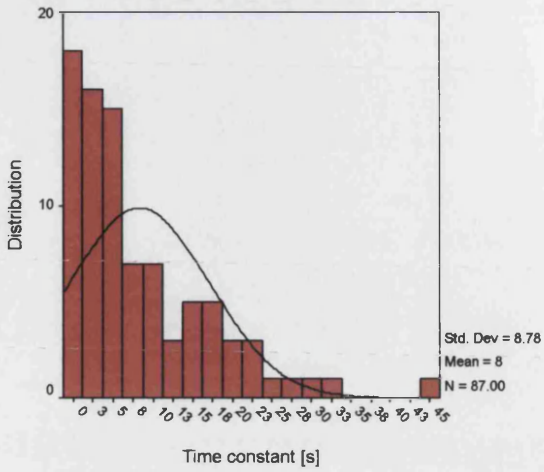

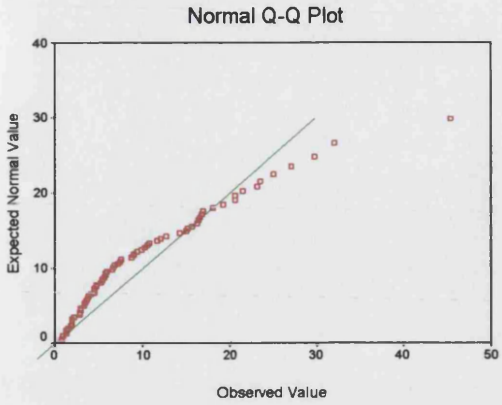

Figure XIV.ix: The distribution of the time constant data on stretching of the epidermis on the PMA.

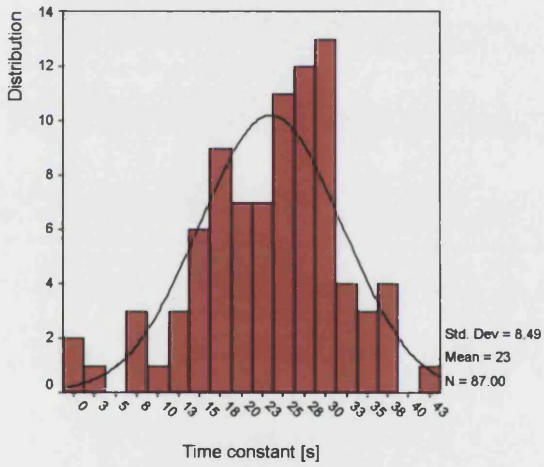

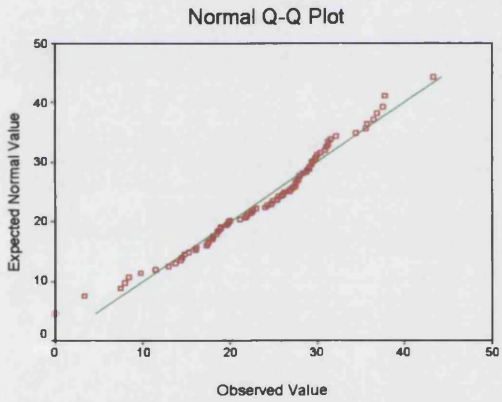

Figure XIV.x: The distribution of the time constant data on retraction of the dorsal epidermis.

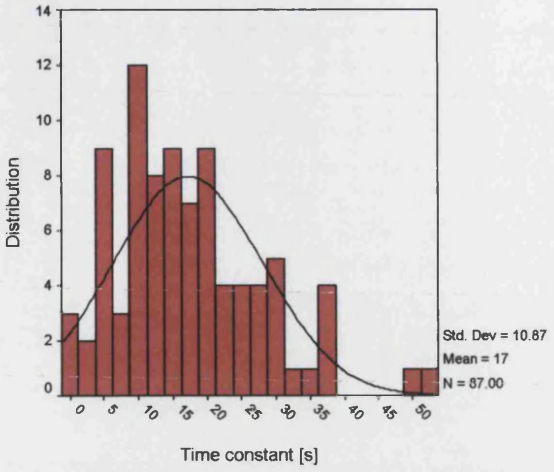

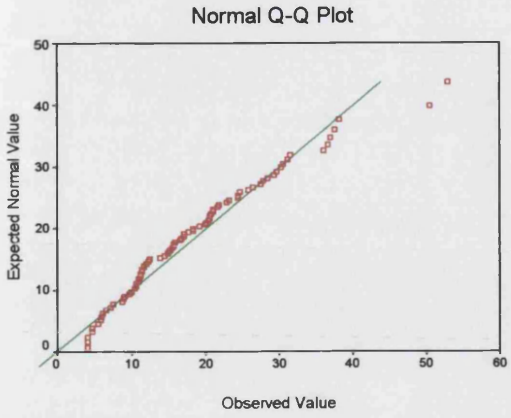

Figure XIV.xi: The distribution of the time constant data on retraction of the epidermis of the MLA.

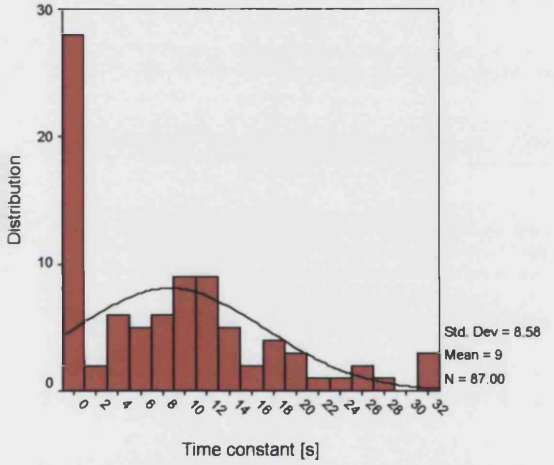

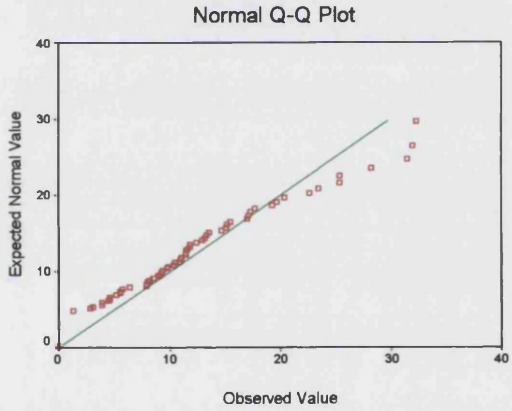

Figure XIV.xii: The distribution of the time constant data on retraction of the epidermis of the PMA.

Appendix XV Distribution of Data from Chapter 8

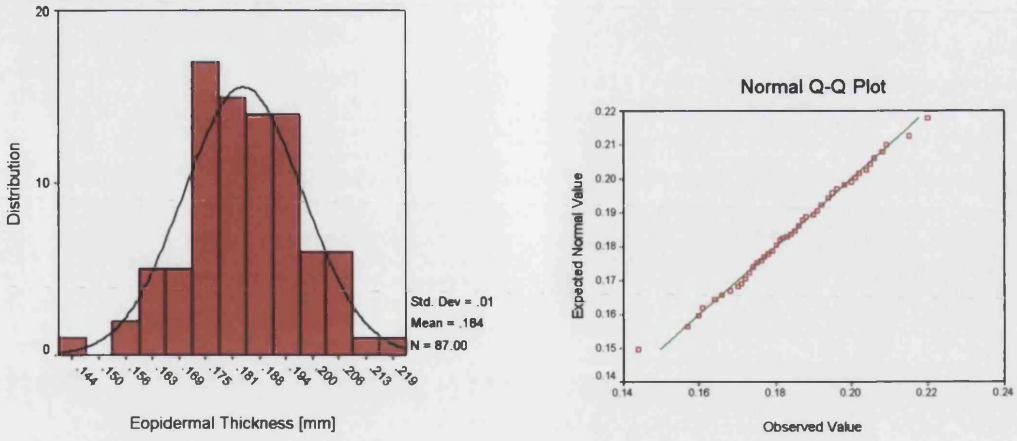

Figure XV.i: The distribution of epidermal thickness data from the dorsal site, v=1580m/s.

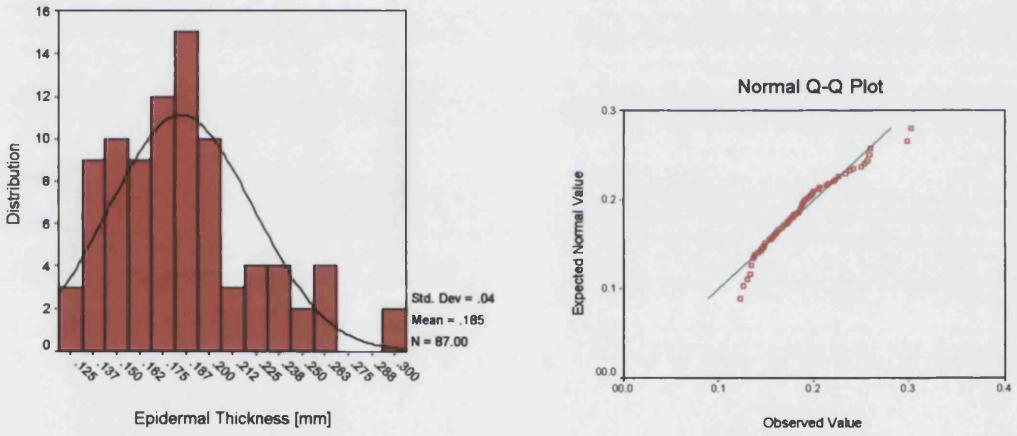

Figure XV.ii: The distribution of epidermal thickness data from the MLA, v = 1580m/s.

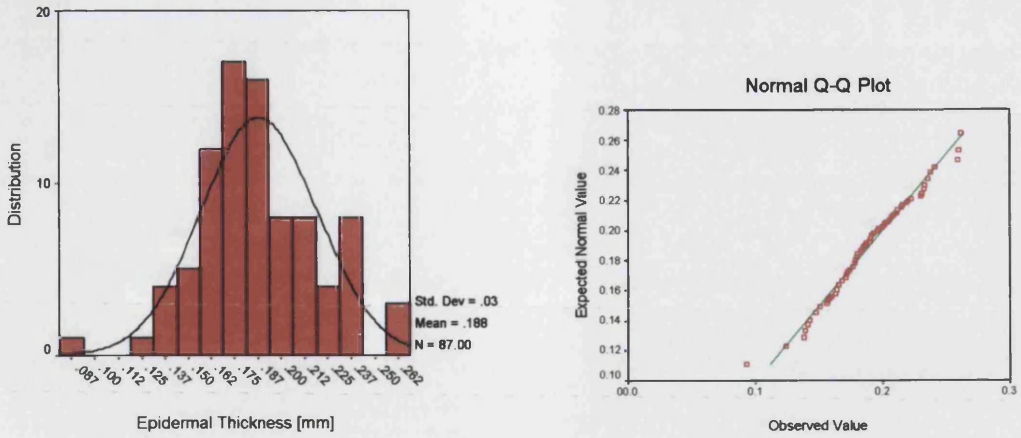

Figure XV.iii: The distribution of epidermal thickness data from the PMA, v = 1580m/s.

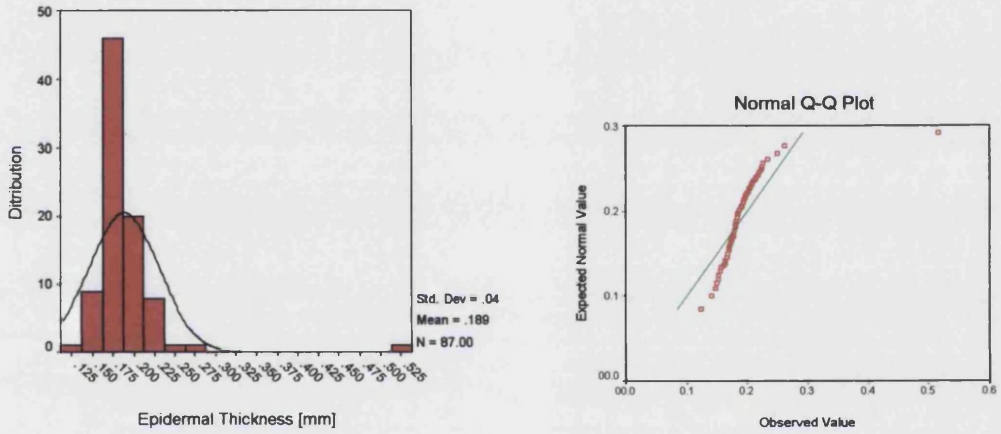

Figure XV.iv: The distribution of epidermal thickness data from the dorsal site, v = 2459m/s.

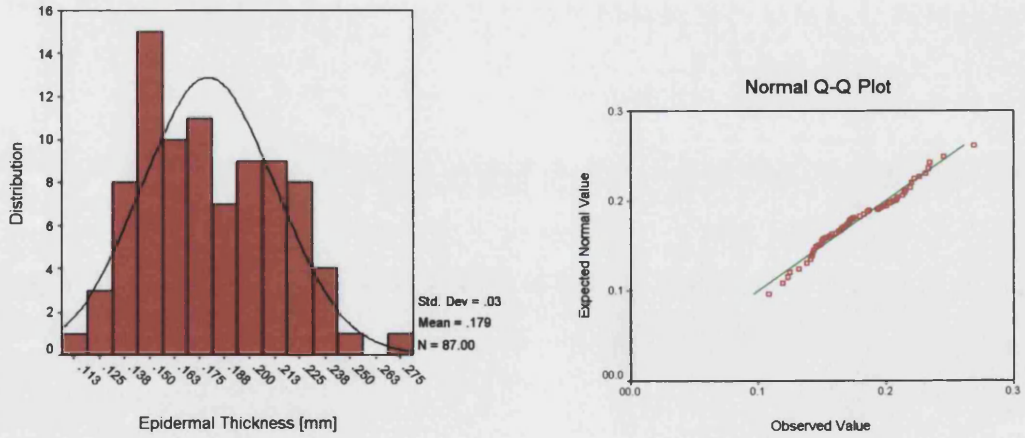

Figure XV.v: The distribution of epidermal thickness data from the MLA, v = 2459m/s.

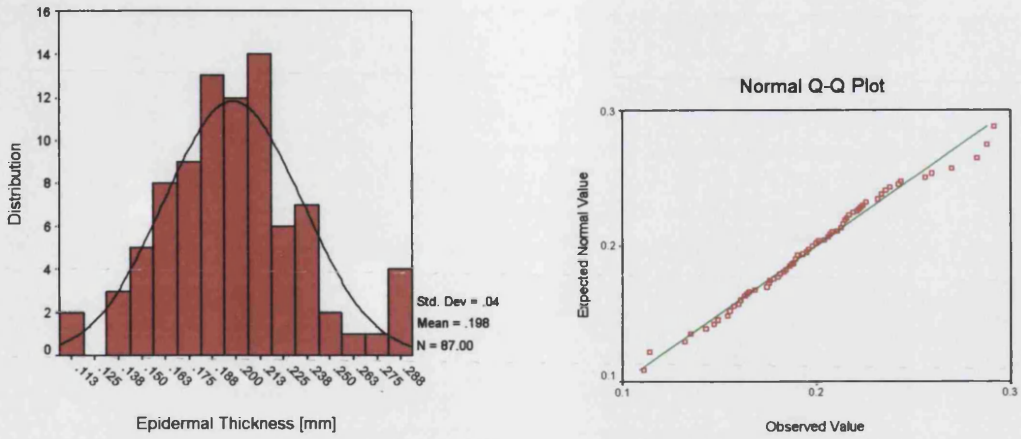

Figure XV.vi: The distribution of epidermal thickness data from the PMA, v = 2459m/s.

Appendix XVI Definition, Diagnosis and Classification of Diabetes Mellitus

In 1999 the World Health Organisation (WHO) published a comprehensive report discussing the definition, diagnosis and classification of diabetes mellitus (DM) [252]. The following reports the criteria for diagnosis according Diabetes UK, who have used the WHO document as their key reference.

Definition

According to the WHOs publication of: '*Definition, Diagnosis and Classification of Diabetes Mellitus and its Complications*', the definition of diabetes is as follows:

> " The term diabetes mellitus describes a metabolic disorder of multiple aetiology characterized by chronic hyperglycaemia with disturbances of carbohydrate, fat and protein metabolism resulting from defects in insulin secretion, insulin action, or both. The effects of diabetes mellitus include long-term damage, dysfunction and failure of various organs. Diabetes mellitus may present with characteristic symptoms such as thirst, polyuria, blurring of vision, and weight loss. In its most severe forms, ketoacidosis or a non-ketotic hyperosmolar state may develop and lead to stupor, coma and, in absence of effective treatment, death. Often symptoms are not severe, or may be absent, and consequently hyperglycaemia sufficient to cause pathological and functional changes may be present for a long time before the diagnosis is made. The long-term effects of diabetes mellitus include progressive development of the specific complications of retinopathy with potential blindness, nephropathy that may lead to renal failure, and/or neuropathy with risk of foot ulcers, amputation, Charcot joints, and features of autonomic dysfunction, including sexual dysfunction. People with diabetes are at increased of cardiovascular, peripheral vascular and cerebrovascular disease.
>
> Several pathogenetic processes are involved in the development of diabetes. These include processes which destroy the beta cells of the pancreas with consequent insulin deficiency, and others that result in resistance to insulin action. The abnormalities of carbohydrate, fat and protein metabolism are due to deficient action of insulin on target tissues resulting from insensitivity or lack of insulin."

Diagnostic Criteria

The criteria for diagnosis differ between patients with and without symptoms, the symptoms being polyuria, polydipsia and unexplained weight loss.

1) Symptoms:

- A random venous plasma glucose concentration ≥ 11.1mmol/l **or**
- A fasting plasma glucose concentration ≥ 7.0mmol/l (whole blood ≥ 6.1mmol/l **or**
- Two hour plasma glucose concentration ≥ 11.1mmol/l two hours after 75g anhydrous glucose in an oral glucose tolerance test (OGTT).

2) No symptoms:

Diagnosis should not be made on one single glucose determination. An additional glucose test result from another day with a value in a diabetic range is required. This test can be any of the tests described above. If the fasting or random glucose tests are not diagnostic, the OGTT should be used.

A diagnosis should never be made on the basis of glycosuria or a stick reading of finger prick blood glucose alone, although these tests are useful for screening purpose. HbA1c measurement is also not recommended for the diagnosis of diabetes.

Diabetes UK recommends that diagnosis be confirmed by a glucose measurement performed in an accredited laboratory on a venous plasma sample. This should mean that there is less need to perform OGTT on the majority of the population. However, in the elderly and some ethnic minority groups the fasting glucose alone may not be a reliable indicator of diabetes. For these individuals, and in the absence if symptoms, the use of a glucose tolerance test would be necessary as a definitive test.

Classification

- Insulin dependent (IDDM) and non-insulin dependent diabetes (NIDDM) are termed Type 1 and Type 2 diabetes, respectively.
- Impaired Glucose Tolerance (IGT) is a stage of impaired glucose regulation. It is characterised by a fasting plasma glucose < 7.0mmol/l and OGTT two hour value ≥ 7.8mmol/l but < 11.1mmol/l..
- Impaired Fasting Glycaemia (IFG) classifies individuals who have fasting glucose values above the normal range but below those diagnostic of diabetes. Fasting plasma glucose ≥ 6.1mmol/ll but < 7.0mmol/l). Diabetes UK recommends that individuals with IFG should have an OGTT to exclude the diagnosis of diabetes.

Gestational diabetes encompasses groups that have formerly been classified as Gestational Impaired Glucose Intolerance (GIGT) and Gestational Diabetes Mellitus (GDM).

Appendix XVII Patient Questionnaires

Record Sheet for diabetics

Name		.....
Hospital number		.....
Patient Identification		.....
Date of Birth		.....
Age in completed years		.....
Weight		.....
Height		.....
Serum Glucose		.....
Date of diagnosis		.....
Duration of diabetes		.....
Therapy for diabetes	Diet controlled = 1 Oral hypoglycaemic = 2 Insulin = 3 Insulin and oral hypoglycaemic = 4 Not known = 9	.....
History of diabetic complications	Renal = 1 Retinopathy = 2 Neuropathy = 3 Vascular insufficiency =4 Skin conditions = 5 Foot pathologies = 6* *Notes	.....
Smoker	Yes = 1 No = 2	....

Record Sheet for Non-Diabetics

Name			.....
Hospital number			.....
Patient Identification			.....
Date of Birth			.....
Age in completed years			.....
Weight			.....
Height			.....
History of foot problems	Yes = 1*	No = 2	.....
	*Notes		
	.....		
Smoker	Yes = 1	No = 2	.....

Structural and Cutaneous Pathologies

Lesser to structure — Hammer = 1 — claw = 2 — Mallet = 3 — .....
Normal = 4 — Other = 5 *
*Notes .....
.....

Hallux structure — HAV = 1 — Trigger = 2 — Hyperextended = 3 — ....
Unilateral = 4 — Bilateral = 5 — Normal = 6 — Other = 7*
*Notes .....
.....

Loss of forefoot arch — Slight = 1 — Moderate = 2 — Marked = 3 — .....
Unilateral = 4 — Bilateral = 5 — Normal = 6 — Other =7*
*Notes .....
.....

General foot structure — Pes Planus = 1 — Pes Cavus = 2 — Unilateral =3 — .....
Bilateral =4 — Normal = 3 — Other = 4*
*Notes .....
.....

Limited range of motion — Yes = 1* — No = 2 — .....
In hands
*Notes .....
.....

Limited range of motion — Yes = 1* — No = 2 — .....
In feet
*Notes .....
.....

Charcot joints — Yes = 1* — No = 2 — .....
*Site .....

Skin pathologies — Corns and callosities = 1 — Fissures = 2 — Tinea Pedis = 3 — .....
Anhydrosis = 4 — Hyperhydrosis = 5
Absence of hair = 6 — Other = 7*
*Notes .....
.....

Nail pathologies — O/C = 1 — O/M = 2 — Yellow nail = 3 — .....
Normal = 5 — Other = 6*
*Notes .....
.....

History of ulceration — Yes = 1* — No = 2 — .....

*Notes .....

.....

Footwear Bespoke = 1 Semi-bespoke = 2 .....

Normal well-fitted = 3 Normal ill-fitted = 4

Other = 5*

*Notes .....

.....

Wear marks on shoes .....

.....

Orthoses Simple Insole = 1 Orthotic = 2 Diabetic Insole = 3 .....

No Orthoses = 4 Other = 5*

*Notes .....

.....

Neurological and Vascular Assessment

Neurological Assessment

Symptoms	Present = 1	Absent = 2		.....
Nature of symptoms	Positive Symptomatology = 1		Negative Symptomatology = 2	.....
Duration of symptoms	<1year = 1 Notes.....		1-3 years = 2	.....
	>3 years = 3 Notes			
Chronic pain	No = 1	Insidious = 2	Intermittent = 3	.....
	Bilateral = 4	Unilateral = 5	Related to treatment = 6	
	Unrelated to treatment = 7		When walking = 8	
	When resting = 9			
History of Ulceration	Yes = 1*	No = 2		.....
	*Notes			
	.....			
Autonomic symptoms	Notes			
	.....			
Acute pain	Neuropathic pain = 1		Contact hyperaesthesia = 2	.....
	No = 3			
Pinprick test	Painful = 1	Unclear = 2	No pain = 3	.....
Light touch test	Yes = 1	Unclear= 2	No = 3	.....
Vibration	Yes = 1	No = 2*		.....
	*Biosthesiometer reading.....			
Pressure perception	Yes =1	Unclear = 2	No = 3	.....
Ankle reflex	L/F Yes = 1	R/F Yes = 2	L/F No = 3	.....
	R/F No = 4			
Knee reflex	L/F Yes = 1	R/F Yes = 2	L/F No = 3	.....
	R/F No = 4			
Muscular atrophy	Yes = 1	Unilateral = 2	Bilateral = 3	.....
	No = 4			
Proprioception	Yes = 1	No = 2		.....
Two point discrimination	Yes = 1	No = 2		

Vascular Assessment

Skin colour	Normal = 1	Hyperaemic = 2	Pallor = 3		.....
	Other = 4*				
	*Notes				
	.....				
Skin texture	Hyperhydrotic = 1	Anhydrotic = 2	Trophic changes = 3		.....
	Normal = 4	Other = 5*			
	*Notes				
	.....				
Skin temperature	Normal = 1	Cold = 2	Warm = 3	Other = 4*	.....
	*Notes				
	.....				
Varicose veins	Yes = 1	Unilateral = 2	Bilateral = 3	No = 4	.....
Odema	Yes = 1	Unilateral = 2	Bilateral = 3	No = 4	.....
History of DVT	Yes = 1	No = 2			.....
Vascular surgery	Yes = 1*	No = 2			.....
	*Notes				
	.....				
Claudication	100 yards or less = 1	No = 2			.....
Heart conditions	Myocardial infarction = 1	Angina = 2	Hypertension = 3		.....
Capillary Refill Time	Immediate = 1	1sec = 2	2sec = 3	3sec = 4	.....
	>3sec = 5				
Pedal pulses palpable	R/FDP = 1	L/FDP = 2	R/FPT = 3	L/FPT = 4	.....
	No = 5*				
*Doppler analysis	Triphasic = 1	Biphasic = 2	Monophasic = 3		.....
	*Notes				
	.....				
AB Index	<0.9 = 1	>0.9 = 2			.....

Callus Information

Description of callus	Distinct area with minimal thickening of keratin layer = 1				.....
	Moderate thickening = 2	Marked thickening = 3			
	Oval = 4	Diffuse = 5	Round = 6	Spongy = 7	
	Glassy = 8	Flaky = 9			
	Associated with corns = 10		Not associated with corns = 11		
Area	..... Cm^2				
Site	.....				
Chiropody treatment for	1-3mths = 1	3-6mths = 2	6-9mths = 3		.....
callus removal	9-12mths = 4	No = 5	Other = 6*		
	*Notes				
	.....				

Appendix XVIII The Distribution of all the Data Collected from the Diabetes

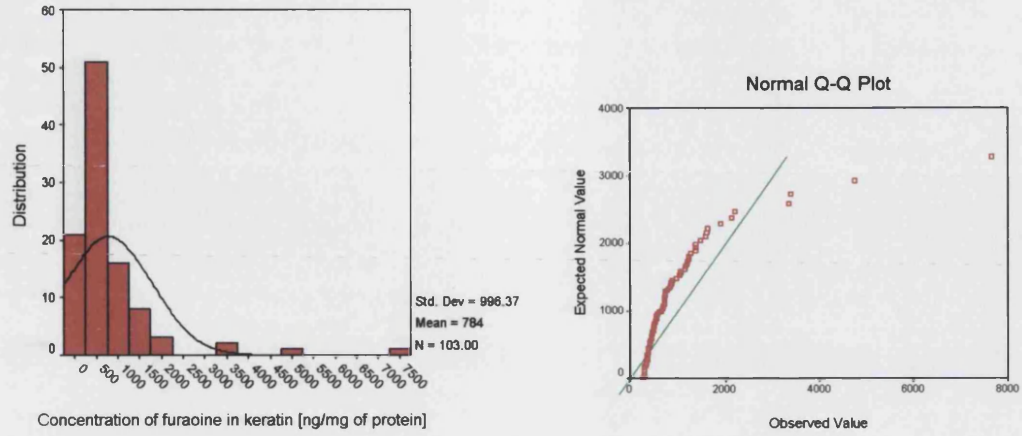

Figure XVIII.i. The distribution of furosine in keratin extracts from 103 diabetic subjects

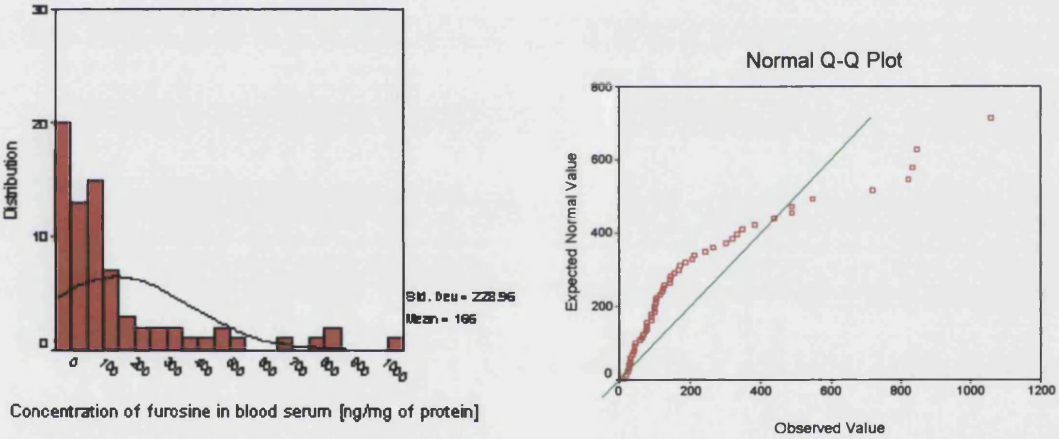

Figure XVIII.ii. The distribution of furosine in blood serum from diabetic subjects

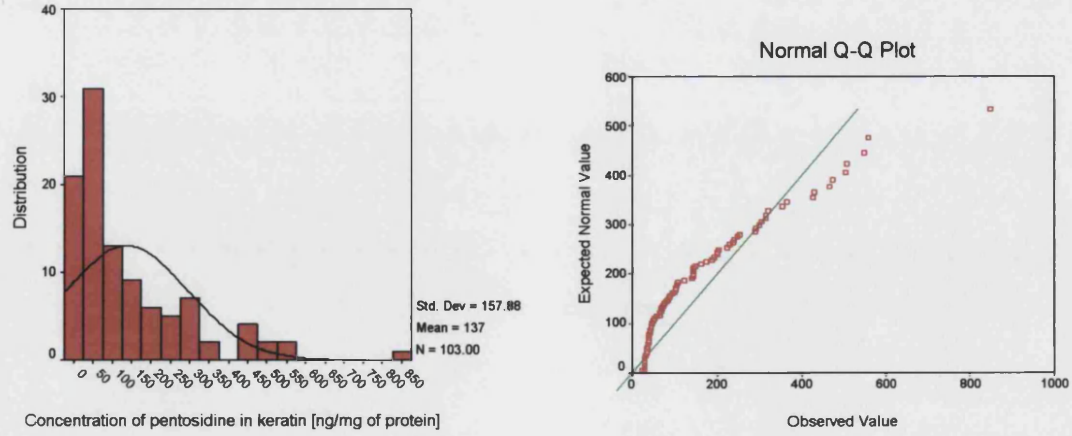

Figure XVIII.iii. The distribution of pentosidine in keratin extracts from103 diabetic subjects

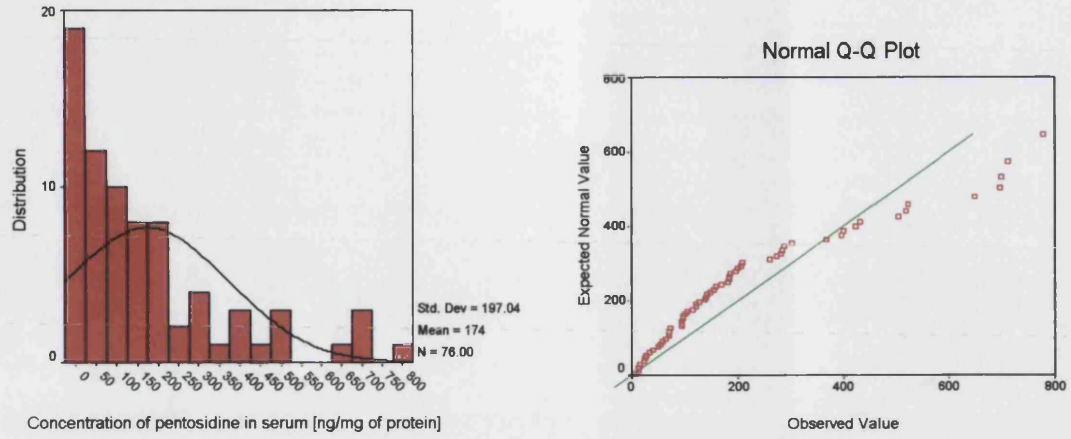

Figure XVIII.iv. The distribution of pentosidine in blood serum from diabetic subjects

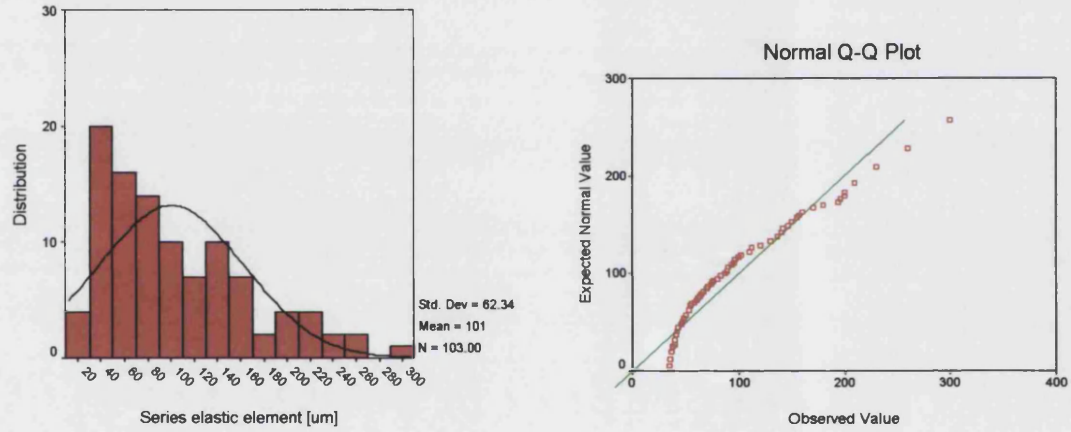

Figure XVIII.v: The distribution of the series elastic element data on stretching of dorsal epidermis.

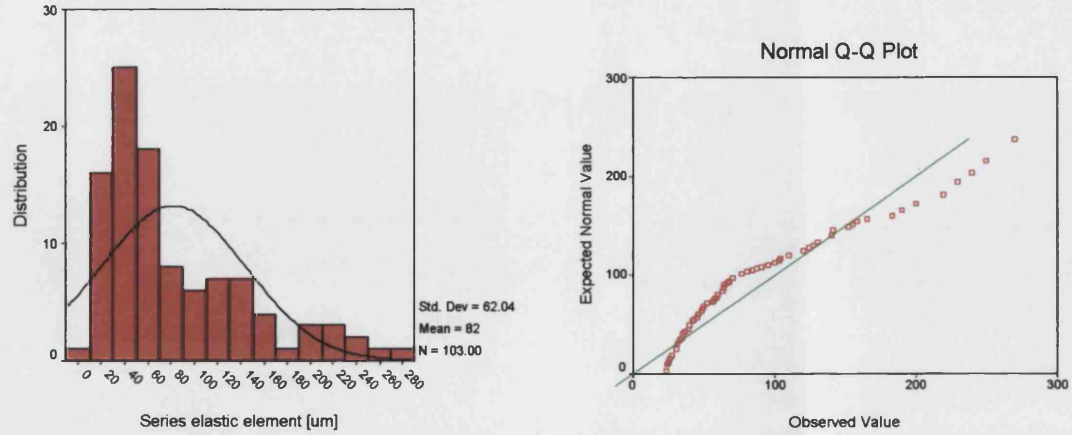

Figure XVIII.vi: The distribution of the series elastic element data on stretching of the epidermis on the MLA.

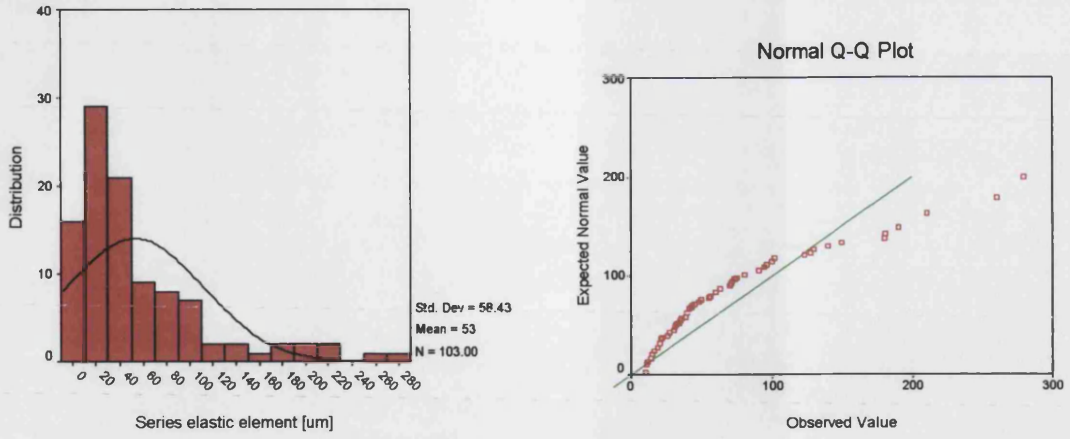

Figure XVIII.vii: The distribution of the series elastic element data on stretching of the epidermis on the PMA.

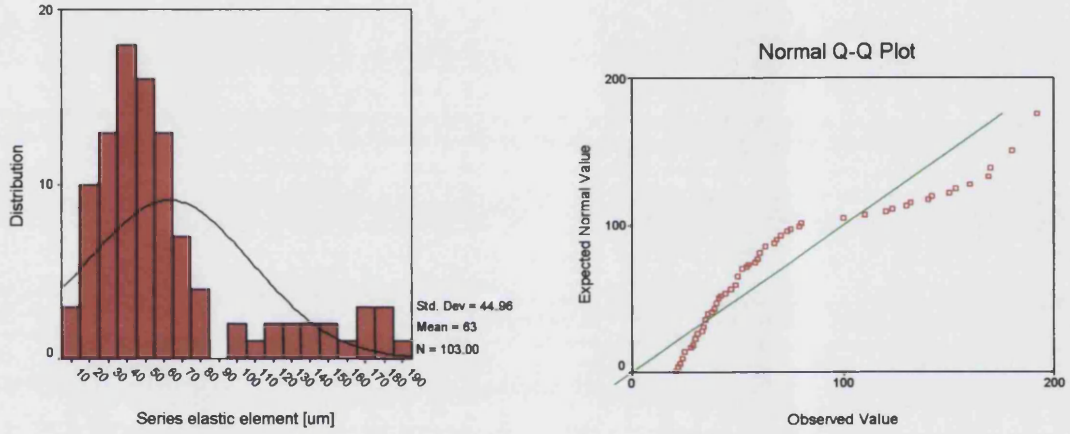

Figure XVIII.viii. The distribution of the series elastic element data on retraction of the dorsal epidermis.

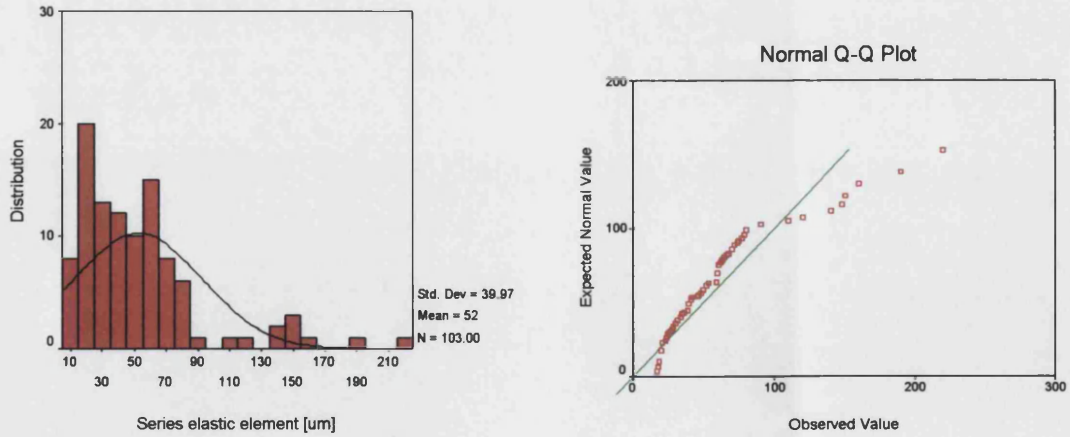

Figure XVIII.ix. The distribution of the series elastic element data on retraction of the epidermis on the MLA.

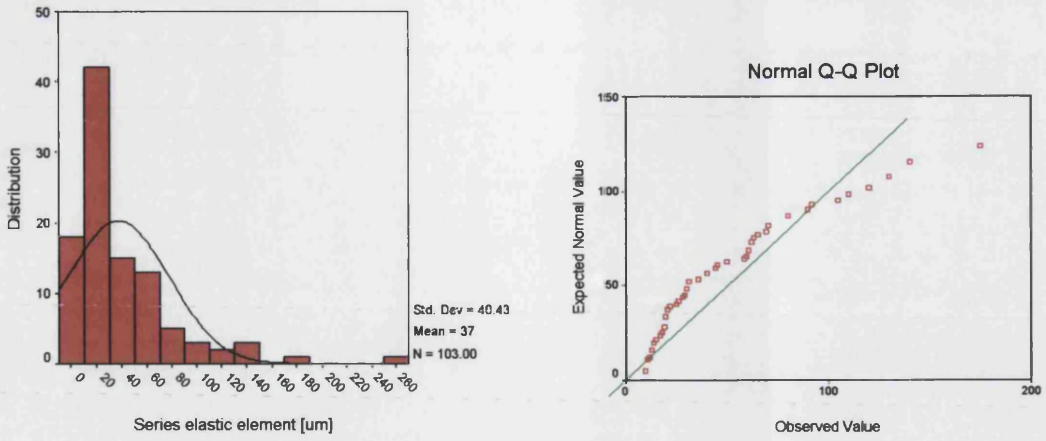

Figure XVIII.x. The distribution of the series elastic element data on retraction of the epidermis on the PMA

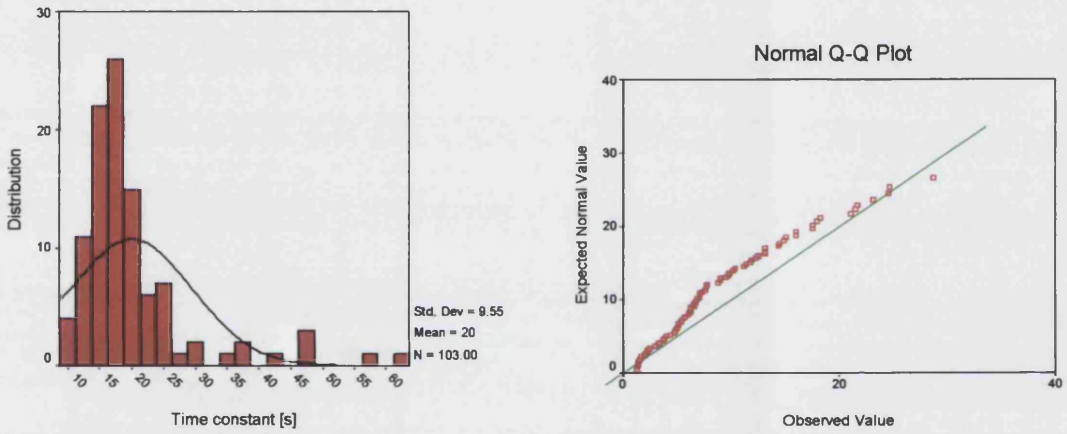

Figure XVIII.xi. The distribution of the time constant data on stretching of the dorsal epidermis

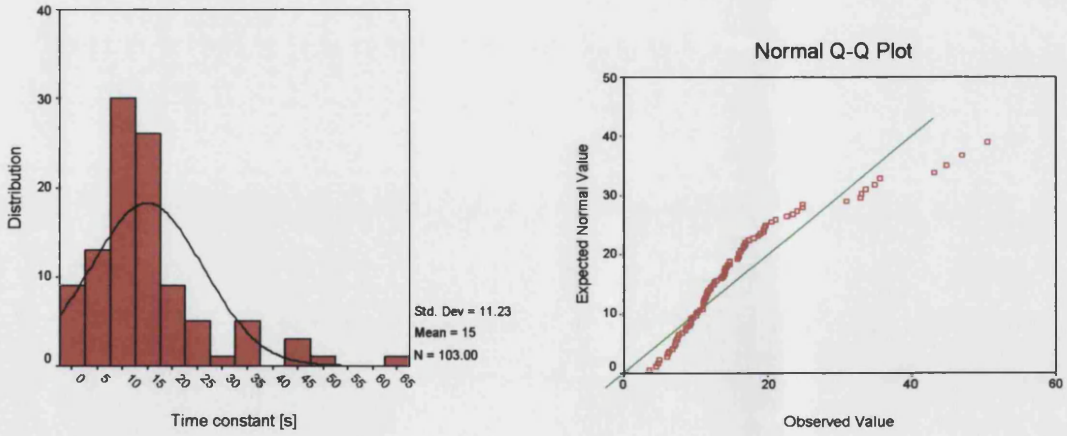

Figure XVIII.xii. The distribution of the time constant data on stretching of the epidermis on the MLA

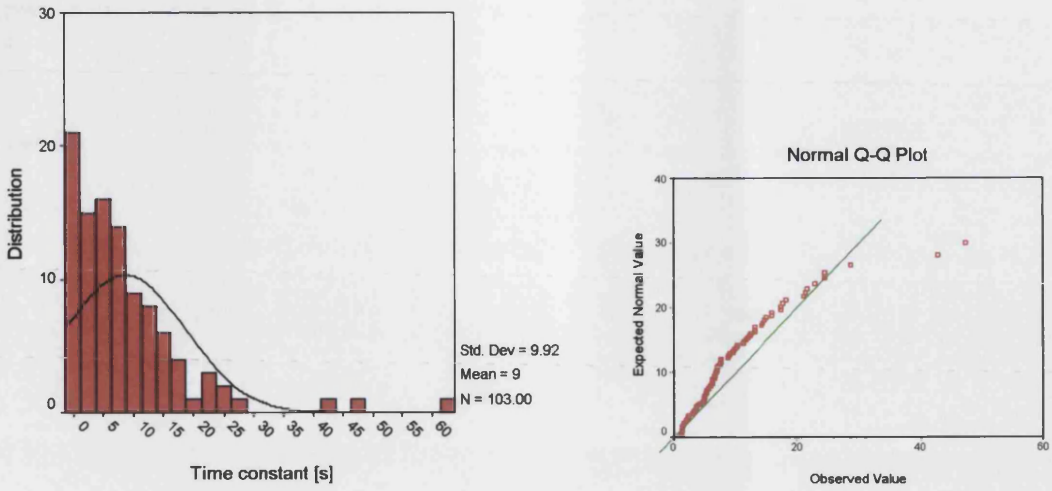

Figure XVIII.xiii. The distribution of the time constant data on stretching of the epidermis on the PMA

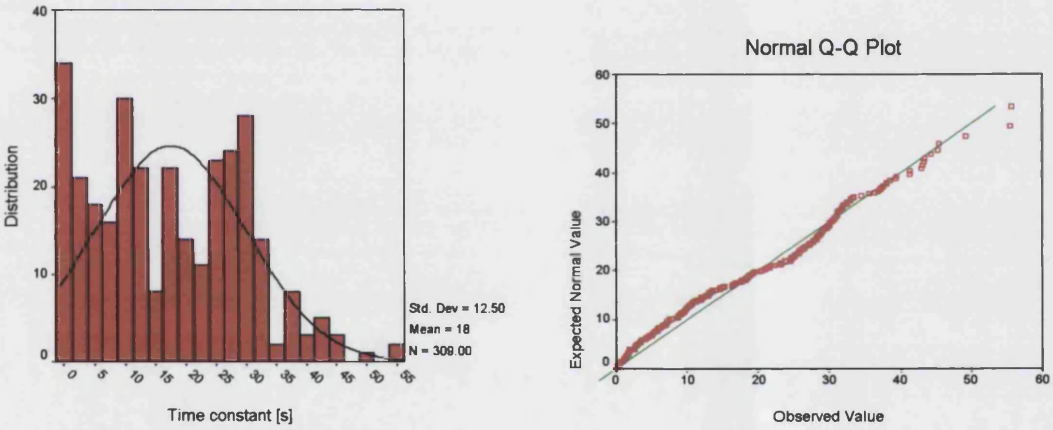

Figure XVIII.xiv. The distribution of the time constant data on retraction of the dorsal epidermis

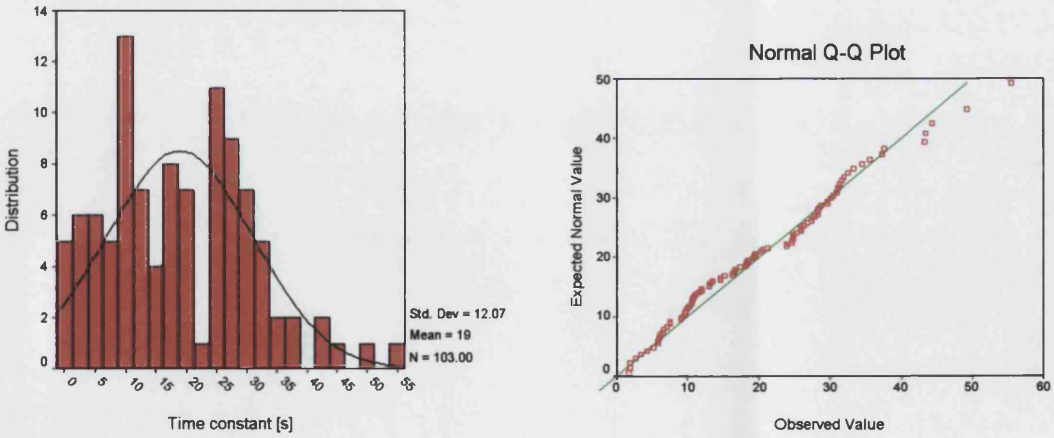

Figure XVIII.xv. The distribution of the time constant data on retraction of the epidermis on the MLA

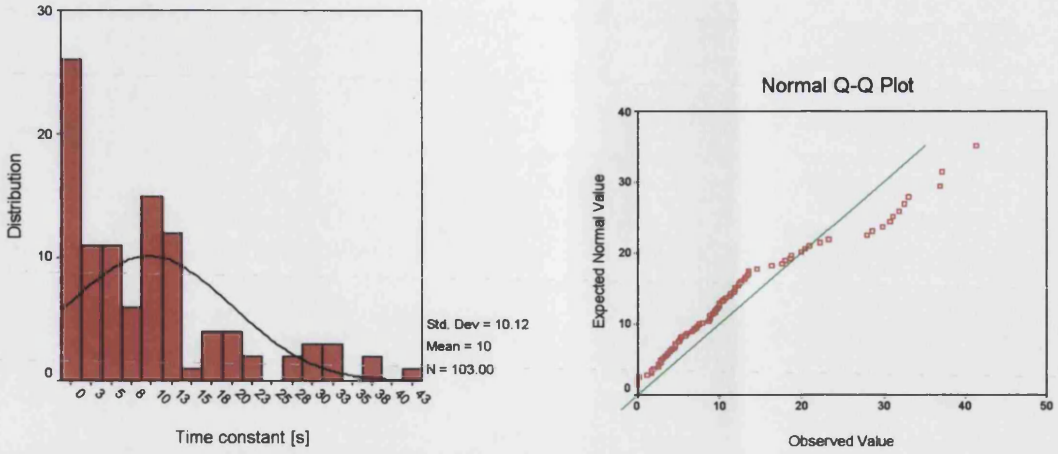

Figure XVIII.xvi. The distribution of the time constant data on retraction of the epidermis on the PMA

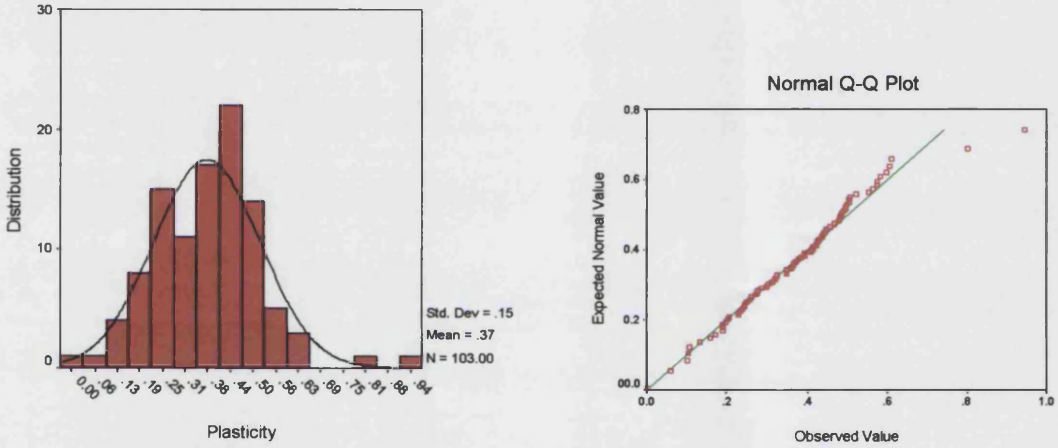

Figure XVIII.xvii. The distribution of the epidermal plasticity data from the dorsum

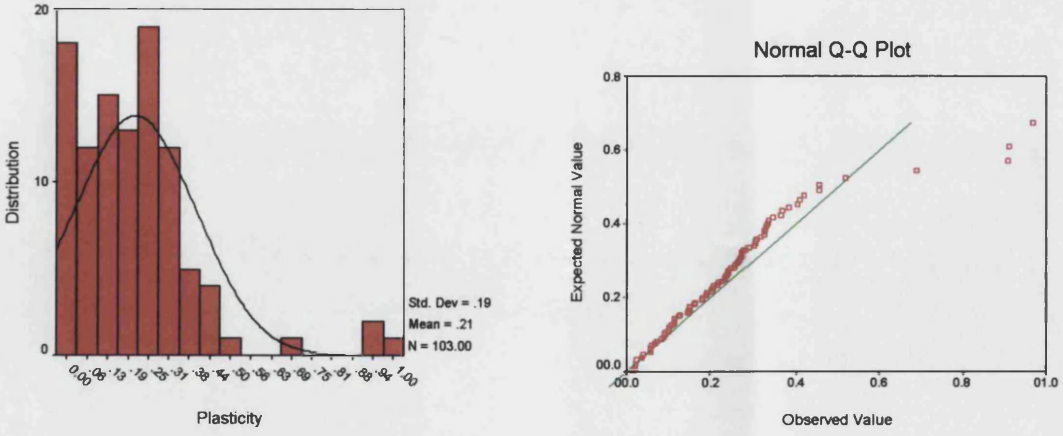

Figure XVIII.xviii. The distribution of the epidermal plasticity data from the MLA

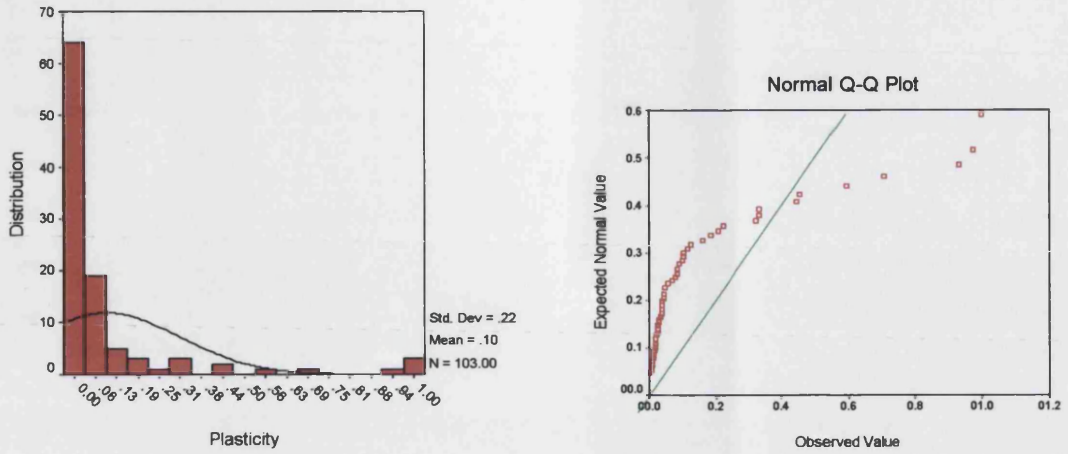

Figure XVIII.xix. The distribution of the epidermal plasticity data from the PMA

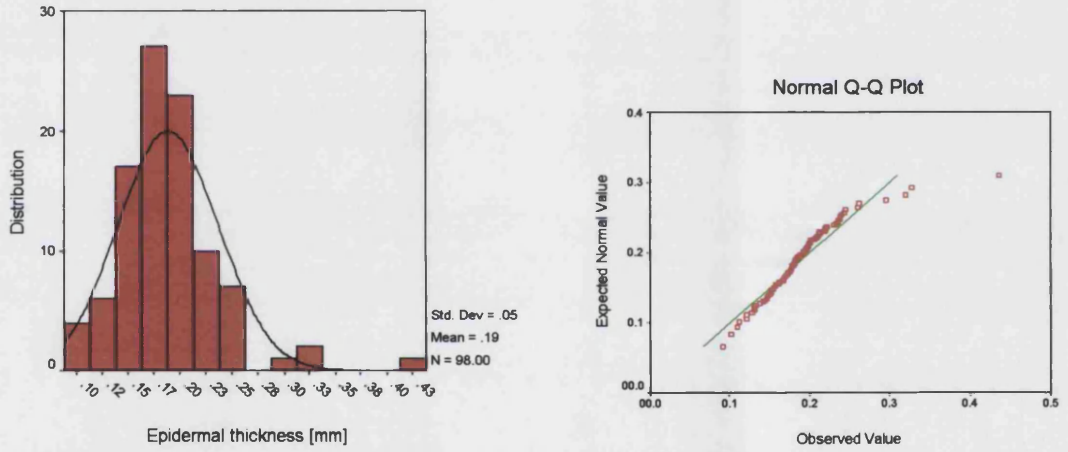

Figure XVIII.xx. The distribution of the epidermal thickness data from the dorsum

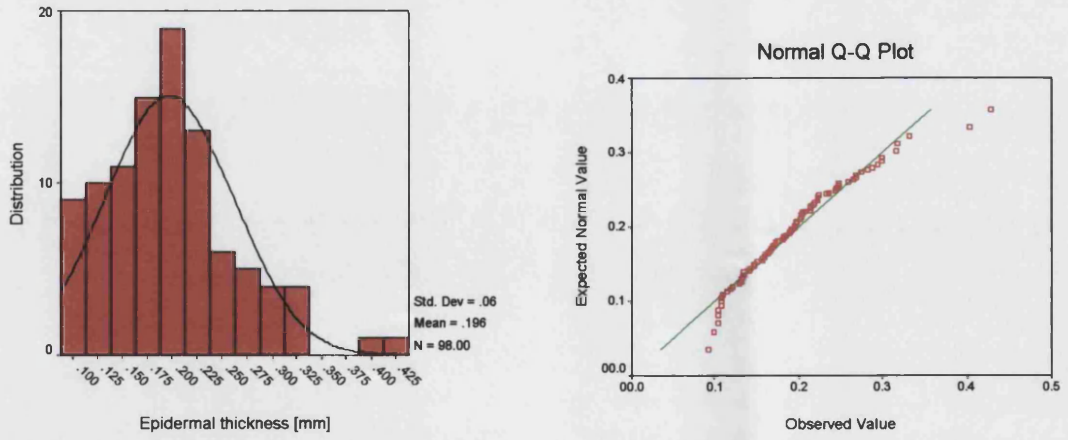

Figure XVIII.xxi. The distribution of the epidermal thickness data from the MLA

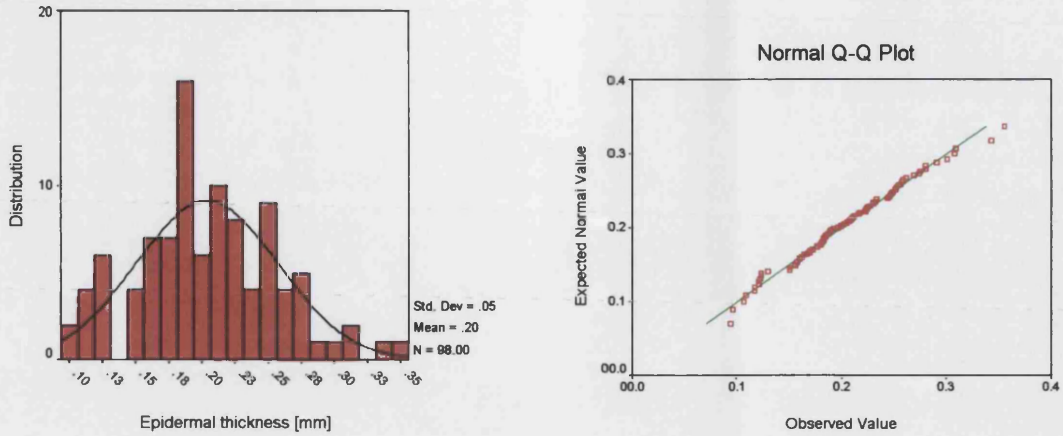

Figure XVIII.xxii. The distribution of the epidermal thickness data from the MLA